

INSTRUMENTATION AND MONITORING OF TIEBACK WALL ON SUM82 AT BRECKSVILLE



Ohio Department of Transportation
Library
1980 West Broad St.
Columbus, OH 43223
614-466-7680

By

Robert Y. Liang
Department of Civil Engineering
The University of Akron
Akron, Ohio 44325-3905

Submitted to

The Ohio Department of Transportation
and
The U.S. Department of Transportation, Federal Highway Administration



TA
770
.L56
2000x

Department of Civil Engineering
The University of Akron
Akron, OH 44325 - 3905

November, 2000

81941



INSTRUMENTATION AND MONITORING OF TIEBACK WALL ON SUM82 AT BTECKSVILLE

Report No.: FHWA/OH-2000/015

State Job No. 14648(0)

Robert Y. Liang, The University of Akron

FOR COPIES OF THIS REPORT, CONTACT:

Ohio Department of Transportation, Mr. Roger L. Green, (614) 275-1381, rgreen@dot.state.oh.us

EXECUTIVE SUMMARY

The instrumentation, monitoring, and analysis of a tieback wall located on the western side of the Cuyahoga valley National Recreation Area (CVNRA) Valley railroad in the vicinity of the State Route 82 bridge over the railroad and the Cuyahoga River, Brecksville, Ohio constitutes the main work of this project. Slope movements on the western wall of the Cuyahoga River valley were noticed, extending excessively to the north and south of the State Route 82 bridge centerline. Slope movements were also occurring within the 80 feet wide bridge right-of-way portion of the embankment. ODOT has conducted an independent investigation of this area and developed plans using tieback walls to stabilize the slope movements.

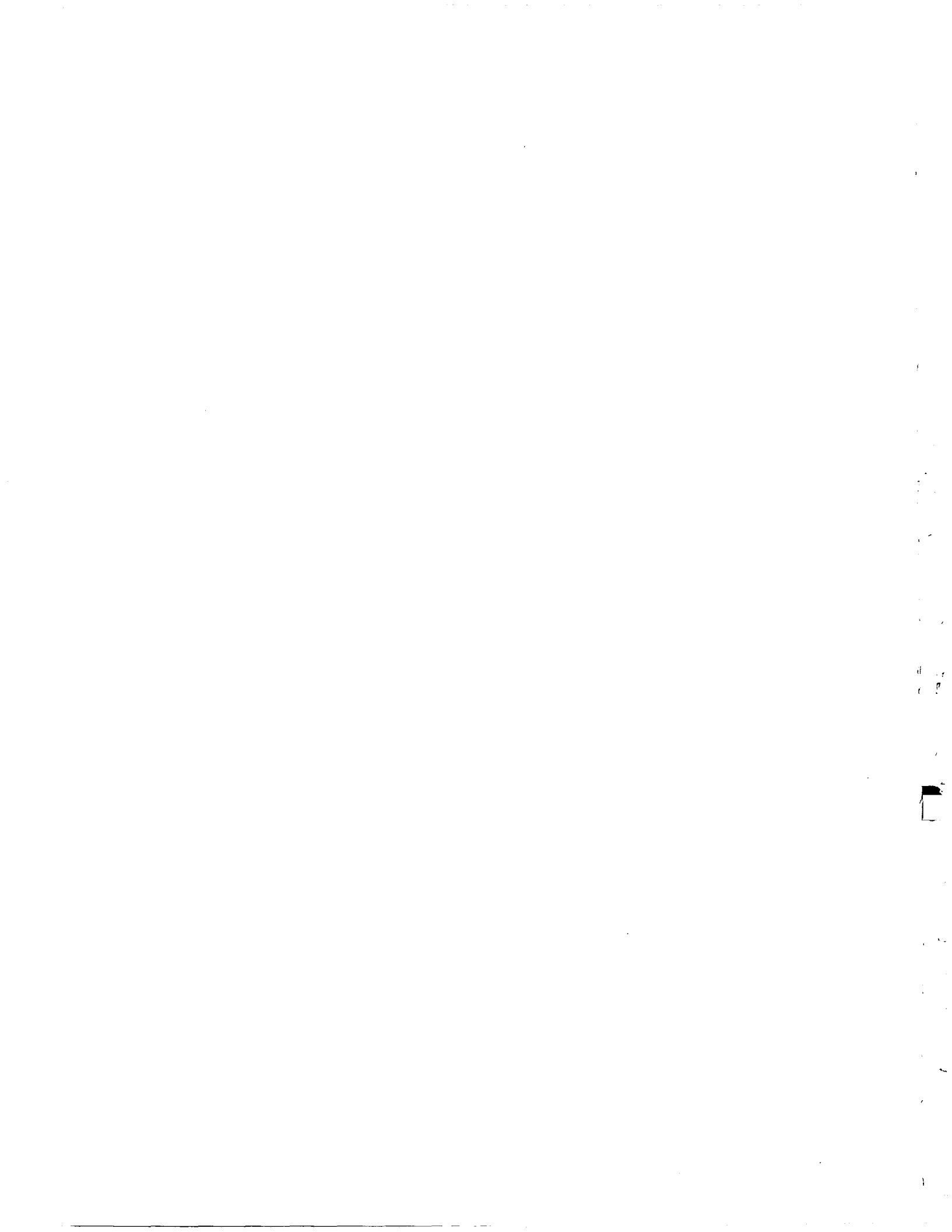
The objectives of this study were to: (a) develop and carry out an instrumentation and monitoring plan for the tieback wall to be constructed on the state Rt. 82, in Brecksville, Ohio (Project No. SUM-82-0.00), (b) plan and carry out load test of tiebacks in shale to determine the load-carrying capacity, load transfer mechanism, and the water effect, (c) plan and carry out creep tests of tiebacks to gain better insight on the time-dependent creep and stress relaxation behavior of tiebacks installed in shale, (d) document the construction sequence and the measured tieback wall responses, (e) monitor tieback wall performance at least for a year after the wall construction is complete, (f) perform a detailed analysis of measured data from the load test results and the monitoring data of instrumented walls, (g) investigate the interrelationships among the magnitude and distribution of the earth pressures, the tieback lock-off loads, the friction between the wall and the backfill, the pile hearing, and the magnitude and nature of ground movements, and (h) to provide recommendations for improved design methods for tieback walls with permanent anchors in shale.

All the elements of the studied tieback wall were provided with instrumentation including strain gages, inclinometers, load cells, and peizometers. The data gathered from all sensors and gages were analyzed, and utilized to validate the developed tieback computer program, and evaluate the present analysis methods.

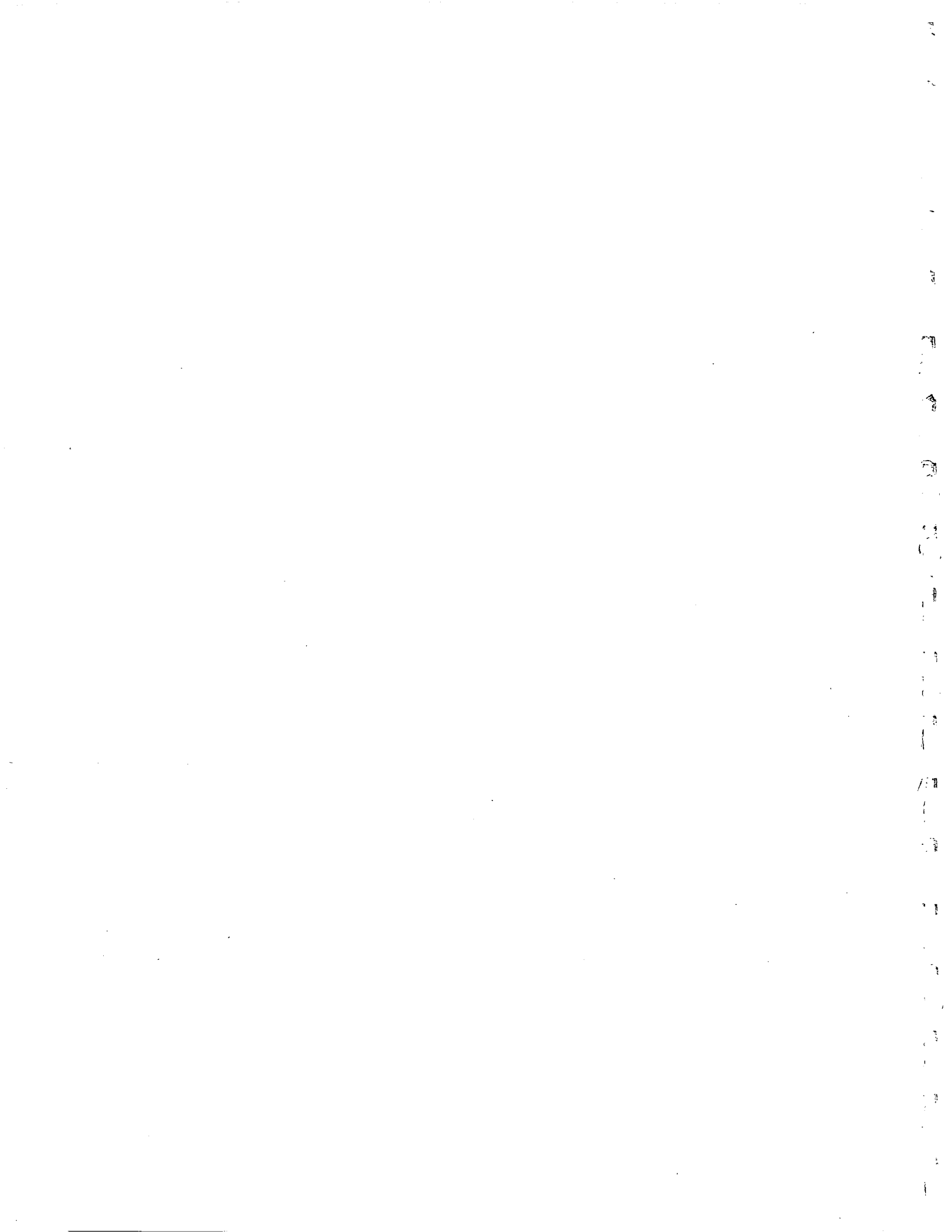
Based on the comparisons of the existing "Earth Pressure Diagram" analysis methods, it was found that these methods result in considerable discrepancies with measured diagrams. The moments measured along the soldier pile were best fitted when a moment was introduced at the anchor-pile point.

A Finite Element Method (FEM) program, PLAXIS, was employed to perform a numerical simulation of the construction of the tieback walls utilizing the inclinometers' readings in the early stage of construction. Then the deduced soil parameters were fixed in the subsequent analysis of various construction stages to accommodate the stress-path dependency of the soil response. The close agreements between the measured and the simulation lend strong support to the validity of the FEM analysis techniques.

Finally, a finite element program developed for the purpose of tieback wall analysis and design was introduced. This program was shown to provide a good predictive and analytic tool for analyzing the structural behavior of the tieback wall, accommodating for the combined effects of construction stage and anchor prestressing. This program is also capable of simulating the anchor-soil response. The anchor-soil model was described and verified and shown to be powerful in both forward and backward calculations encountered in the anchor-soil system.



1. Report No. FHWA/OH-2000/015	2. Government Accession No.	3. Recipient's Catalog No. 3 1980 00021 8624	
4. Title and Subtitle INSTRUMENTATION AND MONITORING OF TIEBACK WALL ON SUM82 AT BRECKSVILLE		5. Report Date August, 2000	
		6. Performing Organization Code	
7. Author(s) Robert Y. Liang		8. Performing Organization Report No.	
9. Performing Organization Name and Address The University of Akron Department of Civil Engineering Akron, OH 44325		10. Work Unit No. (TRAIS)	
		11. Contract or Grant No. State Job No. 14648(0)	
12. Sponsoring Agency Name and Address Ohio Department of Transportation 1980 West Broad Street Columbus, OH 43223		13. Type of Report and Period Covered Final Report	
		14. Sponsoring Agency Code	
15. Supplementary Notes Prepared in cooperation with the U.S. Department of Transportation, Federal Highway Administration			
16. Abstract The instrumentation, monitoring, and analysis of a tieback wall located on the western side of the Cuyahoga valley National Recreation Area (CVNRA) Valley railroad in the vicinity of the State Route 82 bridge over the railroad and the Cuyahoga River, Brecksville, Ohio constitutes the main work of this project. All the elements of the studied tieback wall were provided with instrumentation including strain gages, inclinometers, load cells, and peizometers. The data gathered from all sensors and gages were analyzed, and utilized to validate the developed tieback computer program, and evaluate the present analysis methods. Based on the comparisons of the existing "Earth Pressure Diagram" analysis methods, it was found that these methods result in considerable discrepancies with measured diagrams. The moments measured along the soldier pile were best fitted when a moment was introduced at the anchor-pile point. A Finite Element Method (FEM) program, PLAXIS, was employed to perform a numerical simulation of the construction of the tieback walls utilizing the inclinometers' readings in the early stage of construction. Then the deduced soil parameters were fixed in the subsequent analysis of various construction stages to accommodate the stress-path dependency of the soil response. The close agreements between the measured and the simulation lend strong support to the validity of the FEM analysis techniques. Finally, a finite element program developed for the purpose of tieback wall analysis and design was introduced. This program was shown to provide a good predictive and analytic tool for analyzing the structural behavior of the tieback wall, accommodating for the combined effects of construction stage and anchor prestressing. This program is also capable of simulating the anchor-soil response. The anchor-soil model was described and verified and shown to be powerful in both forward and backward calculations encountered in the anchor-soil system.			
17. Key Words Tieback, Instrumentation, Monitoring, Anchor, Pile, Finite Element Method		18. Distribution Statement No Restrictions. This document is available to the public through the National Technical Information Service, Springfield, Virginia 22161	
19. Security Classif. (of this report) Unclassified	20. Security Classif. (of this page) Unclassified	21. No. of Pages	22. Price



DISCLAIMER STATEMENT

The contents of this report reflect the views of the author who is responsible for the facts and the accuracy of the data presented herein. The contents do not necessarily reflect the official views or policies of the Ohio Department of Transportation or the Federal Highway Administration. This report does not constitute a standard, specification or regulation.



1
2
3
4
5
6
7
8
9
10
11
12
13
14
15
16
17
18
19
20
21
22
23
24
25
26
27
28
29
30
31
32
33
34
35
36
37
38
39
40
41
42
43
44
45
46
47
48
49
50
51
52
53
54
55
56
57
58
59
60
61
62
63
64
65
66
67
68
69
70
71
72
73
74
75
76
77
78
79
80
81
82
83
84
85
86
87
88
89
90
91
92
93
94
95
96
97
98
99
100

ACKNOWLEDGMENT

The completion of this study comes as a result of the efforts of numerous individuals and organizations. The Ohio Department of Transportation (ODOT) is gratefully acknowledged for providing financial support for this work.

The author also is indebted to the following individuals and organizations for their technical support:

Frank Martin, and Bulent Bilgin of ODOT District 4; Vik Dalal of ODOT Research and Development; Eugene Geiger of ODOT Geotechnical Division; Rick Engel, and Jawdat Siddiqi of ODOT Structures Division; Rob Bobel of Cuyahoga Valley National Recreation Area; National Engineering and Contracting Company; Gannet Fleming Corddry & Carpenter Engineers and Planners; Geotech Services Inc.; The department of Civil Engineering at the University of Akron, for providing services of Roger Buck, engineering technician.

Special thanks go to Dr. Jamal Nusairat for leading the field instrumentation team, Sanping Zeng for the Finite Element Simulation, and the graduate students at the University of Akron who assist in the field testing.

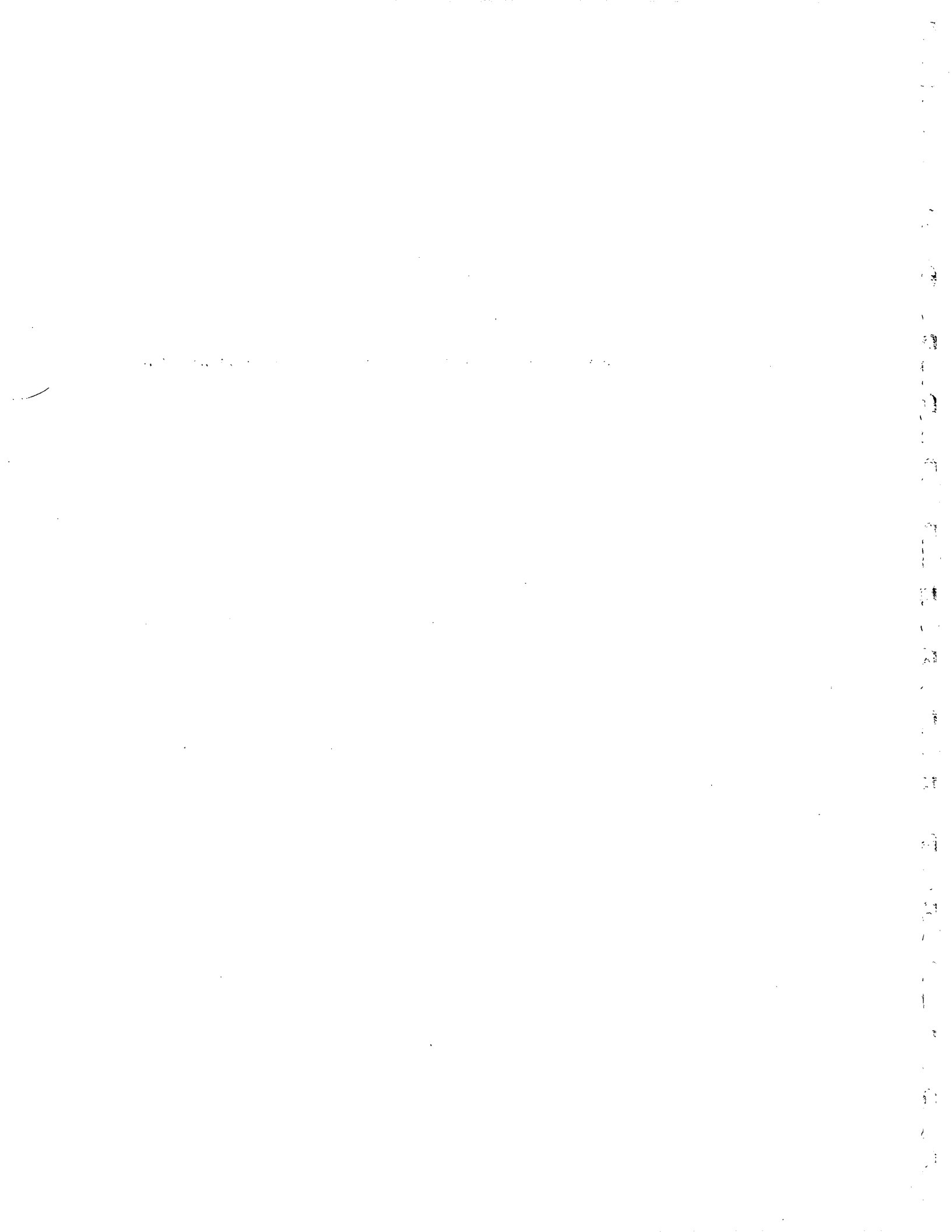


TABLE OF CONTENT

	<u>Page</u>
EXECUTIVE SUMMARY	i
AKNOLEDGEMENT	ii
TABLE OF CONTENT	iii
LIST OF TABLES	viii
LIST OF FIGURES	ix
I. INTRODUCTION	I-1
I.1 STATEMENT OF THE PROBLEM	I-1
I.2 OBJECTIVES OF THE STUDY	I-3
I.3 ORGANIZATION OF THE REPORT	I-4
II. BACKGROUND OF THE PROJECT	II-1
II.1 INTRODUCTION	II-1
II.2 INITIAL SITE INVESTIGATION	II-2
II.2.1 Upper Soil Deposits	II-5
II.2.2 Lower Soil Deposits	II-5
II.2.3 Shale Stratum	II-6
II.2.4 Groundwater	II-7

II.3	PROBLEM DESCRIPTION	II-7
II.4	DESIGN OF TIEBACK WALLS	II-10
III.	INSTRUMENTATION/MONITORING PROGRAM	III-1
III.1	INTRODUCTION	III-1
III.2	INSTRUMENTATION PLAN	III-1
III.3	SLOPE MOVEMENT MONITORING	III-2
III.4	TIEBACK STRUCTURAL BEHAVIOR	III-3
III.4.1	Soldier Piles	III-3
III.4.2	Ground Anchors	III-3
III.5	INSTRUMENTATION INSTALLATION DETAILS	III-4
III.5.1	Sequence of Installation	III-4
III.5.2	Techniques of Installing Instruments and Monitoring	III-7
III.6	DATA ACQUISITION PLANS	III-9
IV.	SHORT AND LONG TERM MONITORING RESULTS	IV-1
IV.1	OVERVIEW OF COLLECTED INFORMATION BEFORE COMMENCEMENT OF CONSTRUCTION	IV-1
IV.2	UPPER AND LOWER TIER ANCHOR FAILURE TESTS	IV-2
IV.3	SOLDIER PILES CONSTRUCTION	IV-3

IV.4	ROCK ANCHOR CONSTRUCTION	IV-4
IV.5	TENSIONING OF ROCK ANCHORS	IV-5
IV.6	GROUTING OF ANCHOR HEADS AND GRADING OF SLOPES	IV-6
IV.7	LONG-TERM MONITORING RESULTS	IV-7
V.	ANALYSIS OF ANCHOR TEST RESULTS	
V.1	INTRODUCTION	V-1
V.2	DEVELOPMENT OF SOIL-ANCHOR INTERFACE MODEL	V-3
V.3	CONSTRUCTION OF INTERFACE LOAD TRANSFER CURVE	V-7
V.4	NUMERICAL STUDIES	V-9
V.5	DEVELOPED ANCHOR-SOIL MODEL PREDICTABILITY	V-11
V.5.1	Anchor Performance by Forward Calculation	V-11
V.5.2	Determination of Interface Model Parameters by Back Calculation	V-12
V.6	VERIFICATION OF THE ANCHOR-SOIL MODEL PREDICTIBILITY	V-16
V.6.1	Comparison between Predictions and Laboratory Test Results	V-16
V.6.2	Tieback 622-1, Outlined in Ludwig Study	V-17
V.7	UPPER AND LOWER TIER FAILURE TESTS AT SUM-82 PROJECT	V-19
V.8	DISCUSSION	V-21
V.9	CONCLUSIONS	V-22

VI.	SIMULATION OF TIEBACK WALL CONSTRUCTION USING FEM PROGRAM PLAXIS	VI-1
VI.1	INTRODUCTION	VI-1
VI.2	FINITE ELEMENT MODELING OF SUM-82 PROJECT	VI.2
VI.3	MATERIAL PROPERTIES OF TIEBACK WALL COMPONENTS	VI.2
VI.4	CALIBRATION STUDY TO DETERMINE SOIL AND BOND INTERFACE PROPERTIES	VI.3
VI.6	SIMULATION OF CONSTRUCTION PROCESSES	VI.6
VI.7	FEM ANALYSIS RESULTS AND DISCUSSION	VI.8
VI.7.1	Stresses and Deformations in Soil Mass	VI.8
VI.7.2	Tieback Wall Structure Response	VI.9
VI.7.2.1	Soldier piles	VI.9
VI.7.2.2	Ground Anchors	VI.11
VI.8	CONCLUSIONS	VI.12
VII.	STRUCTURAL ANALYSIS OF TIEBACK WALL SYSTEM	VII-1
VII.1	INTRODUCTION	VII-1
VII.1.1	Lateral Earth Pressure	VII-3
VII.2	NUMERICAL COMPUTATIONAL ALGORITHMS	VII-11

VII.2.1	Soil Reaction Model	VII-14
VII.2.2	Representation of Tiebacks	VII-15
VII.2.3	Case Study	VII-16
VII.2.4	Parametric Study	VII-18
VII.3	ANALYTICAL STUDY OF SUMMIT 82, SOLDIER PILES	VII-21
VII.4	SUMMARY AND CONCLUSIONS	VII-23
VIII.	SUMMARY AND CONCLUSIONS	VIII-1
IX	REFERNCES	IX-1
	APPENDIX A	A-1

LIST OF TABLES

Table	Description	Page
2.1	Detailed information about soldier piles and anchors.	II-12
4.1	Major construction events.	IV-2
5.1	Soil data for Tieback 622-1	V-23
5.2	Load-displacement measurements for Tieback 622-1 (Ludwig, 1984)	V-24
6.1	Properties of Tieback Wall Components	VI-3
6.2	Typical Combinations of Soil and Interface Properties	VI-5
6.3	Incremental steps for nonlinear calculation	VI-8
6.4	Comparisons between maximum bending moments	VI-11

LIST OF FIGURES

<u>Figure</u>	<u>Description</u>	<u>Page</u>
2.1	Location of boreholes for site investigation.	II-14
2.2	Site plan of the project.	II-15
2.3	Elevation view of the project.	II-16
2.4	Plan and profile for the upper tier wall.	II-17
2.5	Cross-section in the upper tier wall.	II-18
2.6	Plan and profile of the lower tier wall.	II-19
2.7	Cross-section in the lower tier wall.	II-20
2.8	Details of the strut and casing for the rock anchors.	II-21
3.1	Plan view of the entire stabilizing system.	III-10
3.2	Upper tier wall, strain gage locations.	III-11
3.3	Lower tier wall, strain gage locations.	III-12
3.4	Locations of earth inclinometers and piezometers.	III-13
3.5	Lower tier wall, soldier pile # 11 strain gage locations and initial readings.	III-14
3.6	Lower tier wall, soldier pile # 12 strain gage locations and initial readings.	III-15
3.7	Upper tier wall, soldier pile # 30 strain gage locations and initial	III-16

	readings.	
3.8	Upper tier wall, soldier pile # 31 strain gage locations and initial readings.	III-17
3.9	Vibrating wire gage been welded to the soldier pile.	III-18
3.10	Vibrating wire gage been calibrated after installation.	III-19
3.11	A series of gages being installed and checked.	III-20
3.12	Protection C bracket been welded to protect the gage.	III-21
3.13	Soldier pile instrumented and ready to be moved to the hole.	III-22
3.14	Details of anchor instrumentation and final setup.	III-23
3.15	Anchors coiled and casing used in the construction.	III-24
3.16	Rock anchor hole drilling.	III-25
3.17	Overview of the anchor drilling operation.	III-26
3.18	Anchor hole drilled and casing installed.	III-27
3.19	Strand gage being installed on the 7-wire strand.	III-28
3.20	Strand gage being installed on the 7-wire strand and calibrated.	III-29
3.21	Strand gage being installed on the 7-wire strand and greased.	III-30
3.22	Anchor being installed and grouted.	III-31
3.23	Anchor testing undergoing.	III-32
3.24	Anchor under testing and Anchor already locked-off.	III-33
3.25	Start time schedule for major construction events.	III-34

3.26	Drilling operation for the earth inclinometers	III-35
3.27	Inclinometer installed and been grouted.	III-36
3.28	Inclinometer protective casing installed and drilling for piezometer.	III-37
3.29	Vibrating wire Piezometer installed.	III-38
3.30	Instrumented soldier piles ready for installation.	III-39
3.31	Instrumented soldier pile being lifted for installation.	III-40
3.32	The inclinometer being attached to the soldier pile.	III-41
3.33	The inclinometer being extended while lowering the pile.	III-42
3.34	The soldier pile being wrapped with plastic sheet to prevent contact with concrete.	III-43
3.35	The instrumented soldier piles are installed.	III-44
3.36	The strain gages being checked after the pile was installed.	III-45
3.37	Soldier piles being installed in the lower tier.	III-46
3.38	Lowering the instrumented tendon for the lower tier failure test.	III-47
3.39	The lower tier failure test anchor installed and grouted.	III-48
3.40	Drilling for the upper tier failure test anchor.	III-49
3.41	The upper tier failure test anchor being installed.	III-50
3.42	Setup for the upper tier anchor failure test.	III-51
3.43	Upper tier anchor failure test.	III-52
3.44	Setup for the lower tier anchor failure test.	III-53

3.45	Lower tier anchor failure test.	III-54
3.46	Anchor #11-B instrumented tendon.	III-55
3.47	Drilling of instrumented anchor #30-B.	III-56
3.48	Testing of instrumented anchor #30-B.	III-57
3.49	Locking-off anchor #30-B after testing.	III-58
3.50	Testing of anchor #30-C in the upper tier wall.	III-59
3.51	Testing of anchor #11-B in the lower tier wall.	III-60
3.52	Digging a trench to access the lower row of anchors in the upper tier wall.	III-61
3.53	Installation of casing for the upper row of anchors in the lower tier.	III-62
3.54	Temporary lagging installed in the upper tier wall.	III-63
3.55	Performance test of anchor #30-C in the upper tier wall.	III-64
3.56	Installation of precast panels.	III-65
3.57	Drainage blanket installed behind the panels.	III-66
3.58	Concrete box installed to house the data collection devices in the lower tier wall area.	III-67
3.59	Concrete box installed to house the data collection devices in the upper tier wall area.	III-68
3.60	Anchor caps been installed and grouted.	III-69
3.61	Installation of vibrating wire piezometer.	III-70
3.62	Vibrating wire piezometer installed and being checked.	III-71

3.63	Details of instrumented anchor head assembly.	III-72
3.64	Final location of data collection devices in the upper tier wall.	III-73
3.65	Final location of data collection devices in the lower tier wall.	III-74
4.1	Schematic of anchor load testing setup.	IV-9
4.2	Upper tier failure test load vs. displacement at anchor head.	IV-10
4.3	Upper tier failure test, deformation at each strand gage location.	IV-11
4.4	Lower tier failure test, load vs. displacement at anchor head.	IV-12
4.5	Lower tier failure test, deformation at each strand gage location.	IV-13
4.6	Soldier pile # 30, strain on side I (backfill side).	IV-14
4.7	Soldier pile # 30, strain on side II (wall face side).	IV-15
4.8	Soldier pile # 31, strain on side I (backfill side).	IV-16
4.9	Soldier pile # 31, strain on side II (wall face side).	IV-17
4.10	Soldier pile # 11, strain on side I (backfill side).	IV-18
4.11	Soldier pile # 11, strain on side II (wall face side).	IV-19
4.12	Soldier pile # 12, strain on side I (backfill side).	IV-20
4.13	Soldier pile # 12, strain on side II (wall face side).	IV-21
4.14	Moment vs. depth in soldier pile # 11 during construction.	IV-22
4.15	Moment vs. depth in soldier pile # 12 during construction.	IV-23
4.16	Moment vs. depth in soldier pile # 30 during construction.	IV-24

4.17	Moment vs. depth in soldier pile # 31 during construction.	IV-25
4.18	Axial force vs. depth in soldier pile # 11 during construction.	IV-26
4.19	Axial force vs. depth in soldier pile # 12 during construction.	IV-27
4.20	Axial force vs. depth in soldier pile # 30 during construction.	IV-28
4.21	Axial force vs. depth in soldier pile # 31 during construction.	IV-29
4.22	Anchor hole drilling.	IV-30
4.23	Drilling an anchor hole in the lower tier wall.	IV-31
4.24	Drilling an anchor hole in the upper tier wall.	IV-32
4.25	Lifting the tendon with the crane for installation.	IV-33
4.26	A permanent vibrating wire load cell installed at the anchor head.	IV-34
4.27	Anchor load test undergoing.	IV-35
4.28	Performance test of anchor #30B, load vs. displacement at anchor head.	IV-36
4.29	Performance test of anchor #30B, deformation at each gage location in the bonded length.	IV-37
4.30	Performance test of anchor #31B, load vs. displacement at anchor head.	IV-38
4.31	Performance test of anchor #31B, deformation at each gage location in the bonded length.	IV-39
4.32	Performance test of anchor #11B, load vs. displacement at anchor head.	IV-40
4.33	Performance test of anchor #11B, deformation at each gage location	IV-41

in the bonded length.

4.34	Performance test of anchor #30C, load vs. displacement at anchor head.	IV-42
4.35	Performance test of anchor #30C, deformation at each gage location in the bonded length.	IV-43
4.36	Performance test of anchor #11A, load vs. displacement at anchor head.	IV-44
4.37	Performance test of anchor #11A, deformation at each gage location in the bonded length.	IV-45
4.38	Performance test of anchor #30A, load vs. displacement at anchor head.	IV-46
4.39	Performance test of anchor #30A, deformation at each gage location in the bonded length.	IV-47
4.40 (a)	Deflection vs. depth using inclinometer in the A+ direction (East) for soldier pile # 11.	IV-48
4.40 (b)	Deflection vs. depth using inclinometer in the B+ direction (South) for soldier pile # 11.	IV-49
4.41 (a)	Deflection vs. depth using inclinometer in the A+ direction (East) for soldier pile # 12.	IV-50
4.41 (b)	Deflection vs. depth using inclinometer in the B+ direction (South) for soldier pile # 12.	IV-51
4.42 (a)	Deflection vs. depth using inclinometer in the A+ direction (East) for soldier pile # 30.	IV-52
4.42 (b)	Deflection vs. depth using inclinometer in the B+ direction (South) for soldier pile # 30.	IV-53
4.43 (a)	Deflection vs. depth using inclinometer in the A+ direction (East) for soldier pile # 31.	IV-54

4.43 (b)	Deflection vs. depth using inclinometer in the B+ direction (South) for soldier pile # 31.	IV-55
4.44 (a)	Deflection vs. depth using inclinometer in the A+ direction (East) for earth inclinometer # 1.	IV-56
4.44 (b)	Deflection vs. depth using inclinometer in the b+ direction (South) for earth inclinometer # 1.	IV-57
4.45 (a)	Deflection vs. depth using inclinometer in the A+ direction (East) for earth inclinometer # 2.	IV-58
4.45 (b)	Deflection vs. depth using inclinometer in the b+ direction (South) for earth inclinometer # 2.	IV-59
4.46 (a)	Deflection vs. depth using inclinometer in the A+ direction (East) for earth inclinometer # 3.	IV-60
4.46 (b)	Deflection vs. depth using inclinometer in the b+ direction (South) for earth inclinometer # 3.	IV-61
4.47	Pore water pressure recorded using the peizometer.	IV-62
4.48	Strain vs. depth for soldier pile # 11, side I, till 1/29/2000.	IV-63
4.48	Strain vs. depth for soldier pile # 11, side II, till 1/29/2000.	IV-64
4.50	Strain vs. depth for soldier pile # 12, side I, till 1/29/2000.	IV-65
4.51	Strain vs. depth for soldier pile # 12, side II, till 1/29/2000.	IV-66
4.52	Strain vs. depth for soldier pile # 30, side I, till 1/29/2000.	IV-67
4.53	Strain vs. depth for soldier pile # 30, side II, till 1/29/2000.	IV-68
4.54	Strain vs. depth for soldier pile # 31, side I, till 1/29/2000.	IV-69
4.55	Strain vs. depth for soldier pile # 31, side II, till 1/29/2000.	IV-70

4.56	Moment vs. depth for soldier pile # 11 till 1/29/2000.	IV-71
4.57	Moment vs. depth for soldier pile # 12 till 1/29/2000.	IV-72
4.58	Moment vs. depth for soldier pile # 30 till 1/29/2000.	IV-73
4.59	Moment vs. depth for soldier pile # 31 till 1/29/2000.	IV-74
4.60	Axial force vs. depth for soldier pile # 11 till 1/29/2000.	IV-75
4.61	Axial force vs. depth for soldier pile # 12 till 1/29/2000.	IV-76
4.62	Axial force vs. depth for soldier pile # 30 till 1/29/2000.	IV-77
4.63	Axial force vs. depth for soldier pile # 31 till 1/29/2000.	IV-78
4.64	Strain vs. time in soldier pile # 11 from gages 4' from top.	IV-79
4.65	Strain vs. time in soldier pile # 11 from gages 10' - 4'' from top.	IV-80
4.66	Strain vs. time in soldier pile # 11 from gages 14' - 4'' from top.	IV-81
4.67	Strain vs. time in soldier pile # 11 from gages 21' - 6'' from top.	IV-82
4.68	Strain vs. time in soldier pile # 11 from gages 26' - 6'' from top.	IV-83
4.69	Strain vs. time in soldier pile # 11 from gages 31' - 6'' from top.	IV-84
4.70	Strain vs. time in soldier pile # 11 from gages 36' - 6'' from top.	IV-85
4.71	Strain vs. time in soldier pile # 11 from gages 41' - 6'' from top.	IV-86
4.72	Strain vs. time in soldier pile # 11 from gages 4' from top.	IV-87
4.73	Strain vs. time in soldier pile # 12 from gages 10' - 4'' from top.	IV-88
4.74	Strain vs. time in soldier pile # 12 from gages 14' - 4'' from top.	IV-89

4.75	Strain vs. time in soldier pile # 12 from gages 21' - 6'' from top.	IV-90
4.76	Strain vs. time in soldier pile # 12 from gages 26' - 6'' from top.	IV-91
4.77	Strain vs. time in soldier pile # 12 from gages 31' - 6'' from top.	IV-92
4.78	Strain vs. time in soldier pile # 12 from gages 36' - 6'' from top.	IV-93
4.79	Strain vs. time in soldier pile # 12 from gages 41' - 6'' from top.	IV-94
4.80	Strain vs. time in soldier pile # 30 from gages 6' - 2'' from top.	IV-95
4.81	Strain vs. time in soldier pile # 30 from gages 9' - 2'' from top.	IV-96
4.82	Strain vs. time in soldier pile # 30 from gages 14' - 6'' from top.	IV-97
4.83	Strain vs. time in soldier pile # 30 from gages 17' - 6'' from top.	IV-98
4.84	Strain vs. time in soldier pile # 30 from gages 22' - 0'' from top.	IV-99
4.85	Strain vs. time in soldier pile # 30 from gages 28' - 0'' from top.	IV-100
4.86	Strain vs. time in soldier pile # 30 from gages 36' - 0'' from top.	IV-101
4.87	Strain vs. time in soldier pile # 30 from gages 44' - 0'' from top.	IV-102
4.88	Strain vs. time in soldier pile # 31 from gages 6' - 2'' from top.	IV-103
4.89	Strain vs. time in soldier pile # 31 from gages 9' - 2'' from top.	IV-104
4.90	Strain vs. time in soldier pile # 31 from gages 14' - 6'' from top.	IV-105
4.91	Strain vs. time in soldier pile # 31 from gages 17' - 6'' from top.	IV-106
4.92	Strain vs. time in soldier pile # 31 from gages 22' - 0'' from top.	IV-107
4.93	Strain vs. time in soldier pile # 31 from gages 28' - 0'' from top.	IV-108

4.94	Strain vs. time in soldier pile # 31 from gages 36`- 0`` from top.	IV-109
4.95	Strain vs. time in soldier pile # 31 from gages 44`- 0`` from top.	IV-110
4.96	Anchor # 11-A, long-term monitoring of load from load cell at anchor head.	IV-111
4.97	Anchor # 11-B, long-term monitoring of load from load cell at anchor head.	IV-112
4.98	Anchor # 30-A, long-term monitoring of load from load cell at anchor head.	IV-113
4.99	Anchor # 30-B, long-term monitoring of load from load cell at anchor head.	IV-114
4.100	Anchor # 30-C, long-term monitoring of load from load cell at anchor head.	IV-115
4.101	Anchor # 11-A, long-term monitoring of movement at gage location in the bonded length.	IV-116
4.102	Anchor # 11-B, long-term monitoring of movement at gage location in the bonded length.	IV-117
4.103	Anchor # 30-A, long-term monitoring of movement at gage location in the bonded length.	IV-118
4.104	Anchor # 30-B, long-term monitoring of movement at gage location in the bonded length.	IV-119
4.105	Anchor # 30-C, long-term monitoring of movement at gage location in the bonded length.	IV-120
4.106	Anchor # 31-B, long-term monitoring of movement at gage location in the bonded length.	IV-121
4.107(a)	Deflection vs. depth using inclinometer in the A+ direction (East) for earth inclinometer # 1 till 1/29/00.	IV-122

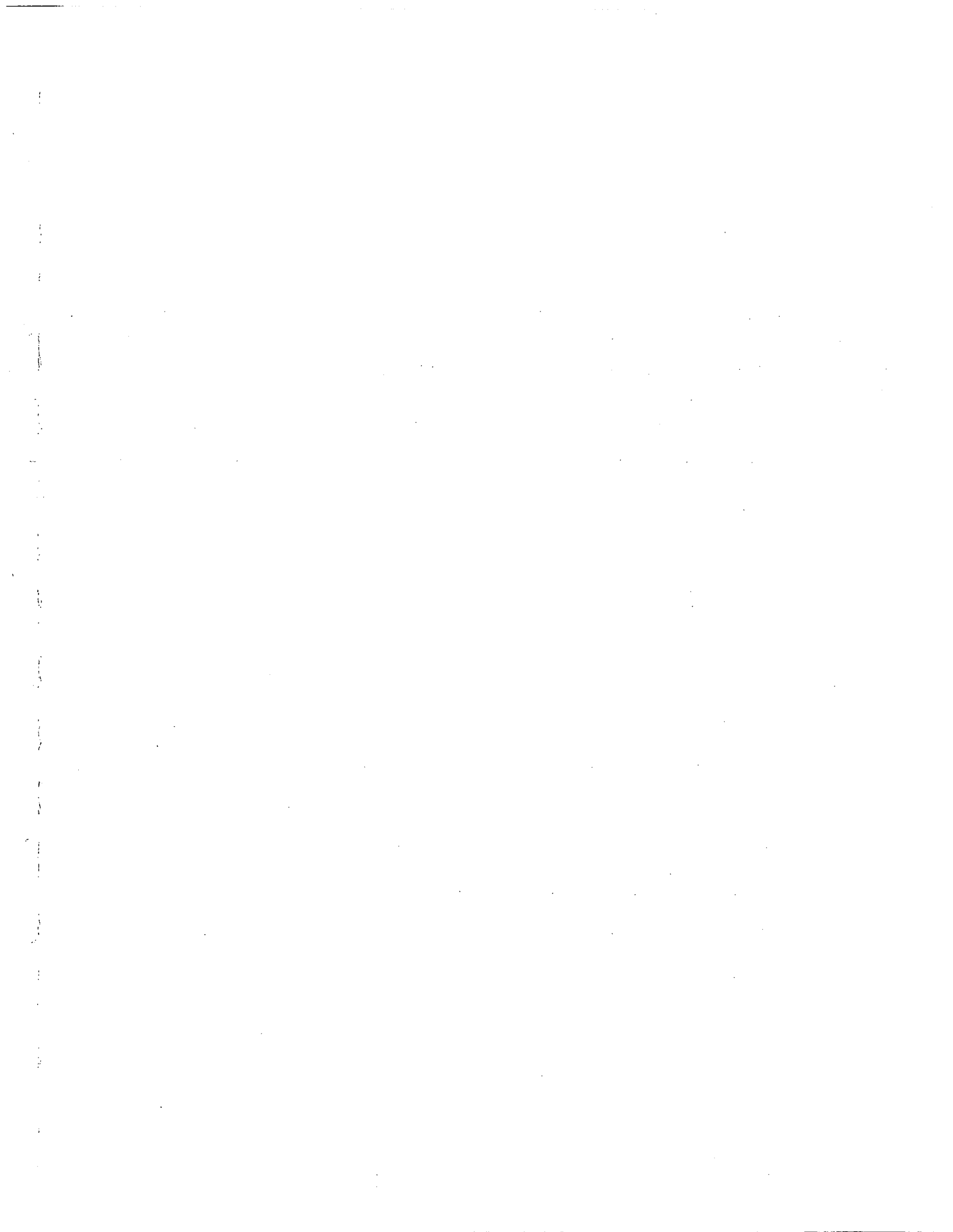
- 4.107(b) Deflection vs. depth using inclinometer in the B+ direction (South) for earth inclinometer # 1 till 1/29/00. IV-123
- 4.108(a) Deflection vs. depth using inclinometer in the A+ direction (East) for earth inclinometer # 2 till 1/29/00. IV-124
- 4.108(b) Deflection vs. depth using inclinometer in the B+ direction (South) for earth inclinometer # 2 till 1/29/00. IV-125
- 4.109(a) Deflection vs. depth using inclinometer in the A+ direction (East) for earth inclinometer # 3 till 1/29/00. IV-126
- 4.109(b) Deflection vs. depth using inclinometer in the B+ direction (South) for earth inclinometer # 3 till 1/29/00. IV-127
- 4.110(a) Deflection vs. depth using inclinometer in the A+ direction (East) for soldier pile # 11 till 1/29/00. IV-128
- 4.110(b) Deflection vs. depth using inclinometer in the B+ direction (South) for soldier pile # 11 till 1/29/00. IV-129
- 4.111(a) Deflection vs. depth using inclinometer in the A+ direction (East) for soldier pile # 12 till 1/29/00. IV-130
- 4.111(b) Deflection vs. depth using inclinometer in the B+ direction (South) for soldier pile # 12 till 1/29/00. IV-131
- 4.112(a) Deflection vs. depth using inclinometer in the A+ direction (East) for soldier pile # 30 till 1/29/00. IV-132
- 4.112(b) Deflection vs. depth using inclinometer in the B+ direction (South) for soldier pile # 30 till 1/29/00. IV-133
- 4.113(a) Deflection vs. depth using inclinometer in the A+ direction (East) for soldier pile # 31 till 1/29/00. IV-134
- 4.113(b) Deflection vs. depth using inclinometer in the B+ direction (South) for soldier pile # 31 till 1/29/00. IV-135

5.1	Schematic of three-stage and two stage models.	IV-110
5.2	Shear deformation pattern in the soil surrounding the anchor.	V-26
5.3	Soil element force equilibrium in vertical and radial directions.	V-27
5.4	Mobilized interface stress versus interface displacement for dilatancy angle from 5° to 25° .	V-28
5.5	Effect of influence zone on the development of interface stress versus interface displacement.	V-29
5.6	Interface stress versus interface displacement for $\gamma = 0^\circ$.	V-30
5.7	Anchor-soil interface behavior for the given maximum mobilized interface strength.	V-31
5.8	Calculation results for the hardening interface model (two stage model), (a) anchor head force vs. anchor head displacement (P-U curve), (b) Anchor tension evolution, (c) anchor-soil interface shear stress evolution.	V-32
5.9	Calculation results for the hardening interface model (three stage model), (a) anchor head force vs. anchor head displacement (P-U curve), (b) Anchor tension evolution, (c) anchor-soil interface shear stress evolution.	V-33
5.10	Effect of anchor relative rigidity factor on the anchor-soil interface shear stress distribution.	V-34
5.11	The relationship between dilatancy angle and the radius ratio.	V-35
5.12	Results of back-calculation of hardening model.	V-36
5.13	Results of back-calculation of softening model.	V-37
5.14	Sensitivity study of the basic interface strength (hardening model).	V-38

7.4	Analysis of Tieback Walls by the Tributary Method Developed by Terzaghi and Peck, 1967.	VII-29
7.5	Analysis of Tieback Walls by the Hinge Method Developed by Lambe, 1970.	VII-30
7.6	Canadian Foundation Engineering manual (Equilibrium Consideration) Method- Canadian Foundation Engineering Manual, 1985.	VII-31
7.7	Schematic of a tieback wall elements and nodes	VII-32
7.8	Elements forces and node forces	VII-33
7.9	Schematic of soil subgrade modulus and soil spring model	VII-34
7.10	Anchor force vs. displacement representation	VII-35
7.11	Typical cross section of the tieback wall.	VII-36
7.12	The relationship between anchor head load and displacement applied for the case history.	VII-37
7.13 (A)	Comparisons between the predicted and the measured pile deflection at stage 1, for one row tieback wall.	VII-38
7.13 (B)	Comparisons between the predicted and the measured pile deflection at stage 2, for one row tieback wall.	VII-39
7.13 (C)	Comparisons between the predicted and the measured pile deflection at stage 2, for one row tieback wall.	VII-40
7.14	Comparison of the pile moments for one row tieback wall at stage 3.	VII-41

7.15	Comparison between the calculated and the measured pile moments at stage 5 for two row tieback wall.	VII-42
7.16	Relationship between anchor head load and displacement applied for parametric study	VII-43
7.17 (a)	Effect of lock-off loads on the structural deflections of the pile.	VII-44
7.17 (b)	Effect of lock-off loads on the soil reaction Forces.	VII-45
7.17 (c)	Effect of lock-off loads on pile moments.	VII-46
7.18	Relationship between anchor working load and anchor lock-off load.	VII-47
7.19 (a)	Effect of anchor locations on the structural deflections of the pile.	VII-48
7.19 (b)	Effect of anchor locations on Pile moments.	VII-49
7.19 (c)	Effect of anchor locations on anchor working loads.	VII-50
7.20 (a)	Effect of pile stiffness on the structural deflections of the pile.	VII-51
7.20 (b)	Effect of pile stiffness on pile moments.	VII-52
7.20 (c)	Effect of pile stiffness on soil reaction forces.	VII-53
7.21 (a)	Effect of internal friction angle on the structural deflections of the pile.	VII-54
7.21 (b)	Effect of internal friction angle on pile moments.	VII-55
7.21 (c)	Effect of internal friction angle on soil reaction forces.	VII-56
7.22 (a)	Effect of cohesion ($j = 0$) on the structural deflections of the pile.	VII-57
7.22 (b)	Effect of cohesion ($j = 0$) angle on pile moments.	VII-58

7.22 (c)	Effect of cohesion ($\phi = 0$) angle on soil reaction forces.	VII-59
7.23	Measured moments on soldier pile no. 30 versus the moments calculated by different methods.	VII-60
7.24	Measured moments on soldier pile no. 30 versus the moments calculated based on the parameters derived from soldier pile no. 30.	VII-61
7.25	Measured moments on soldier pile no. 31 versus the moments calculated based on the parameters derived from soldier pile no. 30.	VII-62
7.26	Measured moments on soldier pile no. 30 versus the moments calculated by different methods.	VII-63



CHAPTER I

INTRODUCTION

1.1 STATEMENT OF THE PROBLEM

Tieback walls have been used as in cuts and bridge abutments for approximately more than 30 years. Recently, there has been an increased interest in the use of tieback walls with permanent anchors for earth retaining and/or soil slope stabilization purposes. The increased popularity of such earth retaining structure may be attributed to several factors: (1) various construction techniques are available for installing tieback walls in almost any type of soil condition, (2) numerous standard tests have been developed for verifying tieback anchor capacity, (3) concerns about long-term resistance to corrosion have diminished over the years due to the successful development of corrosion seals, (4) the use of tieback walls seems to offer a faster construction technique and less costly approach, compared to other types of earth retaining techniques.

Basically, tieback walls are consisted of three elements: earth retaining units such as sheet pile and lagging, anchorage, and the connection of these two elements. Despite various combinations of the assemblage of three elements, the working principle of a tieback wall remains essentially the same. In deep excavation, wall movement results in the development of certain earth pressure behind the wall, which are eventually transferred to the anchorage through the connection of the tieback and the wall. In the case of slope stabilization, tieback walls provide resistance to the driving forces caused

by the factors such as change of ground water regime, increased surcharge, and slope cut. It is in the latter case that great complexities may exist due to the nature of a great variation of geological settings in a site. For this reason, instrumentation and monitoring of tieback walls for stabilizing natural slope has been recommended by the experts (Dunnicliff, 1990; Nicholson, 1982).

One of the major concerns in a tieback wall design is the estimation of the earth pressure acting on the wall. Unfortunately, the development of earth pressure behind a earth retaining structure is influenced by the wall deformation modes, however, vary from one wall system to the other, depending on the wall stiffness, the anchor spacing, the anchor yield, and the lock-off loads. There is particularly a need for a better understanding of the earth pressure development as affected by the construction techniques and construction sequence.

The design of a tieback wall calls for a global stability to prevent failure of the supported soil mass, and structural capacity to resist bending moments developed in the soldier piles due to the earth pressure. There have been numerous literatures providing a wide range of information on the tieback wall (e.g., Terzaghi and Peck, 1967; Schnabel, 1982; Goldberg et al, 1976; Clough et al, 1974; Lambe and Wolfskill, 1970; Hanna, 1982; Otta et al, 1982; Cheney, 1988; Xanthakos, 1991, among others); nevertheless, there is still a need for more data from fully instrumented tieback walls with detailed documentation of construction techniques and sequence. The data of a carefully monitored tieback wall should provide necessary information for investigating the

interrelationship among the magnitude and distribution of earth pressure, the tieback anchor lock-off loads, the friction developed between the wall and the backfill material, the bearing of soldier pile, and the magnitude and nature of ground movements. An instrumentation and monitoring of a tieback wall construction project (SR. 82 Bridge, near Brecksville, Summit County, Ohio) has been carried out to generate much needed data that would fill the knowledge gap exists between field performance and design assumptions.

In addition to fill the general knowledge gap on tieback walls, the research also would address some unique concerns pertinent to this particular tieback wall project. These concerns include the following: (1) the tieback anchors are to be located in the shale, which potentially can be disintegrated due to the presence of water, (2) shale is believed to exhibit strong creep tendency, leading to some concern about the bond loss after some service period. Since shale is rather abundant in Ohio, the knowledge gained from this instrumentation research project should help design engineers in designing tieback walls with permanent anchors in the shale.

1.2 OBJECTIVES OF THE STUDY

The objectives of this study are as follows.

- (a) Develop and carry out an instrumentation and monitoring plan for the tieback wall to be constructed on the state Rt. 82, in Brecksville, Ohio (Project No. SUM-82-0.00).

- (b) Instrument and carry out load test of tiebacks in shales to determine the load-carrying capacity, load transfer mechanism, and the water effect.
- (c) Instrument and carry out creep tests on tiebacks to gain better insight on the time-dependent movement and stress relaxation behavior of tiebacks installed in shales.
- (d) Document the construction sequence and the measured tieback wall responses.
- (e) Monitor tieback wall performance after the completion of wall construction.
- (f) Perform a detailed analysis of measured data from the load test results and the monitoring data of instrumented walls.
- (g) Investigate the inter-relationships among the magnitude and distribution of the earth pressures, the tieback lock-off loads, the friction between the wall and the backfill, the pile bearing, and the magnitude and nature of ground movements.
- (h) Provide recommendations for improved design methods for tieback walls with permanent anchors in shales.

1.3 ORGANIZATION OF THE REPORT

Chapter I provides an introduction, objectives of the project, and outline of the final report.

Presented in chapter II is a summary of background information on the project site prior to the start of the construction. The background information includes a discussion of

the nature of the problem of the project site, soil profile data, prior slope stabilization schemes, and design of the permanent tieback wall.

Chapter III provides a detailed description of the instrumentation plan, types of sensors used, locations of sensors and inclinometers, and the special plans for load testing of ground anchors. Instrumentation installation techniques are detailed in the chapter as well.

Chapter IV presents the bulk of measured data prior to, during, and after construction. The measured data, including strains, loads, and deflections are plotted as a function of time to provide a time history of structural responses of the constructed wall. In addition, the measured data are plotted as a function of locations, providing a spatial representation of the structure elements during different stages of construction. Together, these comprehensive plots of the measured data formed the basis for interpreting the structural behavior of the constructed wall.

Chapter V presents the newly developed interface models for the specific applications to ground anchors. The theoretical interface models taking into consideration of the effects of confining pressure, dilatancy, influence zone, and relative rigidity of the anchor and the soil, have been formulated. In addition, both forward calculation and back calculation computational algorithms have been successfully formulated. The validity of the developed models has been provided by a favorable comparison with both laboratory experimental data and field cases. The interface models have been applied to the two pullout tests conducted in this research project.

Chapter VI presents a detailed description of a finite element (FEM) simulation of the construction of the wall. The FEM program, PLAXIS, was employed to determine the stress and deformation fields of the slope at various stages of construction, as well to calculate the structural responses of the tieback wall elements, including the soldier piles, and the tiebacks. When applicable, a comparison was made between the computed results and the actual measured results. The FEM PLAXIS simulation has proven to be a valuable tool that would enable engineers to gain detailed insights on the interactions of the tieback walls structure elements.

Chapter VII provides a description of an efficient computational algorithm for the tieback wall structures. The algorithm was based on beam on elastic springs, with capabilities for simulation of pre-stress in anchor and stage constructions (e.g., excavation, installation of soldier piles and pre-stress of anchors). The developed algorithm has been added into a PC based computer program with a user-friendly input interface module and powerful post-analysis graphical representation (post-processing). This computer program has been validated by a comparison with instrumented tieback walls at Texas A&M University's Geotechnical Experiment Sites. This chapter also presents a comparative study of various simplified analysis methods for calculating the maximum bending moments developed in the soldier piles. Furthermore, the measured tieback wall structure response is compared with calculations based on these simplified methods, and the deviations between the calculated and the measured are analyzed.

Finally chapter VIII presents summaries and conclusions of the project.

CHAPTER II

BACKGROUND OF THE PROJECT

II.1 Introduction

The project site is located on the western side of the Cuyahoga Valley National Recreation Area (CVNRA) Valley Railroad in the vicinity of the State Route 82 bridge over the railroad and the Cuyahoga River, in Brecksville, Ohio. The slope movements are on the western wall of the Cuyahoga River valley, and extend for distances of approximately 200 and 400 feet to the north and south of the State Route 82 bridge centerline, respectively. Three independent geotechnical studies have been conducted to investigate the site conditions and appropriate remedial measures to stabilize the slope. Messmore/Timmerman Services, Inc. did two of those studies in the areas south and north of the bridge right-of-way. Slope movements are also occurring within the 80 feet wide bridge right-of-way portion of the embankment; however, ODOT has conducted an independent investigation of this area, and developed plans for stabilization of the right-of-way zone.

Within the project area, the Valley Railroad was constructed by cutting a bench into the toe of the western river valley side wall. An untitled and undated topographic drawing of the area prepared by Environmental Design Group, shows the resulting existing embankment to rise sharply from the railroad for a change in elevation of 40 to 50 feet over a horizontal distance of 50 to 60 feet; to continue to rise at a moderate slope for an elevation change of 30 to 40 feet over a horizontal distance of 100 to 200 feet; then to again rise steeply with a change in elevation of 30 feet over a distance of 30 to 60 feet.

II.2 Initial Site Investigation

As indicated above, ODOT has conducted a study of the slope movement within the State Route 82 bridge right-of-way, and developed plans for stabilizing that portion of the general problem area. Five (5) test borings were advanced by ODOT in May and June 1993, with laboratory tests performed on the collected soil and rock samples.

Four test borings were advanced at the project site by Messmore/Timmerman Services, Inc., between September 30 and October 4, 1994, using a medium capacity rotary drill rig. All test positions were selected as shown on the attached Location Plan in Fig. 2.1. Ohio Department of Transportation (ODOT) had advanced test borings within and near the State Route 82 bridge right-of-way prior to this investigation, and the subsurface data obtained was provided to our office. The test boring locations for that investigation was selected to complement the ODOT data, and to further investigate the area beyond the bridge right-of-way zone.

Standard penetration and Shelby tube sampling was performed at the depth intervals shown on the Test Boring Logs that are provided in Appendix A. Water level readings and hole depth soundings were made on completion of each boring, and water level readings were again made in two boreholes at later times. All holes were backfilled following completion of water level determinations. The ground surface elevation shown on each log was interpolated to the nearest one foot from elevation data shown on the topographic drawing in Fig. 2.1.

Supplemental investigation was conducted by Messmore/Timmerman Services, Inc., to obtain additional subsurface data to better define the rock surface elevation in the immediate vicinity of the slide face, and to present any revisions or additions to their original conclusions and recommendations deemed necessary based on the new data. Four (4) Wildcat dynamic cone penetrations were performed at the project site on July 25, 1995 for this supplemental investigation.

The test positions were selected and advanced as shown approximately on the attached location plan in Fig. 2.1, and identified as P-1 through P-4. Also shown on the location plan are test positions of borings advanced during the previous investigation and of borings advanced by the Ohio Department of Transportation (ODOT) in 1993.

Dynamic cone testing was performed by advancing a cone having a 10 square centimeter projected end area into the subsoils using a controlled dynamic energy produced by the drop of a 35 pound hammer through a height of 15 inches. The data was recorded as the number of blows required to advance the cone through each succeeding 10 centimeters of penetration.

The field cone penetration data and results are shown on the attached Wildcat Dynamic Cone Logs in Appendix A. The logs show the relative density of the soil being penetrated for each 10 centimeter increment, if the soil being penetrated were sand or silt; and the stiffness of the soil being penetrated if it was clay. The value shown on the log as "IN" for each test interval is the approximate equivalent standard penetration blow count for the soil being tested, i.e., the equivalent blows per foot required to advance a standard split spoon sampler into that soil using an 140 pound hammer, freely falling from a height of 30 inches. This correlation between the two types of testing becomes inaccurate under high penetration resistance conditions, thus, the equivalent blow count is not given where such conditions exist.

The ground surface elevation shown on each cone penetration log was determined to the nearest one (1) foot by standard surveying methods, using a reference elevation of 638 for the railroad bed in the vicinity of the field testing.

The general nature of the subsurface profile found and reported in the ODOT investigation is similar to that found in the investigations by Messmore/Timmerman Services, Inc. The primary difference between the sets of data is that more soil variability is shown in the ODOT data. Of

particular significance is that "sandy silt" zones were found at greater depths in the ODOT investigation.

The combined subsurface data of the Messmore/Timmerman Services, Inc., and the ODOT investigations indicate that the soil portion of the profile is fairly variable with respect to the soil types found, and the relative horizontal and vertical locations of the specific soil types identified. However, the soil zones containing significant percentages of granular material (sand or gravel) were generally found within the upper approximately 25 to 30 feet of the profile, with the underlying soils being predominantly mixtures of silt and clay, occurring in varying combinations.

In addition to the variability in soil types within the profile, the consistency or density (and resulting strength) of the respective soils was also found to vary horizontally and vertically across the site. As would be anticipated, the soils generally become more stiff or dense (higher strength) with depth. However, zones of relatively low strength were found at large depths in some borings.

The underlying shale surface appears to have a gentle downward slope in a southerly direction. The rock surface was present at an elevation of 672 in the northernmost part of the investigated area (Boring B-1), at 658 to 668 near the bridge (ODOT boring / data), and at 655 at a distance of 150 feet to the south of the bridge (Boring B-3). In the southernmost part of the area, the shale was below the boring termination elevation of 639 (Boring B-2). Based on the ODOT data, the shale surface also appears to have a slight downward slope in a westerly direction, away from the railroad.

Test boring data collected at the site indicate the subsurface to be composed generally of fine grained silt and clay soils with some sandy zones, overlying shale. These can be described for engineering purposes as the following:

II.2.1 Upper Soil Deposits

The uppermost 5.0 to 7.5 feet of soil in Borings B-1 and B-4, and the uppermost 22.5 to 28.0 feet of soil in B-2 and B-3 of the soil profile at the test locations consisted of sand, silt, and clay, occurring in varying combinations, and with no identifiable horizontal or vertical sequencing pattern. This upper soil zone was brown or gray in color, and generally consisted of either mixtures of fine sand and silt, or silt with minor amounts of clay. Where sampled, the sand/silt soils were loose or medium-dense, and the clayey-silt soils were medium stiff to very stiff. These upper soils were mostly damp or moist, except for wet seams found in Borings B-2 and B-3 at depths of 13 and 11 feet, respectively.

II.2.2 Lower Soil Deposits

The remaining lower part of the soil zone consisted predominantly of gray silty clay or clayey silt. Where sampled, these fine grained soils were typically stiff or very stiff. Exceptions were found in Boring B-4 where the soil was medium stiff in the 8.5 to 10.0 and 13.5 to 15.5 foot sampling intervals, and in Boring B-2 where the soil samples below 58.5 feet depth had a slight shaley structure, and were hard. The soil was damp to moist, except in Boring B-3 where a saturated seam was penetrated between 54.0 and 58.0 feet depth. The gray silt/clay soils extended to depths of 38.0 and 58.0 feet (elevations 672 and 655) in Borings B-1 and B-3, respectively. Borings B-2 and B-4 were terminated in the soil stratum at depths of 70.0 and 30.5 feet (elevations 639 and 669), respectively.

II.2.3 Shale Stratum

The combined subsurface data of the two studies by Messmore/Timmerman Sevcics, Inc., and the ODOT investigation indicate that the shale surface can be defined as a north-south trending narrow ridge located at or near the steep slope face along the western side of the railroad; with the

shale surface both to the west and east lying at a significantly lower elevation. The elevation of the probable "ridge top" appears to be fairly constant in the vicinity of the State Route 82 bridge, and decreases to the south. Shale surface elevations, as determined from the various referenced investigations, are shown on the attached Location Plan. Where testing was terminated without encountering the shale, the testing termination elevation is given.

The shale ridge is visible as an outcrop on the steep slope along the railroad, beginning about 100 feet south of the bridge, and continuing to the north beyond the area under investigation. The top of the outcrop is at approximately 695 elevation. Based on the ODOT boring data, the shale surface in the vicinity of the bridge drops sharply to 668 elevation within a 30 to 40 feet distance to the west of the outcrop (steep slope face), with the rock elevation continuing to drop gently to 658 over the next 70 to 80 feet.

The presence of the ridge is also evident in the vicinity of Penetration P-2 in the southern part of the project area. The shale was apparently encountered at elevation 659 at P-2, with the shale being at lower elevations both to the east and west in Penetrations P-1 and P-3. The ridge at this location, however, is beneath 10 feet of soil overburden; and at least 13 feet of overburden is present in Penetration P-4 which is located along the probable ridge alignment, approximately 80 feet north of P-2.

Beginning under the silt/clay soils in Borings B-1 and B-3, and continuing to the boring termination depths of 48.8 and 65.0 feet, was gray, severely weathered or weathered shale. The shale was compact in the sampling intervals, and was dry or damp except for a 1 inch thick wet seam in Boring B-1 at 44.0 feet depth. Shale and siltstone was present in Boring B-3 in the 58.8 to 60.0 feet sampling interval.

II.2.4 Groundwater

Upon completion of drilling and sampling, and removal of the augers from the ground, water was present in Boring B-2 and B-3 test holes at depths of 11.5 and 50.0 feet, with the other two boreholes being dry. Probing indicated that the holes had remained open to depths ranging from 13.5 to 63.5 feet below the ground surface. Free groundwater was initially encountered during drilling at depths of 13.0 and 11.0 feet in B-2 and B-3, as well as in the thin wet seam in B-4 at a depth of 44.0 feet.

Water level readings were taken again in Borings B-2 and B-3 at 41 and 18 hours following completion of drilling, respectively. Water was found in B-2 borehole at 9.8 feet depth, with the hole having collapsed at 10.0 feet; and at 4.5 feet in a 5.0 feet deep hole in B-3. Based on the groundwater observations made during and following drilling at the two locations, and the moisture contents of the collected samples, the water present appeared to have entered the holes from the wet seams penetrated at 13 and 11 feet depths; and became trapped and rose in the boreholes upon hole collapse.

II.3 Problem Description

The side slope of the embankment to the west of CVNRA train tracks underneath State Route 82 was unstable and in a need for support to preserve the foundation of the bridge and to control the erosion of the surface soil and blockage of the train tracks. Moreover, several types of slope movement are evident within the project area, including surface erosion, relatively shallow block movements, and deep seated movements. Significant slope movements have occurred within northern and southern limits of the project area as defined above, and for distances of 200 to 300

feet to the west of the railroad. Evidence of minor slope movements can also be seen to the south of the investigation area.

Surface erosion has been generally limited to the lower, steep slope adjacent to the railroad. Shallow block movements or slumps have occurred throughout the project area, and evidence of deep seated movements are present along the higher elevation, western side of the area. On the steep slope along the western side (west of the State Route 82 main bridge abutment), there appears to be a scarp or scarp system resulting from deep seated earth movement(s).

Attempts by ODOT to stabilize the upper slope within the right-of-way of the bridge by placing large stone rip-rap, bound with reinforced concrete on the ground surface, has not been successful in stopping the movements.

Computer analysis of the stability of the general project area using laboratory determined and assumed engineering properties of the subsoils indicates that large portions of the area are only marginally stable; i.e., the factor of safety against both shallow and deep seated earth movement is low. However, due to the variability in the subsurface conditions, no specific predictable mode of potential slope movement, having a well defined factor of safety against failure, could be established. This lack of predictability is consistent with the site observations that many local movements are occurring throughout the area.

It is likely that water is the primary reason for the continued erosion and shallow slope movements. Thus, it was suggested that provision of some form of positive control of both surface runoff and shallow subsurface water would significantly reduce the surface erosion and shallow earth movements. However, such water control would probably not improve the factor of safety against deep-seated movements.

each anchor location into the soil and penetrated 3 feet into the shale to prevent the anchor hole from collapsing, and to act as a support for the jacking during tensioning of the rock anchors.

The design load for the lower tier wall rock anchors was 110 kips, except anchors 14A, 15A, and 16A where the load was 88 kips. Four 7 wire strands were used in each of these anchors. A five-inch diameter casing was driven through the strut opening at each anchor location into the soil and penetrated 3 feet into the shale to prevent the anchor hole from collapsing, and to act as a support for the jacking during tensioning of the rock anchors. In the lower tier wall, the casing was used in the upper row of anchors only, because of the fact that the bedrock was very close to the piles, and the hole for the anchor will not collapse.

Table 2.1: Detailed information about soldier piles and anchors.

SOLDIER PILE DATA				ANCHORAGE DATA (SEE NOTES 2 THRU 5)				
PILE NO.	PILE TOP CUTOFF ELEVATION	PILE SIZE	6x4x1/2 ANGLE ELEVATION	TIE-BACK NO.	DESIGN LOAD TP (KIPS)	TIEBACK ELEVATION	FREE LENGTH (FEET/ (M))	DEFLECTION ANGLE DOWNWARD
1	667.0	HP 14x73	657.07 (N)	-				
2	667.0	HP 14x73	657.07 (S) 652.80 (N)	2A -	88.0	640.75	5	5°
3	667.0	HP 14x73	652.80 (S) 647.0 (N)	3A -	88.0	640.75	5	5°
4	667.0	HP 14x73	647.0 (S) 642.6 (N)	4A -	88.0	640.75	5	5°
5	667.0	CHANNEL SHAPE	642.6 (S) 640.50 (N)	5A 5B -	100.0 100.0	640.75 640.25	5 5	5°
6	667.0	HP 14x73	640.50 (N45)	6A 6B -	100.0 100.0	640.75 640.25	5 5	5°
7	667.0	HP 14x73	640.50 (N45)	7A 7B -	100.0 100.0	640.75 640.25	5 5	5°
8	667.0	HP 14x73	640.50 (N45)	8A 8B -	100.0 100.0	640.75 640.25	5 5	5°
9	667.0	HP 14x73	640.50 (N45)	9A 9B -	100.0 100.0	640.75	5	5°
10	667.0	HP 14x73	640.50 (N45)	10A 10B -	100.0 100.0	640.75	5	5°
11	667.0	HP 14x73	640.50 (N45)	11A 11B -	100.0 100.0	640.75	5	5°
12	667.0	HP 14x73	640.50 (N45)	12A 12B -	100.0 100.0	640.75 640.25	5 5	5°
13	667.0	CHANNEL SHAPE	640.50 (S) 645.47 (N)	13A 13B -	100.0 100.0	640.75 640.25	5 5	5°
14	667.0	HP 14x73	645.47 (S) 650.44 (N)	14A -	88.0	640.75	10	5°
15	667.0	HP 14x73	650.44 (S) 653.75 (N)	15A -	88.0	640.75	10	5°
16	667.0	HP 14x73	653.75 (S) 650.72 (N)	16A -	88.0	640.75	10	5°
17	667.0	HP 14x73	650.72 (S)	-				
18	650.0	HP 14x73	660.16 (N)	-				
19	650.0	HP 14x73	660.16 (S) 665.57 (N)	19A -	71.0	633.83	24	45°
20	650.0	HP 14x73	665.57 (S) 674.89 (N)	20A 20B -	71.0 71.0	633.83 660.5	24 10	45°

Table 2.1: Detailed information about soldier piles and anchors (Cont'd).

SOLDIER PILE DATA				ANCHORAGE DATA (SEE NOTES 2 THRU 5)				
PILE NO.	PILE TOP CUTOFF ELEVATION	PILE SIZE	6x6x12 ANGLE ELEVATION	TI-BACK NO.	DESIGN LOAD T (KIP-F)	TIEBACK ELEVATION	FREE LENGTH (FEET) (T _{BL})	DEFLECTION ANGLE DOWNWARD
21.	630.0	HP 14x13	674.05 (S) 673.25 (N)	71A 71B -	T1.0 T1.0 -	633.03 605.5	24 0	45°
22.	630.0	CHANNEL SHAPE	673.23 (S) 671.57 (N)	72A 72B 72C	T1.0 T1.0 T1.0	633.03 605.5 671.1	24 0 0	45°
23.	630.0	HP 14x13	671.57 (N45)	23A 23B 23C	T1.0 T1.0 T1.0	633.03 605.5 671.1	24 0 0	45°
24.	630.0	HP 14x13	671.57 (N45)	24A 24B 24C	T1.0 T1.0 T1.0	633.03 605.5 671.1	24 0 0	45°
25.	630.0	HP 14x13	671.57 (N45)	25A 25B 25C	T1.0 T1.0 T1.0	633.03 605.5 671.1	24 0 0	45°
26.	630.0	HP 14x13	671.57 (N45)	26A 26B 26C	T1.0 T1.0 T1.0	633.03 605.5 671.1	24 0 0	45°
27.	630.0	HP 14x13	671.57 (N45)	27A 27B 27C	T1.0 T1.0 T1.0	633.03 605.5 671.1	24 0 0	45°
28.	630.0	HP 14x13	671.57 (N45)	28A 28B 28C	T1.0 T1.0 T1.0	633.03 605.5 671.1	24 0 0	45°
29.	630.0	HP 14x13	671.57 (N45)	29A 29B 29C	T1.0 T1.0 T1.0	633.03 605.5 671.1	24 0 0	45°
30.	630.0	HP 14x13	671.57 (N45)	30A 30B 30C	T1.0 T1.0 T1.0	633.03 605.5 671.1	24 0 0	45°
31.	630.0	HP 14x13	671.57 (N45)	31A 31B 31C	T1.0 T1.0 T1.0	633.03 605.5 671.1	24 0 0	45°
32.	630.0	CHANNEL SHAPE	671.57 (S) 673.23 (N)	32A 32B 32C	T1.0 T1.0 T1.0	633.03 605.5 671.1	24 0 0	45°
33.	630.0	HP 14x13	673.23 (S) 676.55 (N)	33A 33B 33C	T1.0 T1.0 T1.0	633.03 605.5 671.1	24 0 0	45°
34.	630.0	HP 14x13	676.55 (S) 681.57 (N)	34A 34B -	T1.0 T1.0 -	633.03 605.5	24 0	45°
35.	630.0	HP 14x13	681.57 (S) 680.00 (N)	35A - -	T1.0 - -	633.03	24	45°
36.	630.0	HP 14x13	680.00 (S)	- - -	- - -	- - -	- - -	- - -

LOCATION PLAN

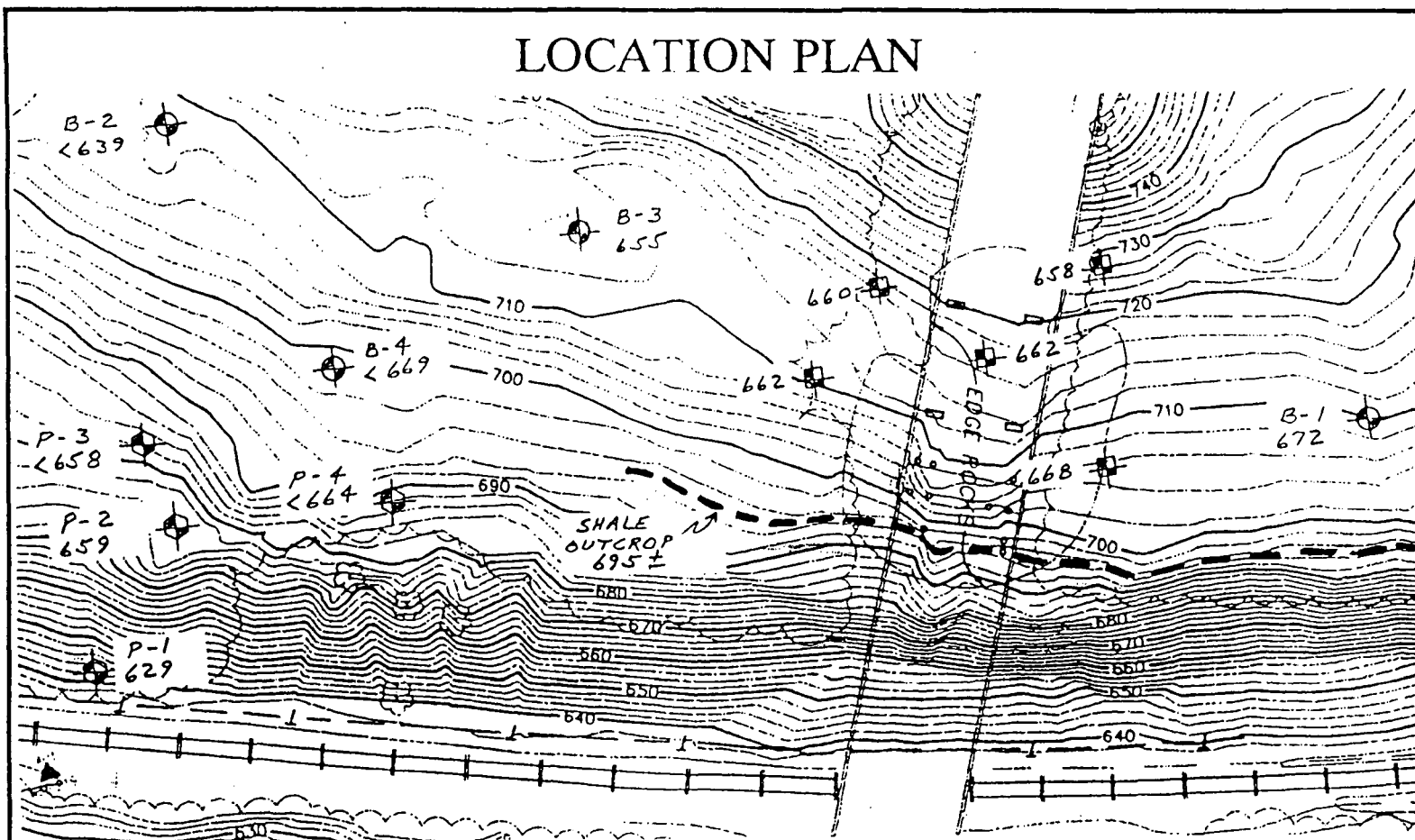


Fig. 2.1: Location of boreholes for site investigation.

II-14

- ⊙ P-() - DYNAMIC CONE PENETRATION
- ⊙ B-() - TEST BORING (1994)
- ⊕ O.D.O.T. BORING (1993)
- 660 - SHALE ELEVATION
- < 660 - SHALE BELOW ELEVATION

SCALE
1" = 50'

PROJECT: C.V.N.R.A. Valley Railroad Slide
 PROJECT NUMBER: 941108A DATE: August 15, 1995
 LOCATION: SR82 Bridge, Brecksville, Ohio

TIMMERMAN
GEOTECHNICAL GROUP, INC.

265 East Market Street ♦ Akron, Ohio 44308 ♦ (216) 434-3494

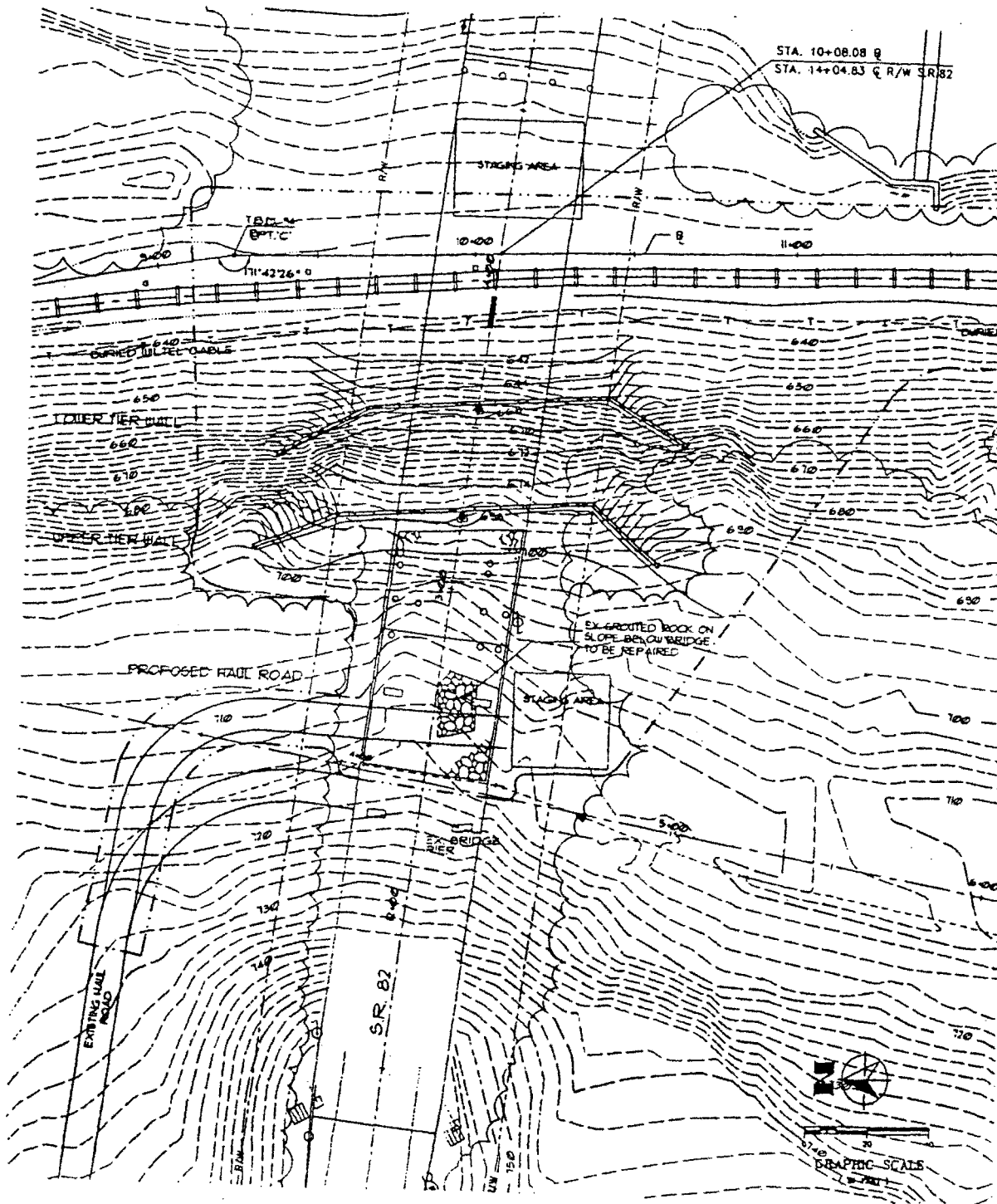


Fig. 2.2: Site plan of the project.

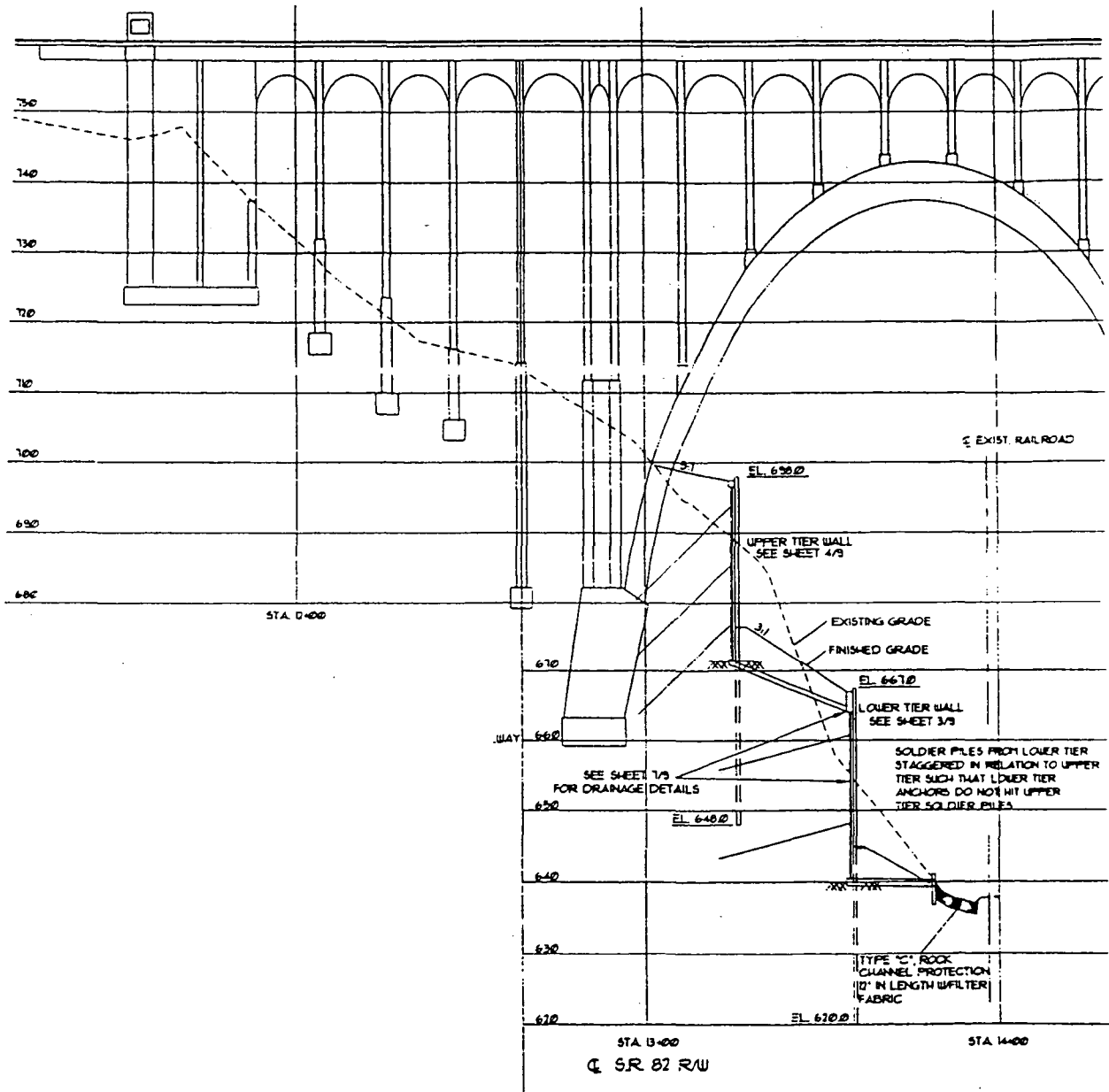
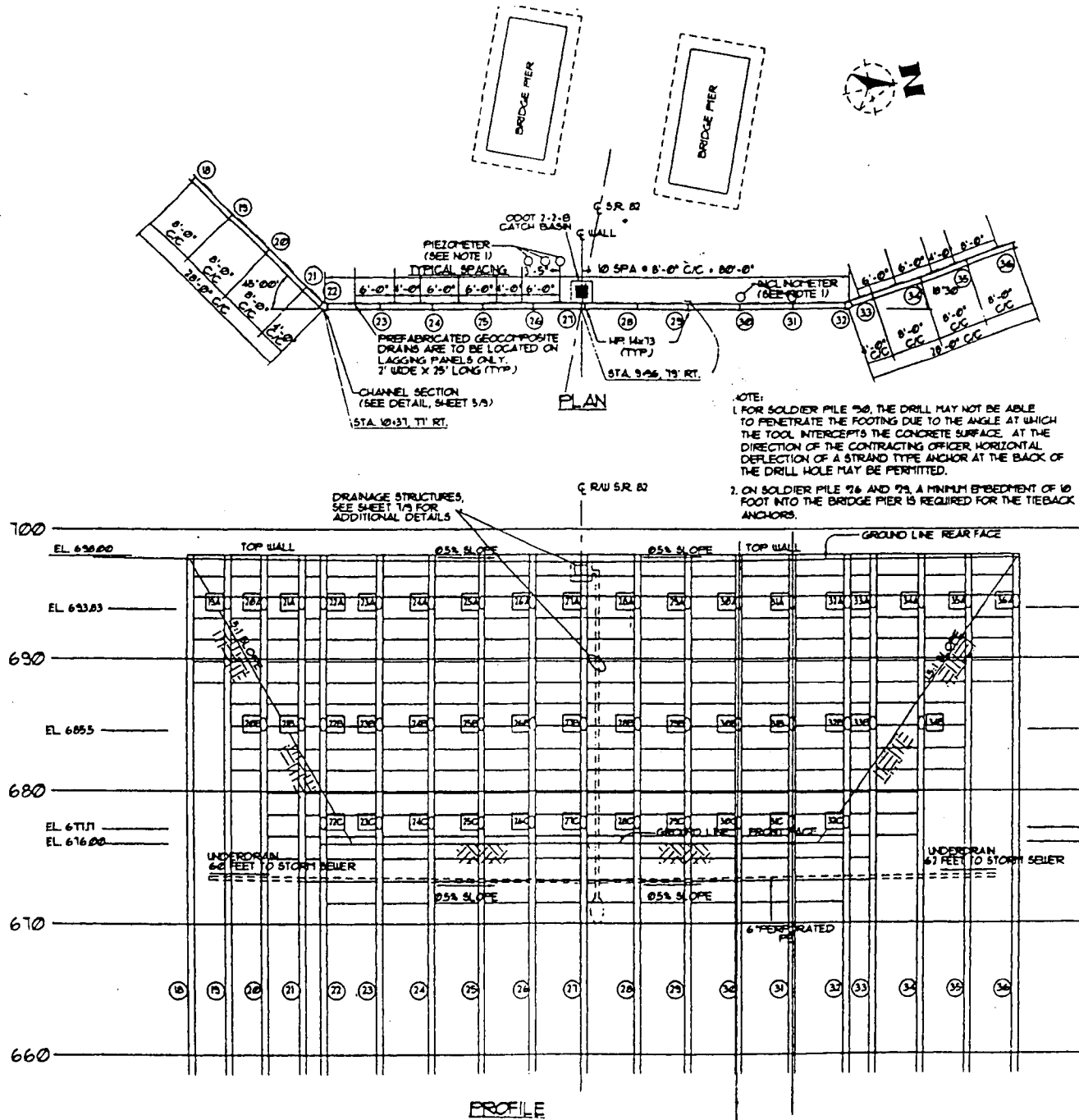


Fig. 2.3: Elevation view of the project.

Fig. 2.4: Plan and profile for the upper tier wall.



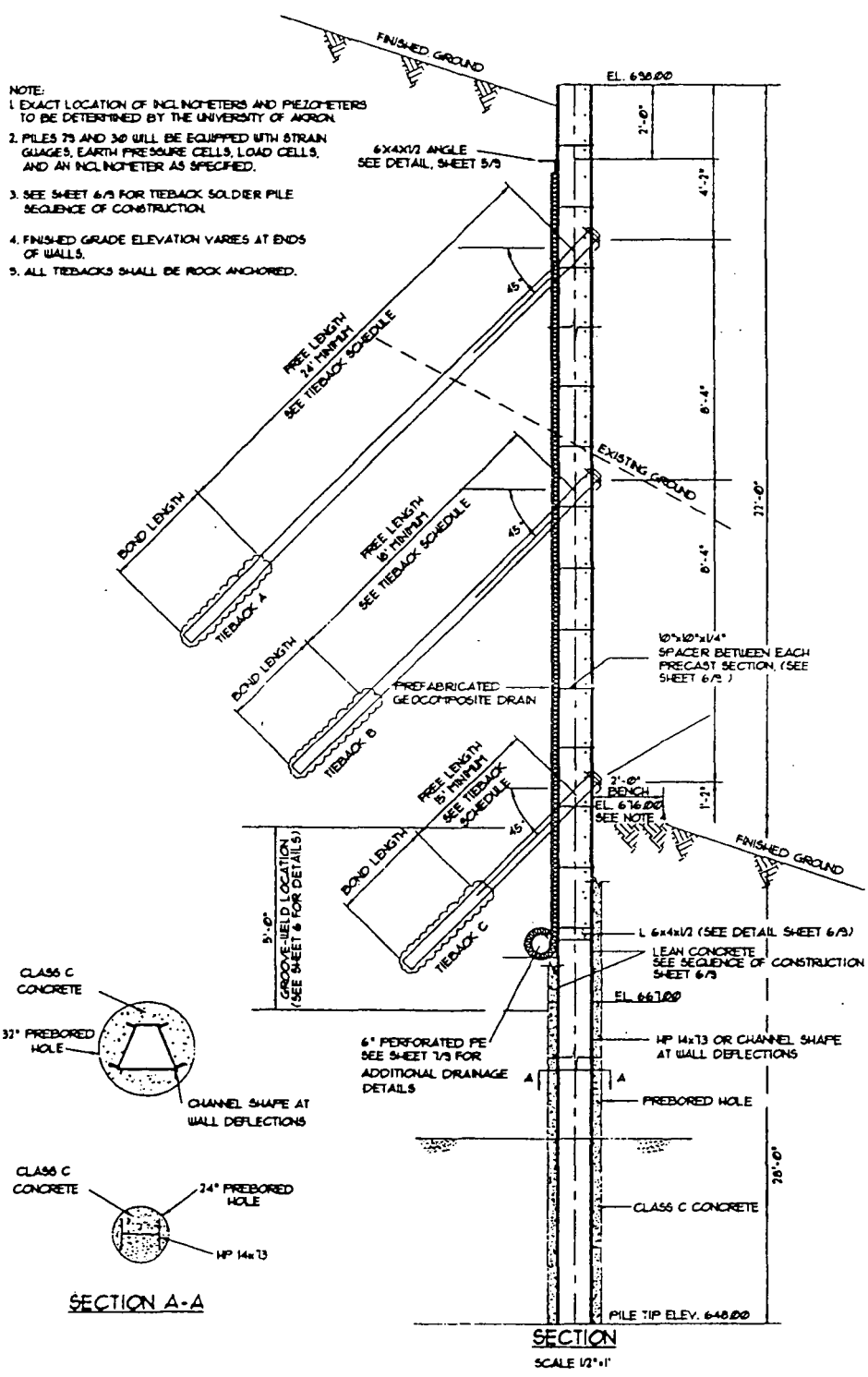
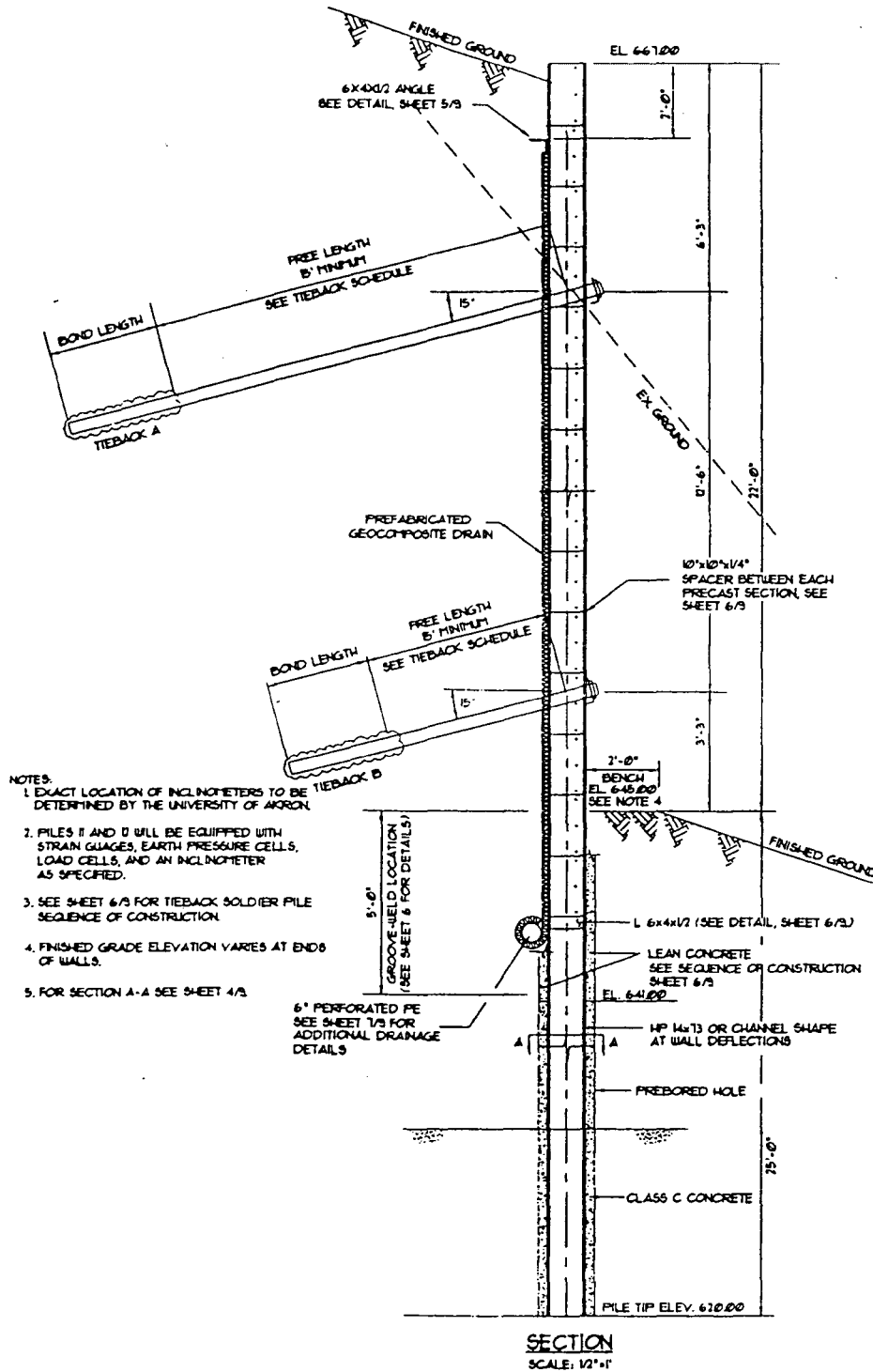
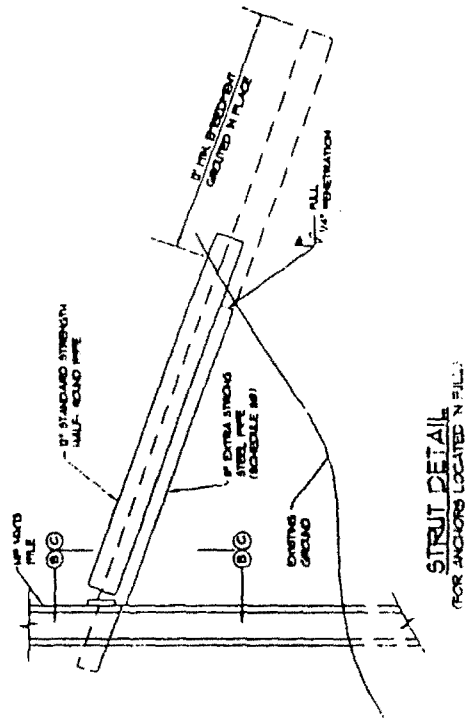


Fig. 2.5: Cross section in the upper tier wall.

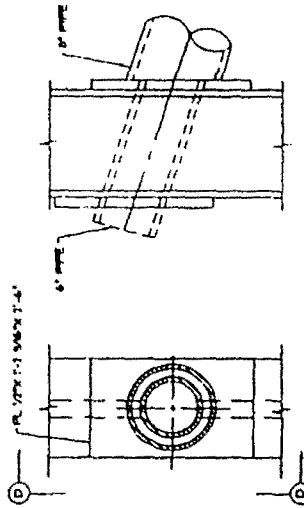


- NOTES:
1. EXACT LOCATION OF INCLINOMETERS TO BE DETERMINED BY THE UNIVERSITY OF AKRON.
 2. PILES II AND D WILL BE EQUIPPED WITH STRAIN GAUGES, EARTH PRESSURE CELLS, LOAD CELLS, AND AN INCLINOMETER AS SPECIFIED.
 3. SEE SHEET 6/3 FOR TIEBACK SOLDIER PILE SEQUENCE OF CONSTRUCTION.
 4. FINISHED GRADE ELEVATION VARIES AT ENDS OF WALLS.
 5. FOR SECTION A-A SEE SHEET 4/3.

Fig. 2.7: Cross section in the lower tier wall.



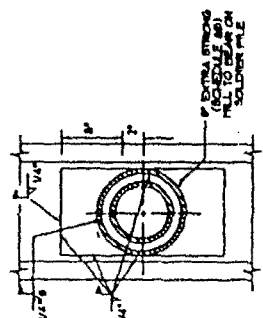
STRUT DETAIL
FOR ANCHORS LOCATED IN FILL



SECTION C-C

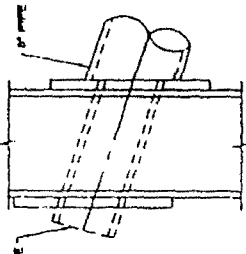
USE WITH SINGLE 1/2\"/>

PILING AND STRUT DETAIL
NOT TO SCALE



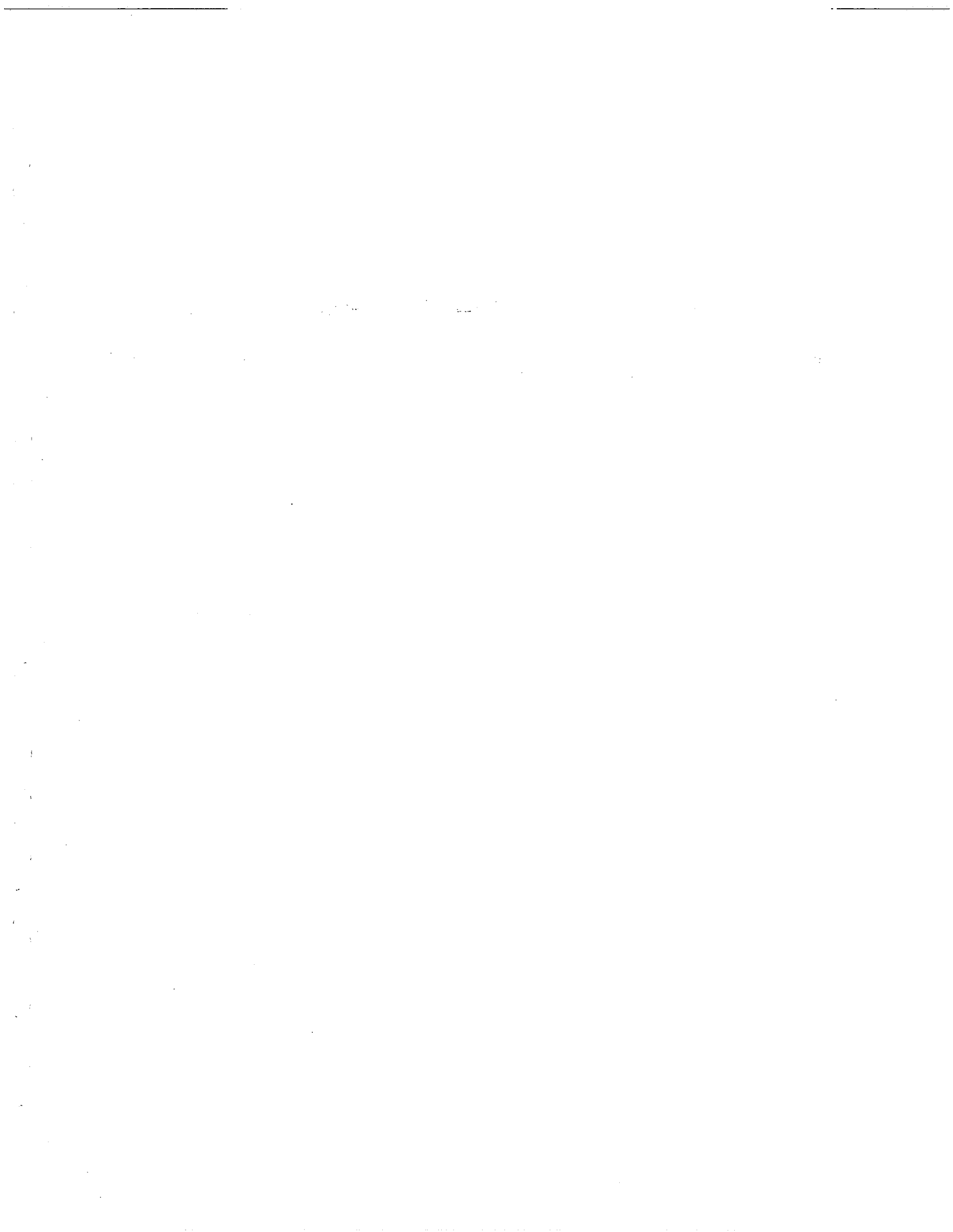
SECTION B-B

USE WITH 2 CHANNELS



VIEW D-D

Fig. 2.8: Details of the strut and casing for the rock anchors.



CHAPTER III

INSTRUMENTATION/MONITORING PROGRAM

III.1 INTRODUCTION

Instrumentation and monitoring of the behavior of the tieback walls used to stabilize the slope was necessary in order to measure the actual stresses and deformations of the stabilized structure and the stabilizing elements, and to further understand the behavior of tieback wall structures. The instrumentation designed for this project was based on questions raised during the design about the behavior of each of the tiebackwall elements and the supported slope. Instruments were installed in the slope, on the soldier piles, and on the rock anchors. The plan of the entire stabilizing system and the locations of the instrumented elements are shown in Fig. 3.1.

III.2 INSTRUMENTATION PLANS

The plan of the instrumented structural elements is shown in Fig. 3.1. The instrumentation includes four soldier piles each with 16 vibrating wire strain gages and an inclinometer. Two of those soldier piles are in the upper tier wall (soldier piles #30 and #31) and two in the lower tier (soldier piles #11 and #12). The strain gages were welded to the piles at 8 locations, 2 gages per location on both sides of the beam as shown in Fig. 3.2 for the upper tier wall and Fig. 3.3 for the lower tier wall. An inclinometer tube was attached to each of the four soldier piles to monitor the deflection of the piles.

Moreover, the rock anchors installed in the soldier pile #11 and #30 were instrumented each with 3 vibrating wire strand gages and a load cell at the anchor head. Additionally, the middle anchor in pile #31 was instrumented with the strand gages only.

Three earth inclinometers were installed in the slope prior to beginning of construction, as part of the instrumentation program, to monitor the movement of the slope. A vibrating wire piezometer was installed in the slope to monitor the ground water elevation. Details of these instruments are discussed in the following sections of this report. The plan locations of those inclinometers and the piezometer are shown in Fig. 3.4.

III.2 SLOPE MOVEMENT MONITORING

The movement of the slope was monitored by The University of Akron prior to the beginning of the construction. Three earth inclinometers were installed to depths of 100', 90', and 85' below ground elevation between the bridge piers as shown in Fig. 3.4 to enable monitoring of the movement in the slope during and after construction. These inclinometers were successfully installed and read bi-weekly since 2/16/1999. The data and explanations of the movement were submitted to ODOT and CVNRA engineers for review on regular basis. The detailed plots of these 3 inclinometer readings are presented in chapter IV. In addition, a vibrating wire piezometer (Geokon Model 4500) was installed in a borehole 3 feet to the west of inclinometer #1 at a depth of 47 feet below ground surface to monitor the ground water elevation in the slope as shown in Fig. 3.4.

III.3 TIEBACK STRUCTURE BEHAVIOR

The study of the behavior of the tieback walls used to support the slope required instrumentation of some elements of the tieback wall. Detailed information about each instrumented structure is summarized below.

III.3.1 Soldier Piles

Four soldier piles were instrumented, each with 16 vibrating wire strain gages (Geokon, model VSM 4000). Two gages were used at each elevation, one on each side of the pile as shown in Figs. 3.5 and 3.6 for piles #11 and #12 in the lower tier, respectively. Figs. 3.7 and 3.8 show the location of the gages on piles #30 and #31 in the upper tier wall, respectively. The detailed locations of these instrumented piles are shown in Fig. 3.1. In addition, Fig. 3.9 to Fig. 3.13 show the pictures of gages attached to these piles. The gages were read manually during construction period. After construction was completed, the Geokon model 8020 datalogger was installed on site and all the gages were connected. Since 8/31/99, continuous collection of the data was done.

III.3.3 Ground Anchors

A total of eight ground anchors were instrumented. Two ground anchors were instrumented for the failure tests and six were instrumented for long term monitoring of the stresses and force in the production anchors. The anchors were inclined at 45 degrees from the horizontal axis in the upper tier and 15 degrees in the lower tier. The failure test anchors were installed and tested before the beginning of the construction of the production anchors. Anchors #11-A and #11-B are on soldier pile #11. Anchors #30-A,

#30-B, and #30-C are on soldier pile #30. Anchor #31-B is on soldier pile #31. Figs. 3.5 and 3.7 show the approximate location of these anchors. All instrumented anchors were each instrumented with three strand meters (Geokon, model 4410) and a vibrating wire load cell (Geokon, model 4900-4-300) with 300 Kips capacity as shown in Fig. 3.14. The construction procedure, installation of the strand gages, and testing is illustrated in pictures shown in Figs. 3.15 to 3.24.

III.4 INSTRUMENTATION INSTALLATION DETAILS

III.4.1 Sequence of Installation

The installation of the instruments were carried out throughout the duration of the entire construction stage. A time-line plot showing the construction progress is shown in Fig. 3.25. The earth inclinometers and the piezometer were the first to be installed in the first week of February 1999, as depicted in Figs. 3.26 through Fig. 3.29. The soldier piles were next instrumented in the second week of February 1999. The gages were welded onto HP14x73 soldier piles #30 and #31 on 2/11/99, and the inclinometers were mounted to the soldier piles on 2/18/99 during lowering of the piles in the holes. The inclinometers were extended 15 feet below the bottom of the soldier piles to monitor if there is any movement at the bottom of the pile. The inclinometers were installed in 10 foot segments during lowering of the soldier pile and were left 10' shorter than the soldier piles to protect them from damage due to construction activities. The top 10 feet were added after completion of installation of all anchors.

Installation of soldier piles for the lower tier started on the week of 2/23/99. Lower tier soldier piles #11 and #12 were instrumented on 2/23/99. Each of the two piles

was instrumented with 16 vibrating wire strain gages that were welded to the pile at 8 locations as shown in Figs. 3.5 and 3.6. The holes for the instrumented piles were drilled 15 feet deeper for the extension of the inclinometer below the bottom of the pile. The inclinometer tubes were assembled and attached to the pile during lowering in the hole. Soldier pile #12 was installed on 2/23/99. Soldier pile #11 was installed on 2/24/99. The strain gage installation, the inclinometer installation, and the pile installation are documented in a series of pictures as shown in Figs. 3.29 to 3.37.

The hole for the lower tier failure test anchor was drilled on 2/10/99, and it was filled with water. The anchor tendon was instrumented, lowered in the hole and grouted on 2/18/99. The drilling for the upper tier failure test was done on 2/25/99. The hole was filled with water till 3/4/99 when the anchor tendon was instrumented, lowered and grouted. A series of pictures documenting these activities are presented in Figs. 3.38 to 3.41. The upper tier failure test was conducted on 3/11/99. The setup for the test and testing process are documented in pictures shown in Figs. 3.42 and 3.44. The lower tier failure test was conducted on 3/15/99. Setup and testing are shown in Figs. 3.44 and 3.45.

The installation of the production anchors started on 4/2/99. Instrumentation of anchor #11-B (lower row in the lower tier) was done on 4/14/99. The hole was drilled, the anchor was installed, and grouted on 4/16/99. Fig. 3.46 show the instrumentation of the tendon. Instrumentation, drilling, installation and grouting of anchors #30-B and #31-B (middle row in the upper tier) was done on 4/21/99. On 4/28/99, performance tests were done on anchors #30-B and 31-B as shown in pictures presented in Figs. 3.47 through 3.50. During the week of 5/3/99, row B anchors in the lower tier were stressed. On 5/7/99, instrumented anchor #11-B was performance tested as shown in Fig. 3.51.

On the week of 5/7 to 5/13/99, 3 feet wide trenches were dug to access the lower row of anchors in the upper tier (row C) as shown in Fig. 3.52. On 5/13/99, anchors #30-C and #11-A were instrumented. During the period from 5/17 to 5/21/99, the casing for upper row of anchors in the lower tier was installed and drilled as shown in Fig. 3.53. Also, the temporary lagging was installed in the upper tier wall area between the soldier piles to support the excavation as shown in Fig. 3.54.

During the week of 5/24 to 5/28/99, drilling, installation, and grouting of anchors in the upper row of the lower tier (row A) were done. Also, stressing of row C in the upper tier was done in the same week. Performance test of instrumented anchor #30-C was done on 5/24/99 as shown in Fig. 3.55. The precast panels installation started on 5/24/99. The drainage blanket was installed behind the panels, as shown in Figs. 3.56 and 3.57.

During the first week of June 99, precast panels were installed up to the elevation which is 10 feet from the top of the soldier piles in the lower tier wall, and the drainage blanket was installed behind the wall as shown in Fig. 3.57. Stressing of the upper row of the anchors in the lower tier (row A) was done during the week of 6/7/99. Instrumented anchor #11-A was performance tested on 6/7/99. During the period from 6/7 to 6/11/99, tensioning of the anchors in the lower tier wall was completed. Concurrently, the upper tier wall precast panel installation was going on.

During the week of 6/14 to 6/28/99, the contractor was grading and cleaning up the lower tier area. The upper row of anchors in the upper tier wall (row A) were drilled, installed and grouted. Instrumentation of anchor #30-A was done on 6/18/99. When they drilled the hole, it came out deeper than the ordered anchor length. A longer anchor was

ordered. The instrumentation was redone on 6/30/99. Anchor #30-A was proof tested on 7/8/99. Anchor testing of row A in the upper tier wall was done on 7/9/99. The wooden mats in front of the lower tier wall were removed on 7/8 and 7/9/99.

During the week of 7/12 to 7/16/99, the wires from the strain gages were run to the concrete boxes installed to house the data collection devices as shown in Figs. 3.58 and 3.59. Installation of the anchor caps and post grouting of all anchor heads was done during the same week as shown in Fig. 3.60. On 7/20/99, grading was done and the construction was completed.

During the period from 8/9/99 to 8/30/99, the gage cables were grouped and connected to the multiplexers. A four feet corrugated PVC pipe was run from the lower tier collection concrete box to the upper tier concrete collection box. The pipe was installed to protect the cable connecting the multiplexers in the lower tier box to the datalogger installed in the upper tier box. The wiring of all sensors to the datalogger was completed on 8/30/99 and the collection of the data on a half-an-hour interval was started on 8/31/99. Figs. 3.58 and 3.59 show these activities.

III.4.2 Techniques of Installing Instruments and Monitoring

The state-of-the-art techniques were used in the installation of the instruments. The instruments consist of vibrating wire sensors that are considered to be the most reliable long-term monitoring gages. The vibrating wire based piezometer installation was done by drilling the hole to the layer where the water was encountered (47' deep from ground elevation at 712). The piezometer was installed at a depth of 42'. The hole was backfilled with clean fine sand to a point 6" below the piezometer tip. The piezometer

was encapsulated in a canvas cloth bag containing clean, saturated sand and then lowered into position as shown in Figs. 3.61 and 3.62. While holding the piezometer in position (a mark was done on the cable to track the right depth), clean sand was placed around the piezometer and to a point 6 inches above it. The borehole was then sealed with impermeable bentonite cement grout mix to the ground surface.

The gages for the soldier piles were mounted to the end blocks (Geokon, Model VSM-4000; RocTest, Model SM-5A). The end blocks were welded first, then the gages were attached and calibrated. The gages were then covered with a steel protection cover to safeguard them during construction and backfill, as shown in Figs. 3.9 through 3.13.

Rock anchor gages were vibrating wire strand type gages (Geokon, Model 4410). At the day of installation, the gages were mounted to the 7-wire strand following the installation procedure recommended by the manufacturer. The installation started by mounting one end block to the strand. After that, the second end block is mounted loose, and the spacer bar is used to have exact distance between the blocks to be equal to the length of the gage and the end block was then tightened. Next, the grease tube is put between the blocks and the gage was inserted and the screws were tightened at the end that is to the side of the wire. A screw was screwed to the other end and the gage wire was hooked to the readout device to calibrate it. The screw was pulled till the gages reading is close to the required reading at the time of installation. When the reading was reached, the tiny screws on the other end block were tightened. A waterproof tape was wrapped around the end blocks to prevent grout from entering the gage. Then, grease was pumped through the grease fit into the pipe and the installation was complete. The gages were read after the contractor lowered the tendon in the hole, to make sure that the gages

were working fine. The procedure is documented in the pictures shown in Figs. 3.19 to 3.21. The gages were installed at the following locations: 4', 8', and 12' from the bottom end of tendon. At each instrumented anchor head, a 300 Kips capacity vibrating wire 4-gage load cell was mounted to measure the anchor force during testing and long-term monitoring. The anchor head assembly is shown in Fig. 3.14 and a picture showing the details is presented in Fig. 3.63.

III.4 DATA ACQUISITION PLANS

The data collection was done by using the Geokon Model 6020 data acquisition systems. The sensors were first hooked to the multiplexers, and then the multiplexers were connected to the main data acquisition box. The time interval for data collection was 10 minutes for the first 7 days, 30 minutes for two weeks, and one hour afterwards. After completion of the tieback construction, all the gages from the soldier piles, the rock anchors, and the load cells were connected to the data acquisition system. A total of 95 gages were hooked to the data acquisition (64 from the soldier piles, 19 from load cells, and 12 from anchor gages). The permanent location for the data acquisition is inside a concrete box in the upper tier area. All gage cables from the lower tier instruments were routed to the collection concrete box in the lower tier bench, where it was connected to the multiplexers. The cables from the multiplexers were run to the upper tier collection box where the datalogger was installed. The pictures showing the final location and the collection boxes are presented in Figs. 3.64 and 3.65.

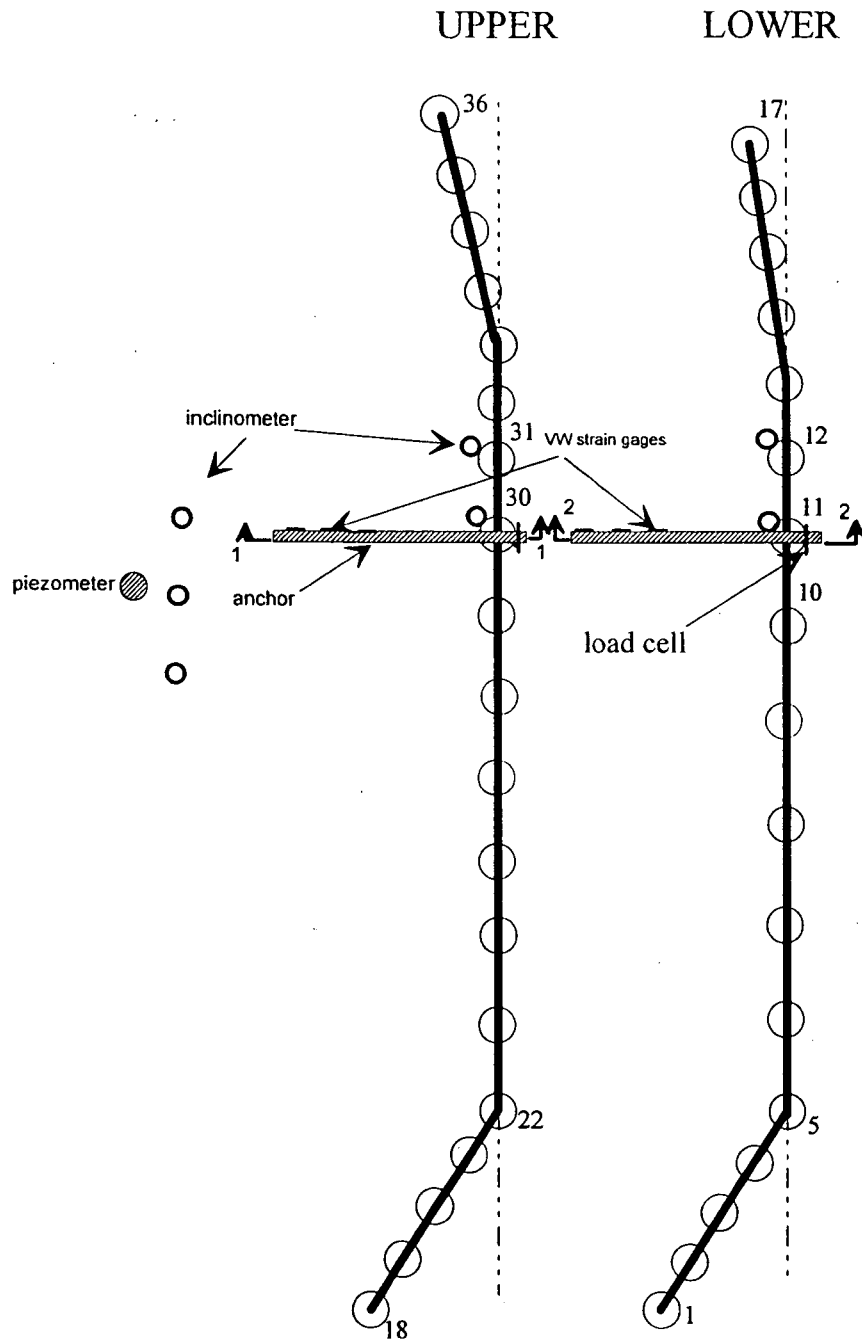


Fig. 3.1: Plan view of the entire stabilizing system.

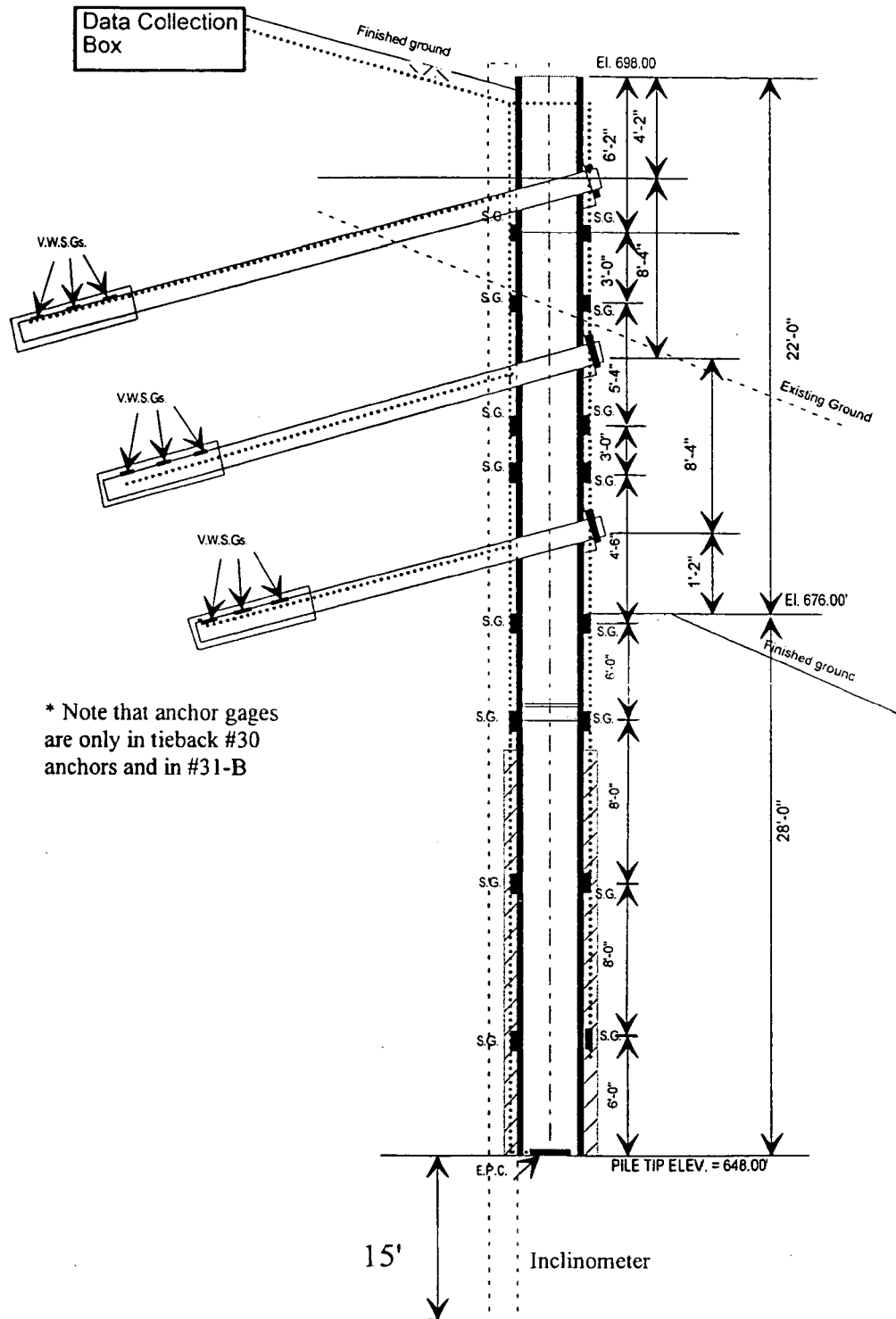


Fig. 3.2: Upper Tier Wall, strain gage locations

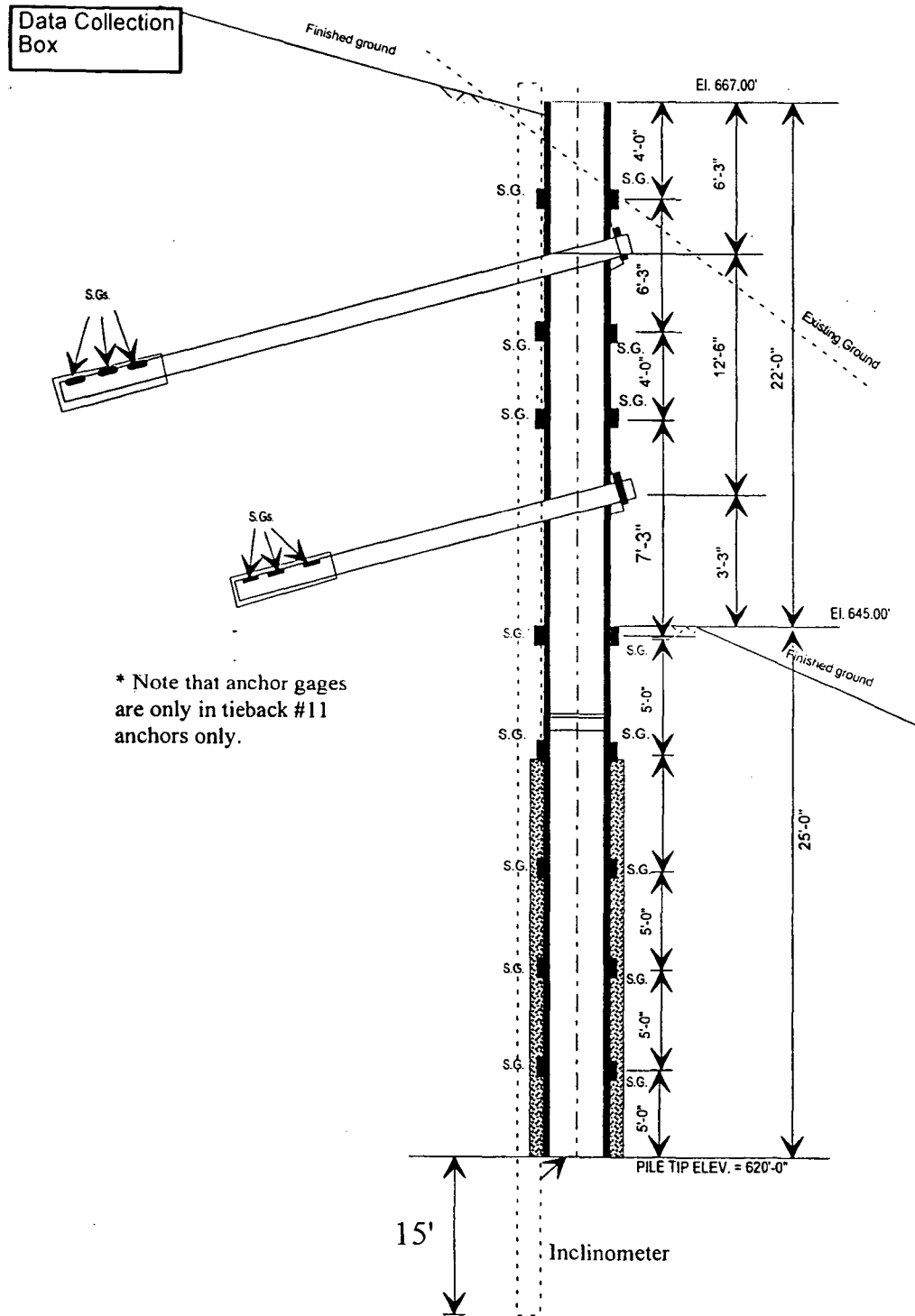


Fig. 3.3: Lower Tier Wall, strain gage locations

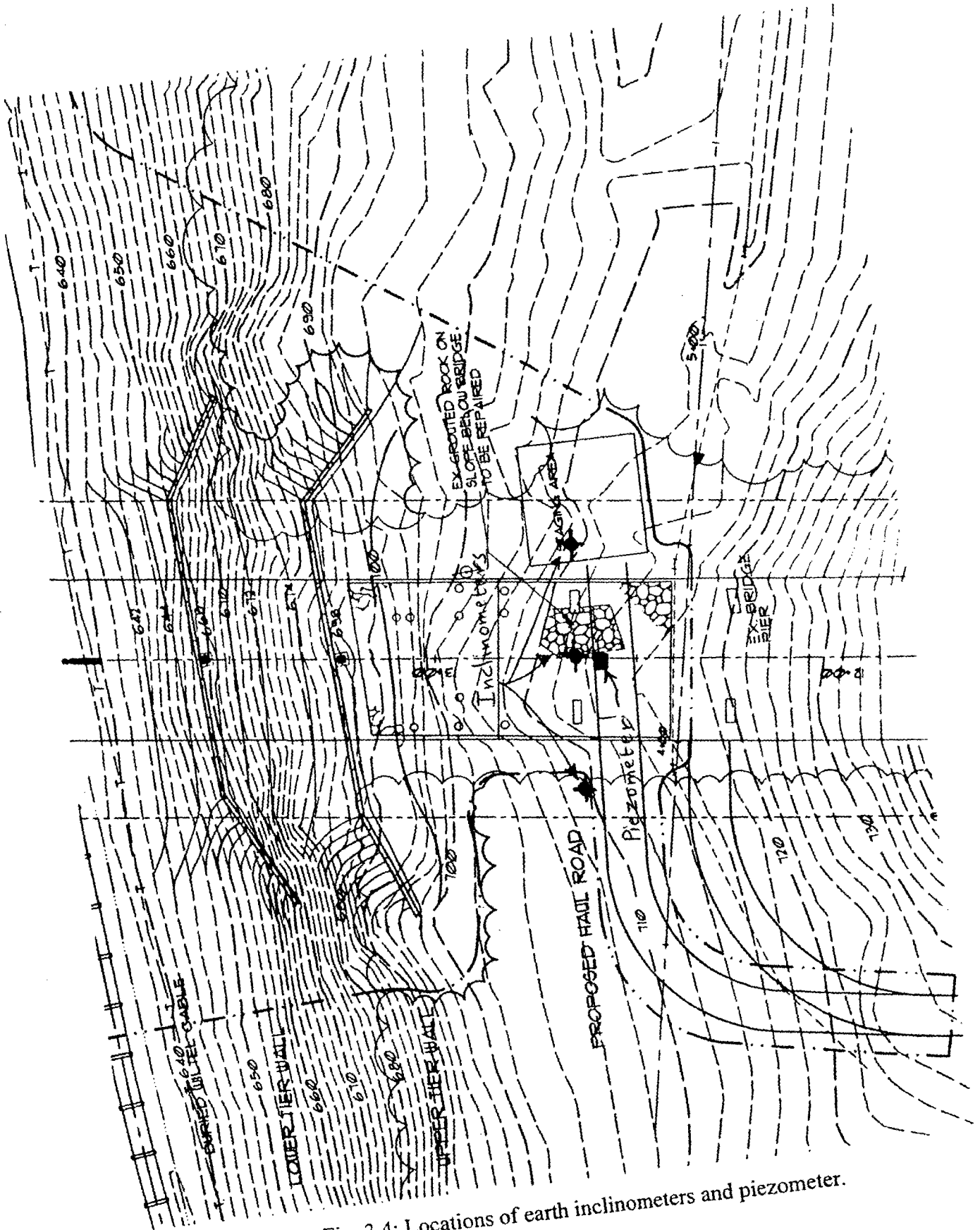


Fig. 3.4: Locations of earth inclinometers and piezometer.

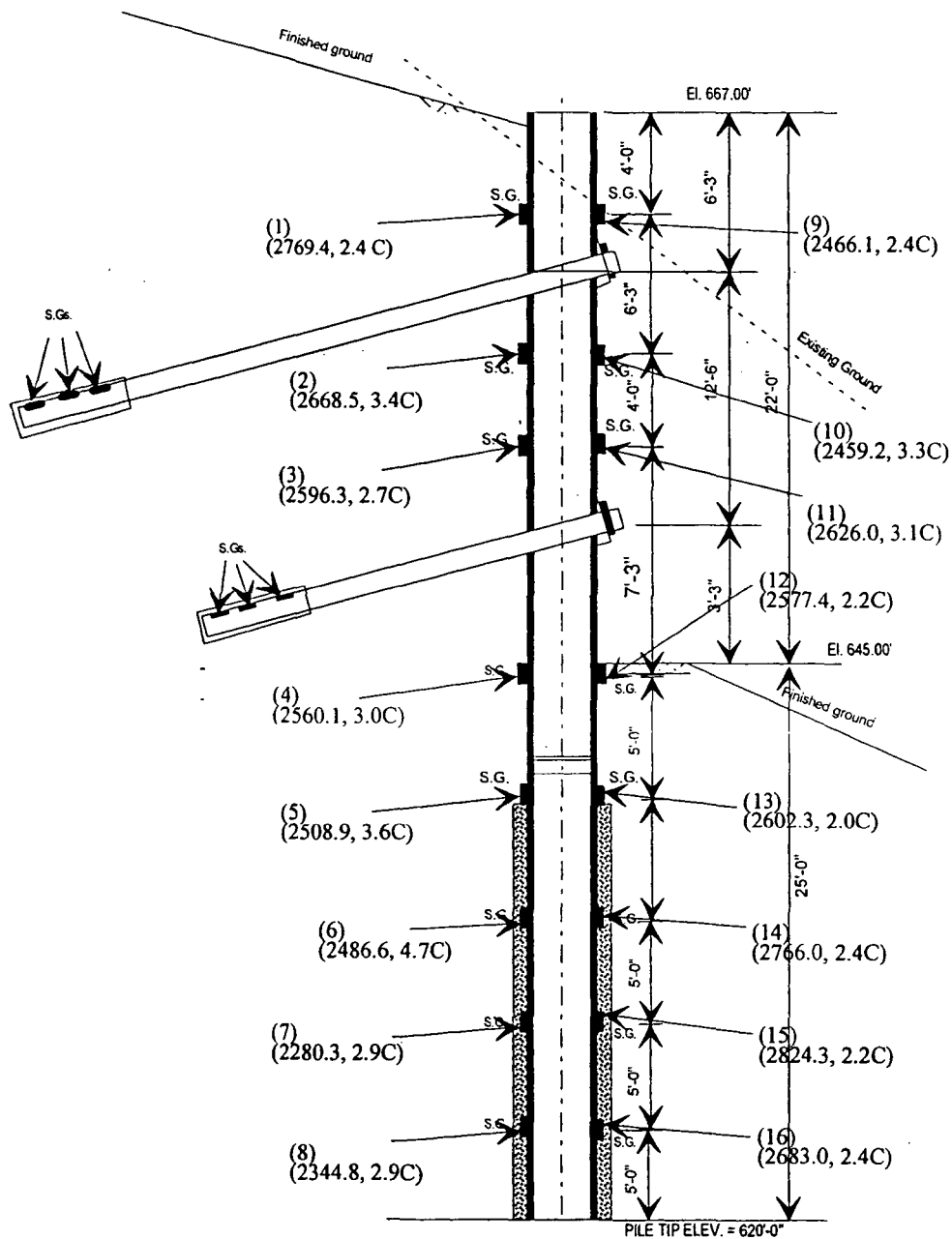


Fig. 3.5: Lower Tier Wall, soldier pile # 11 strain gage locations and initial readings.

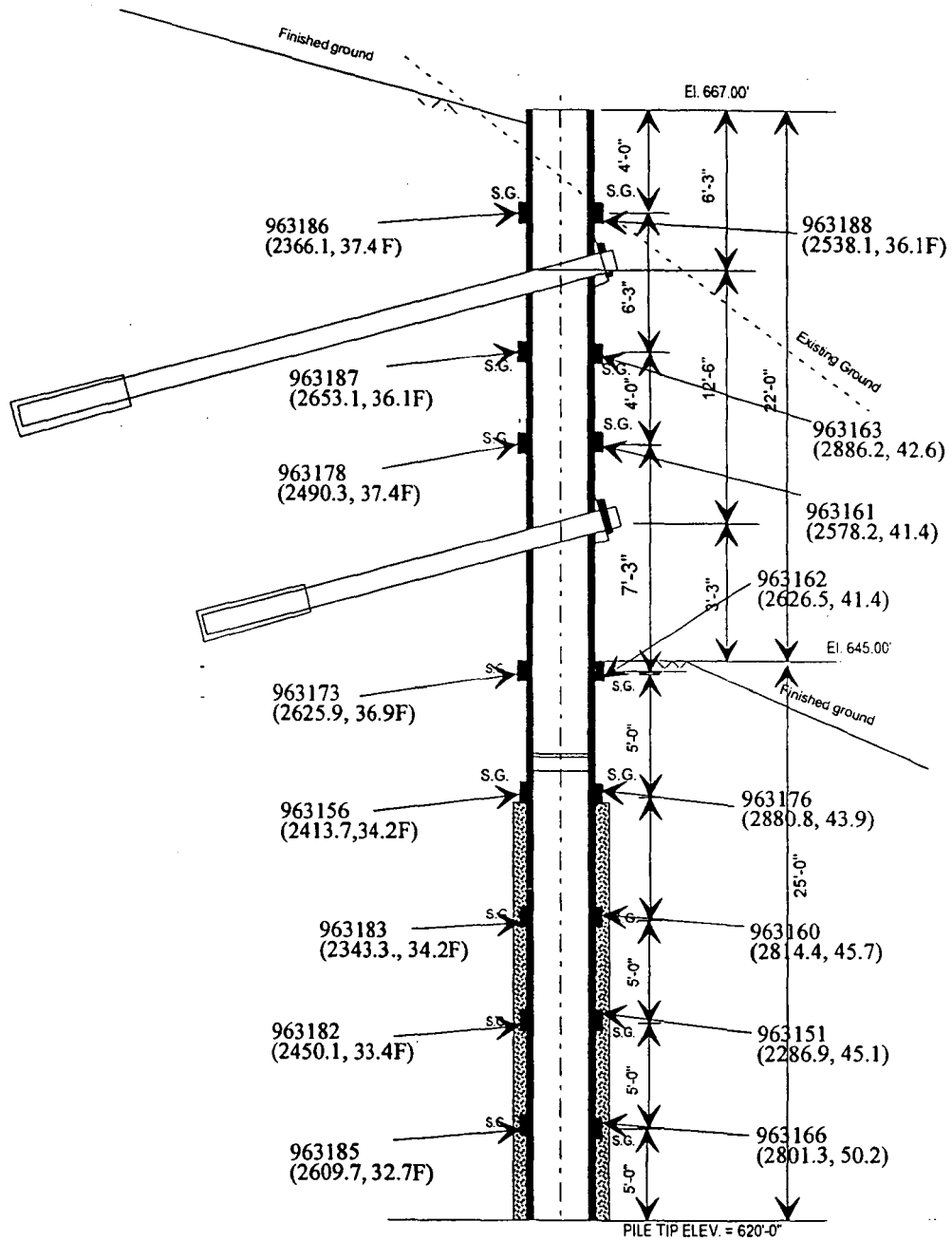


Fig. 3.6: Lower Tier Wall, soldier pile # 12 strain gage locations and initial readings.

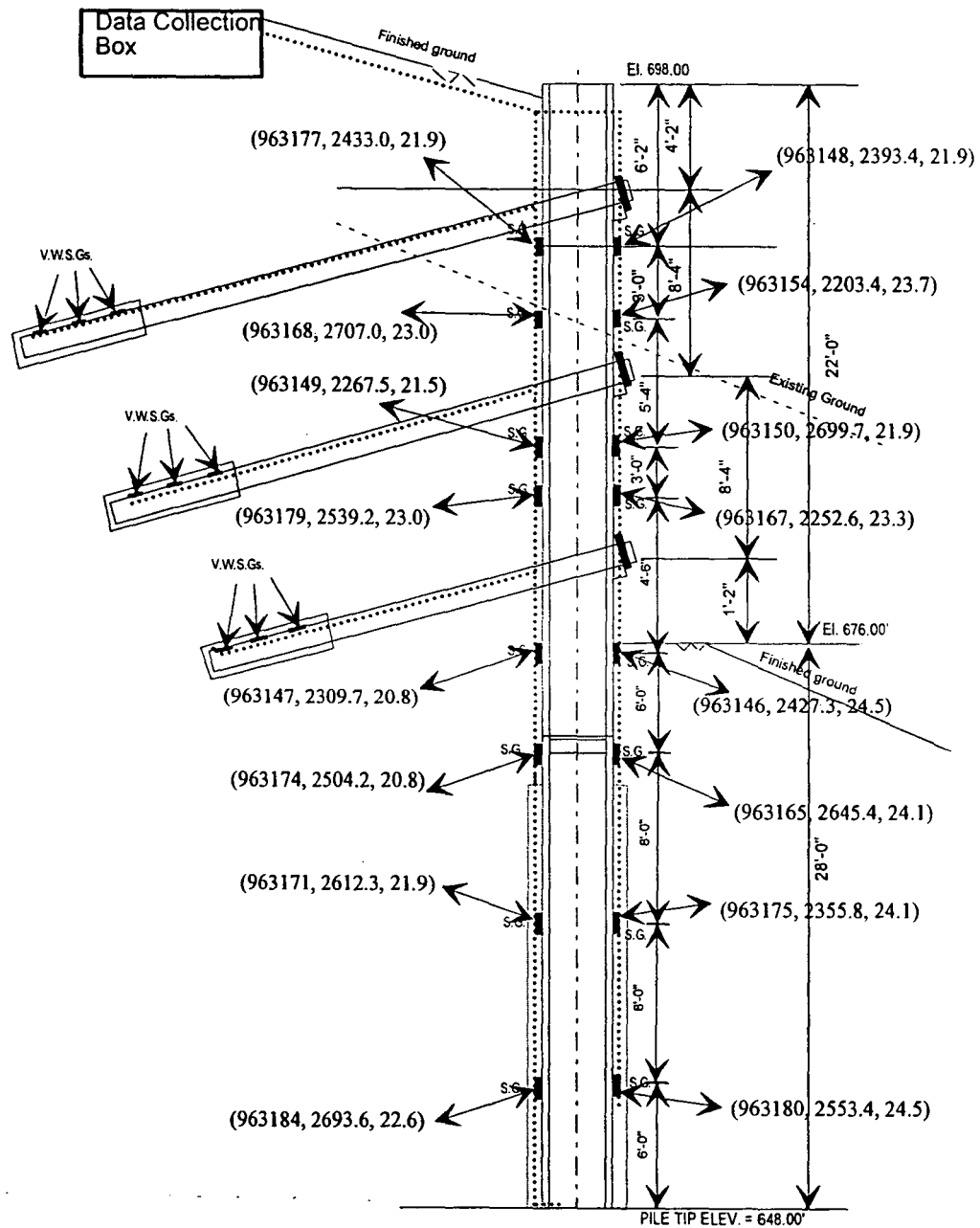


Fig. 3.7: Upper Tier Wall, soldier pile # 30 strain gage locations and initial reading.

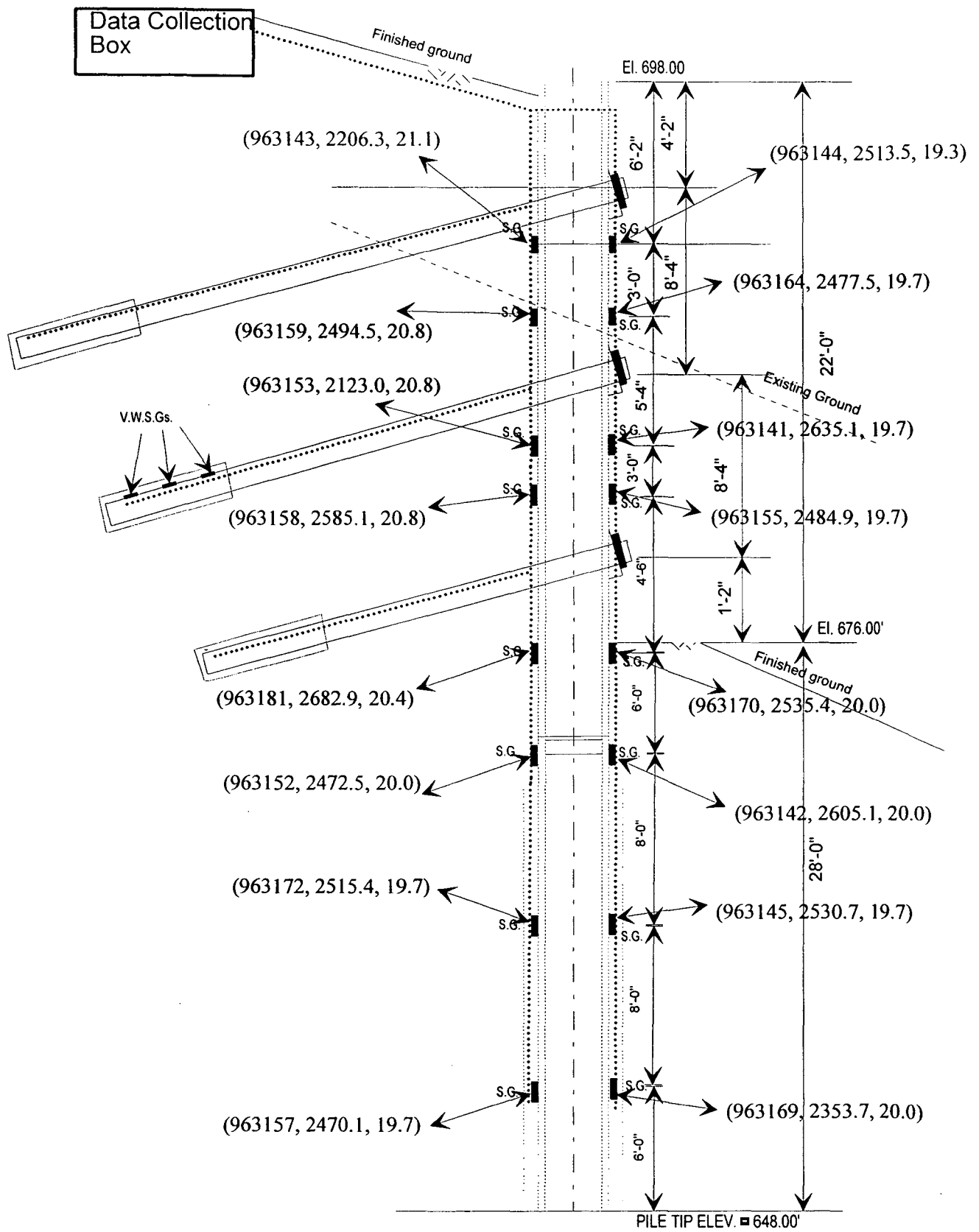


Fig. 3.8: Lower Tier Wall, soldier pile # 31 strain gage locations and initial reading.

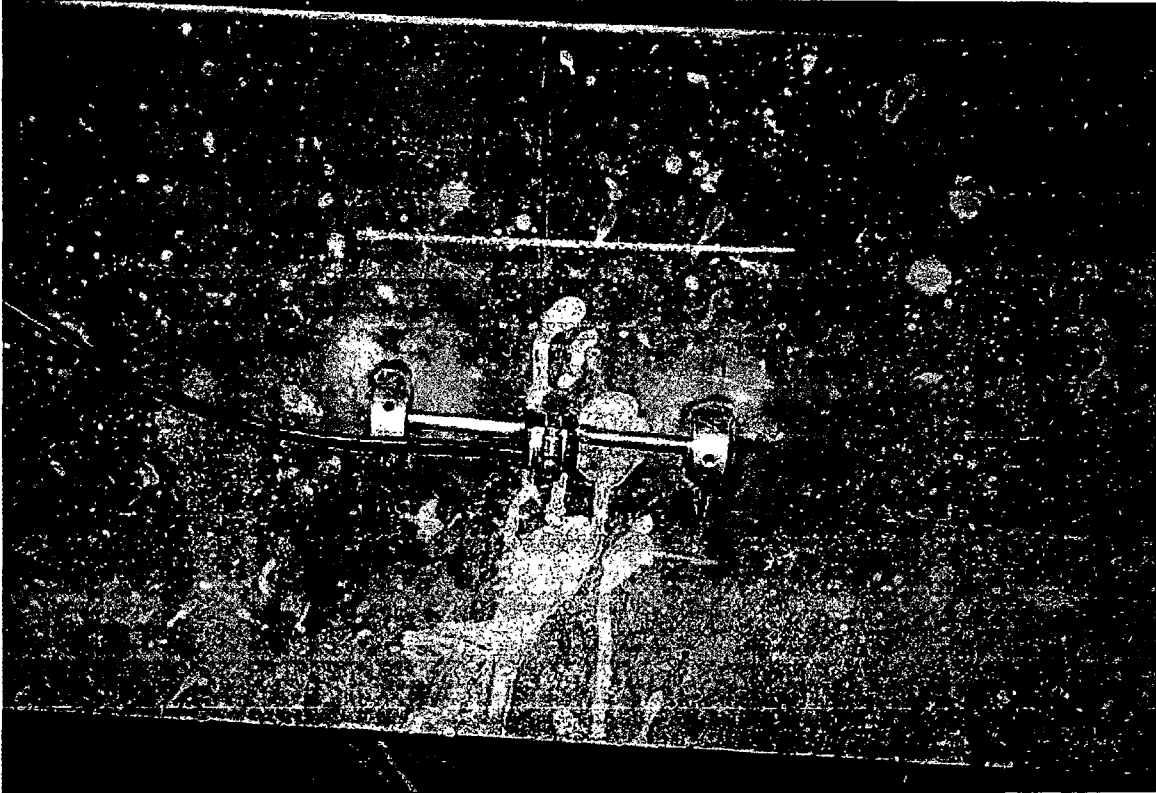


Fig 3.9: Vibrating wire gage been welded to the soldier pile.

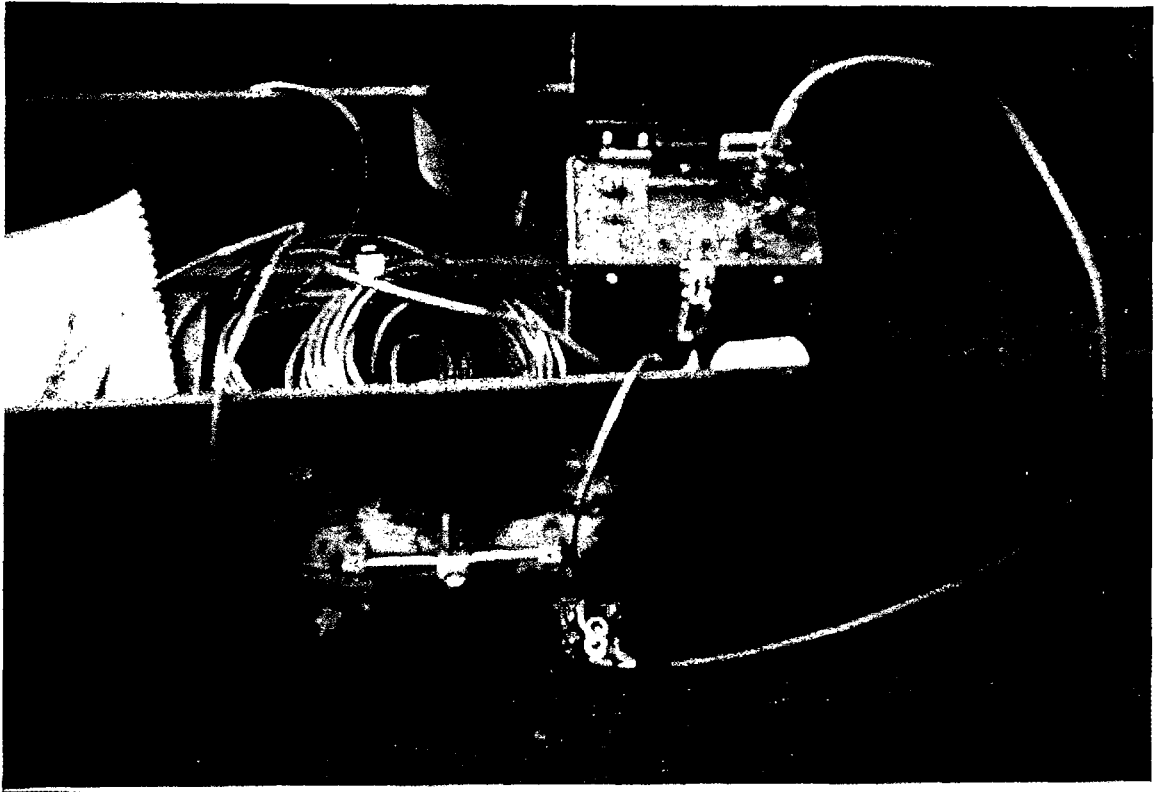


Fig 3.10: Vibrating wire gage been calibrated after installation.



Fig 3.11: A series of gages being installed and checked.

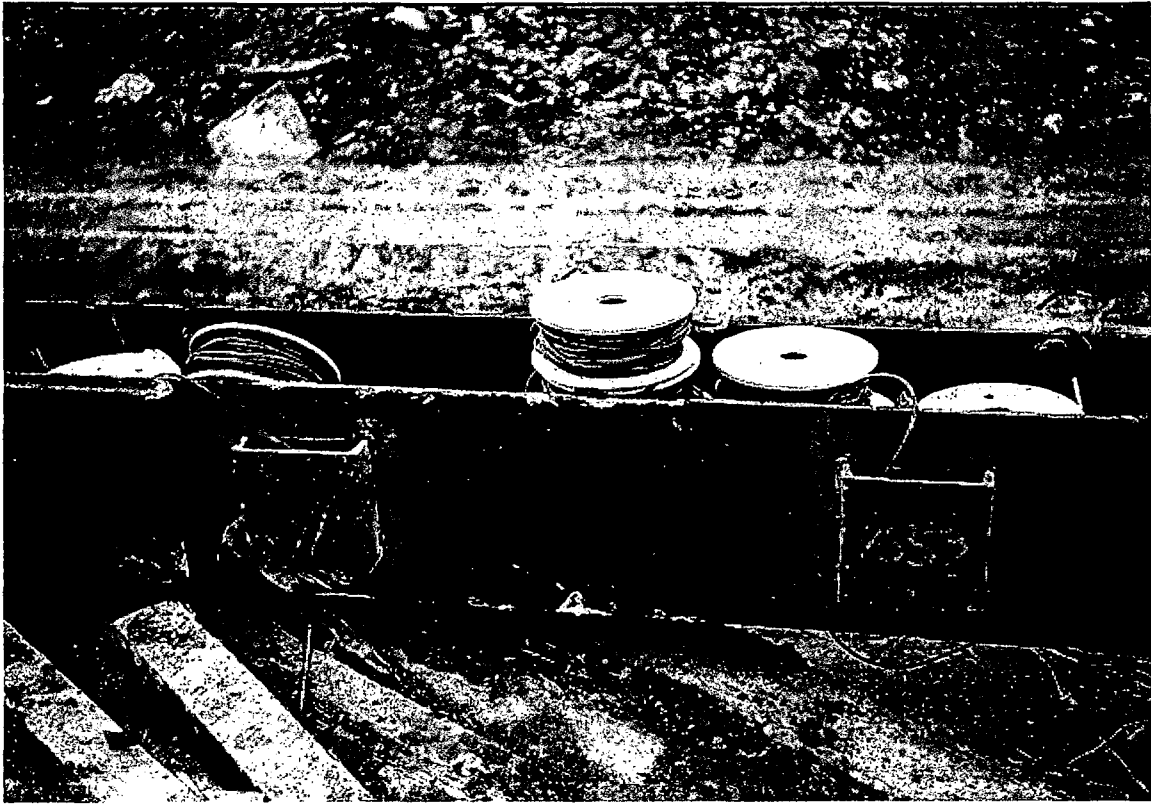


Fig 3.12: Protection C bracket been welded to protect the gage.

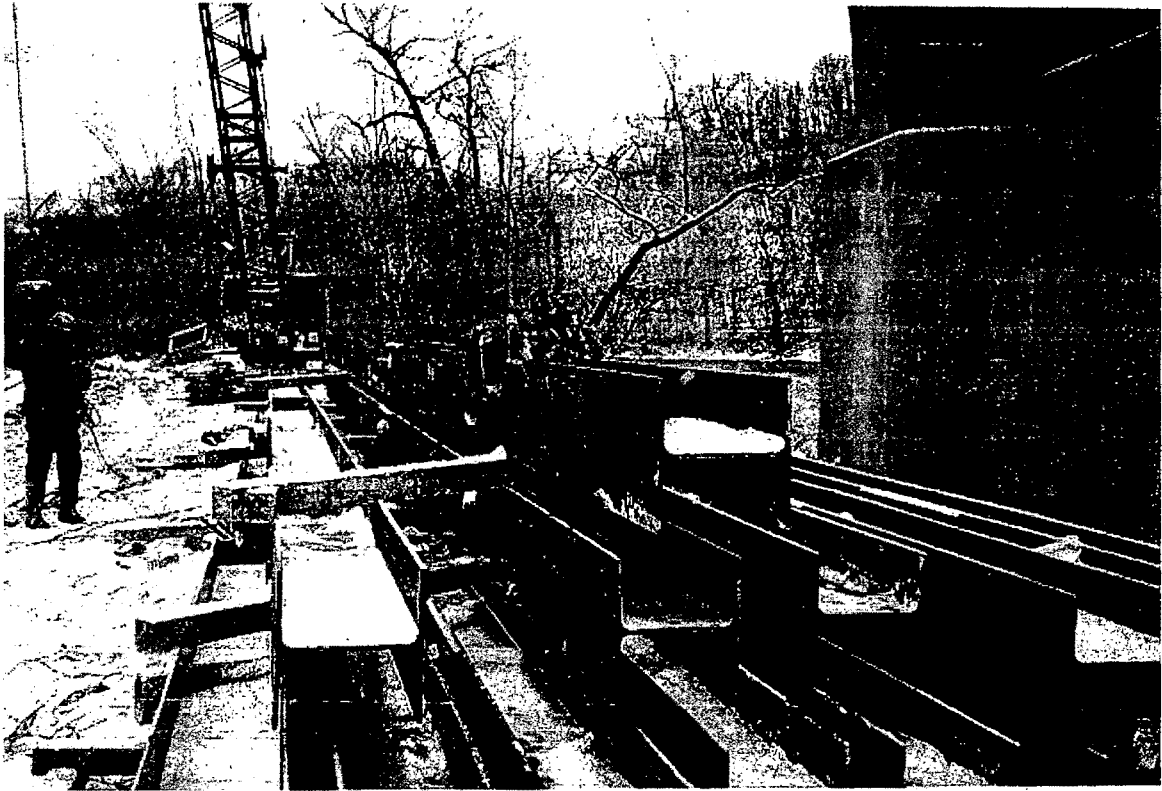


Fig 3.13: Soldier pile instrumented and ready to be moved to the hole.

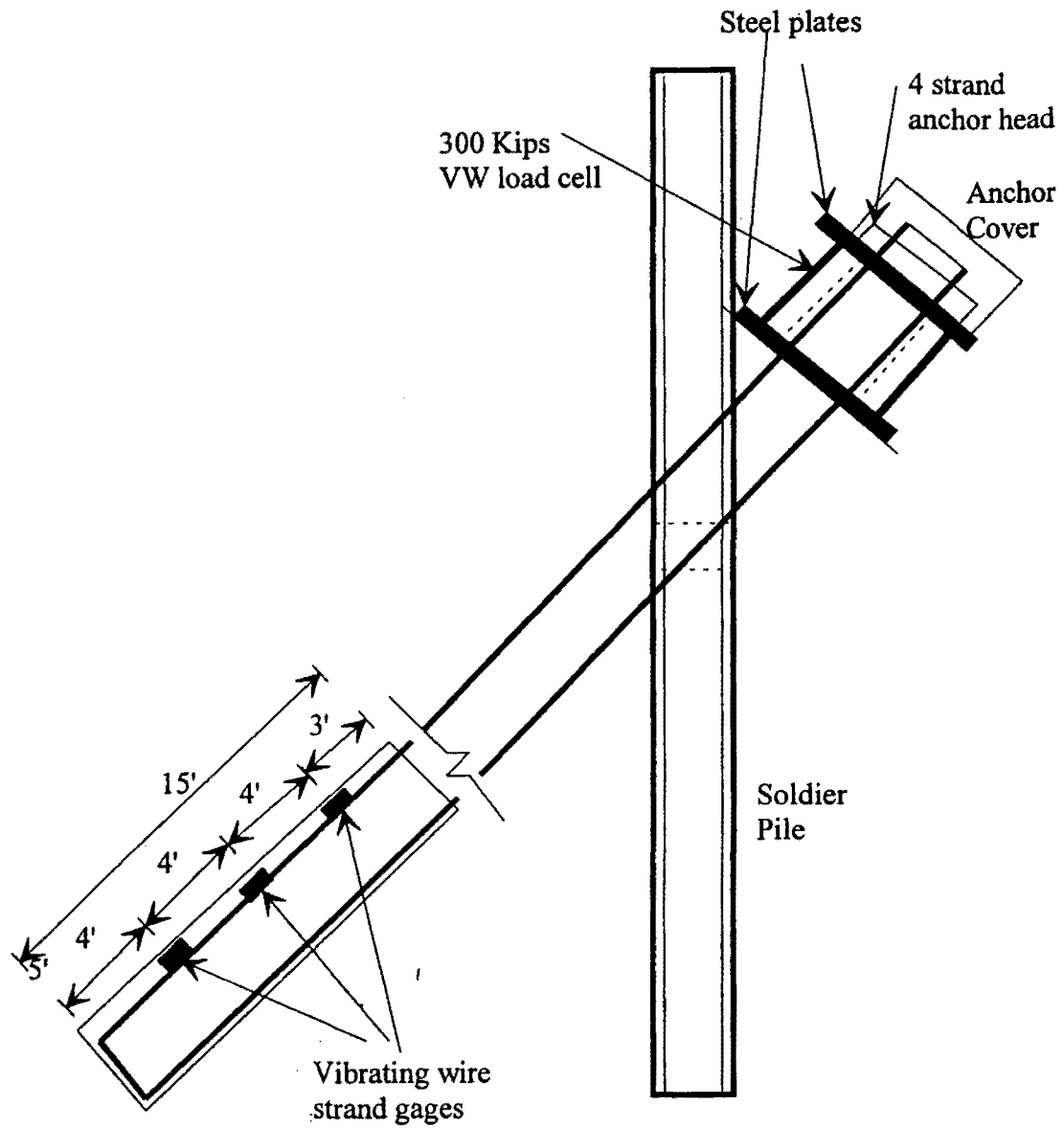


Fig. 3.14: Details of anchor instrumentation and final setup.

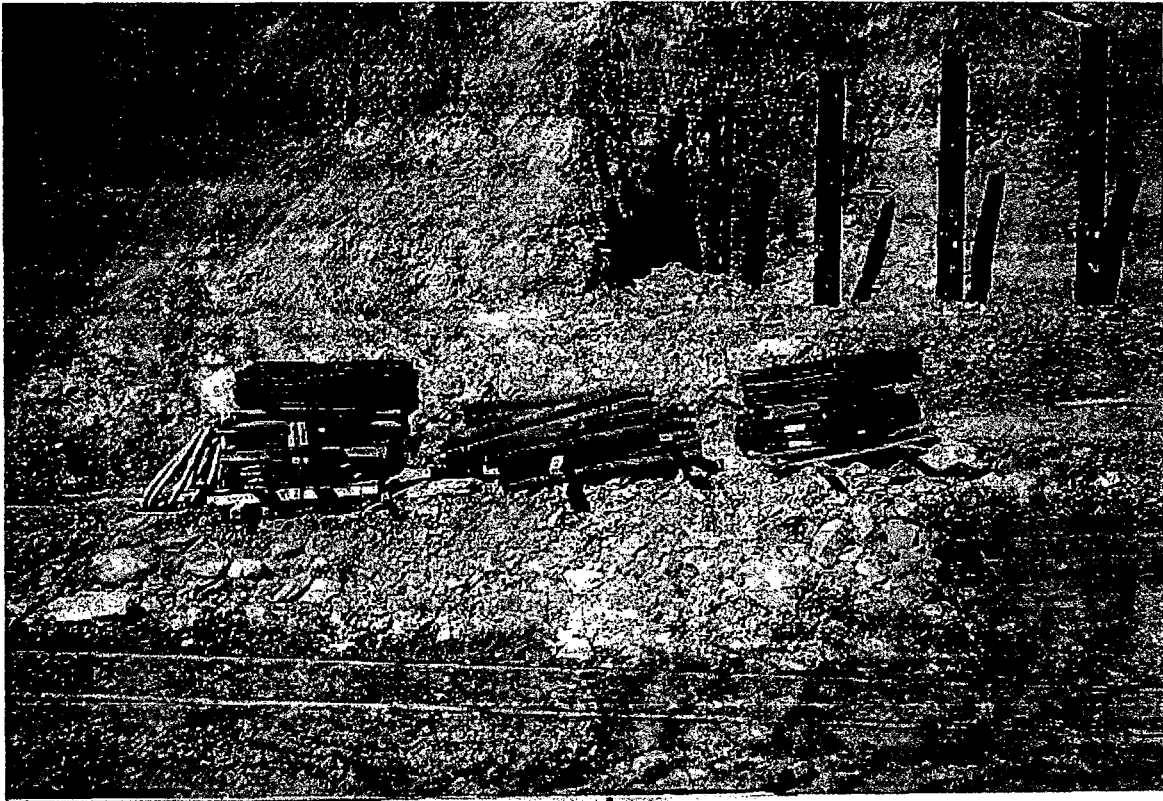


Fig 3.15: Anchors coiled and casing used in the construction.



Fig 3.16: Rock anchor hole drilling.



Fig 3.17: Overview of the anchor drilling operation.



Fig 3.18: Anchor hole drilled and casing installed.



Fig 3.19: Strand gage being installed on the 7-wire strand.



Fig 3.20: Strand gage being installed on the 7-wire strand and calibrated.



Fig 3.21: Strand gage being installed on the 7-wire strand and greased.

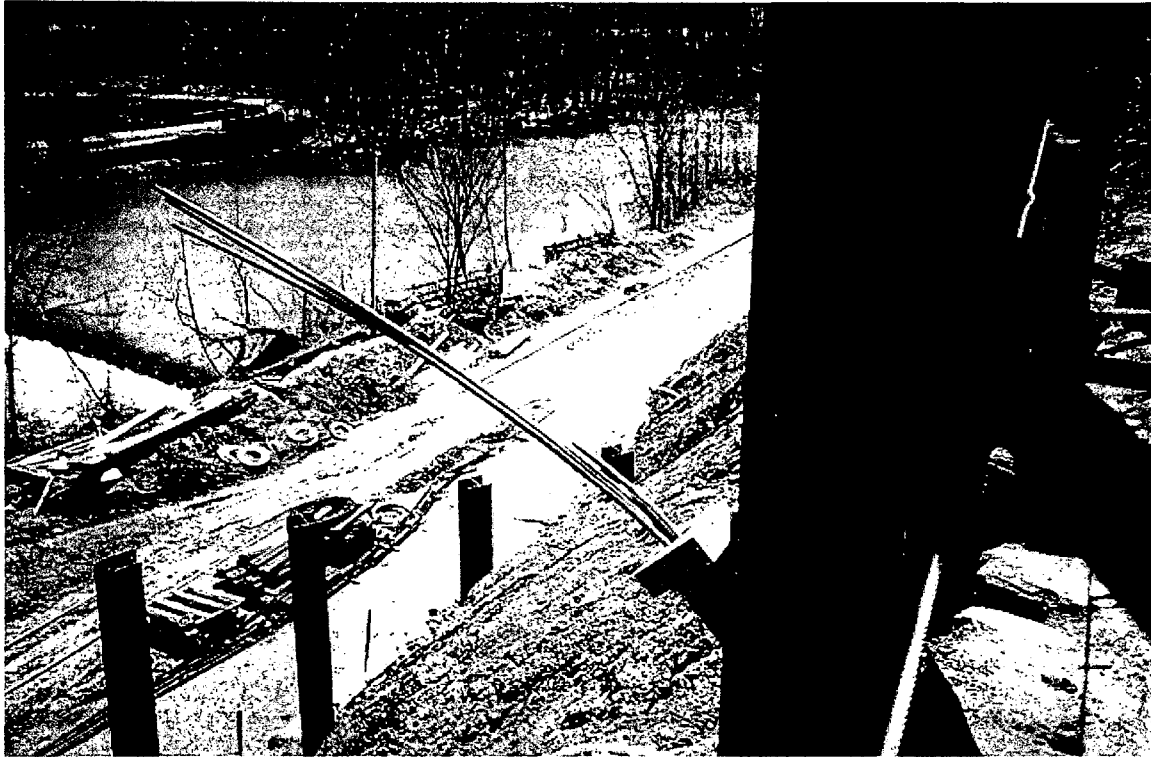


Fig 3.22: Anchor being installed and grouted.

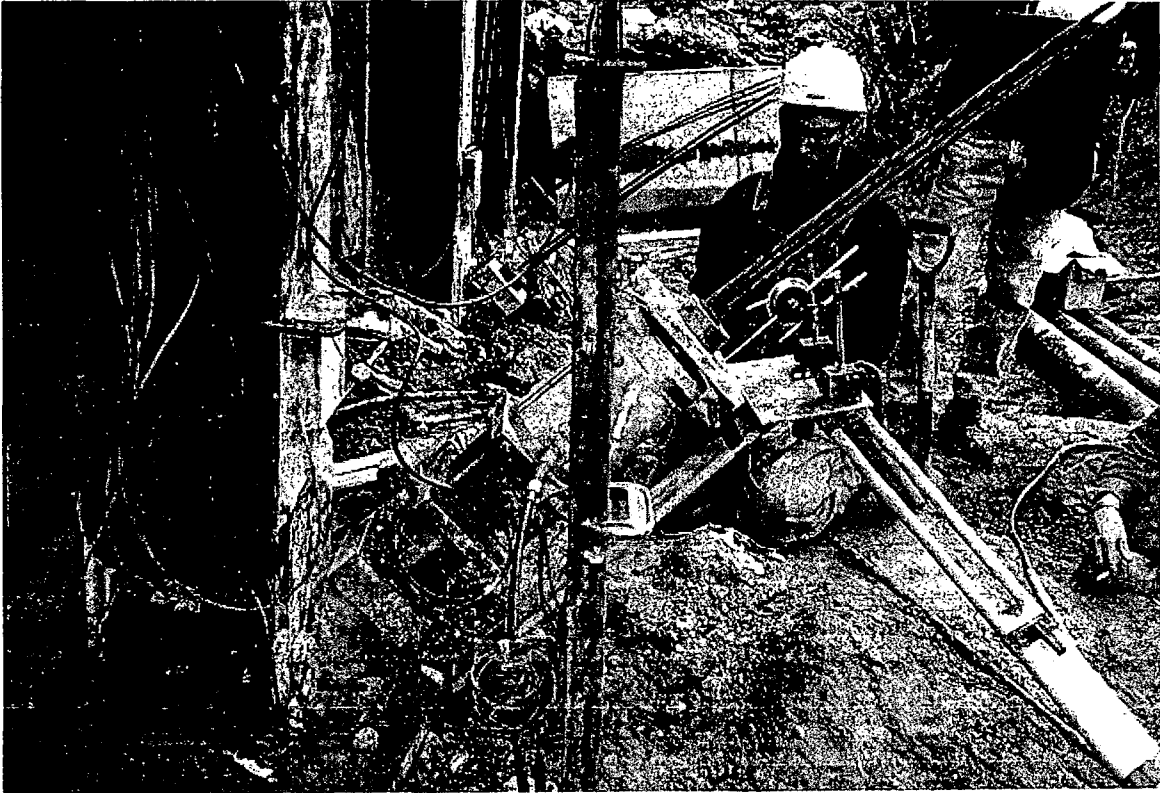


Fig 3.23: Anchor testing undergoing.

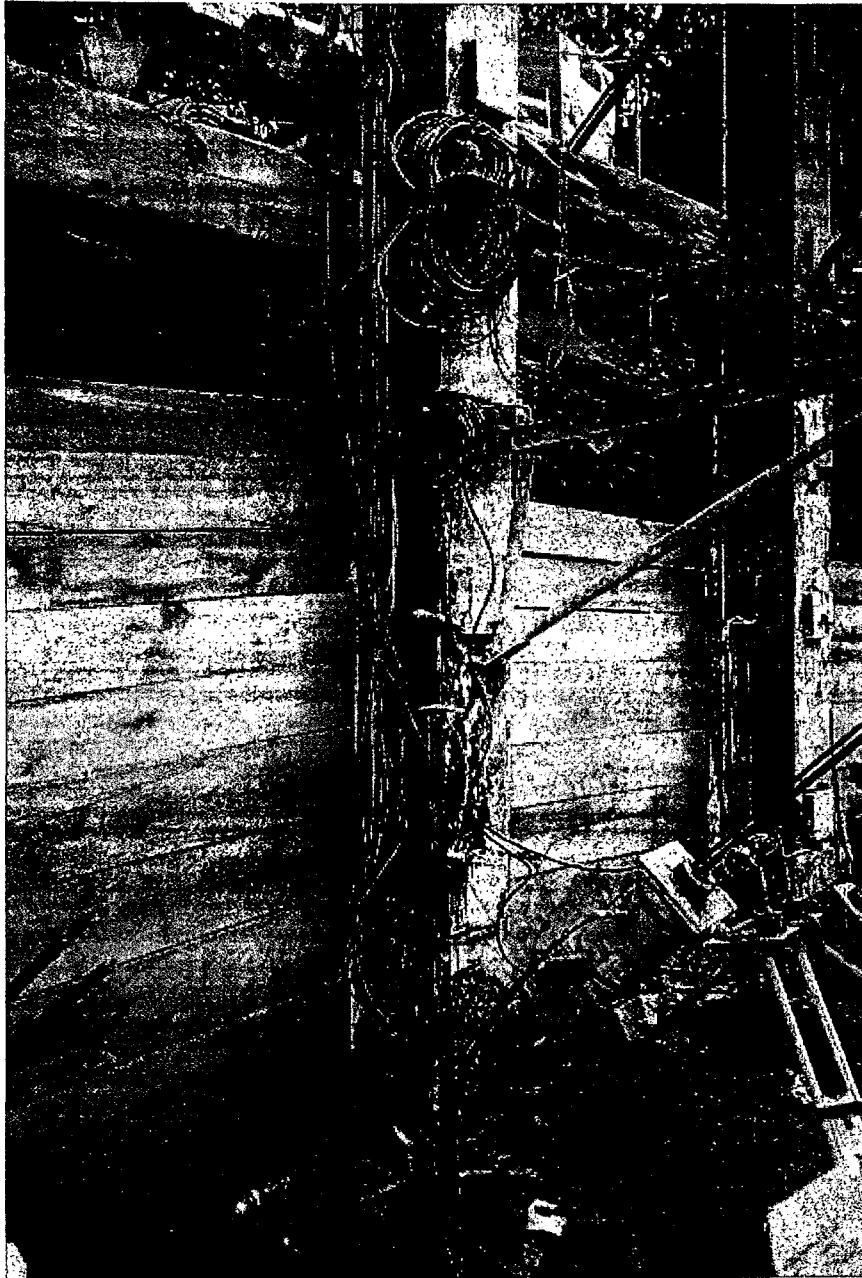
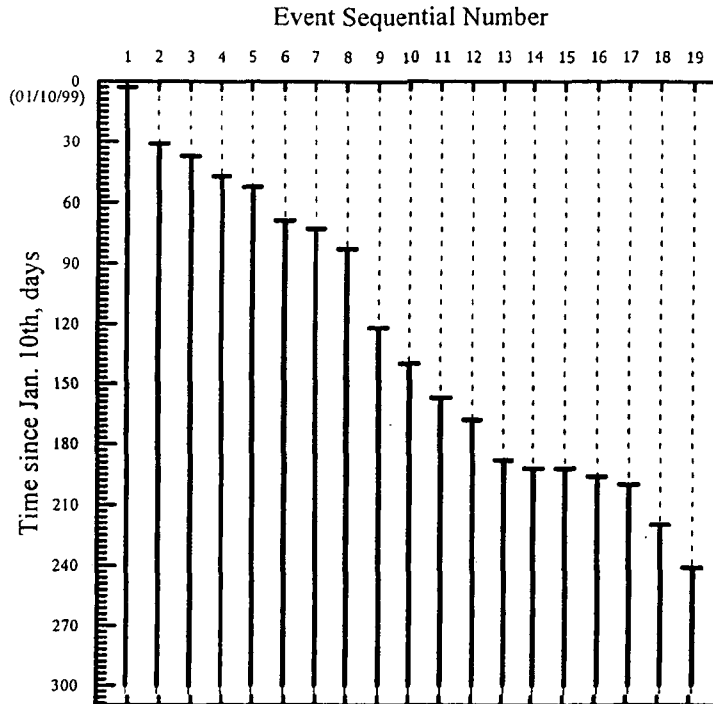


Fig 3.24: Anchor under testing and Anchor already locked-off.



Event	Event Description
1	Establishment of upper and lower benches for soldier pile installation
2	Earth inclinometers and piezometer installation
3	Installation of upper tier soldier piles
4	Installation of lower tier soldier piles
5	Upper tier failure test
6	Lower tier failure test
7	Rock anchor installation and testing was started
8	Installation of precast panels for lower tier was started
9	Start installation of precast panels for upper tier
10	Rock anchor installation and testing was completed for lower tier
11	Installation of precast panels for lower tier was completed
12	Finish tensioning of rock anchors for upper tier wall
13	Start of backfilling the lower tier wall to the proposed final grade
14	Installing the concrete boxes to house the instrumentation wire and the datalogger
15	Start rough grading the upper tier wall area
16	Rough grading the lower tier was completed
17	Installing post grout, anchor caps, and complete project
18	Start wiring gages to the multiplexers
19	Finish wiring gages and connect the datalogger for long-term monitoring

Figure 3.25 Start time schedule for major construction events.



Fig 3.26: Drilling operation for the earth inclinometers



Fig 3.31: Instrumented soldier pile being lifted for installation.



Fig 3.32: The inclinometer being attached to the soldier pile.



Fig 3.33: The inclinometer being extended while lowering the pile.



Fig 3.34: The soldier pile being wrapped with plastic sheet to prevent contact with concrete.



Fig 3.35: The instrumented soldier piles are installed.



Fig 3.36: The strain gages being checked after the pile was installed.



Fig. 3.41: The upper tier failure test anchor being installed.



Fig. 3.42: Setup for the upper tier anchor failure test.

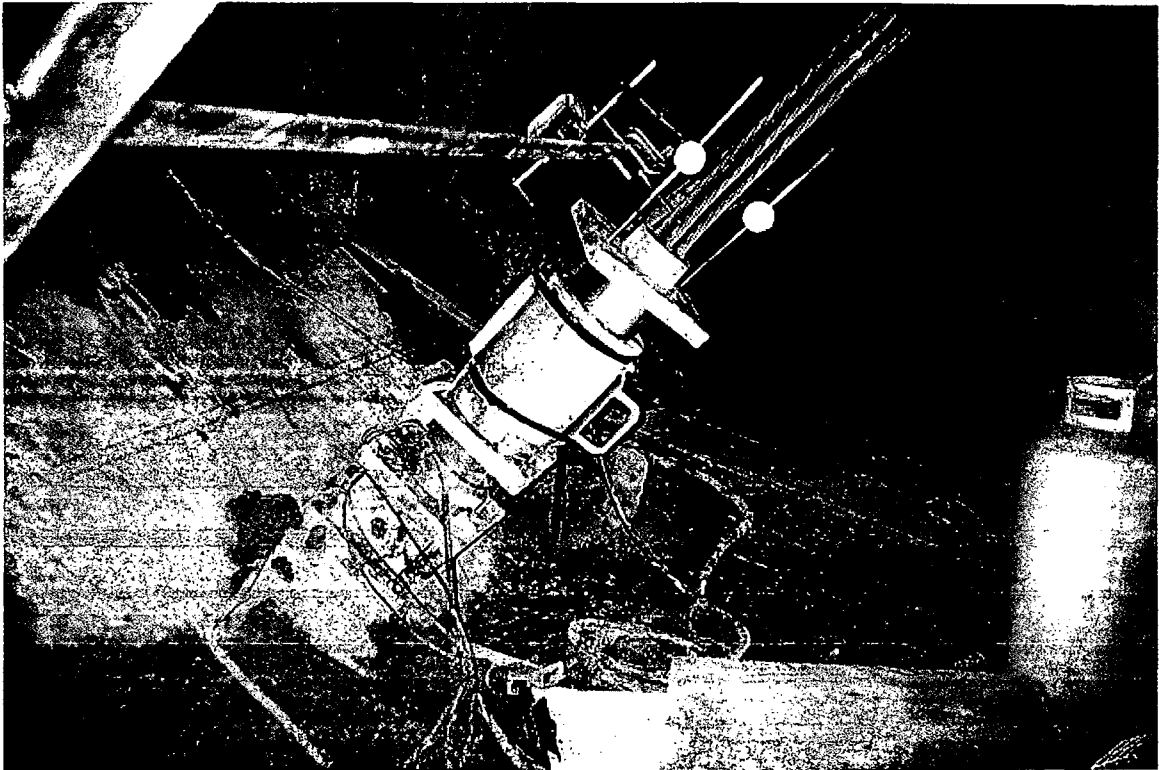


Fig. 3.43: Upper tier anchor failure test.



Fig. 3.44: Setup for the lower tier anchor failure test.



Fig. 3.45: Lower tier anchor failure test.

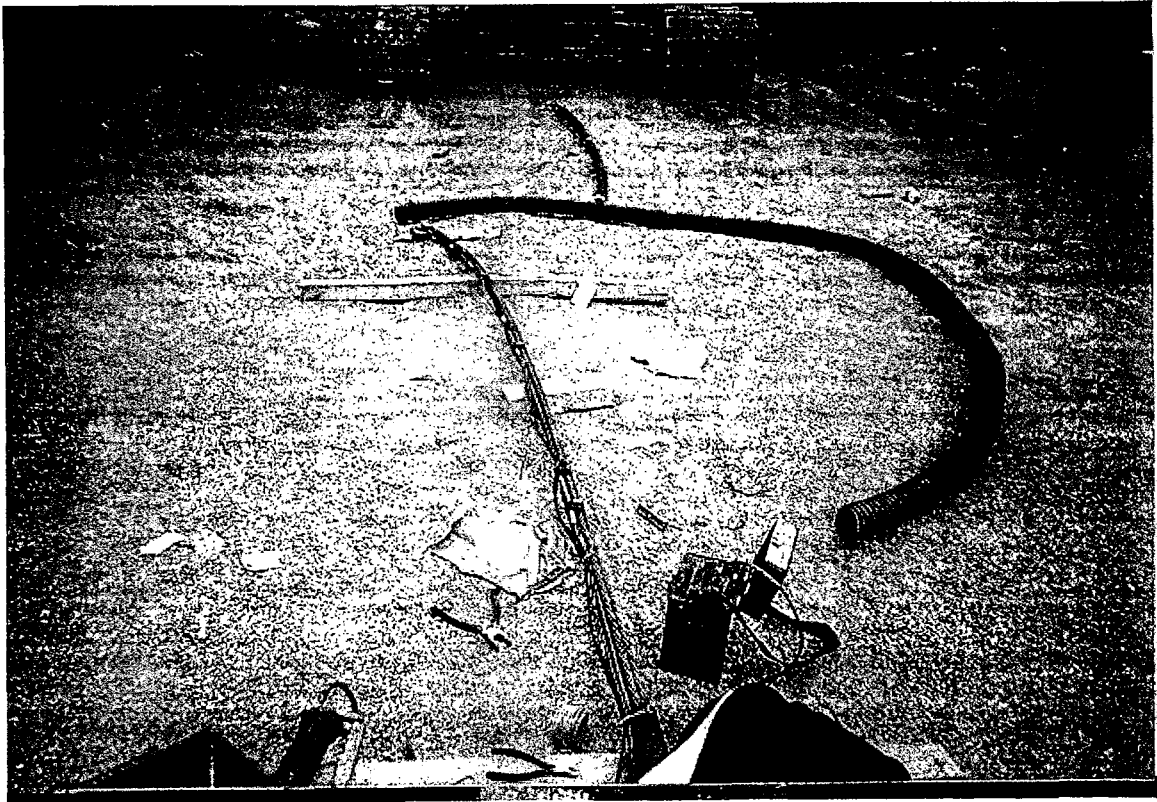


Fig. 3.46: Anchor #11-B instrumented tendon.

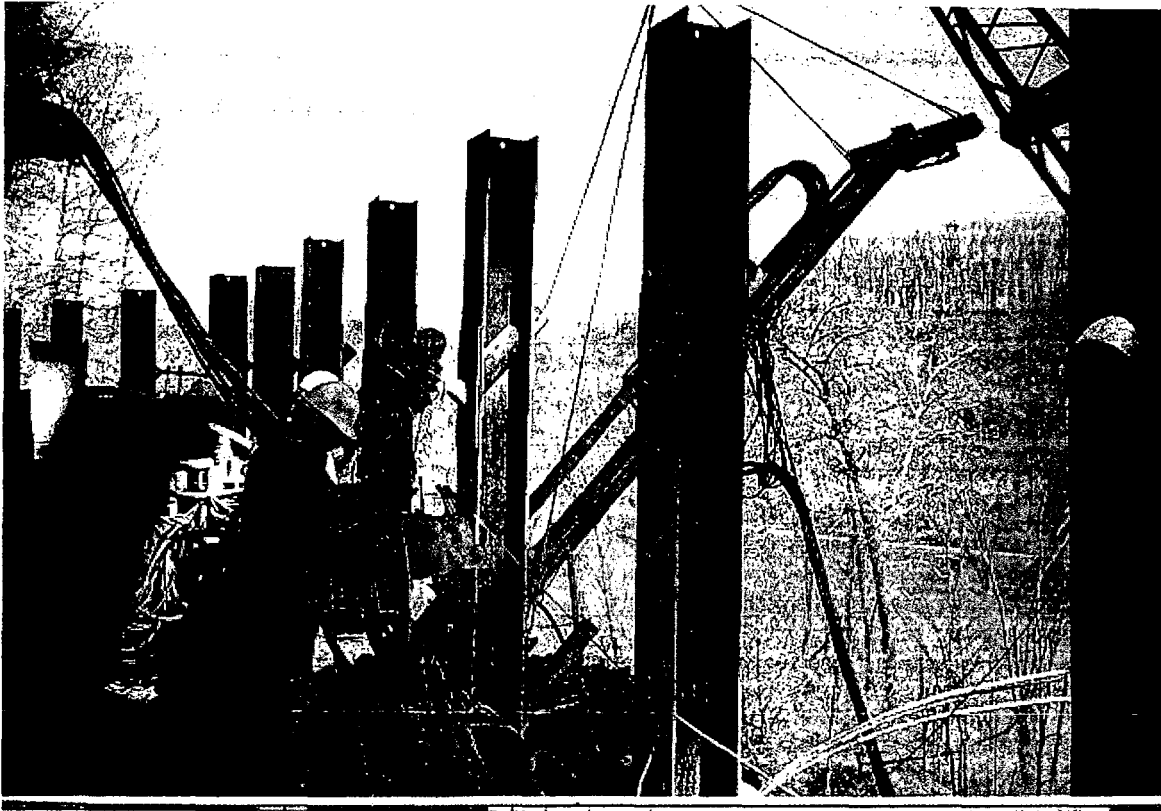


Fig. 3.47: Drilling of instrumented anchor #30-B.



Fig. 3.48: Testing of instrumented anchor #30-B.

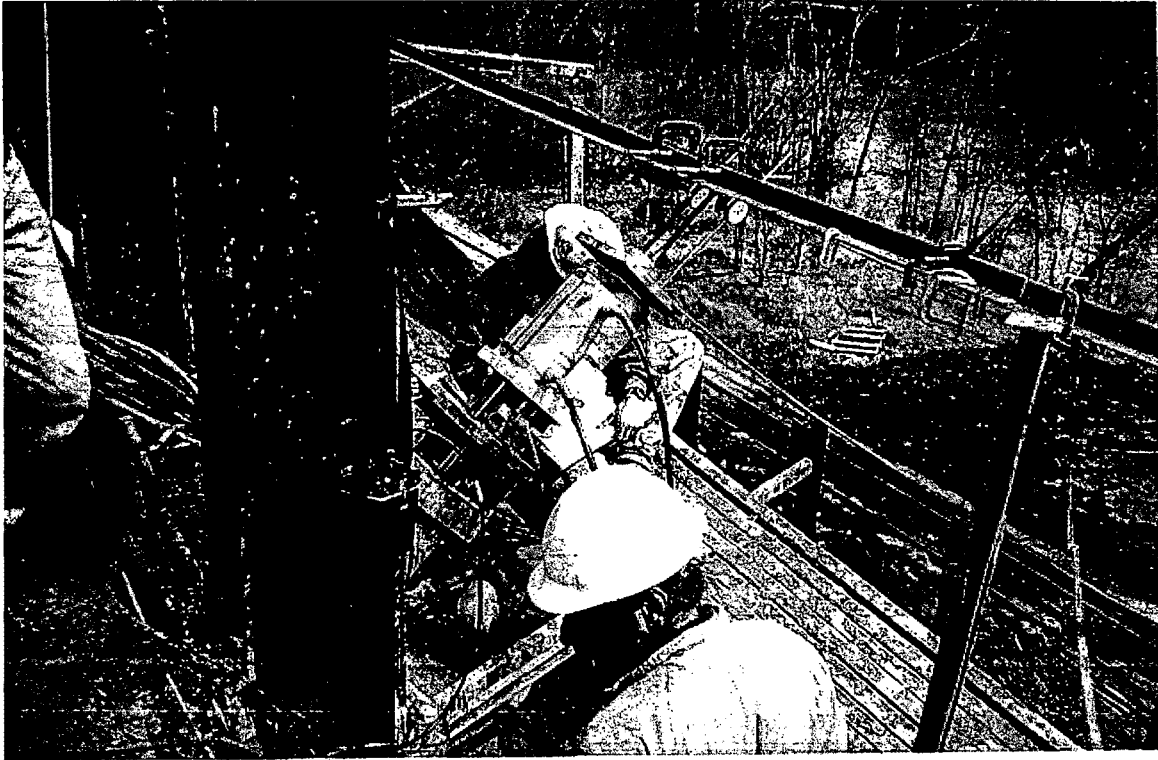


Fig. 3.49: Locking-off anchor #30-B after testing.

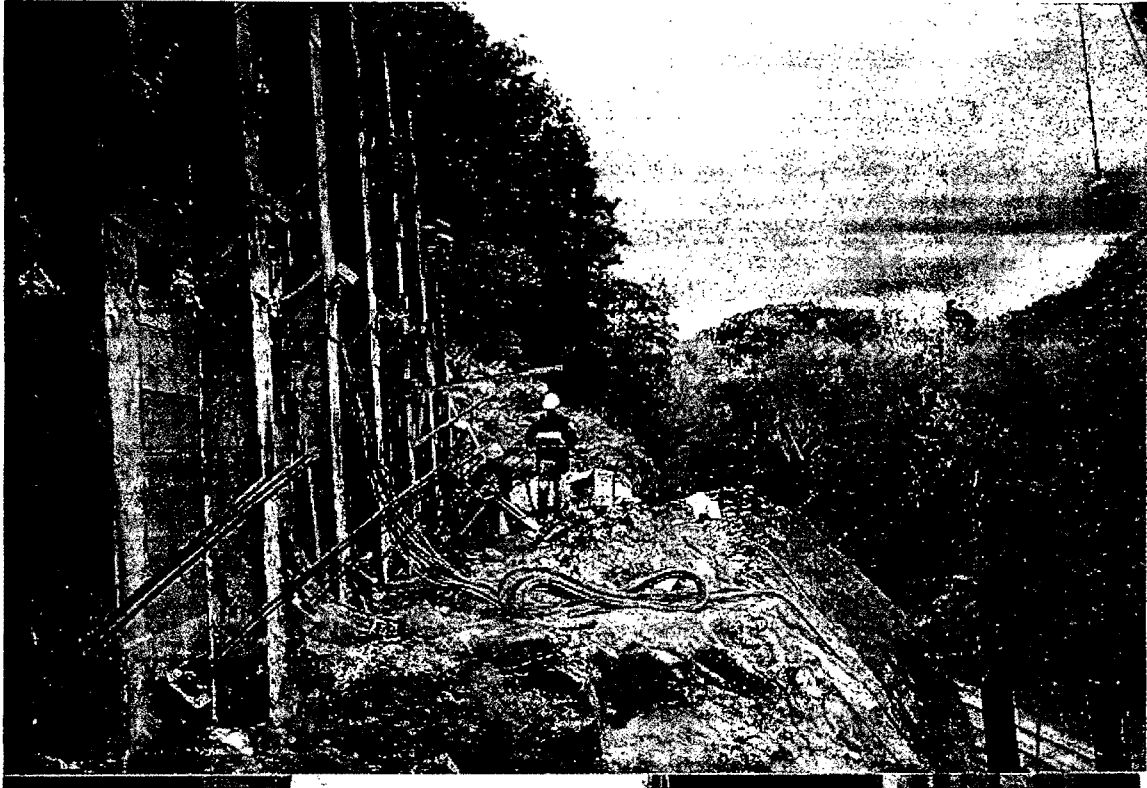


Fig. 3.50: Testing of anchor #30-C in the upper tier wall.

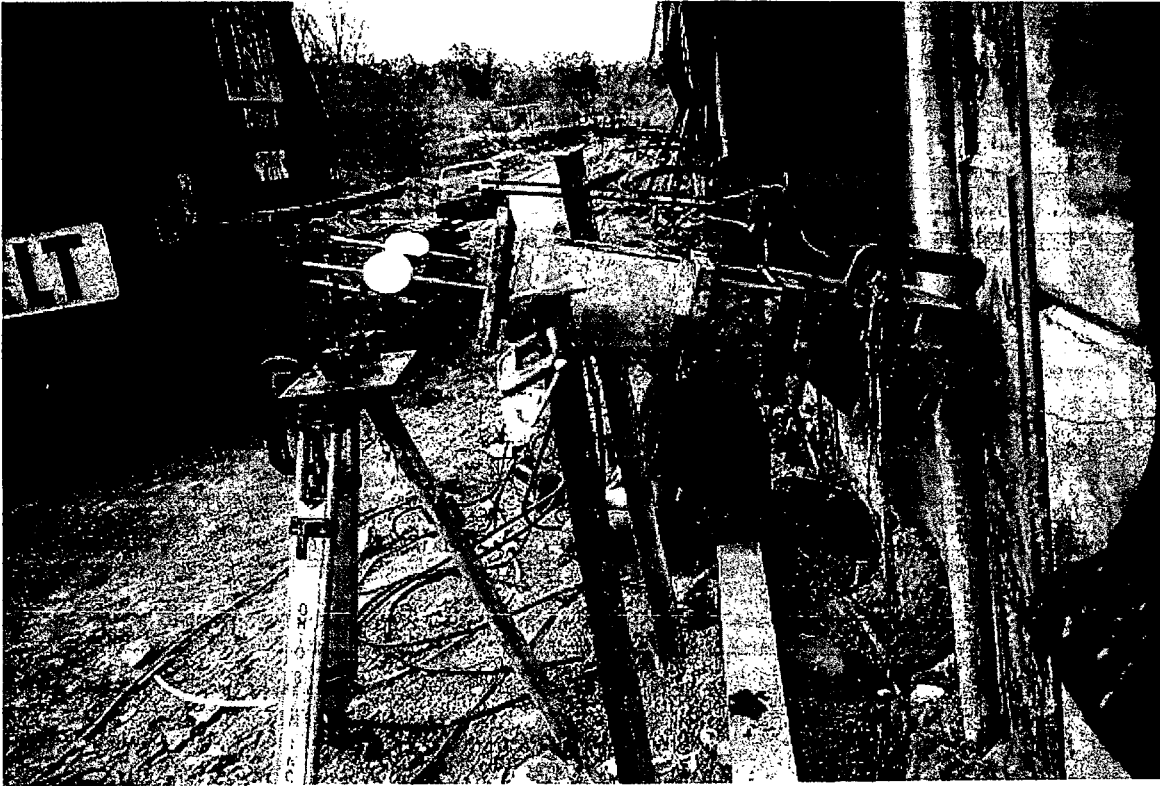


Fig. 3.51: Testing of anchor #11-B in the lower tier wall.

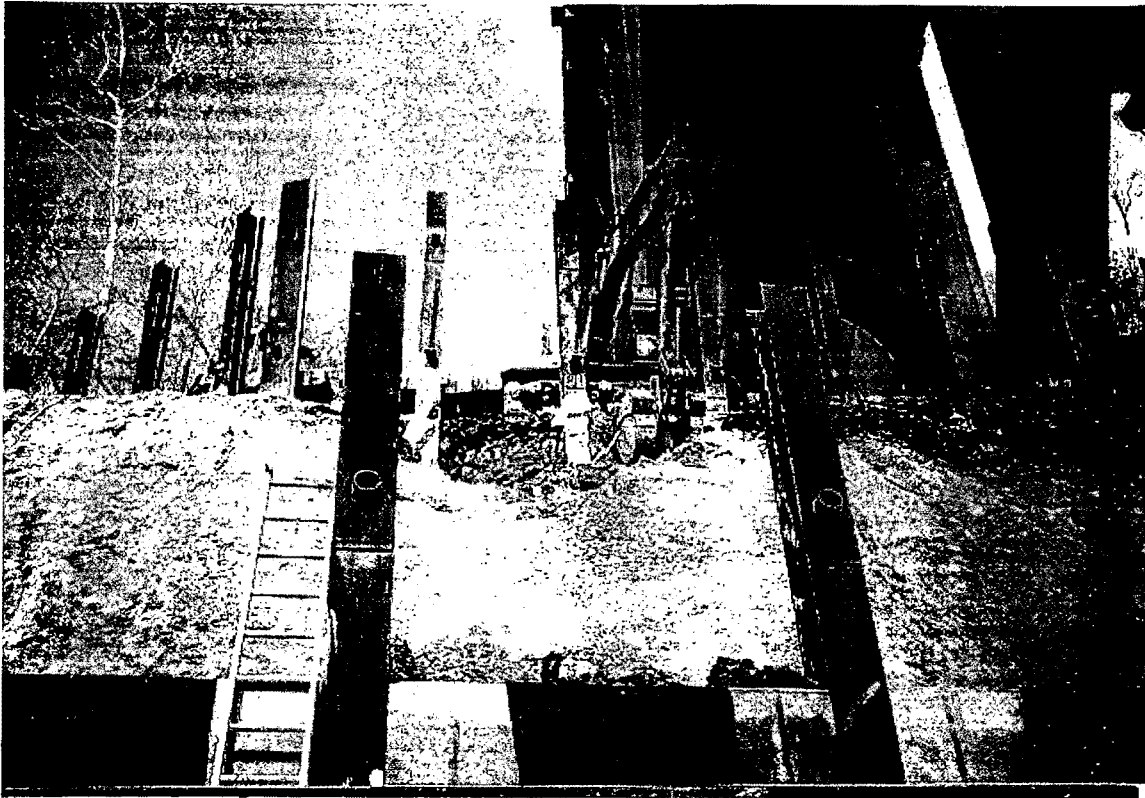


Fig. 3.52: Digging a trench to access the lower row of anchors in the upper tier wall.



Fig. 3.53: Installation of casing for the upper row of anchors in the lower tier.



Fig. 3.54: Temporary lagging installed in the upper tier wall.



Fig. 3.55: Performance test of anchor #30-C in the upper tier wall.

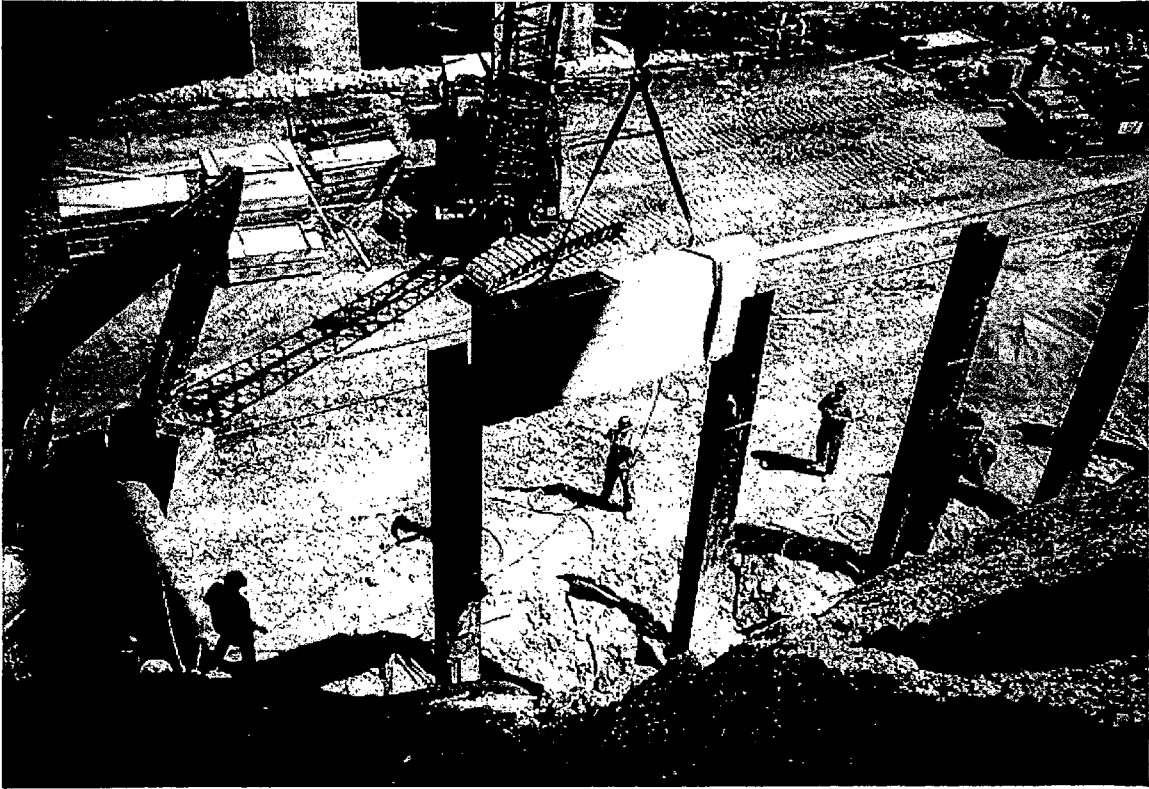


Fig. 3.56: Installation of precast panels.

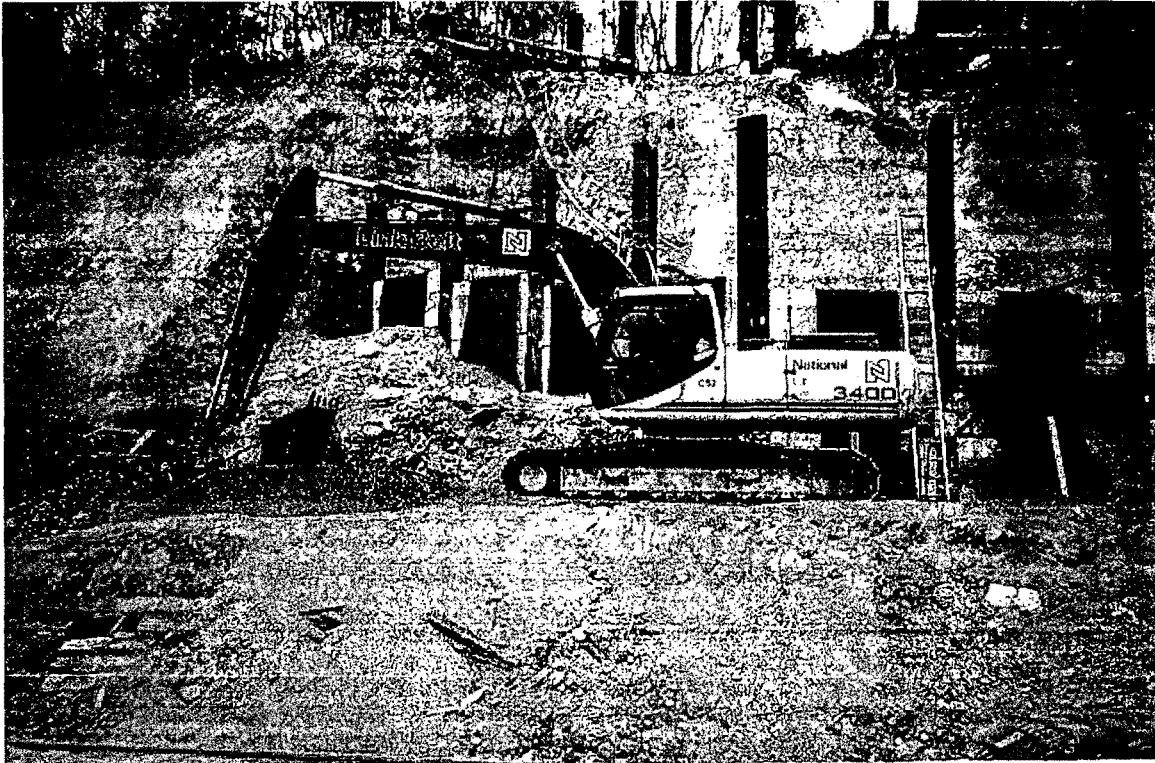


Fig. 3.57: Drainage blanket installed behind the panels.

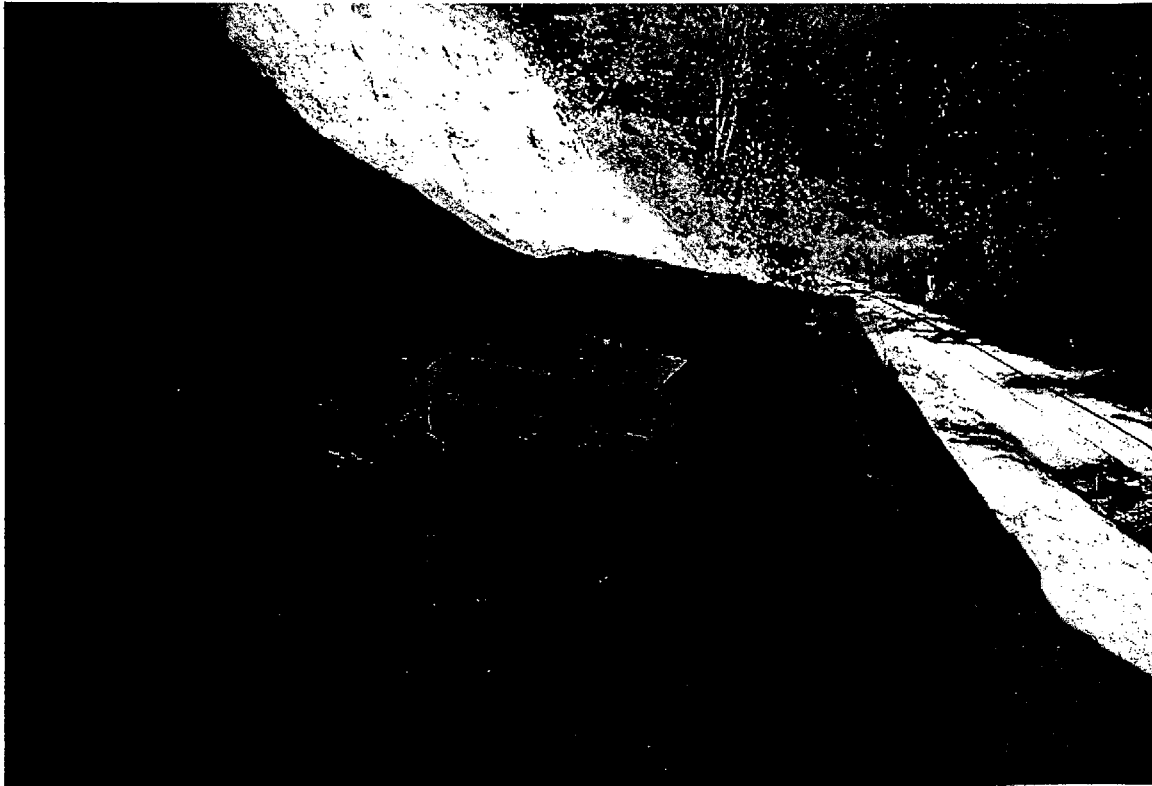


Fig. 3.58: Concrete box installed to house the data collection devices in the lower tier wall area.



Fig. 3.59: Concrete box installed to house the data collection devices in the upper tier wall area.

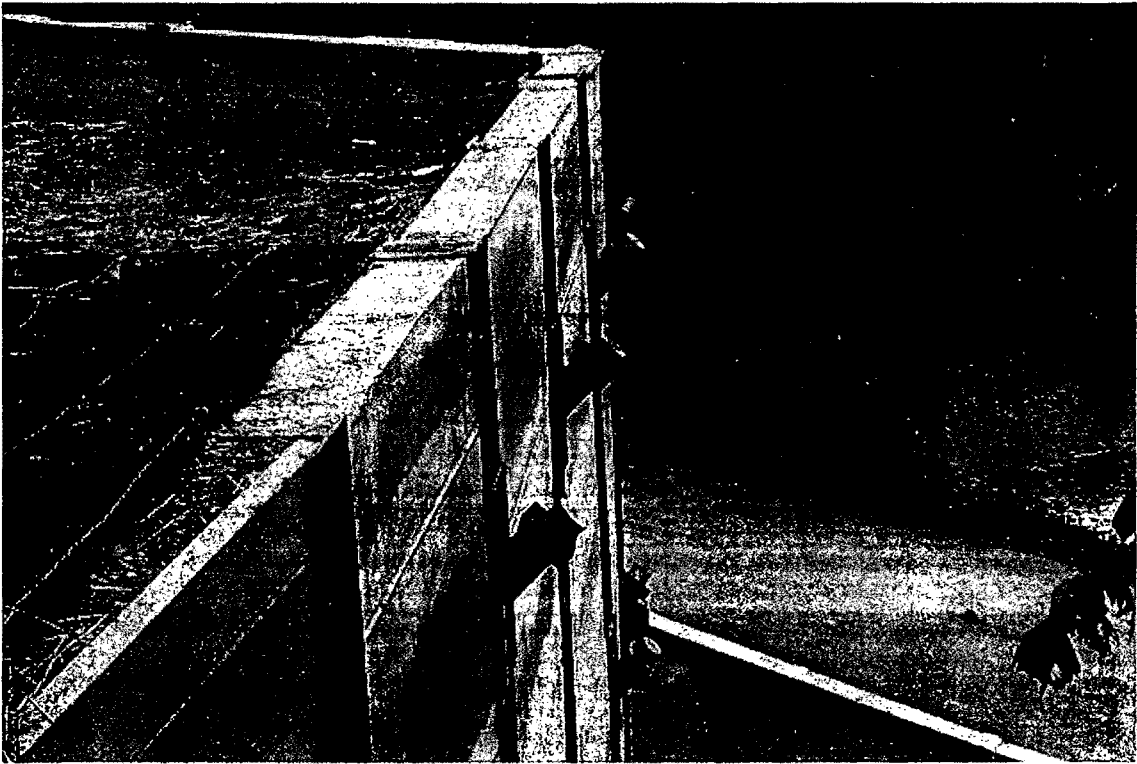


Fig. 3.60: Anchor caps been installed and grouted.



Fig. 3.61: Installation of vibrating wire piezometer.

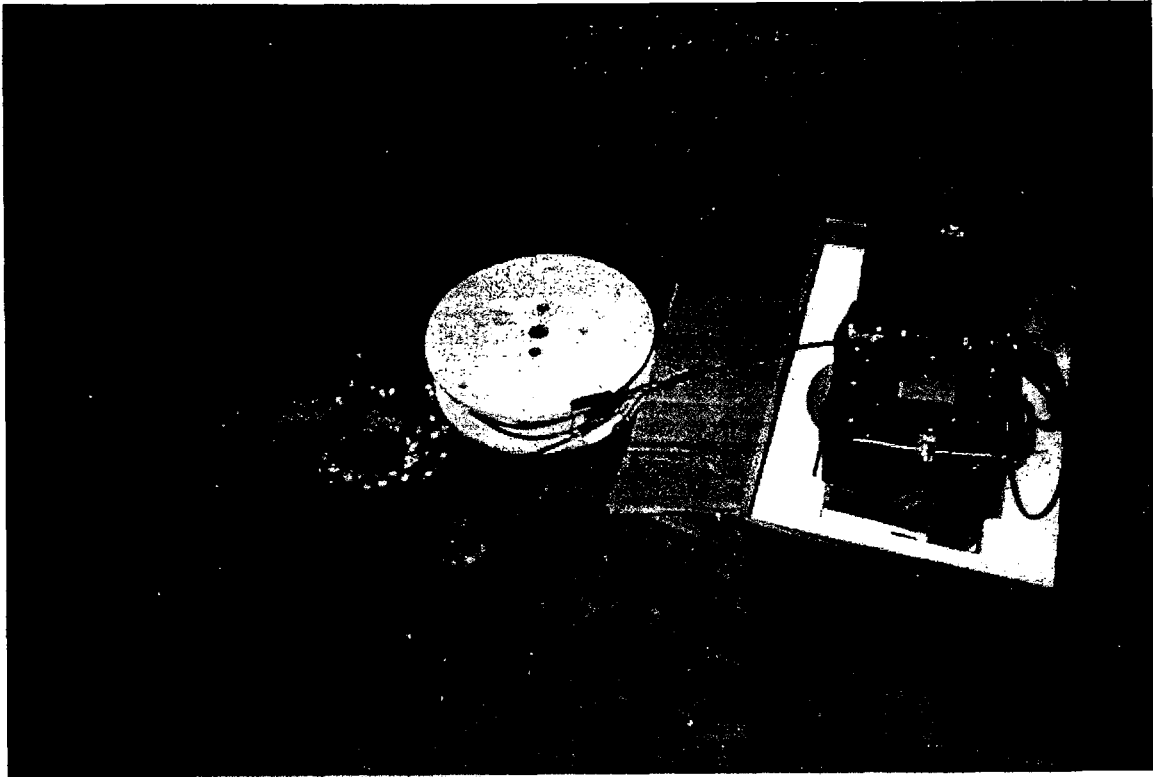


Fig. 3.62: Vibrating wire piezometer installed and being checked.



Fig. 3.63: Details of instrumented anchor head assembly.

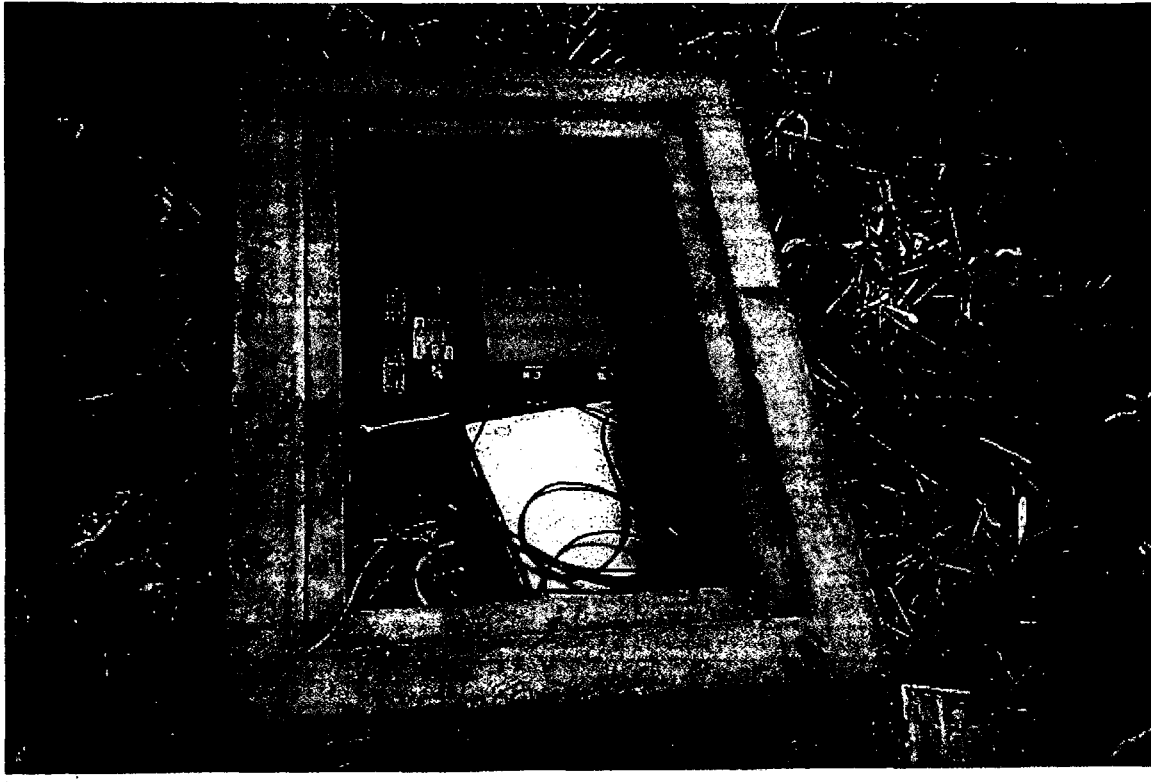


Fig. 3.64: Final location of data collection devices in the upper tier wall.



Fig. 3.65: Final location of data collection devices in the lower tier wall.

CHAPTER IV

SHORT AND LONG TERM MONITORING RESULTS

IV.1 OVERVIEW OF COLLECTED INFORMATION BEFORE COMMENCEMENT OF CONSTRUCTION

Since the beginning of this research project, the Cuyahoga Valley National Recreation Area (CVNRA) has kindly provided the University of Akron's (UA) team with all the information collected including previous site investigation done during the years of 1993 through 1995. The information was compiled and the design soil parameters were selected to check on the slope stability analysis, the tieback analysis and design. This was done to assure that the tieback wall design is safe and to help in designing the instrumentation plans. The UA team worked with CVNRA engineers and the design firm on the plans of instrumentation and testing specifications for the project manual. Three earth inclinometers were installed during the first week of the project to begin the monitoring of the movement of the slope. A vibrating wire based piezometer was also installed to measure the pore water pressure. For clarity of data presentation, the major construction stages are summarized in Table 4.1, and the corresponding instrument monitoring results are presented in the remaining part of the chapter.

Table 4.1: Major construction events.

Event #	Event Description	Starting Date
1	Establishment of upper and lower benches for soldier pile installation	1/13/1999
2	Earth inclinometers and piezometer installation	2/1/1999
3	Installation of upper tier soldier piles	2/8/1999
4	Installation of lower tier soldier piles	2/23/1999
5	Upper tier failure test	3/11/1999
6	Lower tier failure test	3/15/1999
7	Rock anchor installation and testing was started	3/25/1999
8	Installation of precast panels for lower tier was started	5/3/1999
9	Start installation of precast panels for upper tier	5/21/1999
10	Rock anchor installation and testing was completed for lower tier	6/7/1999
11	Installation of precast panels for lower tier was completed	6/18/1999
12	Finish tensioning of rock anchors for upper tier wall	7/8/1999
13	Start of backfilling the lower tier wall to the proposed final grade	2/18/1999
14	Installing the concrete boxes to house the instrumentation wire and the datalogger	7/12/1999
15	Start rough grading the upper tier wall area	7/12/1999
16	Rough grading the lower tier was completed	7/16/1999
17	Installing post grout, anchor caps, and complete project	7/20/1999
18	Start wiring gages to the multiplexers	8/9/1999
19	Finish wiring gages and connect the datalogger for long-term monitoring	8/31/1999

III.2 UPPER AND LOWER TIER ANCHOR FAILURE TESTS

Two failure tests on fully instrumented non-production rock anchors were suggested to be carried at the start of the project to ensure the load carrying capacity of the rock anchors and to study the load transfer mechanism of the anchor. During the design stage, the drilled holes for those anchors were proposed to be filled with water for a minimum of 24

hours to check if the shale will absorb water and to study the effect of saturation on the load carrying capacity of the anchors. Drilling of the hole for the lower-tier failure test anchor was completed on 2/11/99. The hole was 4 inches in diameter and was filled with water until 2/18/99, when the instrumented tendon was installed and grouted. The tendon was composed of seven 7-wire strands. Testing of the lower tier failure anchor was done on 3/15/1999. The testing procedure was in accordance with the Post Tensioning Institute specifications for anchor testing (creep testing procedure) with extension after 1.33P as follows: 1.5P, 1.75P, 2.0P, 2.25P, 2.5P, and 2.75P. The setup and testing devices are shown in the schematic sketch in Fig. 4.1. The displacement at anchor head vs. applied load is presented in Fig. 4.2. The deformation at each gage location vs. time is presented in Fig. 4.3.

Drilling of the hole for the upper-tier failure test anchor was completed on 2/25/99. The hole was 4 inches in diameter and was filled with water until 3/4/99, when the instrumented tendon was installed and grouted. The tendon was composed of seven 7-wire strands. Testing of the upper tier failure anchor was done on 3/11/1999. The testing procedure was in accordance with the Post Tensioning Institute specifications for anchor testing (creep testing procedure) with extension after 1.33P as follows: 1.5P, 1.75P, 2.0P, 2.25P, 2.5P, and 2.75P. The displacement at anchor head vs. applied load is presented in Fig. 4.4. The deformation at each gage location vs. time is presented in Fig. 4.5.

IV.3 SOLDIER PILES CONSTRUCTION

Construction of the soldier piles started on 2/9/1999 and completed on 3/4/1999. The upper tier soldier piles were installed first. The holes were drilled 30 inches in diameter and 20 feet deep in the shale. The length of each of the upper tier soldier piles is 50 feet. The instrumented soldier pile holes were extended 15' below the tip of the pile to account for the

extension of the inclinometer casing. The piles were carried by the crane and lowered in the hole to the specified depth. The pile was fixed to a supporting frame to keep it in place and aligned, and then concrete was poured. The data from the strain gages during the construction period until 8/31/99 is presented in Figs. 4.6 and 4.7 for Pile #30 and in Figs. 4.8 and 4.9 for Pile #31

The Lower tier soldier piles were installed after the completion of the upper tier piles installation. The holes were drilled 30 inches in diameter and 20 feet deep in the shale. The length of each of the upper tier soldier piles is 45 feet. The instrumented soldier pile #11 and #12 holes were extended 15' below the tip of the pile to account for the extension of the inclinometer casing. The pile was carried by the crane and lowered in the hole to the specified depth. The pile was fixed to a supporting frame to keep it in place and aligned, and then concrete was poured. The strain data from the strain gages during the construction period until 8/31/99 is presented in Figs. 4.10 and 4.11 for Pile #11 and in Figs. 4.12 and 4.13 for Pile #12.

The bending moment reduced from the measured strain along the length of the soldier pile is presented in Figs. 4.14 to 4.17 for soldier piles #11, #12, #13, and #14, respectively. The axial force calculated from the deduced strain data at each gage location is presented in Figs. 4.18 to 4.21 for soldier piles #11, #12, #13, and #14, respectively.

IV.4 ROCK ANCHOR CONSTRUCTION

A total of sixty eight rock anchors were installed. The casing was installed to a depth ranging from 2 ~ 5 ft. into the shale to prevent the opening from collapsing, due to overburden soil weight, and to support the jacking system while testing the anchors. The free

length of the anchors ranges from 17 feet to 56 feet and the bond length is 15 ft. Six rock anchors were instrumented each with 3 vibrating wire strand meters (Geokon Model 4410). The gages were read before and after installation. In addition, a total of five anchors were instrumented with a permanent load cell to measure the load at the anchor head during tensioning and service life of the structure. Five of the instrumented anchors (anchors #30B, #30C, #31B, #11A and #11B) were performance tested and one anchor (anchor #30A) was proof tested. The pictures showing the sequence of anchor hole drilling and installation of tendons are shown in Figs. 4.22 to 4.25.

IV.5 TENSIONING OF ROCK ANCHORS

The tensioning of production rock anchors was started on April 19, 1999. Anchor #30B was performance tested on 4/28/99. A total of three strand gage cables were attached to the strands and connected to the data acquisition system. The sampling rate was set at a 1-minute interval. A permanent vibrating-wire based load cell was installed between the bearing plate and the anchor head to measure the applied load on the anchor as shown in Fig. 4.26. The anchor head movement was recorded using two dial gages, in accordance with the standard performance test procedure. The load test setup and testing assembly are shown in Fig. 4.27. The plot of the load versus dial gage reading is presented in Fig. 4.28. The strain readings versus time is plotted in Figs. 4.29(a)~(c) for each of the three strand gages.

Moreover, on April 28, 1999, another performance test was conducted on anchor #31B. The same setup and testing procedure as for anchor #30B was followed. The head movement for anchor #31B is presented in Figs. 4.30. The strain data from anchor #31B are presented in Figs. 4.31(a)~(c).

A performance test was conducted on anchor #11B on May 7, 1999. The anchor head movement is presented in Fig. 4.32. The jack pressure and the load from the load cell were recorded. The strain data from the strand gages were reduced and plotted in Fig. 4.33(a)~(c).

On May 24, 1999, a performance test was conducted on anchor #30C. The anchor head movement is presented in Fig. 4.34. The jack pressure and the load from the load cell were recorded. The strain data from the strand gages were reduced and plotted in Fig. 4.35(a)~(c).

A performance test was conducted on anchor #11A on June 7, 1999. The anchor head movement is presented in Fig. 4.36. The jack pressure and the load from the load cell were recorded. The strain data from the strand gages were reduced and plotted in Fig. 4.37(a)~(c).

A proof test was conducted on anchor #30A on July 8, 1999. The anchor head movement is presented in Fig. 4.38. The jack pressure and the load from the load cell were recorded. The strain data from the strand gages were reduced and plotted in Fig. 4.39(a)~(c).

IV.6 GROUTING OF ANCHOR HEADS AND GRADING OF SLOPES

Upon completion of anchor tensioning and precast panel installation in the lower tier wall, the area behind the wall and in-front-of the upper tier wall was backfilled and graded to the final elevation on July 16, 1999. The upper tier wall anchor testing was completed on July 9, 1999. The area behind the wall was graded and completed by July 20, 1999. The plots of deflection versus depth from the soldier pile inclinometers are shown in Figs. 4.40 to 4.43 for the period until 8/30/1999. The deflection vs. depth from the earth inclinometers are shown in Figs. 4.44 to 4.46. The pore water pressure recorded by the piezometer is shown in

Fig. 4.47. The piezometer wire was damaged during grading the area behind the upper tier wall, and no readings were taken after 8/9/1999.

The data from soldier pile strain gages for the period until 8/30/1999 were shown previously in Figs. 4.6 to 4.13 for soldier piles #11, #12, #30, and #31, respectively.

IV.7 LONG-TERM MONITORING RESULTS

After the completion of grouting the anchor heads, the electrical wires from the soldier pile gages, the rock anchor gages and the load cells of the rock anchors were run through a PVC pipe to the permanent concrete boxes designed to house the data collection devices. The two concrete boxes located on the lower tier and the upper tier wall vicinity, respectively. All the wires were connected to the dataloggers and long-term monitoring of the entire instruments was on-line on August 31, 1999.

The collected data until the end of monitoring phase on 2/1/2000 from all sensors are presented in this section. Strains from soldier pile gages since 8/31/1999 are presented in Figs. 4.48 to 4.55. The moment along the soldier piles is presented in Figs. 4.56 to 4.59 for soldier piles #11, #12, #30, and #31, respectively. Axial force along pile depth is presented in Figs. 4.60 to 4.63 for soldier piles #11, #12, #30, and #31, respectively. Strains in soldier pile #11 at each gage location are presented in Figs. 4.64 to 4.71. Strains in soldier pile #12 at each gage location are presented in Figs. 4.72 to 4.79. Strains in soldier pile #30 at each gage location are presented in Figs. 4.80 to 4.87. Finally, strains in soldier pile #31 at each gage location are presented in Figs. 4.88 to 4.95. The load from the load cell at each anchor head is plotted against time in Figs. 4.96 to 4.100. The movement in the bonded length of each instrumented anchor at the location of every strand gage is presented as a function of

time in Figs. 4.101 to 4.106. A total of three additional sets of inclinometer readings were taken during long-term monitoring phase and the measured results are presented in Figs. 4.107 to 4.109 separately for each of the earth inclinometers, and in Figs. 4.110 to 4.113 for the soldier pile inclinometers.

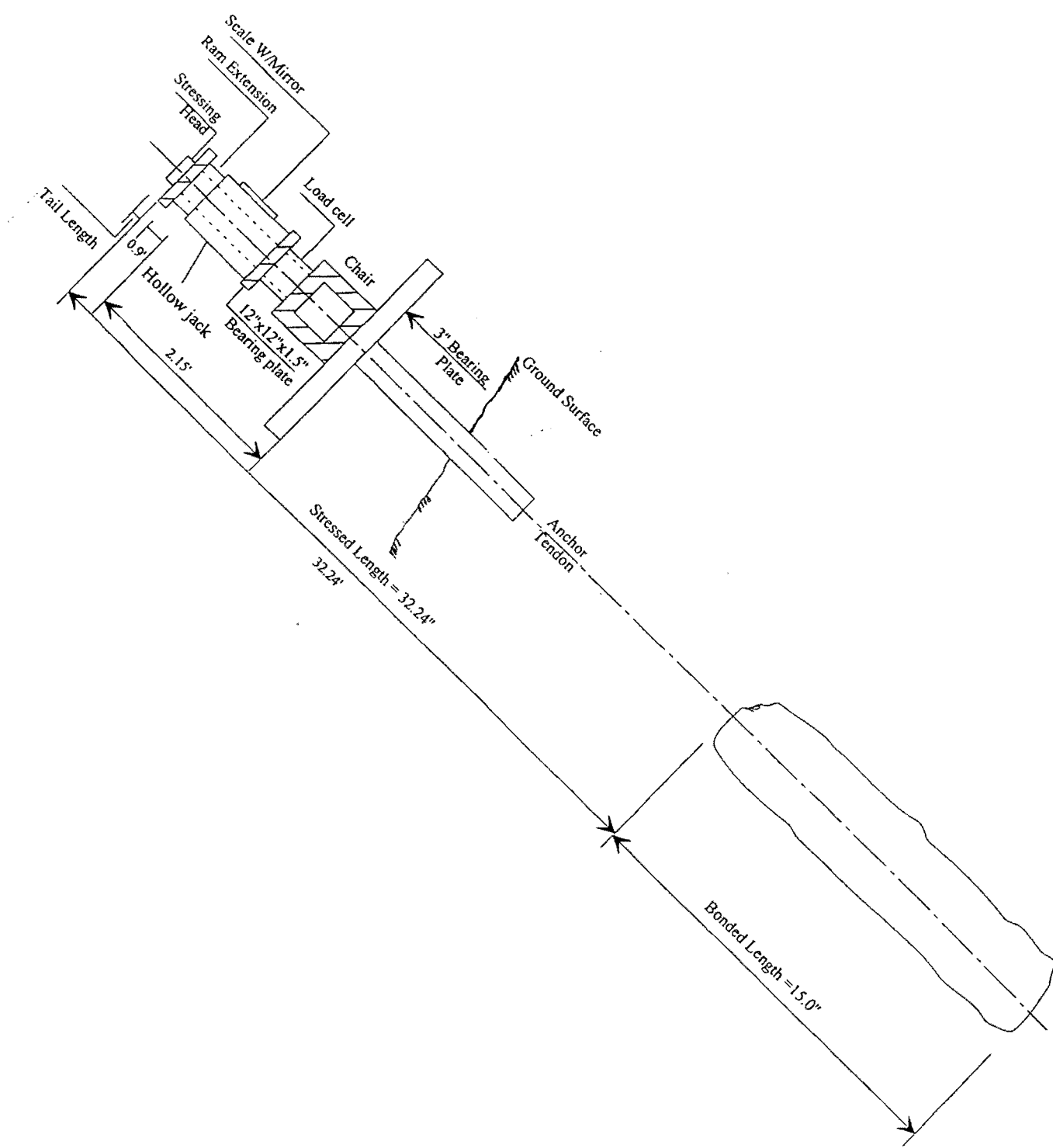


Fig. 4.1: Schematic of anchor load testing setup.

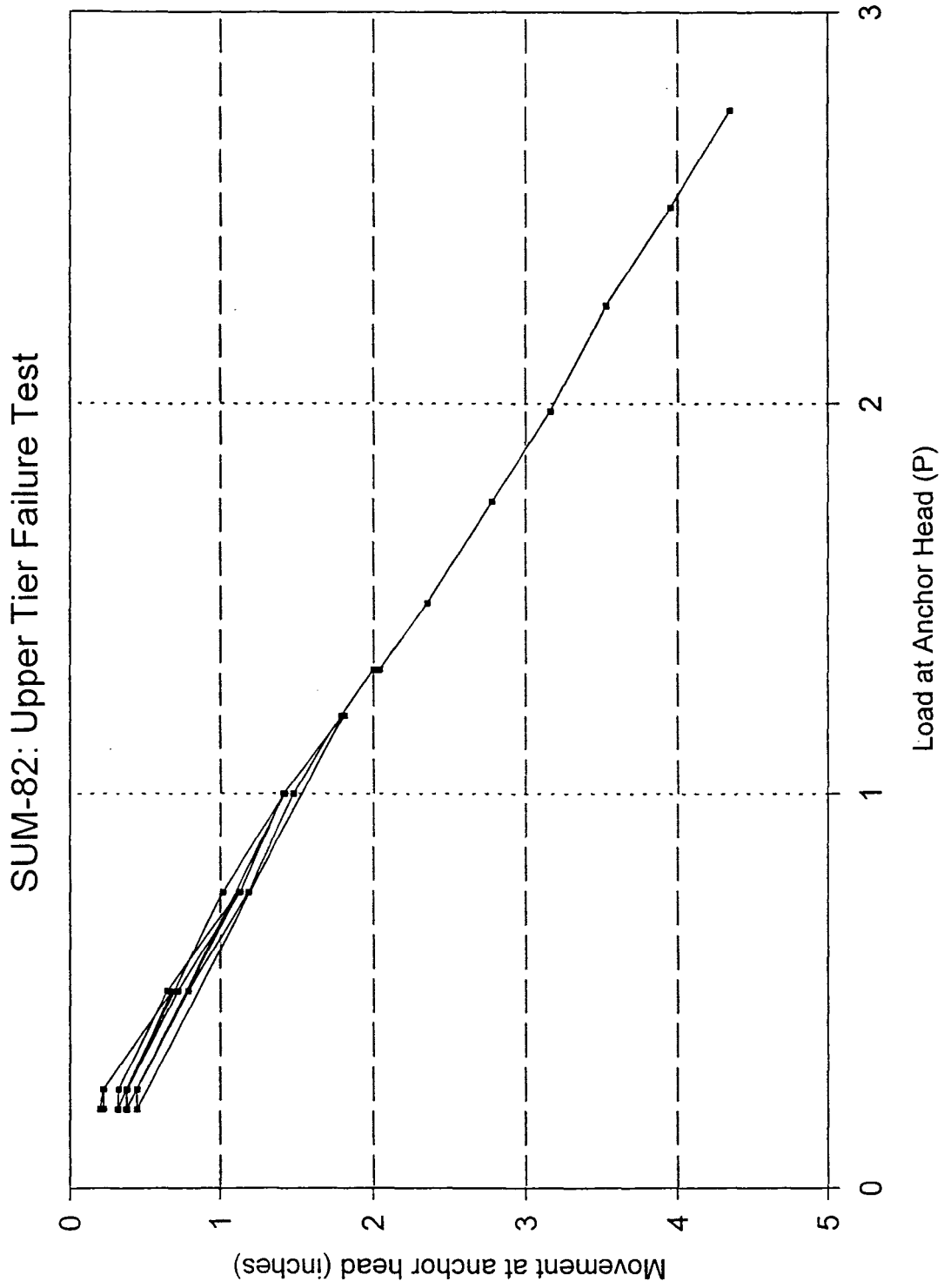


Fig. 4.2: Upper tier failure test, load vs. displacement at anchor head.



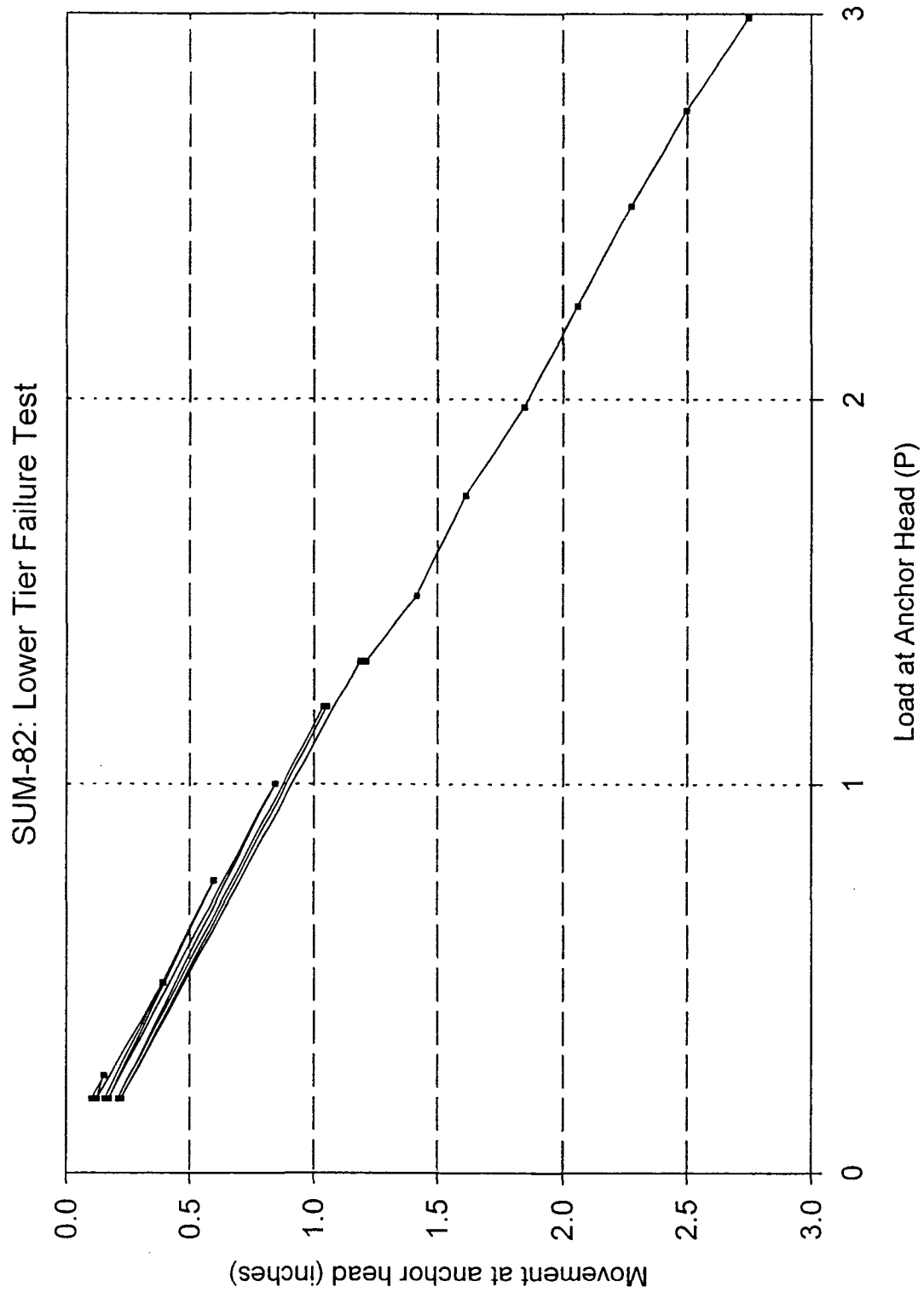


Fig. 4.4: Lower tier failure test, load vs. displacement at anchor head.

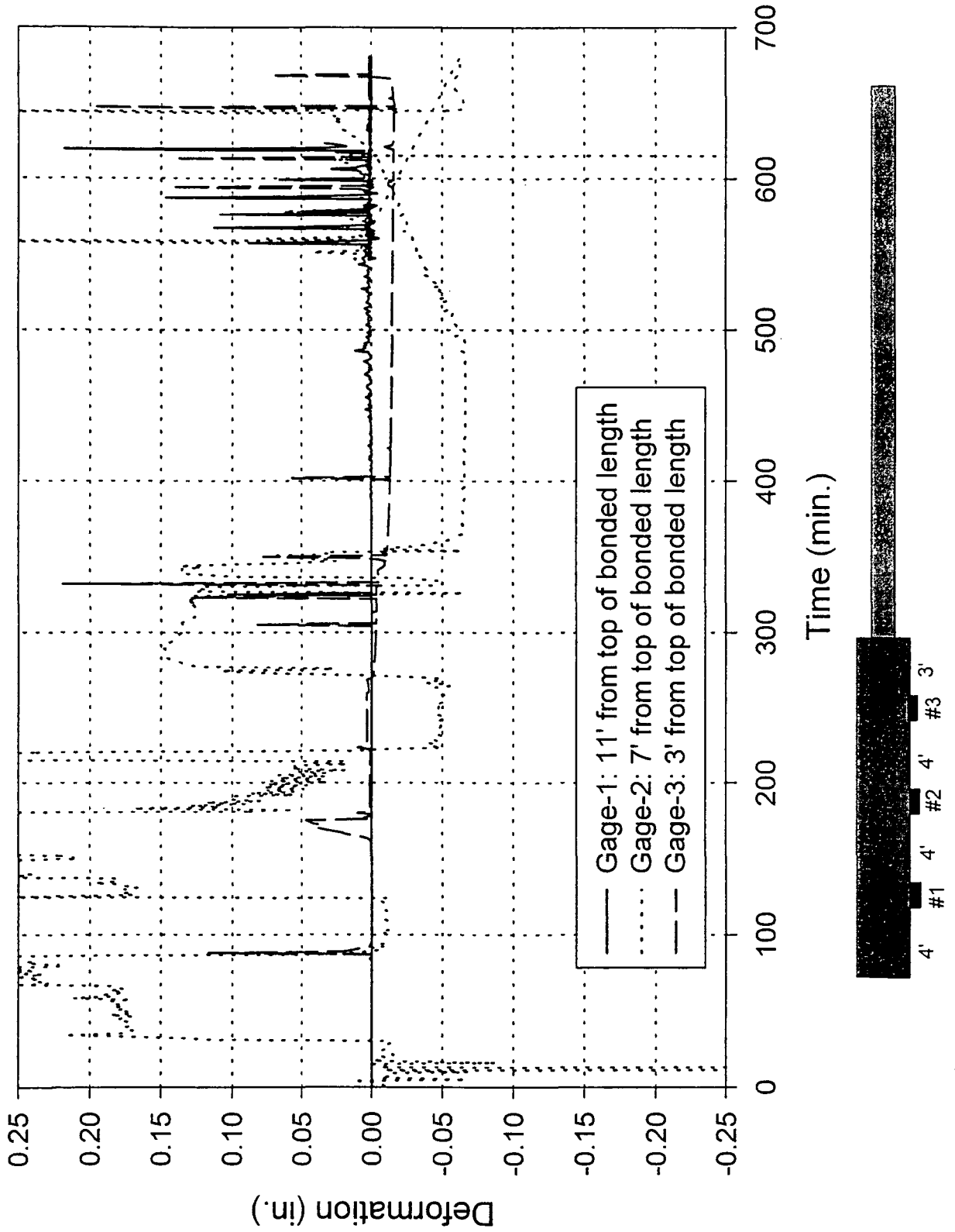


Fig. 4.5: Lower tier failure test, deformation at each strand gage location.

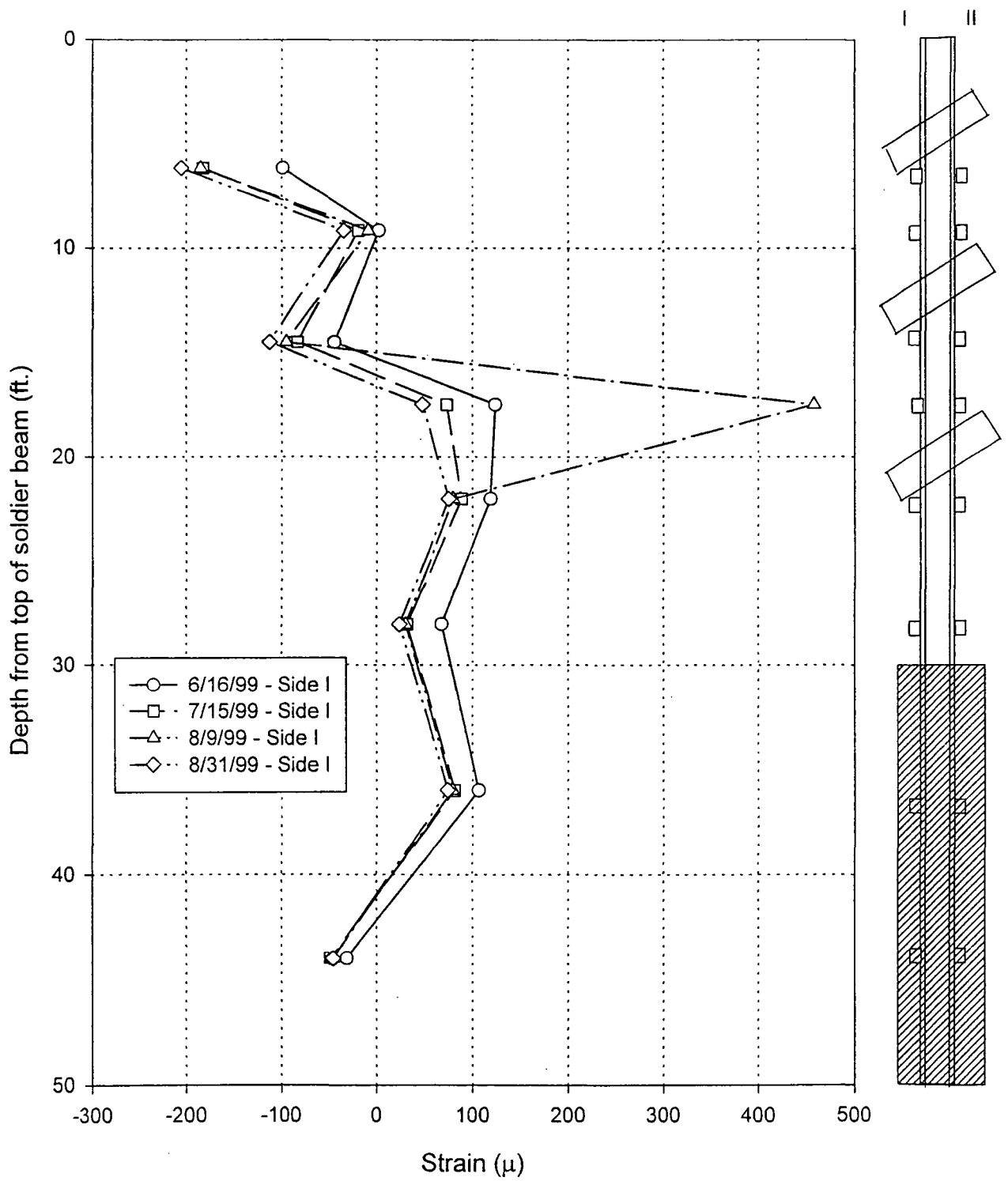


Fig. 4.6: Soldier pile # 30, strain on side I (backfill side).



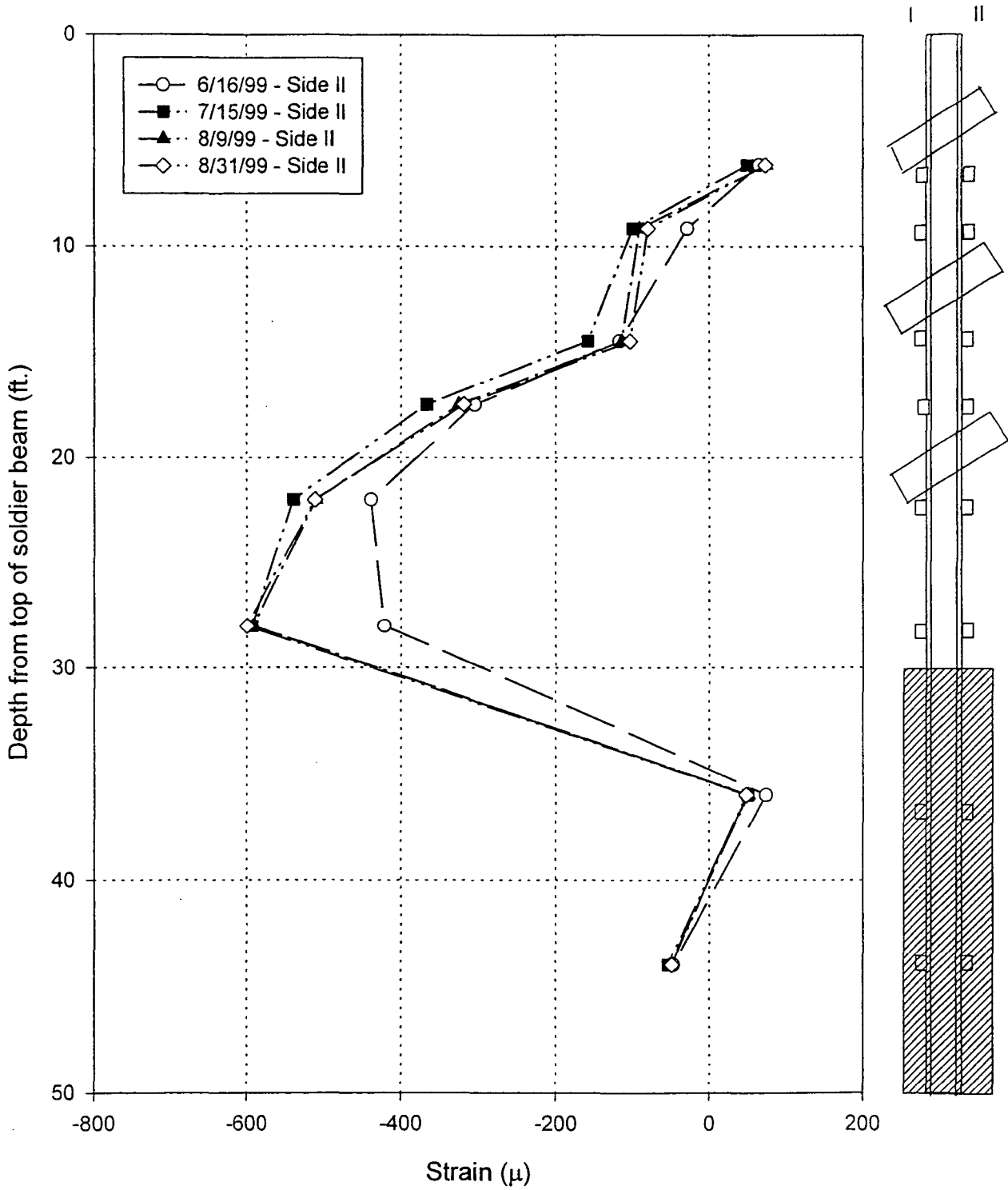
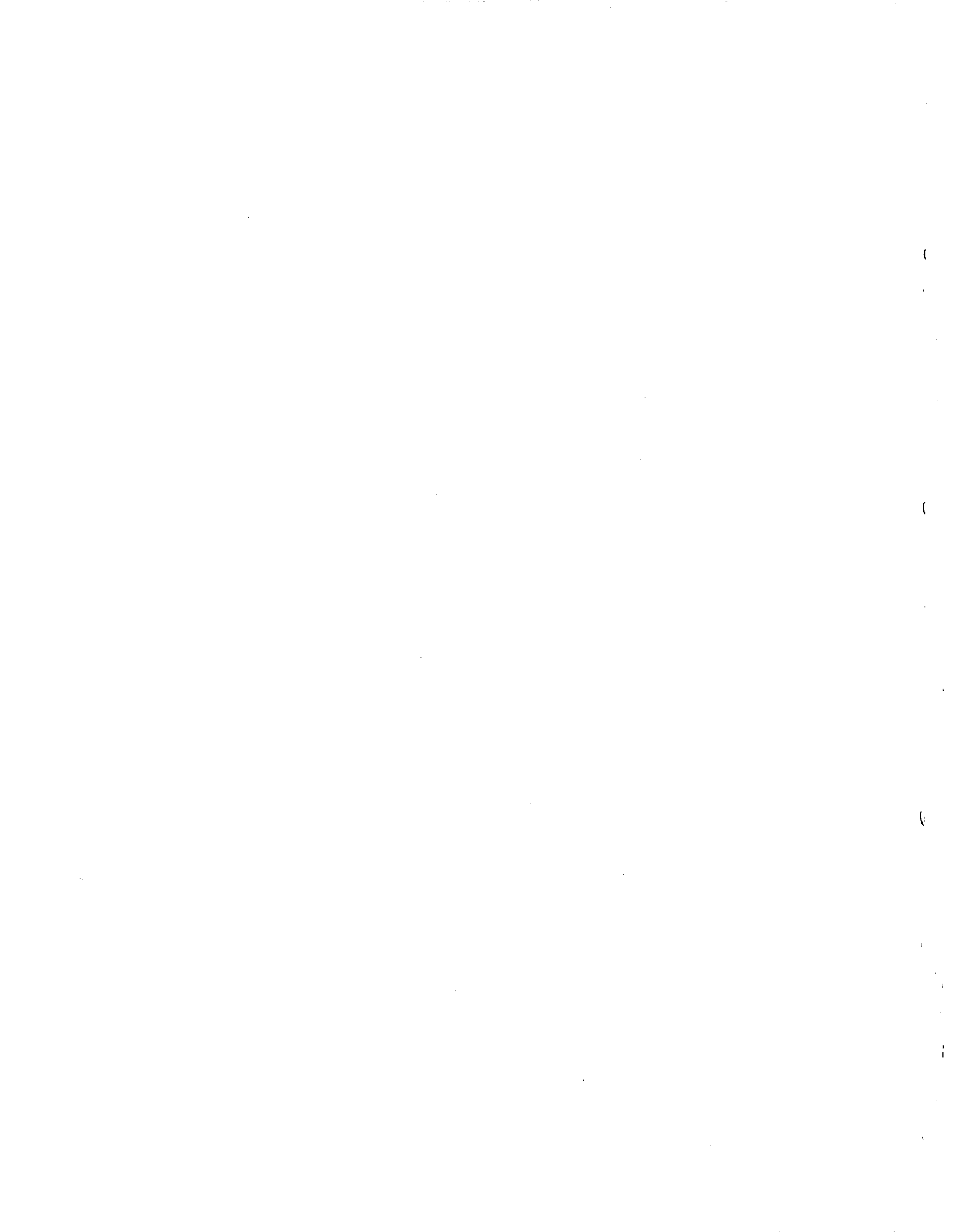


Fig. 4.7: Soldier pile # 30, strain on side II (wall face side).



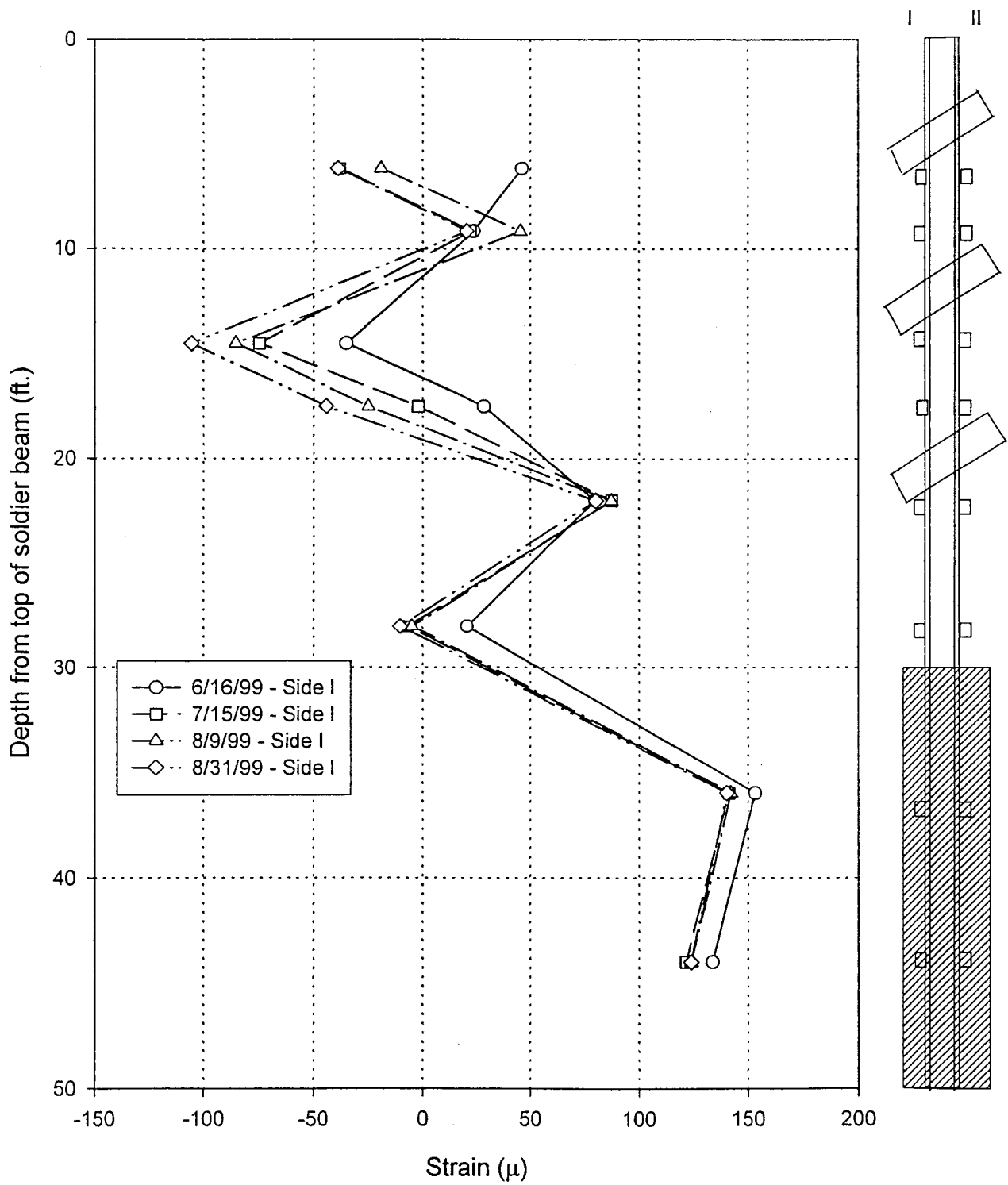
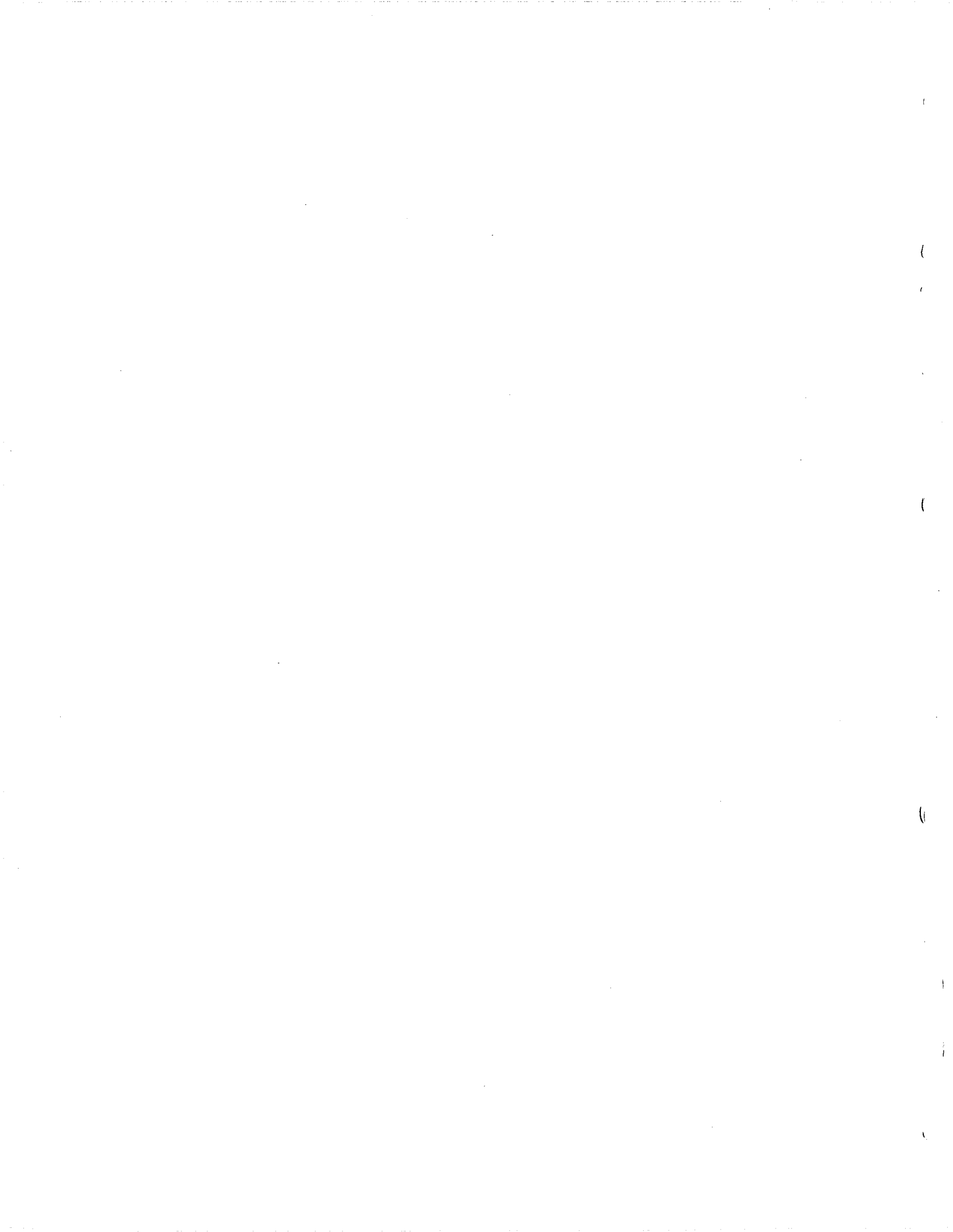


Fig. 4.8: Soldier pile # 31, strain on side I (backfill side).



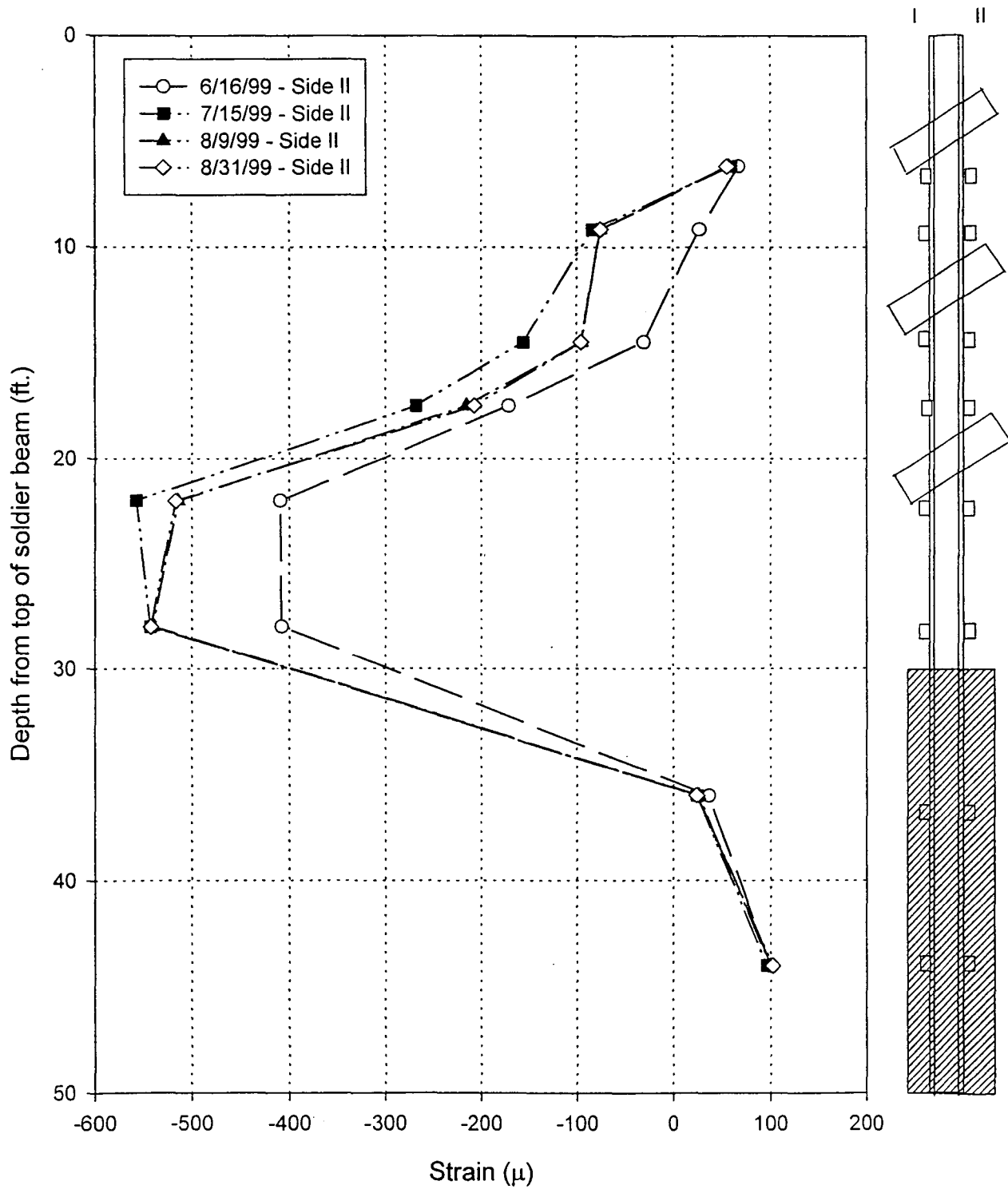


Fig. 4.9: Soldier pile # 31, strain on side II (wall face side).

(

(

(

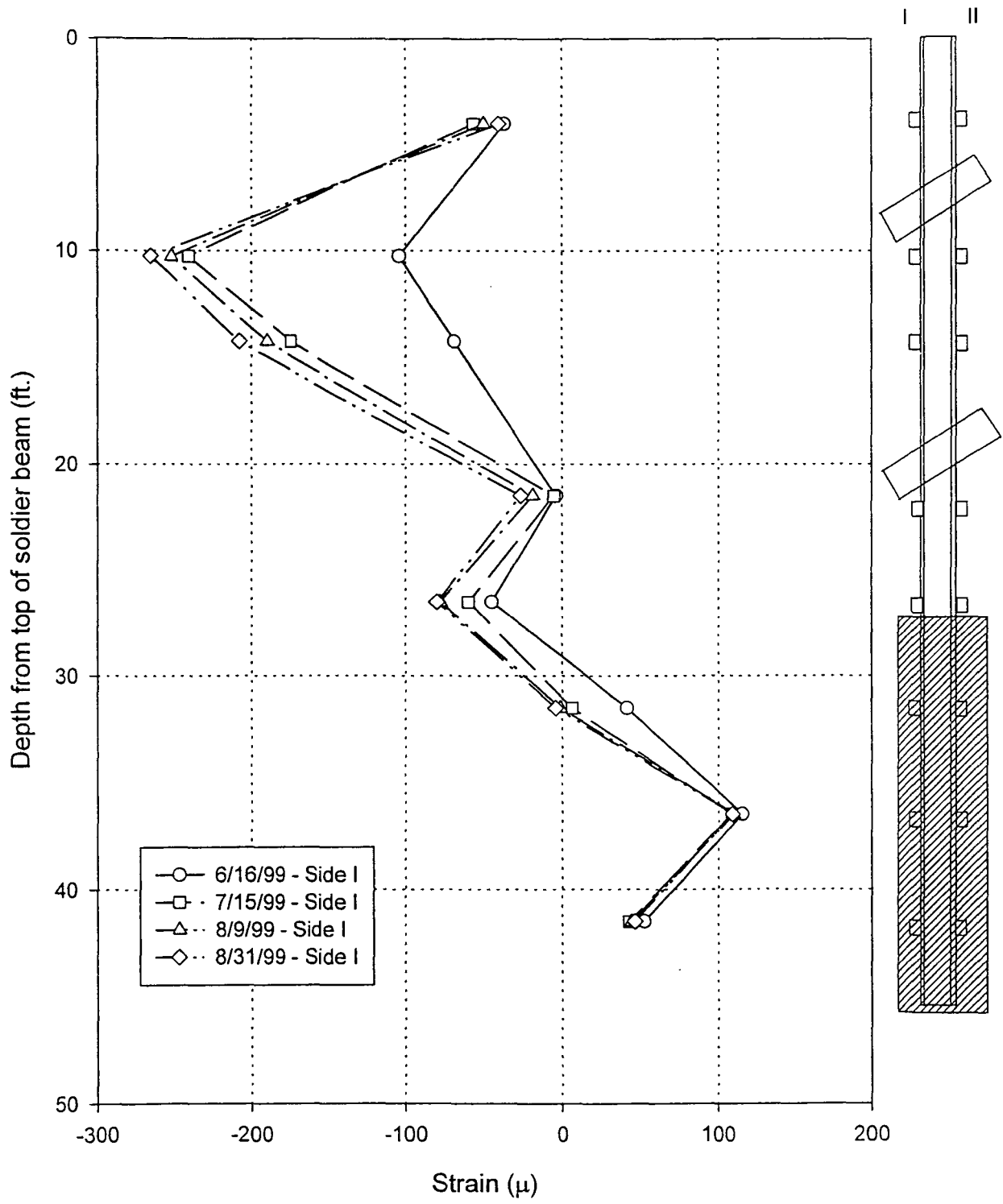


Fig. 4.10: Soldier pile # 11, strain on side I (backfill side).



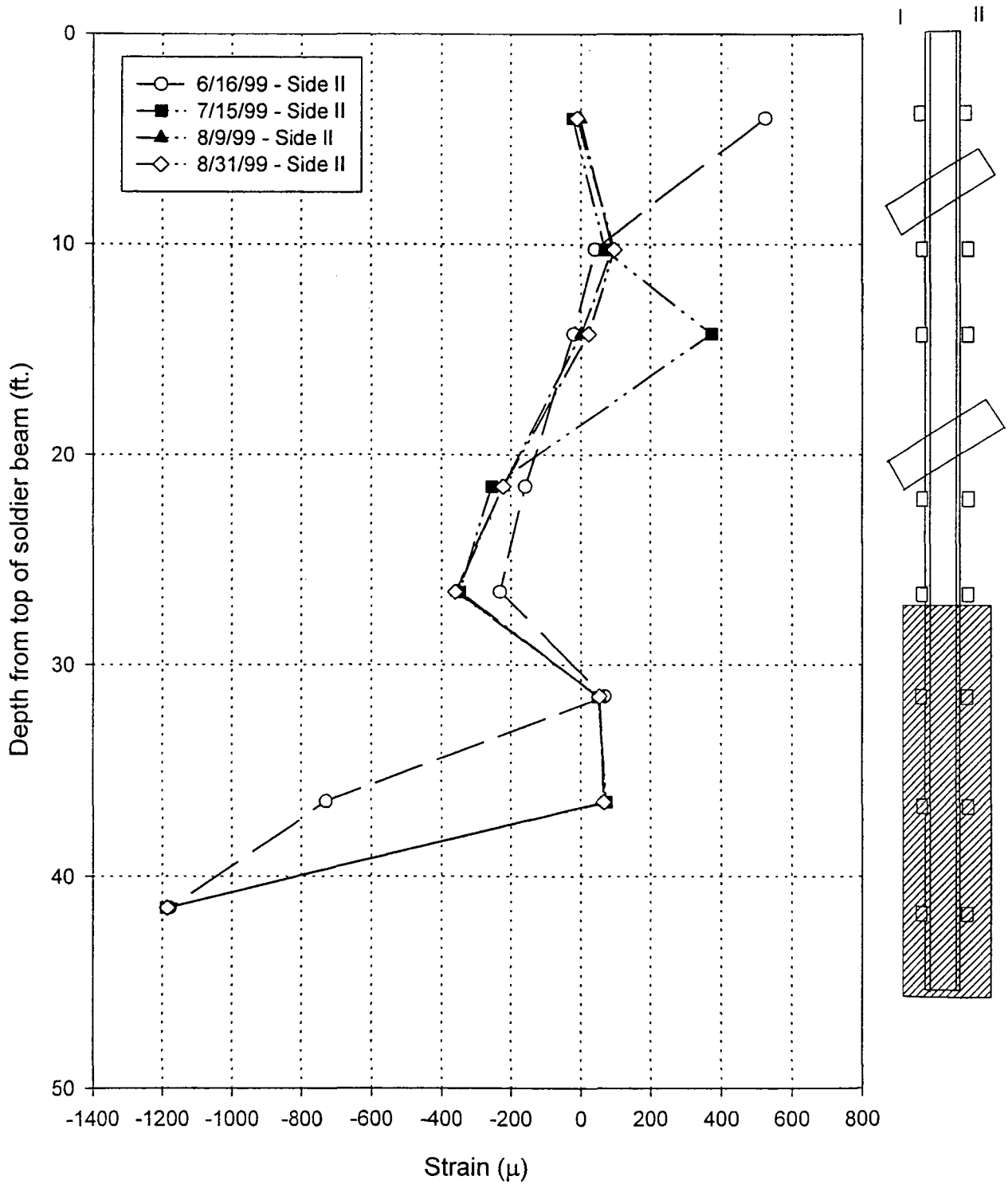
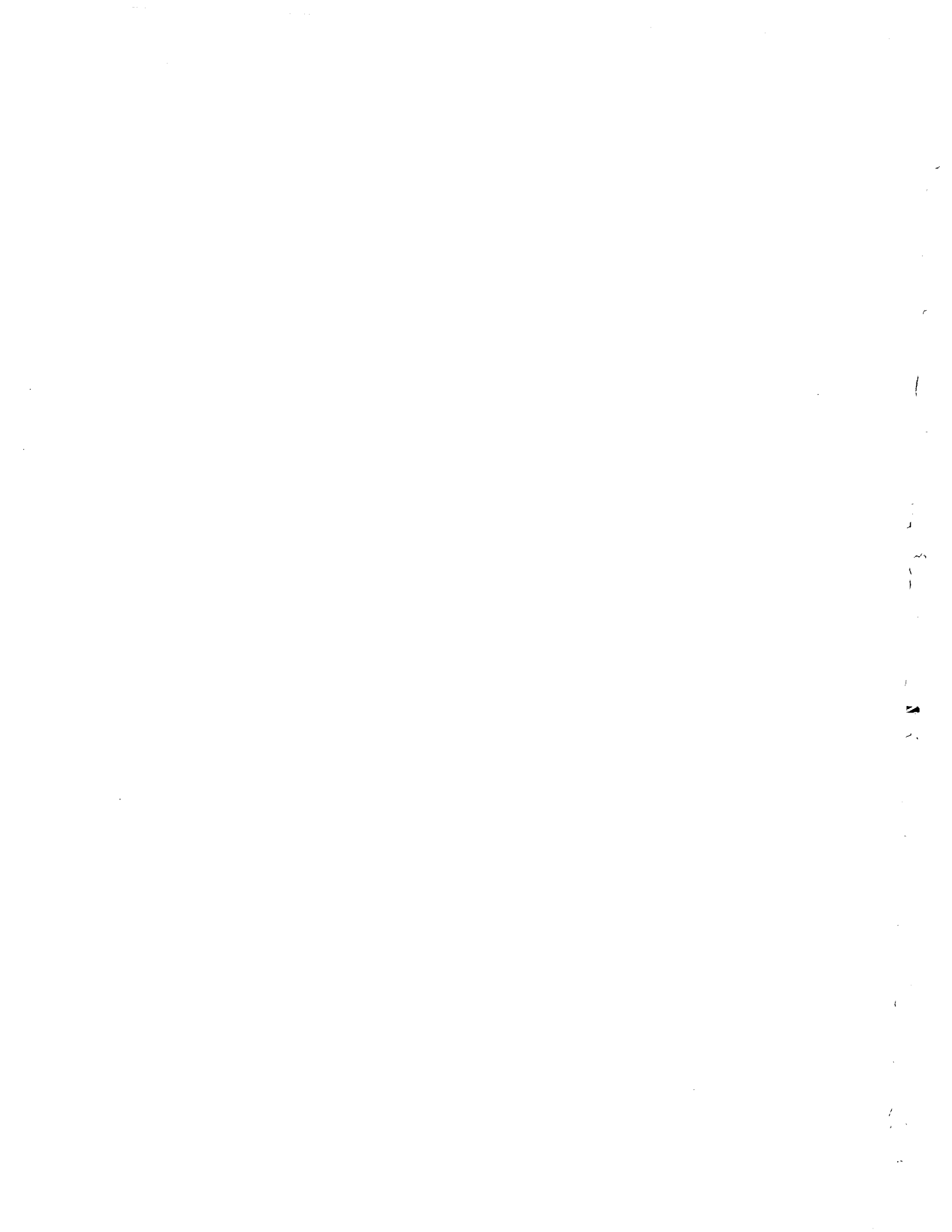


Fig. 4.11: Soldier pile # 11, strain on side II (wall face side).



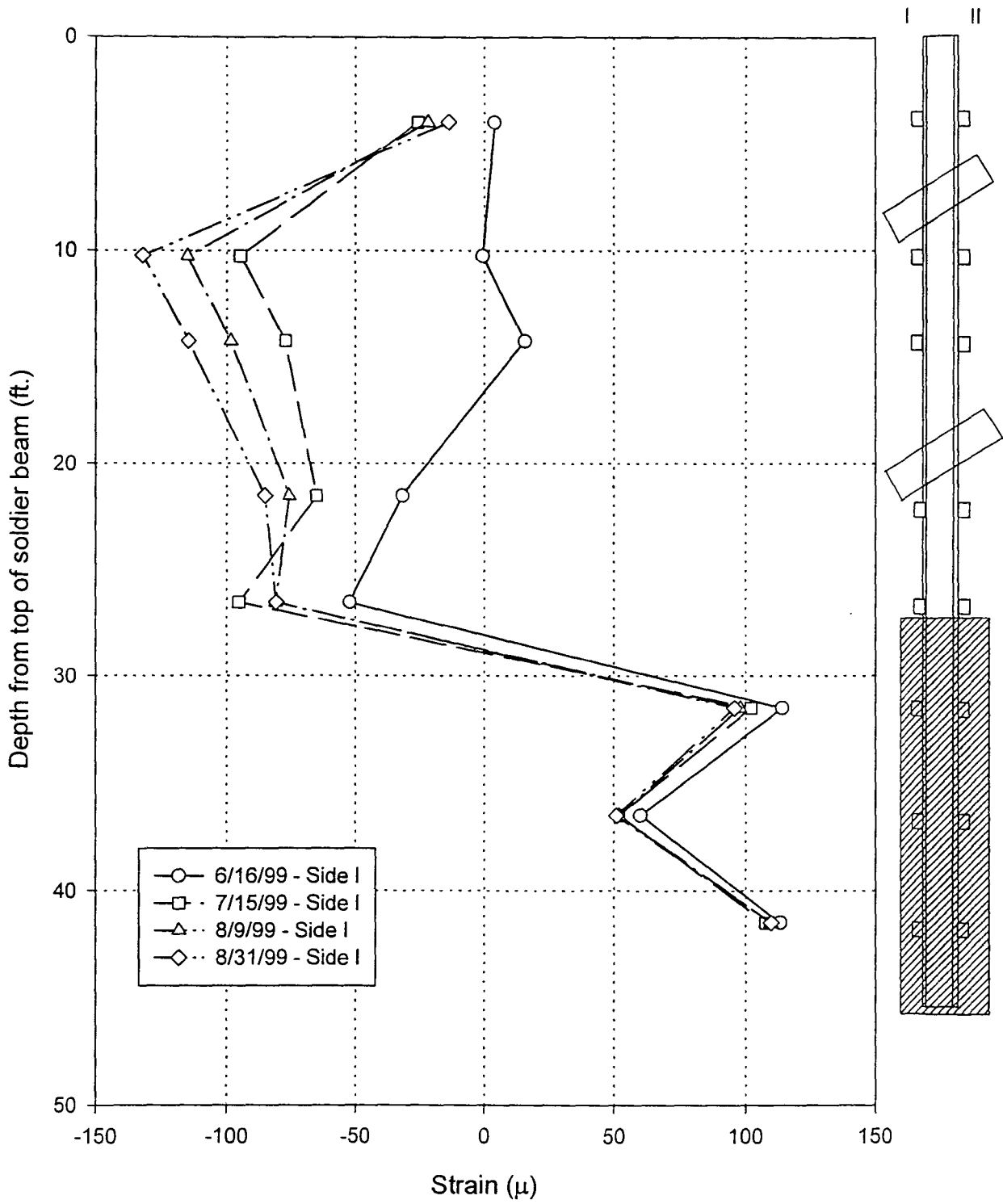


Fig. 4.12: Soldier pile # 12, strain on side I (backfill side).



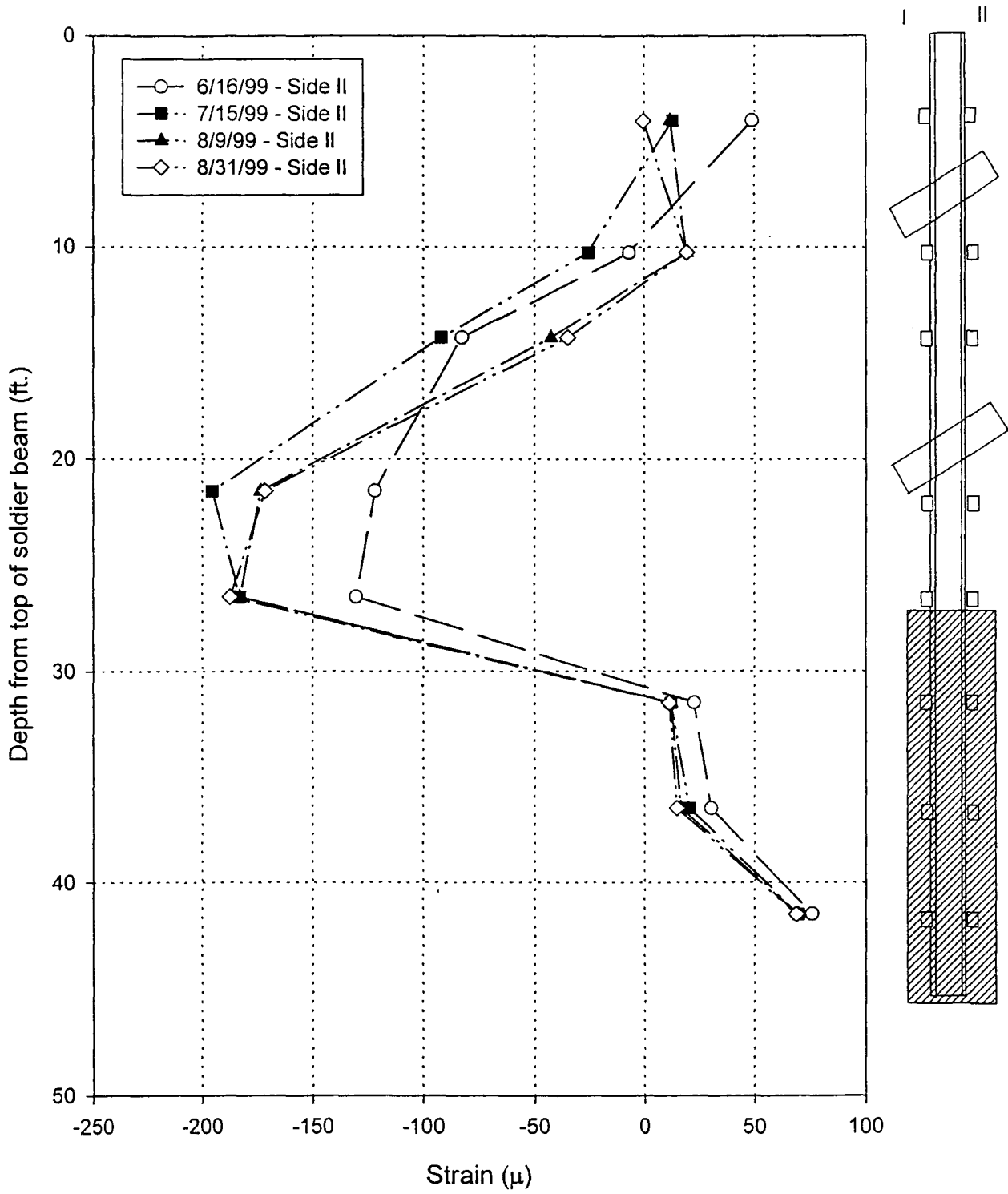


Fig. 4.13: Soldier pile # 12, strain on side II (wall face side).

1
2
3
4
5
6
7
8
9
10
11
12
13
14
15
16
17
18
19
20
21
22
23
24
25
26
27
28
29
30
31
32
33
34
35
36
37
38
39
40
41
42
43
44
45
46
47
48
49
50
51
52
53
54
55
56
57
58
59
60
61
62
63
64
65
66
67
68
69
70
71
72
73
74
75
76
77
78
79
80
81
82
83
84
85
86
87
88
89
90
91
92
93
94
95
96
97
98
99
100

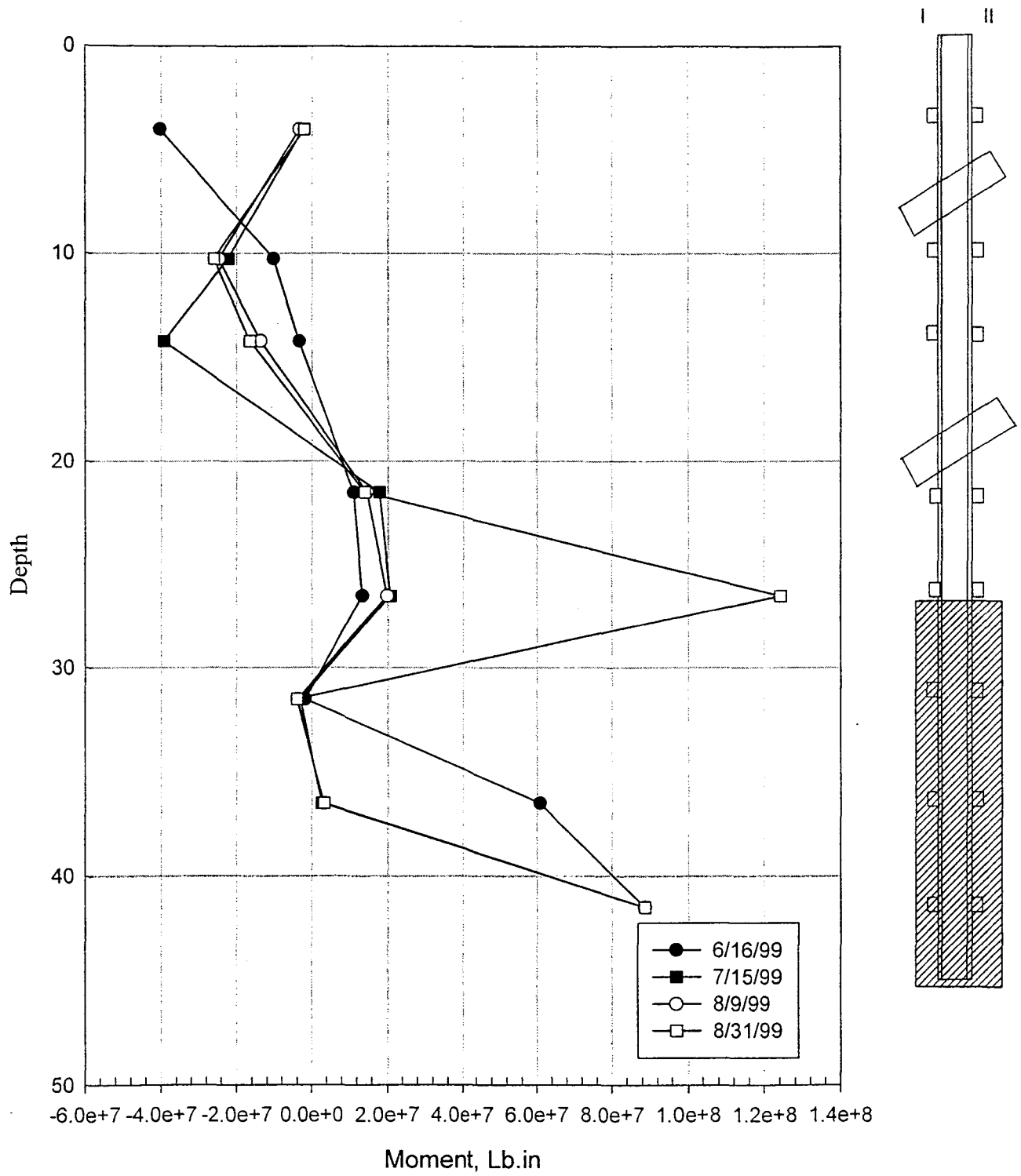


Fig. 4.14: Moment vs. depth in soldier pile # 11 during construction.



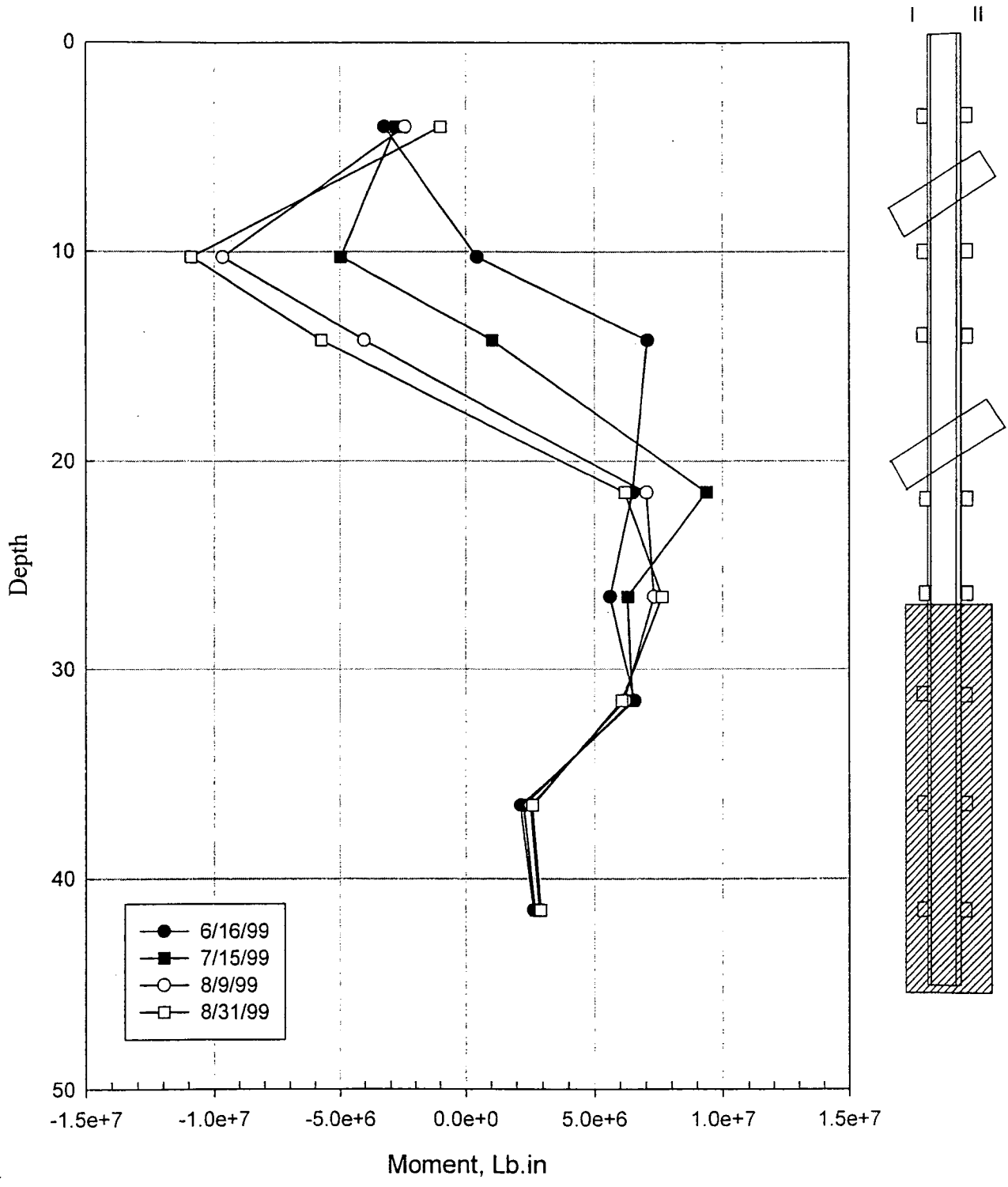


Fig. 4.15: Moment vs. depth in soldier pile # 12 during construction.



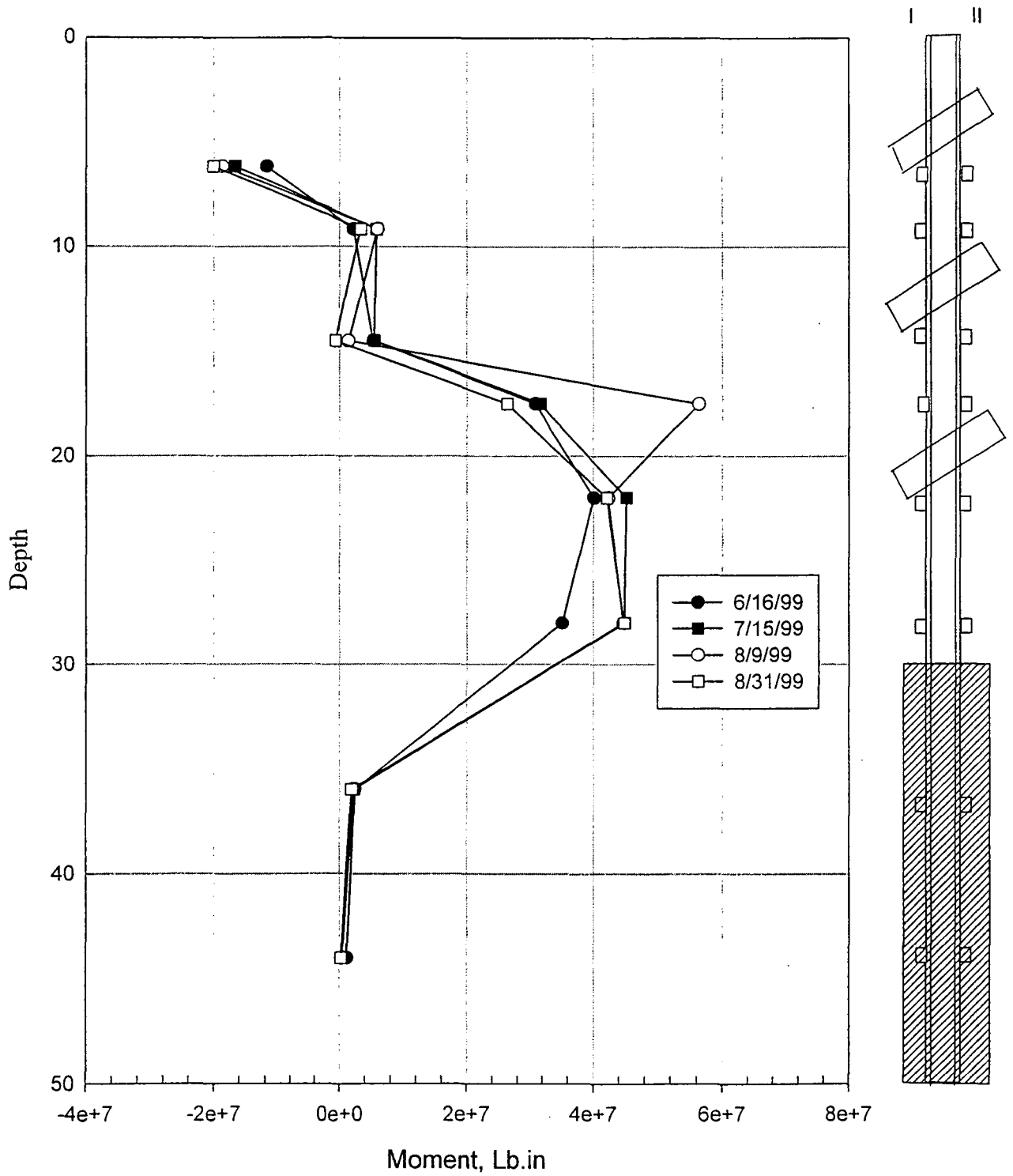


Fig. 4.16: Moment vs. depth in soldier pile # 30 during construction.



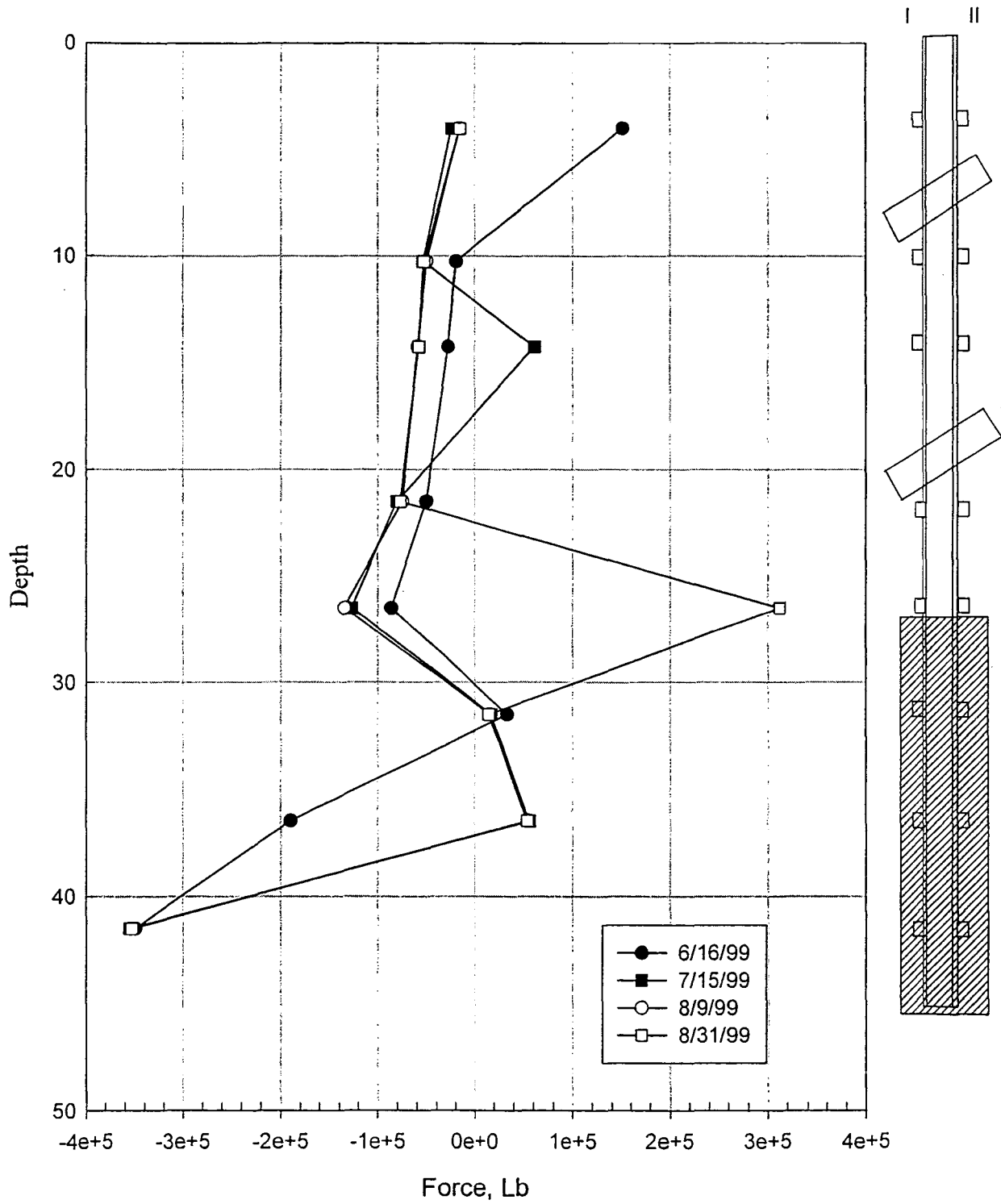


Fig. 4.18: Axial force vs. depth in soldier pile # 11 during construction.



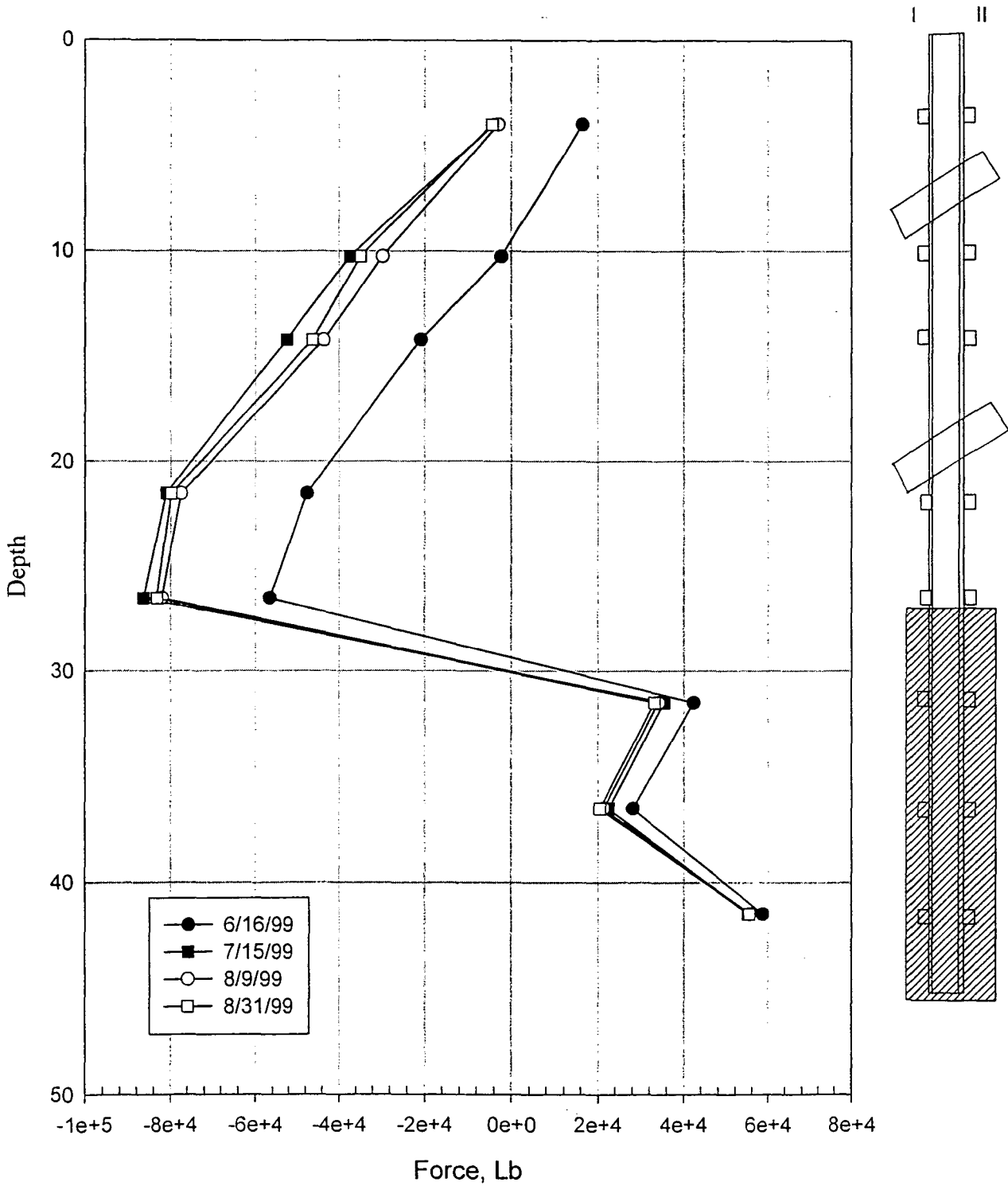


Fig. 4.19: Axial force vs. depth in soldier pile # 12 during construction.

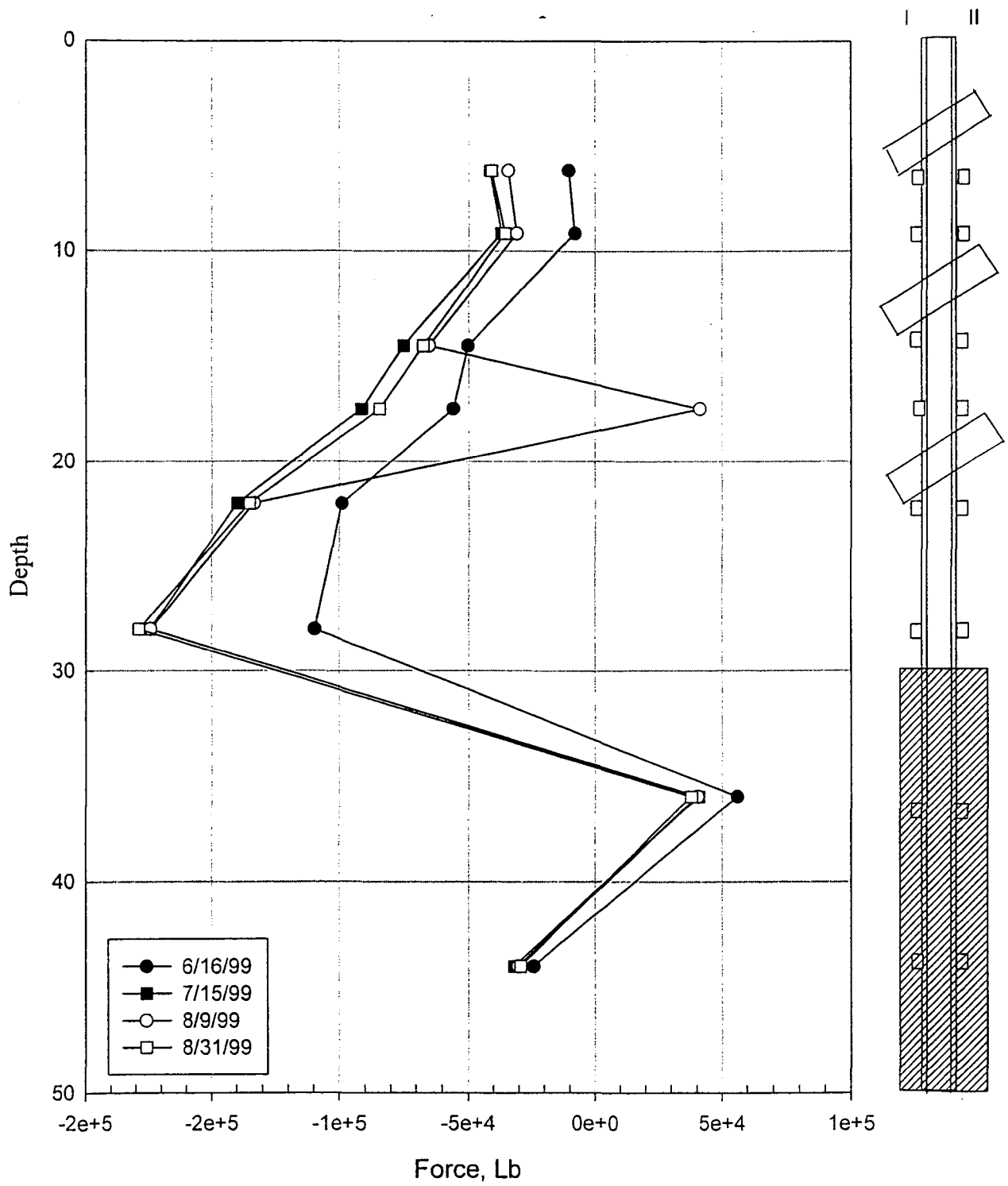


Fig. 4.20: Axial force vs. depth in soldier pile # 30 during construction.



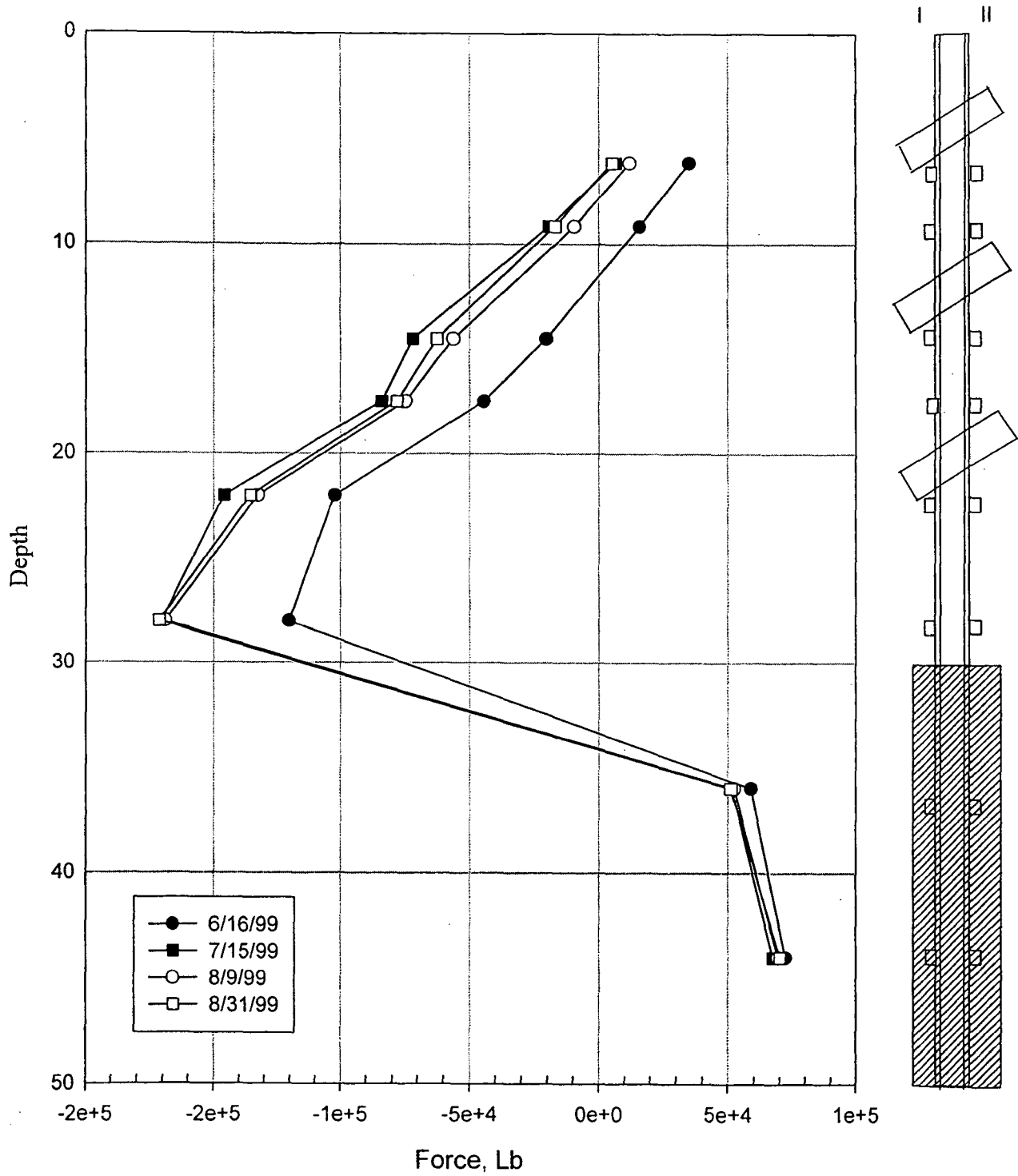


Fig. 4.21: Axial force vs. depth in soldier pile # 31 during construction.

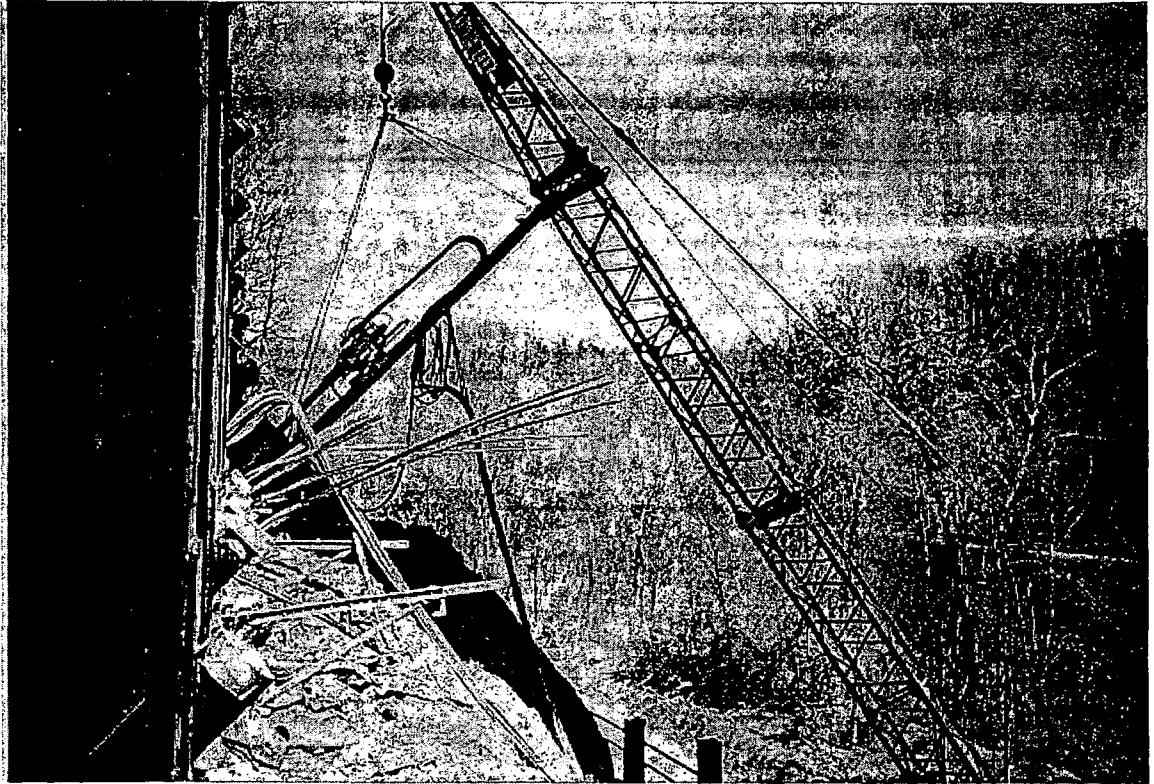


Fig. 4.22: Anchor hole drilling.

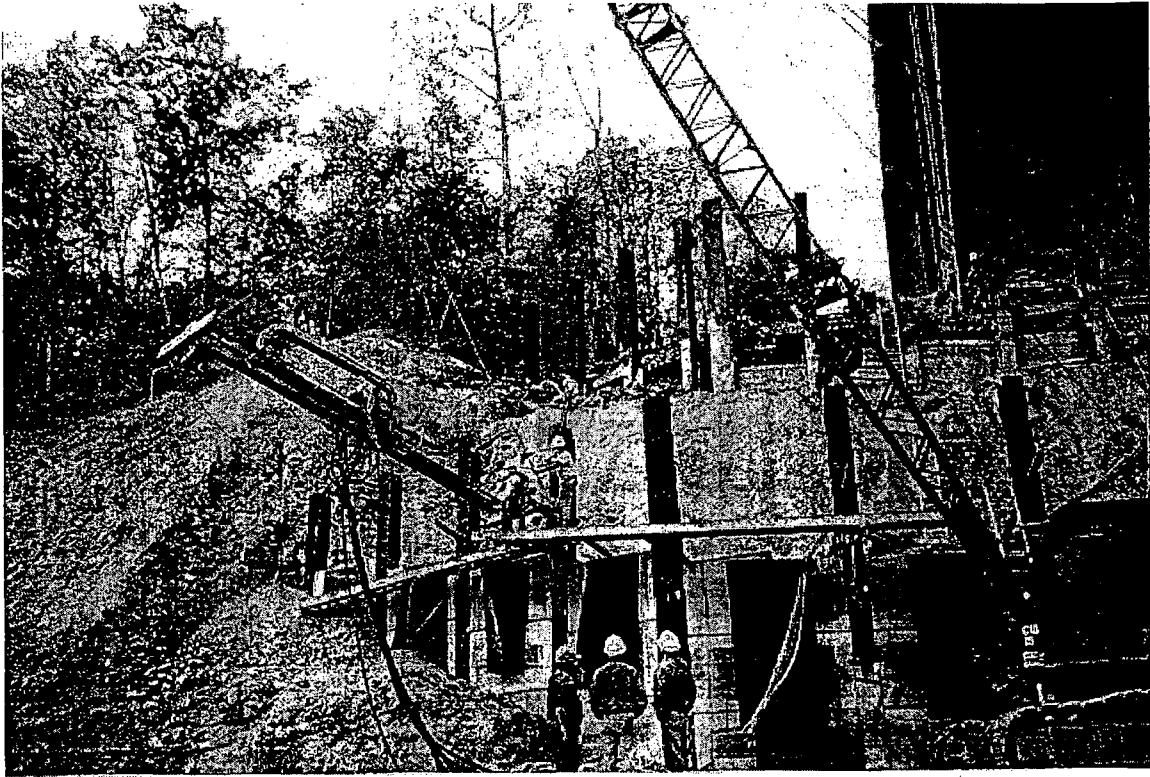


Fig.4.23: Drilling an anchor hole in the lower tier wall.

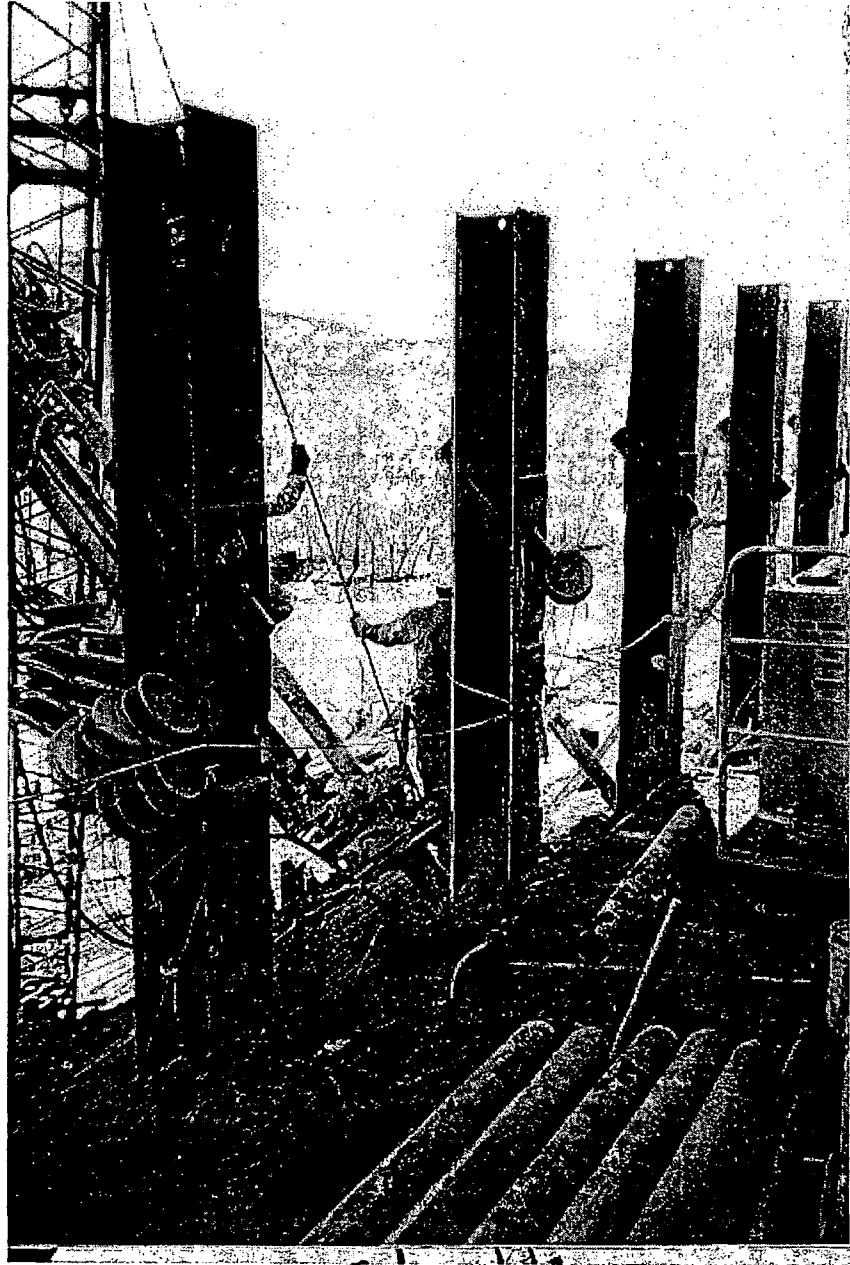


Fig. 4.24: Drilling an anchor hole in the upper tier wall.

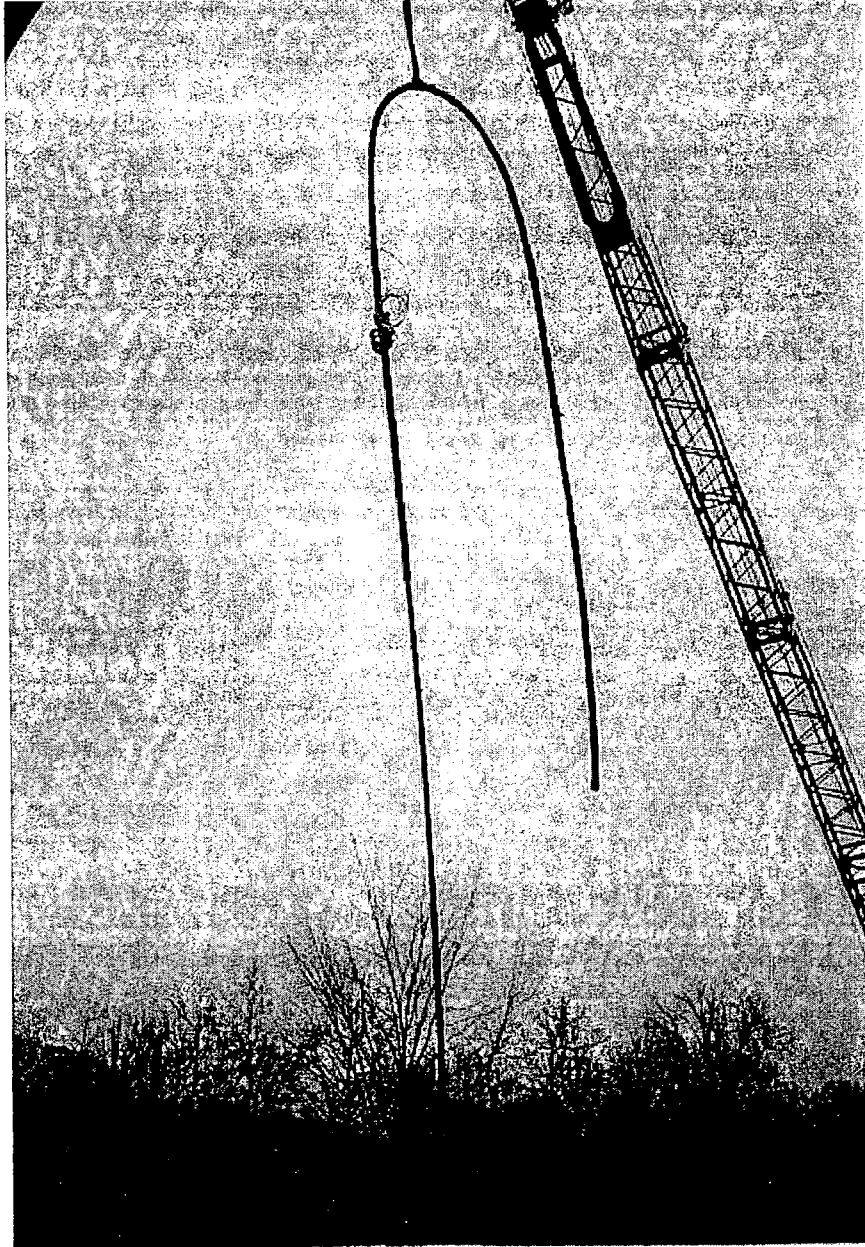


Fig. 4.25: Lifting the tendon with the crane for installation.



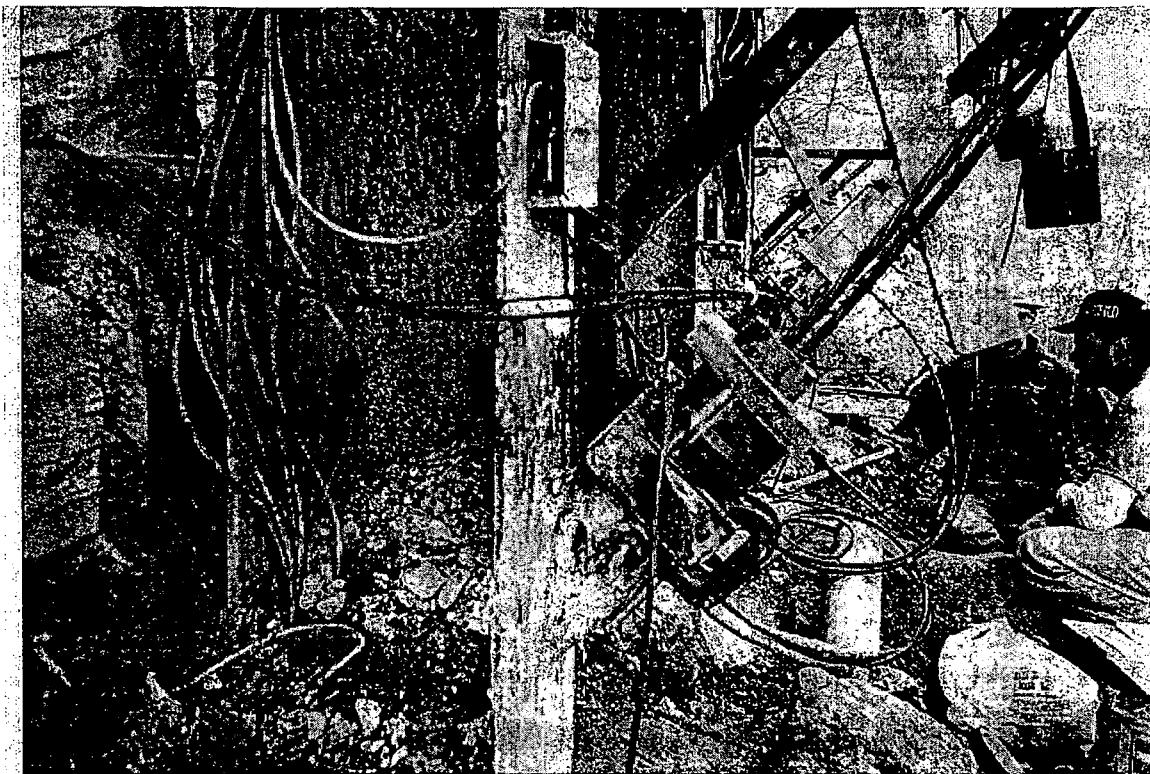


Fig. 4.26: A permanent vibrating wire load cell installed at the anchor head.



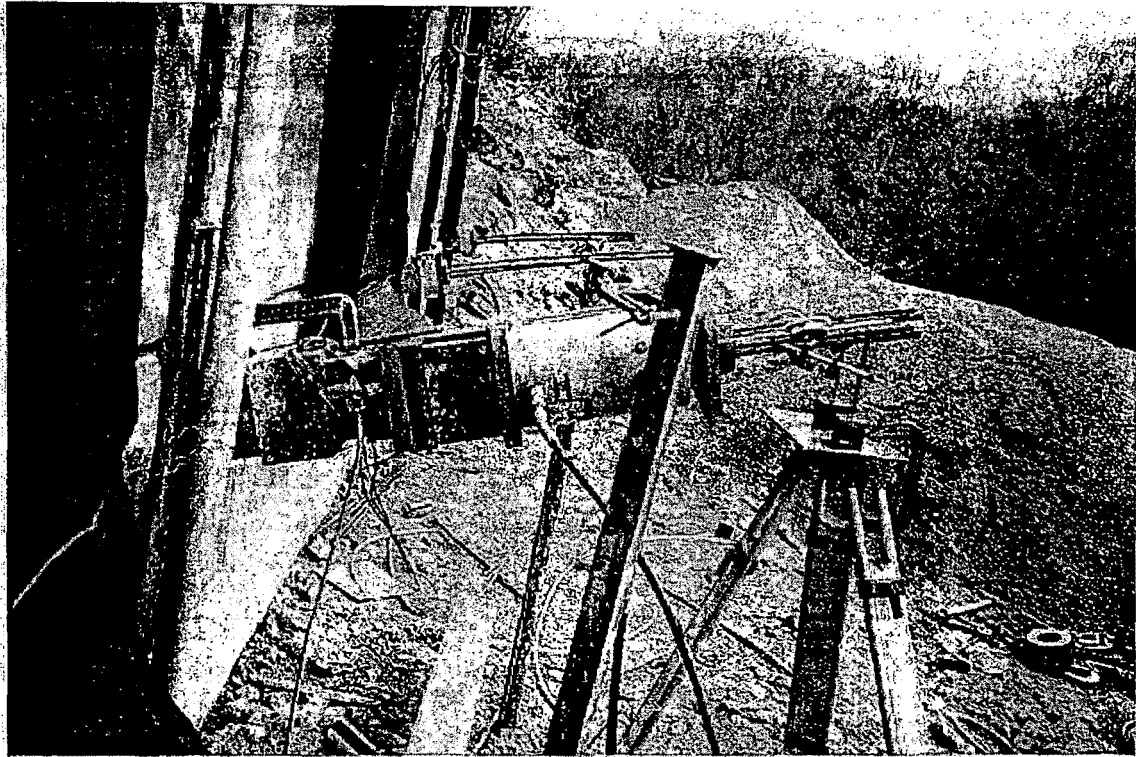


Fig. 4.27: Anchor load test undergoing.

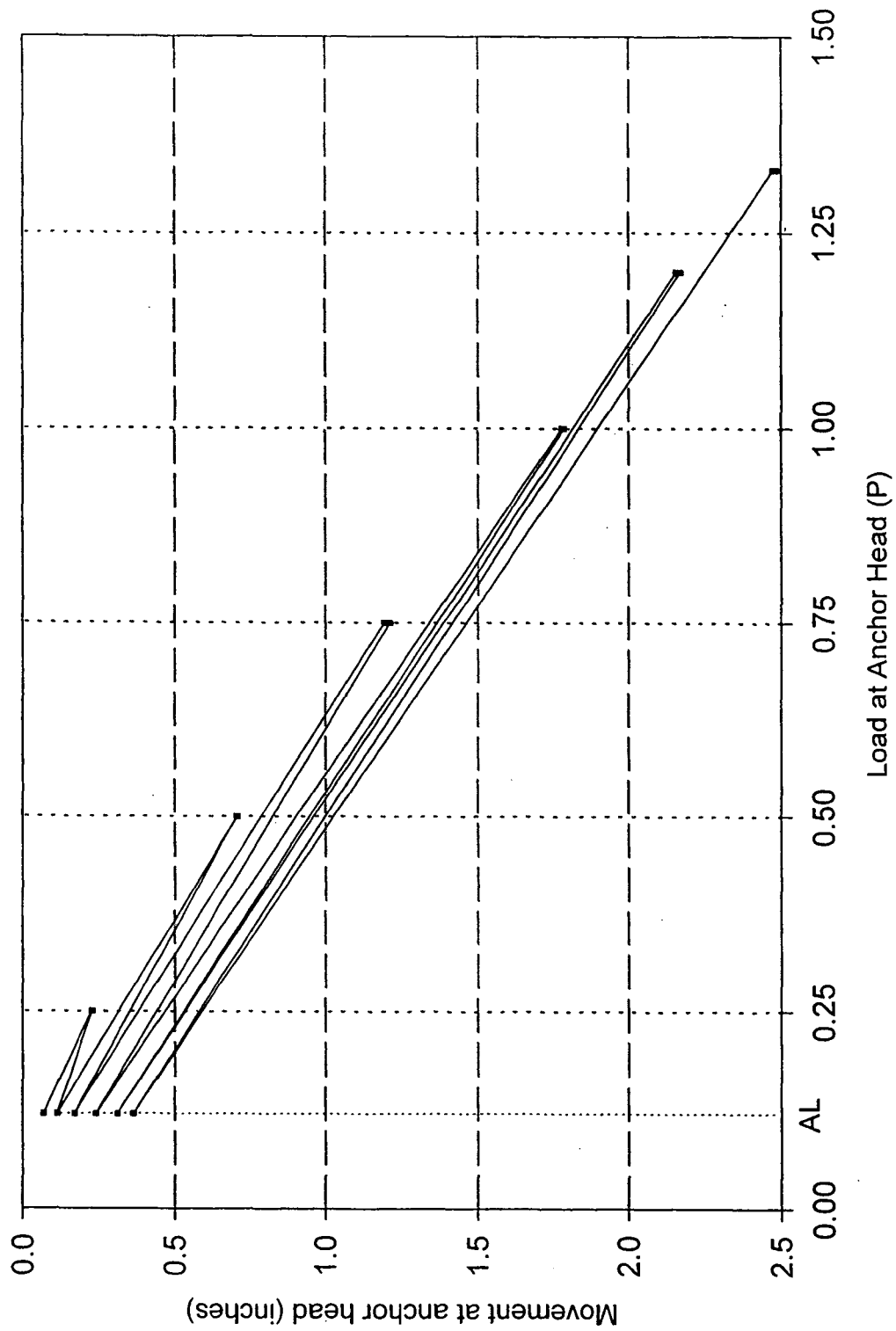


Fig. 4.28: Performance test of anchor #30B, load vs. displacement at anchor head.

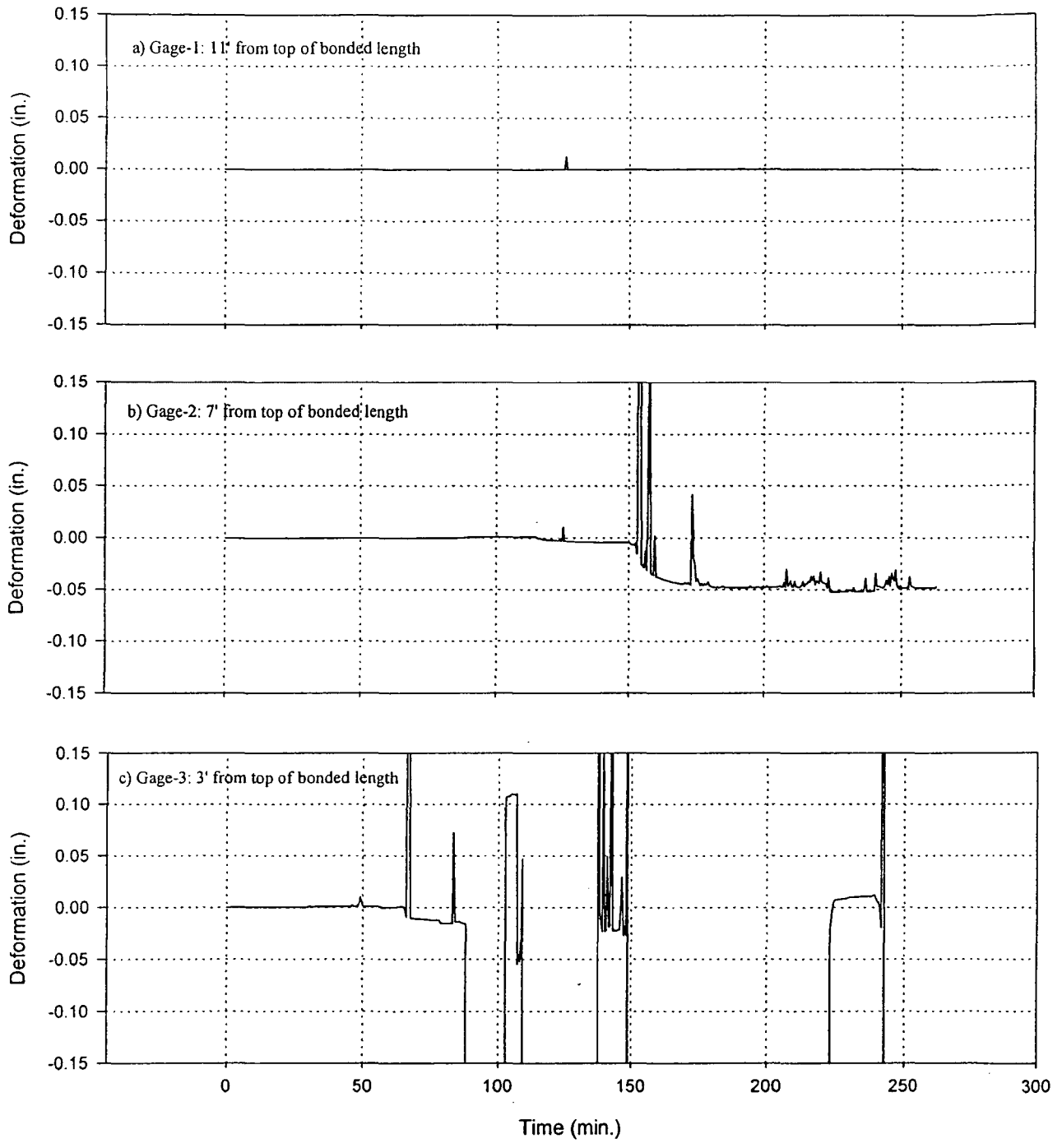


Fig. 4.29: Performance test of anchor #30B, deformation at each gage location in the bonded length.



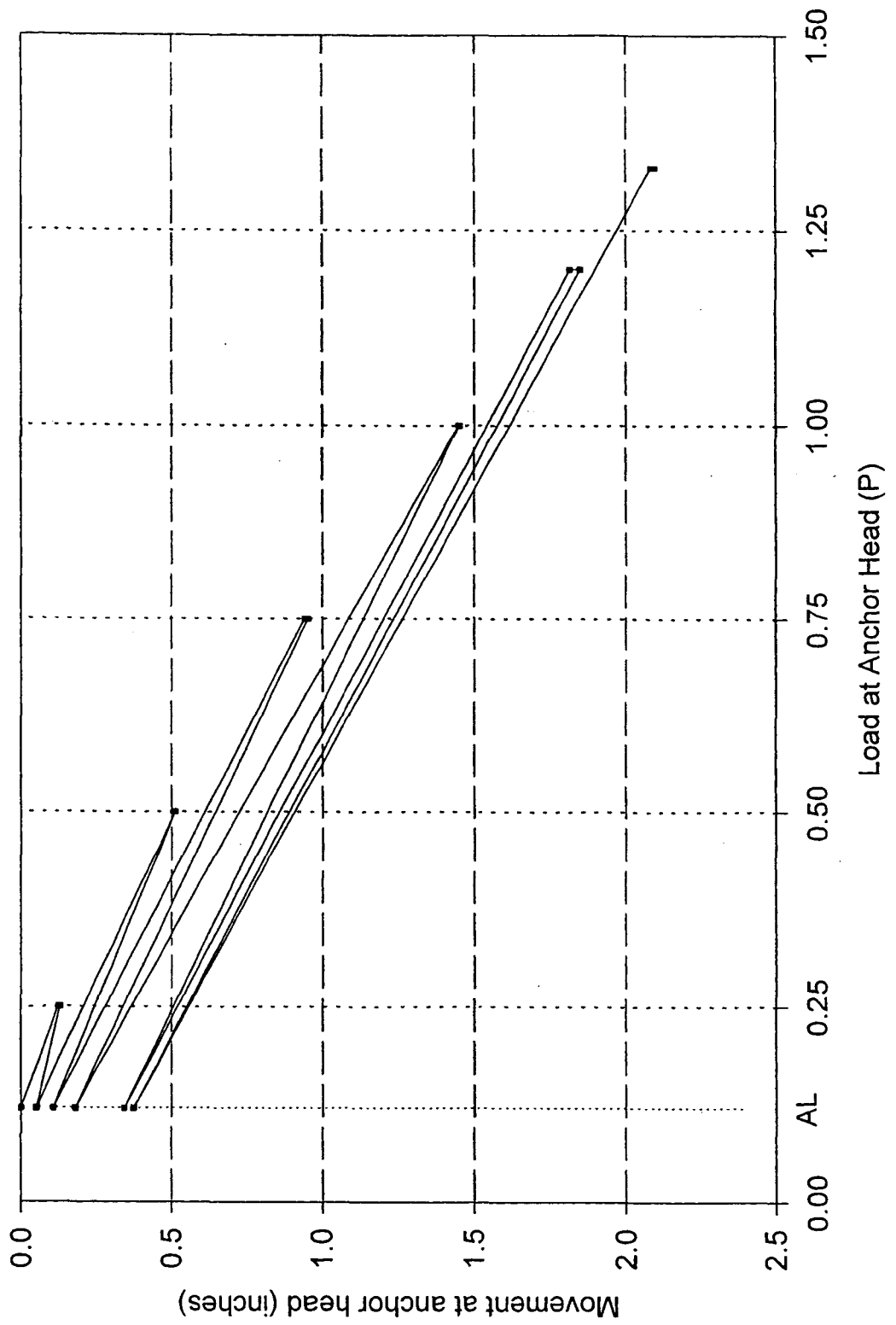


Fig. 4.30: Performance test of anchor #31B, load vs. displacement at anchor head.



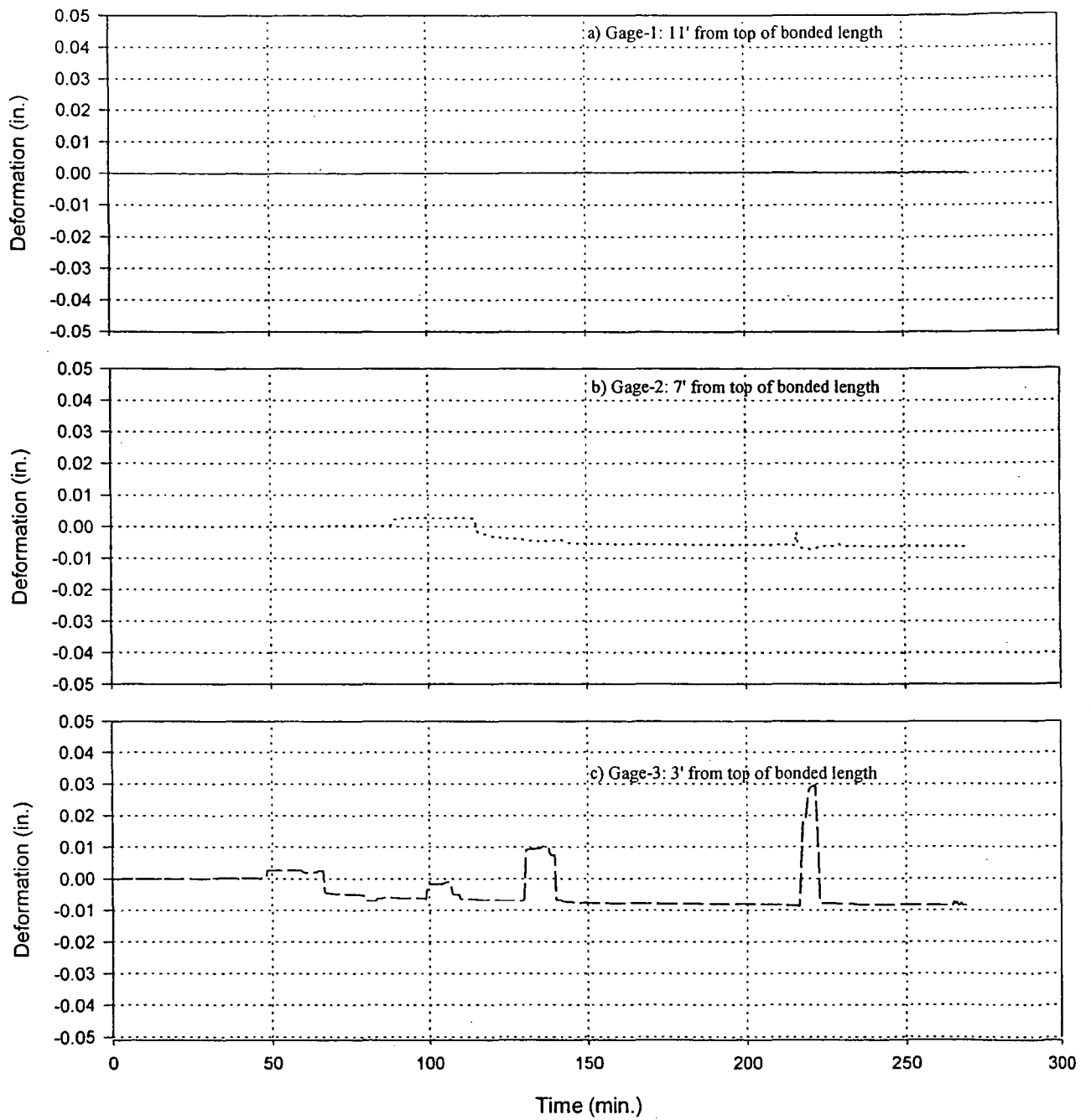


Fig. 4.31: Performance test of anchor #31B, deformation at each gage location in the bonded length.

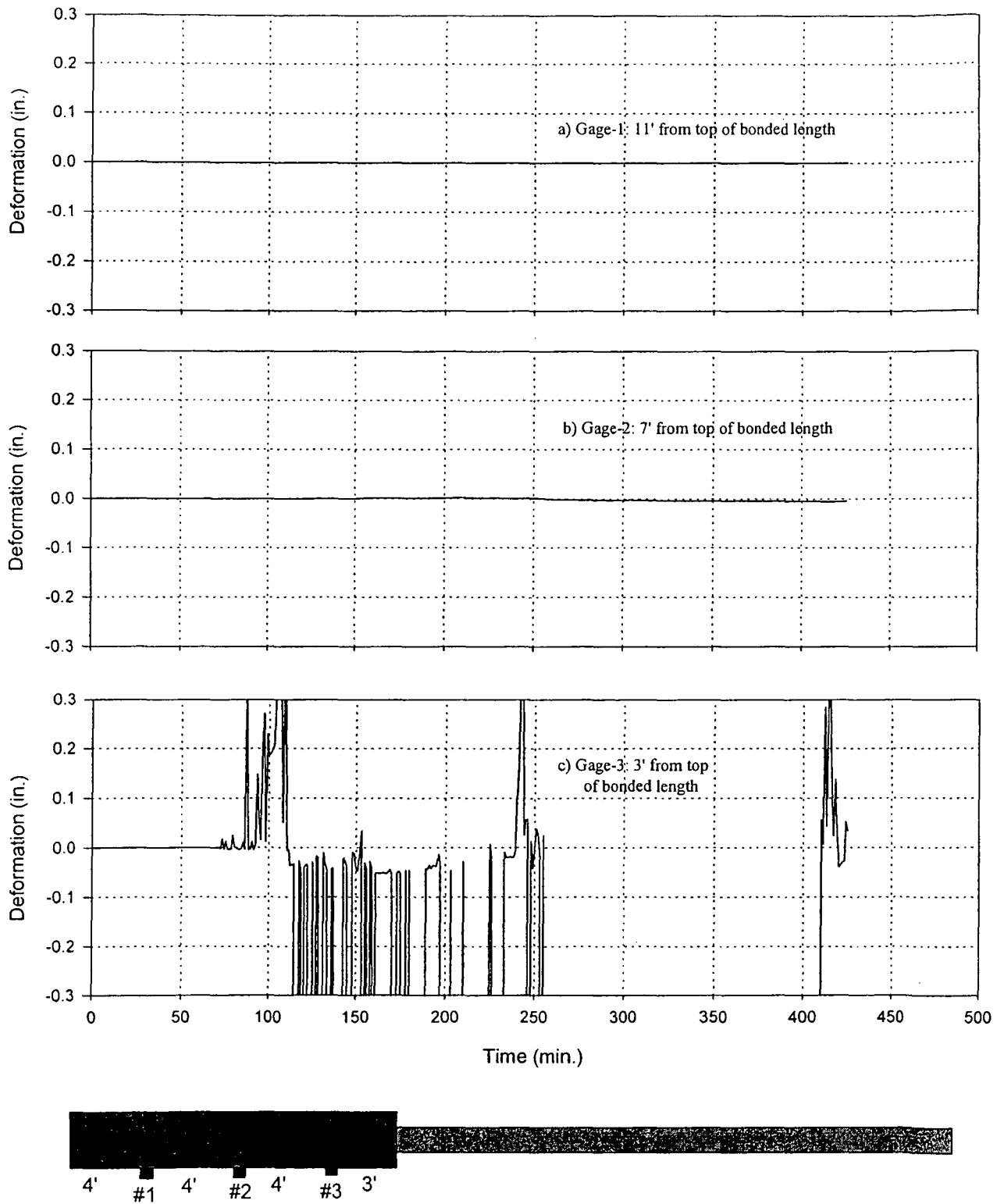


Fig. 4.33: Performance test of anchor #11B, deformation at each gage location in the bonded length

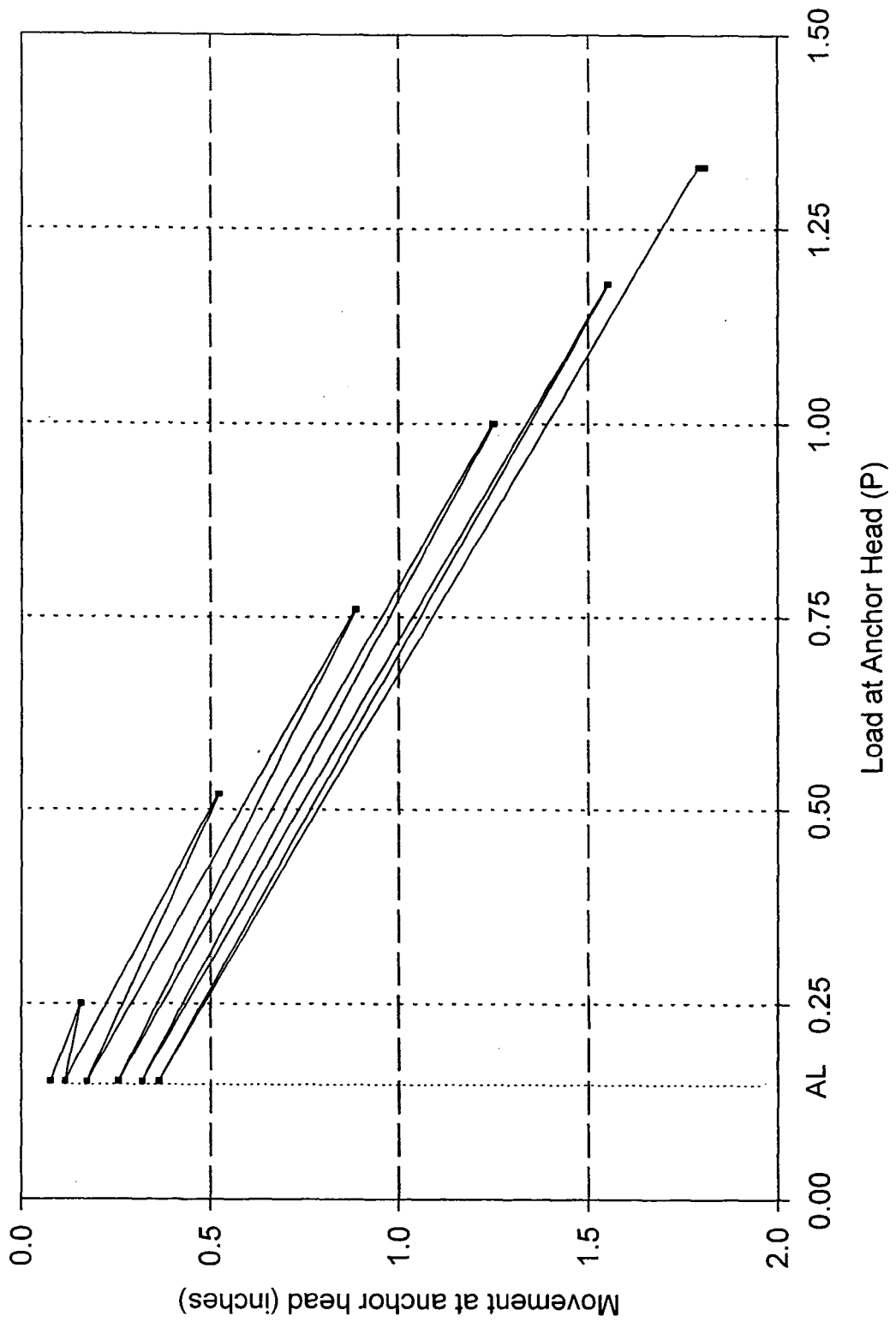


Fig. 4.34: Performance test of anchor #30C, load vs. displacement at anchor head.



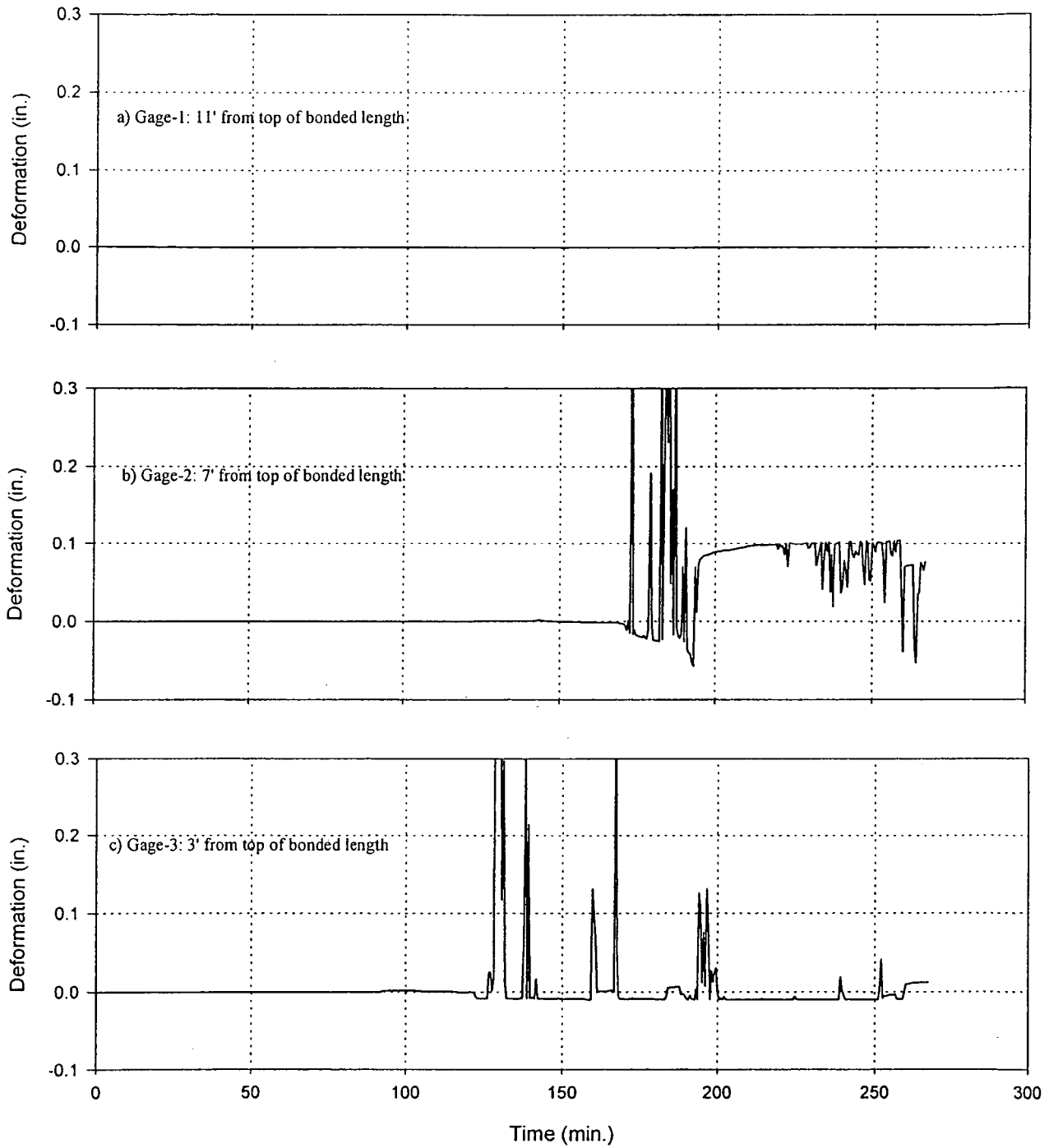


Fig. 4.37: Performance test of anchor #11A, deformation at each gage location in the bonded length.



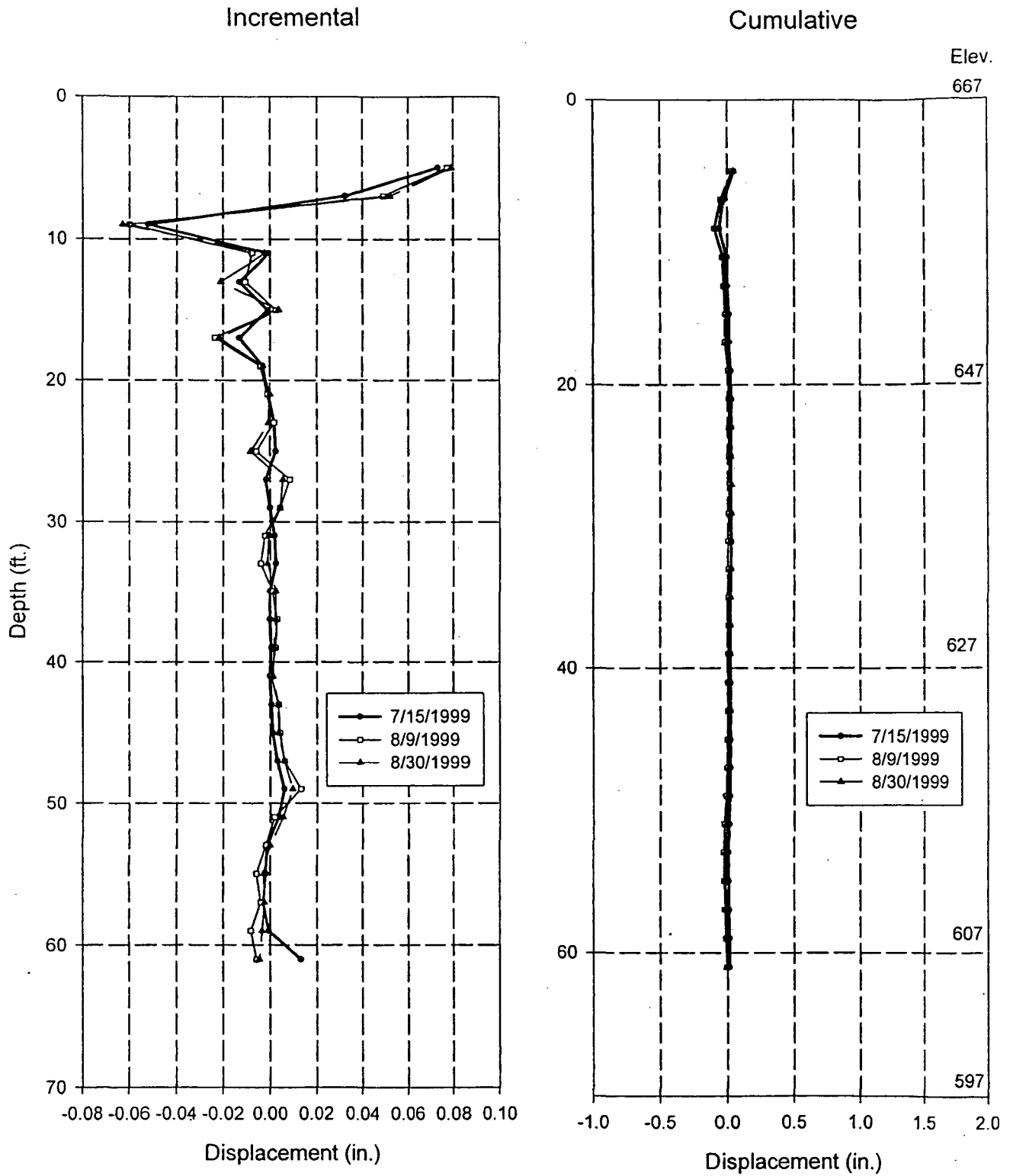


Fig. 4.41(b): Deflection vs. depth using inclinometer in the B+ direction (South) for soldier pile # 12.

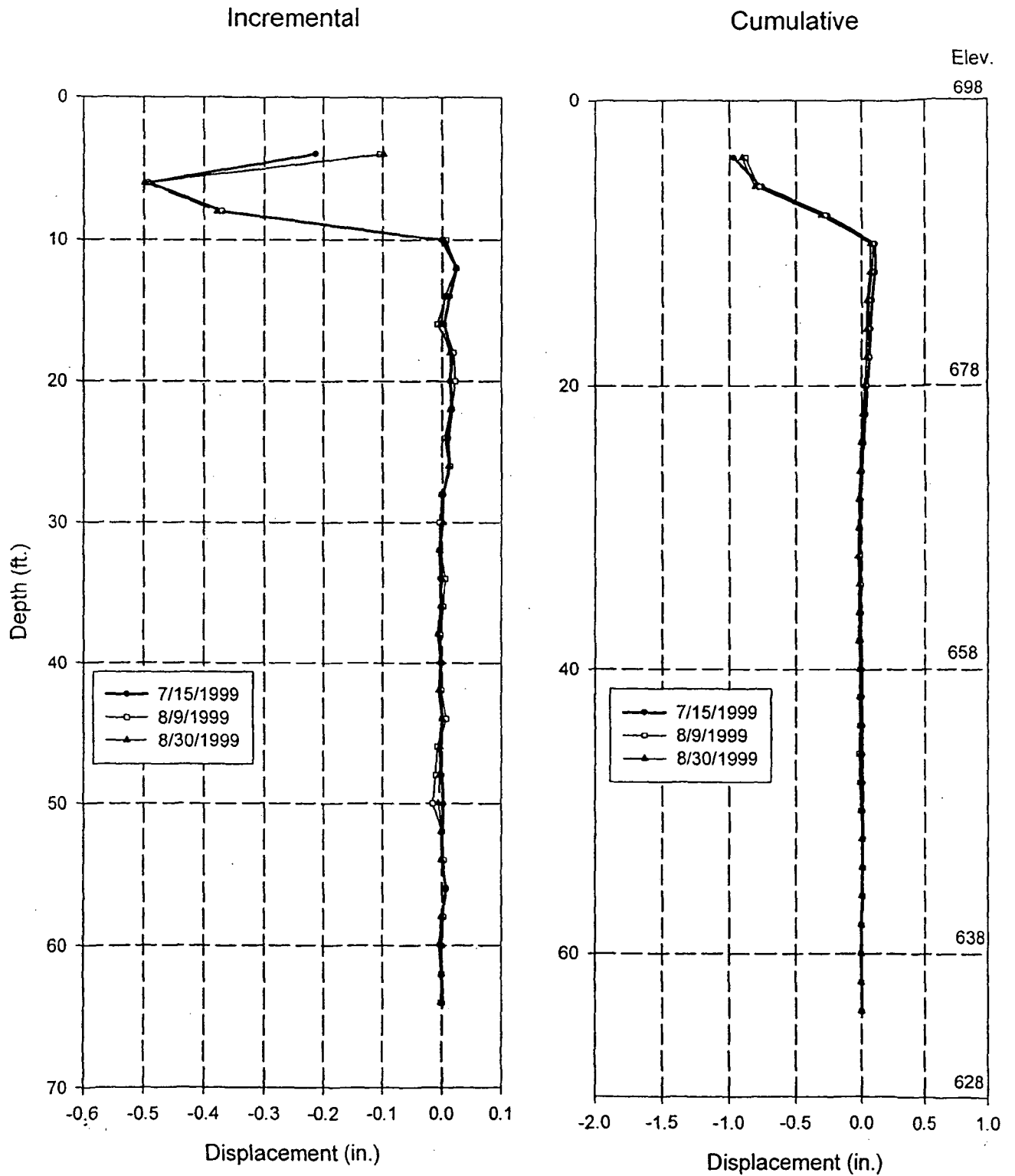


Fig. 4.42(a): Deflection vs. depth using inclinometer in the A+ direction (East) for soldier pile # 30.



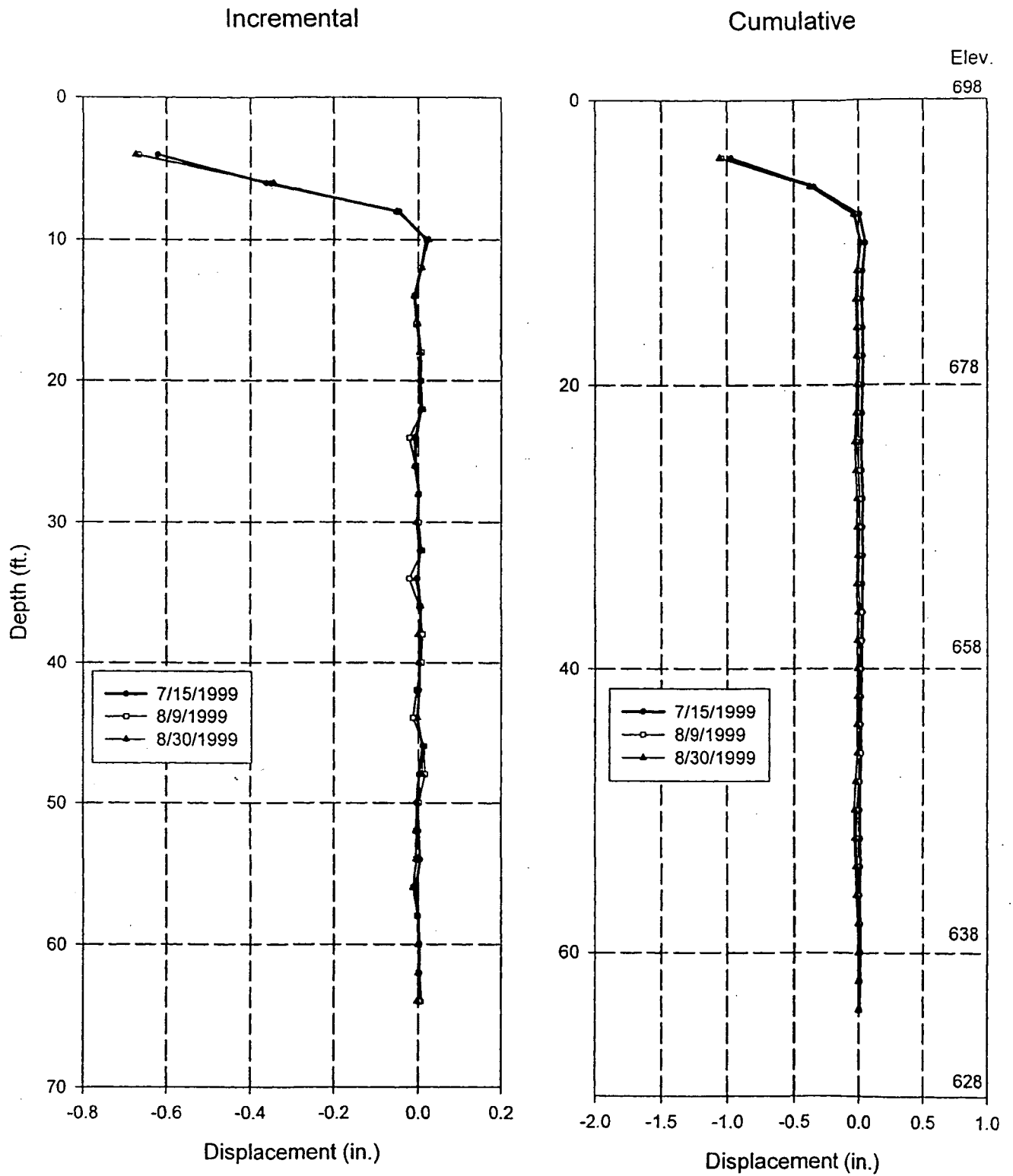


Fig. 4.42(b): Deflection vs. depth using inclinometer in the B+ direction (South) for soldier pile # 30.



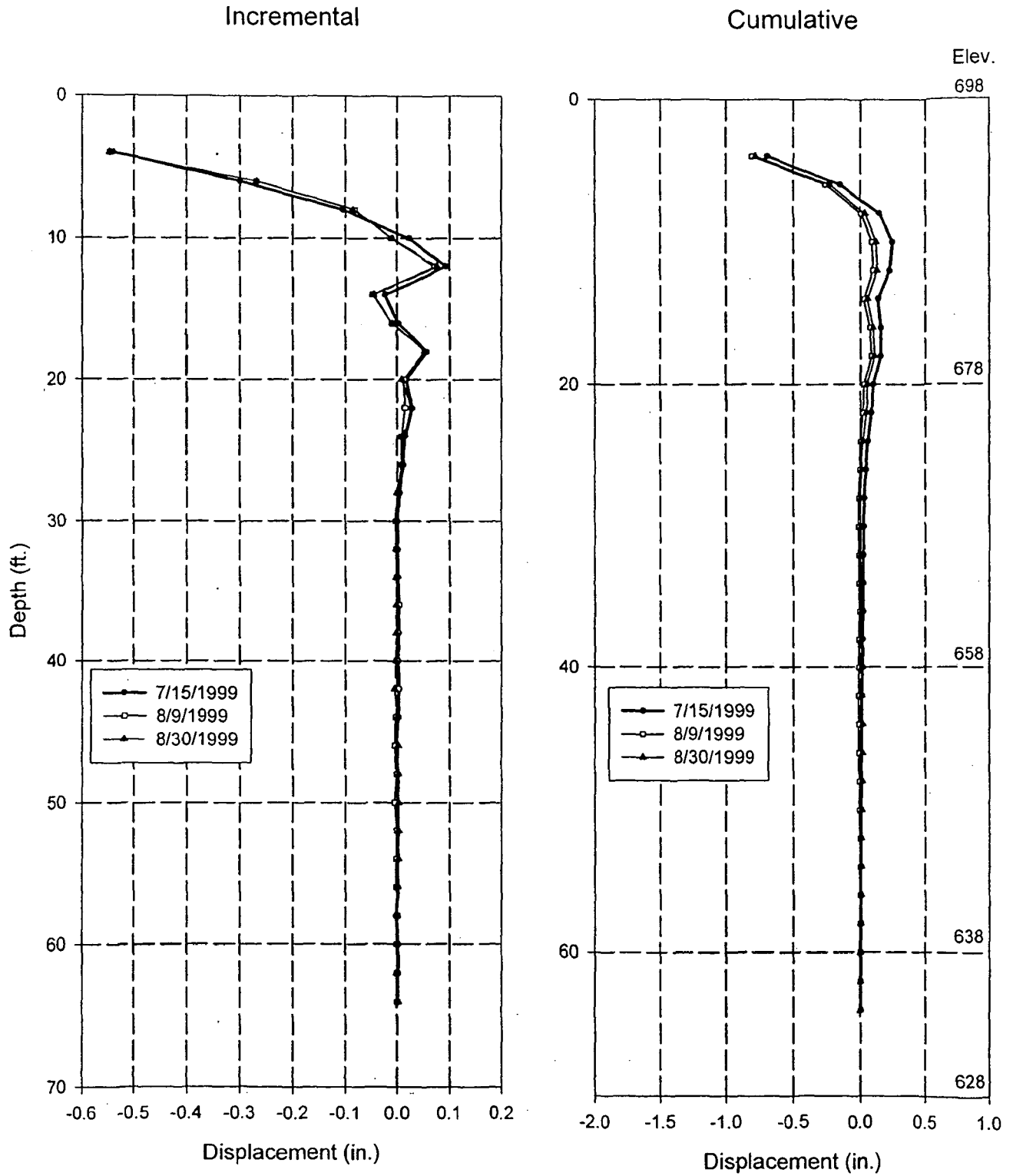


Fig. 4.43(a): Deflection vs. depth using inclinometer in the A+ direction (East) for soldier pile # 31.



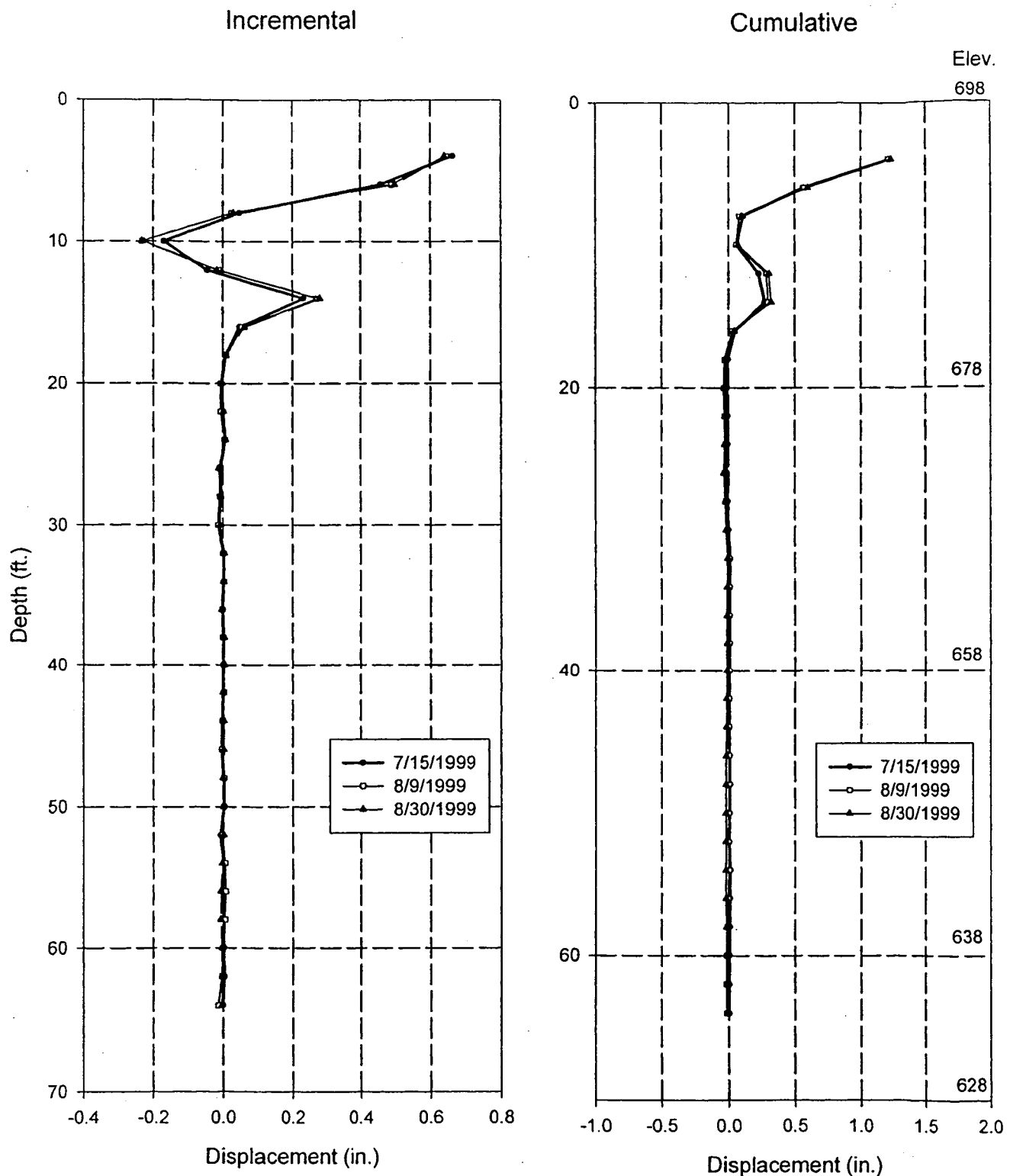


Fig. 4.43(b): Deflection vs. depth using inclinometer in the B+ direction (South) for soldier pile # 31.

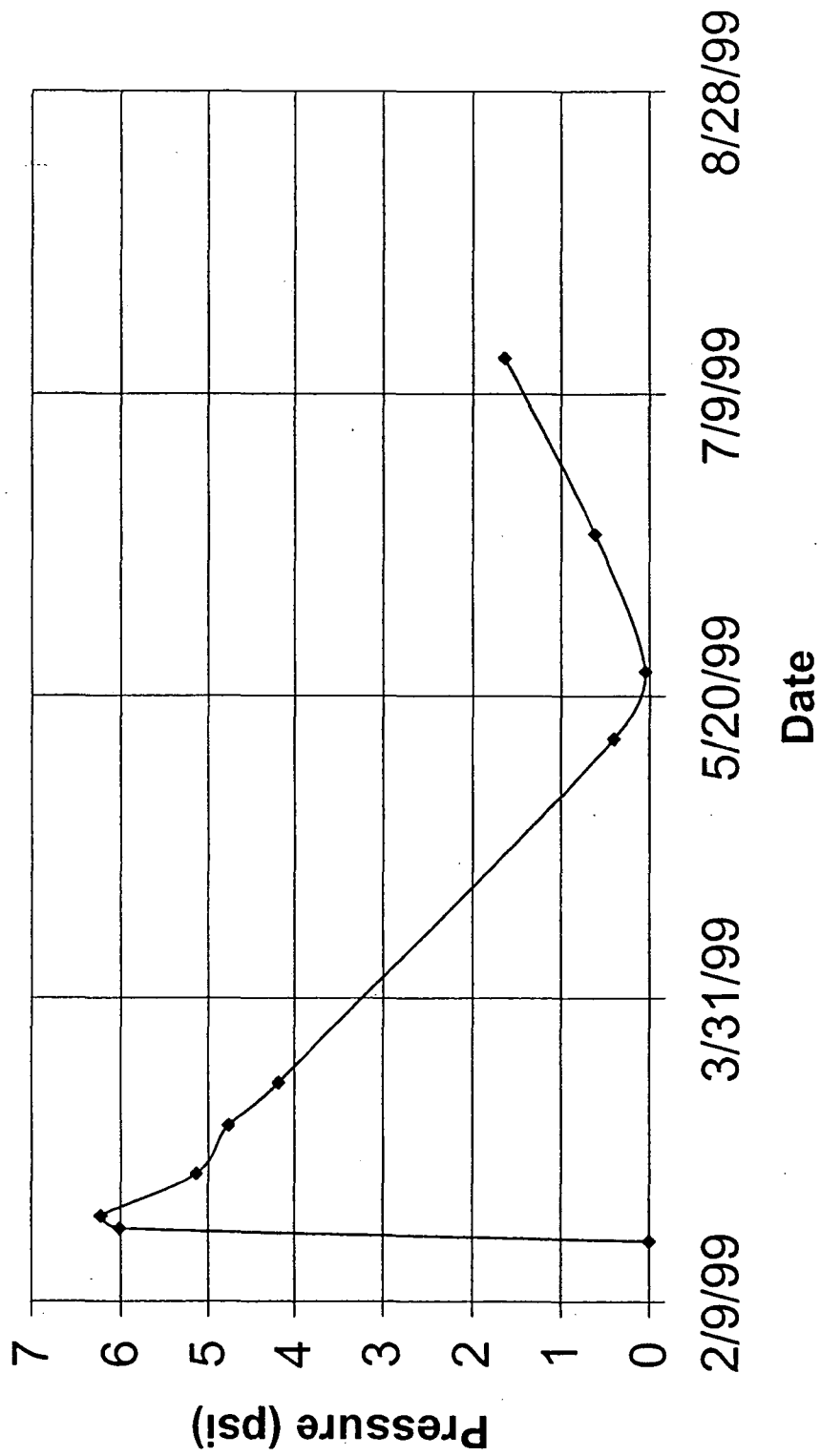


Fig. 4.47: Pore water pressure recorded using the piezometer.



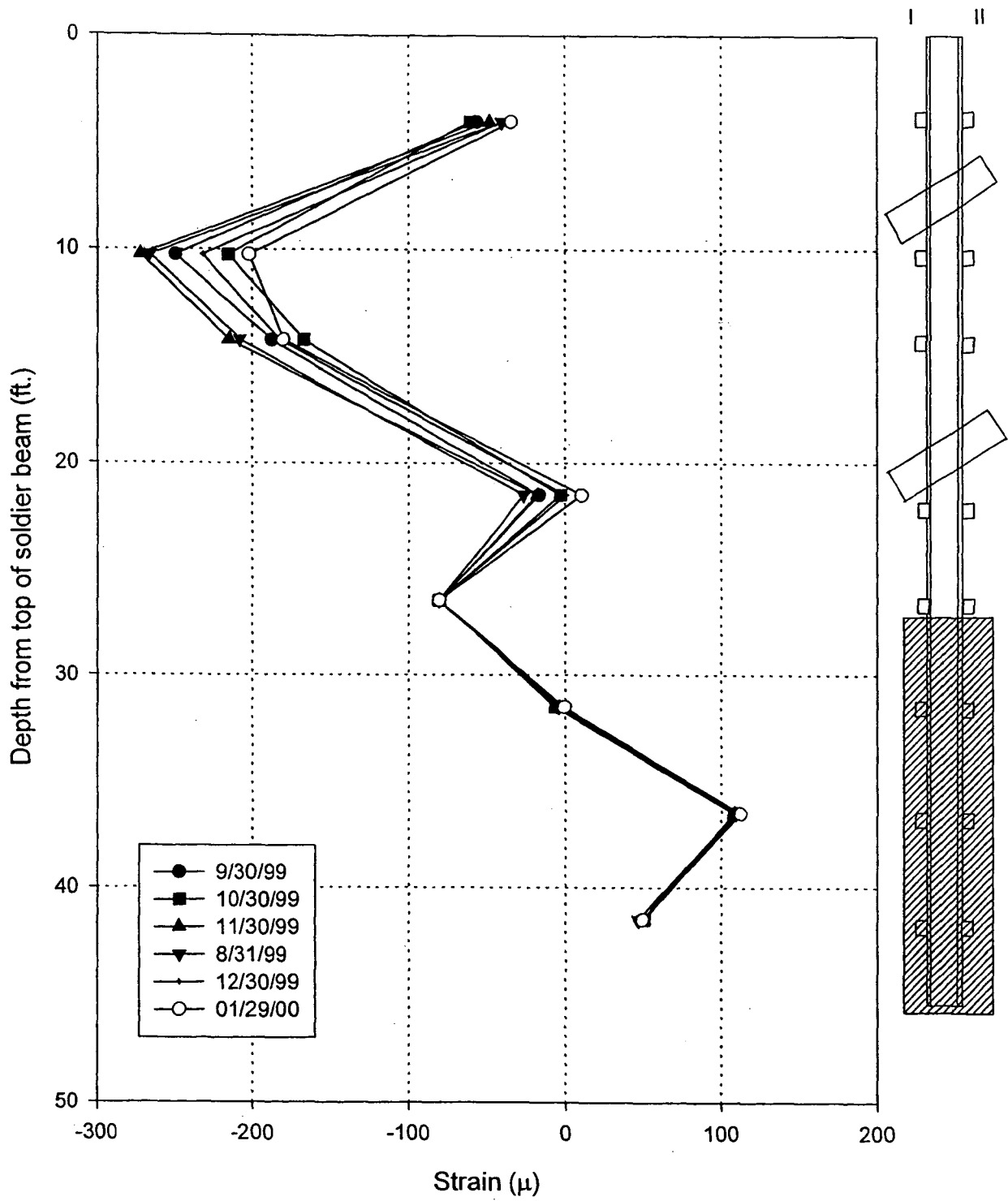


Fig. 4.48: Strain vs. depth for soldier pile # 11, side I, till 1/29/2000.



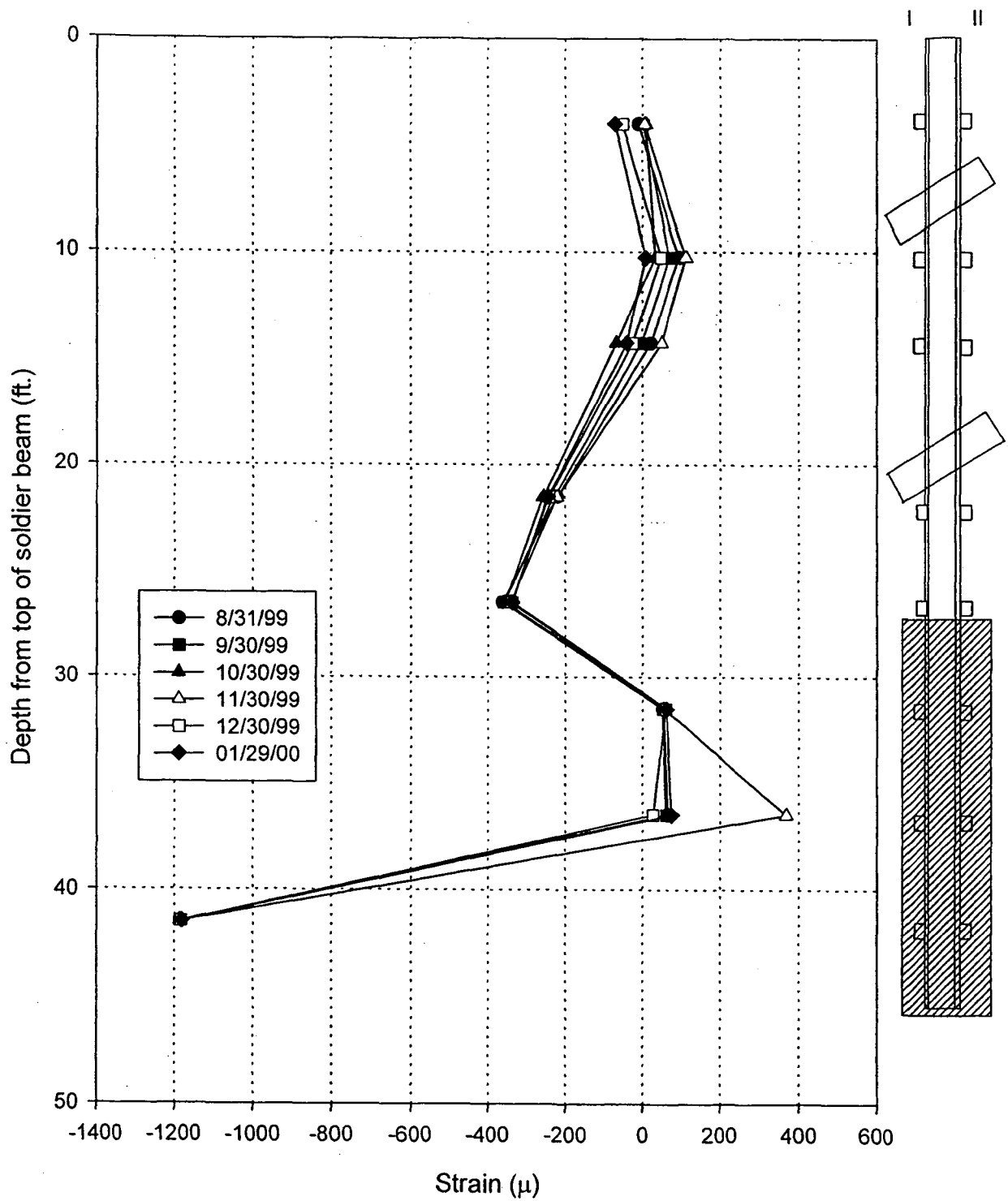


Fig. 4.49: Strain vs. depth for soldier pile # 11, side II, till 1/29/2000.

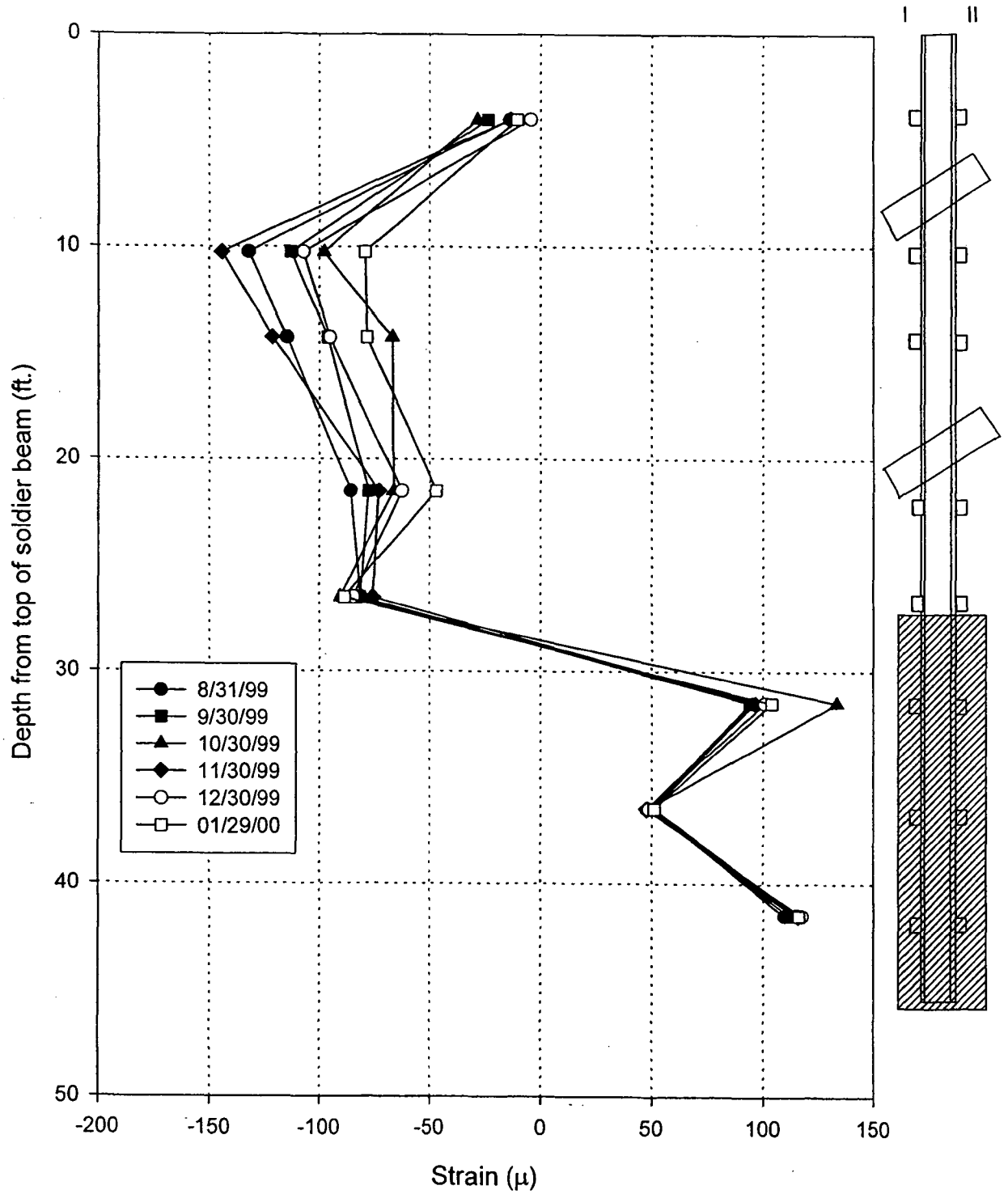


Fig. 4.50: Strain vs. depth for soldier pile # 12, side I, till 1/29/2000.

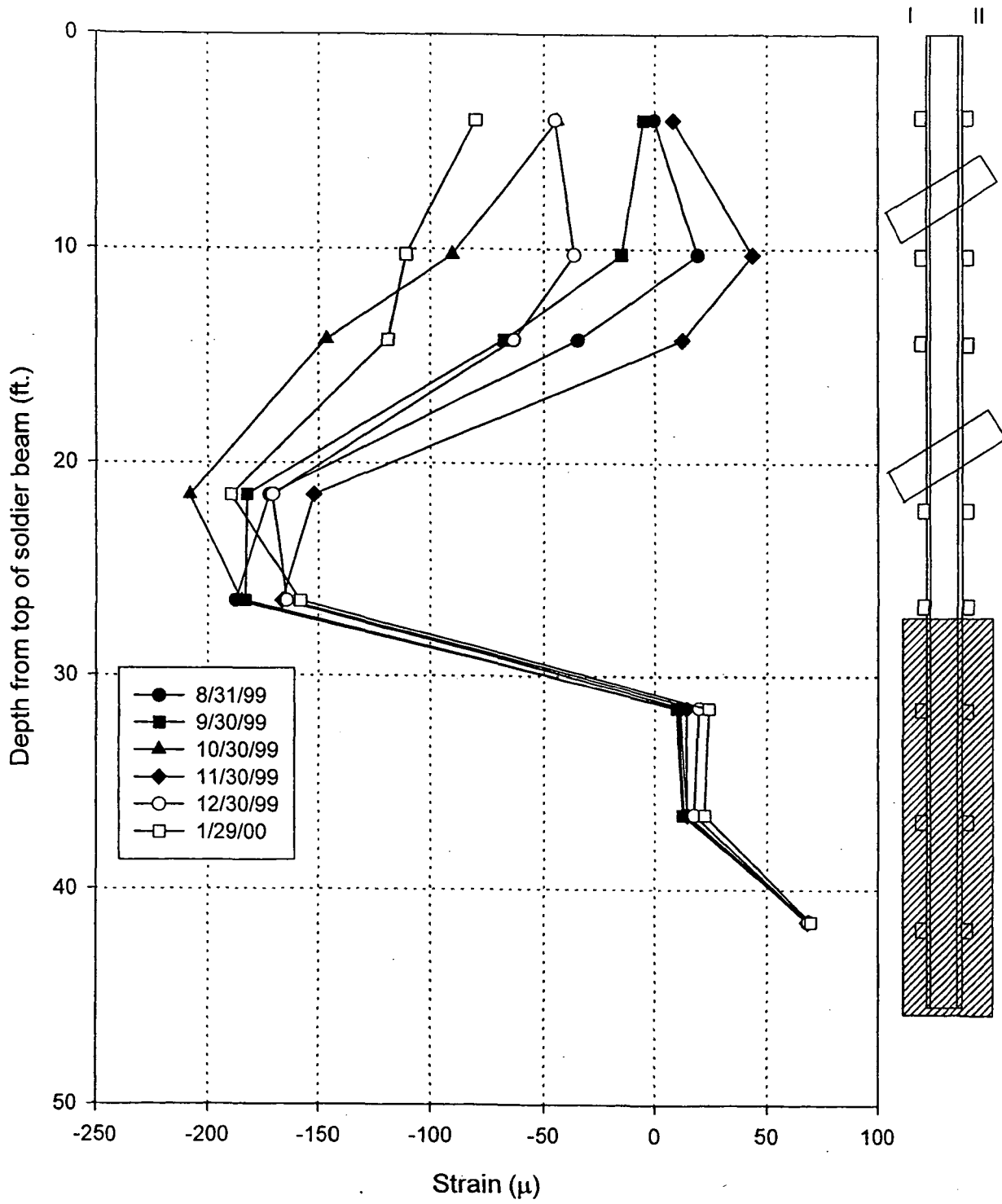


Fig. 4.51: Strain vs. depth for soldier pile # 12, side II, till 1/29/2000.

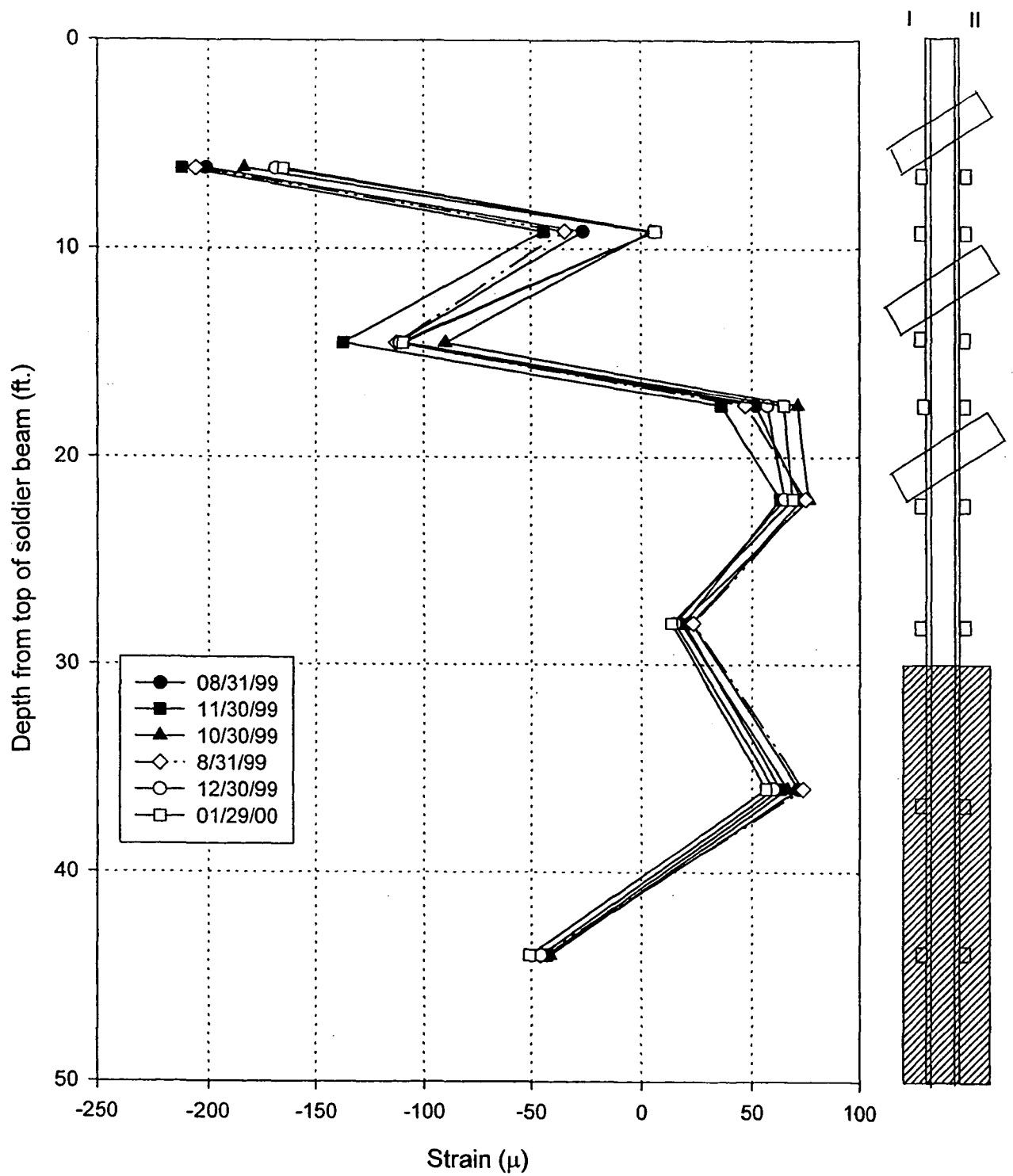


Fig. 4.52: Strain vs. depth for soldier pile # 30, side I, till 1/29/2000.

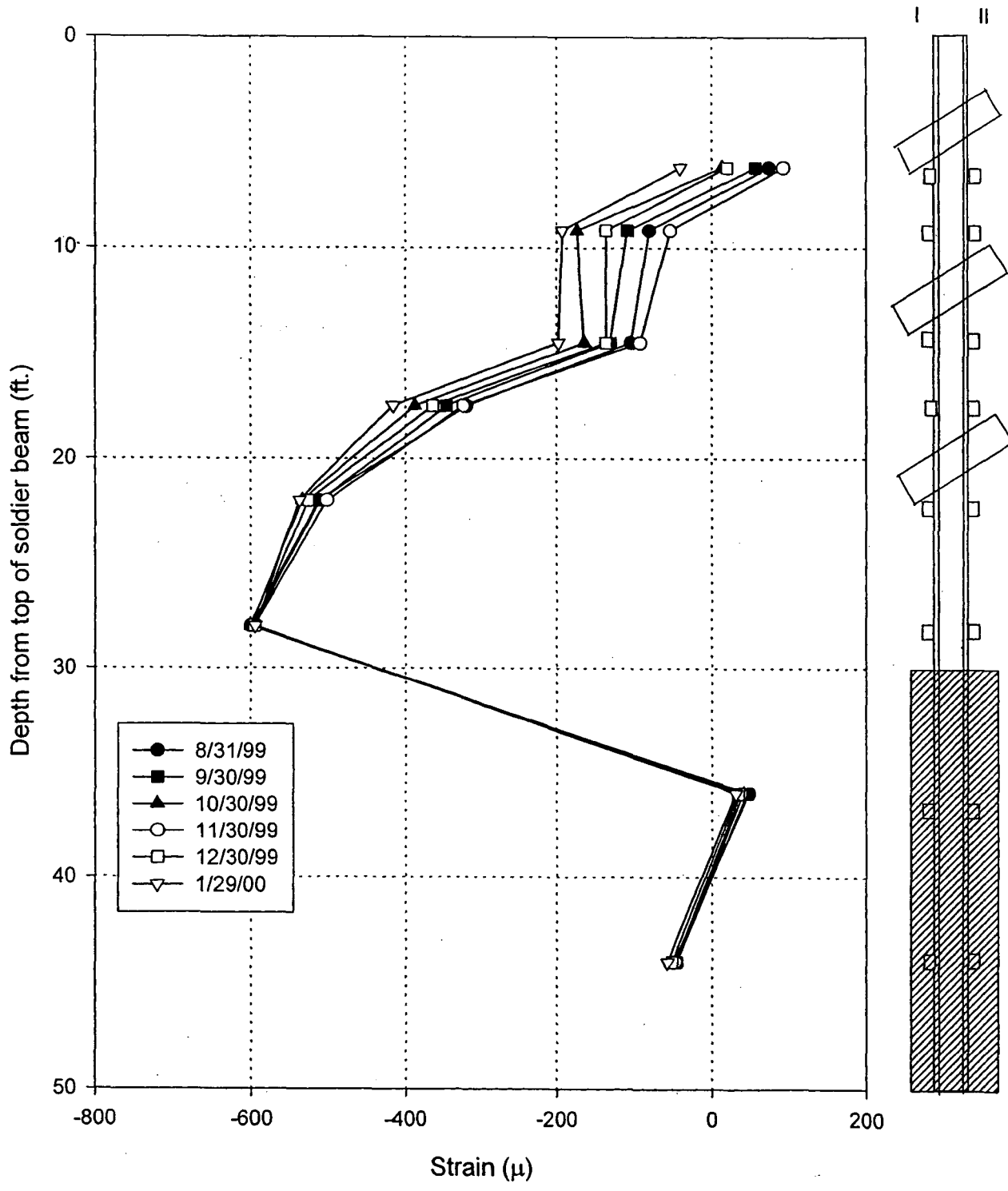


Fig. 4.53: Strain vs. depth for soldier pile # 30, side II, till 1/29/2000.

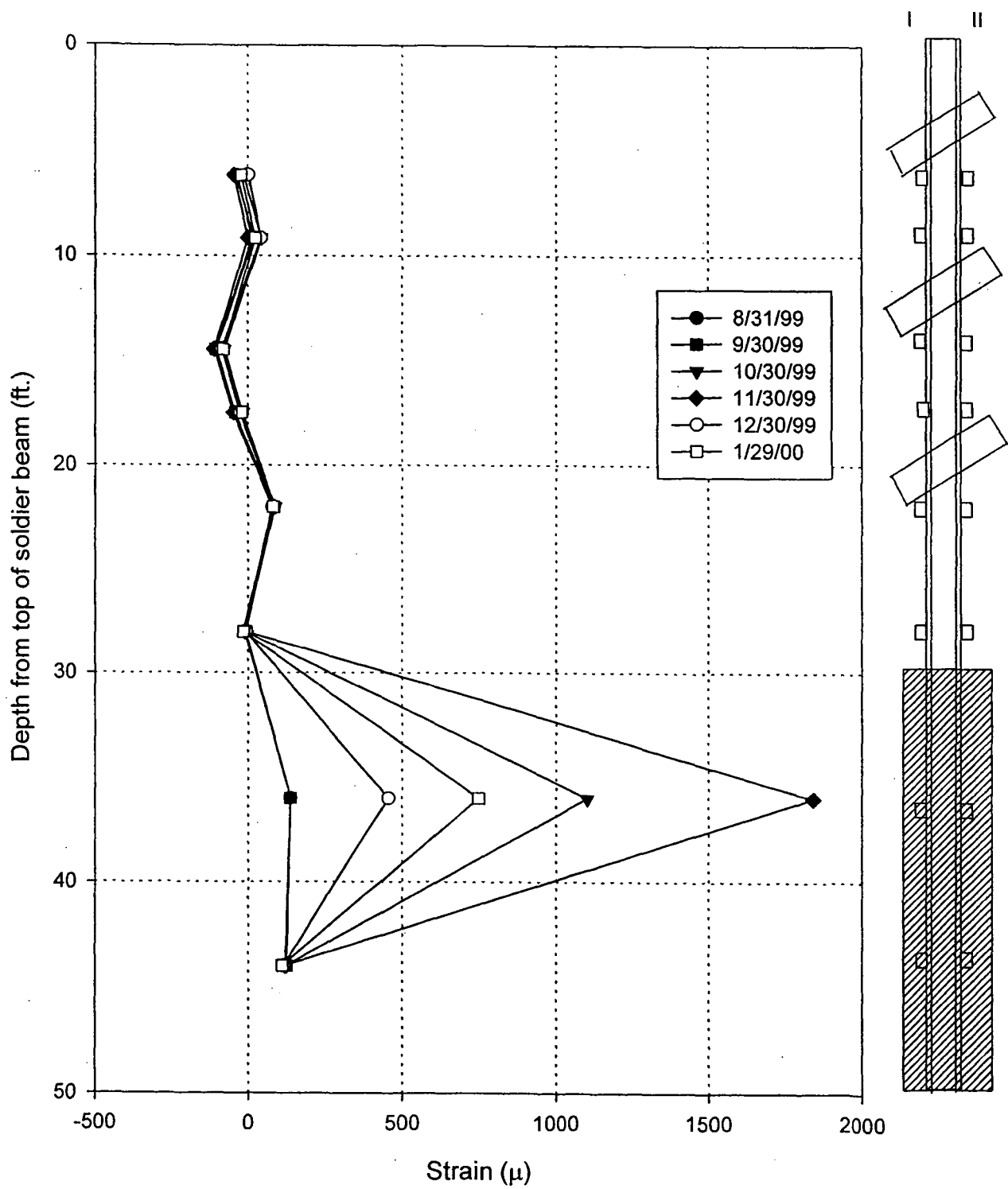


Fig. 4.54: Strain vs. depth for soldier pile # 31, side I, till 1/29/2000.

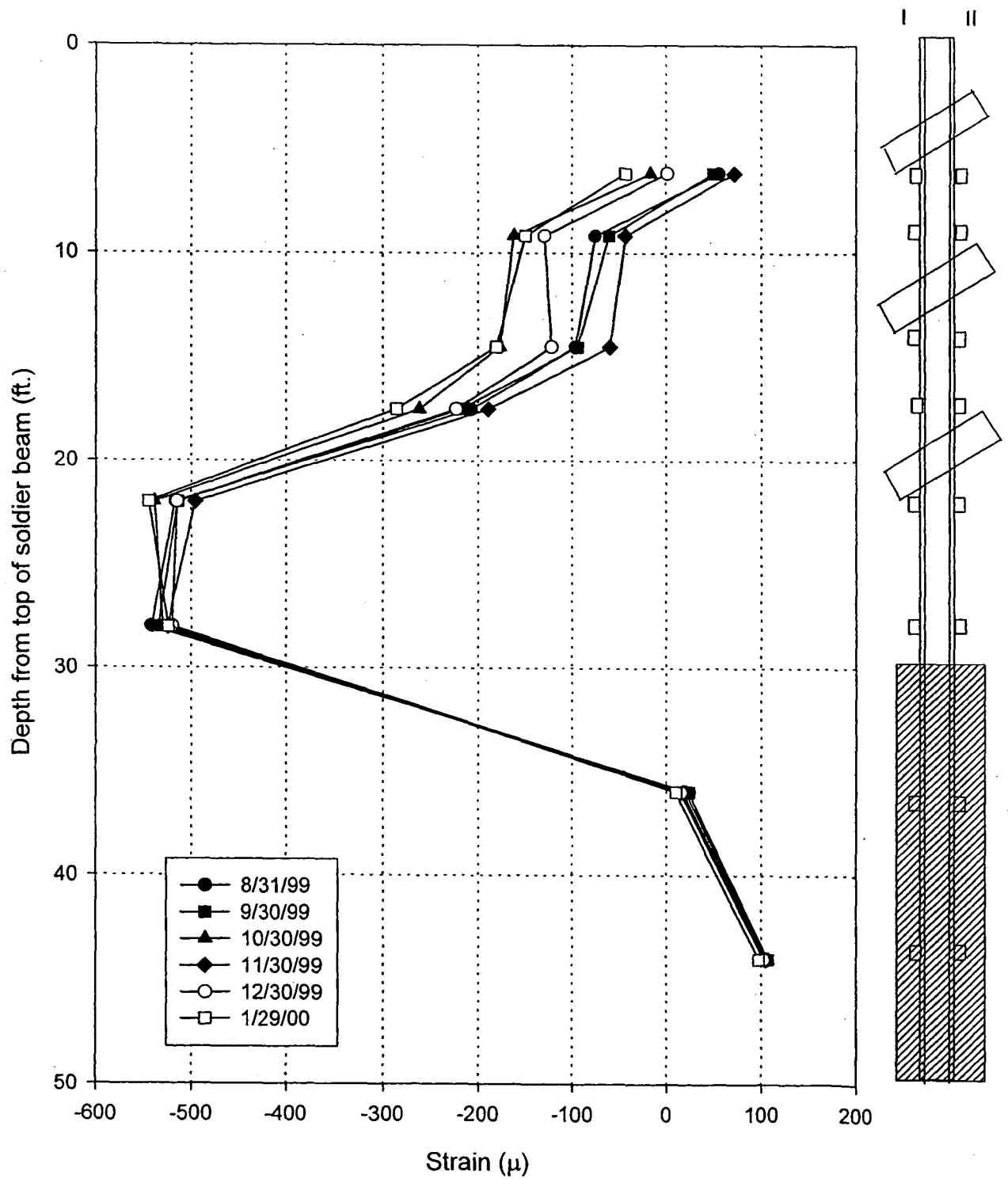


Fig. 4.55: Strain vs. depth for soldier pile # 31, side II, till 1/29/2000.

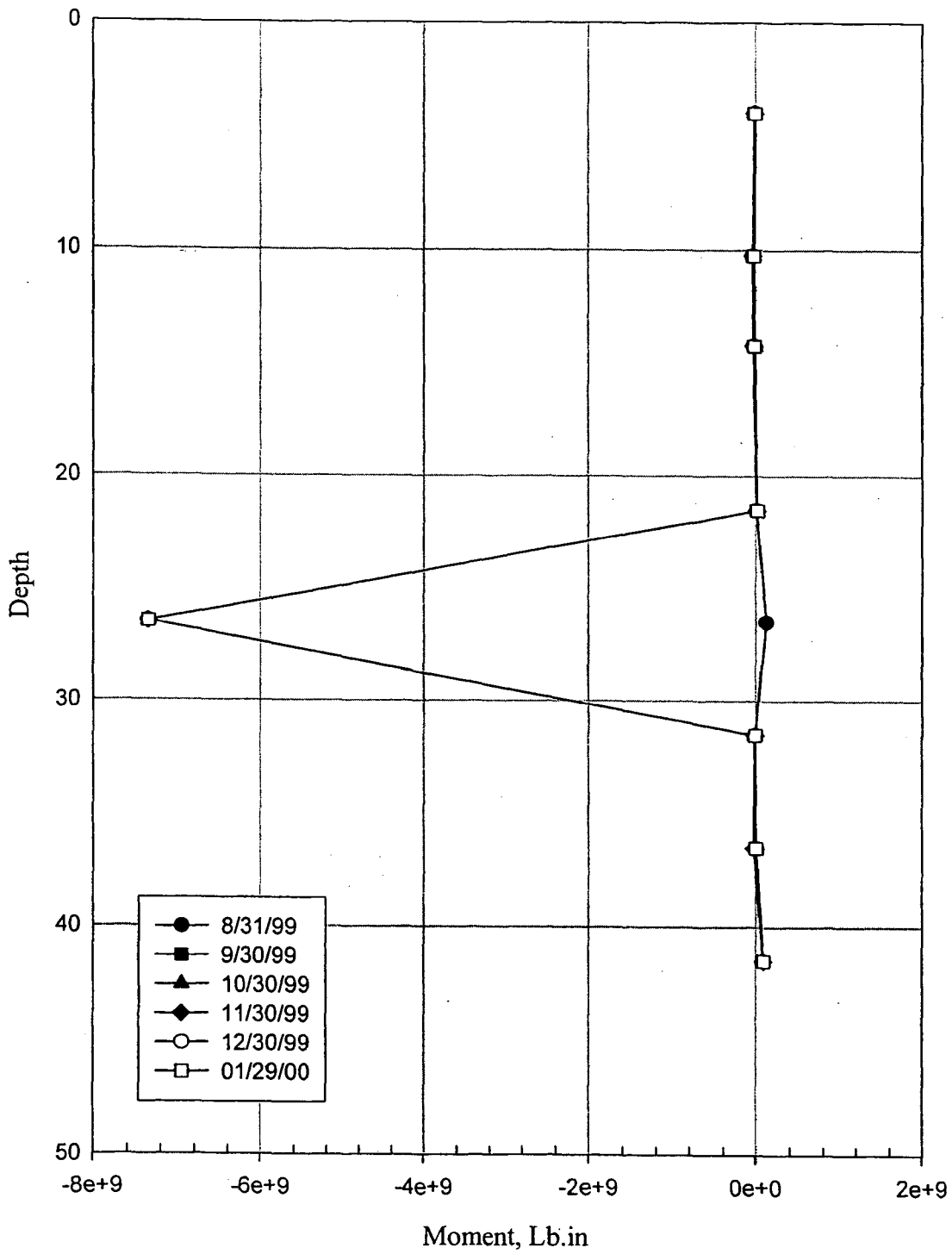


Fig. 4.56: Moment vs. depth for soldier pile # 11 till 1/29/2000.

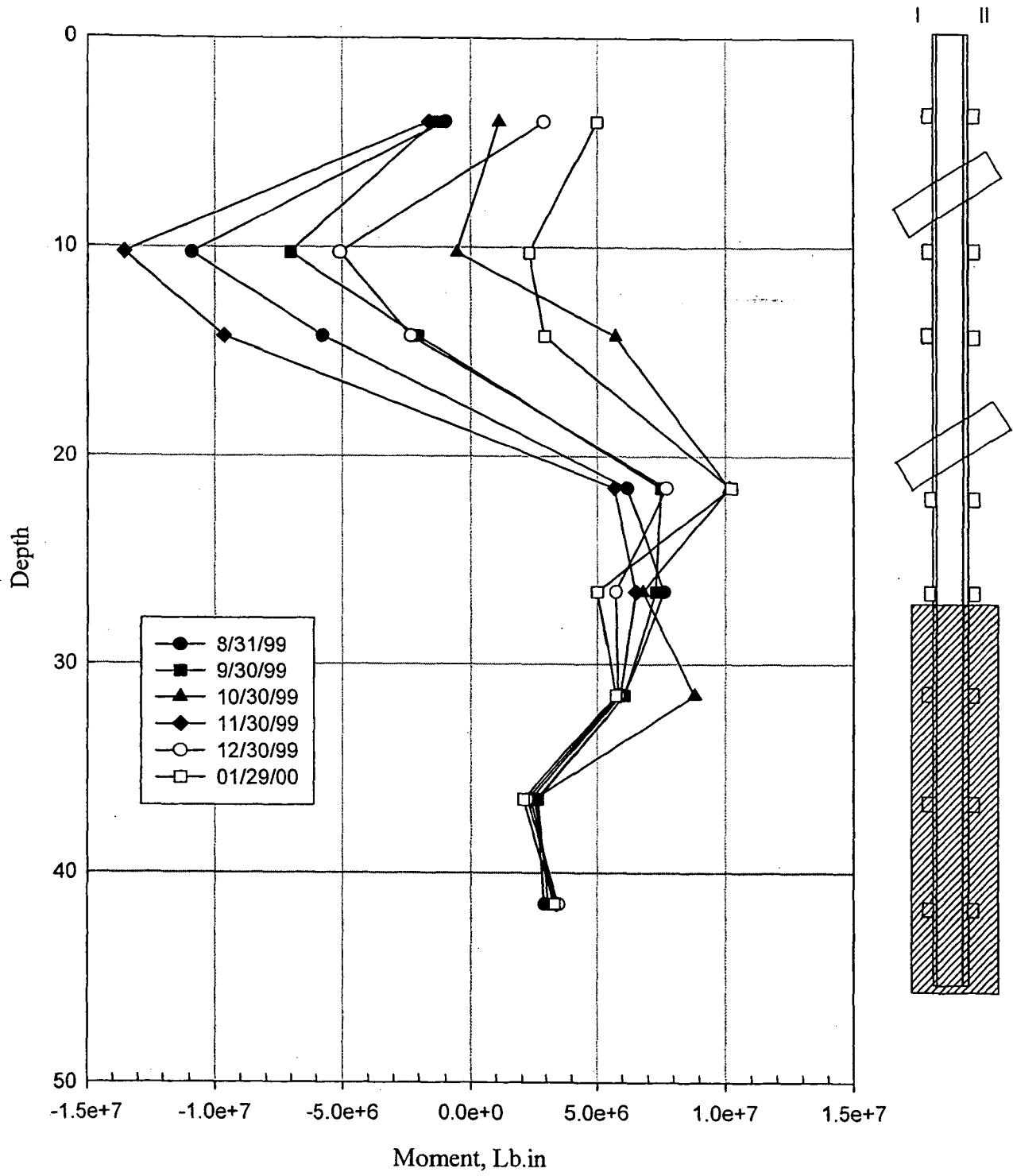


Fig. 4.57: Moment vs. depth for soldier pile # 12 till 1/29/2000.

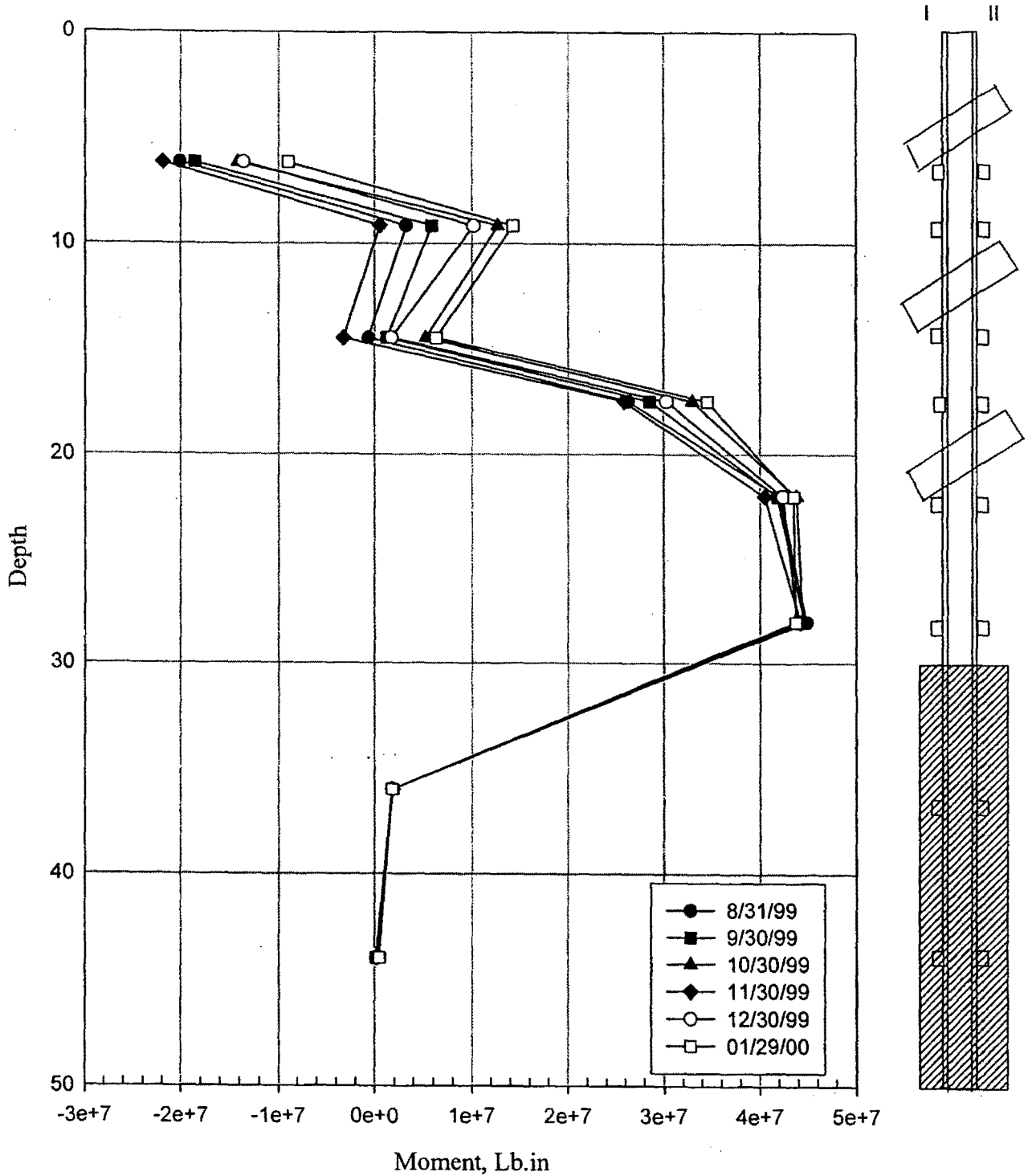


Fig. 4.58: Moment vs. depth for soldier pile # 30 till 1/29/2000.

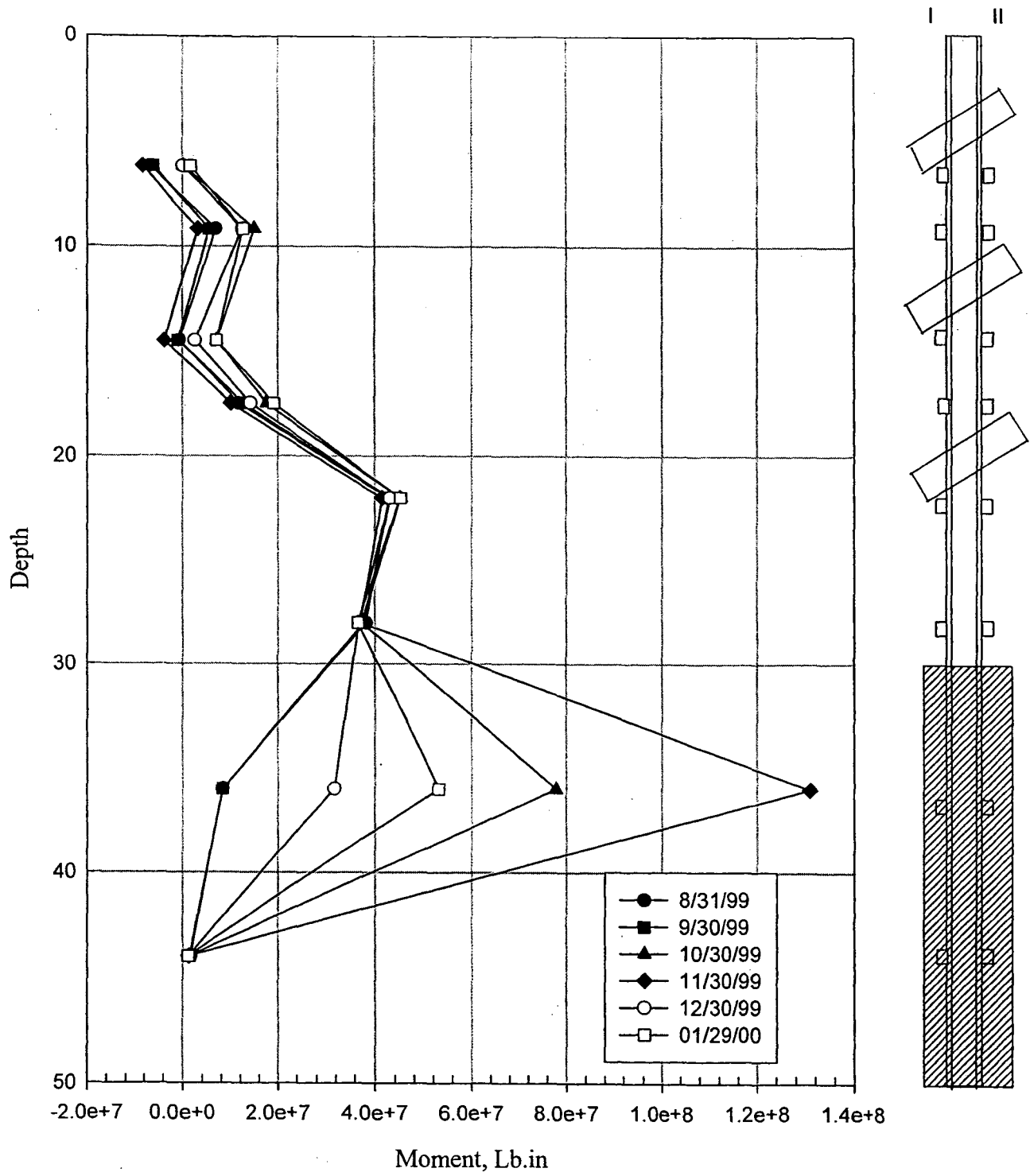


Fig. 4.59: Moment vs. depth for soldier pile # 31 till 1/29/2000.

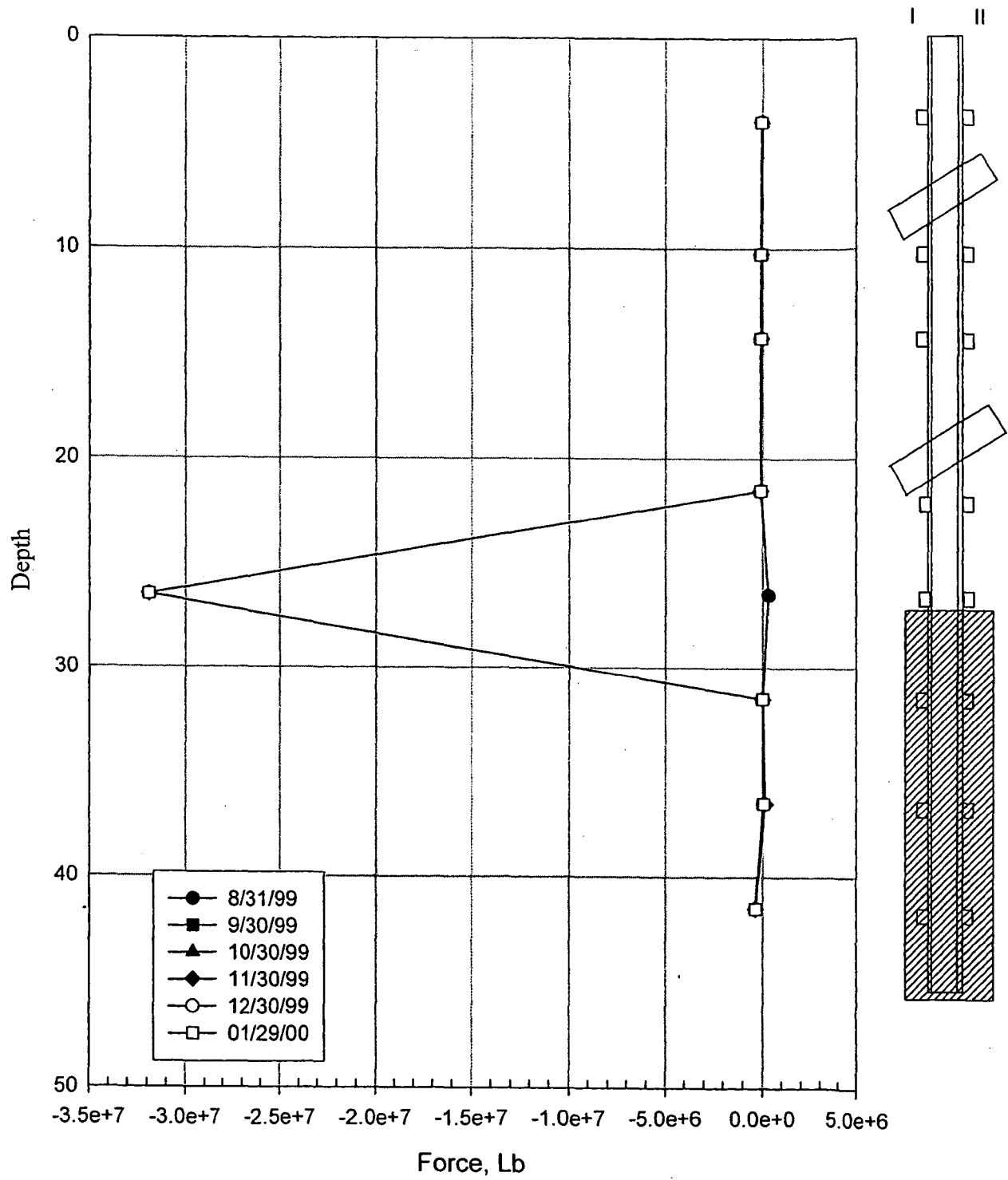


Fig. 4.60: Axial force vs. depth for soldier pile # 11 till 1/29/2000.



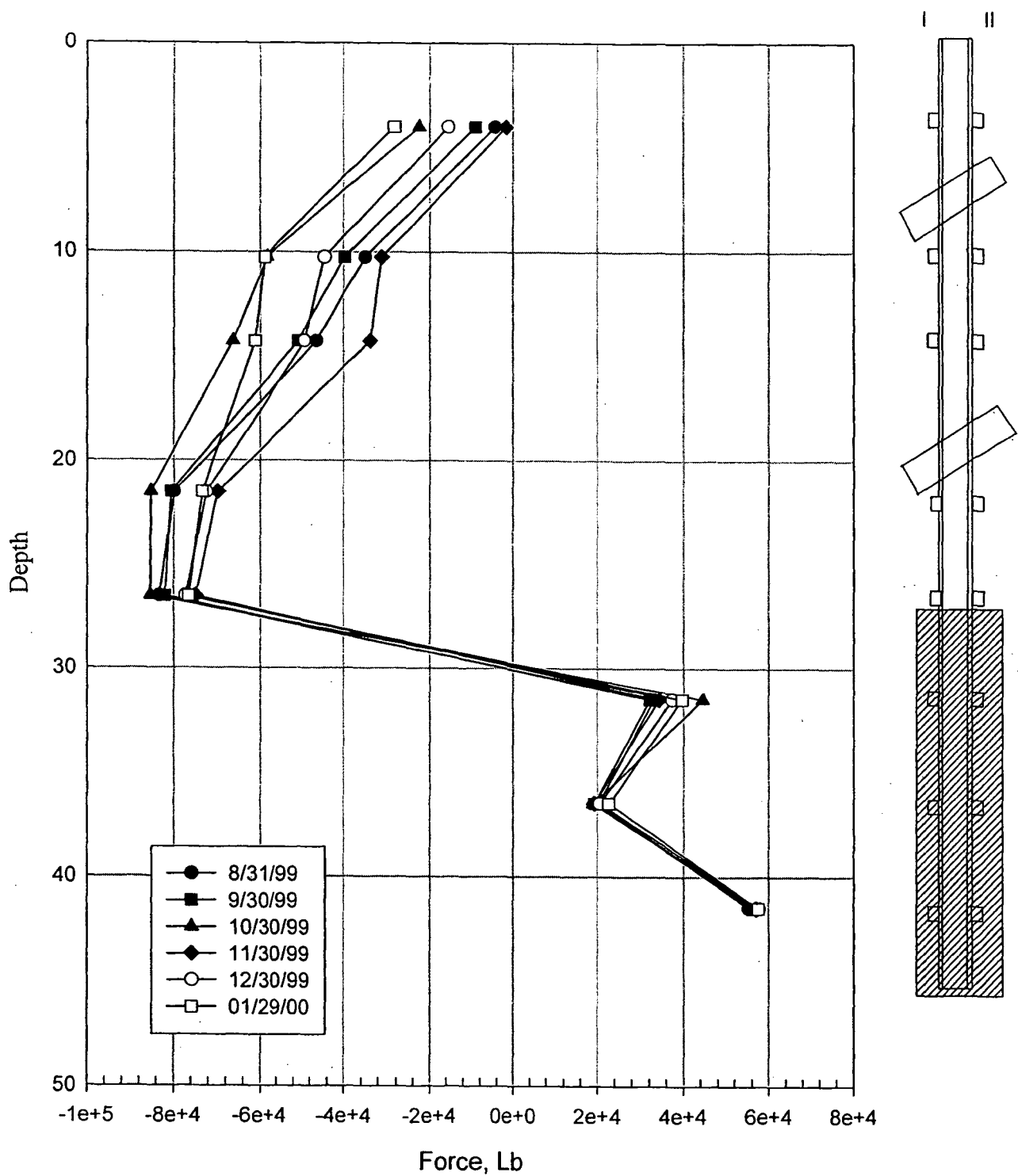


Fig. 4.61: Axial force vs. depth for soldier pile # 12 till 1/29/2000.

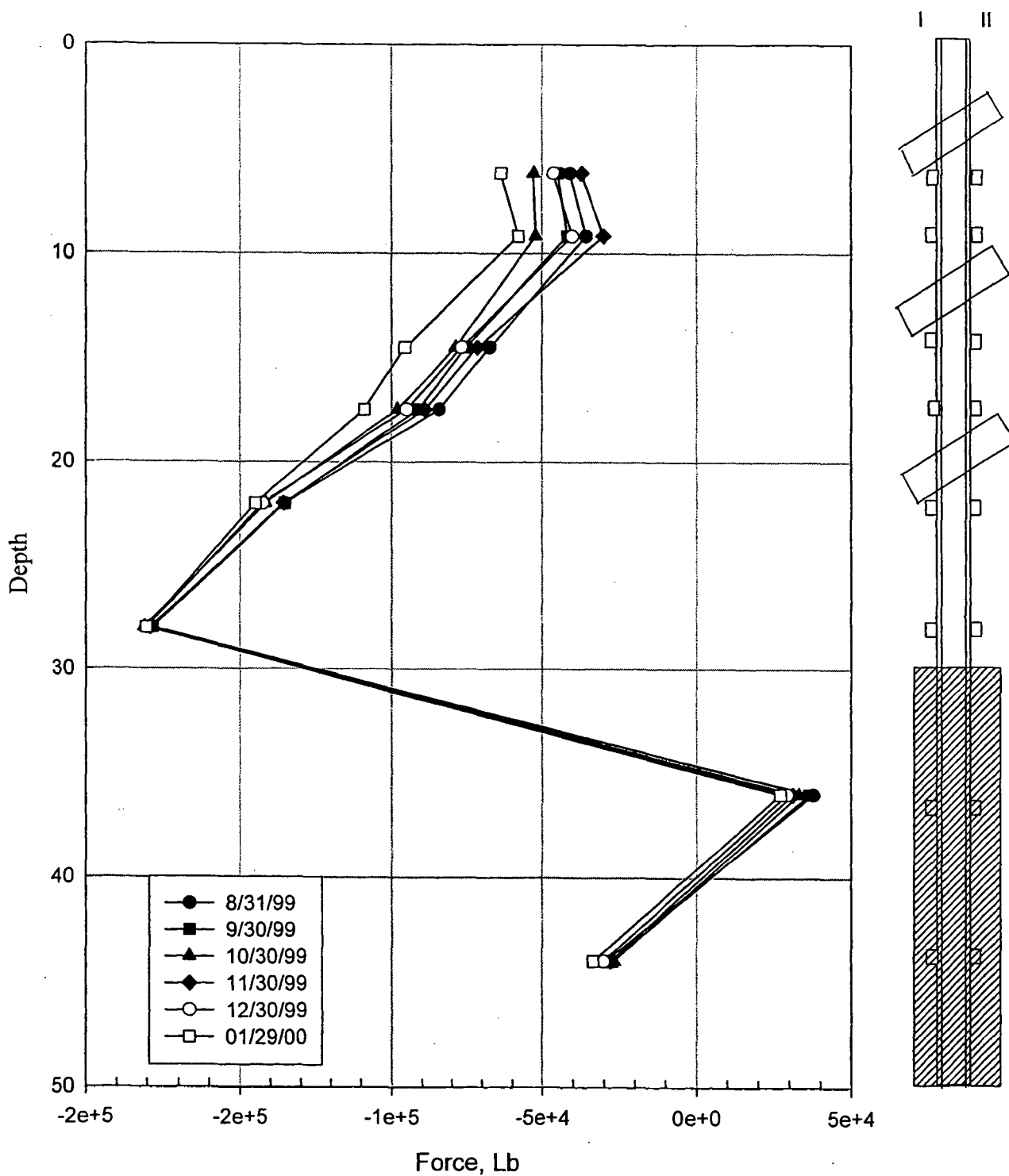
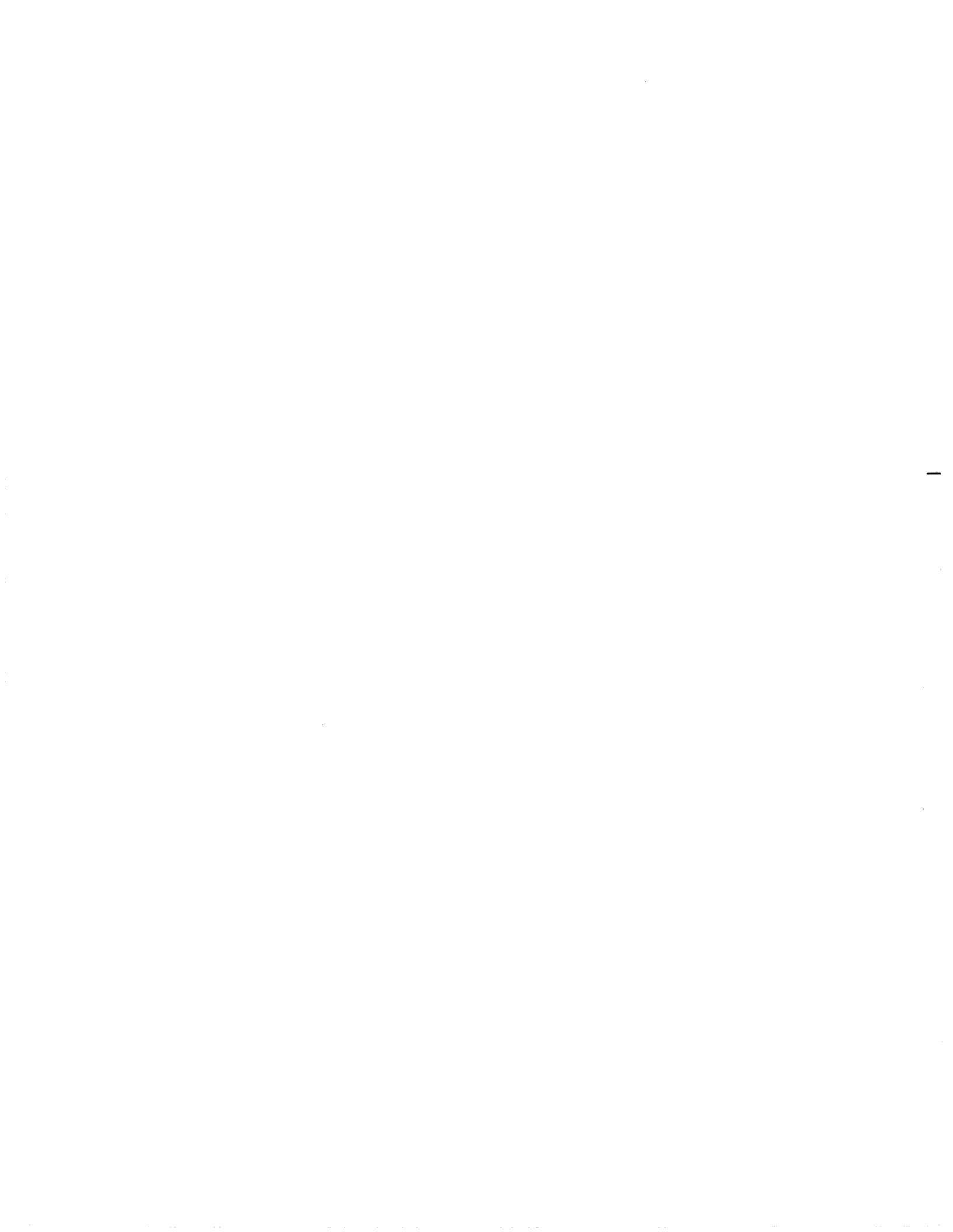


Fig. 4.62: Axial force vs. depth for soldier pile # 30 till 1/29/2000.



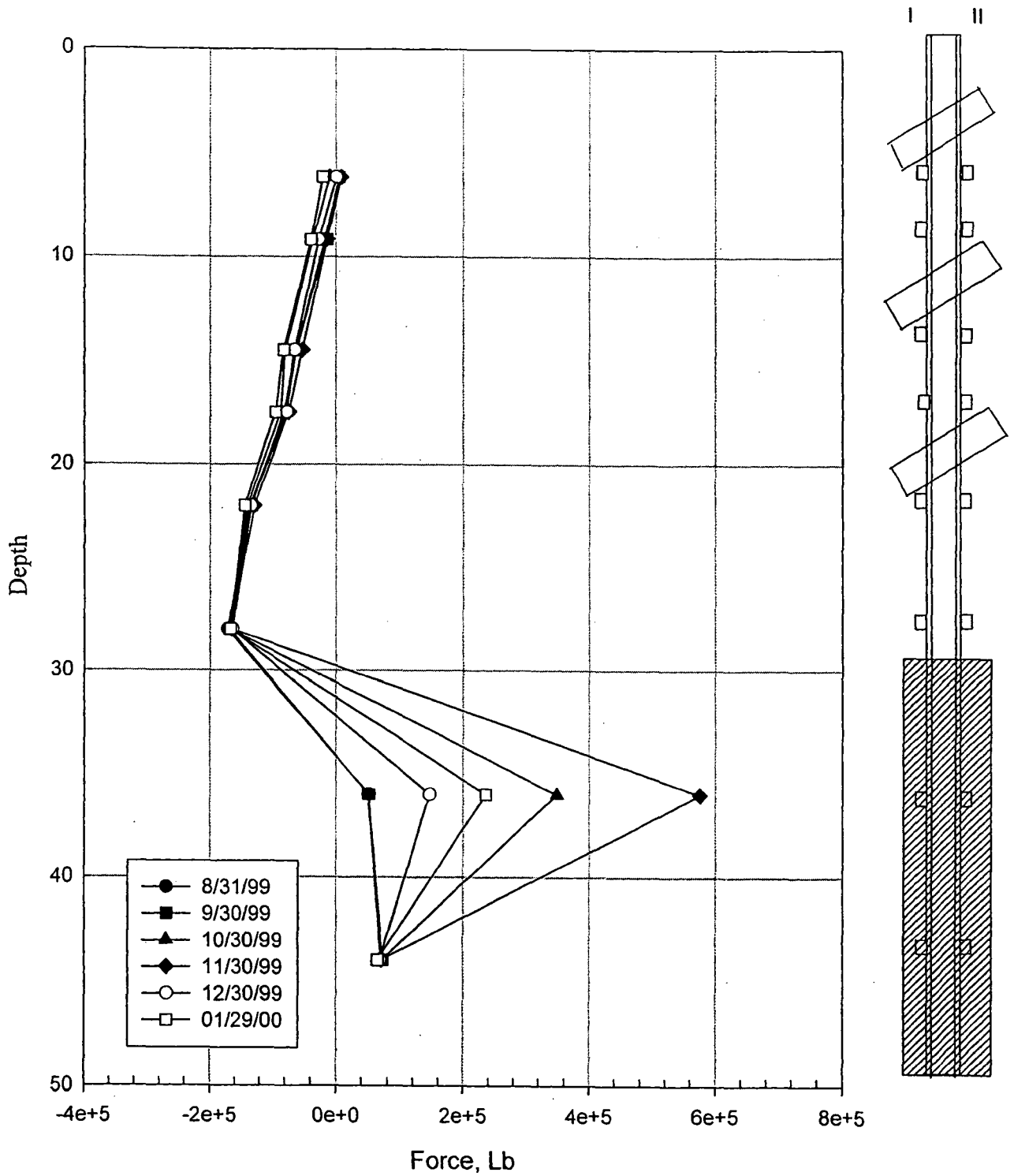


Fig. 4.63: Axial force vs. depth for soldier pile # 31 till 1/29/2000.



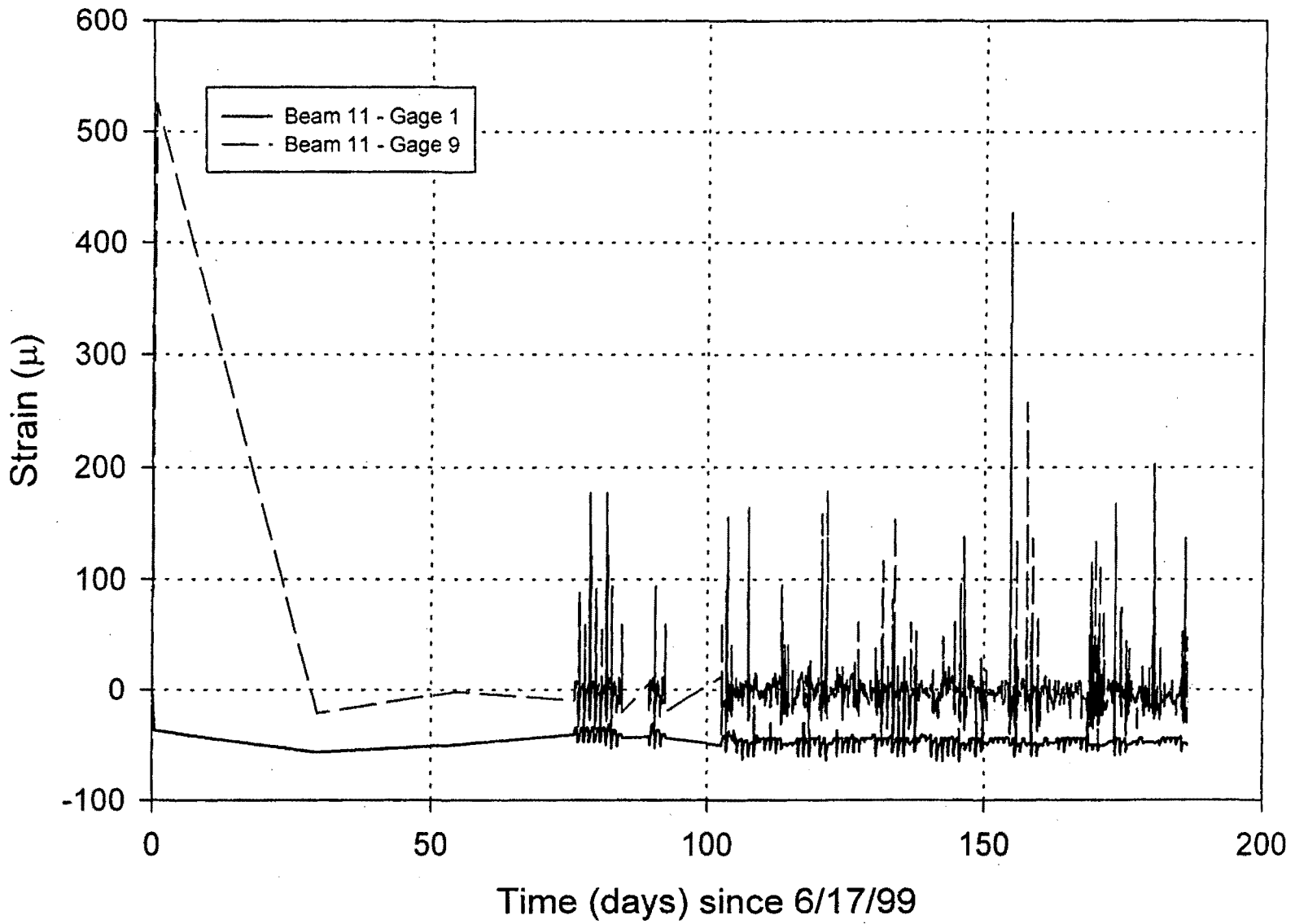


Fig. 4.64: Strain vs .time in soldier beam # 11 from gages 4' from top.

5

08-VI

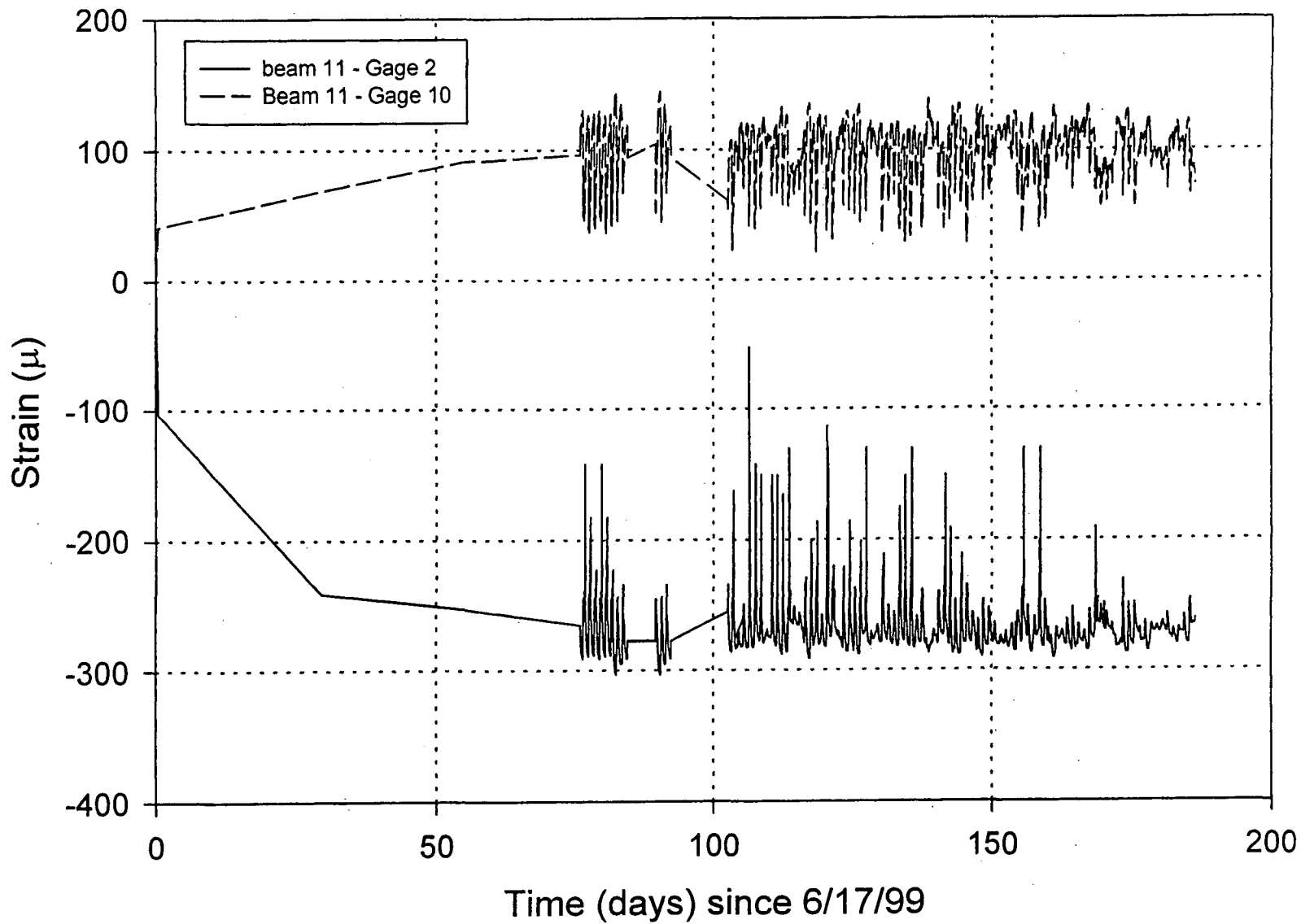


Fig. 4.65: Strain vs .time in soldier beam # 11 from gages 10'- 4" from top.



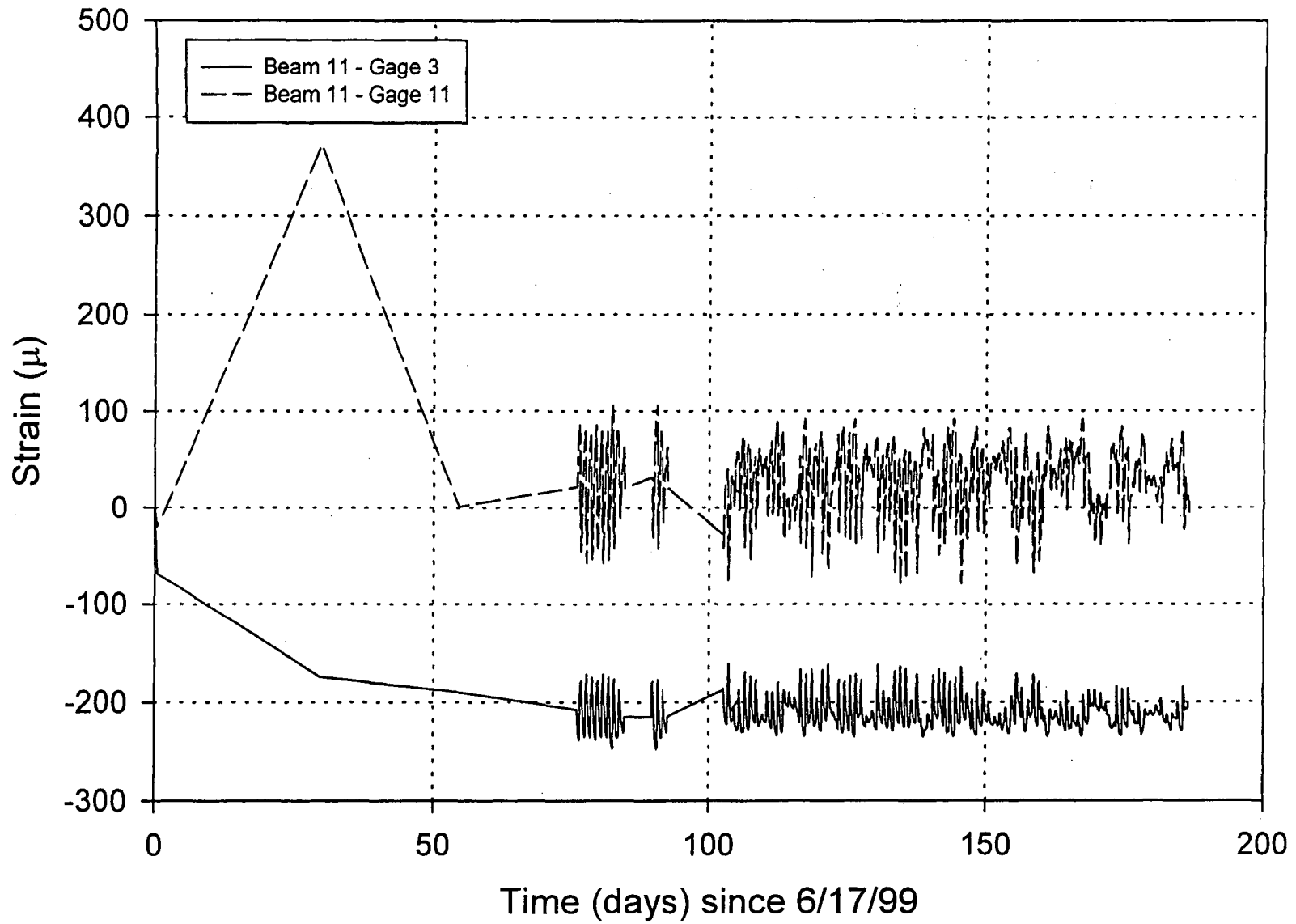


Fig. 4.66: Strain vs .time in soldier beam # 11 from gages 14'- 4" from top.



IV-85

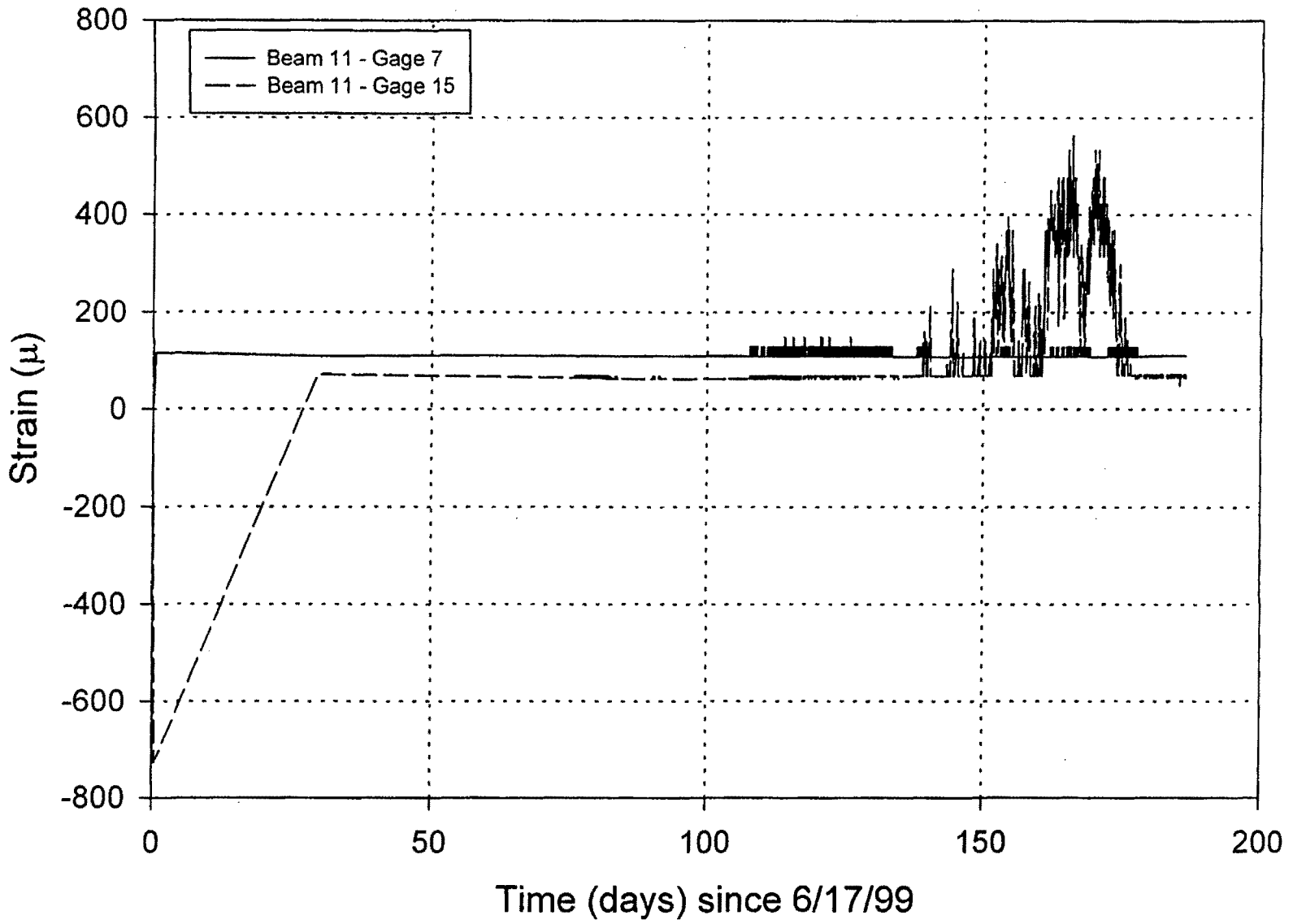


Fig. 4.70: Strain vs .time in soldier beam # 11 from gages 36'- 6" from top.



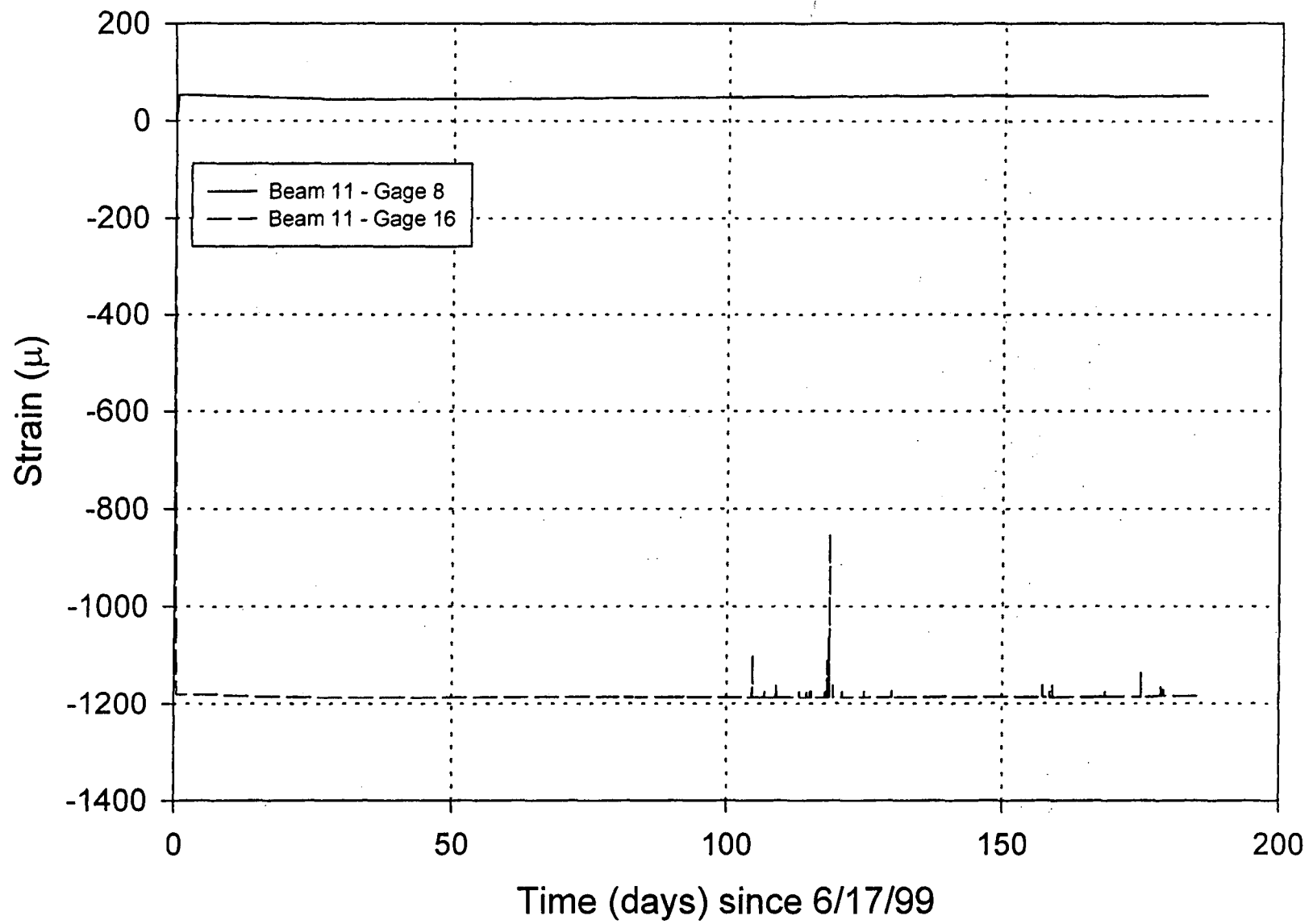


Fig. 4.71: Strain vs .time in soldier beam # 11 from gages 41'- 6" from top.



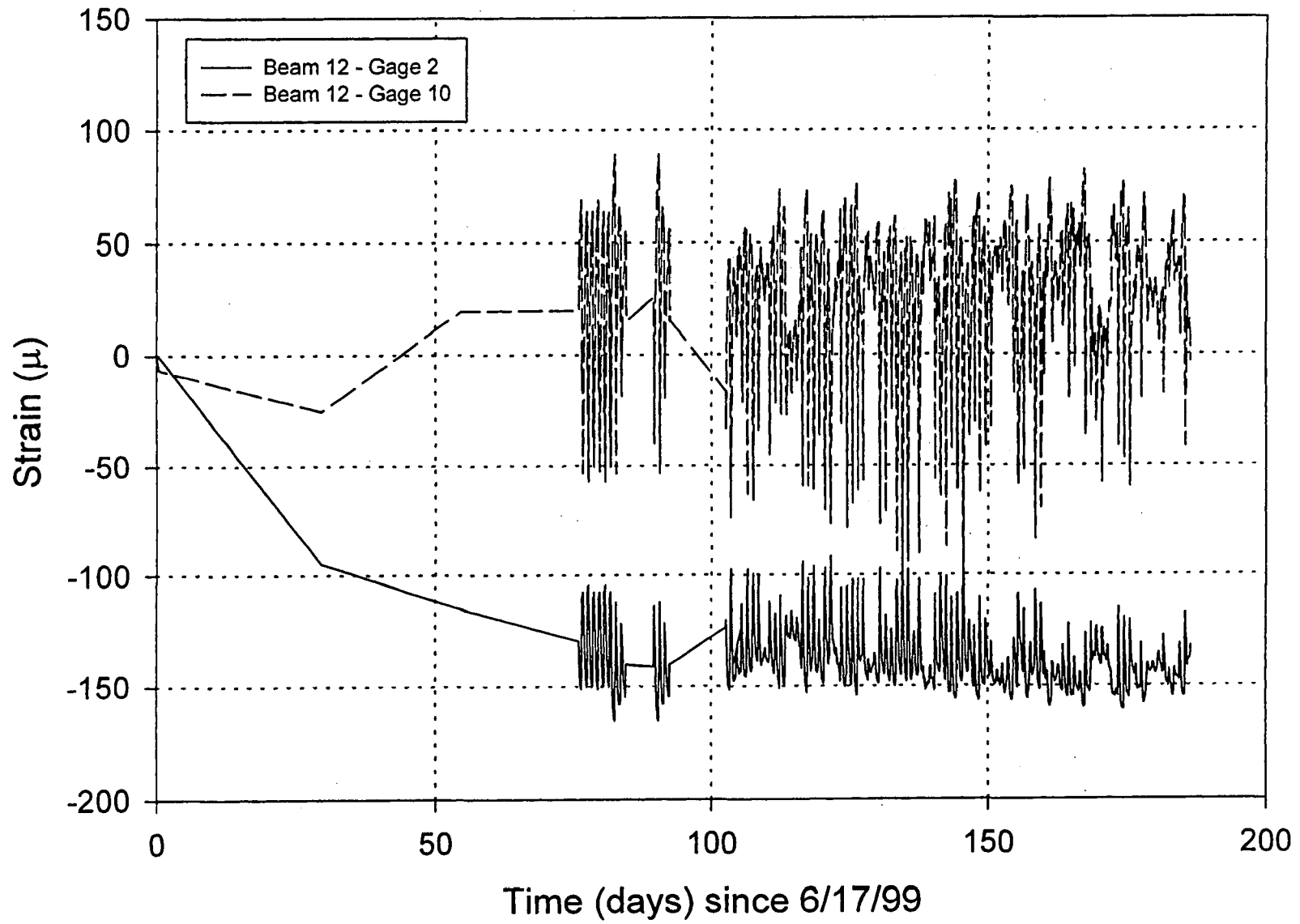


Fig. 4.73: Strain vs .time in soldier beam # 12 from gages 10'- 4" from top.



06-11

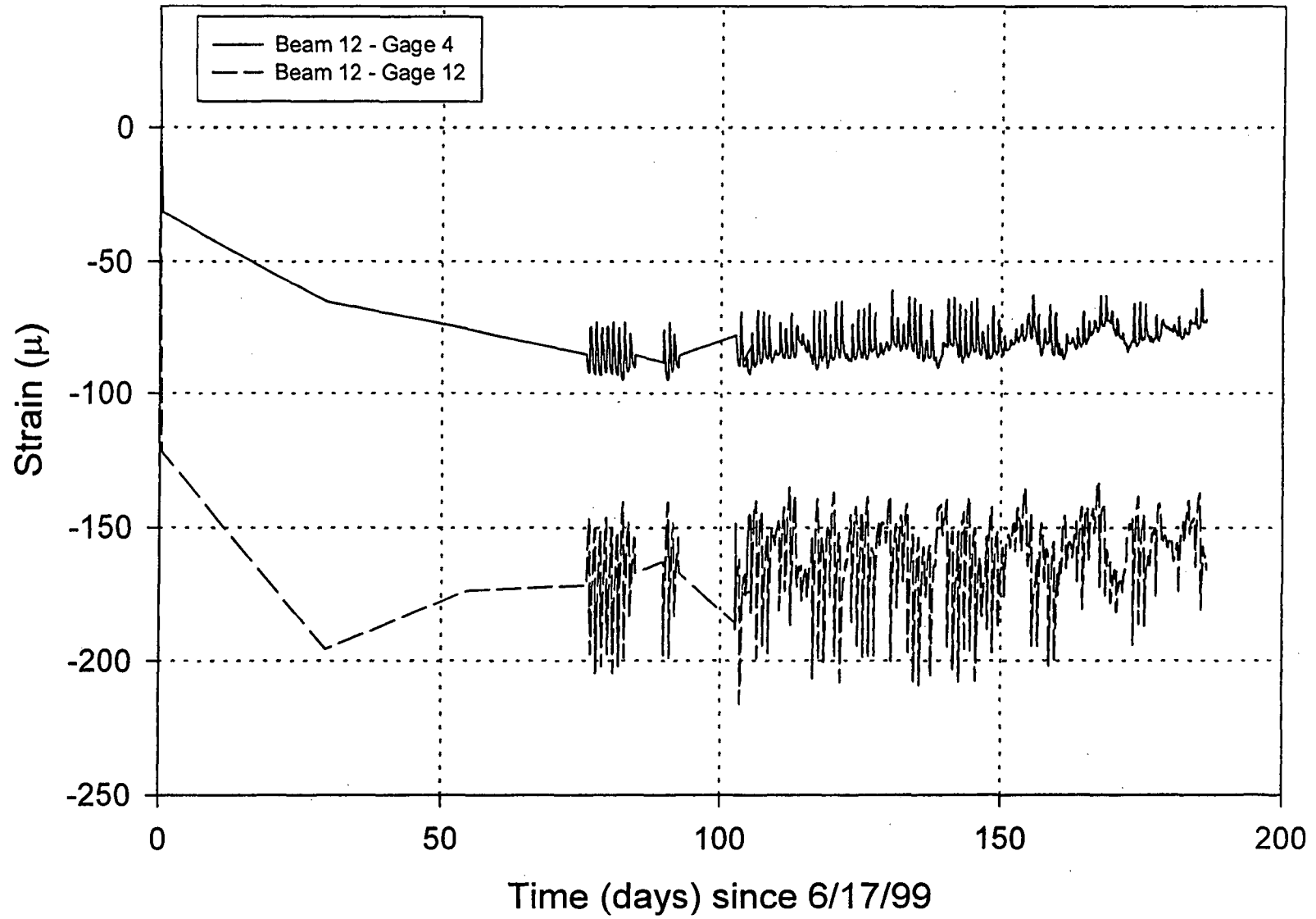


Fig. 4.75: Strain vs .time in soldier beam # 12 from gages 21'- 6" from top.

1
2
3
4
5
6
7
8
9
10
11
12
13
14
15
16
17
18
19
20
21
22
23
24
25
26
27
28
29
30
31
32
33
34
35
36
37
38
39
40
41
42
43
44
45
46
47
48
49
50
51
52
53
54
55
56
57
58
59
60
61
62
63
64
65
66
67
68
69
70
71
72
73
74
75
76
77
78
79
80
81
82
83
84
85
86
87
88
89
90
91
92
93
94
95
96
97
98
99
100

IV-91

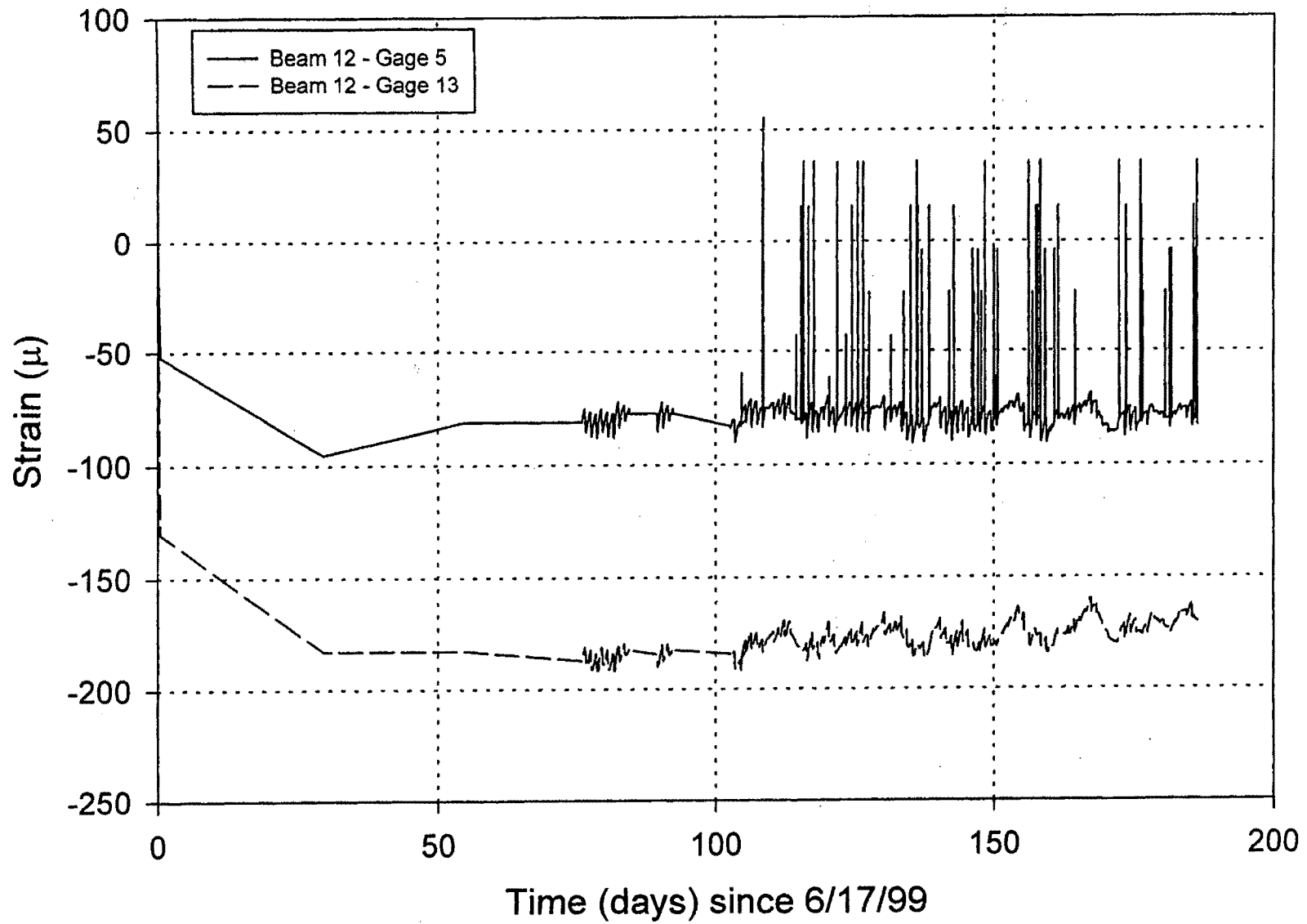


Fig. 4.76: Strain vs .time in soldier beam # 12 from gages 26'- 6" from top.



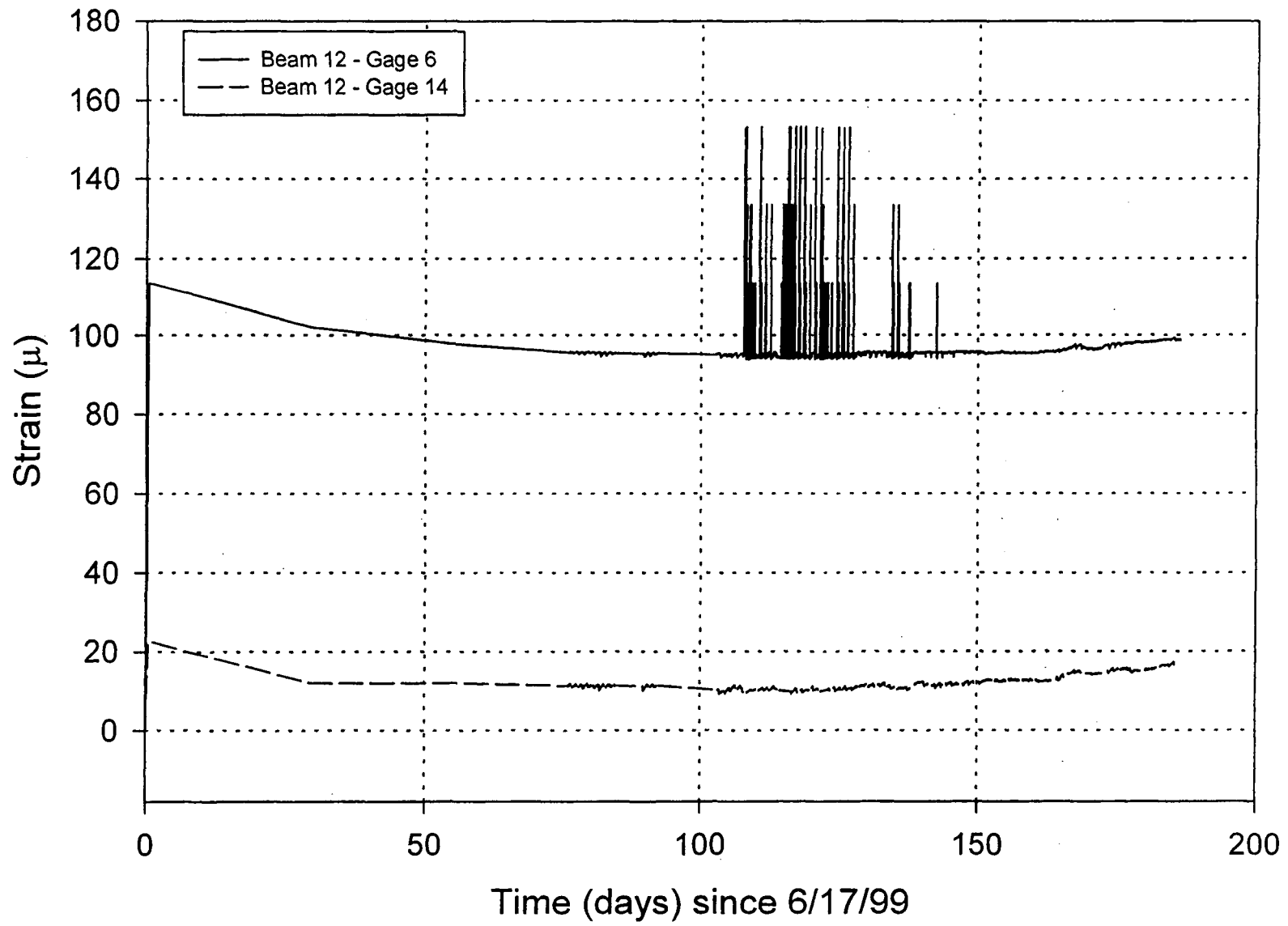


Fig. 4.77: Strain vs. time in soldier beam # 12 from gages 31'- 6" from top.



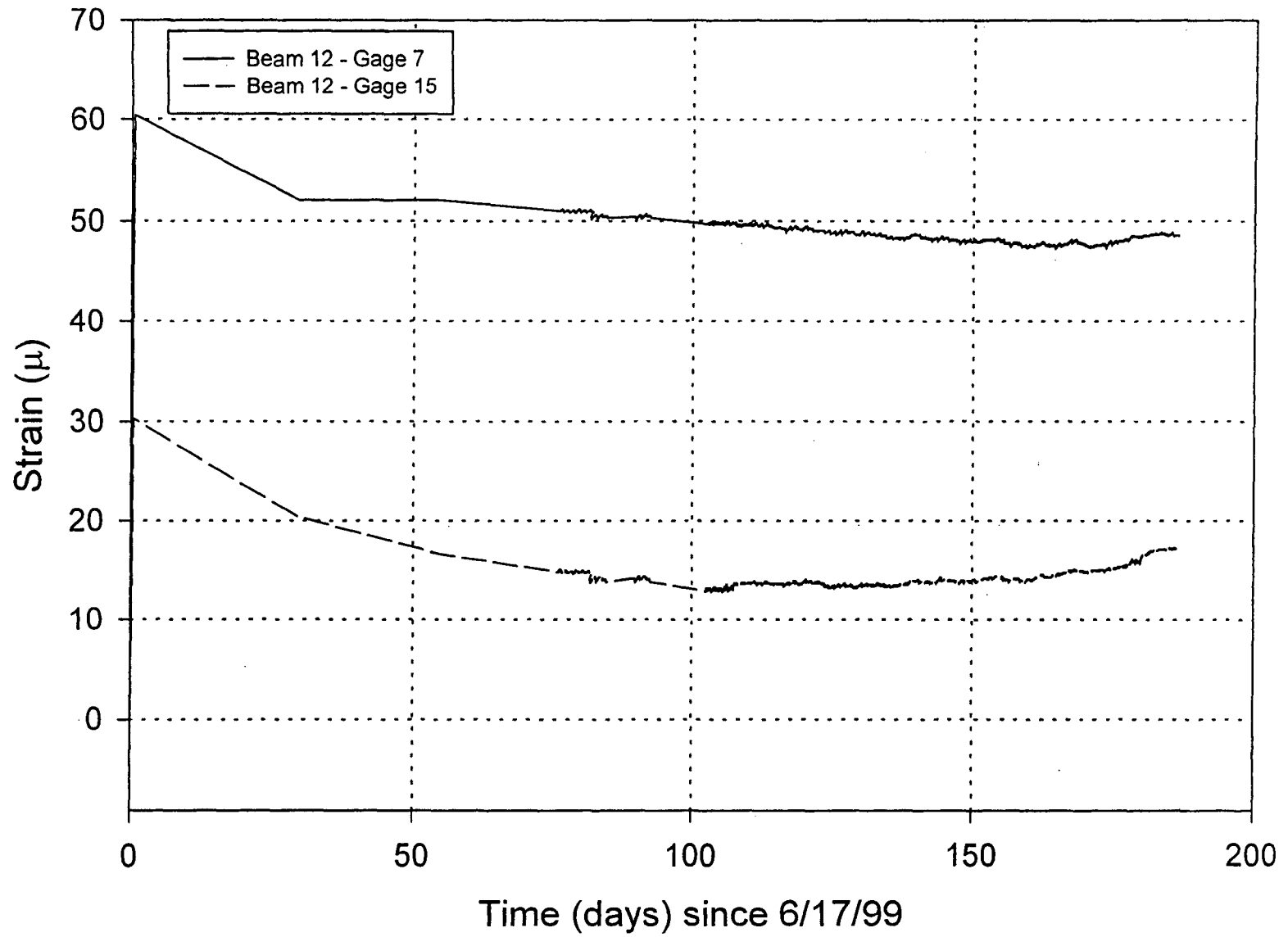


Fig. 4.78: Strain vs .time in soldier beam # 12 from gages 36'- 6" from top.

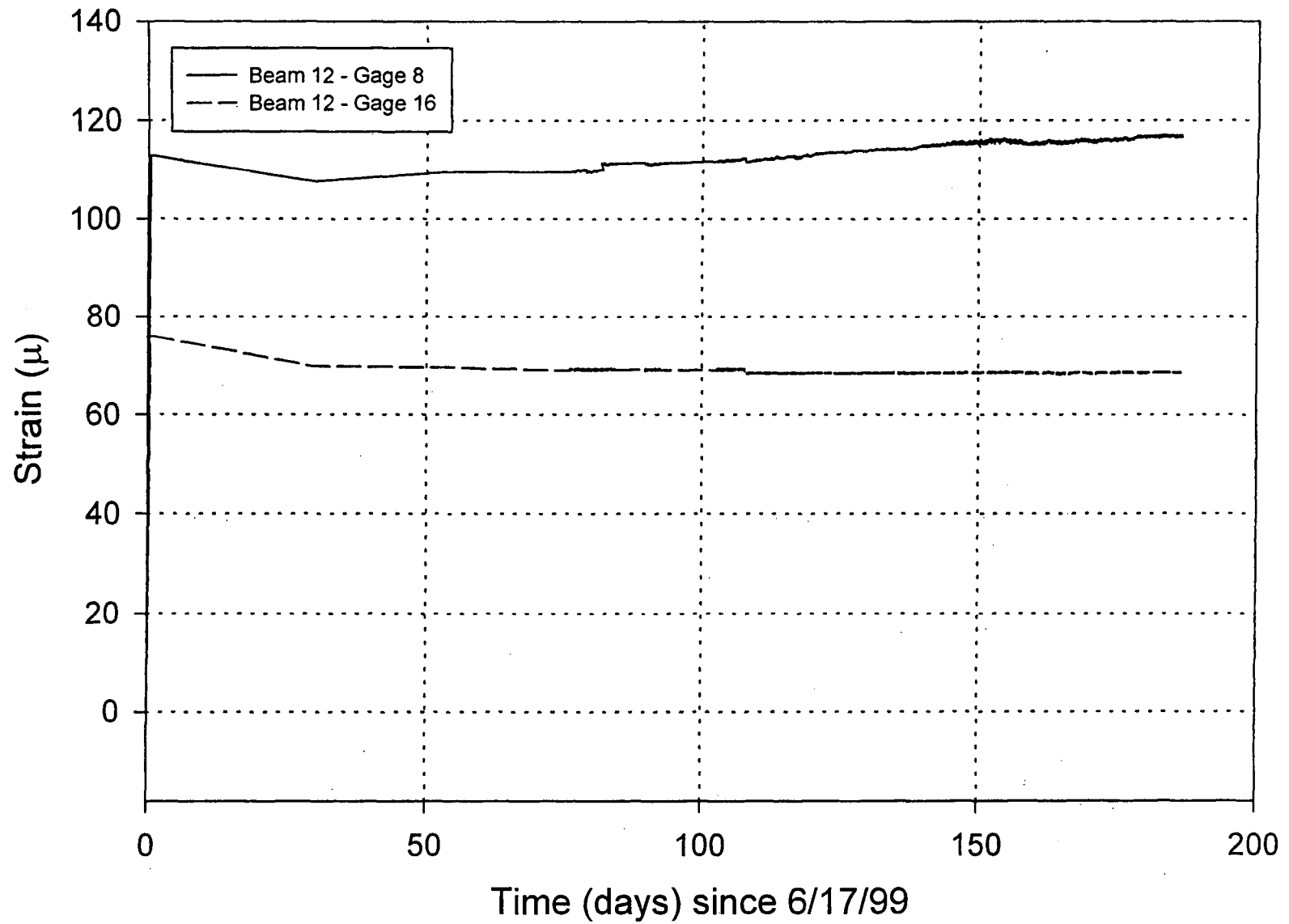


Fig. 4.79: Strain vs .time in soldier beam # 12 from gages 41'- 6" from top.

S6-VI

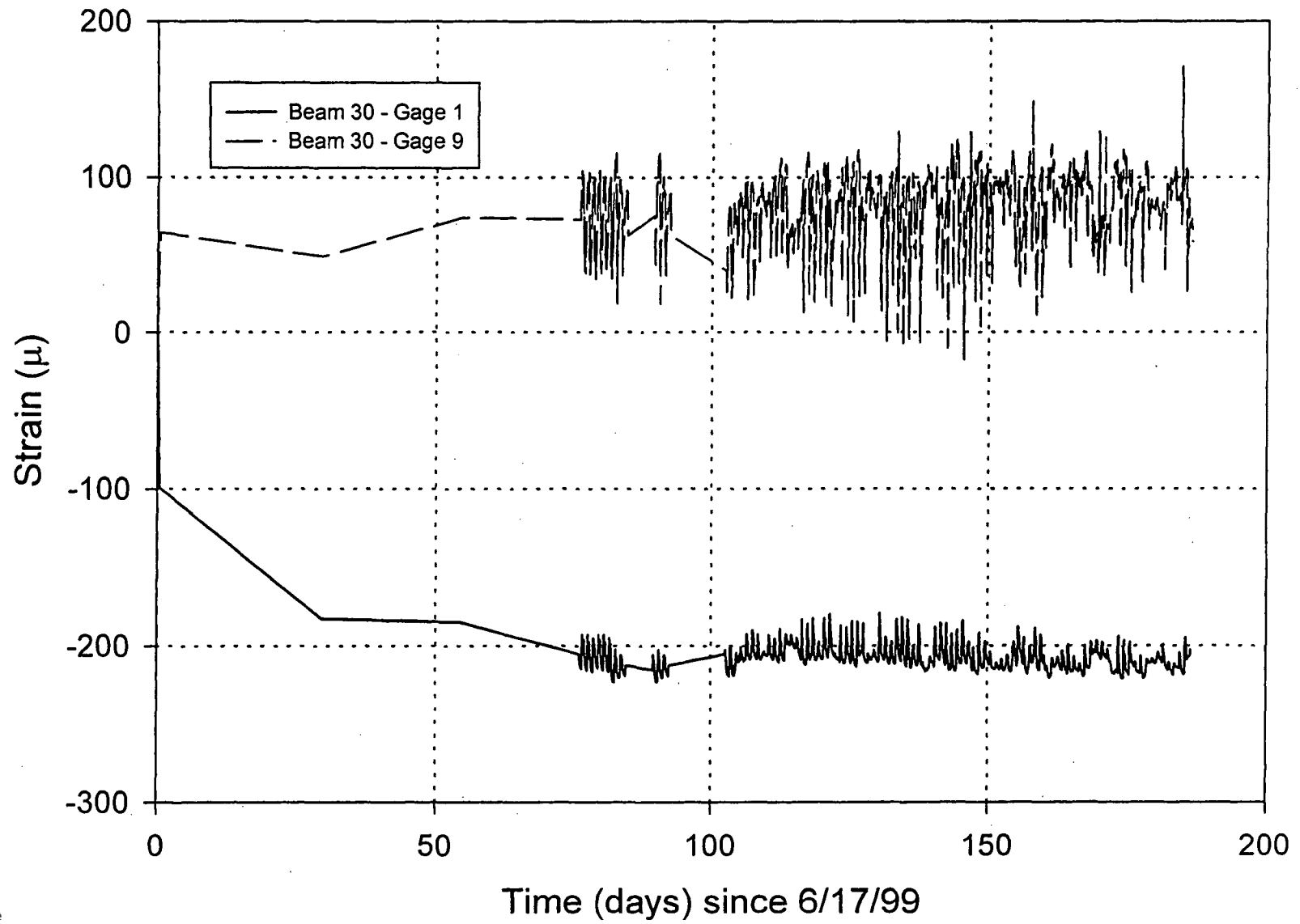


Fig. 4.80: Strain vs .time in soldier beam # 30 from gages 6'-2" from top.

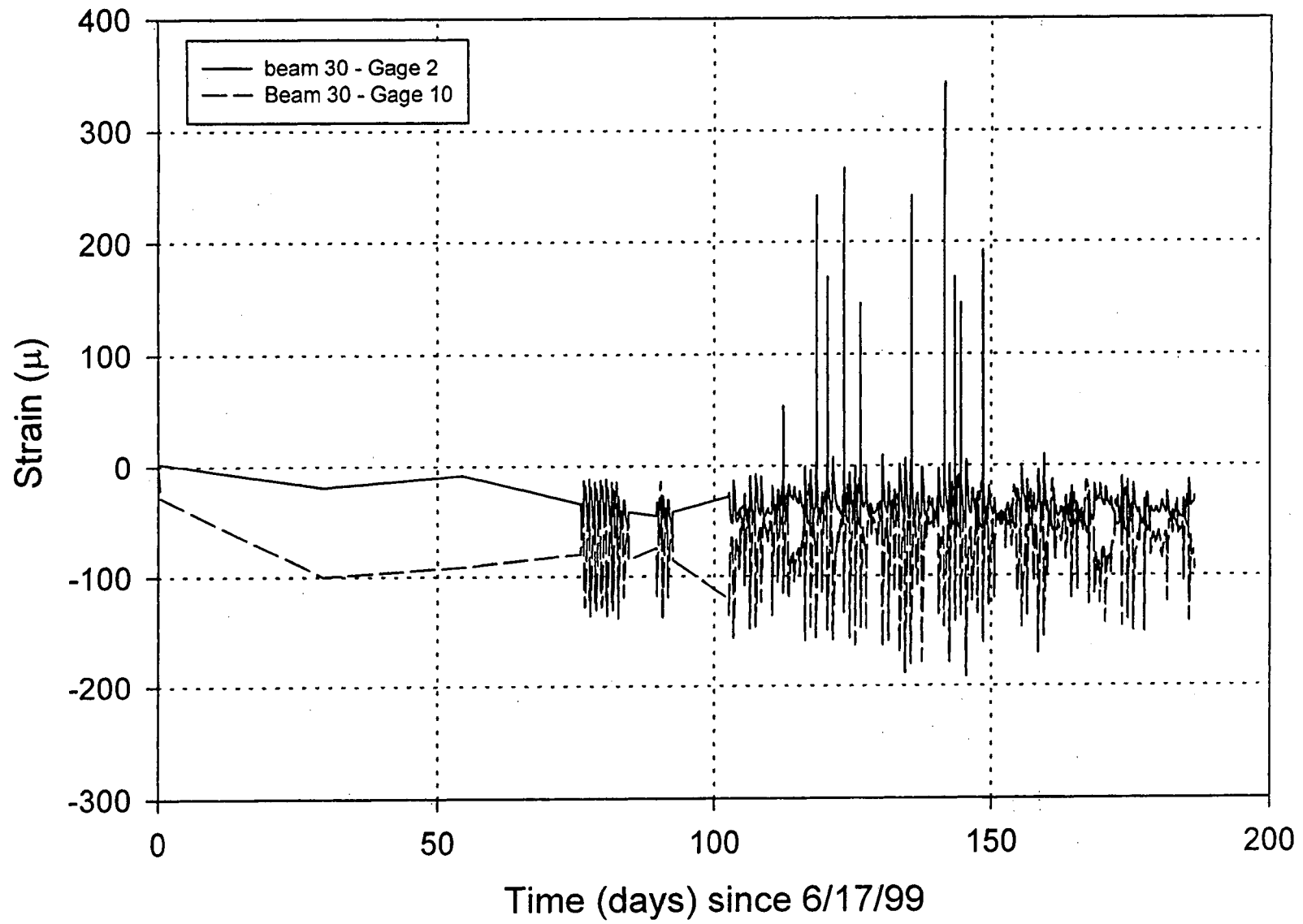


Fig. 4.81: Strain vs .time in soldier beam # 30 from gages 9'- 2" from top.

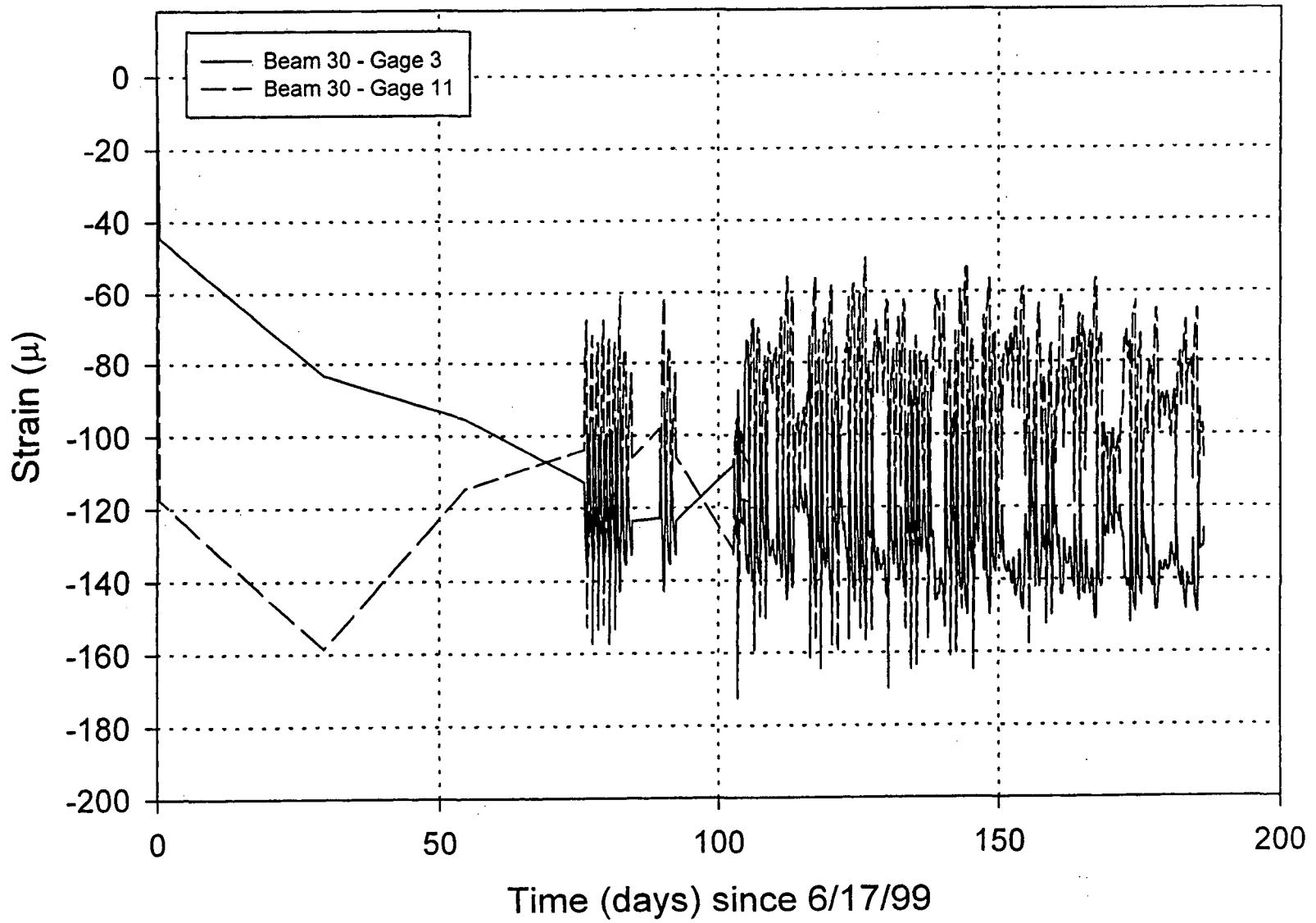


Fig. 4.82: Strain vs. time in soldier beam # 30 from gages 14'- 6" from top.

86-11

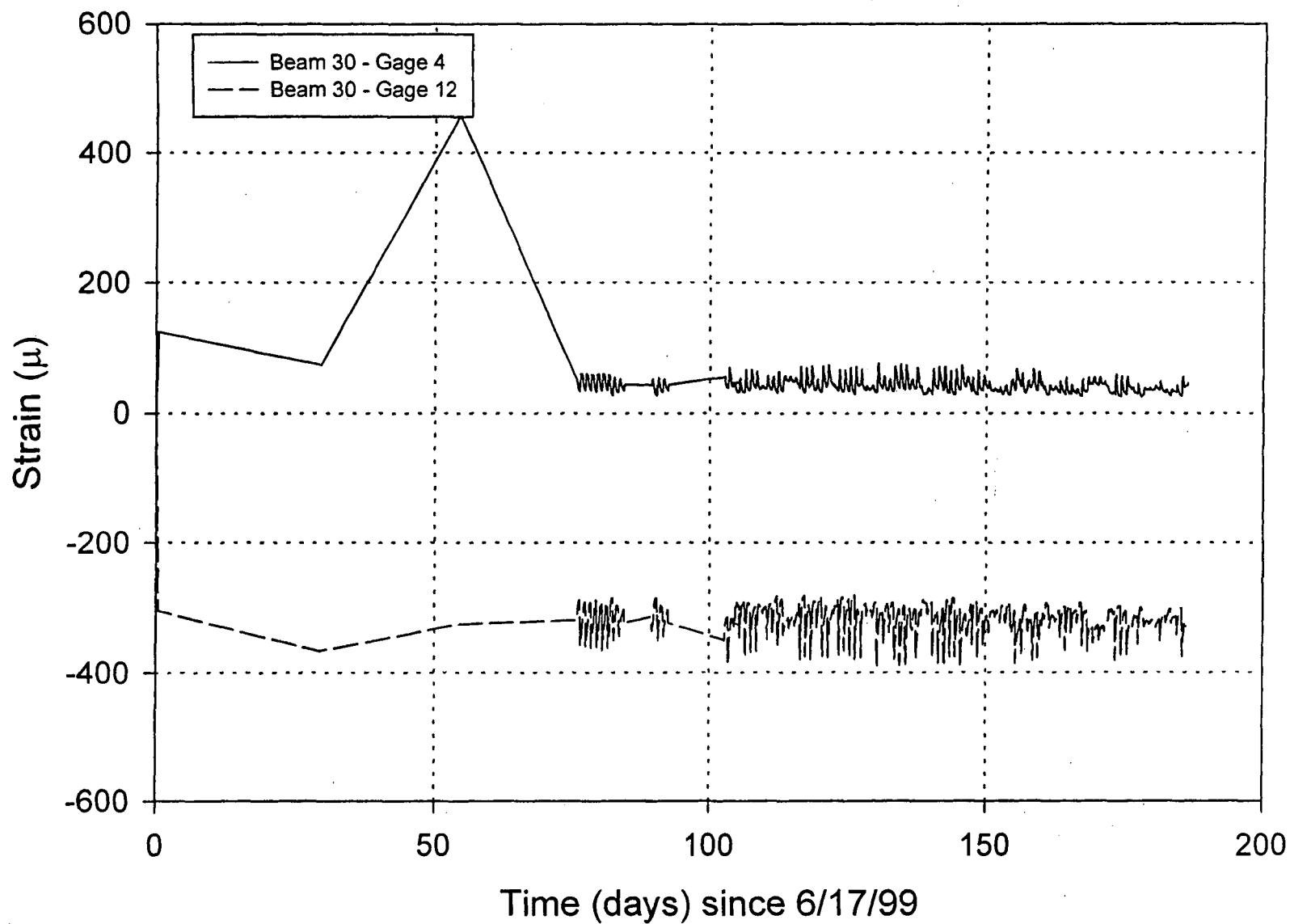


Fig. 4.83: Strain vs .time in soldier beam # 30 from gages 17'- 6" from top.



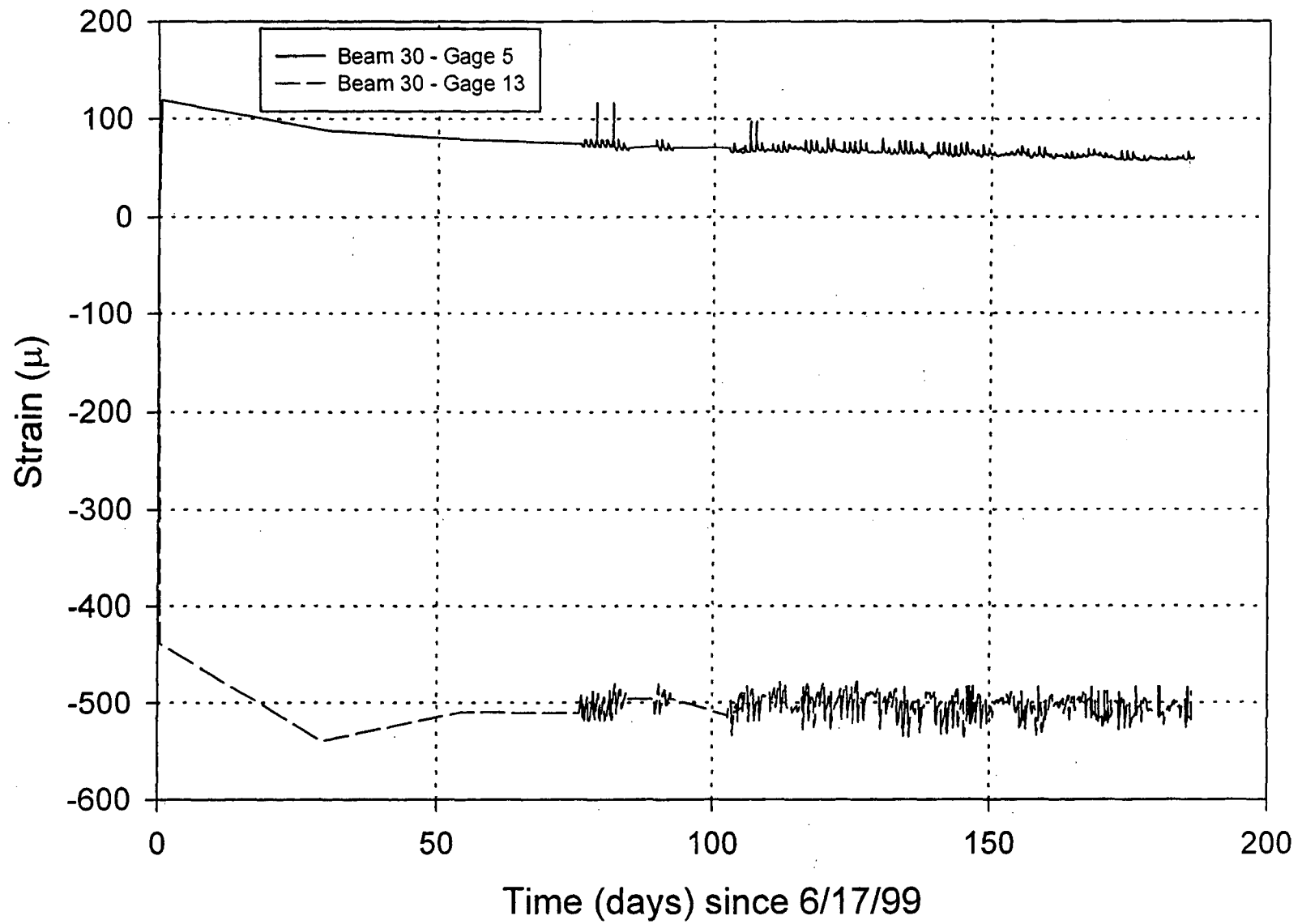


Fig. 4.84: Strain vs. time in soldier beam # 30 from gages 22'- 0" from top.



IV-100

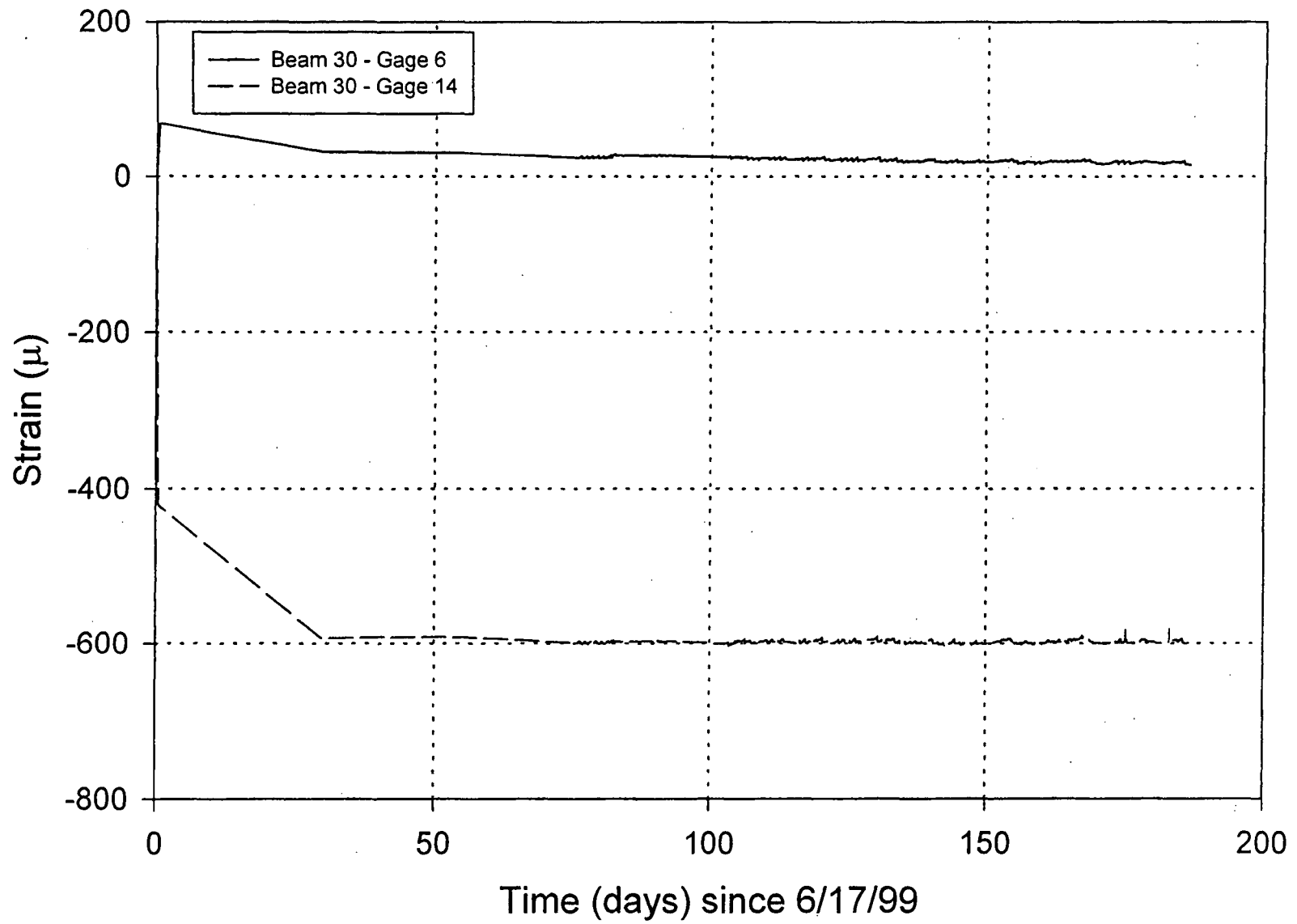


Fig. 4.85: Strain vs .time in soldier beam # 30 from gages 28'- 0" from top.



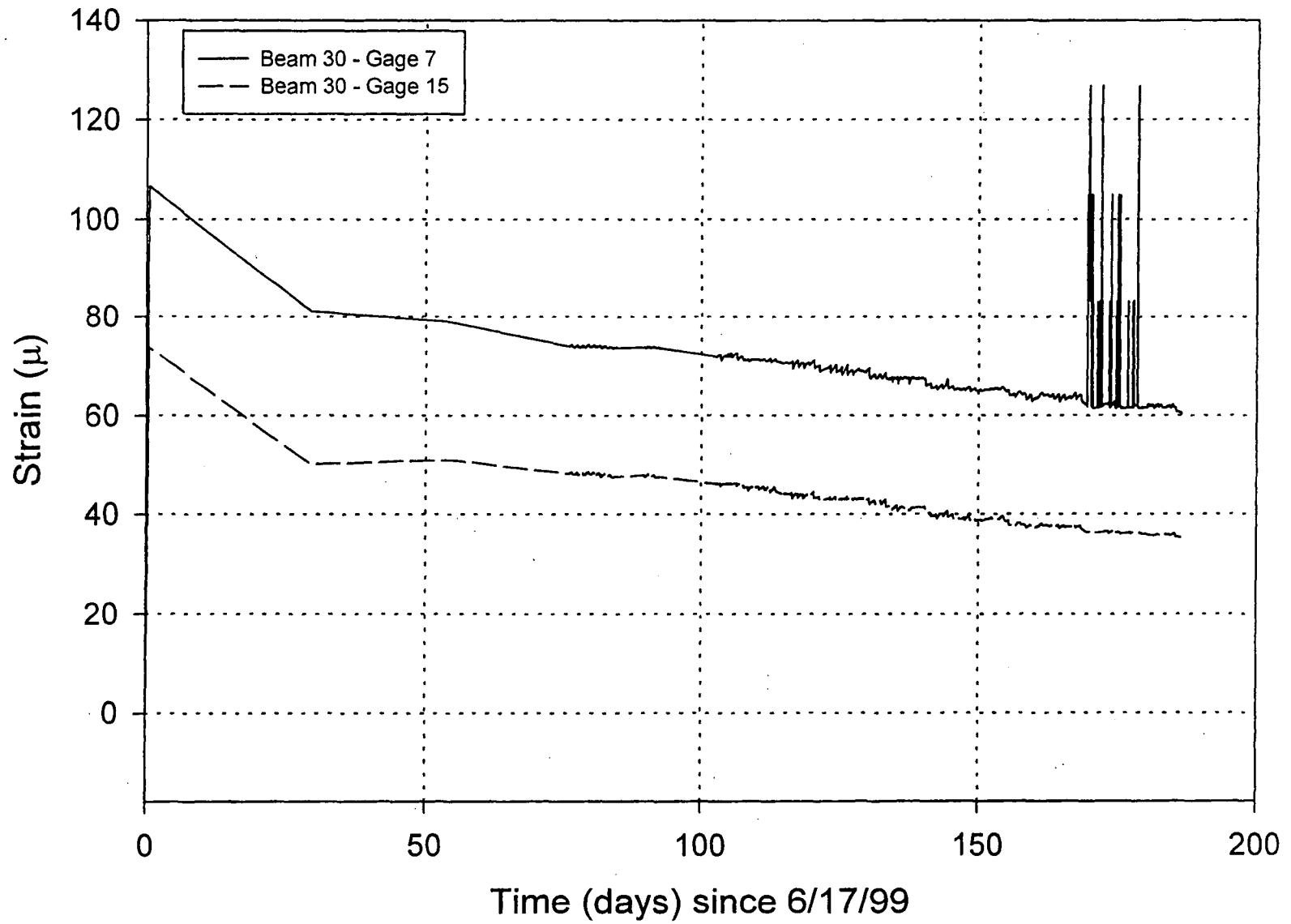


Fig. 4.86: Strain vs .time in soldier beam # 30 from gages 36'- 0" from top.

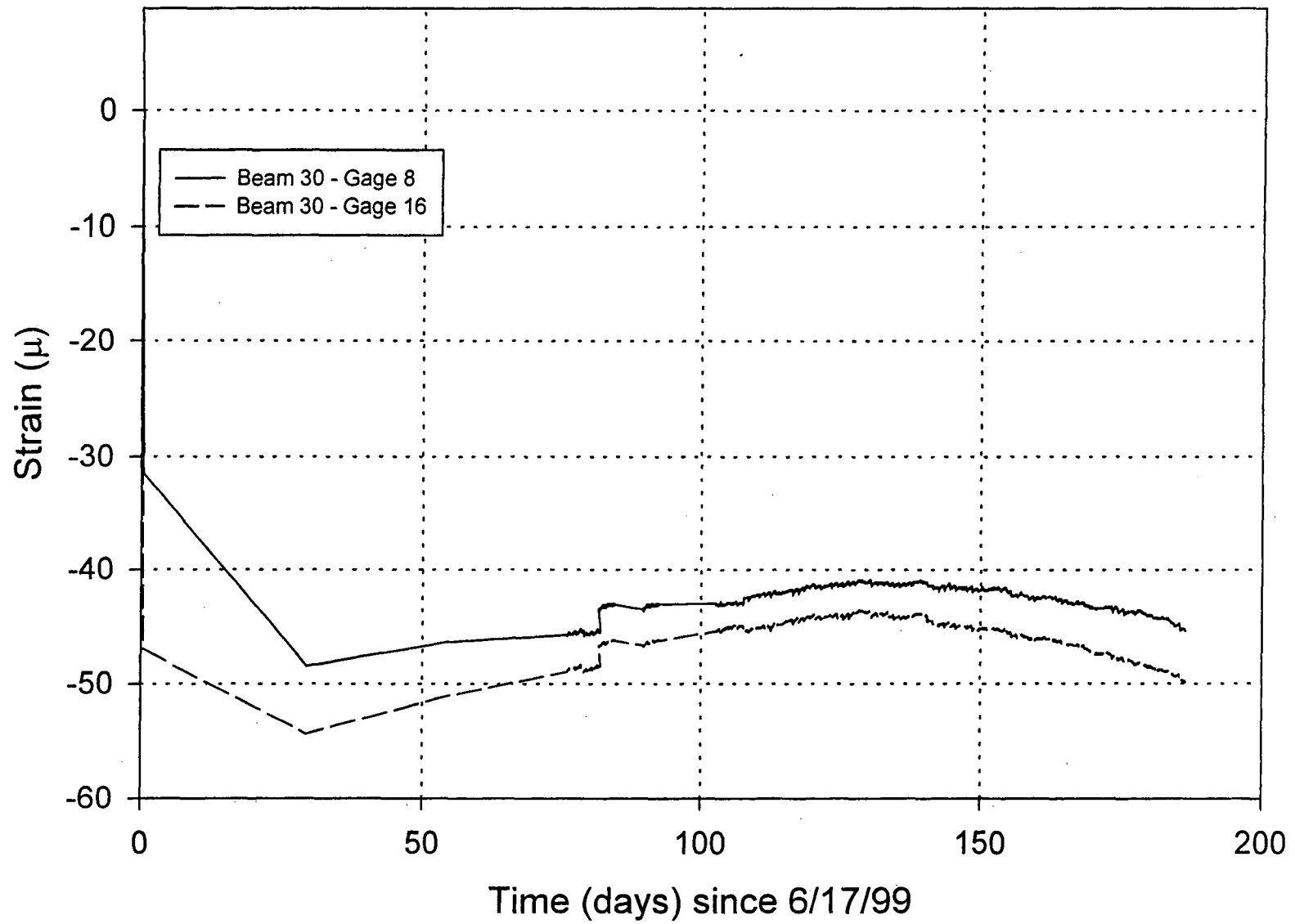


Fig. 4.87: Strain vs .time in soldier beam # 30 from gages 44'- 0" from top.

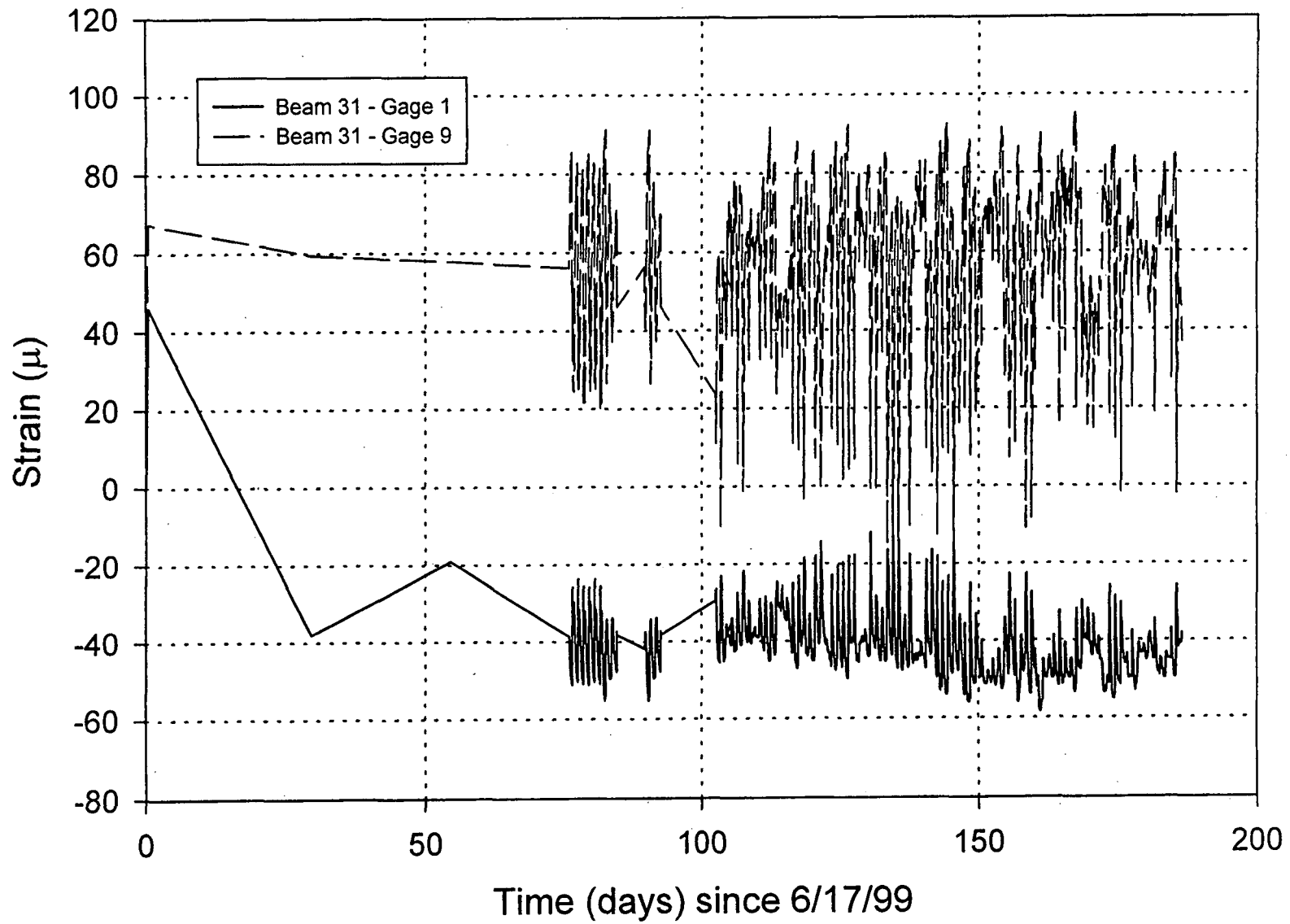
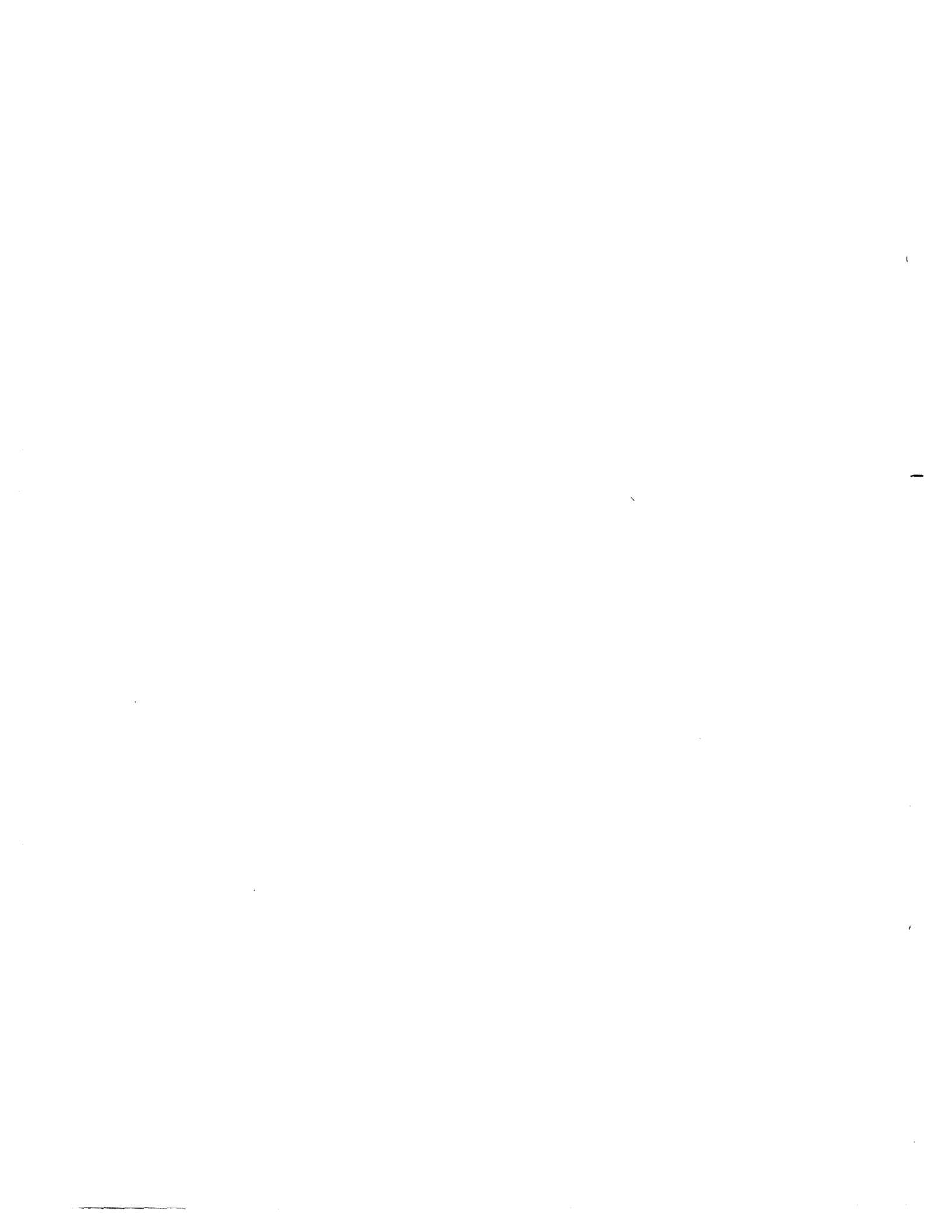


Fig. 4.88: Strain vs .time in soldier beam # 31 from gages 6'-2" from top.



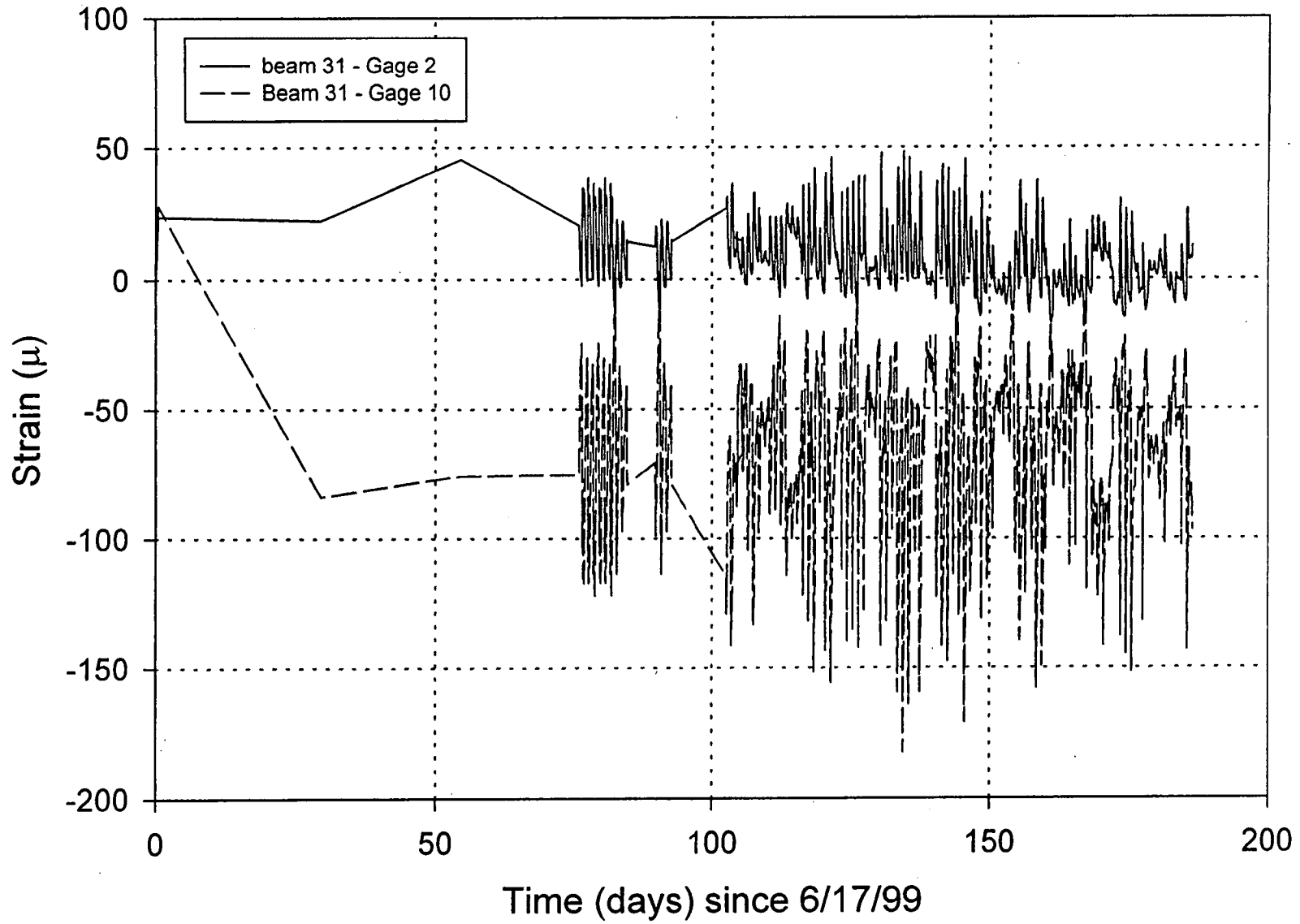


Fig. 4.89: Strain vs .time in soldier beam # 31 from gages 9'- 2" from top.

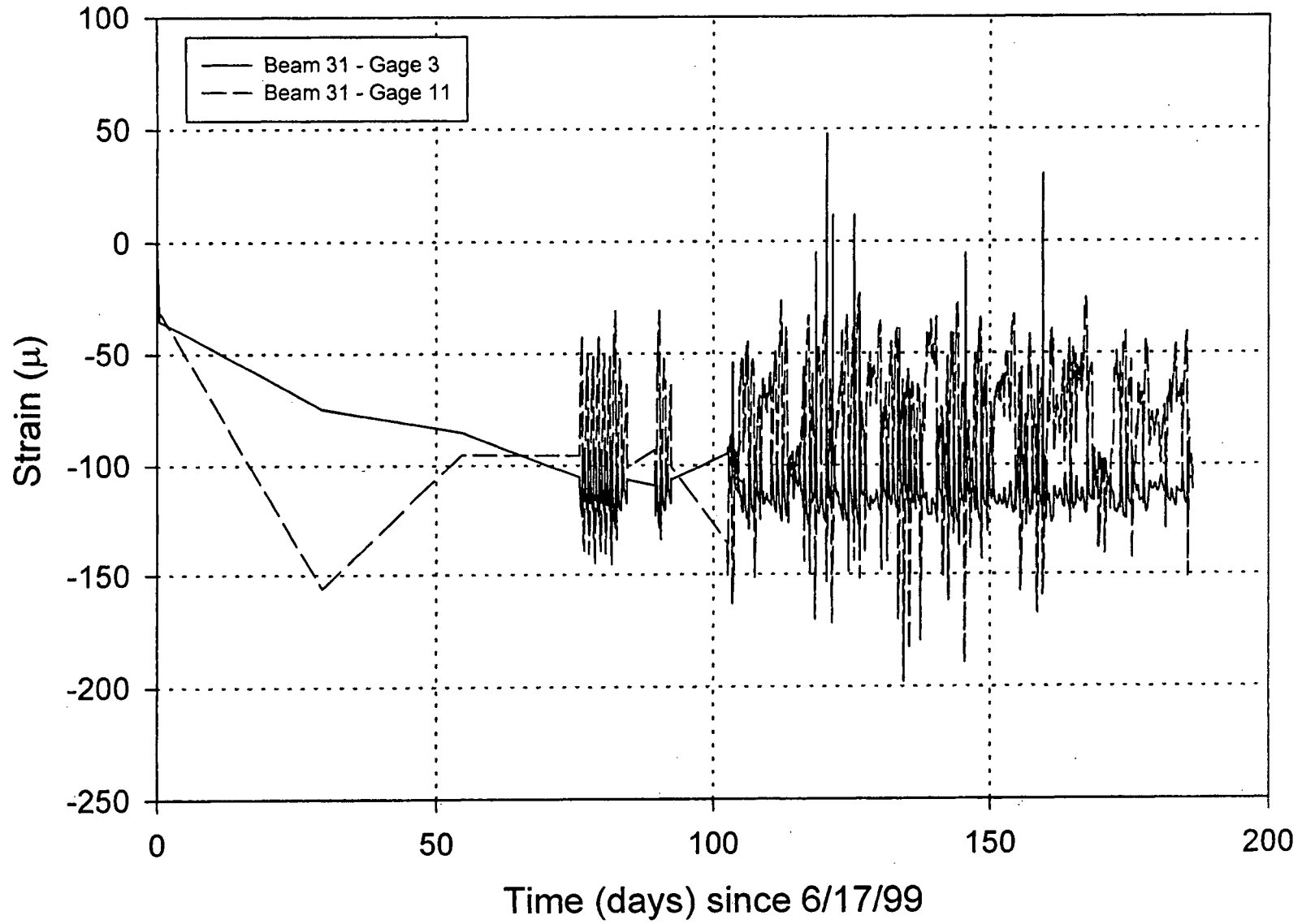


Fig. 4.90: Strain vs. time in soldier beam # 31 from gages 14'- 6" from top.

90I-VI

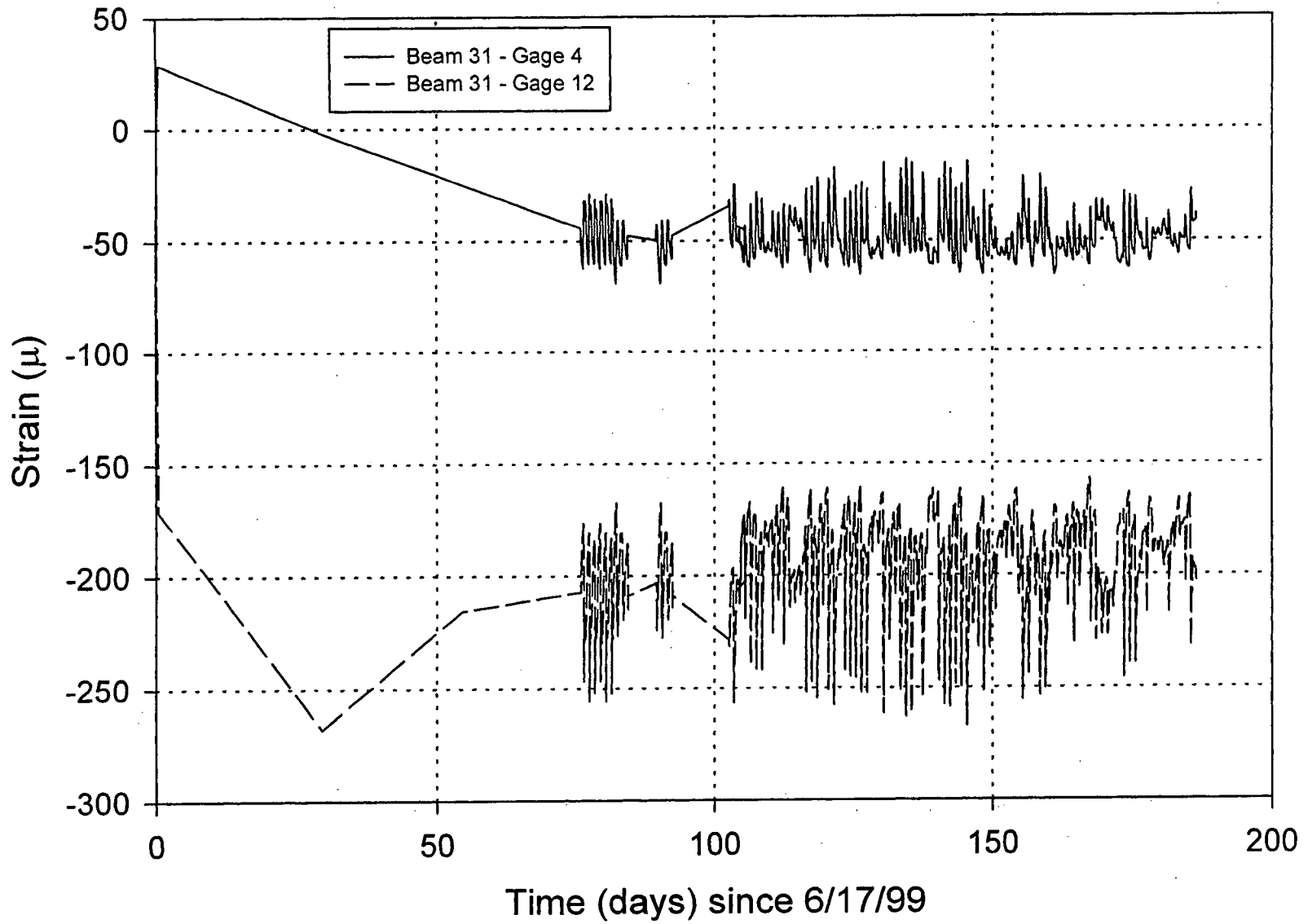
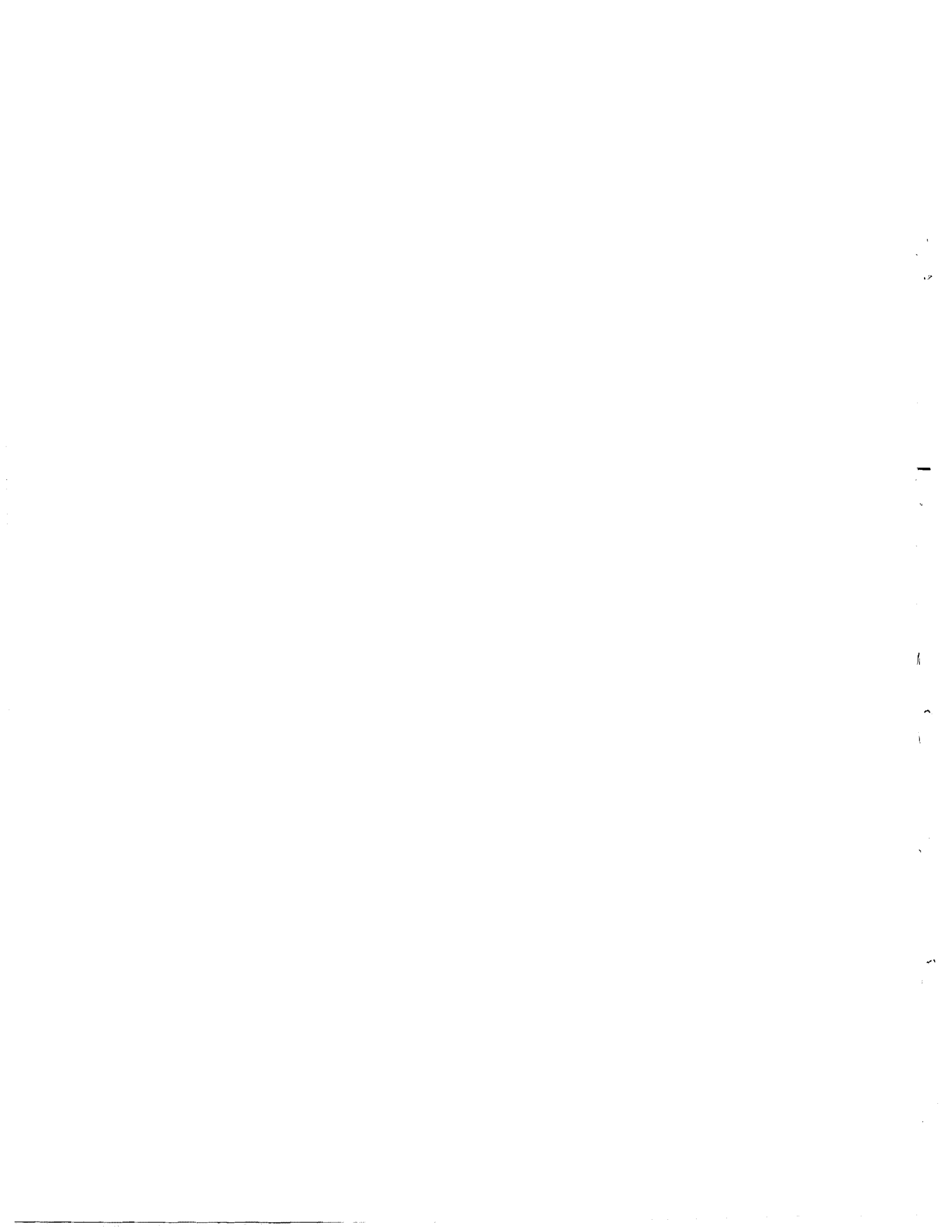


Fig. 4.91: Strain vs. time in soldier beam # 31 from gages 17'- 6" from top.



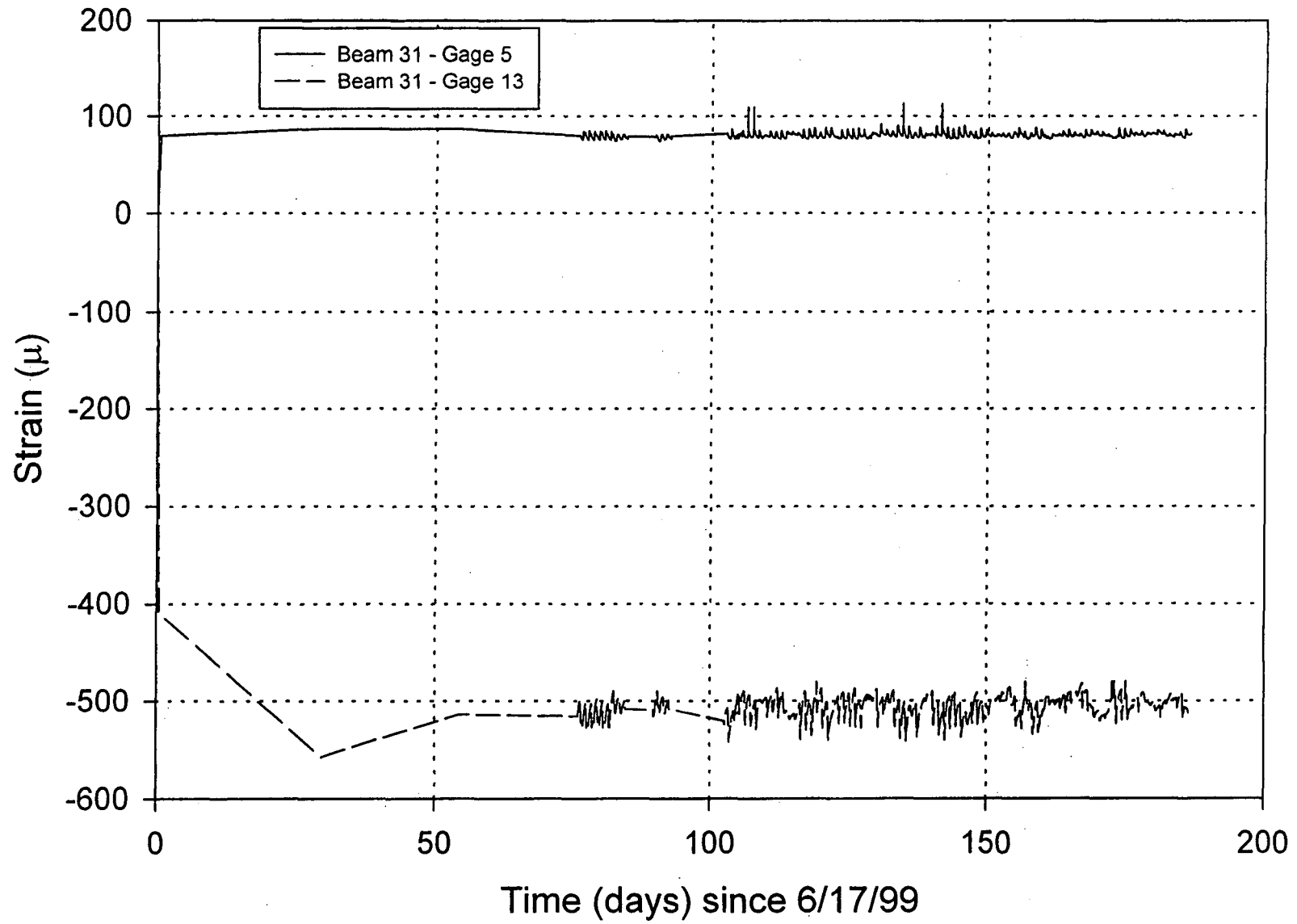


Fig. 4.92: Strain vs. time in soldier beam # 31 from gages 22'- 0" from top.



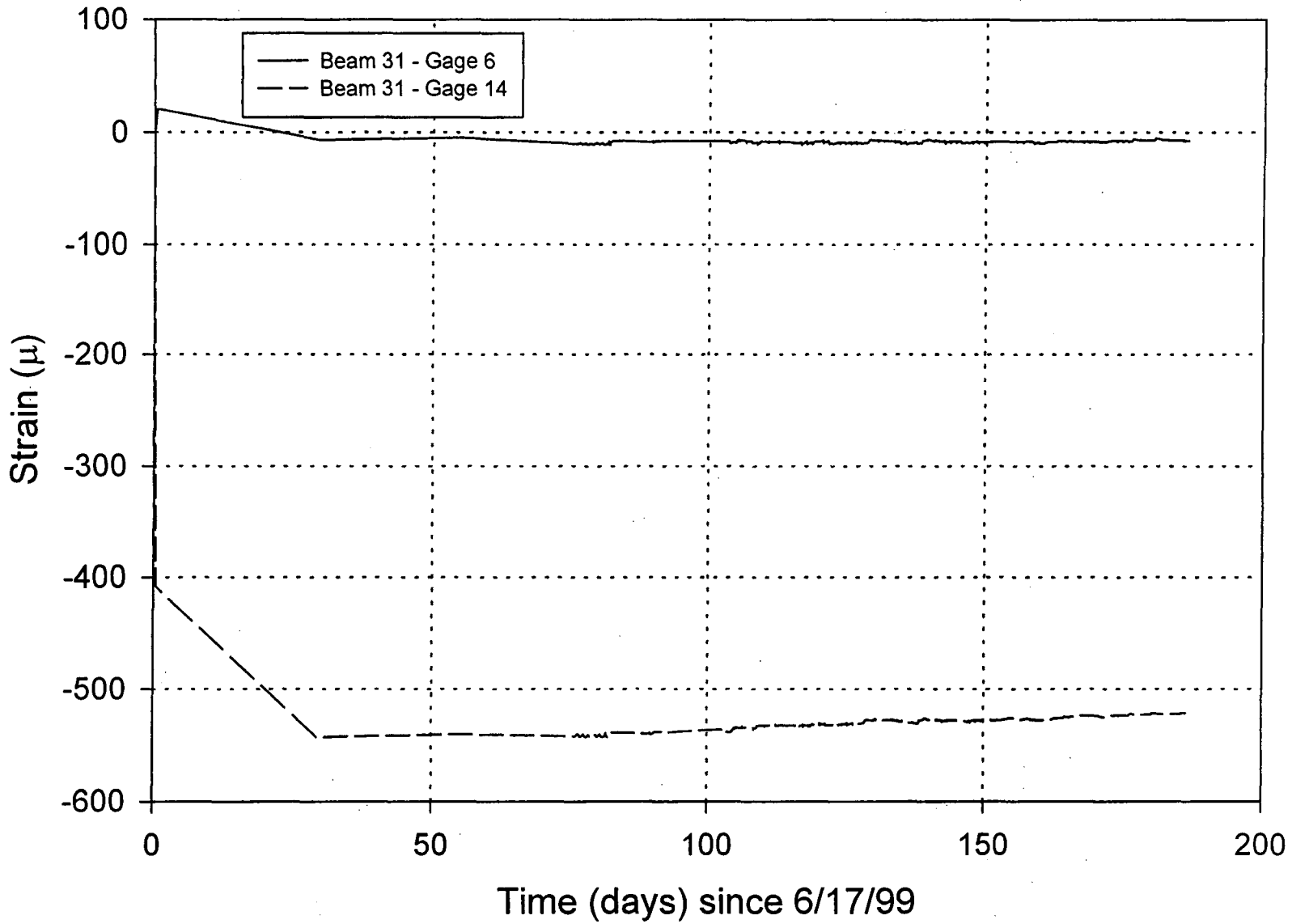


Fig. 4.93: Strain vs. time in soldier beam # 31 from gages 28'- 0" from top.



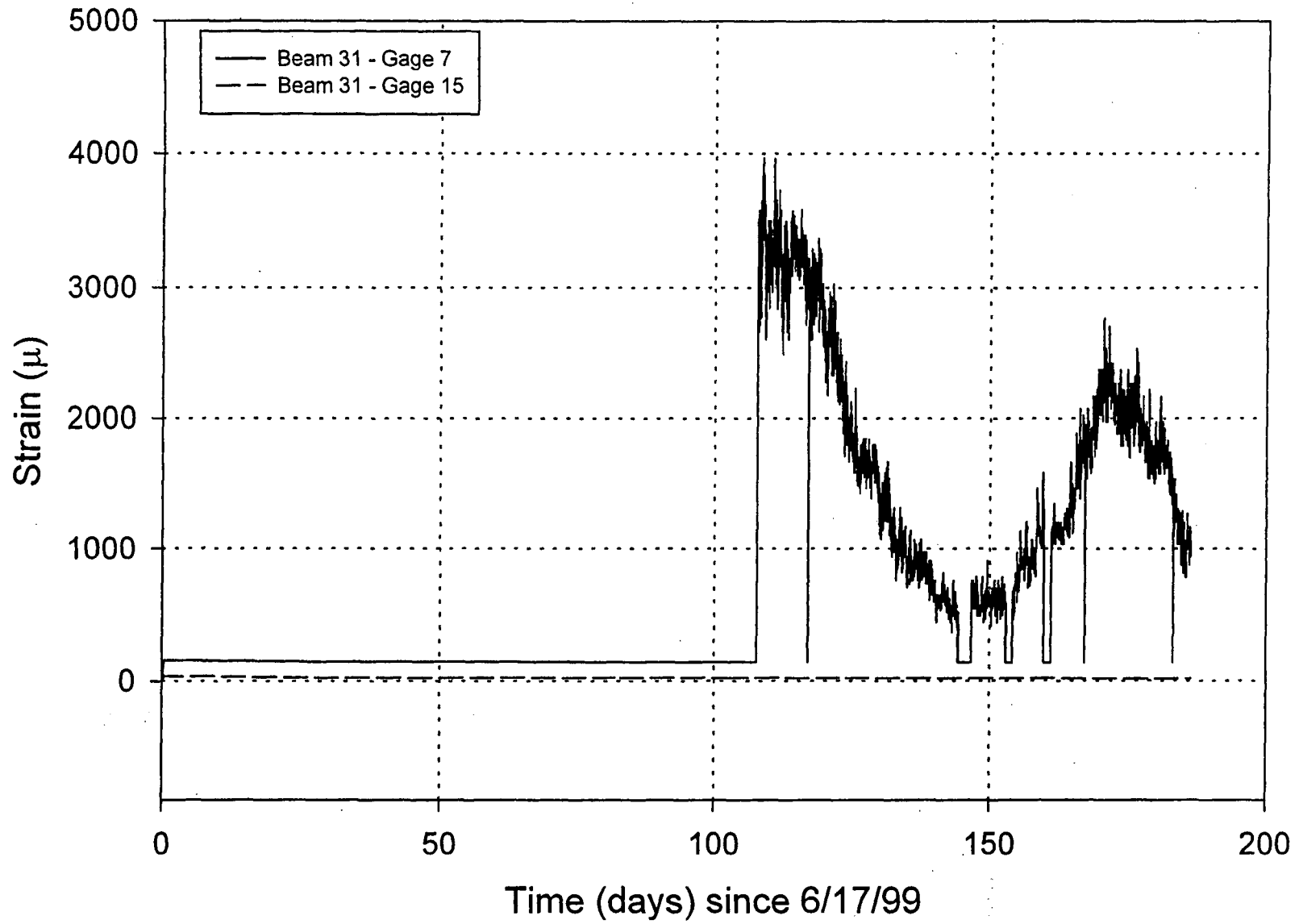


Fig. 4.94: Strain vs. time in soldier beam # 31 from gages 36'- 0" from top.



011-11

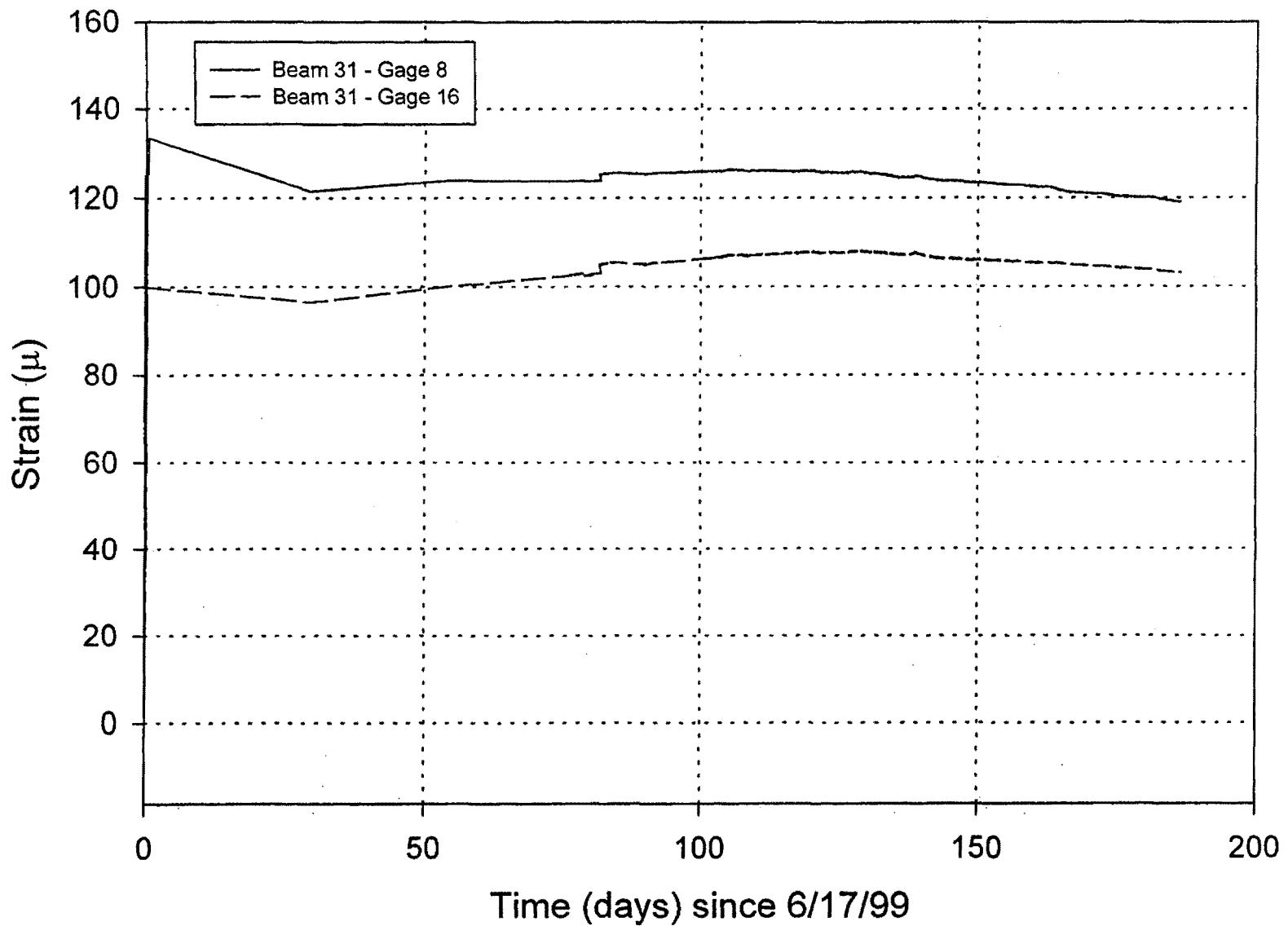


Fig. 4.95: Strain vs. time in soldier beam # 31 from gages 44'- 0" from top.



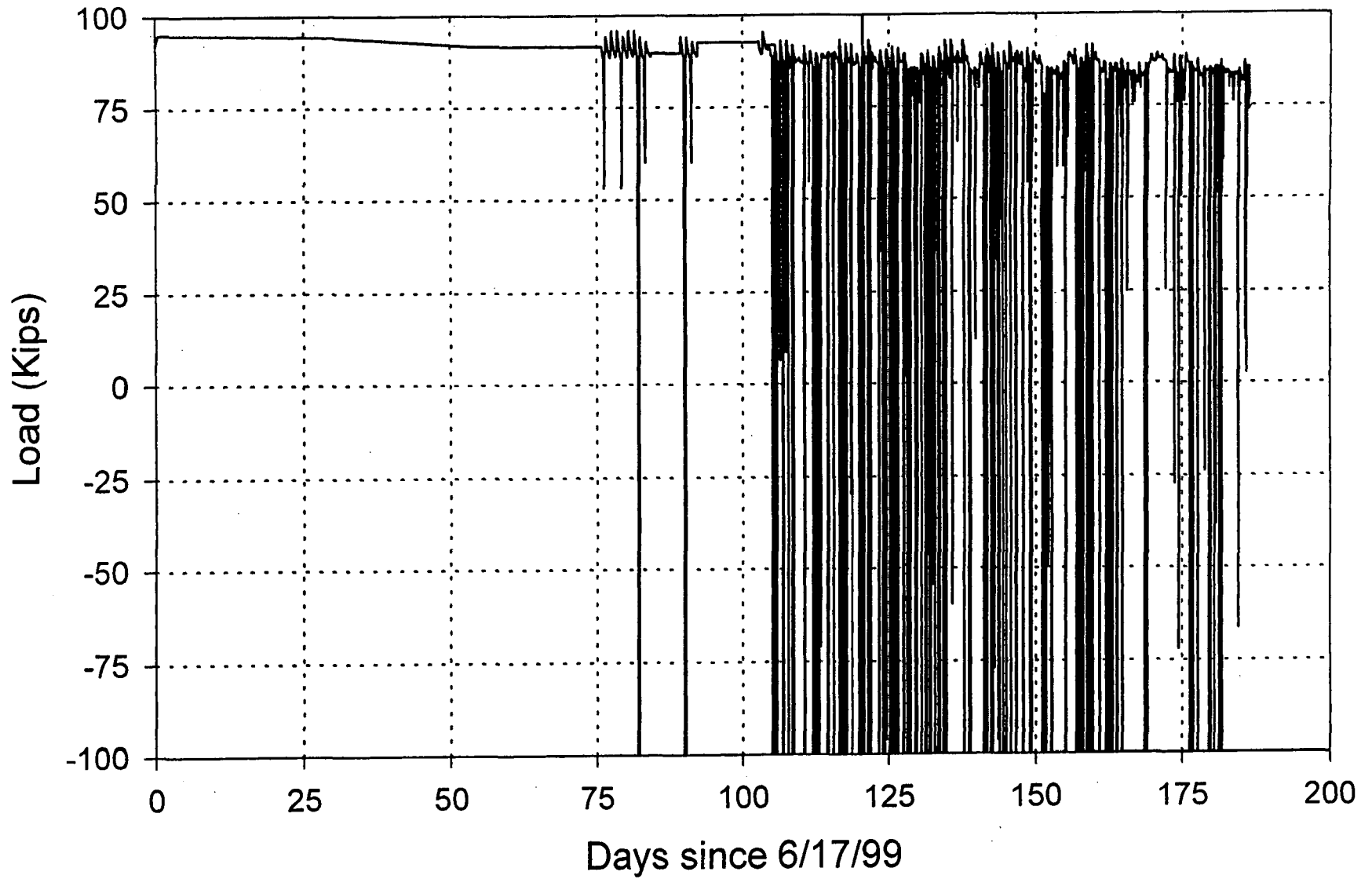
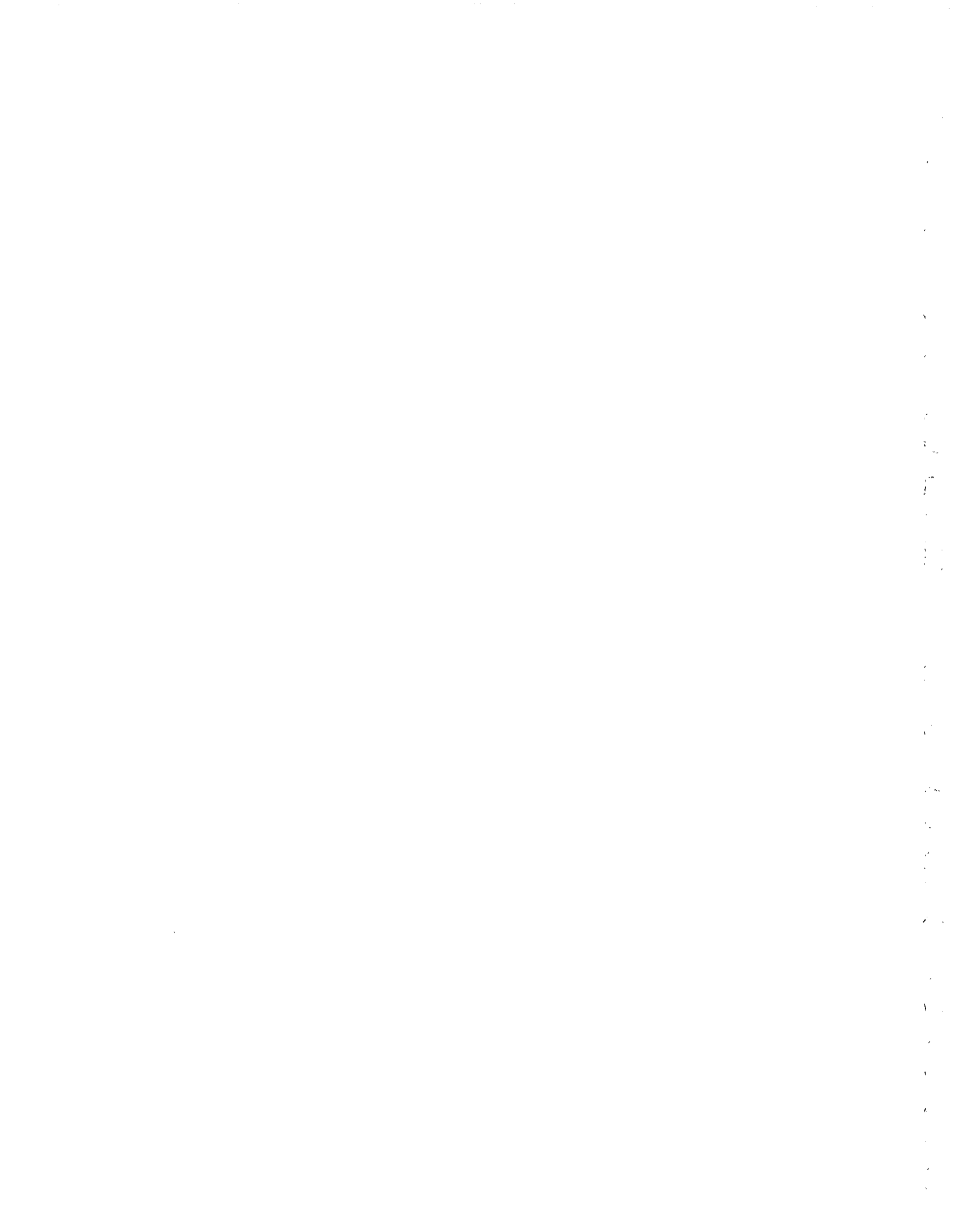


Fig. 4.96: Anchor #11-A, long-term monitoring of load from load cell at anchor head.



IV-112

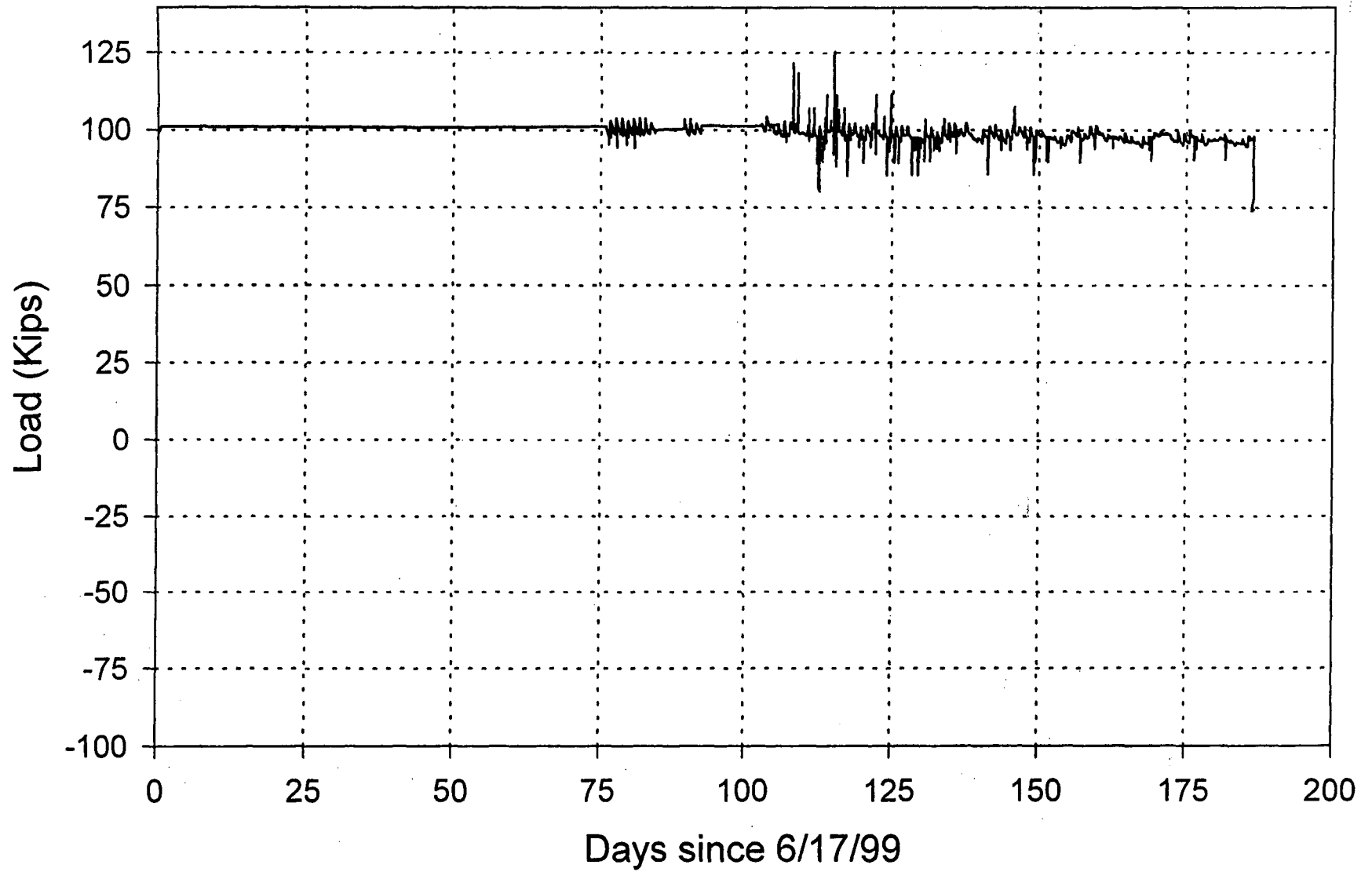


Fig. 4.97: Anchor #11-B, long-term monitoring of load from load cell at anchor head.

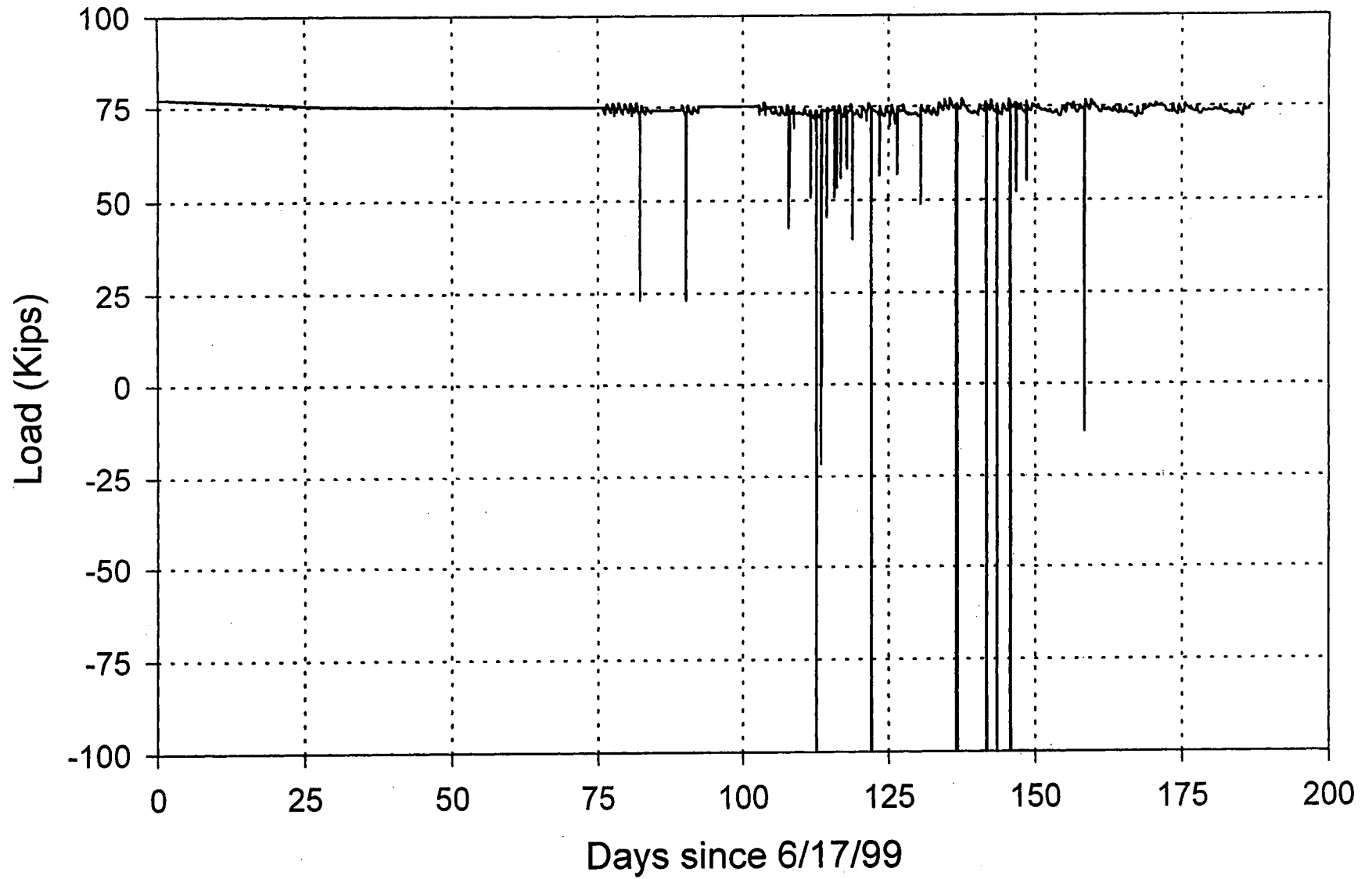


Fig. 4.98: Anchor #30-A, long-term monitoring of load from load cell at anchor head.

IV-114

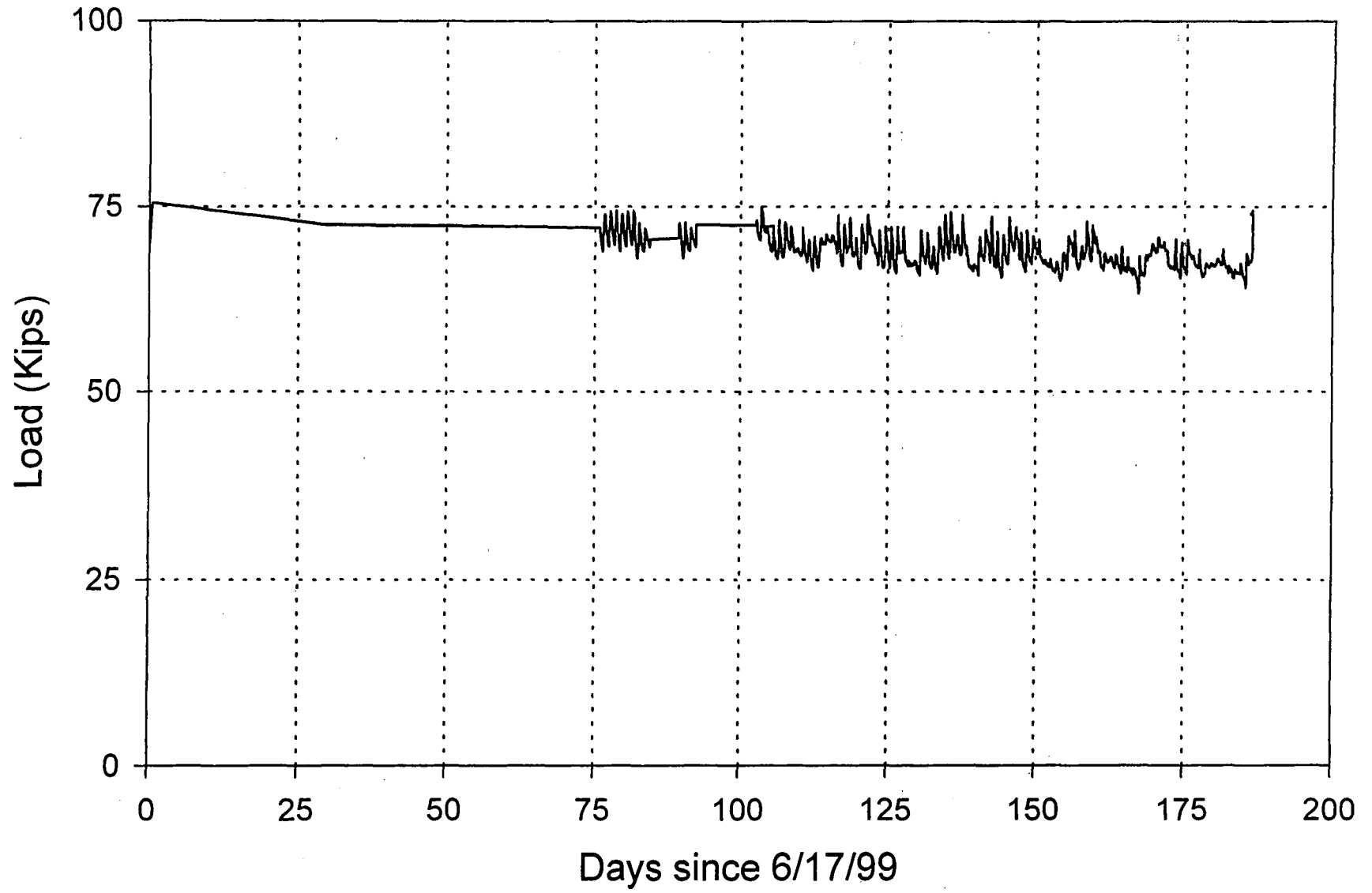


Fig. 4.99: Anchor #30-B, long-term monitoring of load from load cell at anchor head.

SII-VI
IV-115

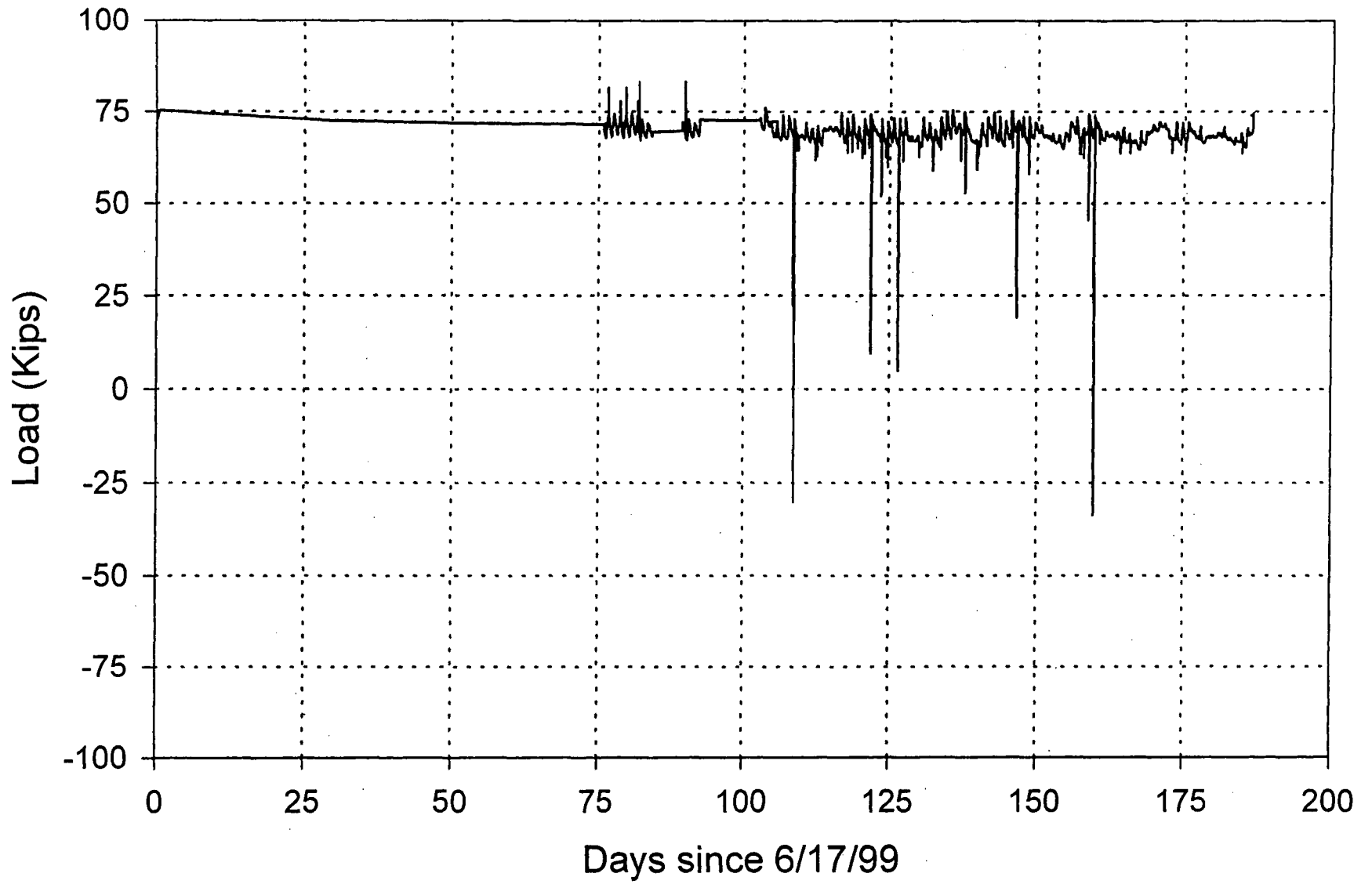


Fig. 4.100: Anchor #30-C, long-term monitoring of load from load cell at anchor head.



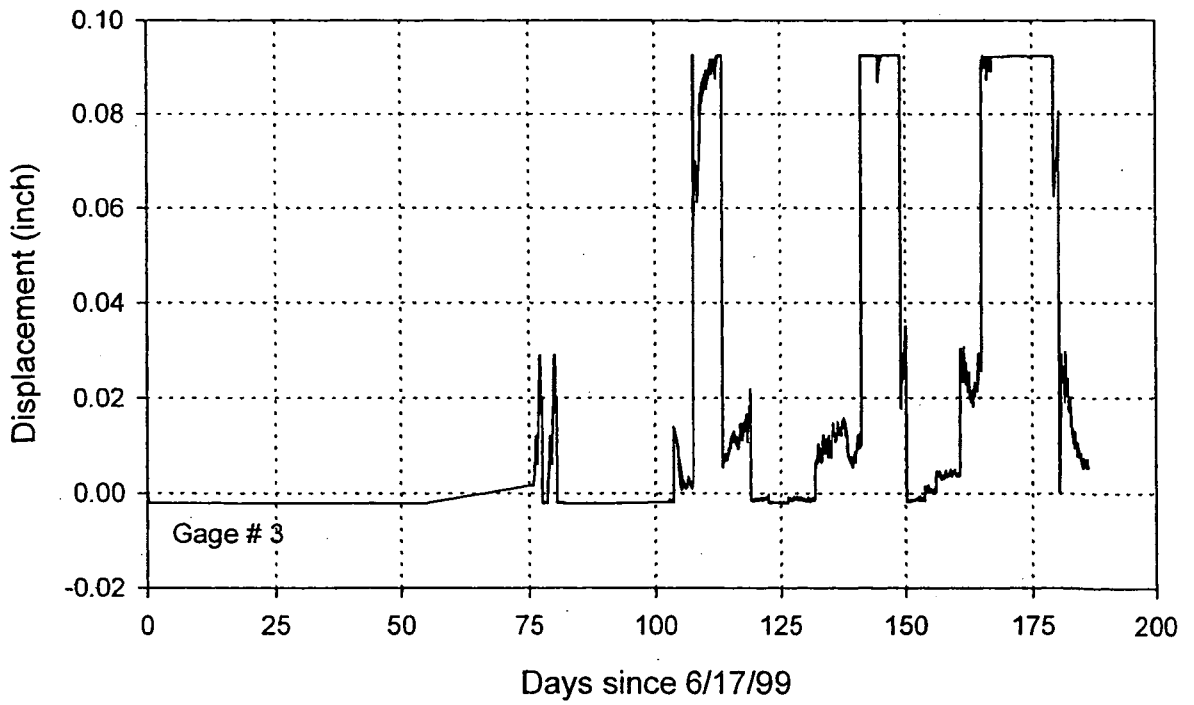
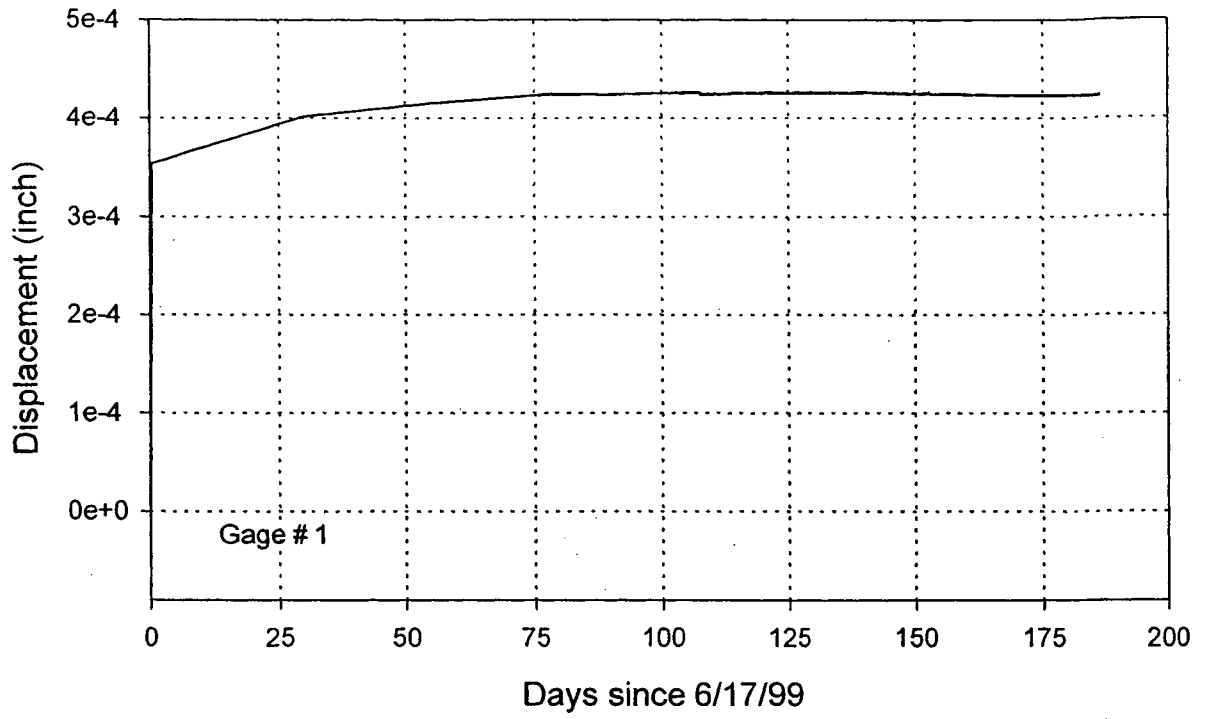


Fig. 4.101: Anchor #11-A, long-term monitoring of movement at gage locations in the bonded length.

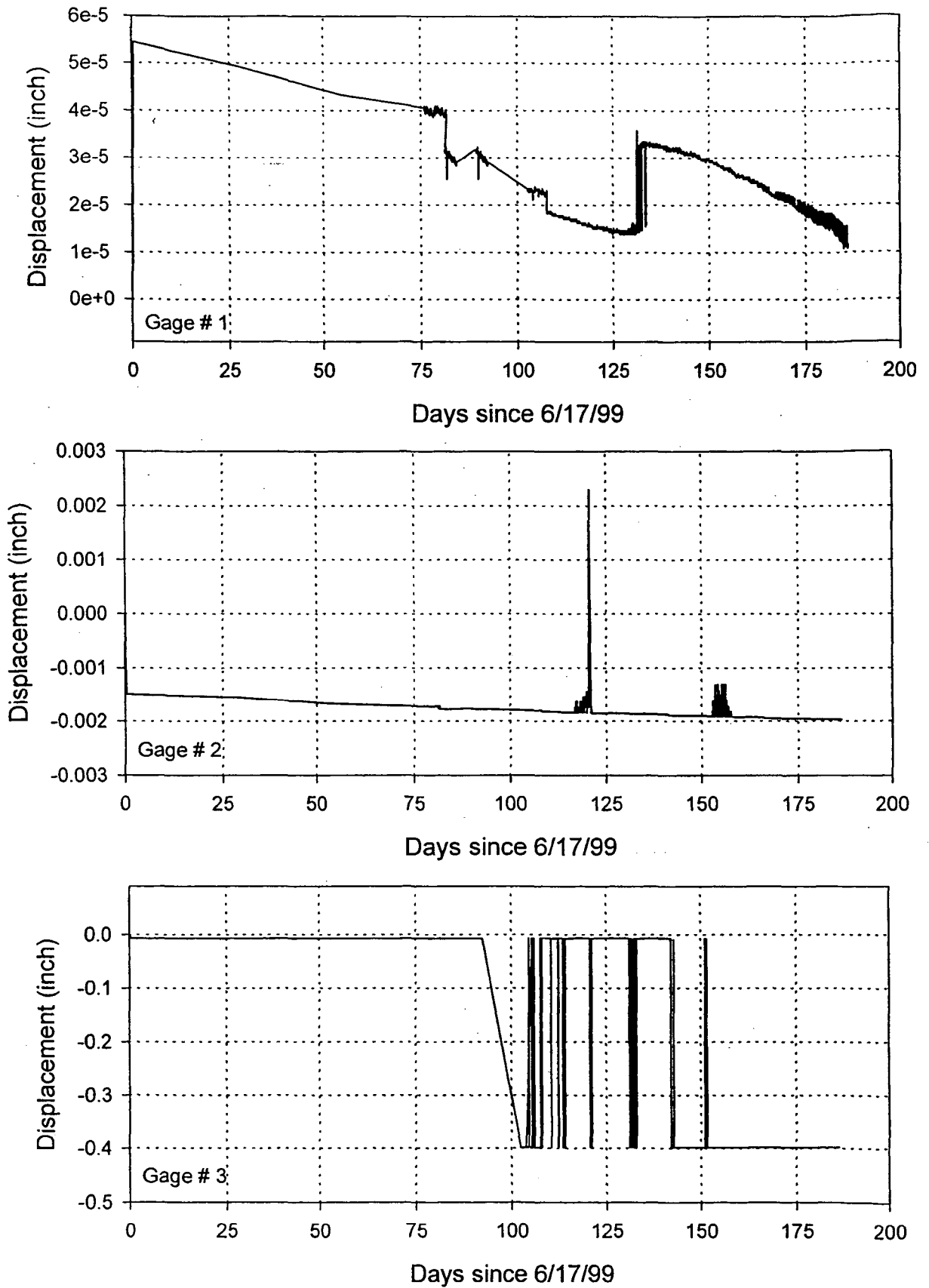


Fig. 4.102: Anchor #11-B, long-term monitoring of movement at gage locations in the bonded length.



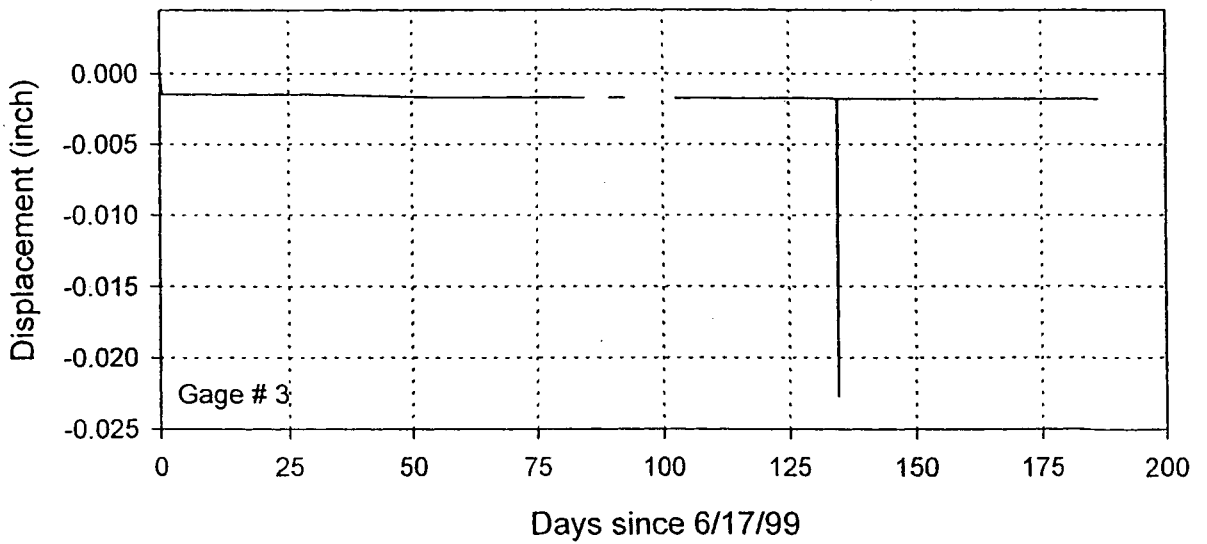
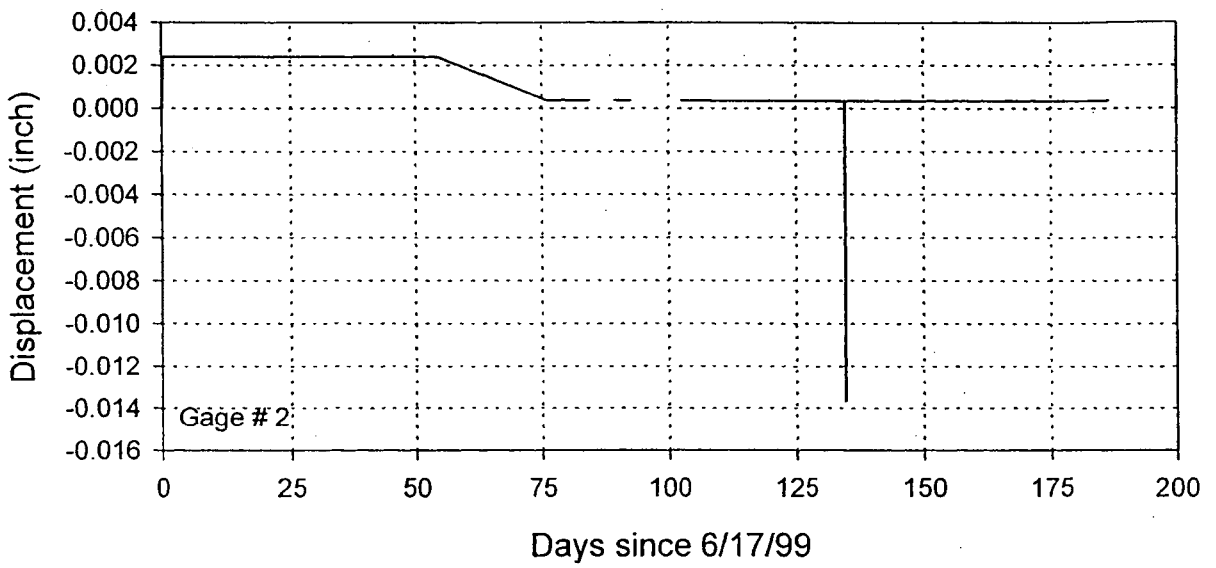
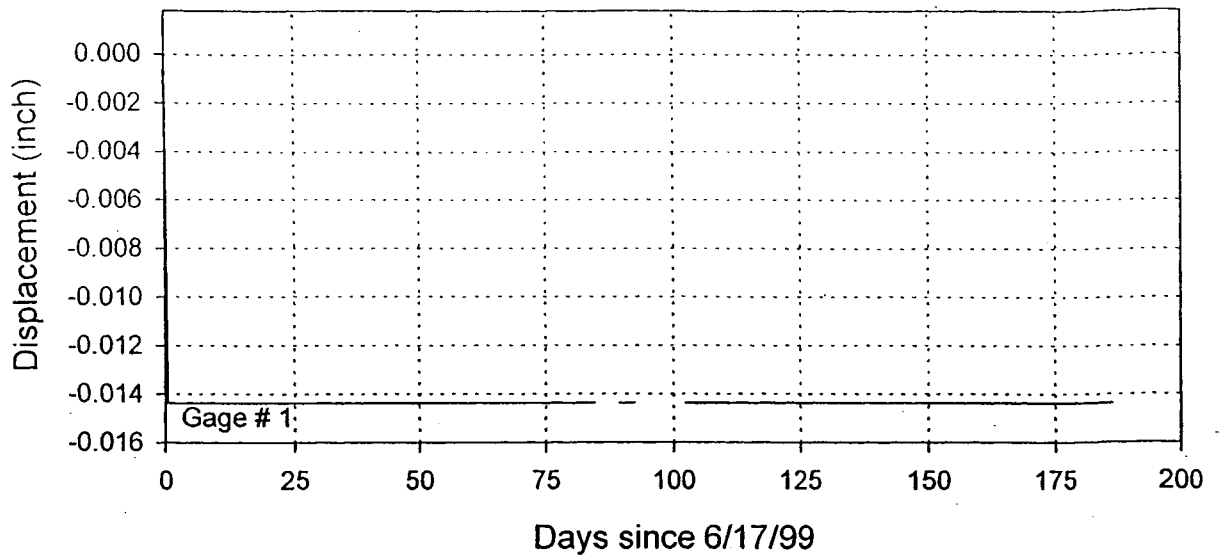


Fig. 4.103: Anchor #30-A, long-term monitoring of movement at gage locations in the bonded length.



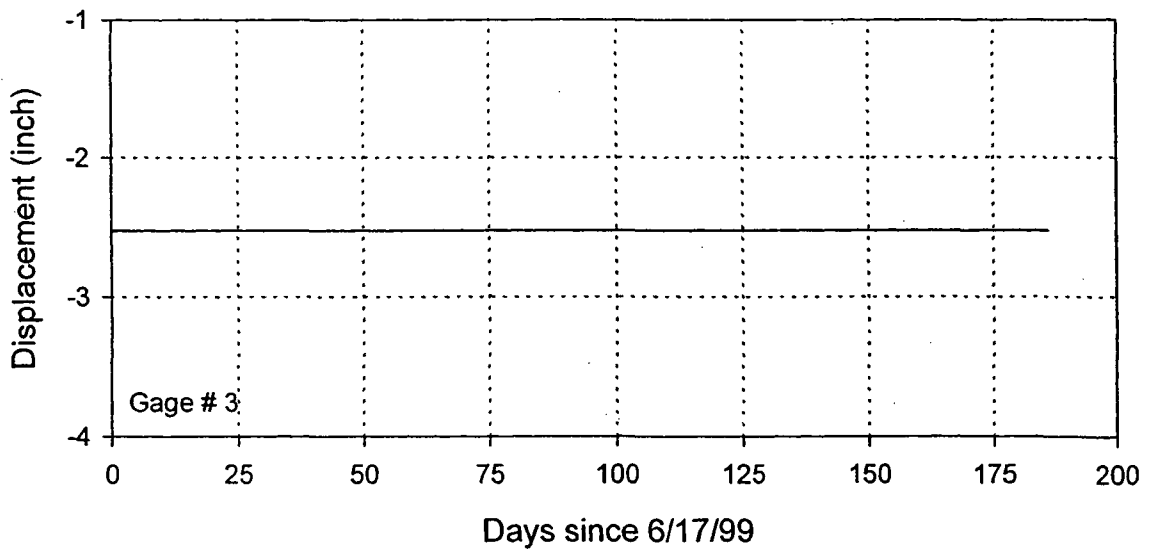
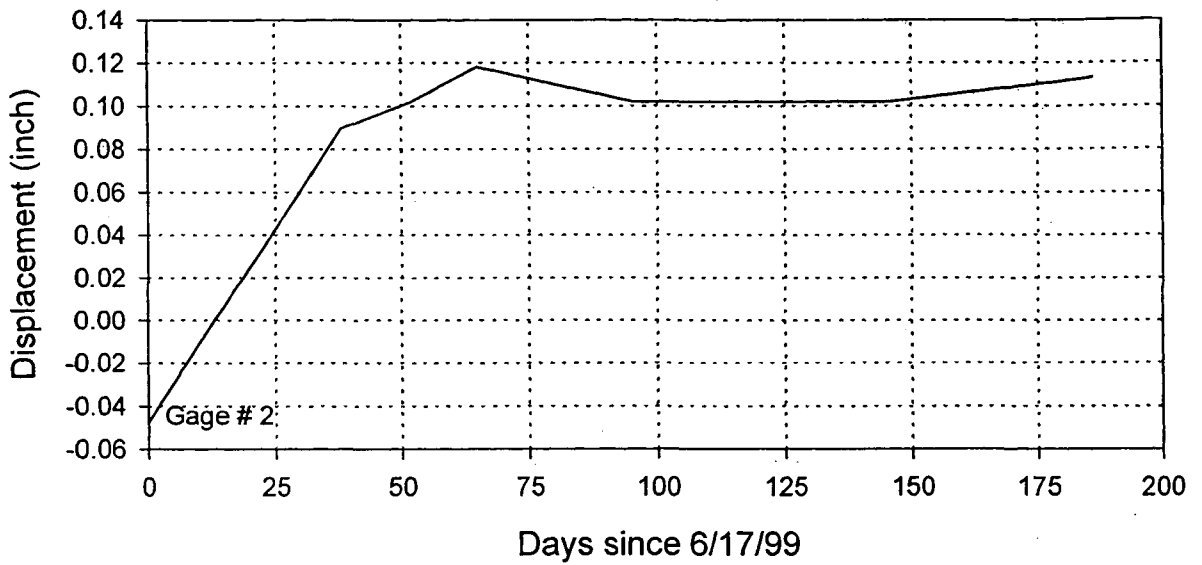
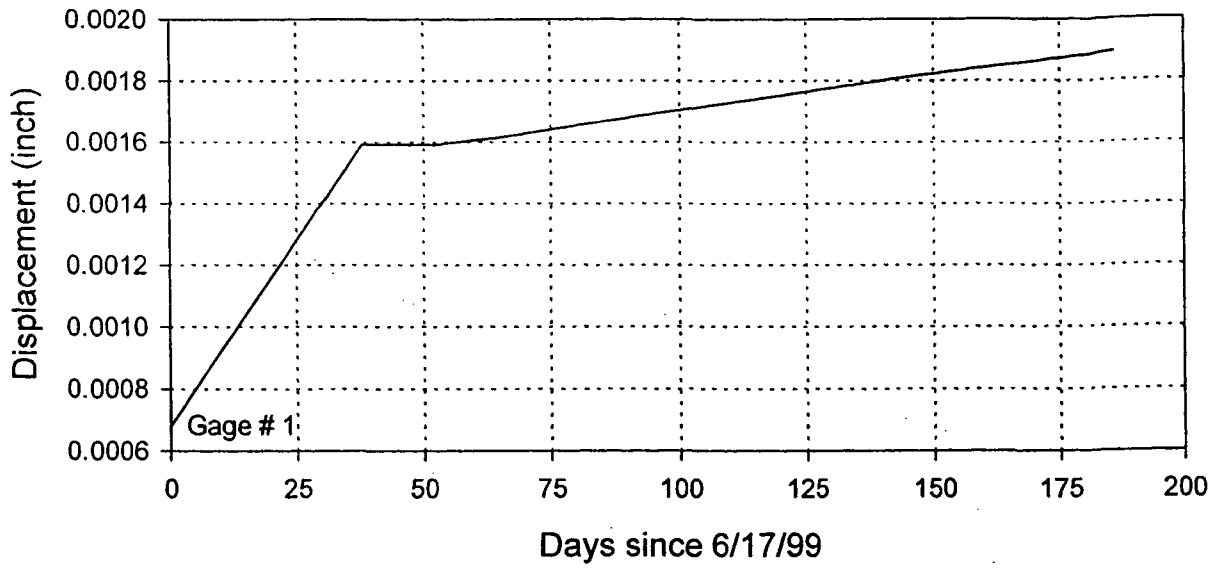


Fig. 4.104: Anchor #30-B, long-term monitoring of movement at gage locations in the bonded length.

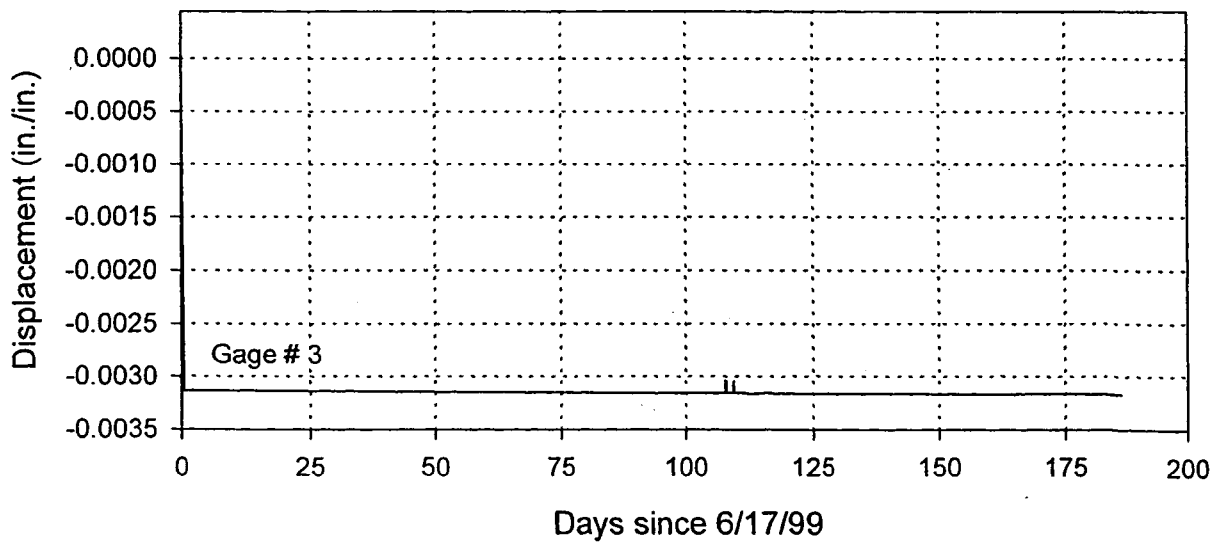
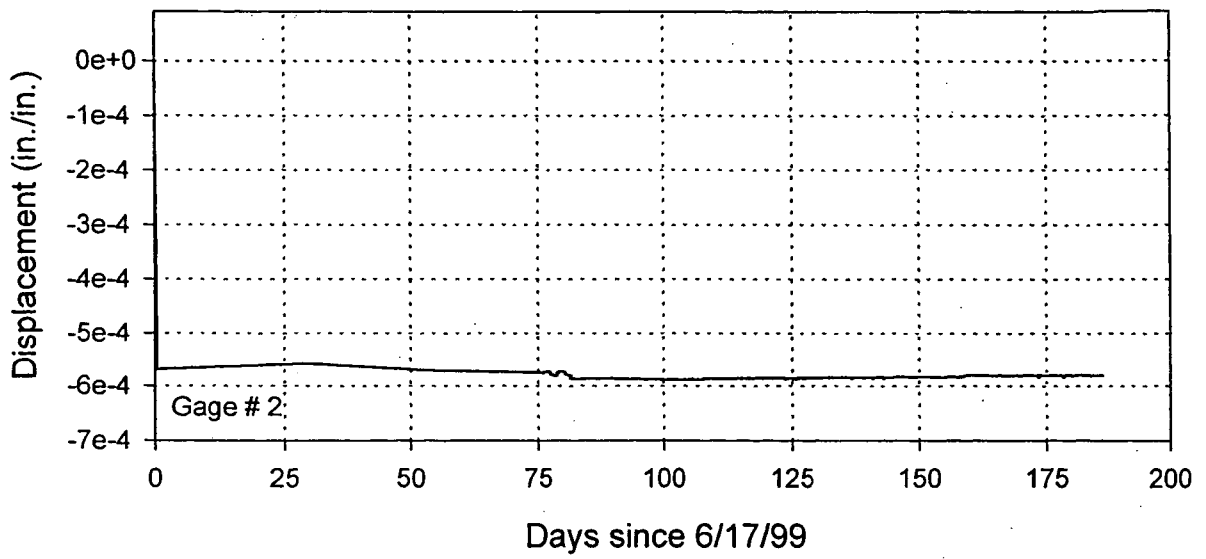
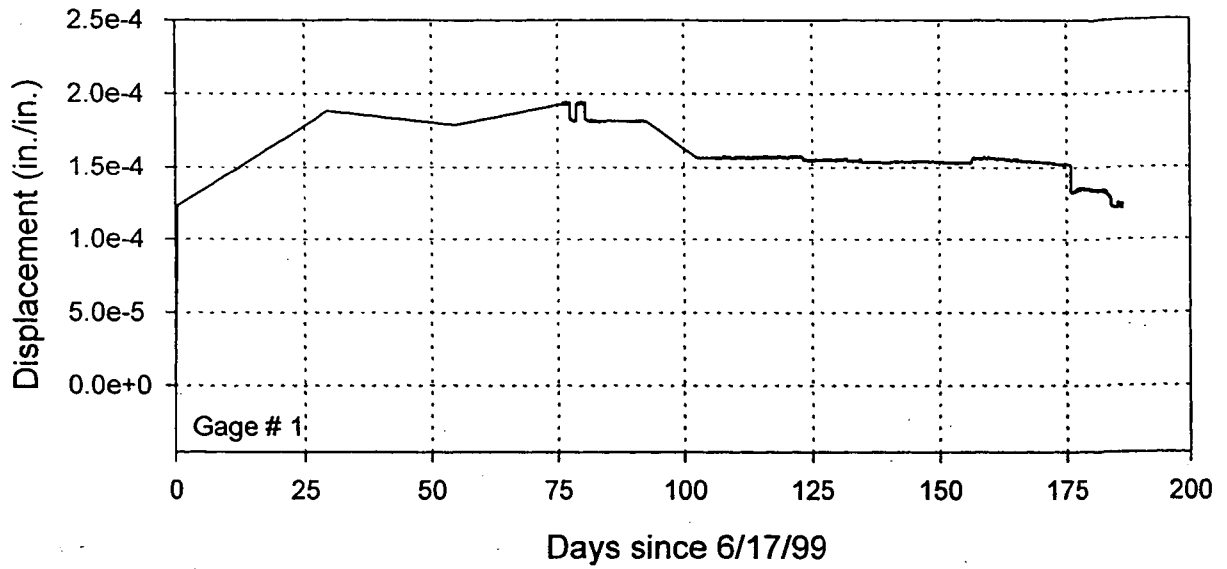
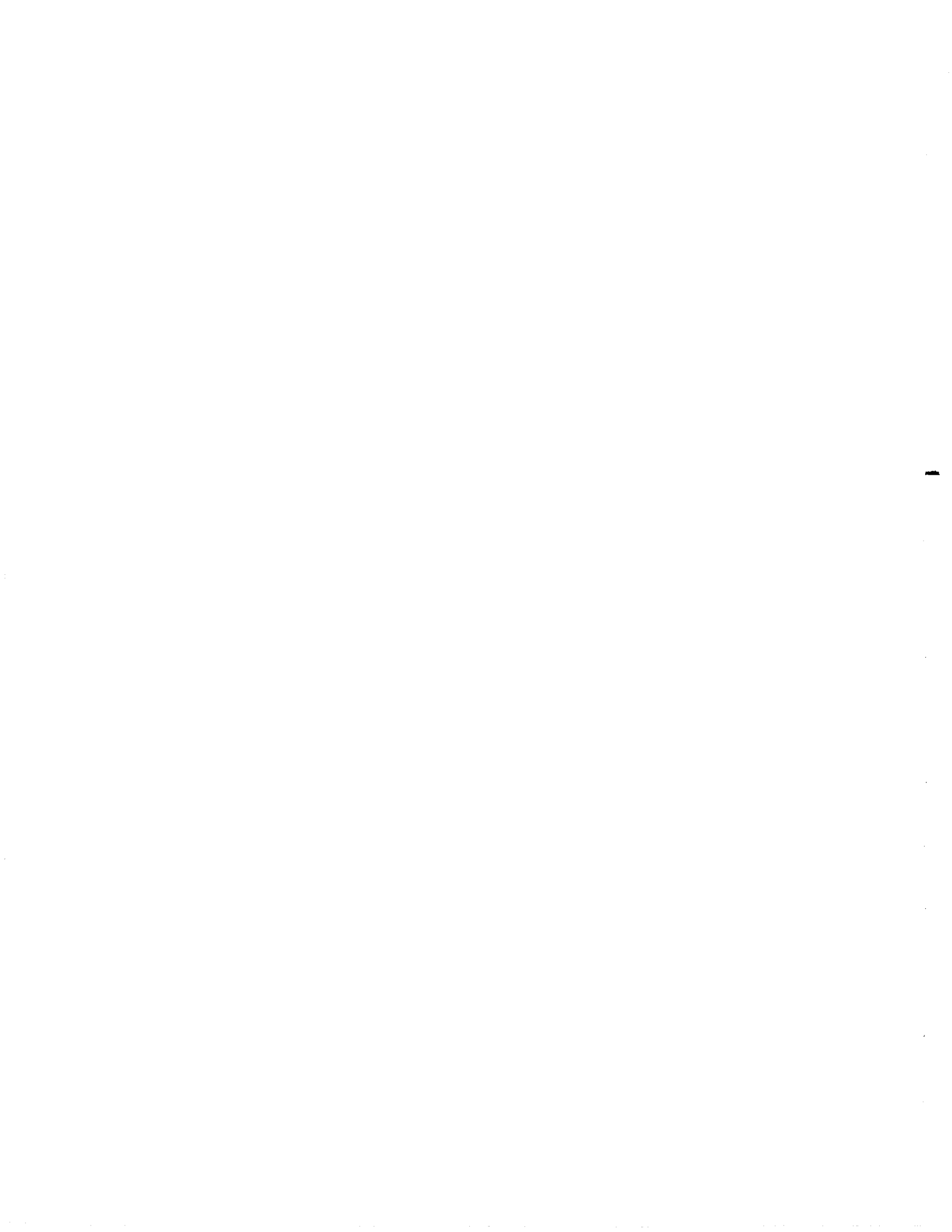


Fig. 4.105: Anchor #30-C, long-term monitoring of movement at gage locations in the bonded length.



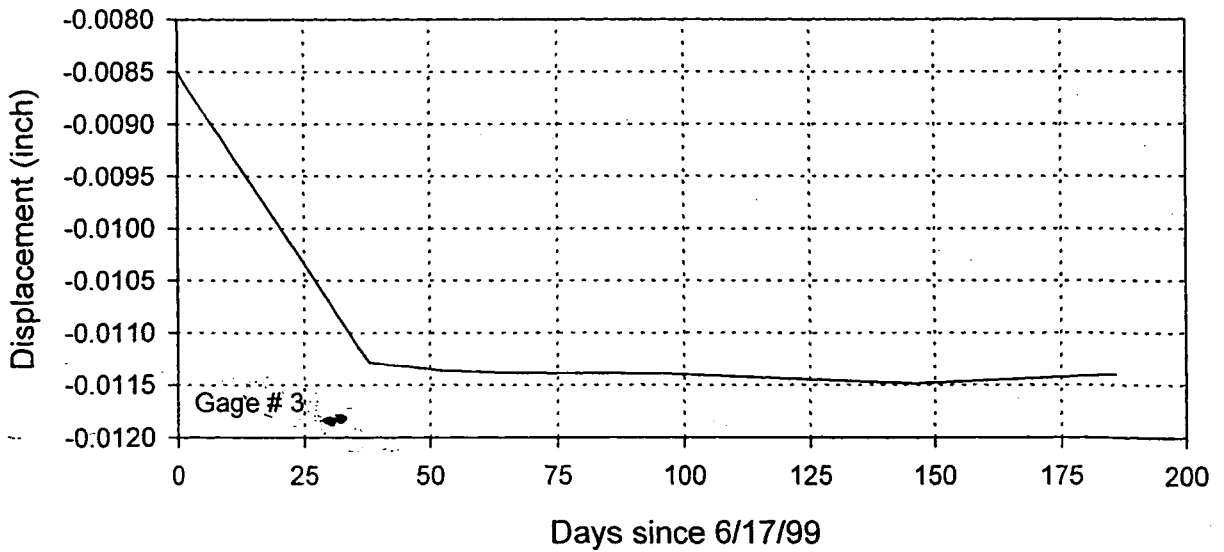
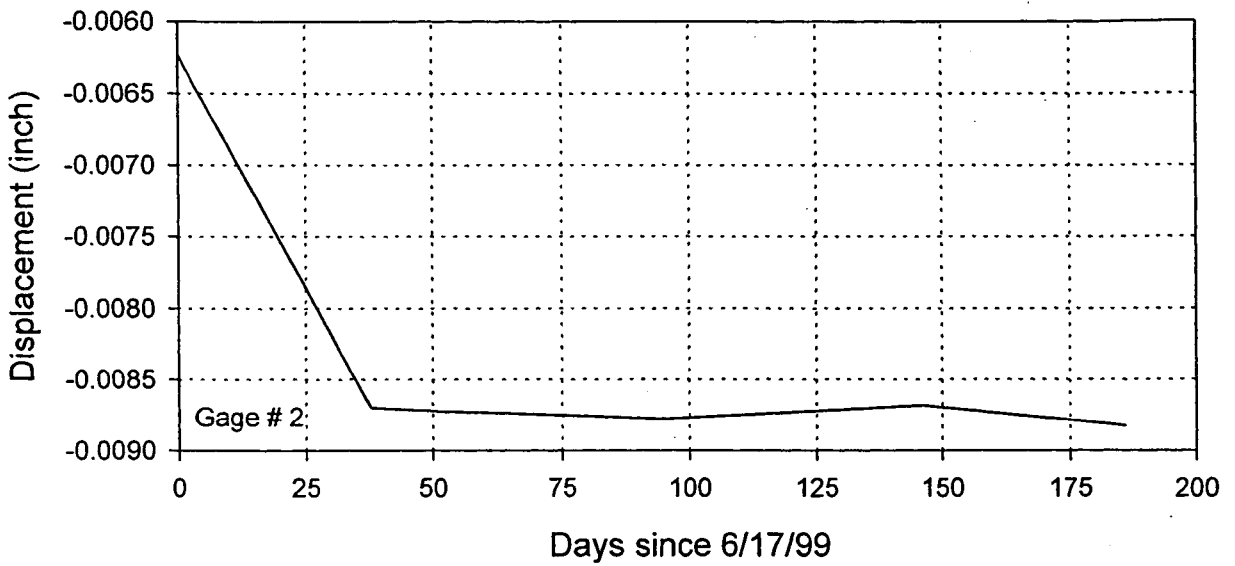
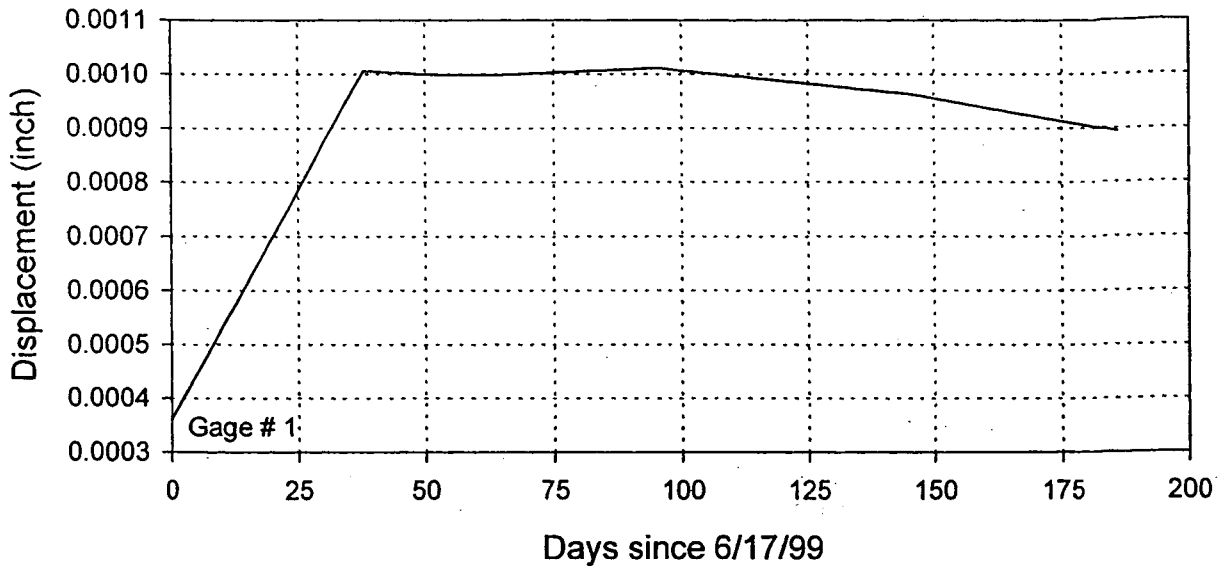


Fig. 4.106: Anchor #31-B, long-term monitoring of movement at gage locations in the bonded length.

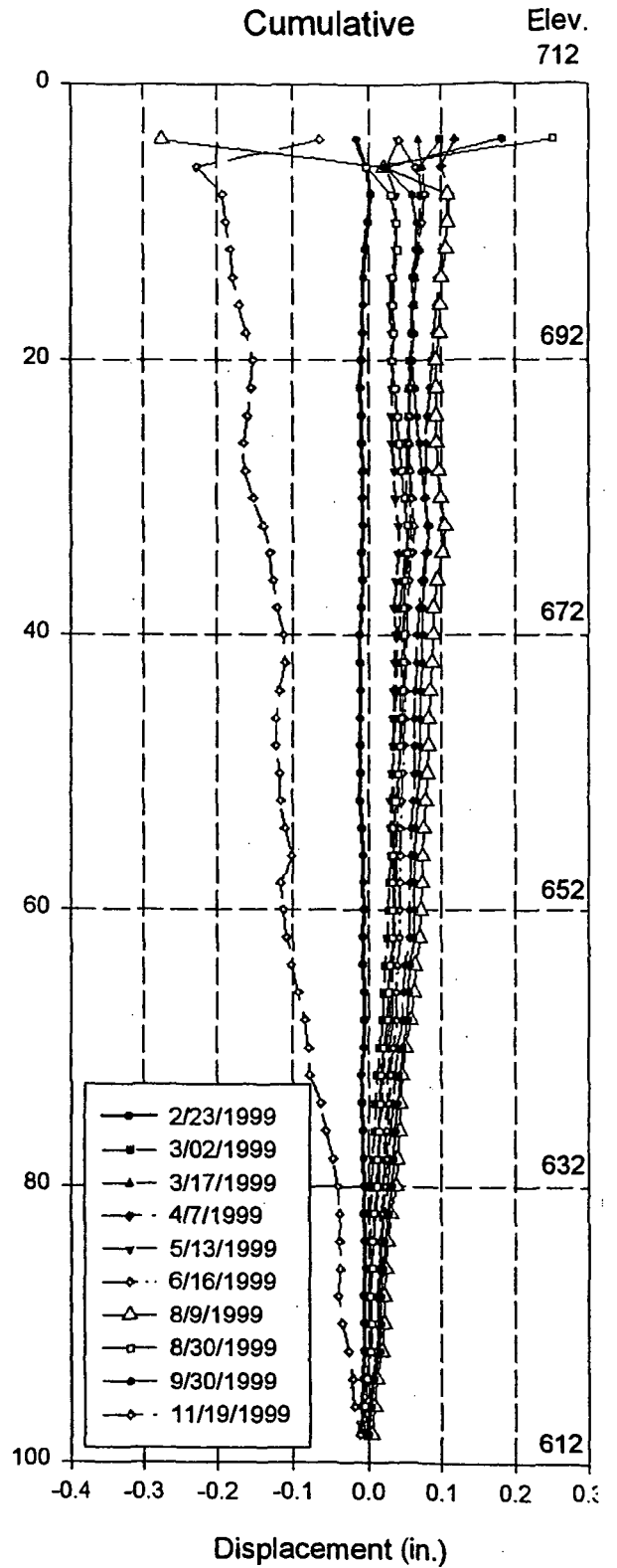
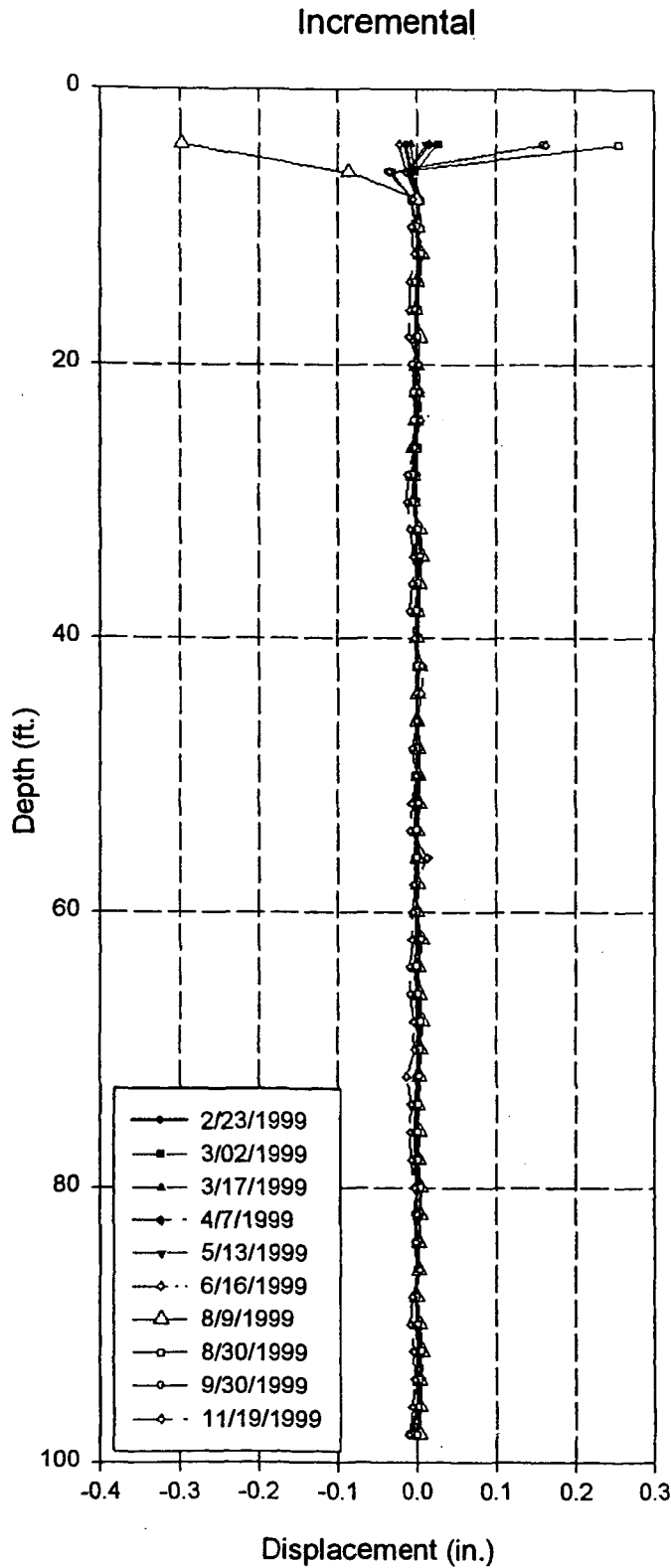


Fig. 107(b): Deflection vs. depth using inclinometer in the B+ direction (South) for earth inclinometer # 1 till 1/29/2000



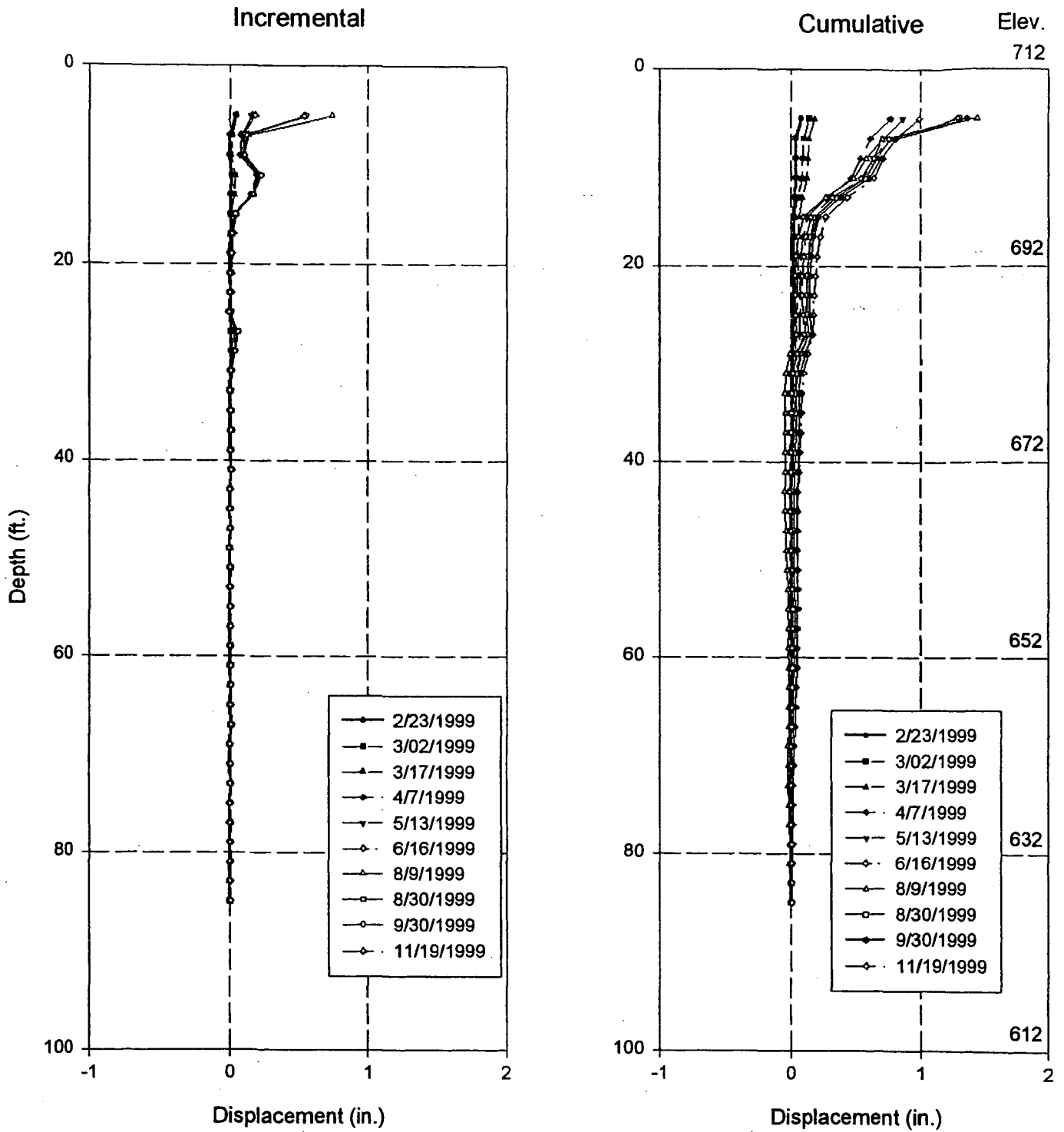


Fig. 108(a): Deflection vs. depth using inclinometer in the A+ direction (East) for earth inclinometer # 2 till 1/29/2000



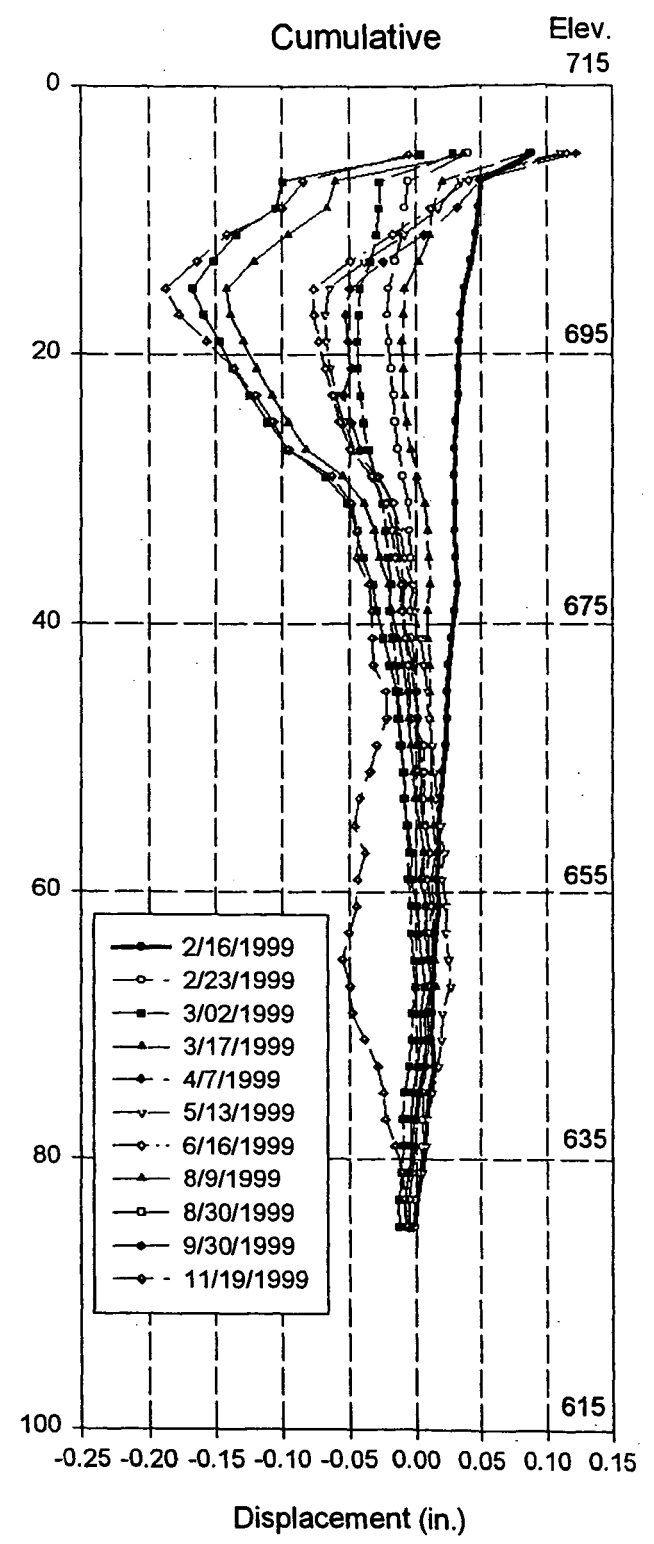
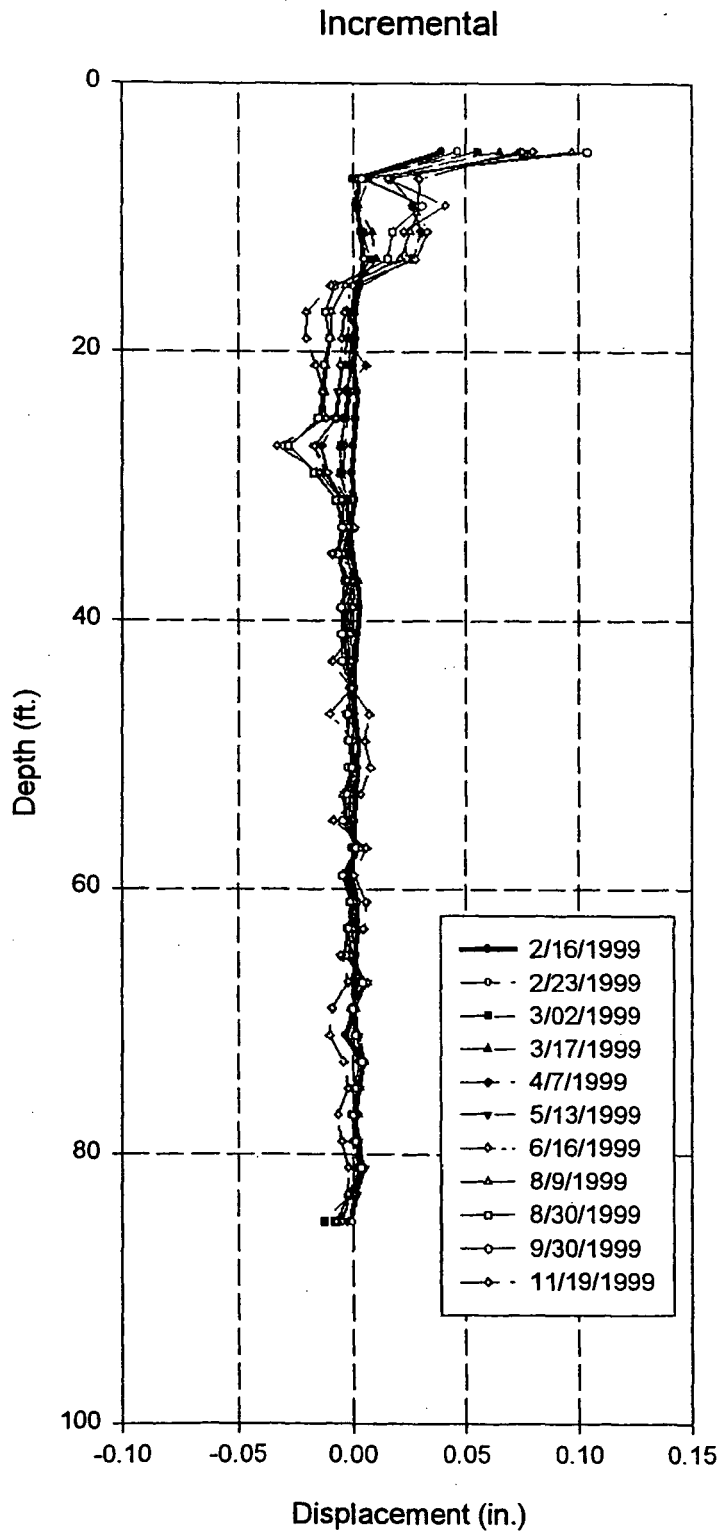
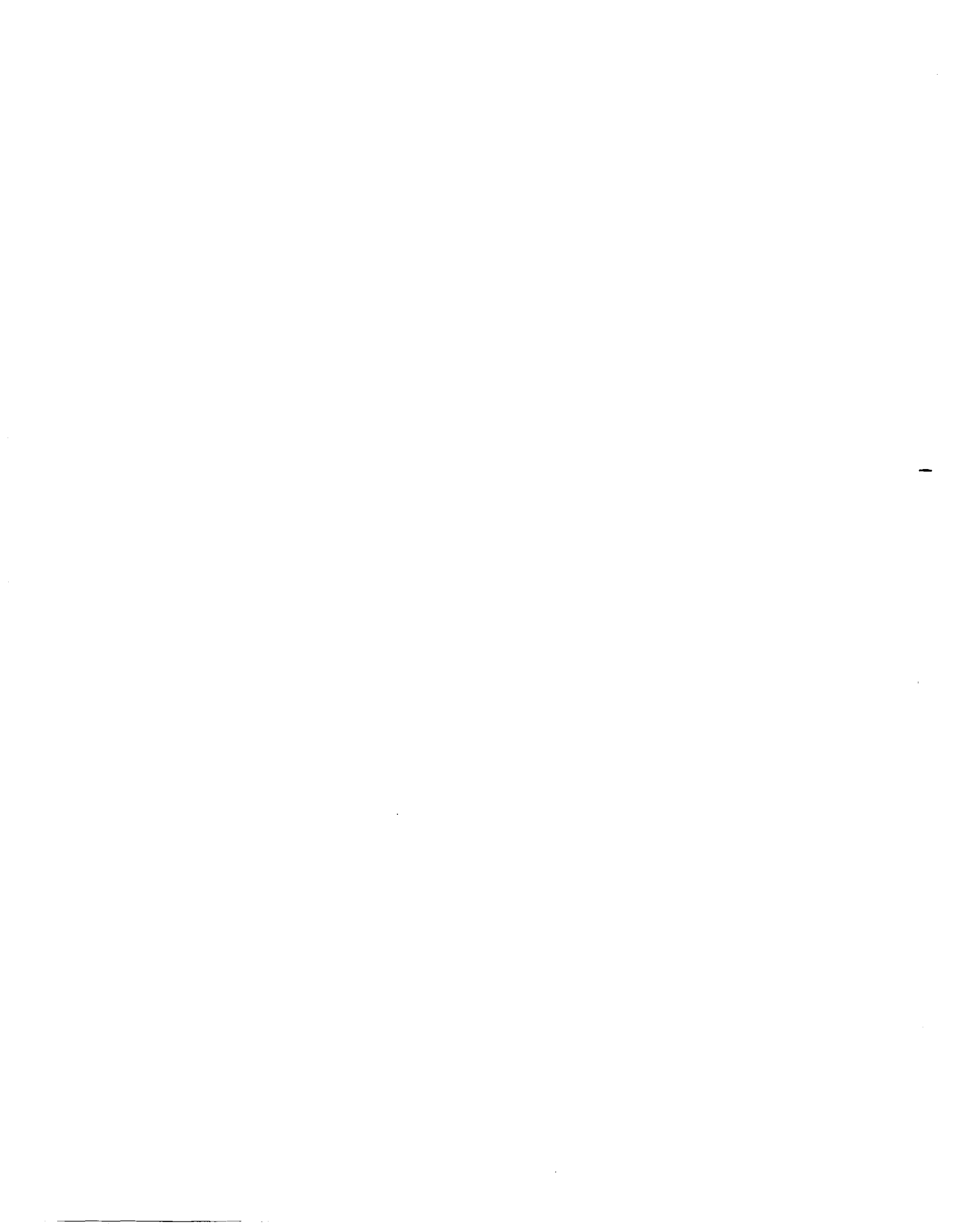


Fig. 108(b): Deflection vs. depth using inclinometer in the B+ direction (South) for earth inclinometer # 2 till 1/29/2000



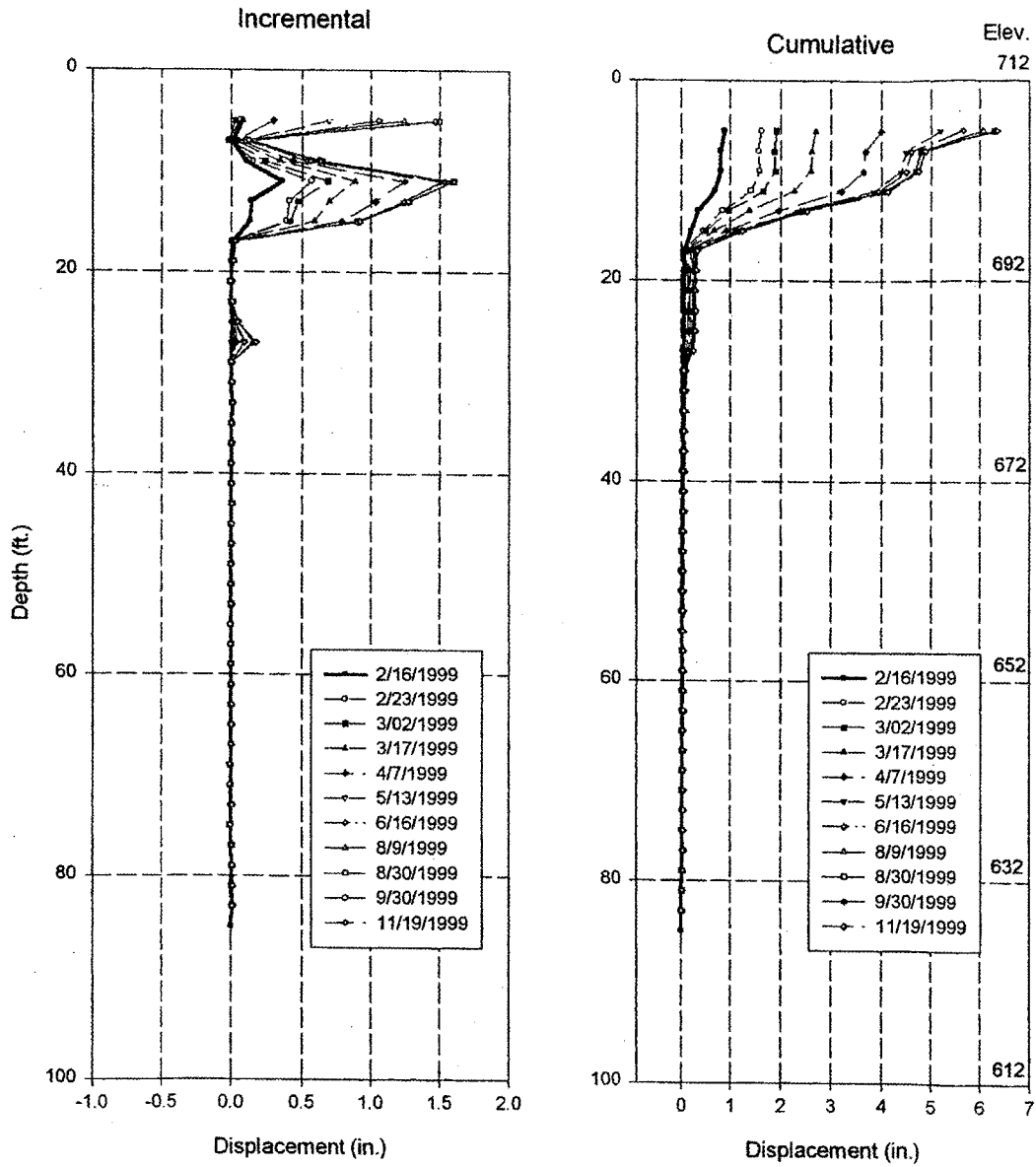


Fig. 109(a): Deflection vs. depth using inclinometer in the A+ direction (East) for earth inclinometer # 3 till 1/29/2000



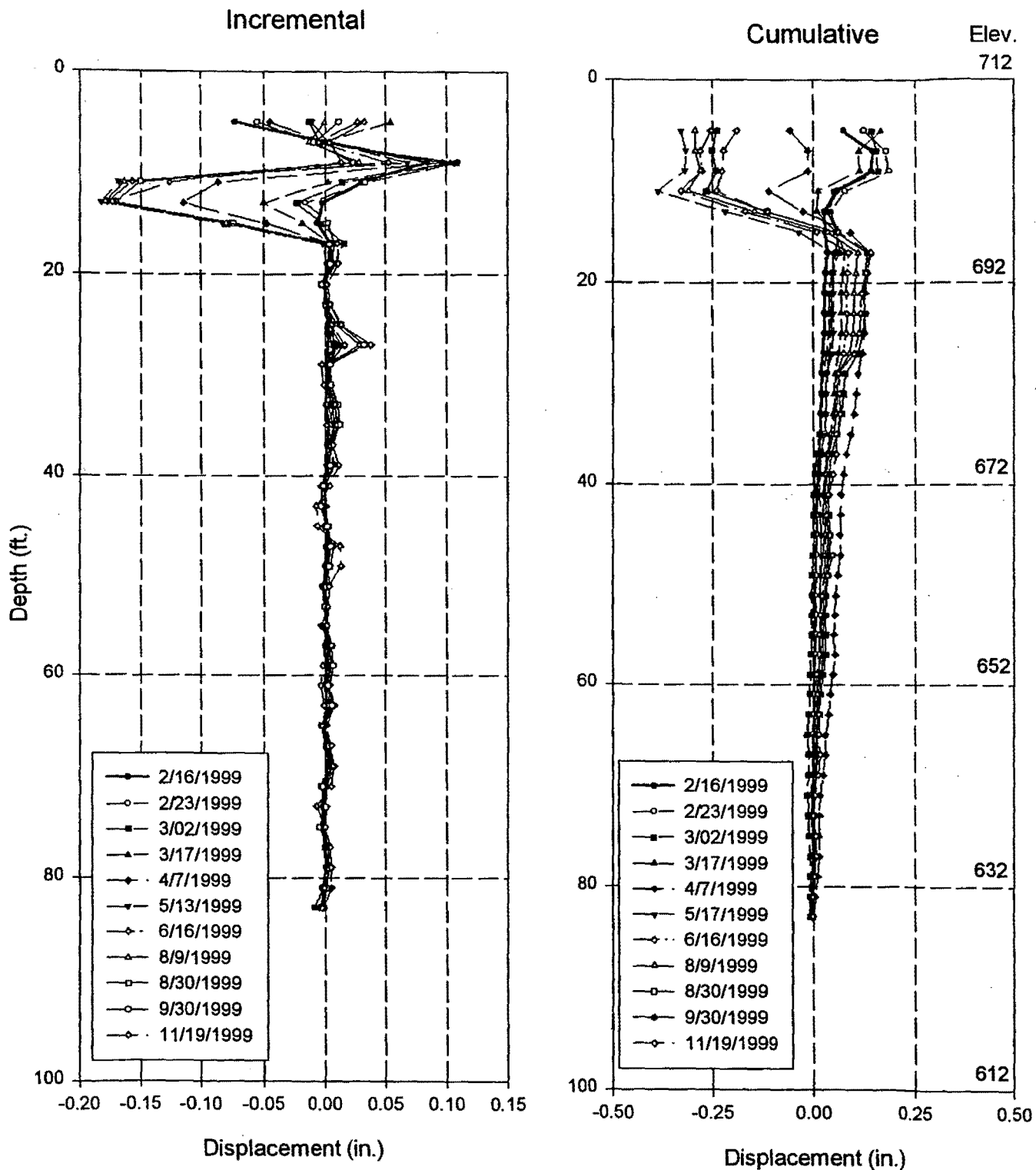


Fig. 109(b): Deflection vs. depth using inclinometer in the B+ direction (South) for earth inclinometer # 3 till 1/29/2000

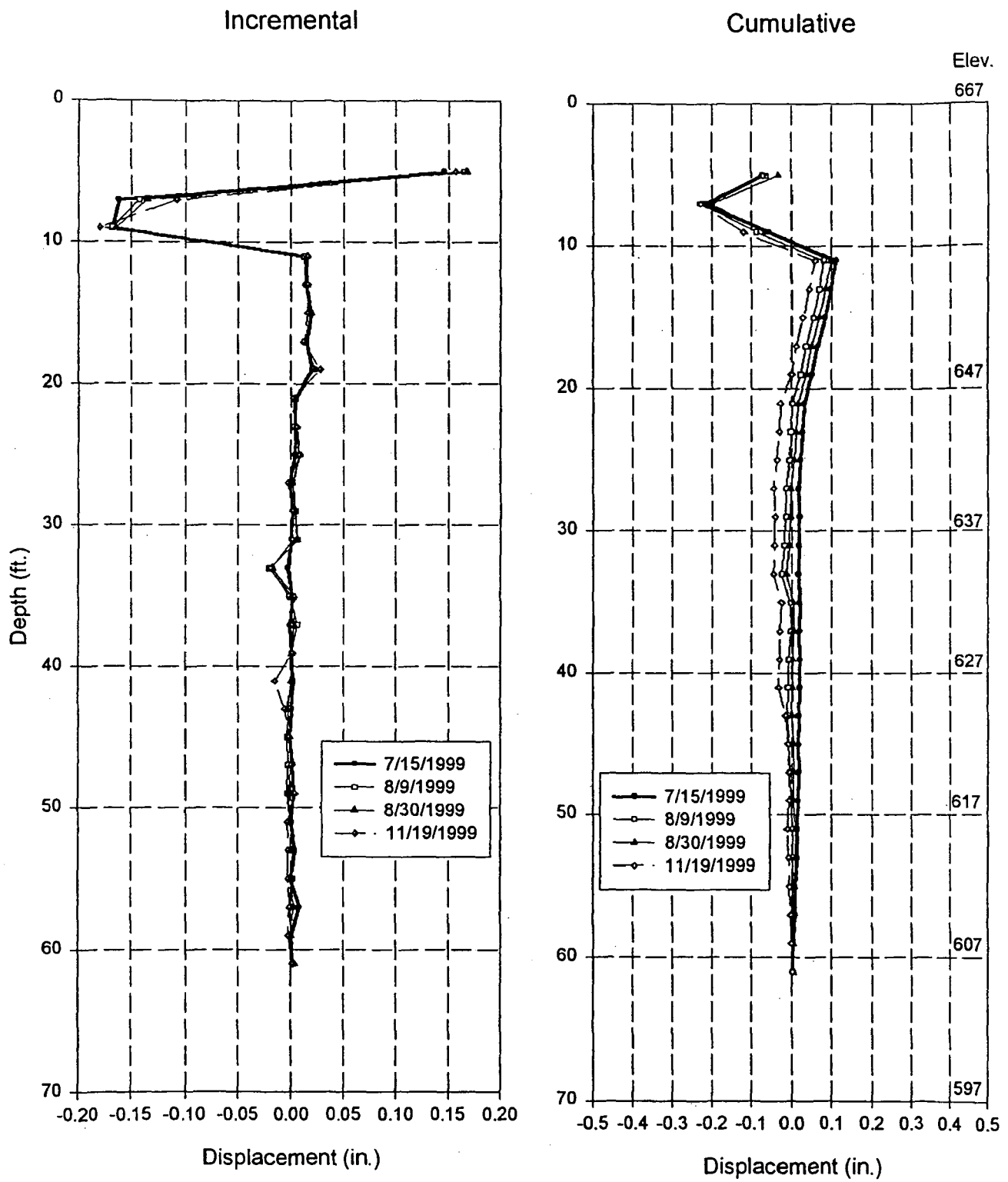


Fig. 110(a): Deflection vs. depth using inclinometer in the A+ direction (East) for soldier pile # 11 till 1/29/2000.

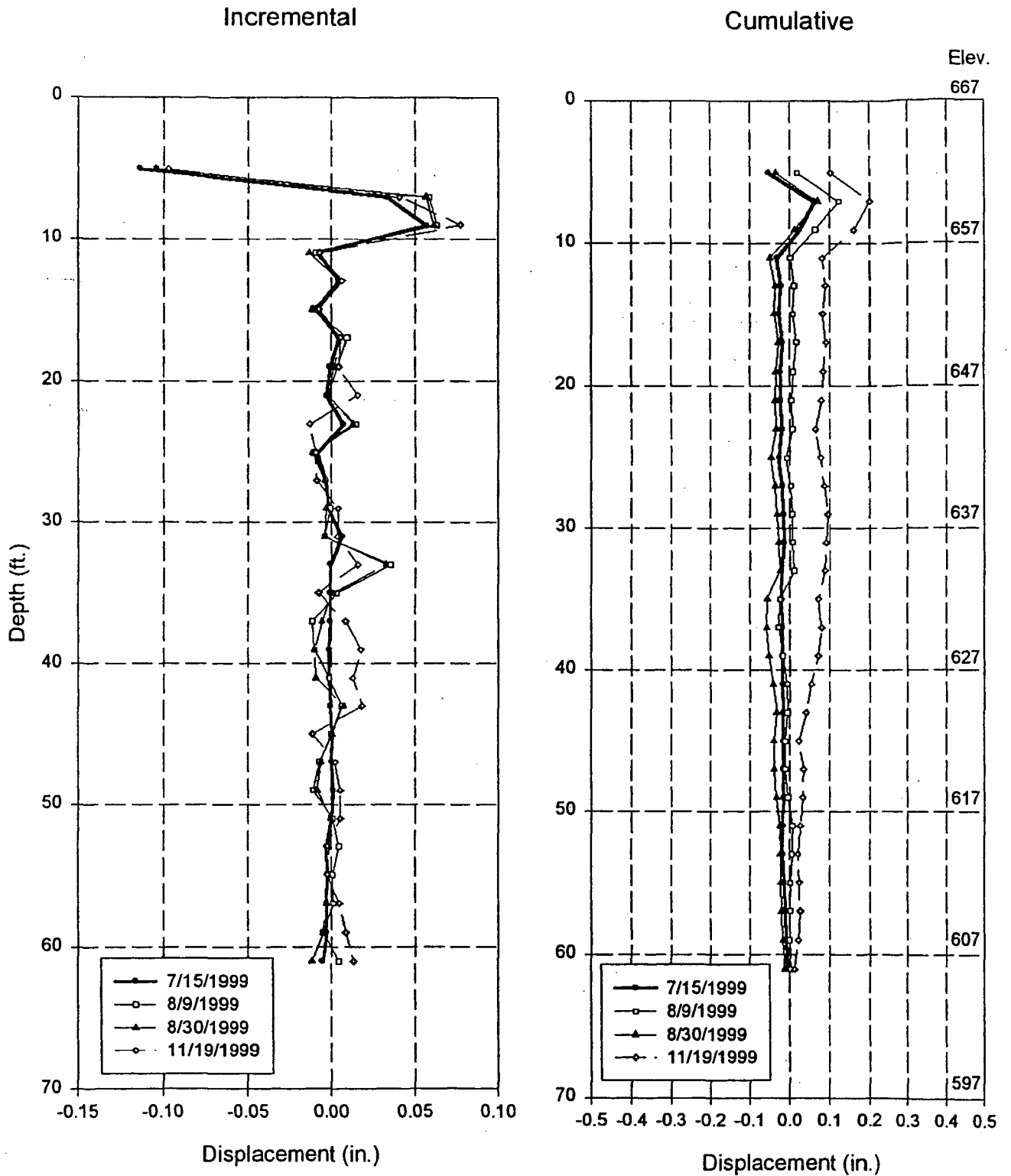


Fig. 110(b): Deflection vs. depth using inclinometer in the B+ direction (South) for soldier pile # 11 till 1/29/2000.



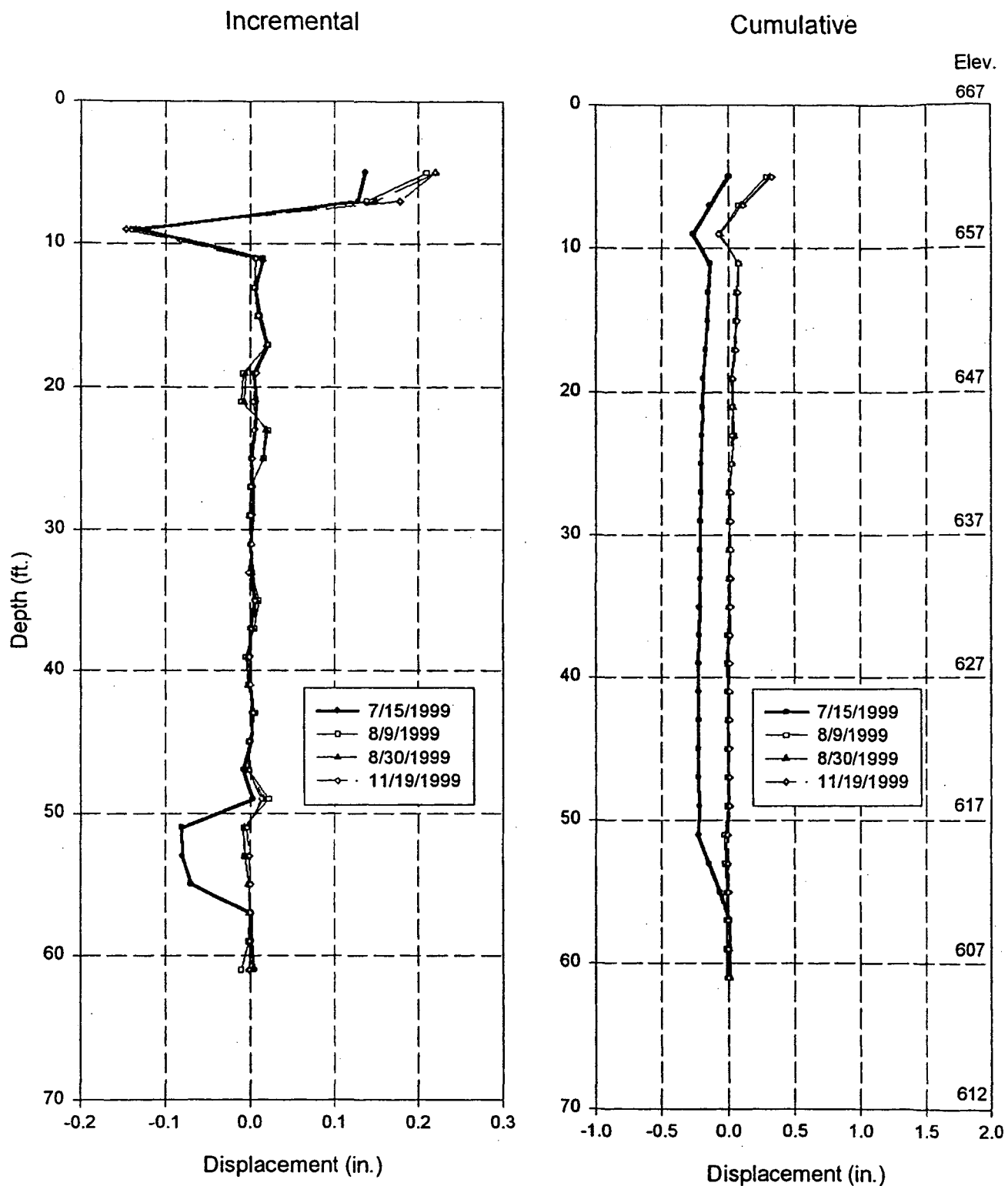


Fig. 111(a): Deflection vs. depth using inclinometer in the A+ direction (East) for soldier pile # 12 till 1/29/2000.



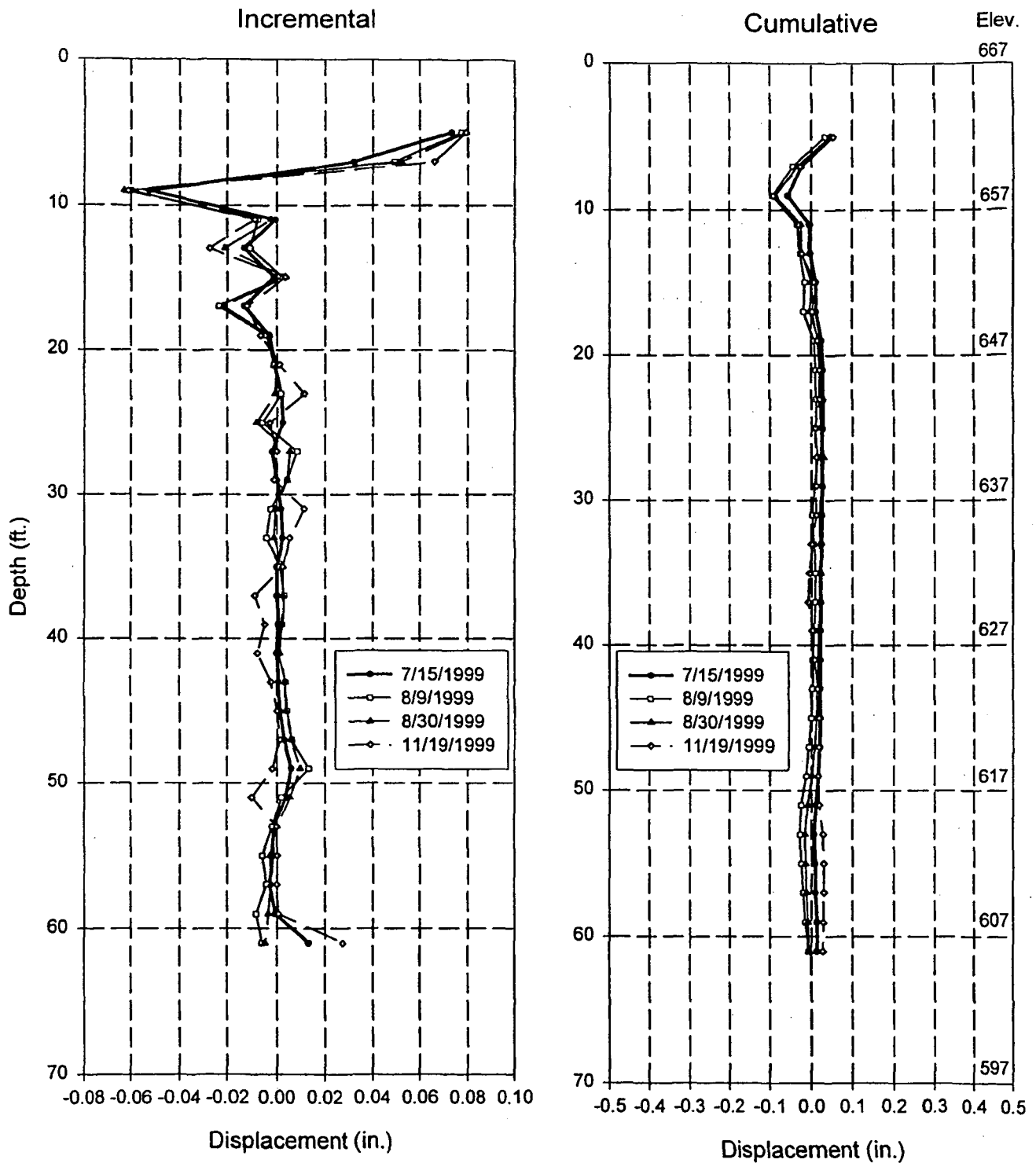


Fig. 111(b): Deflection vs. depth using inclinometer in the B+ direction (South) for soldier pile # 12 till 1/29/2000.

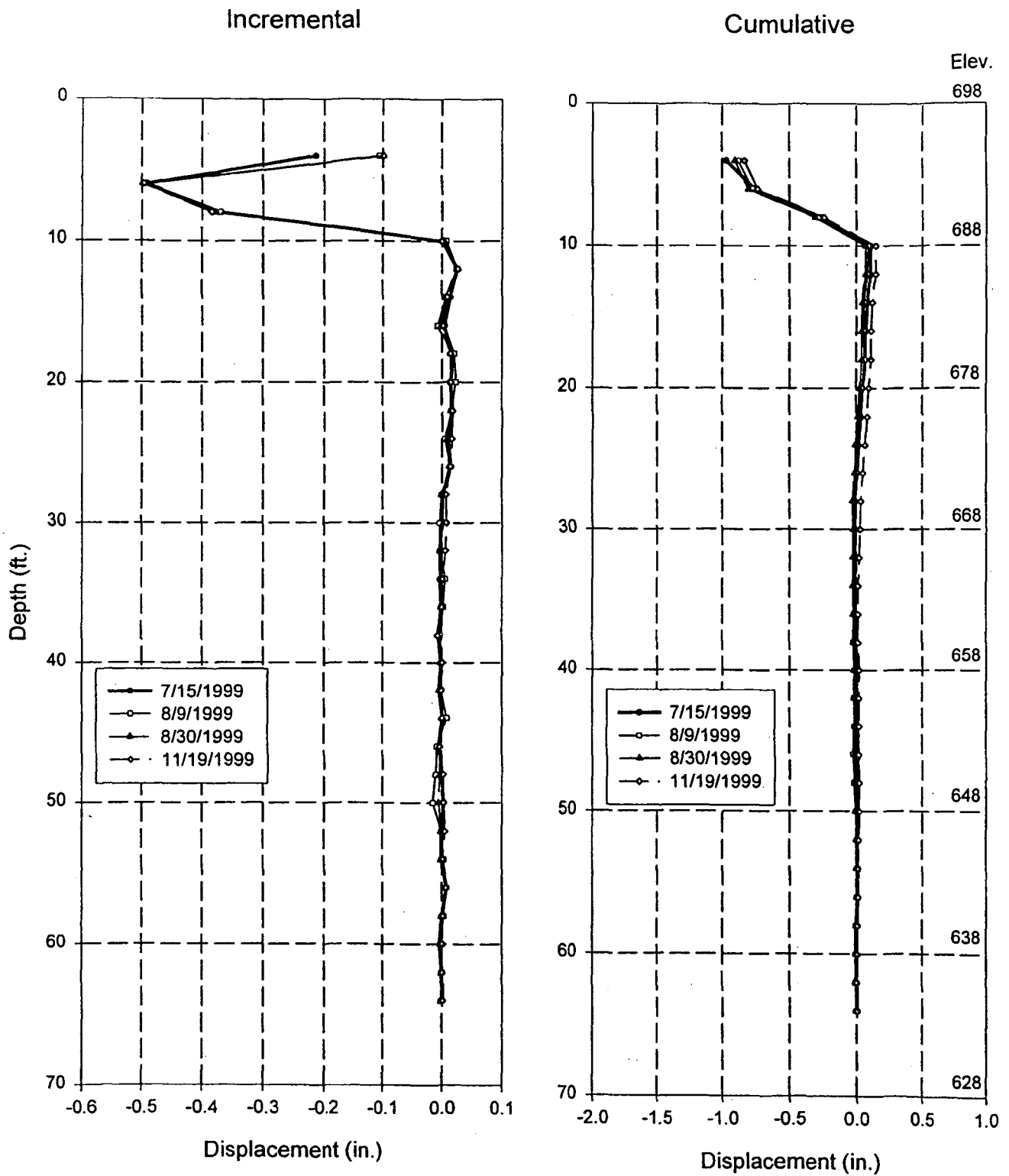


Fig. 112(a): Deflection vs. depth using inclinometer in the A+ direction (East) for soldier pile # 30 till 1/29/2000.



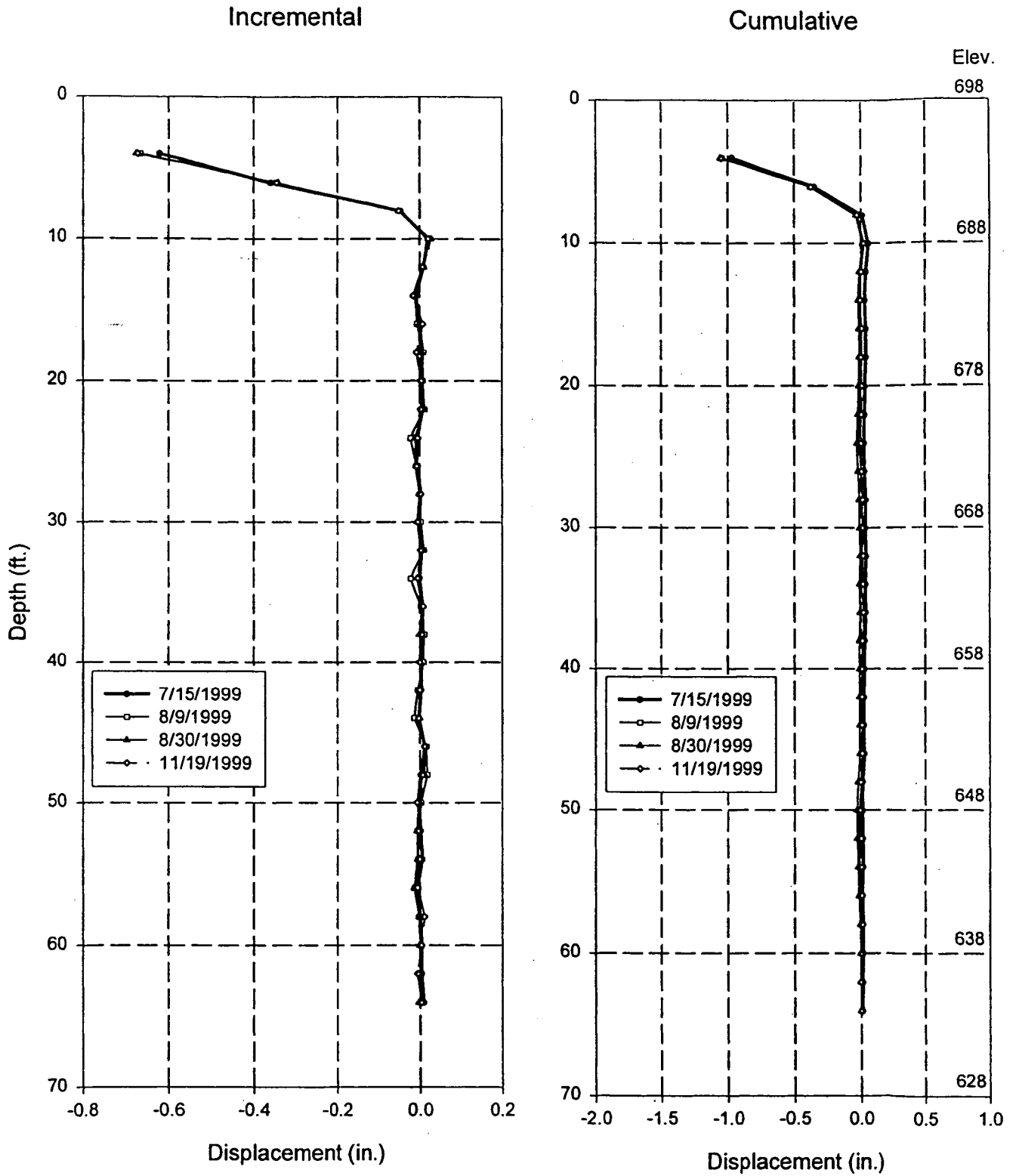
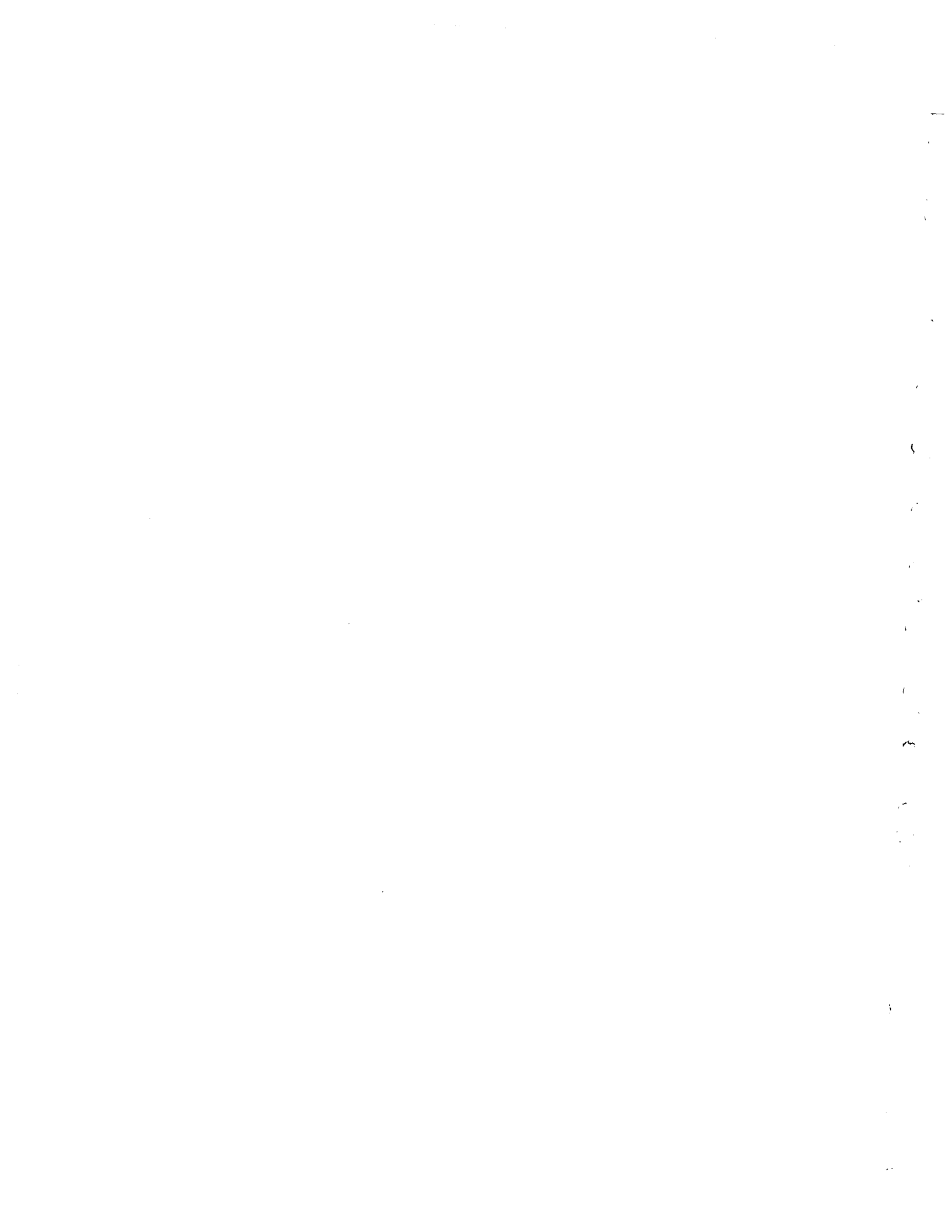


Fig. 112(b): Deflection vs. depth using inclinometer in the B+ direction (South) for soldier pile # 30 till 1/29/2000.



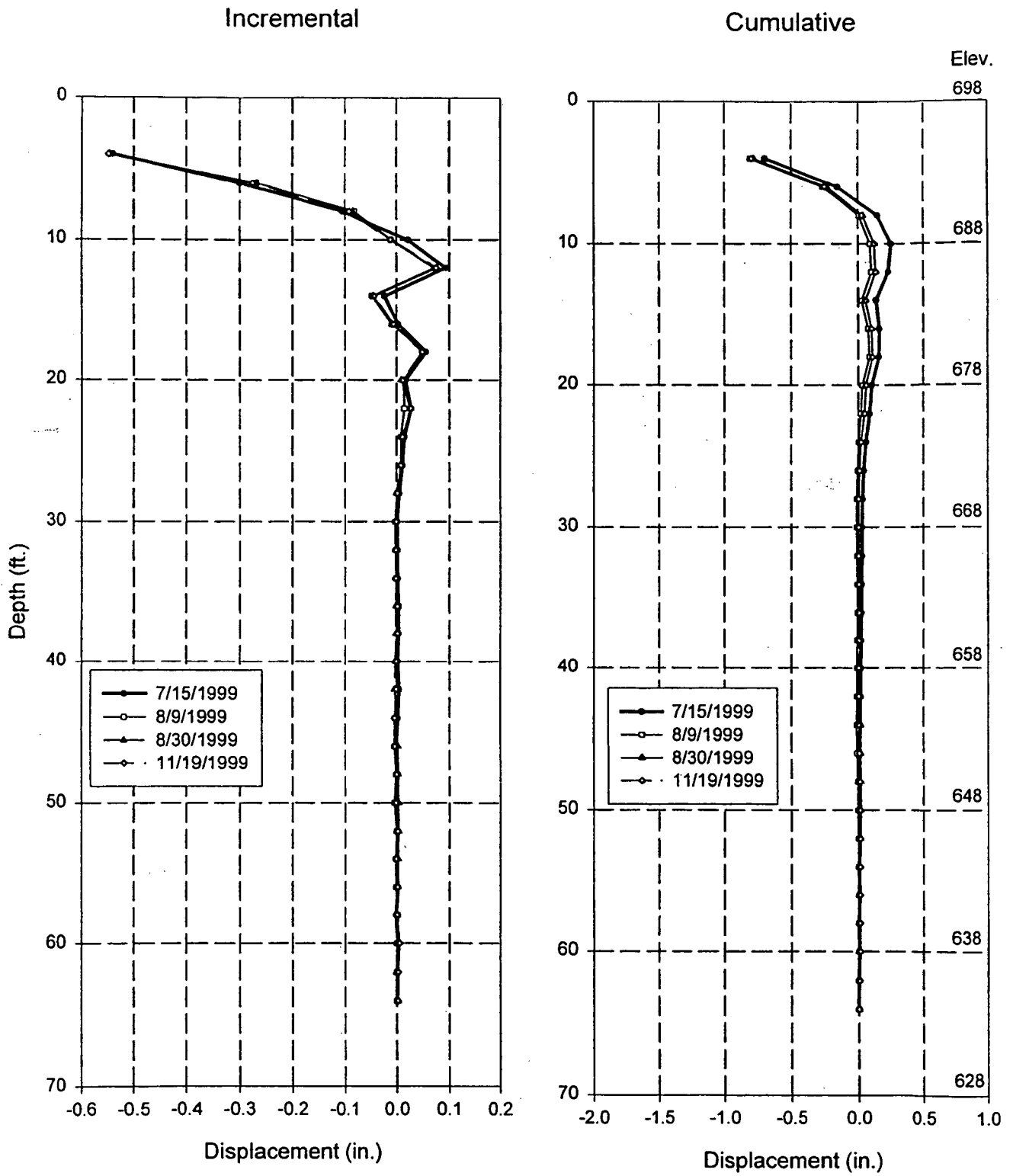


Fig. 113(a): Deflection vs. depth using inclinometer in the A+ direction (East) for soldier pile # 31 till 1/29/2000.



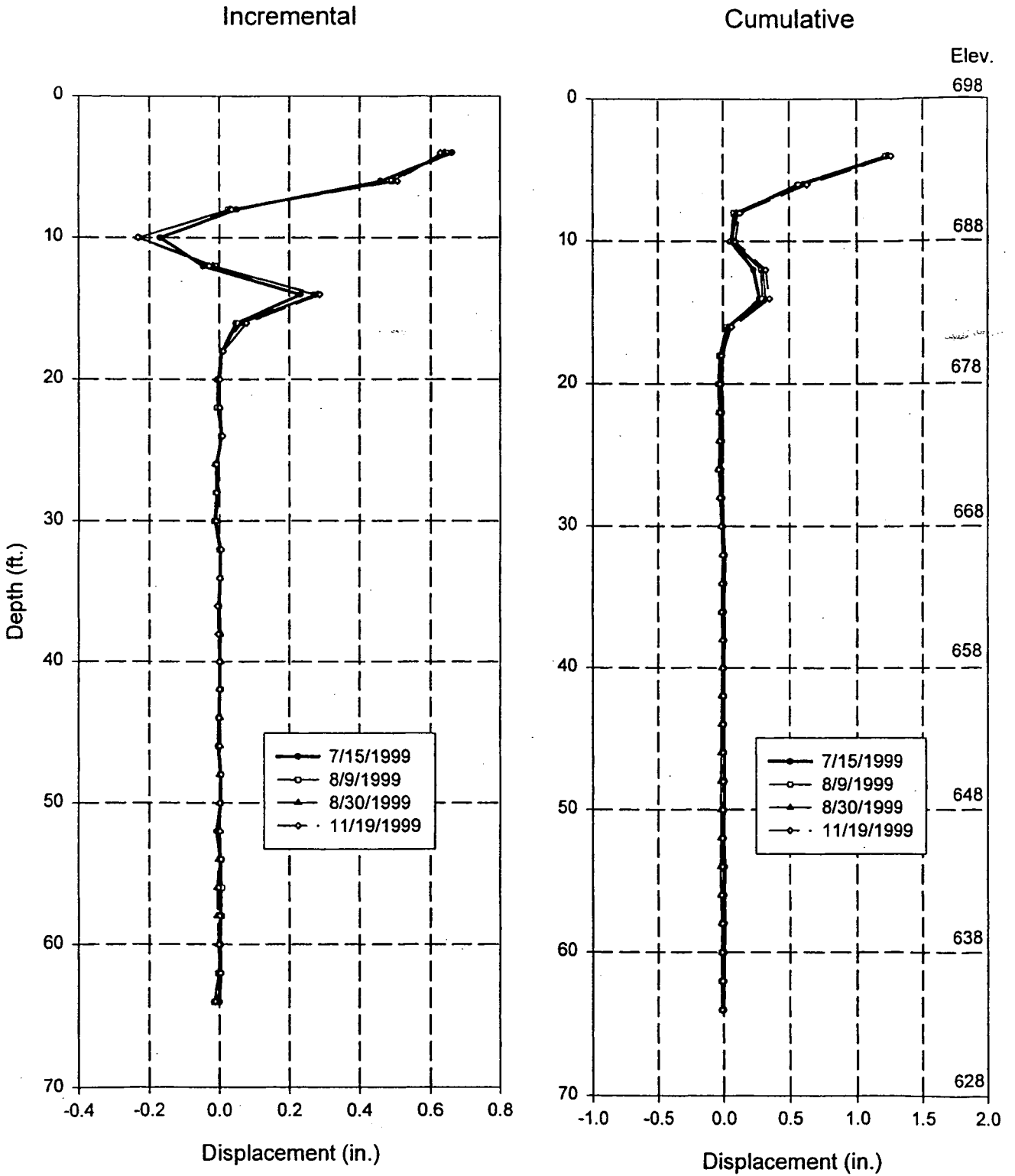


Fig. 113(b): Deflection vs. depth using inclinometer in the B+ direction (South) for soldier pile # 31 till 1/29/2000.

1
2
3
4
5
6
7
8
9
10
11
12
13
14
15
16
17
18
19
20
21
22
23
24
25
26
27
28
29
30
31
32
33
34
35
36
37
38
39
40
41
42
43
44
45
46
47
48
49
50
51
52
53
54
55
56
57
58
59
60
61
62
63
64
65
66
67
68
69
70
71
72
73
74
75
76
77
78
79
80
81
82
83
84
85
86
87
88
89
90
91
92
93
94
95
96
97
98
99
100

CHAPTER V

ANALYSIS OF ANCHOR TEST RESULTS

5.1 INTRODUCTION

Understanding the anchor-soil interface behavior is essential to determining the anchor pull-out capacity and predicting the deformation of the anchor-reinforced system under working load conditions. Numerous anchor pull-out tests under both laboratory and field conditions have generally yielded extremely high apparent interface strength, which cannot be explained by conventional theory using interface friction between the anchor material and the soil. In this study, the mechanism and the phenomena of the anchor-soil interaction were studied, and the soil dilatancy due to shearing was considered as the main factor contributing to the increase of the anchor-soil interface friction. Considering this dilatancy effect, along with the adoption of a cylindrical shear deformation pattern of the soil, anchor-soil interface models have been developed for either hardening or softening behavior. Using the developed interface models, forward and backward calculation algorithms have been formulated and applied to predict the anchor performance for the given interface parameters and to determine the interface parameters from the given anchor pullout test, respectively. The prediction of the anchor pullout performance was compared favorably with two hypothetical cases, two laboratory test results, and one field case.

The properties of the interface between the soil and the inclusion (e.g., ground anchor, pile, and geosynthetic) plays an important role in governing the response of the composite (soil/inclusion) system under applied loads. The load transfer behavior of the interface in terms of the relationship between shear stress and displacement is particularly important if one needs

to understand accurately the deformation behavior of the system under the working load conditions. In the area of ground anchor analysis/design, the attention paid to the interface shear stress-displacement properties has been very limited. In general, the practice (e.g., tieback wall anchors) calls for all of the installed anchors to be proof tested and at least 3-5% of the total number of the installed anchors be subjected to the performance test (Nicholson, et al, 1982; Otta, et al, 1982; Pfister, et al, 1982). All of these tests, however, only serve the purpose of verifying the design load for the safety against ultimate load-carrying capacity. These test results have not been used in such a way that they can provide information on the deformation of the system under the working loads.

The majority of research on ground anchors has been on the determination of the anchor pullout capacity under a variety of conditions, such as the embedded depth, the inclination angle, and the types of anchors and soils. In a few cases where the anchor load versus the anchor head displacement has been studied, the interface models used were mostly empirical in nature (Vijayvergiya, 1977; Coyle and Reese, 1966; Coyle and Sulaiman, 1967), or derived based on the pure shear test results of soils (Su and Fragaszy, 1988; Kraft, et al, 1981).

The existing interface models (e. g., Randolph and Wroth, 1978; Kraft, et al, 1981) developed for simulating the pile behavior under axial load assume that the surrounding soil is subjected to pure shear and under constant confining pressure. This assumption cannot be applied directly to modeling the anchor pull-out behavior, as both laboratory tests and field tests indicate significant soil dilatancy during anchor pull-out (Su and Fragaszy, 1988; Yoshimi and Kishida, 1982; Shields, et al, 1984). Due to shear dilatancy of the soil, the radial stress can reach as high as 20 times the overburden pressure. Because of the pronounced dilatancy effect, the use of the existing soil-pile interface model to predict ground anchor pullout behavior

would be erroneous. A soil-anchor interface model that is capable of taking into account the effects of dilatancy and confining pressure is needed.

During the course of this research, the following have been achieved:

- a. Development of soil-anchor interface models that explicitly include the effect of soil dilatancy, the confining pressure acting on the anchor, the relative stiffness between the anchor and the soil, and the size of the influence zone. Furthermore, both 'hardening' and 'softening' types of load transfer mechanism at the interface are considered.
- b. Presentation of a series of parametric study results to shed insights on the importance of the soil dilatancy, the relative rigidity, and the influence zone size on the anchor pullout behavior.
- c. Development of back-calculation algorithms to extract important soil-anchor interface properties from anchor pullout test results. The proposed back-calculation techniques can be used in practice to allow engineers to achieve more confidence and efficiency in predicting anchor performance.

5.2 DEVELOPMENT OF SOIL-ANCHOR INTERFACE MODEL

Generally, when the pullout force is applied to the anchor head, the soil surrounding the anchor will be subjected to shear. Consequently, three stages of soil particle movement can be identified (Morimich, et al; 1988, 1990): (i) the particles' relative movement (shear deformation of soil), (ii) transition of the particles' relative movement to rigid body movement (mixed shear deformation and sliding), (iii) rigid body movement (sliding). Each stage is associated with different interface behavior: stage 1 indicates that only shear deformation is developed in the

soil mass; in stage 2, yielding occurs at the interface with the accompanying shear deformation; and stage 3 indicates the onset of rigid body sliding along the interface. Correspondingly, two types of interface models are adopted, the hardening model (two stage model) and the softening model (three stage model), as shown in Fig. 5.1.

Some basic assumptions in the mathematical derivation of the interface models are summarized as follows: First, the dilatancy of the soil is considered as an average value during the entire range of loading. Second, the shear deformation pattern in the soil surrounding the anchor resembles a concentric cylindrical pattern, as shown in Fig. 5.2. Third, the work (energy) equation is applied. Last, the nonlinear behavior for the soil is represented by a hyperbolic equation. It should be noted that the above basic assumptions are adopted so that a simple mathematical equation can be developed. If desired, some of these assumptions can be relaxed or removed, resulting in a more complex equation.

$$\tau = R_0 \tau_0 / R \quad (5.1)$$

where:

R_0 = radius of the anchor, which is the distance from the central axis of the anchor to the interface surface.

τ_0 = basic shear strength of the interface without the effect of soil dilatancy.

From obtained mobilized shear stress (τ), the shear strain in the soil can be obtained from the following equation

$$\gamma = \tau / G \quad (5.2)$$

Where:

G = shear modulus of the soil.

γ = shear strain in the soil.

To simplify the dilatancy computation, the overall average dilatancy angle is used and the analogy is drawn between the condition and the cylindrical stresses and deformation as in the anchor condition. Thus, based on the concept of the soil dilatancy and referring specifically to Fig.5.3 (b). the following relationship can be established with:

$$\frac{\delta R}{\delta x} = \tan \psi \quad (5.3)$$

i.e.:

$$\frac{\frac{\delta R}{R}}{\frac{\delta x}{R}} = \tan \psi \quad (5.4)$$

where:

ψ = the average dilatancy angle of the soil within the stress range of interest

δR = the displacement in the radial direction

δx = the displacement in the direction of the anchor axis

Note that $\epsilon_R = \delta R/R$, and $\gamma = \delta x/R$, thus $\epsilon = \gamma \tan \psi$. Consequently,

$$\epsilon_R = \frac{R_0 \tau_0}{GR} \tan \psi \quad (5.5)$$

$$\sigma_R = \frac{ER_0}{GR} \tau_0 \tan \psi \quad (5.6)$$

Assuming that the external work is completely transferred to the deformation of the soil, we have,

$$w_e = w_p + w_s \quad (5.7)$$

where:

w_e = external work done by the applied load

w_p = energy stored in the soil body due to the radial stress

w_s = energy stored in the soil body due to shear deformation

The energy equation can be expanded as follows.

$$w_e = \frac{1}{2} T \frac{\tau_0 R_0}{G} \ln \frac{R_l}{R_0} \quad (5.8)$$

$$w_p = \frac{\pi R_0^2 \tau_0^2}{G} \ln \frac{R_l}{R_0} \frac{E}{G} \tan^2 \psi + 2\pi \sigma_0 \frac{R_0 \tau_0}{G} \tan \psi (R_l - R_0) \quad (5.9)$$

$$w_s = \frac{\pi \tau_0^2 R_0^2}{G} \ln \frac{R_l}{R_0} \quad (5.10)$$

where:

R_l = the radius of the influence zone

T = the axial force per unit length in the anchor

If one inserts these expressions in the energy equation, the mobilized maximum interface shear strength can be obtained as follows.

$$\tau_{\max} = \tau_0 \left(1 + \frac{E}{G} \tan^2 \psi \right) + 2\sigma_0 \tan \psi \frac{\frac{R_l}{R_0} - 1}{\ln\left(\frac{R_l}{R_0}\right)} \quad (5.11)$$

where:

τ_{\max} = maximum mobilized interface shear strength

It can be seen that the mobilized shear strength of the anchor-soil interface is a function of the basic anchor-soil interface strength, τ_0 , the size of the influence zone (R_l/R_0), and the dilatancy angle ψ .

Based on the adopted concentric cylindrical shear deformation pattern, the relative shear displacement at the interface, u , can be calculated as:

$$u = \int_{R_0}^{R_l} \frac{\tau}{G} dR \quad (5.12)$$

The hyperbolic nonlinear stress versus shear strain relationship for this interface can be described as follows.

$$G = (\tau, \sigma) = G_i \left(1 - \frac{\tau R_f}{\tau_f}\right)^2 \quad (5.13)$$

$$G_i = k p_a \left(\frac{\sigma}{p_a}\right)^n \quad (5.14)$$

where:

G_i = initial shear modulus

p_a = atmosphere pressure

k, n, R_f = hyperbolic soil model parameters

Thus, the expression of the interface displacement, u , as a function of the mobilized interface shear stress, τ , can be expressed as:

$$u = \frac{\tau R_0}{k p_a^{1-n} \sigma_0^n} \int_{R_0}^{R_f} R (1 + R_G R_R^{-1} R_\tau \tan \psi) (1 - R_R^{-1} f_\tau) dR \quad (5.15)$$

$$R_G = 2(1 + \nu) \quad (5.16)$$

$$R_R = \frac{R_L}{R_0} \quad (5.17)$$

$$R_\tau = \frac{\tau}{\sigma_0} \quad (5.18)$$

$$f_\tau = \frac{\tau_0}{\tau_f} \quad (5.19)$$

where ν = Poisson's ratio

5.3 CONSTRUCTION OF INTERFACE LOAD TRANSFER CURVE

For the hardening (two-stage) model, the derived relationship of the interface displacement vs. interface stress (Eq. 5.15) can be used directly to construct the interface load

transfer curve. Once the maximum mobilized interface strength is reached, the shear stress vs. displacement curve becomes horizontal (refer to Fig. 5.1). However, for the softening (three stage) model, the post peak portion of the curve cannot be evaluated by Eq. 5.15. Several empirical methods have been proposed by analogy to the direct shear test on soils (Su and Frigaszy, 1988; Kraft, et al, 1981). However, the condition of the direct shear test cannot truly represent the condition that exists at the soil-anchor interface. This is mainly because in a direct shear test the confining stress remains constant while the soil is allowed to dilate or compress, whereas in the anchor-soil interface the constant volume condition is maintained while the confining stress is varied. Thus, for all practical purpose, a straight line connecting between the peak point and the residual state is used to represent the post failure portion. Two parameters representing this post-peak straight portion are needed: the slope, m , and the ratio of the residual strength over the maximum strength, τ_{res}/τ_{max} , respectively. Kraft, et al. (1981) suggested the following values: the strength ratio, $\tau_{res}/\tau_{max} = 0.9$, and the displacement that occurs from τ_{max} to $\tau_{res} = 0.03 - 0.05$ inch (0.0762 cm – 0.127 cm) for sand, and about 0.1 inch (0.254 cm) for clay. It will be demonstrated in a later section that these parameters can be determined by back calculation, if the anchor pullout test results are given.

As discussed above, the parameters required to construct the anchor-soil interface load transfer curves are as follows: (1) the hyperbolic soil model parameters, k , n , R_p , (2) the influence zone radius ratio, R_i/R_0 , and the soil dilatancy angle, ψ , and (3) basic interface strength, τ_0 and confining pressure, σ_0 acting on the anchor-soil interface. If the softening model is used, two more parameters are needed: strength ratio, τ_{res}/τ_{max} , and post-peak straight line slope, m . Obviously, the model behavior will vary with the different combinations of these parameters, which will be presented in detail in the later sections.

Studies on the pile-soil interfaces have been carried out for more than two decades, a more representative contribution to the study of the stress transfer between the soil and pile is Kraft's theoretical $t - z$ curve (Kraft, et al, 1981). However, in their theoretical derivation, an empirical influence zone size and constant interface strength were used. As a result, the model cannot be used to account for the higher anchor capacity generally observed in laboratory and field tests (Shield, et al, 1984). When one compares the developed model with Kraft's equation, it can be observed that when the soil dilatancy is not considered, the interface stress vs. displacement curves exhibits the same trend for both models. However, once the dilatancy is included, the present model predicts an increase in the interface strength, which is enhanced by the size of influence zone.

5.4 NUMERICAL STUDIES

The developed nonlinear interface model is used to perform a series of parametric studies to gain insight into the influences of the various factors on the anchor behavior. The factors investigated include the dilatancy angle, ψ , the size of the influence zone as represented by R_f/R_o , and the relative rigidity α defined by the following expression.

$$\alpha = \sqrt{\frac{E_A A}{KL}} / L \quad (5-20)$$

where:

L = anchor bond length

K = average value of the interface modulus for the loading range from zero to yielding

A = anchor cross section area

E_A = modulus of anchor material

To demonstrate the importance of considering the dilatancy effect on the interface behavior, the dilatancy angle is varied between 5° and 25° , while maintaining other properties constant as follows: $\tau_o = 4 \text{ lb/in}^2$ (27.58 Kpa), $\sigma_o = 10 \text{ lb/in}^2$ (68.95 Kpa), $R_1/R_o = 20$, hyperbolic model parameters for the soil: $k = 500$, $n = 0.8$, $R_f = 0.9$, and the anchor properties: $D=1 \text{ inch}$ (2.54 cm), $E_A=29000000 \text{ lb/in}^2$ ($2.0 \cdot 10^5 \text{ Mpa}$).

As shown in Fig. 5.4, the mobilized interface stress increases dramatically as the dilatancy angle increases from 5° to 25° .

The effect of the size of the influence zone, represented by the ratio R_1/R_o , is shown in Fig. 5.5 (a) and (b) for the dilatancy angle of 5° and 25° , respectively. In general, an increase of R_1/R_o leads to an increase in the mobilized interface shear strength and a decrease in the interface stiffness. However, based on the cases studied, it is seen that the change of the interface stiffness caused by the change of the influence zone size is insignificant compared to the effect of the dilatancy angle.

For the case where the dilatancy angle is zero (the conventional approach), the interface stress versus the interface displacement is shown in Fig. 5.6. The parameters used in the analysis are also given in Fig. 5.6. The results indicate, in this case, that the ultimate interface strength is the same regardless the size of the influence zone (R_1/R_o). However, the size of the influence zone has greater effects on the stiffness of the stress versus the displacement. Theoretically, $R_1/R_o=1$ implies a perfectly rigid relative displacement at the interface (or lack of the influence zone); the interface stress versus interface displacement is a vertical line along the y axis in Fig. 5.6. From the above discussions, it is apparent that any design referring only to the maximum anchor pull-out capacity, τ_{max} , without taking into account the load transfer curve, is incomplete, especially when the working load and the related deformation are concerned.

Furthermore, when both the dilatancy angle, ψ , and the size of the influence zone, R_f/R_o , are accounted for, as shown in Fig. 5.7, the shear stress versus displacement relationships are quite different, even though the maximum interface strength is forced to be the same as shown in Fig. 5.7.

5.5 DEVELOPED ANCHOR-SOIL MODEL PREDICTABILITY

5.5.1 Anchor Performance by Forward Calculation

Based on the above anchor-soil interface model, a numerical iteration procedure is devised to analyze anchor performance. The iteration procedure is as follows: (i) divide the anchor bond length into segments and assume that the anchor-soil interface of each segment is represented by the middle point, (ii) calculate the force and the corresponding displacement of each segment, ensuring that force equilibrium and displacement compatibility are met, (iii) if the calculated anchor head force matches the given externally applied load, go to next load stage; otherwise, adjust the initial condition (anchor tip displacement), and repeat step (ii).

The conditions for the case studied are as follows:

Anchor parameters: $L=220$ in (588.8 cm), $D=1.0$ in (2.54 cm)

Soil parameters: $k=200$, $n=0.8$, $R_f=0.7$, $\nu=0.25$

Interface parameters: $\tau_0 = 4$ lb/in² (27580 pa) $\sigma_0 = 10$ lb/in² (58690 Pa) $\psi = 10$, $R_f/R_o = 50$

For the softening model: $\tau_{res}/\tau_{max} = 0.8$, $m = 0.4$ Pa/in²/in (2.76 Kpa/cm)

The calculation results for the hardening interface model (two stage model) are obtained and shown in Fig. 5.8(a) ~ (c). It is expected, as shown in Fig. 5.8(c), that the maximum pullout capacity of the anchor will be developed when the entire bond length of the anchor is at the state of yielding. At this state, the relationship between the applied anchor head force and the

anchor head displacement becomes horizontal, as shown in Fig. 5.8(a). Before reaching this state, the mobilized anchor-soil interface stress and the anchor tension are distributed along the anchor length as shown in Figs. 5.8(b) and 5.8(c), respectively.

The calculated results for the softening model (three stage model) are plotted in Figs. 5.9(a) ~ (c). Due to the drop of the shear strength after reaching the peak value, the maximum pull-out capacity of the anchor depends on a number of factors, such as the ratio of residual strength over the maximum strength, τ_{res}/τ_{max} , anchor bond length, L_b , and the slope of interface strength drop, m .

The pattern of the load transfer (or the mobilization of the interface stress) has been found to depend greatly on the relative rigidity, α , defined previously. The larger the relative rigidity factor, the smaller the relative elongation of the anchor in the system. Thus, an increase of the relative rigidity factor leads to a more linear pattern of load transfer along the anchor, as illustrated in Fig 5.10. When the relative rigidity of the anchor is high enough, uniformly distributed interface stress will be obtained. Further computations showed that when the relative rigidity of the anchor is greater than $1/10$, the anchor elongation is negligible; it implies that the anchor can be simply treated as a rigid bar.

5.5.2 Determination of Interface Model Parameters by Back Calculation

The previous section has provided numerical examples to show the capability of the developed anchor-soil interface models to predict the anchor performance, provided that the representative anchor-soil interface model parameters are given. The determination of the representative interface model parameters from the traditional soil testing techniques is difficult, due to the fact that numerous factors tend to affect the interface behavior. These

pull-out force vs. displacement were obtained through the forward calculation. The calculated results are compared with test results in Fig. 5.12(b) and Fig. 5.13(b) for the hardening and softening models, respectively. It can be seen that the interface parameters by the developed back calculation algorithm will yield anchor pull-out performance close to the given test results for both hardening and softening models.

It is worth noting that only two interface parameters are used in the back calculation: a dilatancy angle and influence zone radius ratio. The basic interface strength τ_0 is considered fairly constant. Generally, the value of basic interface strength is referred to as the friction on the interface between the soil and anchor, as expressed by:

$$\tau_0 = \mu \sigma_0 \quad (5.24)$$

where:

μ = interface basic friction factor

σ_0 = confining pressure acting on the anchor-soil interface

For the magnitude of σ_0 , it is normally determined by the overburden pressure or the grouting pressure. On the other hand, the value of μ might vary from 0.3 to more than 1.0 according to the reports by previous investigators (Vitto, 1991; Littlejohn 1980). However, the value of μ ranging from 0.4 to 0.8 has been suggested. Therefore, in the following sensitivity analysis, the value of μ was varied from 0.3 to 1.1, while the other parameters were kept constant as follows:

(i) Anchor parameters: $D=1.0$ inch (2.54 cm), $L = 240$ inch (60.9.6 cm), $E_A=29000000$ lb/in² ($2.0 * 10^5$ Mpa);

(ii) Interface parameters: $R_i/R_0 = 80$, $\psi = 10^0$,

(iii) Hyperbolic model parameters for soil: $k=200$, $n=0.8$, $R_f=0.95$,

The hardening interface model is used in this sensitivity analysis. The calculated results are shown in Figs. 5.14(a), and 5.14(b) for the interface shear stress vs. interface displacement, and anchor head force vs. anchor head displacement, respectively. In both cases, the change in basic interface strength does not seem to alter greatly the calculated results. For practical purposes, it is reasonable and sufficient to choose the value of basic friction factor between 0.5 and 0.9.

5.6 VERIFICATION OF THE ANCHOR-SOIL MODEL PREDICTIBILITY

5.6.1 Comparison between Predictions and Laboratory Test Results

In this section, the laboratory tests conducted by Vitton (1991) are used to evaluate further the capability of the back-calculation and forward prediction algorithm of the developed interface models.

The results of a group of a 0.5 inch diameter rebar with 36 inch embedment under the confining pressure of 5 psi (34.5Kpa), 10 psi (68.9 Kpa), 15 psi (103.0Kpa) are used in this comparison study. The soil used in the test is 20-30 Ottawa loose sand, with $k=100$, $n=1.2$, $R_f=0.7$, and $\nu=0.25$.

First, the results of the pull-out test under the confining pressure of 5 psi (34.5Kpa) were used to determine the anchor-soil interface parameters via the back calculation algorithm. Next, with these interface parameters as input, the anchor performance was predicted for the cases where the confining pressures are 10 psi (68.9Kpa) and 15 psi (103.0Kpa), respectively. The comparisons between the predictions and the test results are shown in Fig. 5.15(a) and 5.15(b), for 10 psi (68.9Kpa) and 15 psi (103.0Kpa) confining pressure, respectively. It can be

seen that the overall agreement between the predictions and test measurements is good, especially when the applied anchor load is relatively small. On the other hand, it can be seen that the difference between the prediction and test measurement becomes more pronounced with an increase of the applied anchor load. At the final state, the prediction yields a little bit higher capacity but smaller displacement compared to the results of the tests. The main reason for the discrepancies is the treatment of the boundary conditions in the model. In the tests, the boundary condition is basically a flexible one with a constant confining pressure. As a result, the effect of confining pressure will not be fully developed in the test chamber. However, in the field condition and in the anchor-soil model, the rigid displacement boundary condition allows for the confining pressure to change due to the shear action, which will enhance the interface strength and interface rigidity as well. Therefore, the higher capacity and smaller displacement predicted by the model are to be expected. Meanwhile, the comparisons indicate that the effect of boundary condition becomes more pronounced when the initial confining pressure is higher.

5.6.2 Tieback 622-1, Outlined in Ludwig Study

Tieback 622-1 outlined in the Ludwig (1984) was a straight-shafted ground anchor installed at Charlotte, North Carolina. Soil conditions at the site are summarized in Table 5.1. The tieback is 60 ft (18.3 m) long, 1-1/4 in (32 mm) diameter threaded bar with an ultimate strength of 93.8 tons (835 KN), grouted inside a 2.5 in (65 mm) corrugated plastic tube. The bonded length of tieback was covered with a smooth plastic tube. The installation of the tieback was done using a 12 in (305 mm) diameter, continuous flight, hollow-stem-auger. The drillhole was grouted to the surface. Grout pressure generally did not exceed 150 psi (1035 Kpa).

Instrumentation used in the study included the Hitec HBW-35-250-6-3VR weldable, electrical resistance strain gages. Both zero shift and drift were taken into account by Ludwig (1984) in reducing the data. In addition to strain gages, extensometers were used to provide the measurement of the performance of the grout column above the anchor of the straight-shafted tiebacks.

In facilitating the computations of the algorithm, a PC based computer program has been developed (Liang and Feng 1997). An interactive feature of the computer program allows the user to input the required parameters easily. In analyzing the current case, the back-calculation method was used to obtain the load-transfer t-z curves along the shaft-soil interface. The following steps were followed.

Step1: Select the interface model type (hardening or softening model) and calculation method (back or forward calculation). In this case, the hardening model with back-calculation scheme was selected.

Step2: Input the required parameters. The parameters for the present case are as follows: (i) anchor parameters: anchor length =590 in (1498.6 cm), anchor diameter =1.375 in (3.49 cm), drillhole diameter =12 in (30.48 cm), (ii) soil parameters: hyperbolic soil parameters $k=100$, $n=0.9$, $R_f=0.8$, Poission ratio=0.2, (iii) interface parameters: soil-grout interface basic strength =1.3 psi (8.96Kpa), interface confining pressure =30 psi (206.85Kpa), modulus of tieback =29000000 psi ($2.0 \cdot 10^5$ Mpa). Also, the user needs to specify the number of segments to be used to divide the bonded length in the numerical calculations. Typically, 20 to 30 segments are used to divide the total bonded length.

Step3: Input load-displacement curve measured at the anchor head from the pullout tests. Table 5.2 summarizes the actual measured load-displacement data for Tieback

622-1. It should be noted that the time-dependent displacement was not considered in the present study.

The back-calculation generates the interface load transfer curve (t-z curves) using the above input information. The output of the current analysis is shown in Fig. 5.16, in which the actual measured t-z curve is shown for a comparison purpose.

Once the back-calculated load transfer curve (t-z curve) is obtained, then the user can choose the forward calculation option to calculate the load-displacement curve at the anchor head and distribution of the load transfer along the anchor. Shown in Fig. 5.17 is the comparison of the load-displacement response of Tieback 622-1 between actual test results and the forward calculation results. In addition, Fig 5.18 shows the distribution of the load transfer along the anchor length at different loads. By and large, the proposed calculation algorithm seems to be able to capture the load transfer behavior quite accurately.

5.7 UPPER AND LOWER TIER FAILURE TESTS AT SUM-82 PROJECT

The failure tests conducted at SUM-82 project were further used as a case study to further judge on the validity of the model in predicting the anchor pullout test results (load deformation) curve.

The interface model parameters are first evaluated through a semi-iterative parametric optimization process, employing a measured load-deformation curve with an assumption of a two stage interaction model. Next, the deduced model parameters are checked by applying them to a different anchor pullout test. In the first step, the upper tier anchor (Anchor No. FT1) load-deformation curve and the associated data were used to back-calculate the interface parameters.

These interface parameters were then used in the lower tier anchor (Anchor No. FT2) to judge on the quality of the predicted versus the measured load-displacement curve at the anchor head.

The back-calculation process aimed at evaluating the interface shear strength, dilation angle, influence ratio, as well as the interface modulus. Due to the number of variables introduced, it was necessary to alternatively assume one of these parameters. The optimum parameters are those resulting in the best fit of the load-deformation curve, and satisfying the range of the measured deformation. For the upper tier, the input data was as follow:

Anchor: total length, $L = 553.2$ in (46.1 ft)
bonded length, $L_b = 180.0$ in (15 ft)
diameter, $D = 1.0$ in.
 $E = 28800$ ksi

Interface: $R_o = 1.5$, $\sigma_o = 3.8$ psi, $\psi = 5^\circ$
Strength, $\tau =$ variable, $R_1/R_o =$ Variable,

Soil: $n = 0.8$, $R_f = 0.9$, $\nu = 0.3$
 $K =$ variable.

Figure 5.18 shows the deduced curve as compared to the measured. The deduced interface parameters are as follows:

Strength, $\tau = 420$ psi, $K = 110$, and $R_1/R_o = 75$.

These parameters were then introduced to the lower tier anchor for which the whole set of parameters would be:

Anchor: total length, $L = 327.6$ in (27.3 ft)
bonded length, $L_b = 180.0$ in (15 ft)
diameter, $D = 1.0$ in. $E = 28800$ ksi

Interface:	$R_o = 1.5,$	$\sigma_o = 50 \text{ psi},$	$\psi = 5^\circ$
	Strength, $\tau = 420 \text{ psi},$	$R_1/R_o = 75,$	
Soil:	$n = 0.8,$	$R_f = 0.9,$	$\nu = 0.3$
	$K = 110.$		

The predicted curve gave a fairly good match with the measured load-deformation curve as shown in Figure 5.19. It was noticed that the deduced curve began to show some signs of yielding, whereas the measured load was still linearly changing with deformation. Due to the very high confining stress at the anchor level, the dilation angle would logically be greater than that in the upper tier. Thus it was decided to alter the dilation angle to obtain a better fit for the lower tier. Changing the dilation angle to 15° resulted in a very good match as can be seen in Figure 5.20.

V.8 DISCUSSION

The field case studies and the previous comparisons with laboratory pullout tests were geared towards uniform soil deposits, in which the load transfer curve (t-z curves) can be considered to be the same for the entire anchor length. In many actual cases, however, a layered soil deposit is likely to be encountered. The proposed algorithm theoretically can take into account the presence of multi-layers by allowing for more than one load transfer curve to be determined via the back-calculation scheme in the program. One of the drawbacks, though, is that the more t-z curves specified in the program, the more difficult it is for the program to attain a convergent solution. There is also a question about the uniqueness of the back-calculated load transfer curves, although the Summit-82 case study indicated that the

uniqueness issue might not be significant. During the parametric optimization process, it was found that all variables exerted a limited influence on the final load-deformation curve.

The emphasis of the current modeling was placed on the interface of the straight-shaft anchor, with the grouting pressure typically small. The failure mode associated with this type of anchor during the pullout test will be along the shaft-soil interface. Other types of failure modes, such as cone shaped or wedge-type, certainly are possible in other anchor types. The consideration of these failure modes is outside the current model's capability.

V.9 CONCLUSIONS

The following conclusions can be drawn from this chapter:

(1) The mobilized interface shear strength is strongly dependent upon the soil dilatancy angle and the size of influence zone. In general, an increase of either one of them would lead to an increase of the mobilized shear strength. The dilatancy, strength, and interface modulus (k) showed very limited contribution after reaching definite limiting values.

(2) The rigidity of the anchor-soil interface increases drastically with an increase of the dilatancy angle, but decreases with an increase of the influence zone size. However, the latter factor is negligible for the dilatancy angle from 5° to 25° .

(3) The distribution of the mobilized anchor force along the anchor bonded length is strongly dependent upon the relative rigidity of the anchor. For the case where the relative rigidity factor is larger than $1/10$, the distribution is linear.

(4) By using the back calculation technique, the important interface model parameters can be determined accurately, which can then be used to predict the performance of the anchors with different design lengths.

(5) a further study may be oriented to evaluating suitable parameters for different soil/rock materials. Based on the cases analyzed earlier in this section, it was clear that the parameters of different materials differ considerably.

Table 5.1 Soil data for Tieback 622-1

Soil properties				
Properties	Values			
Degree of saturation	84%			
Liquid limit	60%			
Plastic limit	46%			
Plasticity index	14%			
Specific gravity	2.87			
Natural water content	56%			
Dry density	1.0 mg/m ³			
Preconsolidation pressure	270 kpa			
Undrained shear strength	54 kpa (vertical)			
(unconfined compression test)	59 kpa (horizontal)			
Grain size distribution				
Sand	28%			
Silt	52%			
Clay	20%			
Soil strength parameters (direct shear test)				
Strength	C _u (Kpa)	φ _u	C' (Kpa)	φ'
Peak soil-soil	49	19.5		
Residual soil-soil	24	18		
Peak grout-soil	25	35		
Residual grout-soil	9	34		
Consolidated undrained triaxial test	67	4	62	8

Table 5.2 Load-displacement measurements for Tieback 622-1 (Ludwig, 1984)

Applied load at anchor head (KN)	Anchor head displacement (cm)
111	0.0076
223	0.0787
334	0.1448
445	0.2540
556	0.3556
668	0.5334
779	1.016

Fig. 5.9: Calculated results for the softening interface model (three stage model).
(a) Anchor head force vs. anchor head displacement (P-U),
(b) Anchor tension evolution,
(c) Anchor-soil interface shear stress evolution.

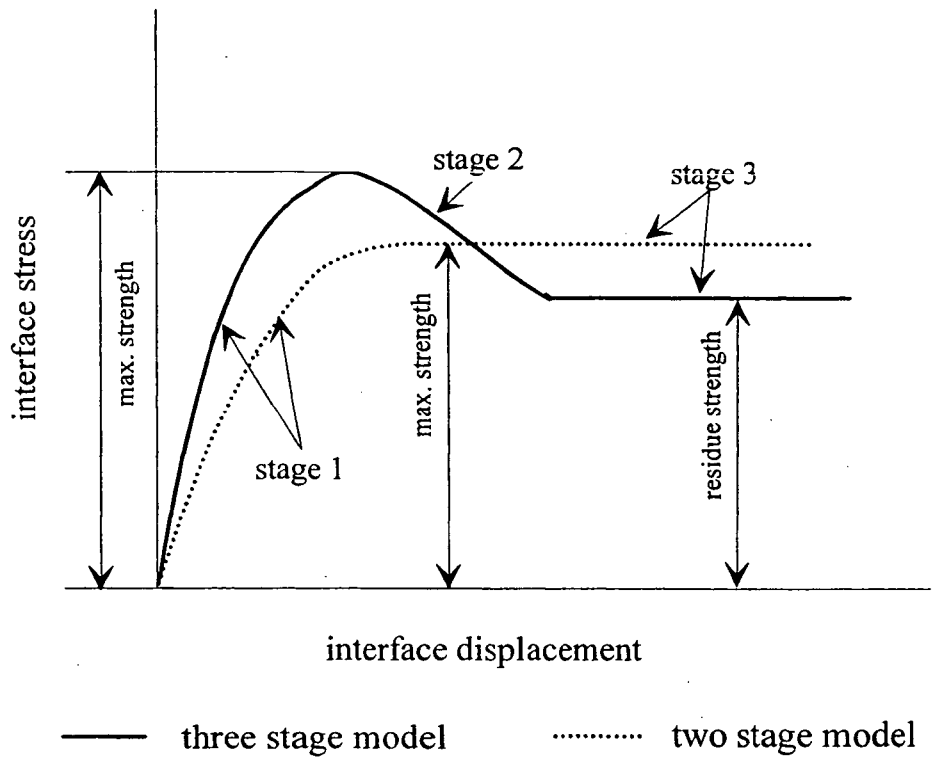


Fig 5-1: Schematics of three stage and two stage models.

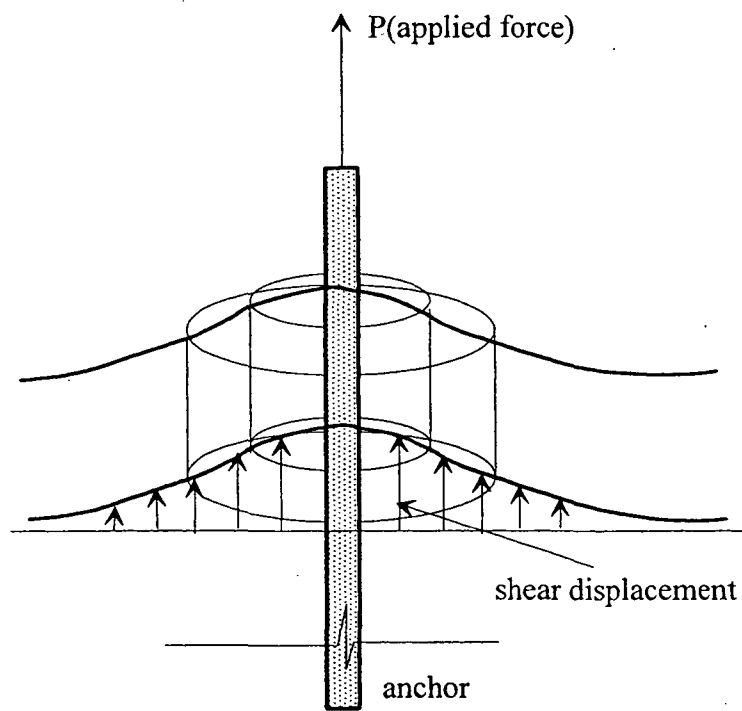
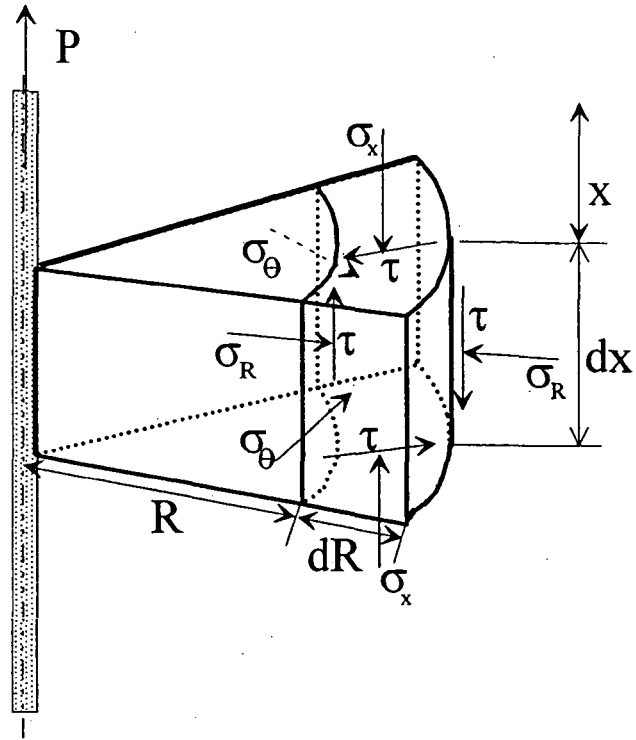
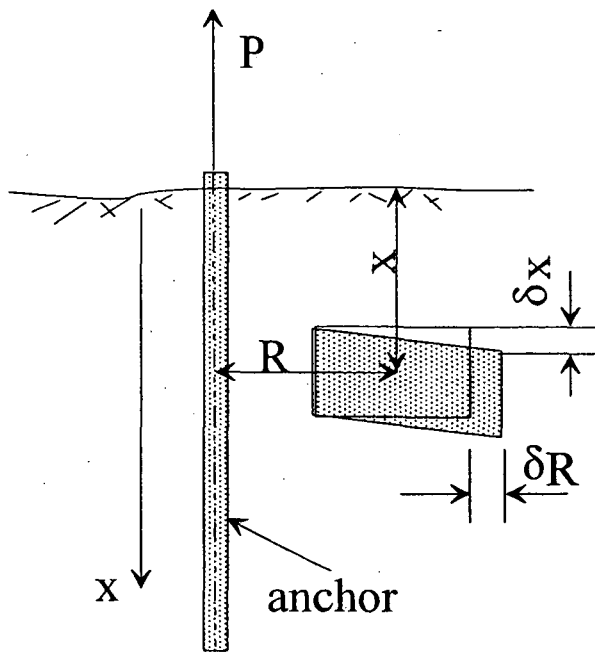


Fig. 5.2: Shear deformation pattern in the soil surrounding the anchor.



(a)



(b)

Fig. 5.3: Soil element force equilibrium in vertical and radial directions.

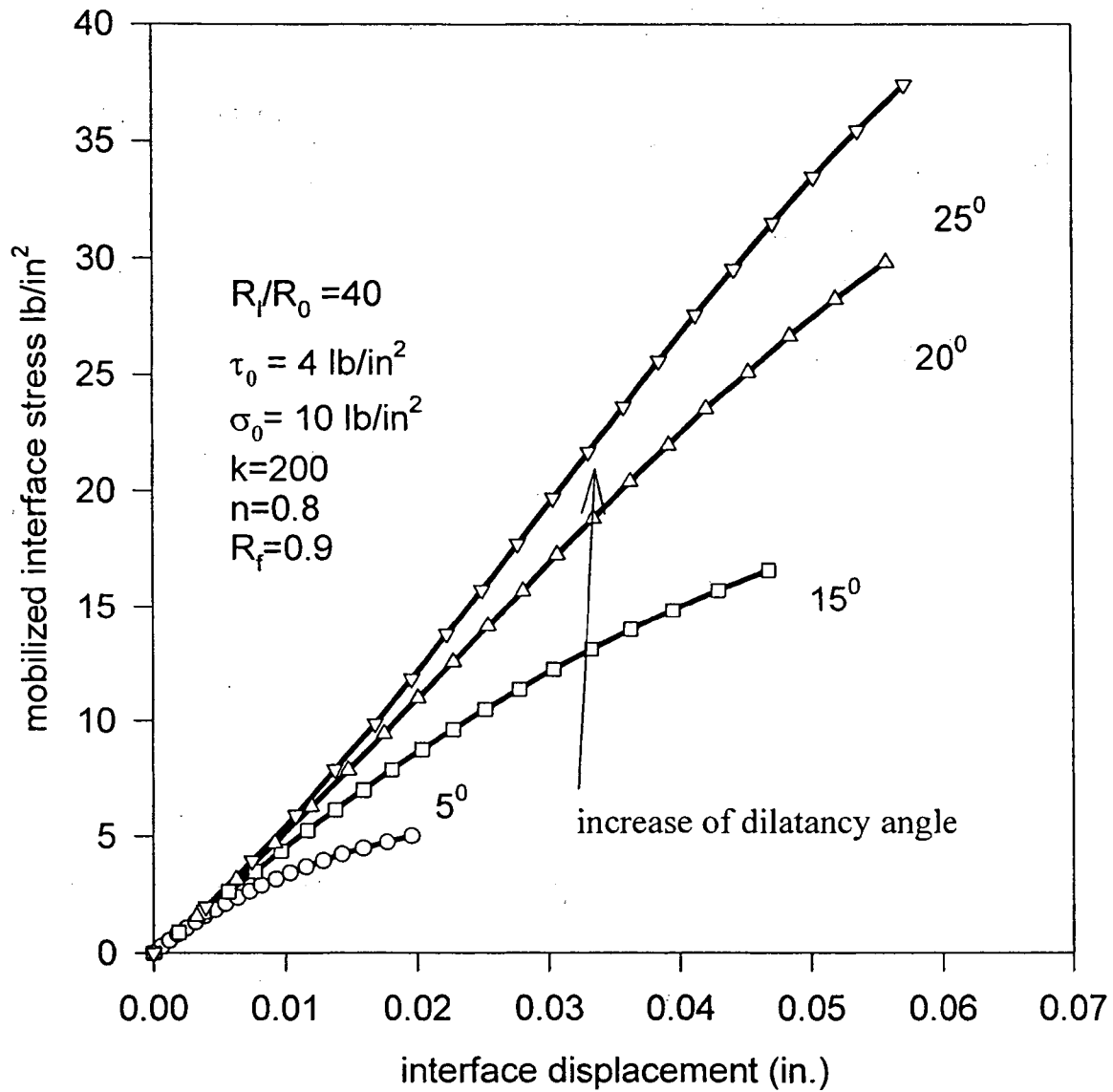


Fig. 5.4: Mobilized interface stress versus interface displacement for dilatancy angle from 5° to 25°.

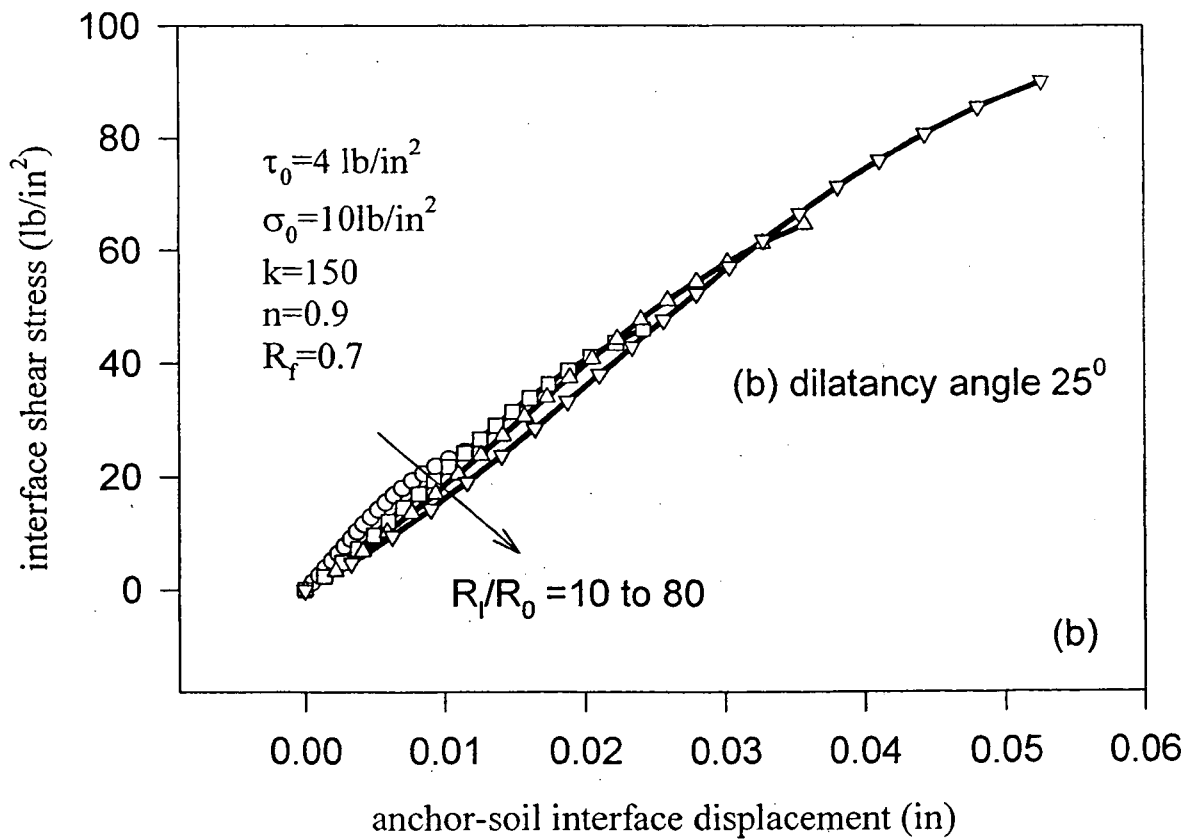
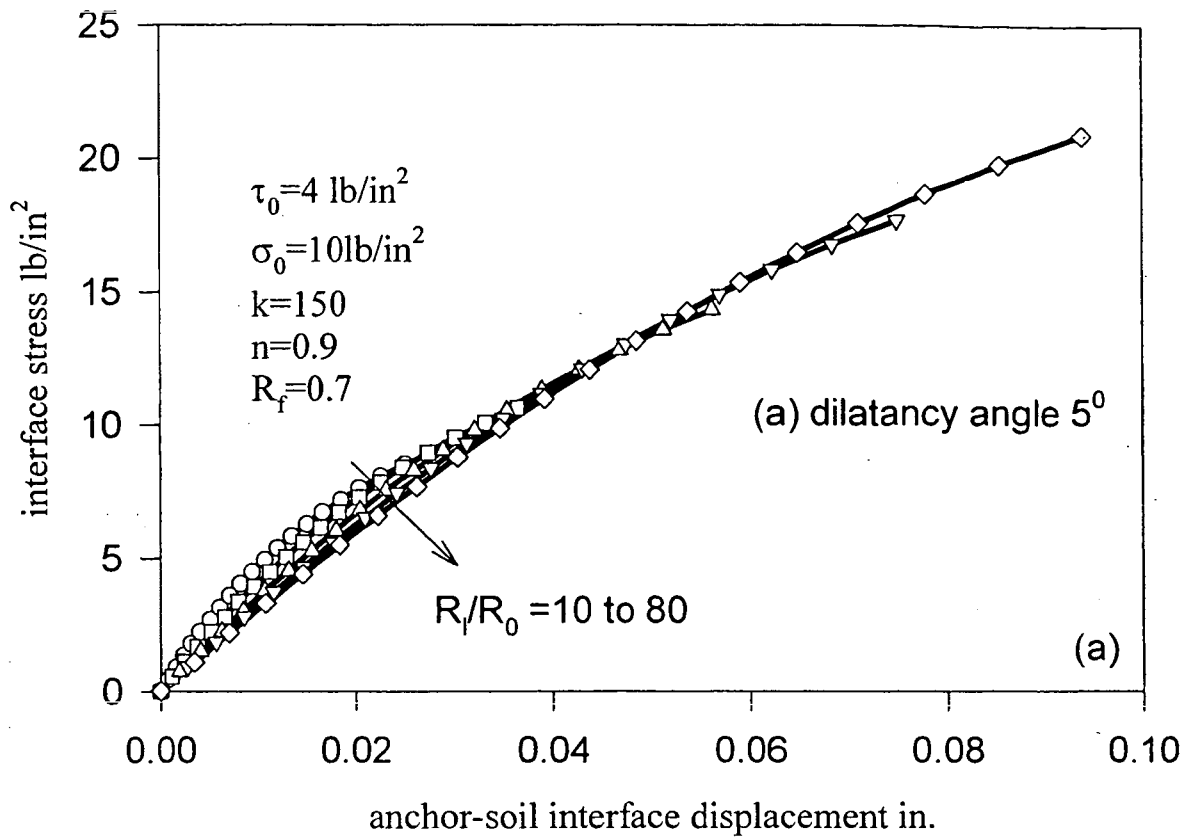


Fig. 5.5: Effect of influence zone on the development of interface stress versus interface displacement.

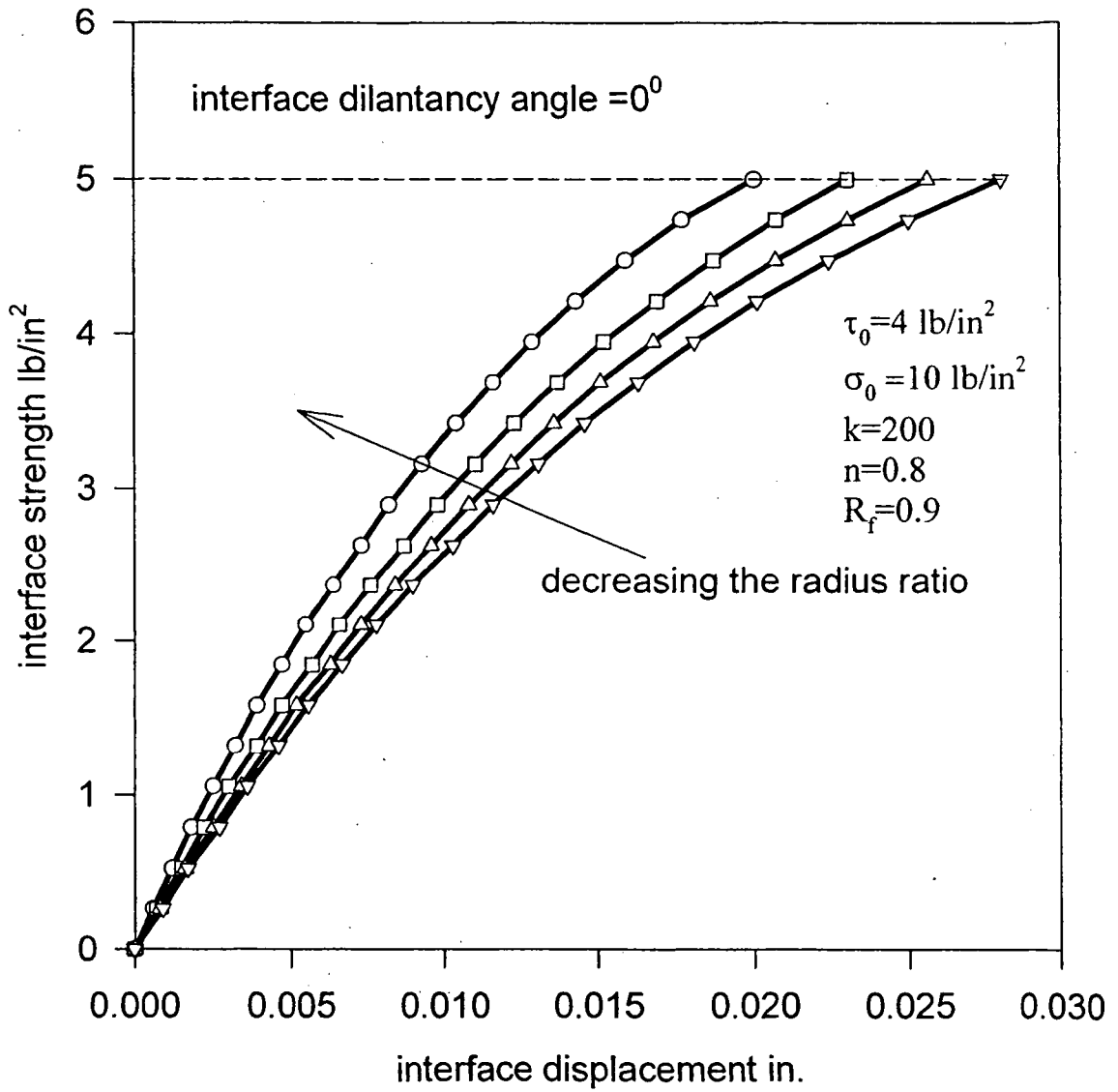


Fig. 5.6: Interface stress versus interface displacement for $\gamma=0^{\circ}$.

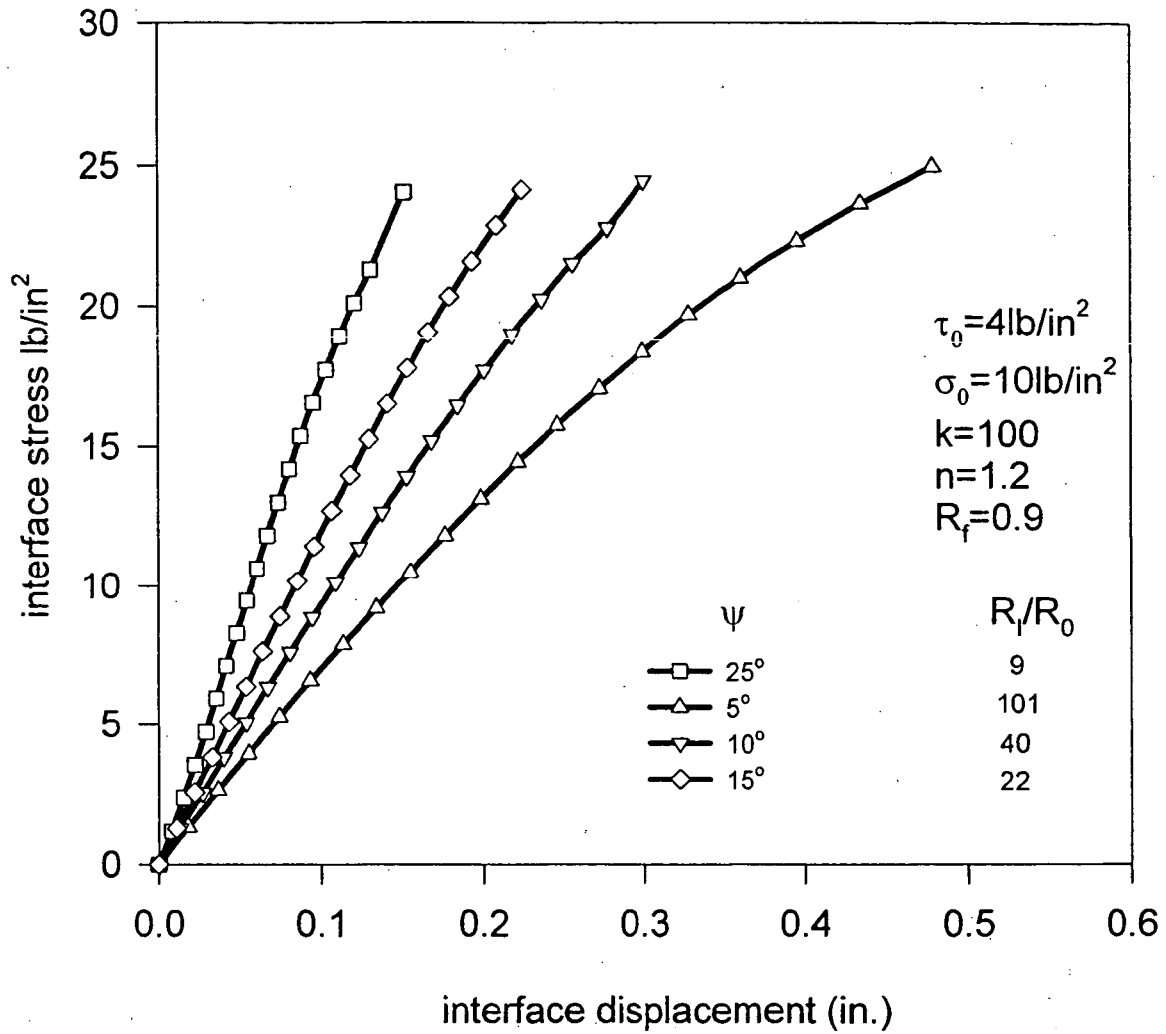


Fig. 5.7: Anchor-soil interface behavior for the given maximum mobilized interface strength

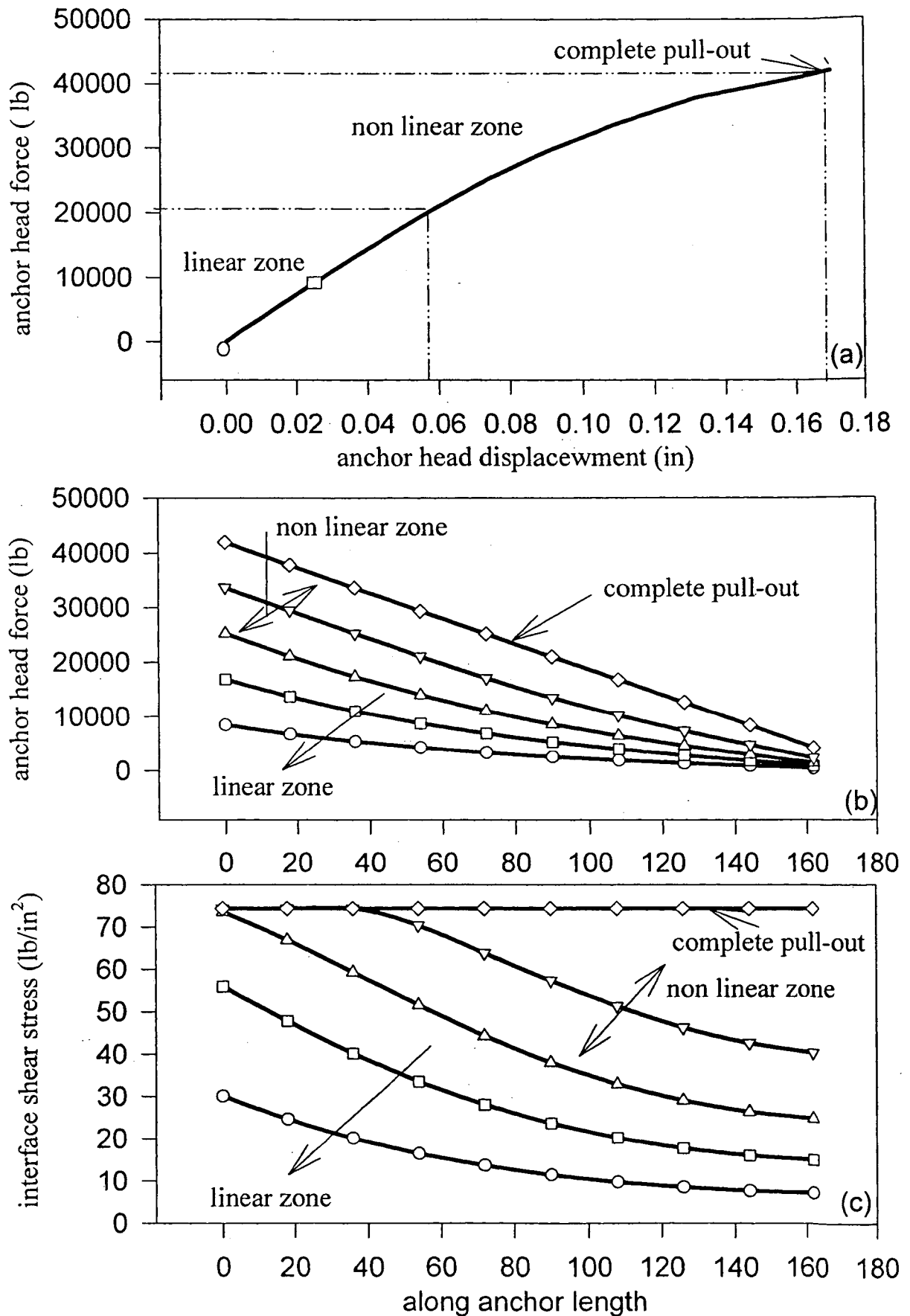


Fig. 5.8: Calculation results for the hardening interface model (two stage model), (a) anchor head force vs. anchor head displacement (P-U curve), (b) Anchor tension evolution, (c) anchor-soil interface shear stress evolution.

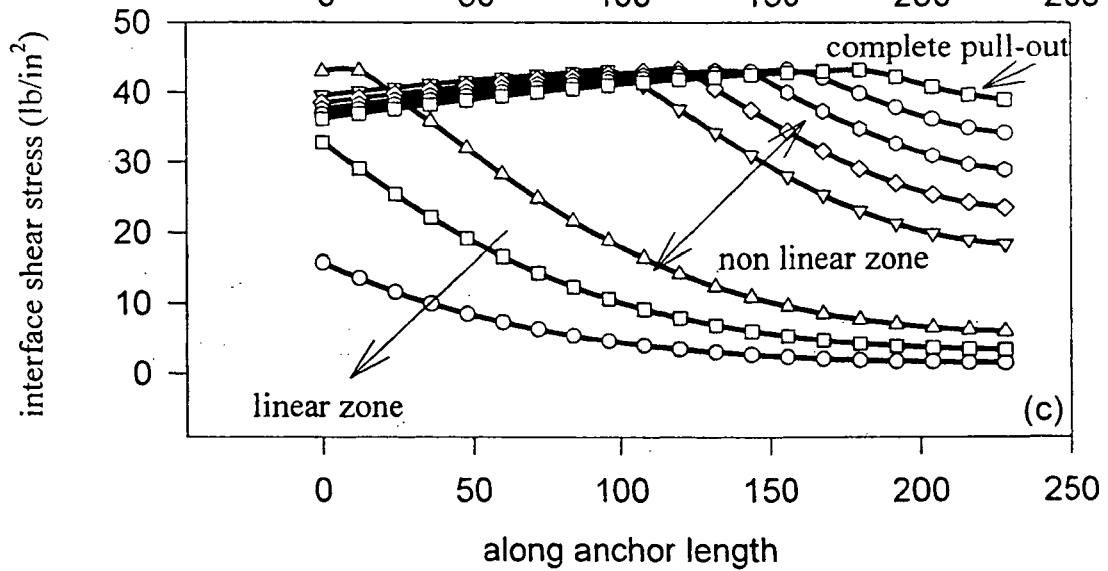
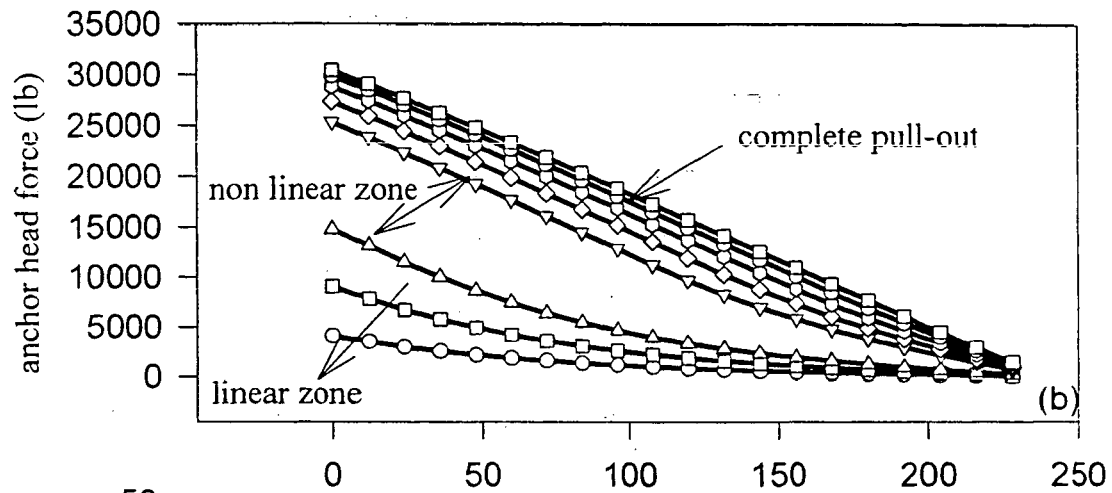
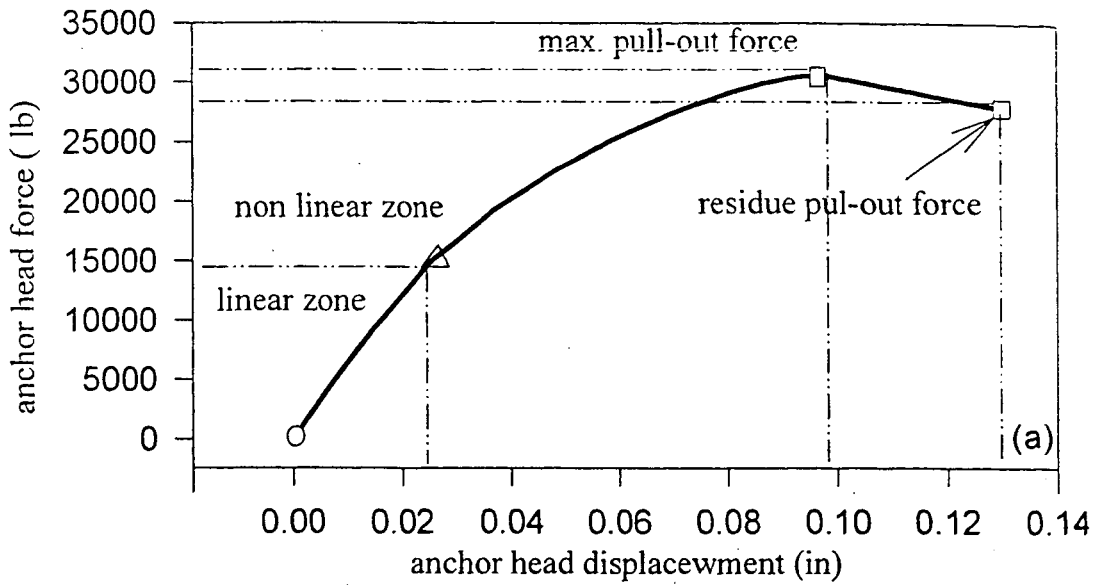


Fig. 5.9: Calculated results for the softening interface model (three stage model).

(a) Anchor head force vs. anchor head displacement (P-U),

(b) Anchor tension evolution,

(c) Anchor-soil interface shear stress evolution.

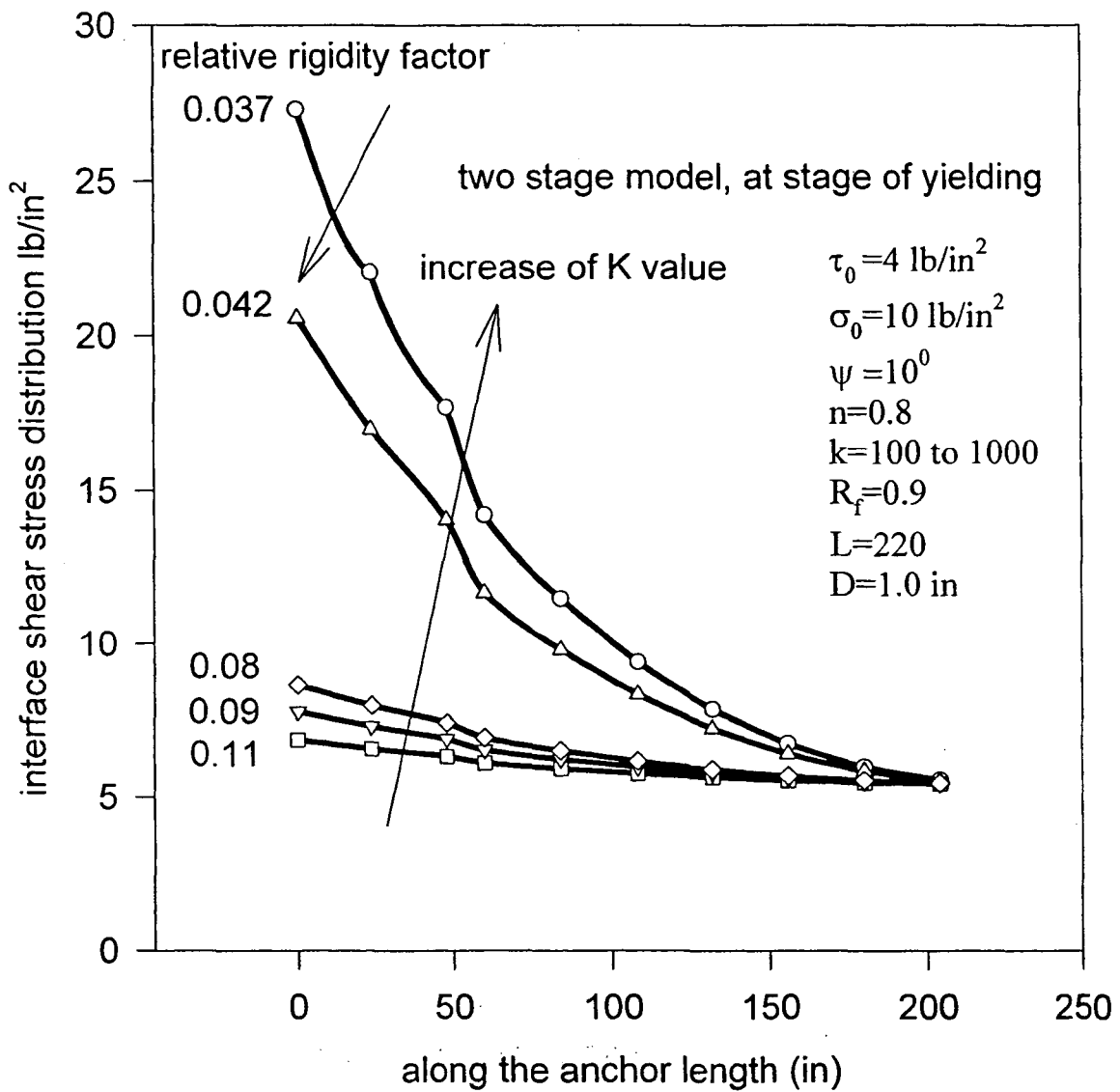


Fig. 5.10: Effect of the anchor relative rigidity factor on the anchor-soil interface shear stress distribution.

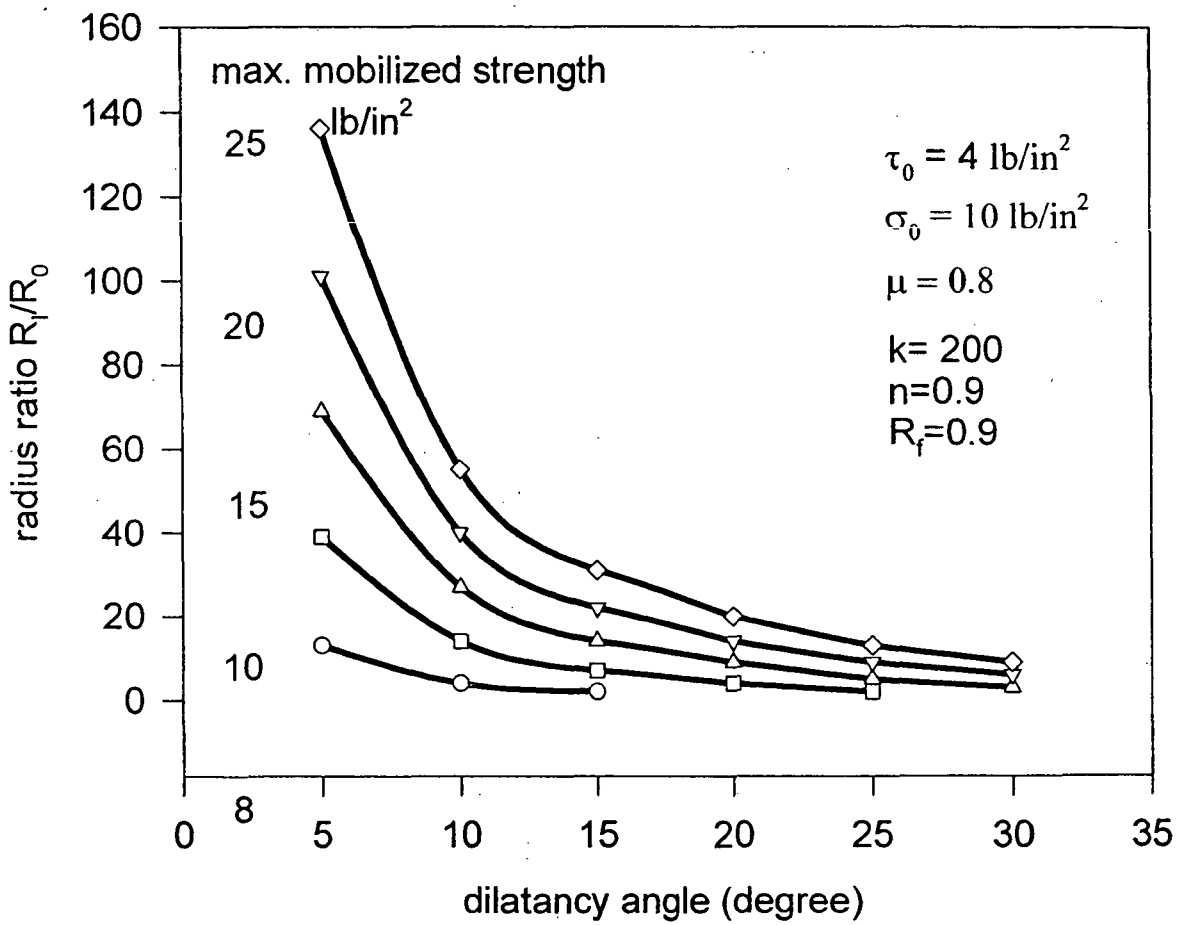


Fig. 5.11: The relationship between dilatancy angle and radius ratio.

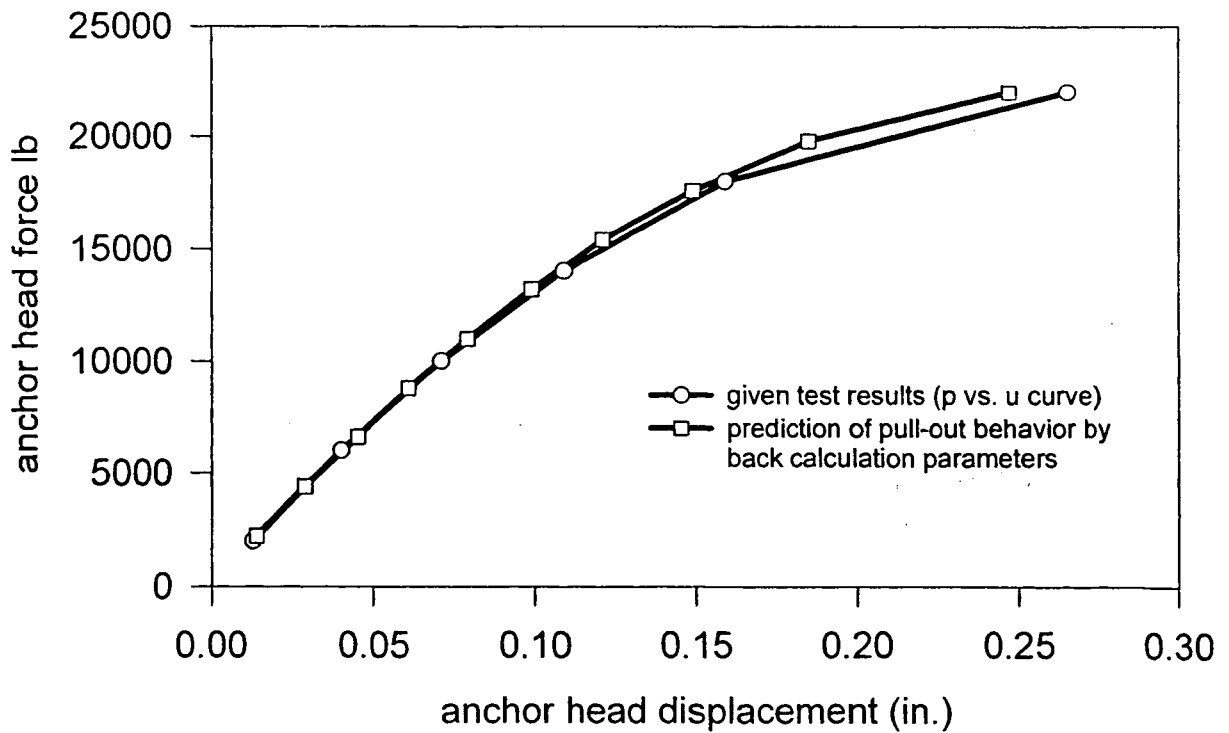
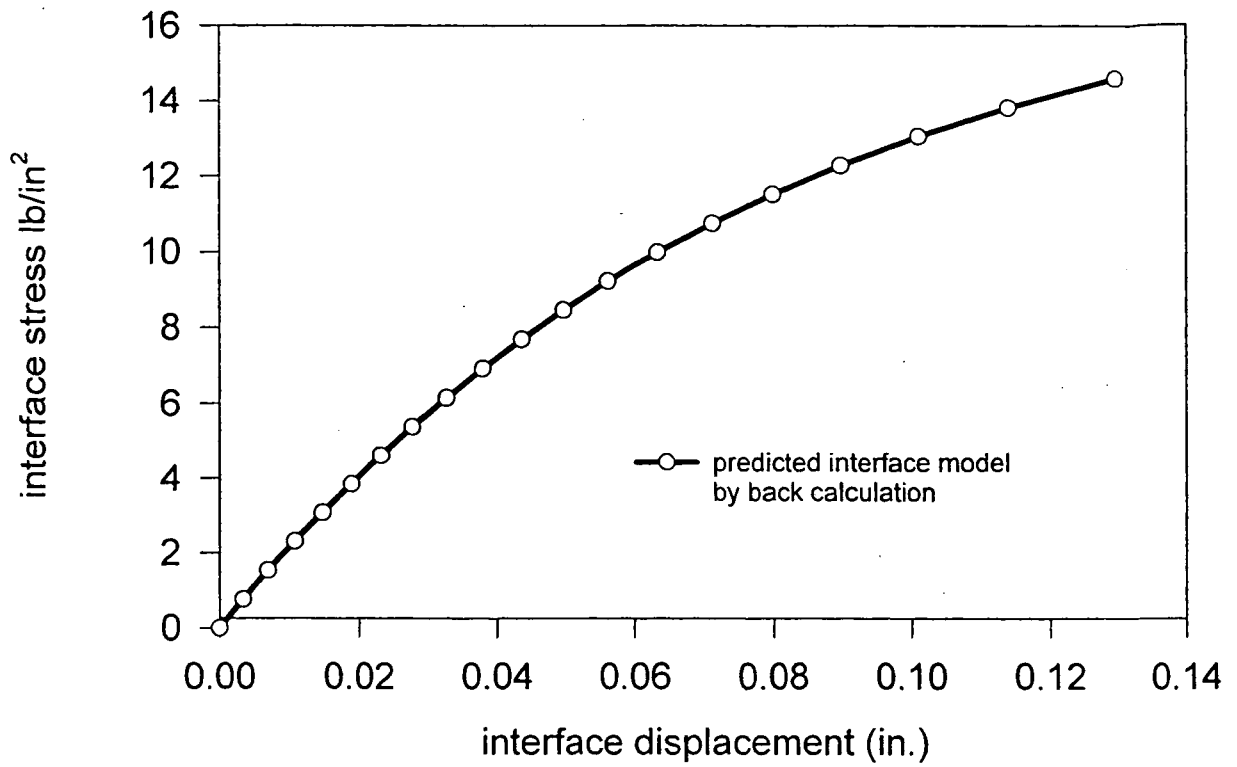


Fig. 5.12: Results of back calculation of hardening model.

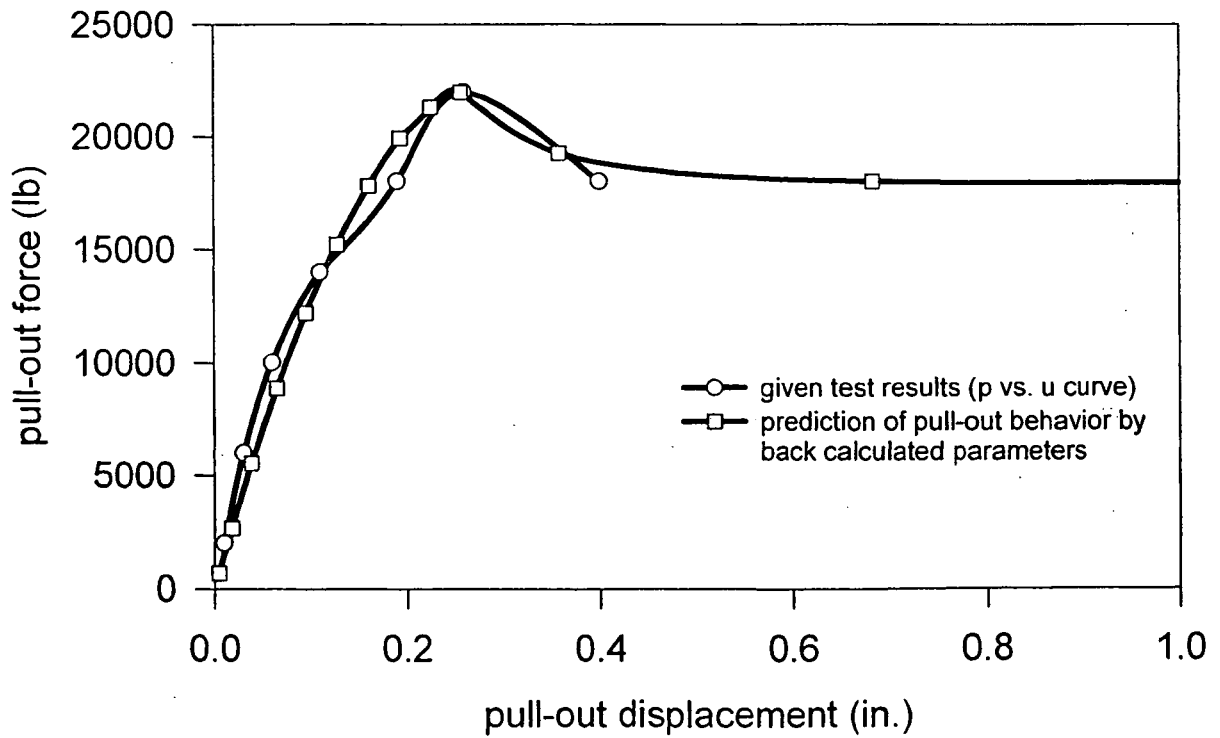
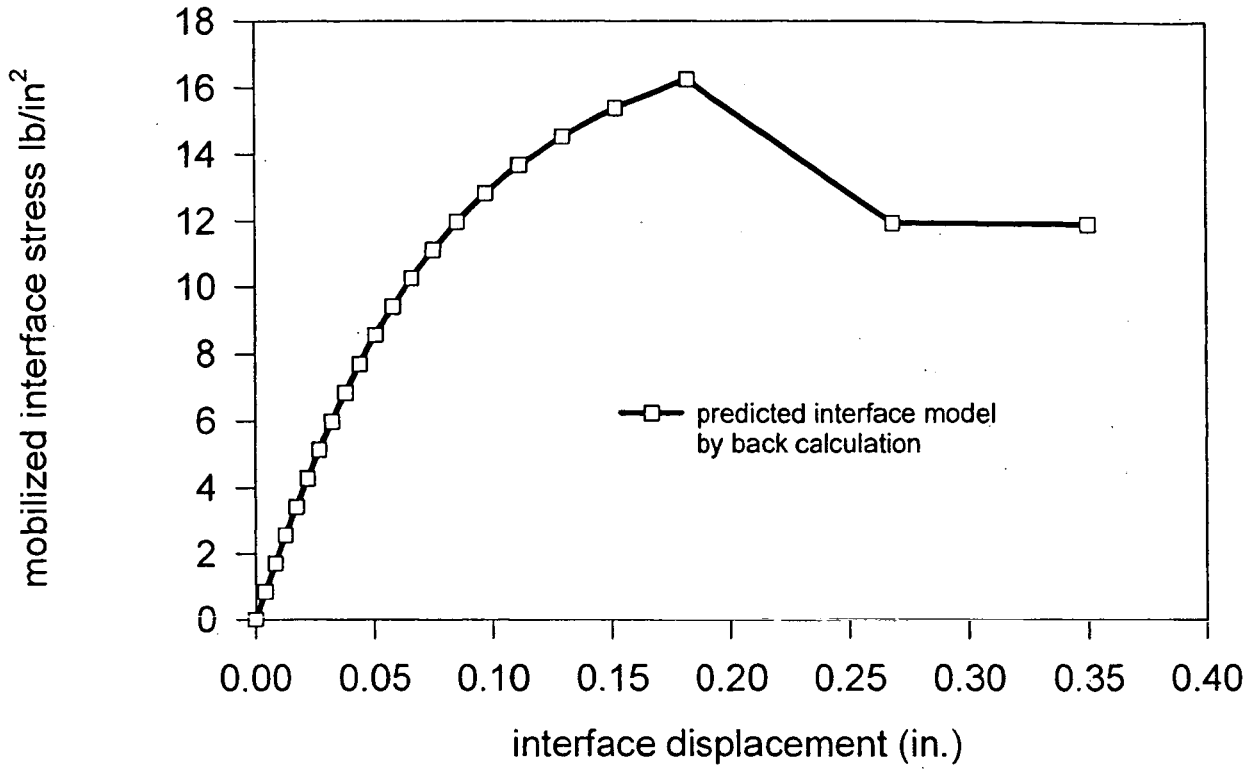


Fig. 5.13: Results of backward calculation of softening model.

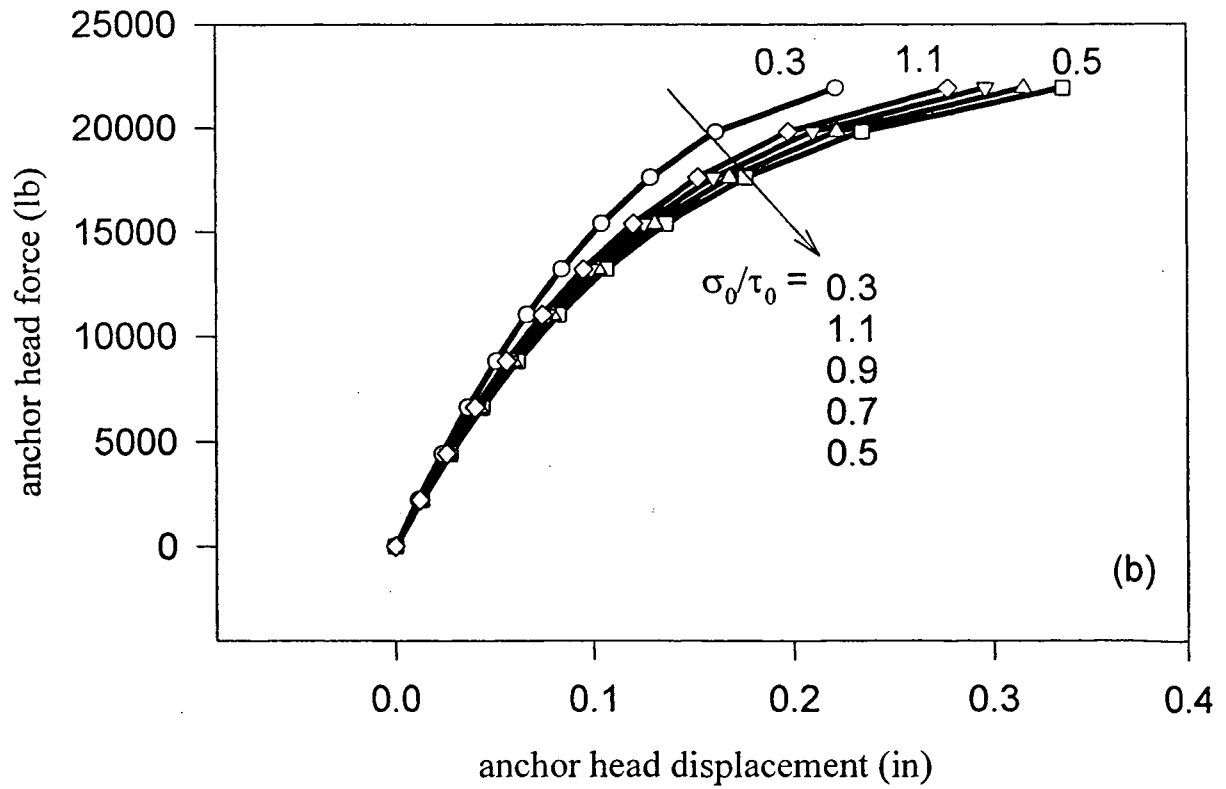
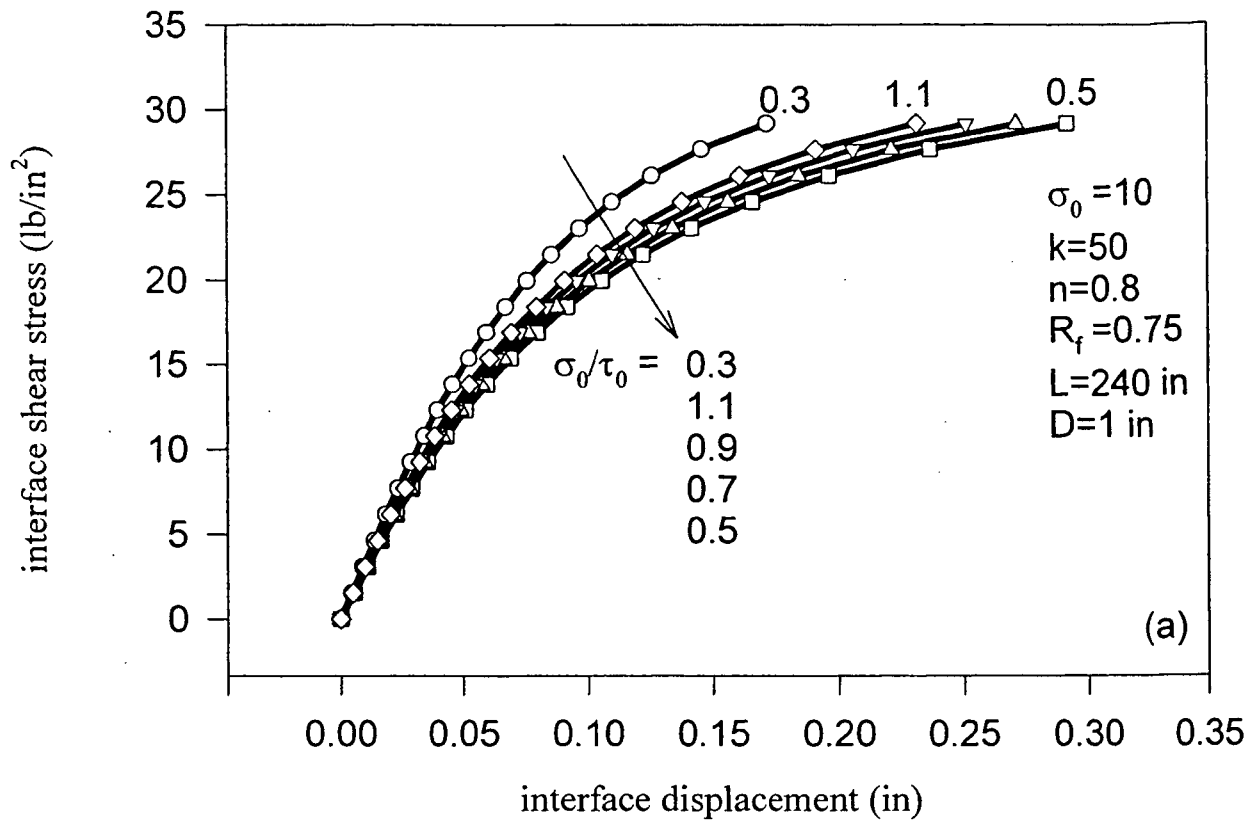


Fig. 5.14: Sensitivity study of the basic interface strength (hardening model).

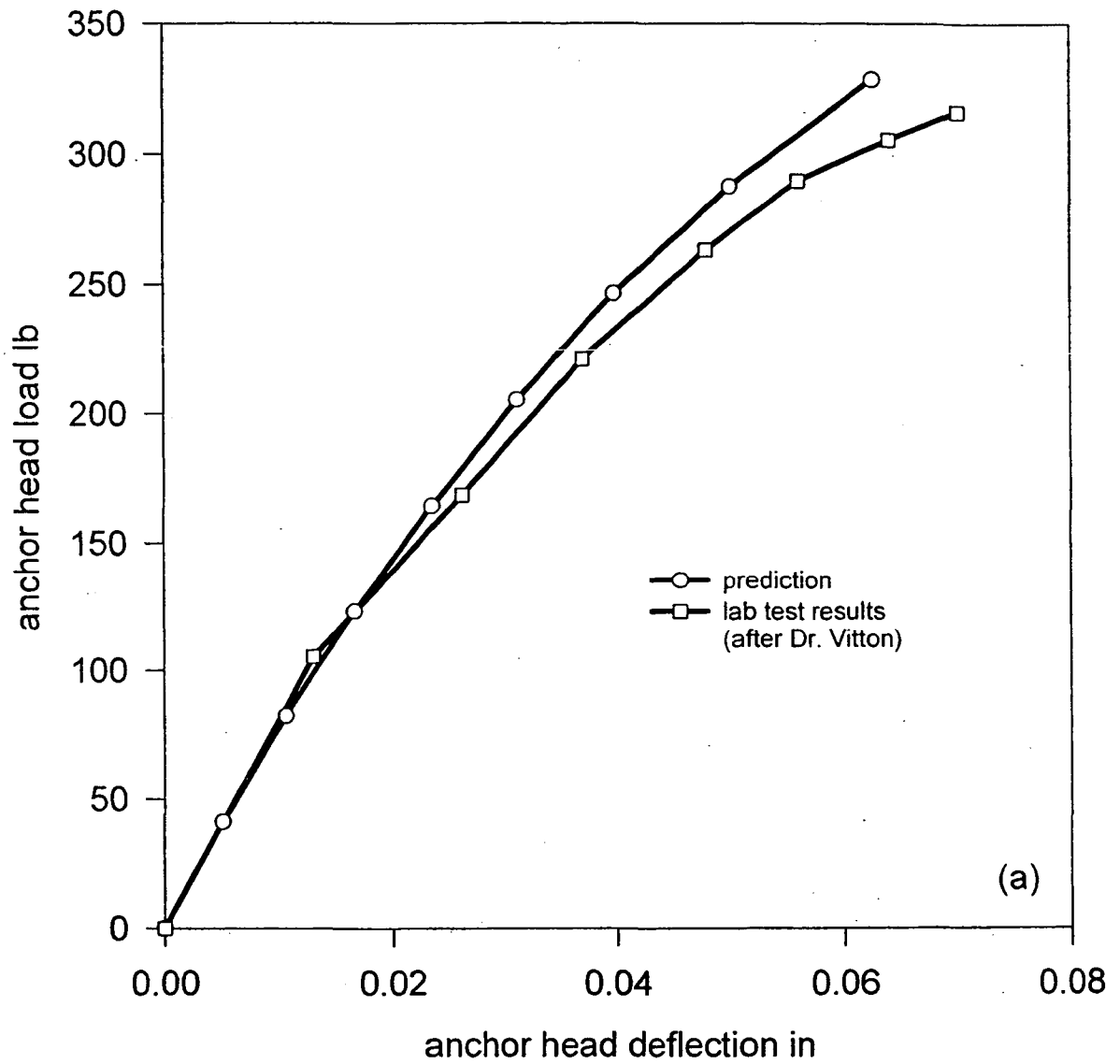


Fig. 5.15(a): Comparison between calculation and test results under confining pressure of 10 psi.

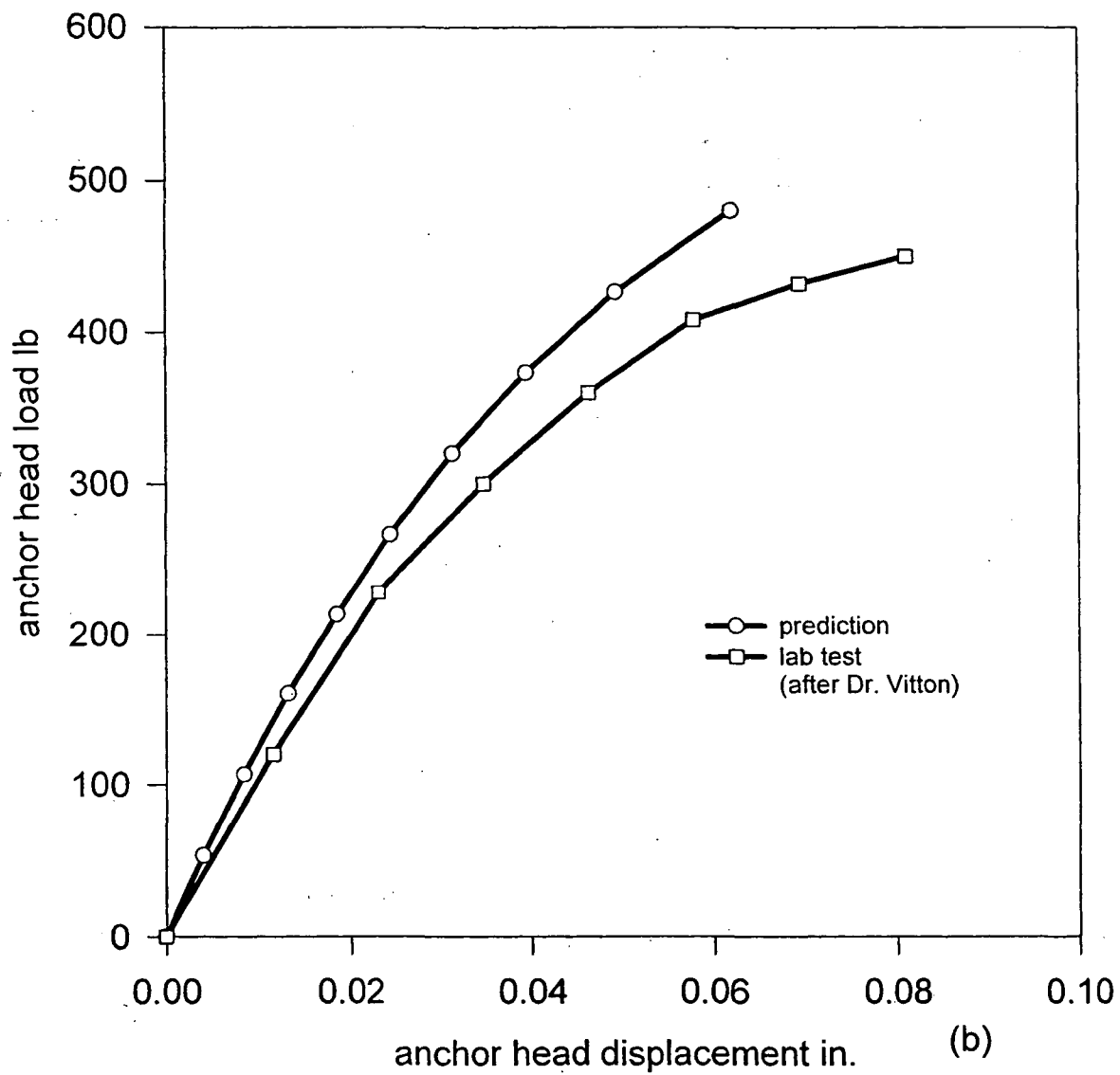


Fig. 5.15(b): Comparison between calculation and test results under confining pressure of 15 psi.

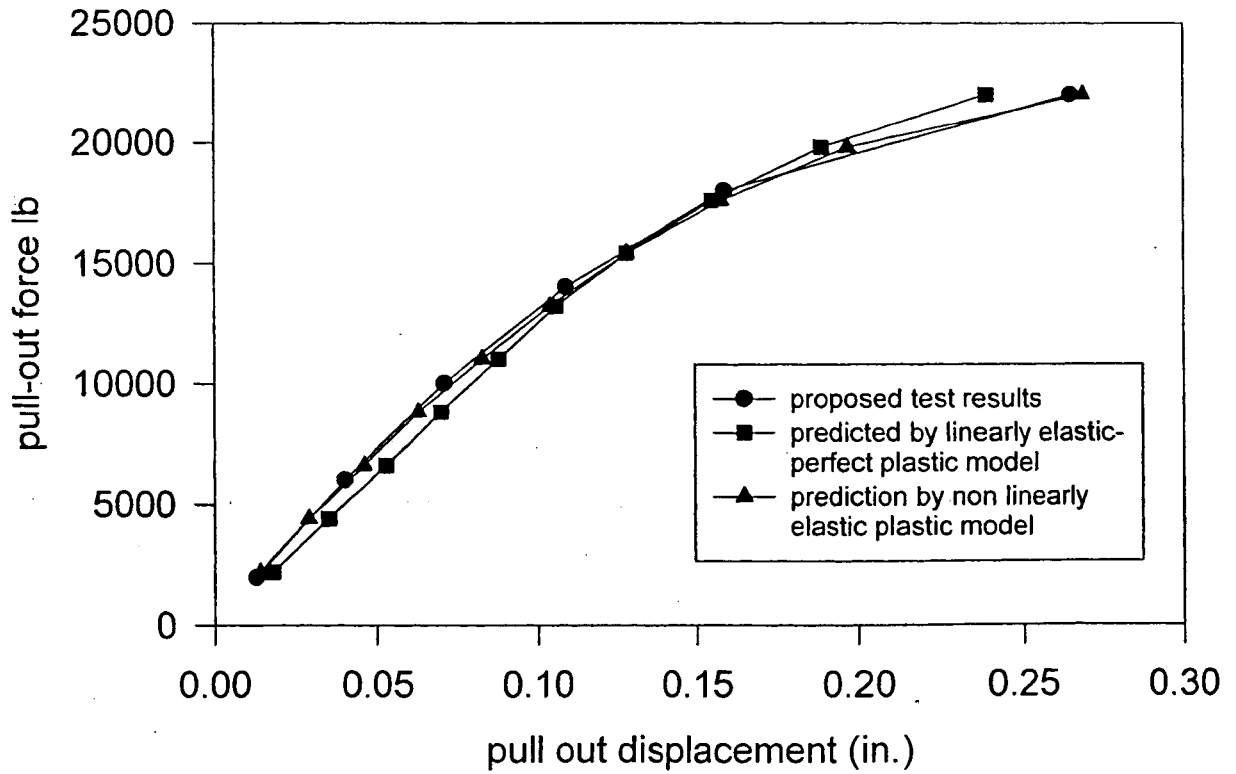
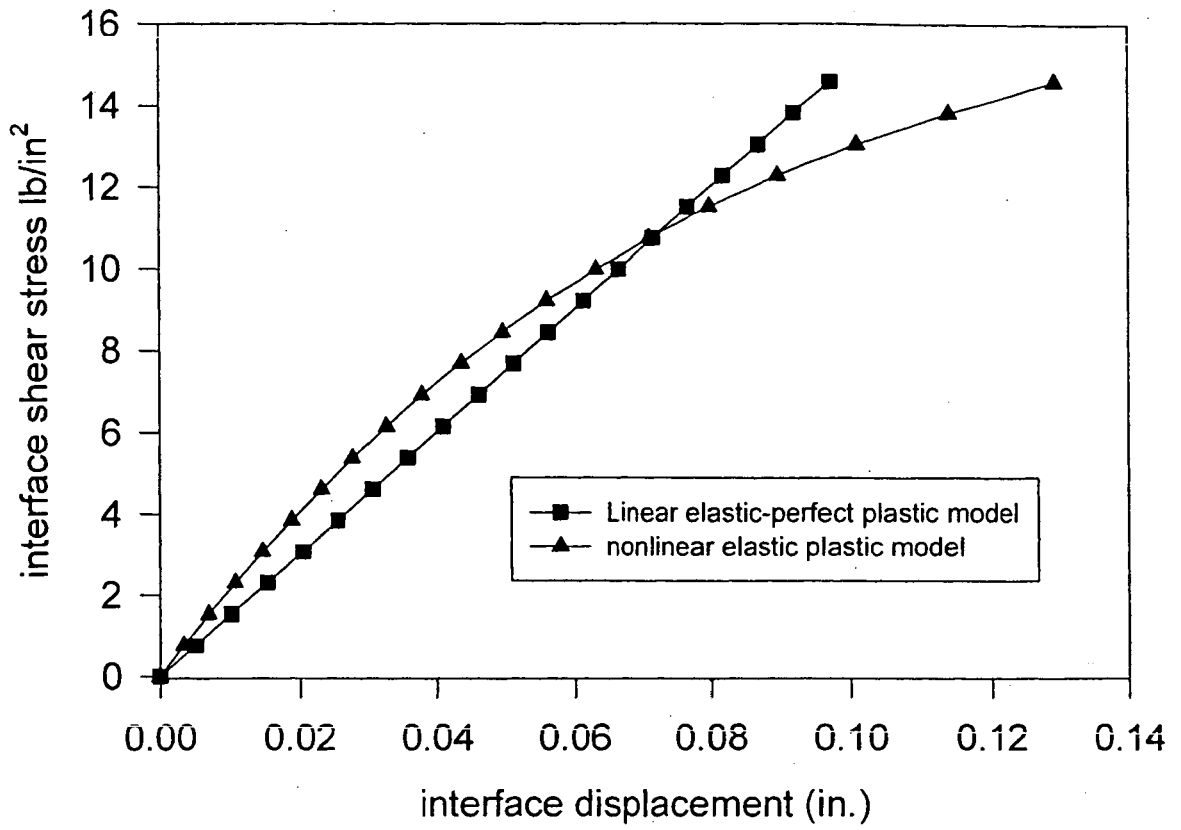


Fig. 5.16: Back-calculation interface load transfer curves (t-z curves)
 (a) comparison of back calculated models.
 (b) comparison of anchor pull-out prediction.

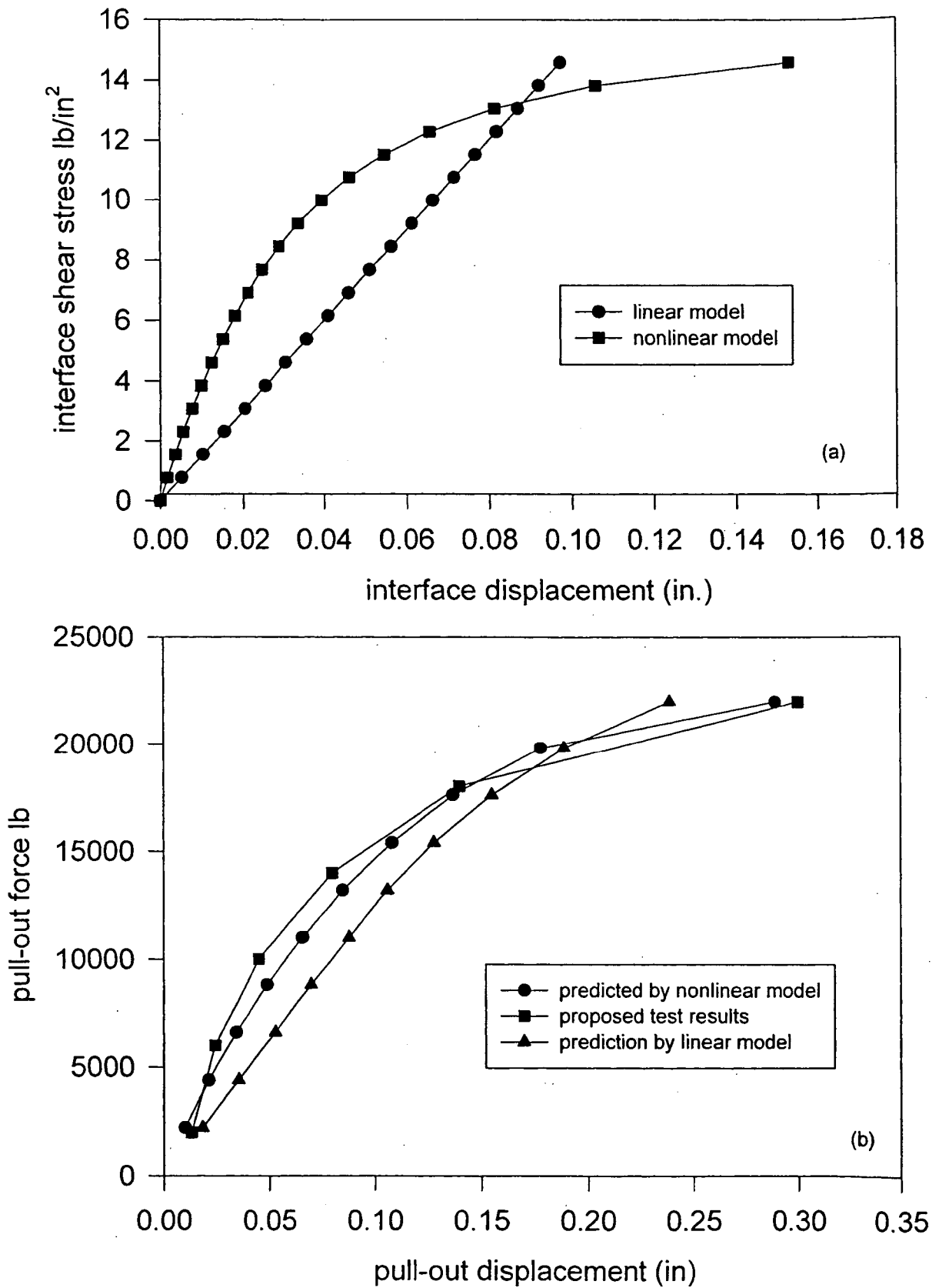


Fig. 5.17: Comparison of the load-displacement response of Tieback 622-1 between actual test results and the forward calculation results.

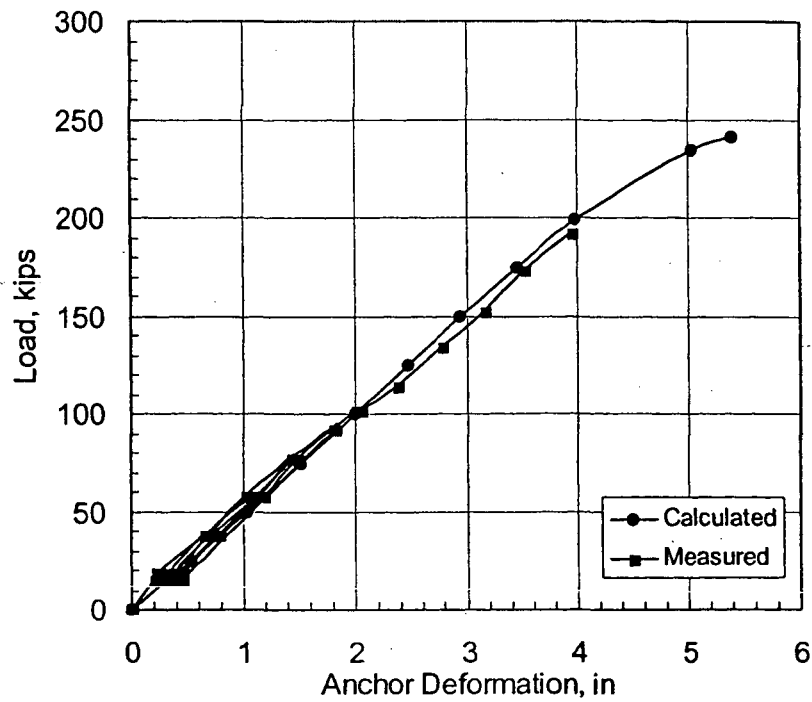


Figure 5.18 Measured versus back-calculated load-deformation curve for upper tier (Anchor FT1).

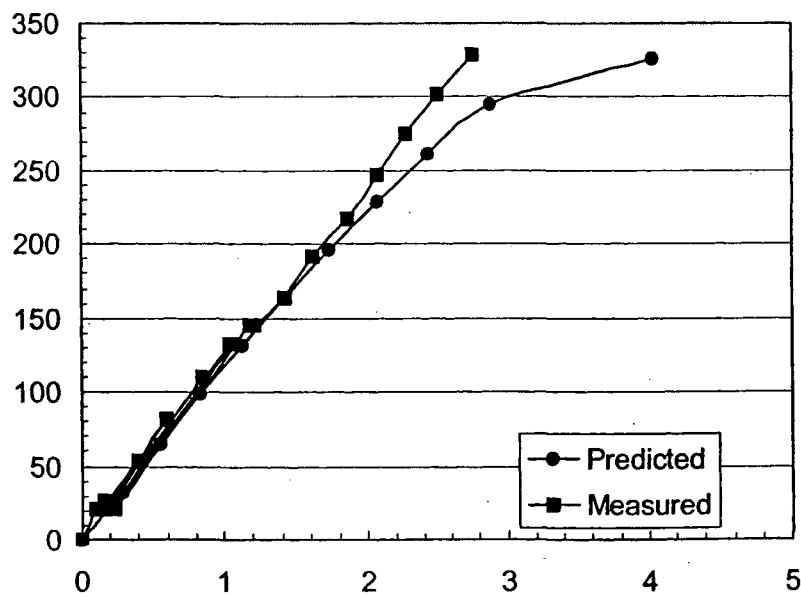


Figure 5.19 Predicted versus measured load deformation curve for the lower tier (Anchor FT2), for $\psi = 5^\circ$.

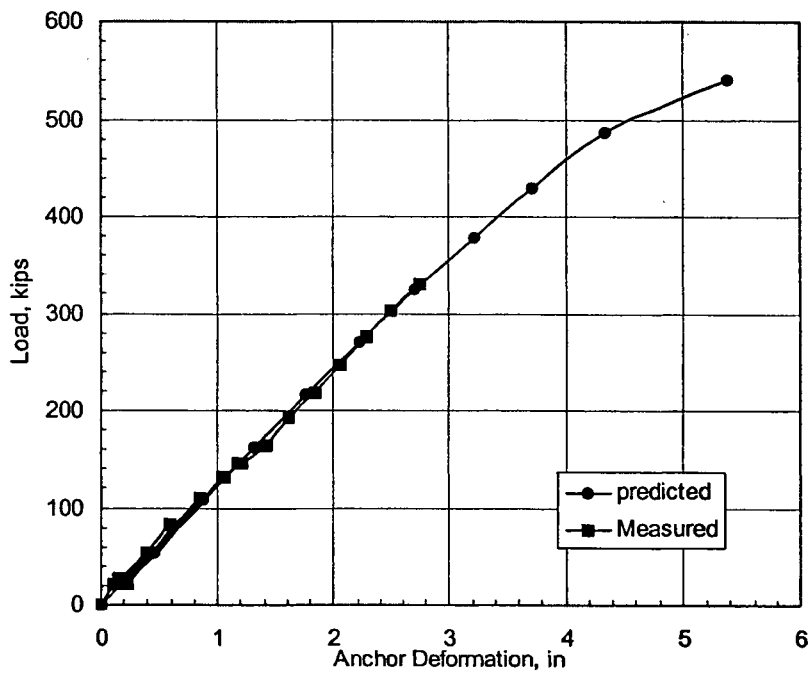


Figure 5.20 Predicted versus measured load deformation curve for the lower tier (Anchor FT2), for $\psi = 15^\circ$.

THE UNIVERSITY OF CHICAGO
LIBRARY
540 EAST 57TH STREET
CHICAGO, ILLINOIS 60637
TEL: 773-936-3000
WWW.CHICAGO.EDU

CHAPTER VI

SIMULATION OF TIEBACK WALL CONSTRUCTION USING FEM PROGRAM PLAXIS

VI.1 INTRODUCTION

The recent advent of finite element analysis methods has provided a powerful analytical tool that can be used for analysis of large-scale and complex geotechnical problems. The employment of the finite element method for analysis of the tieback wall behavior offers the following advantages:

- (a) The versatility of elements makes available the representation of the geometry complexities involved in the slope profile, construction sequence and various kinds of structure components of the tieback wall.
- (b) The versatility of constitutive models makes it capable of accounting for such complexities as nonlinear material behavior and discontinuities due to possible slip along the anchor bond interface.
- (c) The availability of high-speed digital computers makes it practical to incorporate all components of tieback wall and the various soil-structure interaction mechanisms.
- (d) The repeated computer runs using various soil parameters make it possible to systematically investigate the various aspects of factors controlling the anchor reinforcement mechanisms.

VI.2 FINITE ELEMENT MODELING OF SUM-82 PROJECT

A two-dimensional finite element program, PLAXIS, is used to simulate the construction of a tieback wall at the SUM-82 project site. A centerline cross-section of the construction area is shown in Fig. 6.1. A finite element domain representing the cross-section between Stat. 11+00 and Stat. 14+80 is shown in Fig. 6.2. This domain includes all tieback wall components: soldier piles, ground anchors, anchor casings and anchor bond zones. Based on the information obtained from soil boring investigation and in situ construction, the soil at the site is represented by three layers: top fill, silty clay and shale, as shown in Fig. 6.2. The finite element mesh of the domain and the pertinent structures are shown in Fig. 6.3. The mesh consists of a total of 859 elements and 1790 nodes. The soldier piles and the anchor casings are modeled with beam elements. The ground anchors are modeled with the node-to-node anchor elements while the bond part of the ground anchor is modeled with the geotextile interface elements.

VI.3 MATERIAL PROPERTIES OF TIEBACK WALL COMPONENTS

Two tiers of tieback walls were installed in this project to enhance the slope stability. The upper tier wall was anchored with three rows of prestressed ground anchors while the lower tier with two rows. Detailed information on the dimensions, properties and layout of those structures can be found in Chapter II. The relevant structure parameters required as input in the PLAXIS are summarized in Table 6.1.

Table 6.1. Properties of Tieback Wall Components

Component	Type	E (lb/ft ²)	ν	EA (lb)	EI (lb-ft ²)
Soldier Pile	HP14x73	4.177e+09	0.3	6.235e+08	1.476e+08
Concreted Soldier Pile	Φ24"/HP14x73	6.251e+08	0.27	1.964e+09	6.385e+08
Anchor Tendon I	Φ0.6x3	4.177e+09	0.3	1.887e+07	/
Anchor Tendon II	Φ0.6x4	4.177e+09	0.3	2.517e+07	/
Anchor Casing	OD55"/THK0.304"	4.177e+09	0.3	1.439e+08	3.384e+06

VI.4 CALIBRATION STUDY TO DETERMINE SOIL AND BOND INTERFACE PROPERTIES

As indicated in the subsurface investigation reports, the soil portion of the profile in this project is fairly variable with respect to soil types found and the relative horizontal and vertical location of the specific soil types identified. In addition to the variability in soil types within the profile, the consistency of the respective soils was also found to vary horizontally and vertically across the site. Therefore, the traditional procedure, in which the soil properties can be determined based on the SPT value and other information from the subsurface investigation, is inadequate to produce reliable representative values for this project. Supplemental measures have to be taken in conjunction with the broad subsurface investigation information to determine the soil properties for finite element analyses.

In addition to soil properties, the parameters of the anchor bond interface are very important for anchored structures and need to be carefully calibrated. It is well known that the interface between the bonded portion of anchor and the surrounding soil is a critical plane to bear shear stresses induced from the anchor loads, and is most likely to experience sliding

under certain circumstances. The reduction of strength along the interface as a result of relative slippage must be incorporated in the finite element model.

The decrease of strength of the interface is represented by a strength reduction factor R_{inter} in the PLAXIS program. The interface properties are calculated from the following equations:

$$c_{inter} = R_{inter} c_{soil}$$

$$\tan \varphi_{inter} = R_{inter} \tan \varphi_{soil}$$

where c_{inter} and φ_{inter} are the cohesion and friction angle of the interface and c_{soil} and φ_{soil} are the cohesion and friction angle of the adjacent soil. In addition to the Coulomb's strength criterion, the tension cut-off criterion also applies:

$$\sigma_{n,inter} < \sigma_{t,inter} = R_{inter} \sigma_{t,soil}$$

where $\sigma_{n,inter}$ is normal stress acting on the interface, and $\sigma_{t,inter}$ and $\sigma_{t,soil}$ are the tensile strength of the interface and soil, respectively. In general, the interface is weaker in strength and stiffness than the adjacent soil layers. Typically, the value of R_{inter} varies between 0 and 1.

For the purpose of determining the soil and interface properties, two additional FEM PLAXIS runs were carried out separately to simulate the failure tests FT1 and FT2, respectively. Figs. 6.4 and 6.6 show the typical cross-sections of FT1 and FT2, respectively, and the corresponding FEM meshes are given in Figs. 6.5 and 6.7. The differences between FT1 and FT2 are the following: (i) FT2 did not have the steel compression tube, and (ii) only shale exists in the bond zone. Therefore, it is used to retrieve the pertinent material properties. Most simulation efforts were concentrated on FT2 while the simulation of FT1 served as a

verification of the material properties derived from FT2 and the techniques for simulating compression tube structures.

The soil and interface properties have been carefully calibrated by matching the FEM predictions with the measurements obtained from the failure tests. Due to the possibility of numerous combinations of material property parameters, the computational efforts on the calibration process were tremendous. Table 6.2 lists an example of typical combinations for the five trials.

Table 6.2. Typical Combinations of Soil and Interface Properties.

Case	γ_{dry} (pcf)	γ_{wet} (pcf)	E(lb/ft ²)	ν	C(lb/ft ²)	ϕ (°)	R_{inter}
1	115	140	2.0e+6	0.20	10000	38	0.500
2	115	140	2.0e+7	0.23	40000	38	0.667
3	115	140	1.2e+7	0.25	13500	38	0.500
4	115	140	7.0e+6	0.25	13500	38	0.667
5	115	140	6.0e+6	0.25	12500	38	0.667

The calculated anchor head movements of FT2 were plotted against the incremental loading history for these five cases in Fig. 6.8 to 6.12, respectively. For the purpose of comparison, the test measurements were also plotted in these figures. As shown in Fig. 6.12, the best match of these comparisons was reached in case 5. Also, the good agreement between the calculated and measured results for FT1, as shown in Fig. 6.13, confirmed that the properties listed for case 5 were acceptable and hence can be used for the subsequent numerical simulations.

VI.6 SIMULATION OF CONSTRUCTION PROCESSES

It is well known that the final stress and deformation state of the nonlinear problems, encountered in most earth structure constructions similar to the project considered here, is highly loading path and initial stress dependent. The stabilization structure construction in the SUM-82 project involves sequentially the following stages: excavation, tieback wall installation and backfill. For a realistic evaluation of stress and deformation in these structures, the construction sequences and initial stress should be simulated as carefully as possible.

For the initial stress, the in situ stress under gravity is first introduced into the finite element mesh. For the numerical simulation, the construction sequences are carefully simulated according to the construction events described in Chapter III. The entire simulation approach involves the following steps in sequence.

- Phase 1. In situ stress under gravity.
- Phase 2. Excavation for soldier pile installation.
- Phase 3. Installation of upper and lower tier soldier piles.
- Phase 4. Installation and tension of anchors in the second row, i.e. 27B, of upper tier tieback wall.
- Phase 5. Installation and tension of anchors in the second row, i.e. 9B, of lower tier tieback wall.
- Phase 6. Installation and tension of anchors in the first row, i.e. 9A, of lower tier tieback wall.
- Phase 7. Installation and tension of anchors in the third row, i.e. 27C, of upper tier tieback wall.

- Phase 8. Installation and tension of anchors in the first row, i.e. 27A, of upper tier tieback wall.
- Phase 9. Backfill to the final grade.

This is a typical sequence procedure that is most commonly used in tieback wall construction. The initial calculated results by following this procedure, however, were found to be much different from the in situ measurements. This discrepancy was attributed to the fact that the anchor tension loads were applied onto the steel casings. Consequently, the soldier piles would not experience any further deformation induced from anchor tension until backfill is complete. In order to model this kind of construction scenario, the typical simulation sequences presented above were adjusted as follows:

- Phase 1. In situ stress under gravity.
- Phase 2. Excavation for soldier pile installation.
- Phase 3. Installation and tension of anchors in the second row, i.e. 27B, of upper tier tieback wall.
- Phase 4. Installation and tension of anchors in the second row, i.e. 9B, of lower tier tieback wall.
- Phase 5. Installation and tension of anchors in the first row, i.e. 9A, of lower tier tieback wall.
- Phase 6. Installation and tension of anchors in the third row, i.e. 27C, of upper tier tieback wall.
- Phase 7. Installation and tension of anchors in the first row, i.e. 27A, of upper tier tieback wall.
- Phase 8. Installation of upper and lower tier soldier piles.

- Phase 9. Backfill to the final grade.

The typical and adjusted construction sequence procedures were both simulated for the purpose of comparison. For the sake of convenience, the former was referred to as Case I and the later Case II in the subsequent discussions.

VI.7 FEM ANALYSIS RESULTS AND DISCUSSION

VI.7.1 Stresses and Deformations in Soil Mass

The execution of computer program PLAXIS requires that the loading path due to construction be strictly followed. For each construction phase, the loading step has to be further divided into several sub-steps, as required by the incremental finite element method to ensure the convergence of nonlinear iteration. Table 6.3 summarizes the number of calculation step for each phase.

Table 6.3 Incremental steps for nonlinear calculation

Phase No.	Case I	Case II
1	17	17
2	9	9
3	1	7
4	5	8
5	4	6
6	6	9
7	6	8
8	7	2
9	11	15

The computer simulation results for each phase are presented in a variety of plots. These plots include: (a) the total displacement vectors indicating the major direction of soil movement, (b) the total displacement contours, (c) the principal stress directions and magnitude, (d) the mean effective stress contours, (e) the relative shear stress ratio contour, where relative shear stress ratio is defined as the shear stress applied over the shear strength available. These plots are presented in Fig. 6.14 to Fig. 6.53.

VI.7.2 Tieback Wall Structure Response

In addition to the stresses and deformations calculated for the soil mass, the computer simulation also generates the resulting forces and moments in the tieback wall components. The calculated results for each component are presented below.

VI.7.2.1 Soldier piles

There are two tieback walls in this project: upper tier wall and lower tier wall. The upper tier wall is anchored with three rows of prestressed ground anchors while the lower tier with two rows. The calculated deflections, bending moments and axial forces of soldier piles of these walls after final construction stage are shown in Fig. 6.54 to 6.59, respectively. For the sake of comparison, similar results due to the typical construction procedure (Case I) are also plotted in those figures.

For the upper tier soldier piles, the driving forces during the final simulation/construction stage are induced from the backfill within upper tier wall area and the excavation for final grading of the lower tier wall area. These forces all caused the soldier

piles to bend to the downslope direction. The calculated and measured deflections along the pile length are shown in Fig. 6.54. It can be clearly seen that the calculated and measured deflection profiles match quite well. The maximum magnitudes are found within the area of 1/3 length below the top of the pile with the values of 0.055 in. for prediction of case I, 0.071 in. for prediction of case II, and 0.049 in. for in situ measurement.

As far as for the lower tier soldier piles, their deflections, as shown in Fig. 6.55, are much smaller due to minor construction activities imposed on them during the final stage. The deflection magnitudes obtained from finite element analysis and inclinometer readings are both within the range less than 0.02 in. One thing needed to be pointed out is the discrepancy between the calculated and measured deflections within the area of top 10 ft. In fact, the measured data within this area are questionable because the backfill soil was loose and likely move the inclinometer tube around.

Figs. 6.56 and 6.57 provides the bending moment comparisons for upper and lower tier soldier piles, respectively. As expected, the FEM analysis results indicate that the construction case II developed less bending moments on both sides of the soldier piles, compared to the typical construction case I. The in situ instrumentation, however, recorded the measurements lying somewhere between the predictions of case I and case II. This implies that even though the lock-off anchor loads were directly applied on to the steel casings, some portion of loads was eventually transferred to the soldier piles after the mounting of the anchor heads to the soldier piles due to some reasons such as the creep effects. This observation can be verified by comparing the calculated and measured axial forces, as shown in the Figs. 6.58 and 6.59.

Table 6.4 Comparisons between maximum bending moments

Soldier piles	M_{+max} (kip-ft)			M_{-max} (kip-ft)			M_{max} (design)
	Case I	Case II	Measured	Case I	Case II	Measured	
Upper tier	91.4	20.5	80.6	-63.1	-24.6	-36.1	340
Lower tier	44.6	7.1	13.7	-30.1	-4.8	-19.6	340

Table 6.4 lists the maximum bending moments for the upper and lower tier piles, where the positive bending moment is defined such that the tension occurs on the side facing the downslope direction. It can be seen that either the maximum positive bending moment or the maximum negative bending moment for each case is small and far from the maximum design bending moment.

VI.7.2.2 Ground Anchors

The calculated axial forces (both case I and case II in FEM simulation) along the ground anchor length for anchor 27A, 27bB, 27C, 9A and 9B are shown in Fig. 6.60 to 6.64, respectively, together with the results from actual measurement.

It can be seen from these figures that the axial force distributions along the bond length of ground anchor for construction case I and II are almost the same. This means that variation in mounting the lock-off loads on the anchor heads does not significantly affect the mechanistic behavior of the other end of anchor, i.e. the bond part of the anchor. Both the FEM predictions and the in situ measurements indicate that only top 1/3 portion of the bond part of the anchors is mobilized to sustain the tension induced from the lock-off loads while

other portion remains motionless with almost zero axial force, which provides an adequate safety reservation for further creep development.

VI.8 CONCLUSIONS

In this chapter, the behaviors of slope and the retaining wall of SUM-82 project have been investigated with the aid of FEM analysis. First of all, some main parameters, such as soil properties, anchor-soil interface properties, and element types characterizing various structure components, as required by the numerical model, were carefully calibrated in a way by matching the FEM predictions with the in situ measurements obtained from two failure tests, i.e., FT1 and FT2. With the calibrated model available, two kinds of construction processes were fully simulated stage by stage in order to incorporate the stress path effects. Based on the results obtained from finite element analysis and their comparisons with in situ measurements, some conclusions can be drawn as follows:

- 1) Good agreement between the calculated predictions and the measured data has verified the validity of the results obtained from FEM PLAXIS analysis.
- 2) Variation in construction sequences has great impact on the bending moment distribution, both the shape and the magnitude, in the soldier piles of the retaining wall. For the project considered, construction case II can significantly reduce the maximum bending moments imposed on the soldier piles compared to the typical construction case I.
- 3) Different construction sequences have little influence on the ground anchor behaviors as long as the lock-off loads remain unchanged.
- 4) The global stability of the slope has been significantly improved by the installation

of the retaining wall, with the calculated relative shear stress ratios decreasing from the range of around 0.4 to the range of 0.1.

- 5) Both the calculated and measured results indicate that the maximum bending moments developed in the upper tier and lower tier wall are less than 1/4 of design capacity and only top 1/3 portion of bond part of the ground anchors are mobilized to sustain the tension induced from the anchor lock-off loads. The structural safety of the retaining wall components is thus guaranteed.

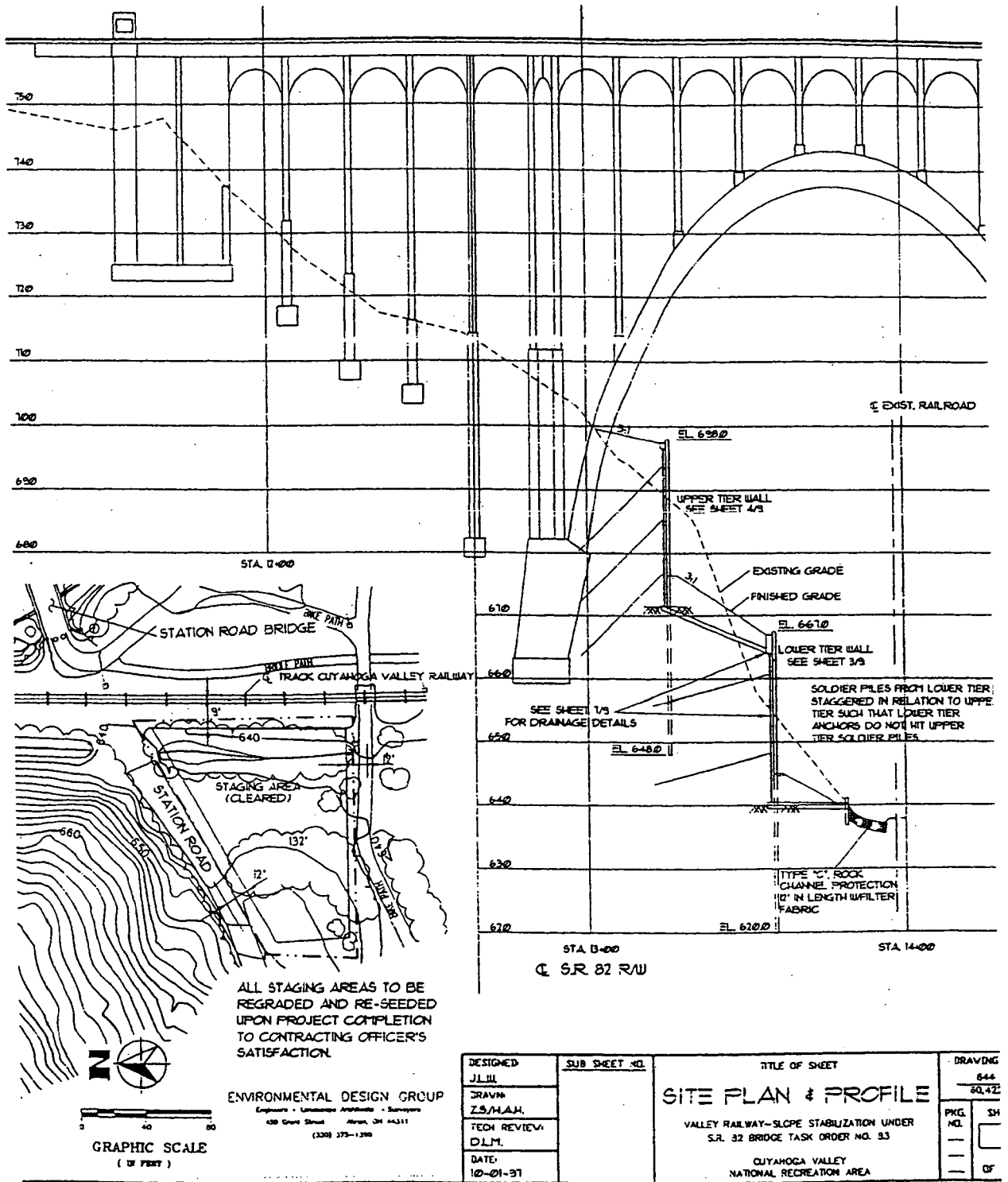


Fig. 6.1: Centerline cross-section of SUM-82 project

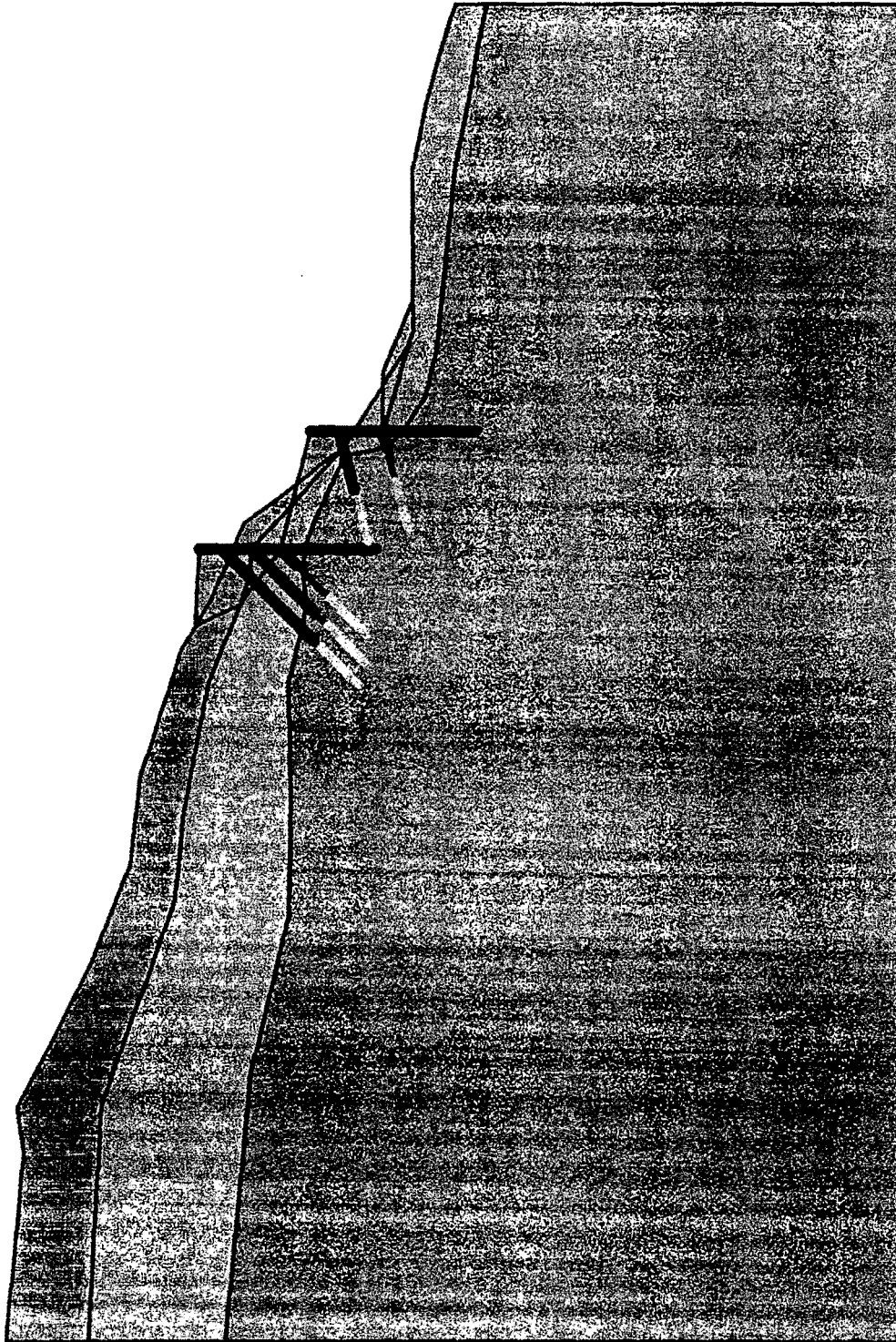


Fig. 6.2: Calculation model



Fig. 6.3: Finite element mesh

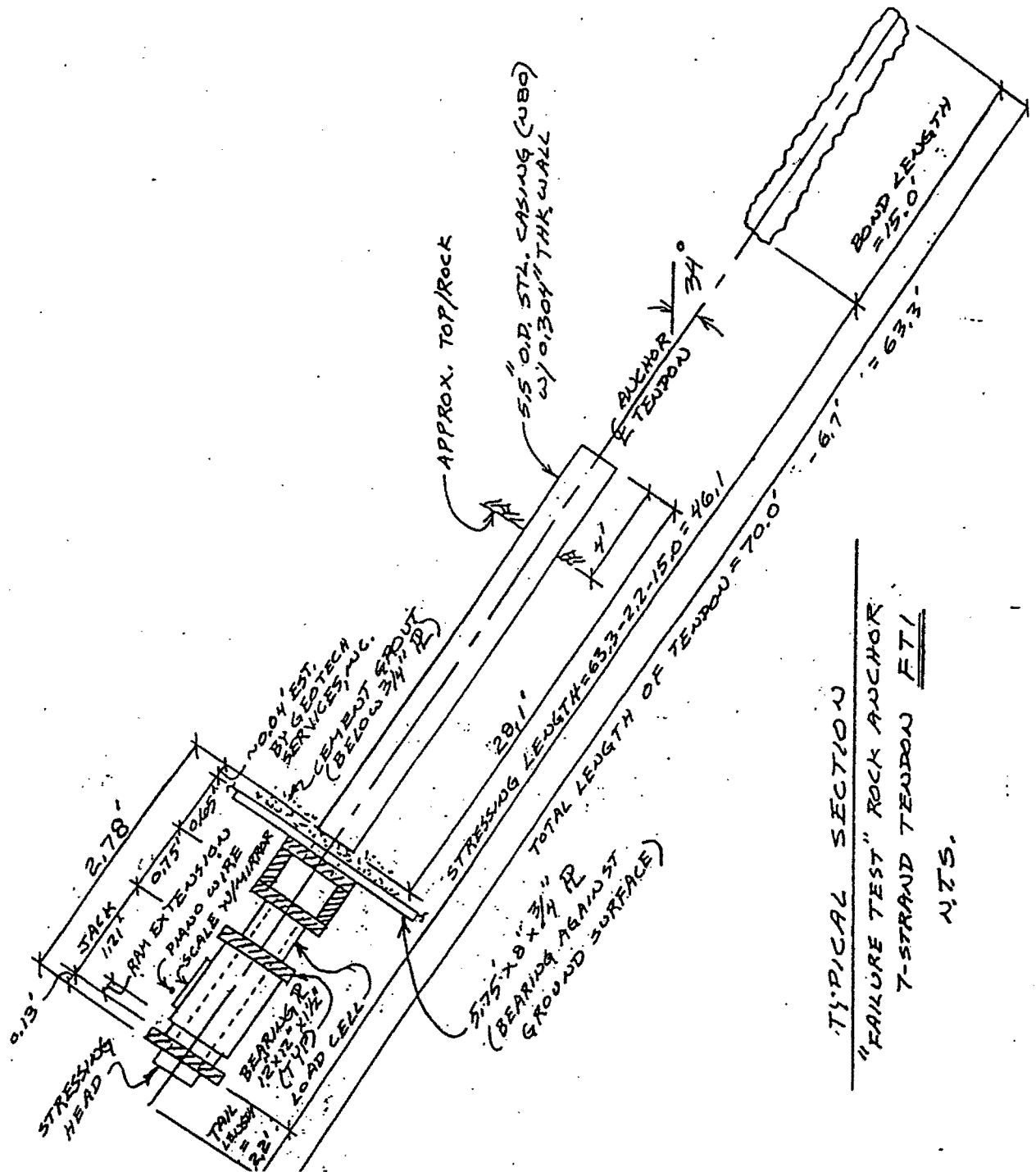


Fig. 6.4: Typical cross-section of failure test FT1

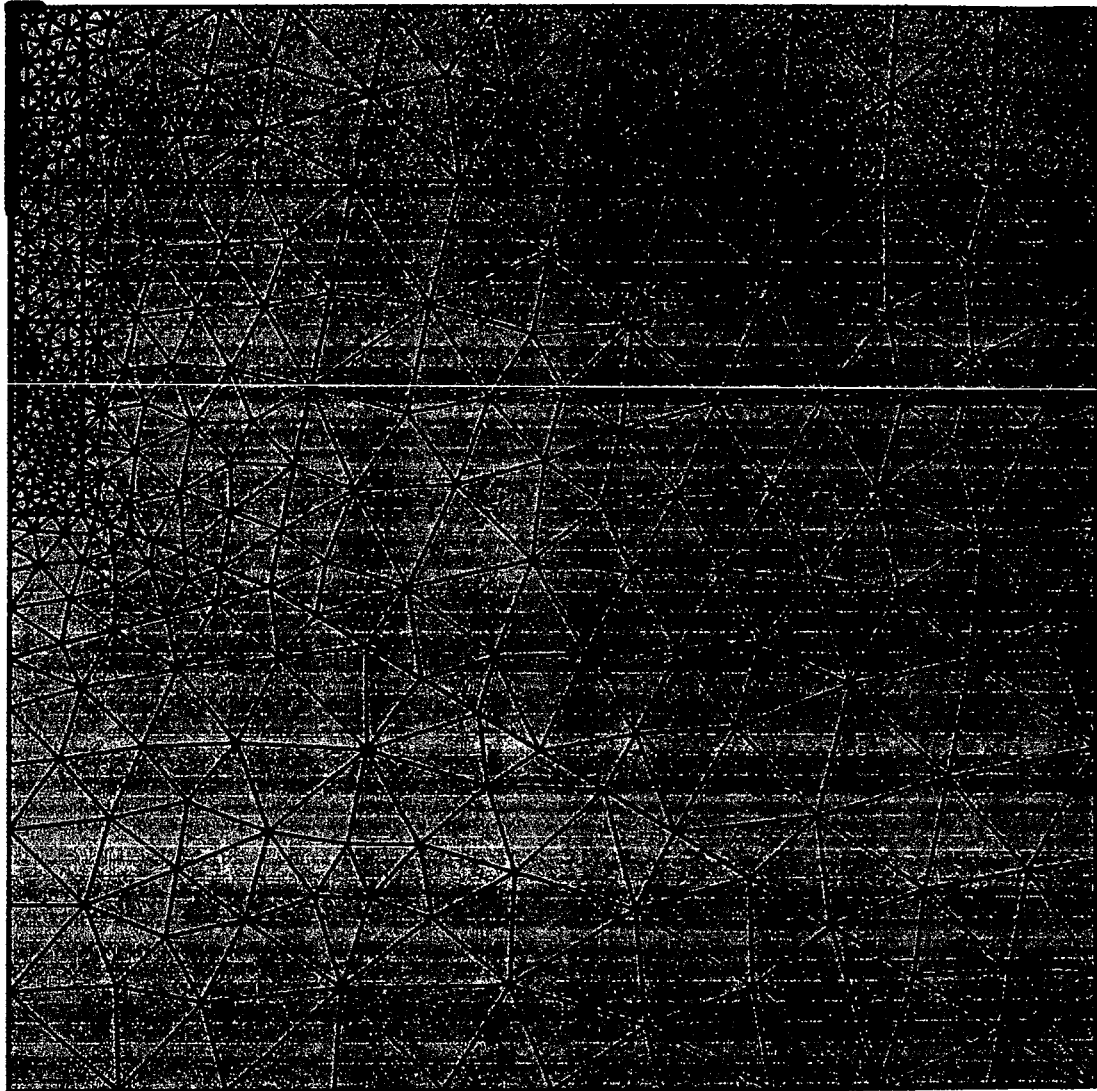


Fig. 6.5: Finite element mesh for FT1

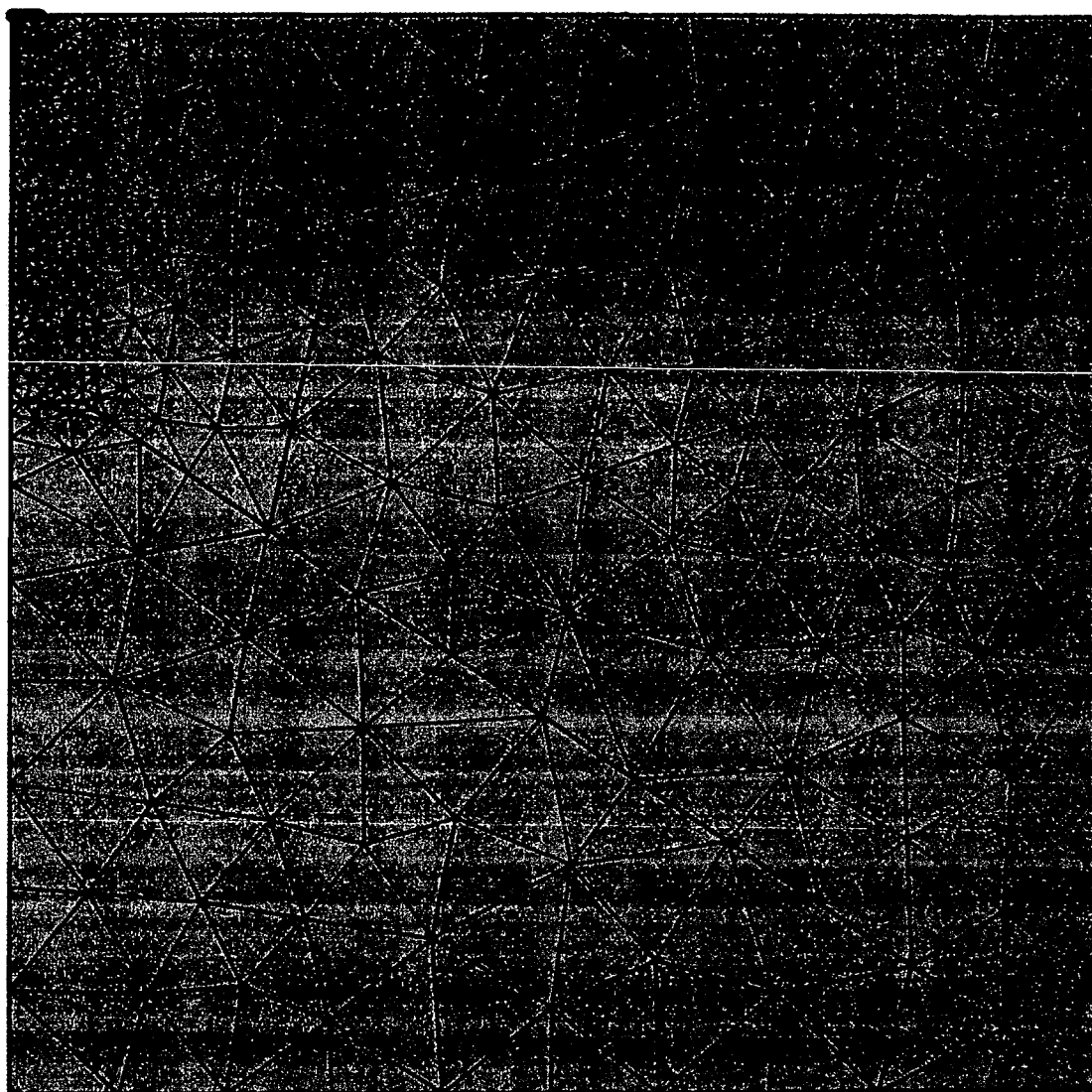


Fig. 6.7: Finite element mesh for FT2

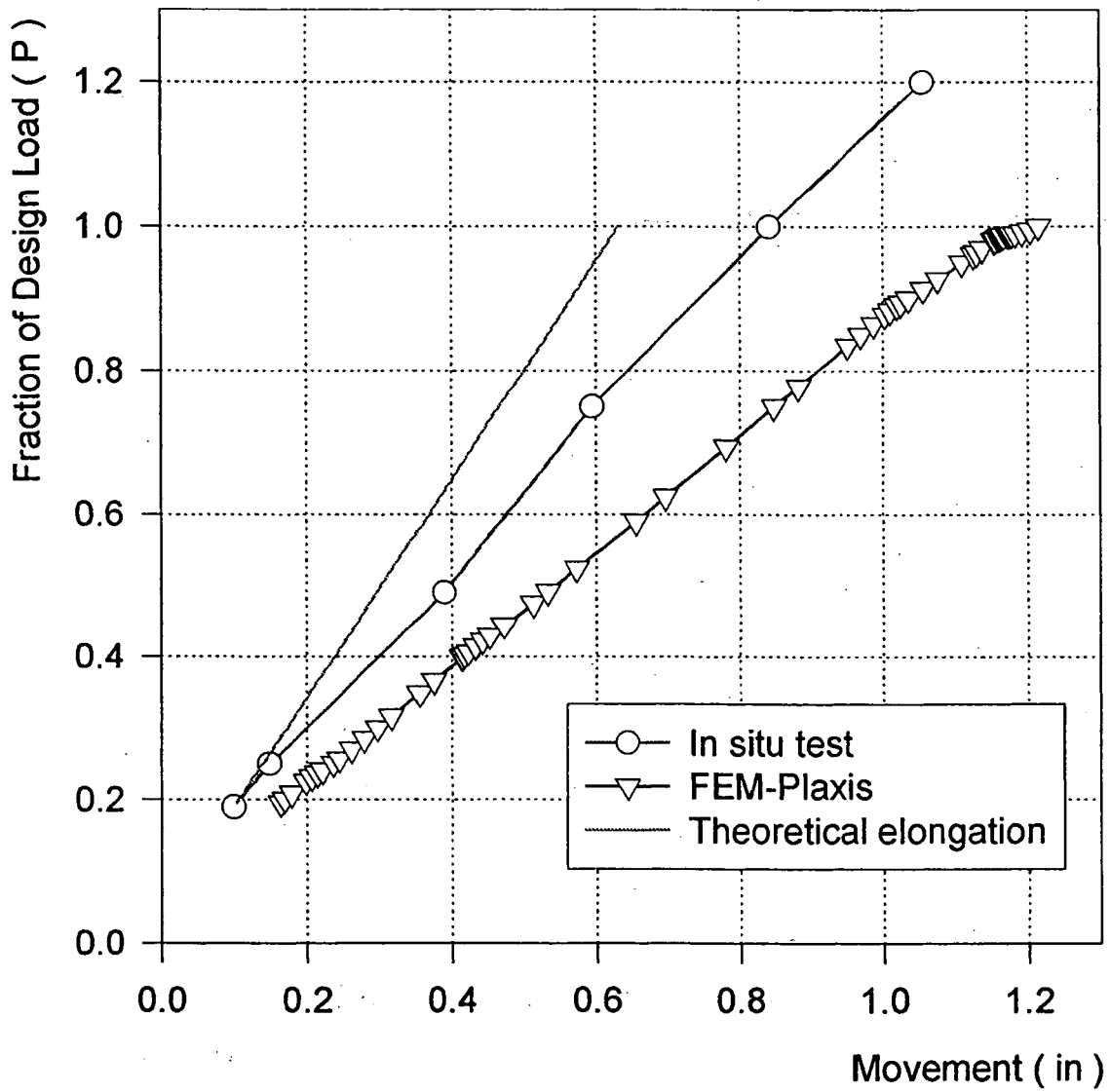


Fig. 6.8: Comparison of anchor head movements in FT2 (Case 1)

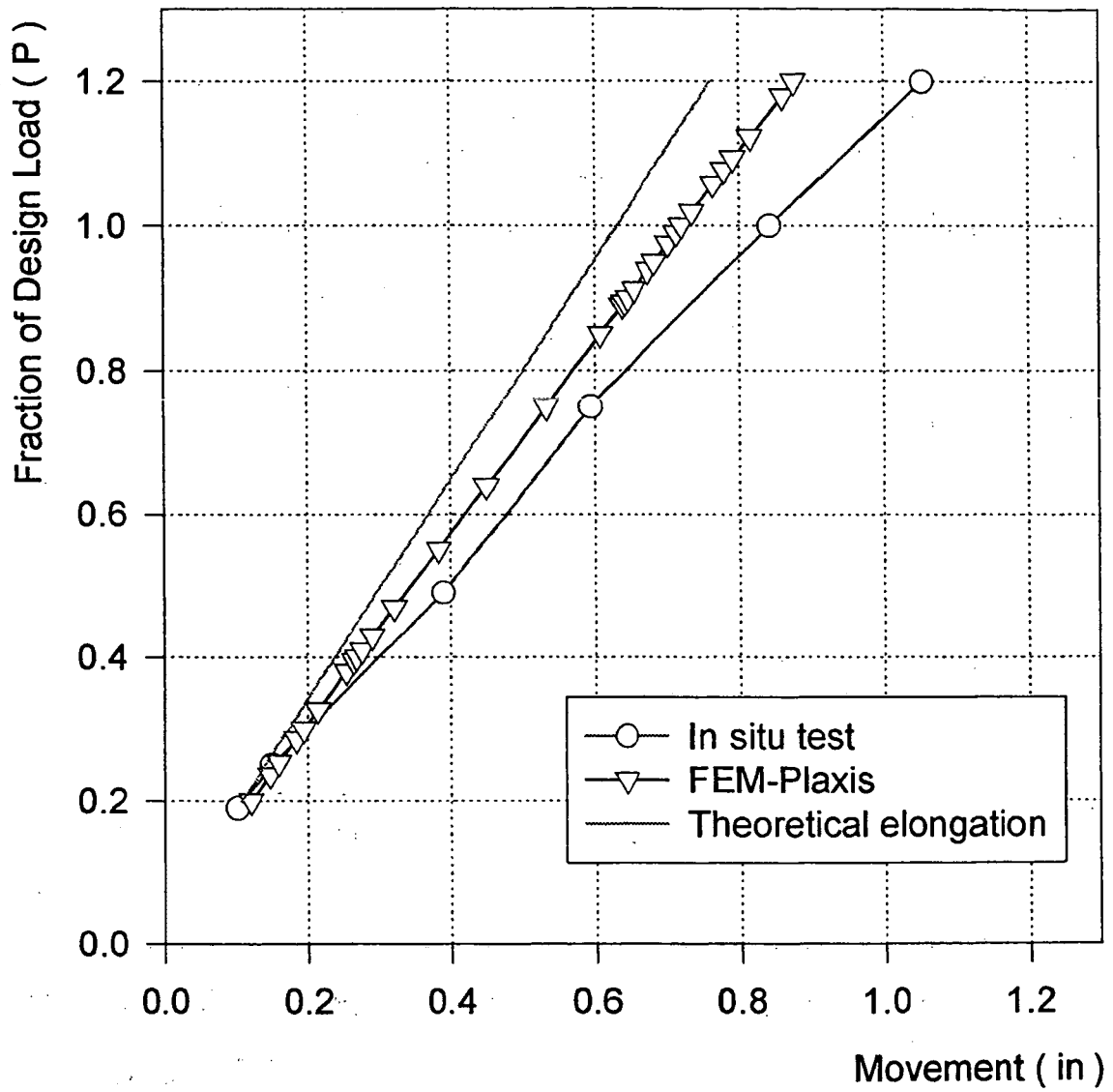


Fig. 6.10: Comparison of anchor head movements in FT2 (Case 3)

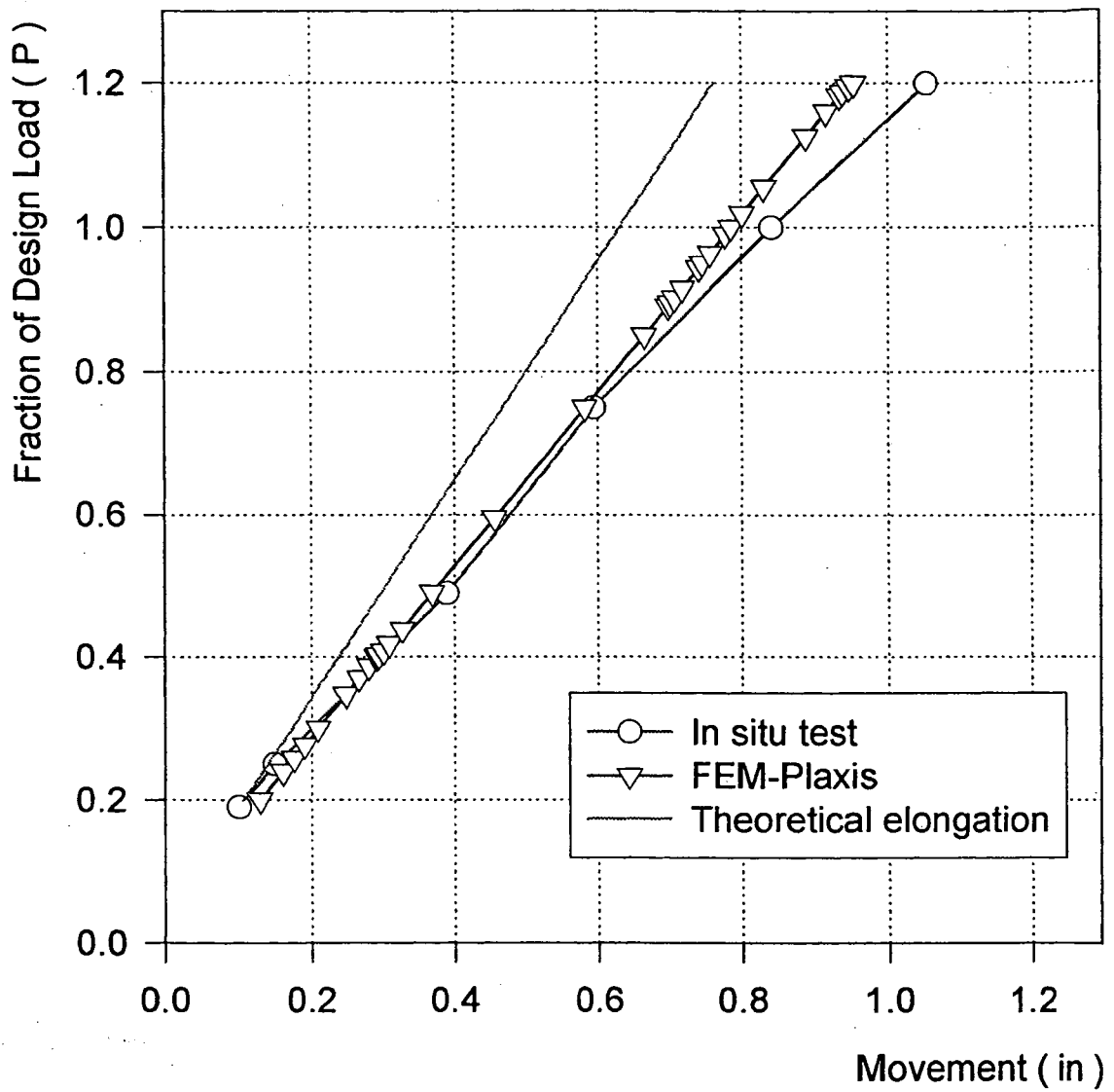


Fig. 6.11: Comparison of anchor head movements in FT2 (Case 4)

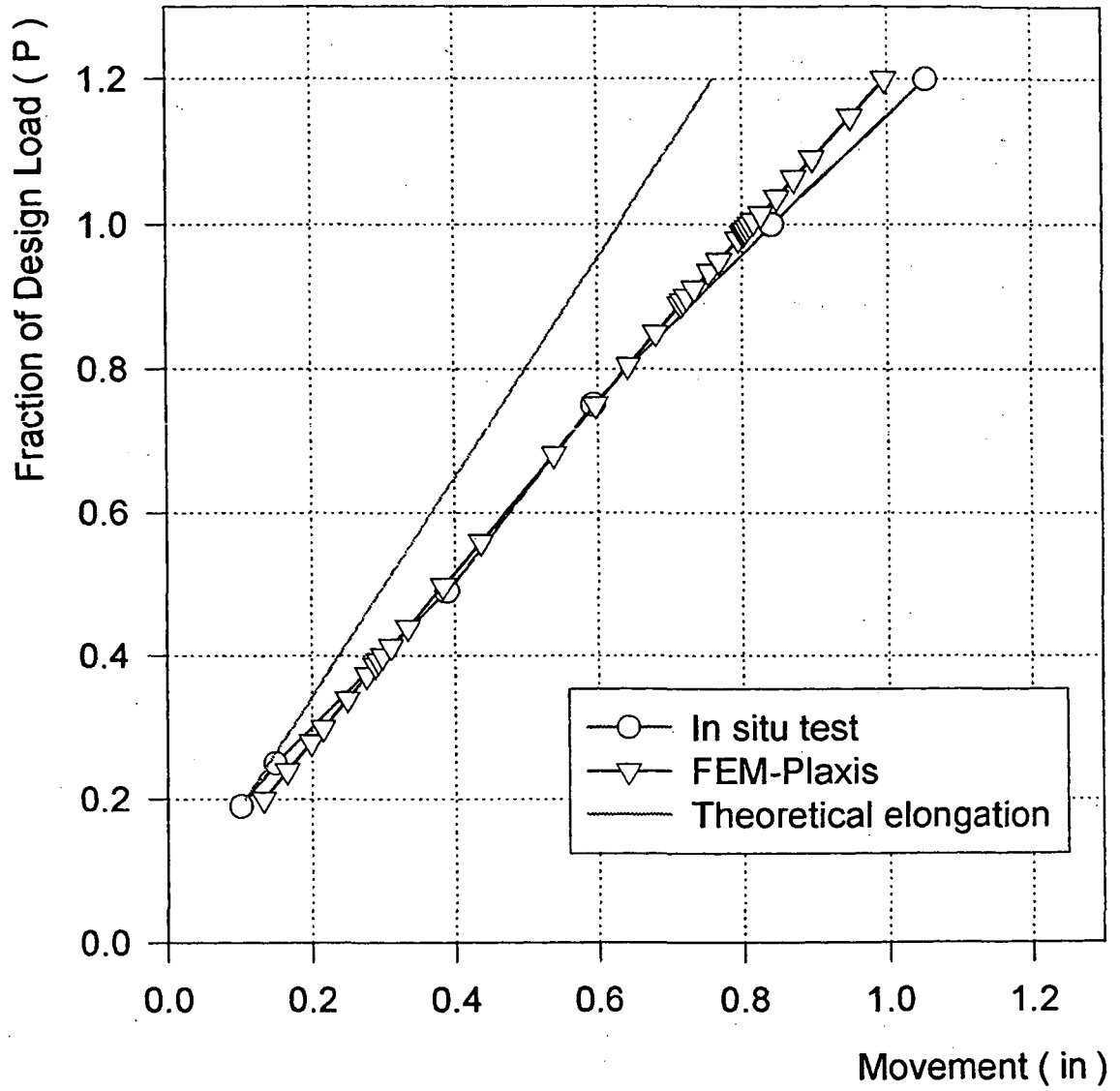


Fig. 6.12: Comparison of anchor head movements in FT2 (Case 5)

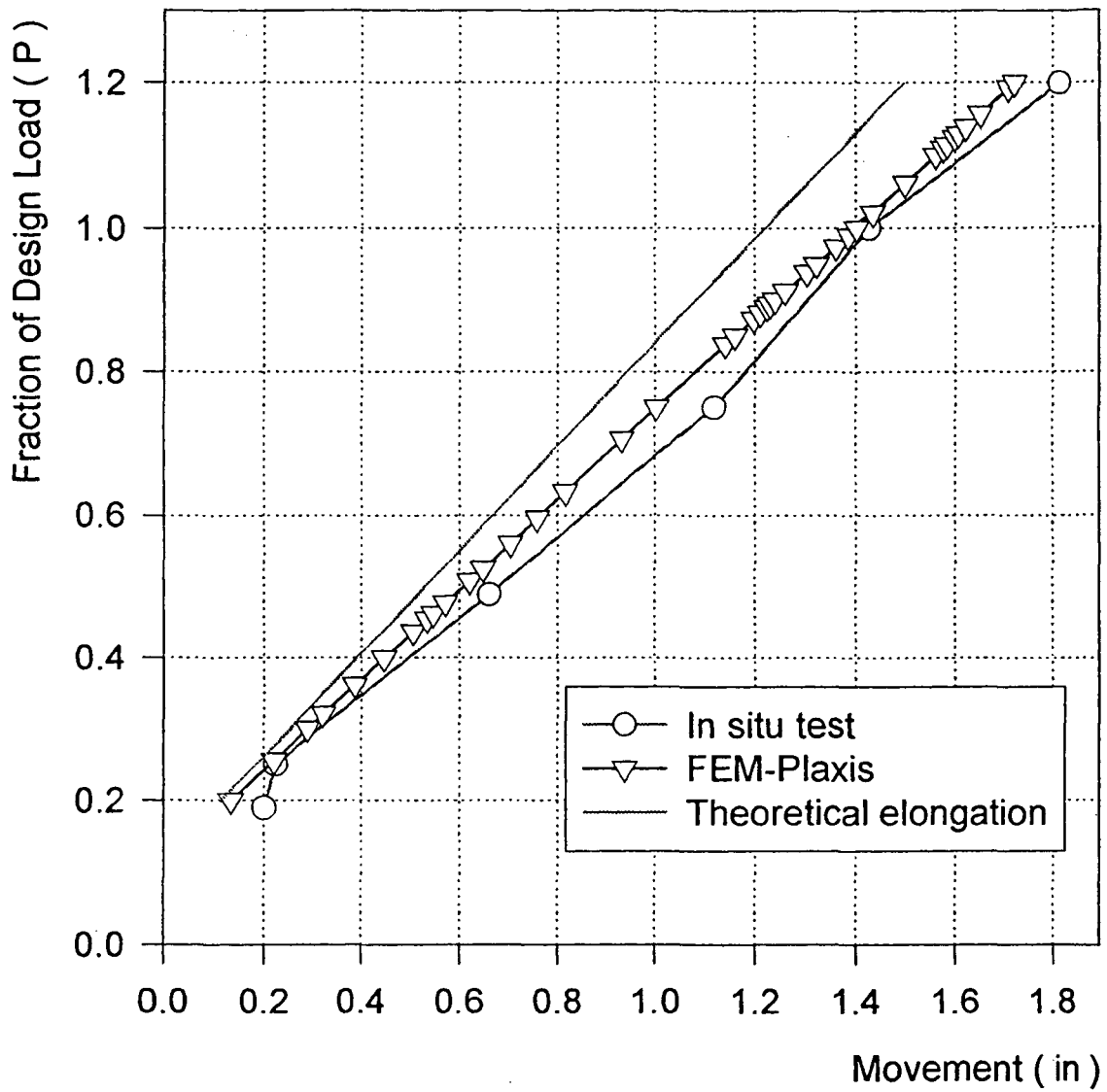


Fig. 6.13: Comparison of anchor head movements in FT1

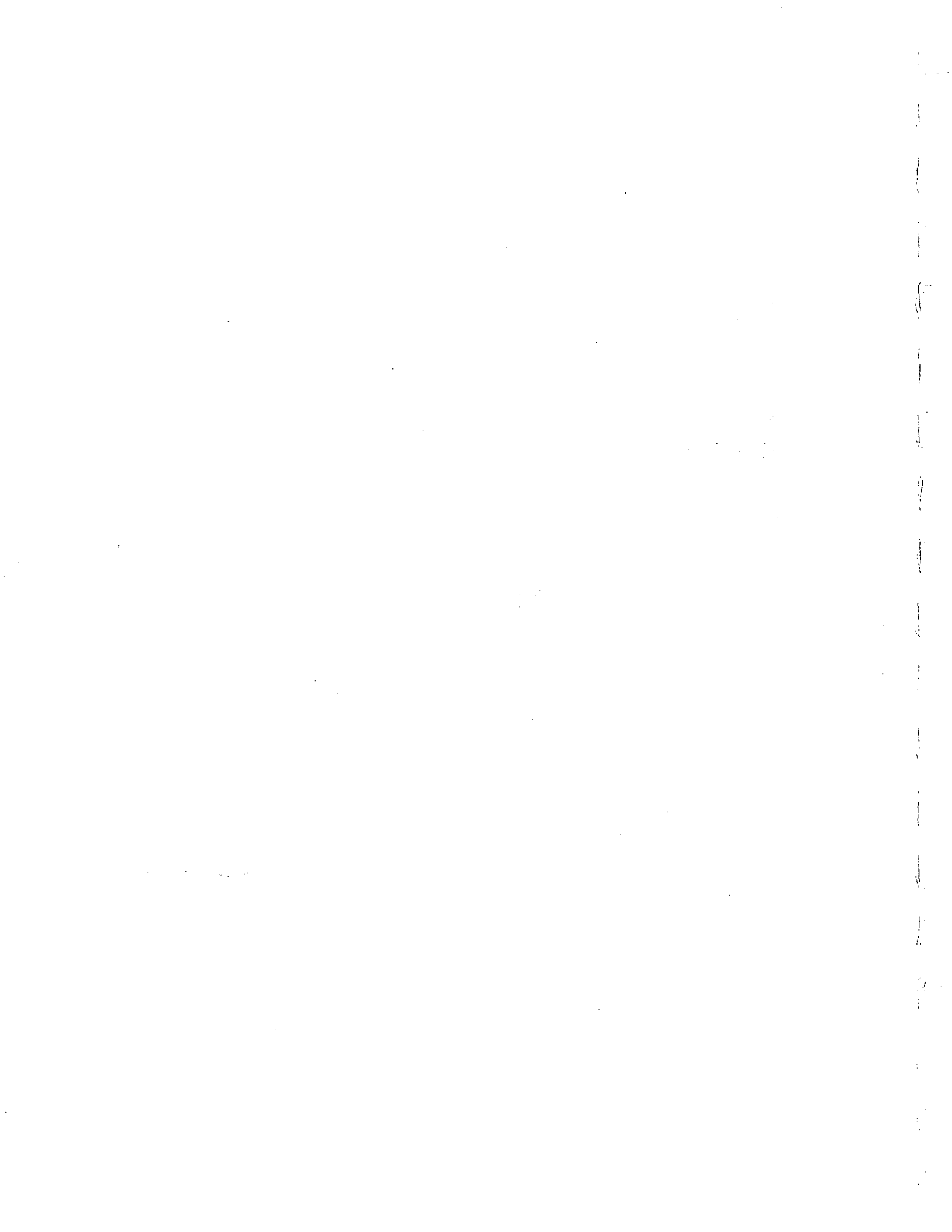




Fig. 6.14: Soil displacement vectors due to phase 1

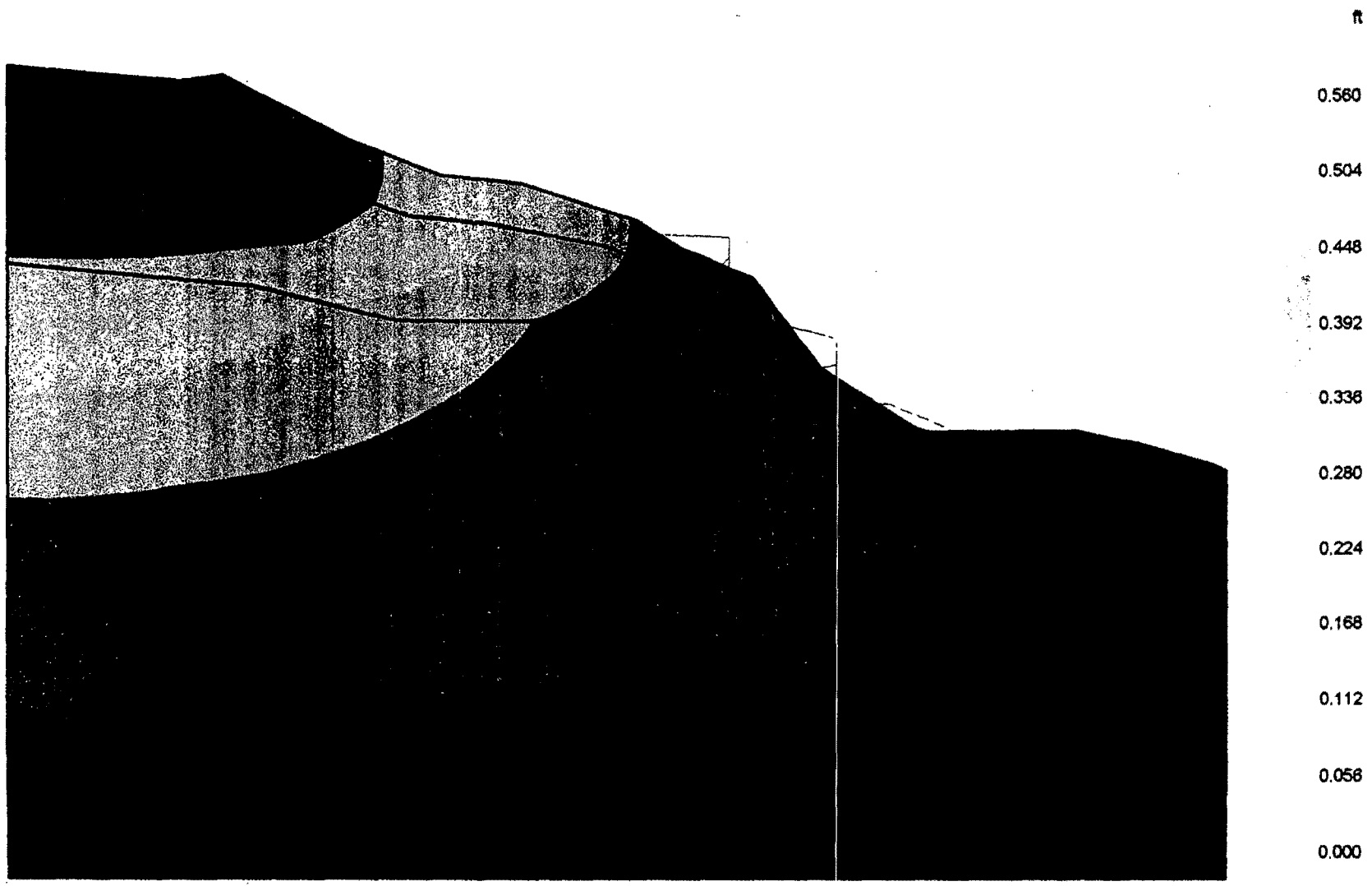


Fig. 6.15: Soil displacement contours due to phase 1

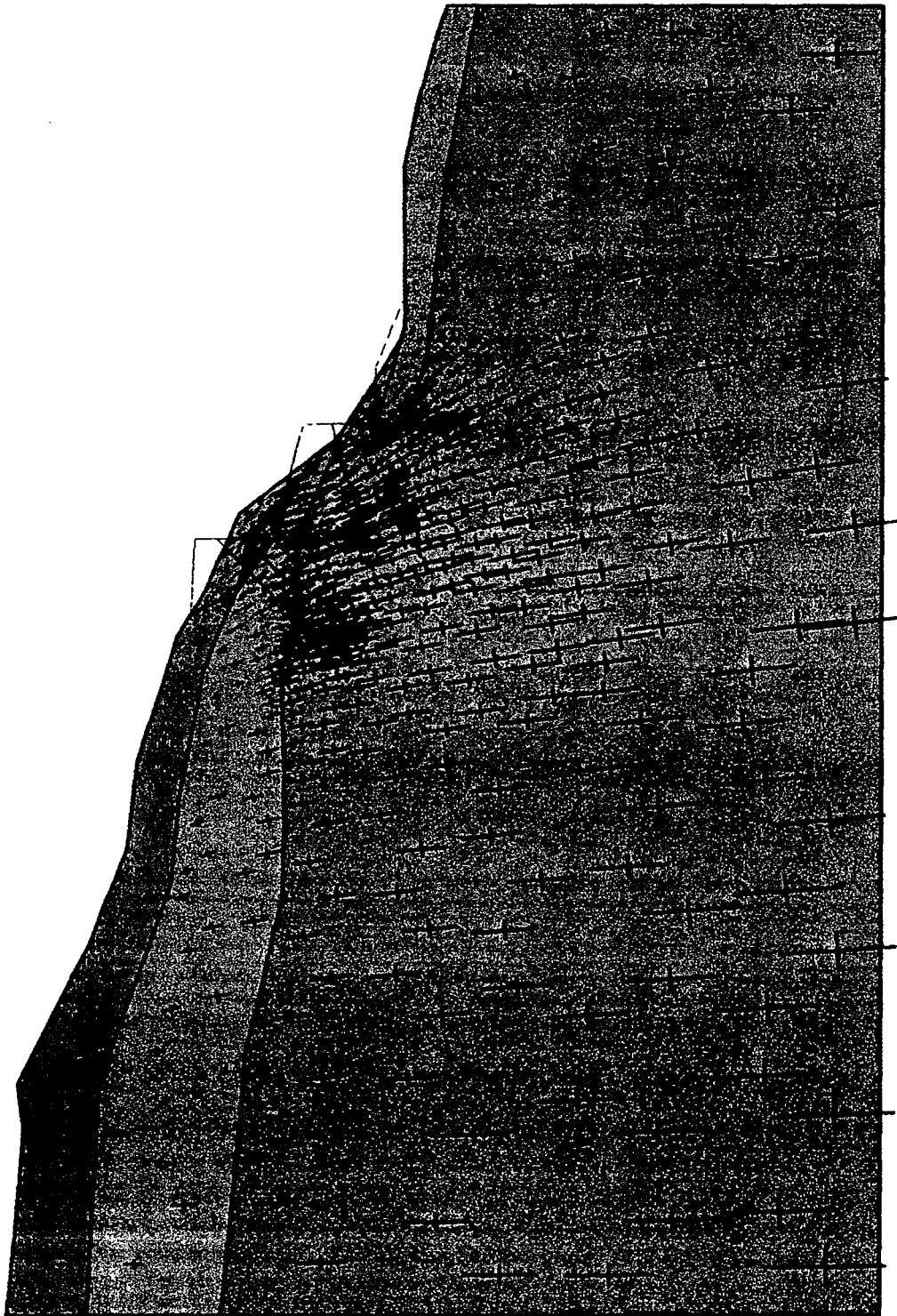


Fig. 6.16: Principal stress direction and magnitude after phase 1

VI-30

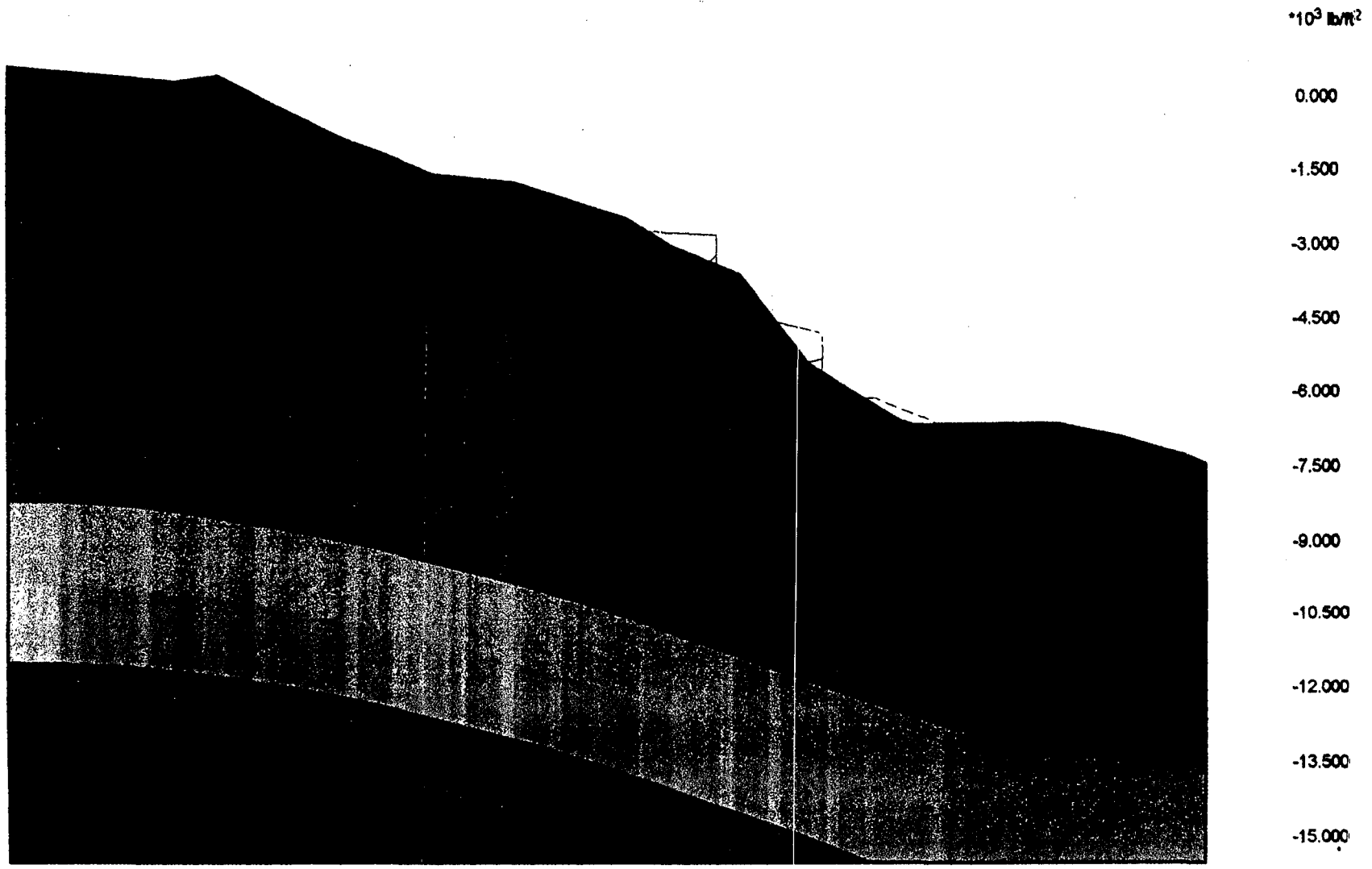


Fig. 6.17: Mean effective stress contours after phase 1

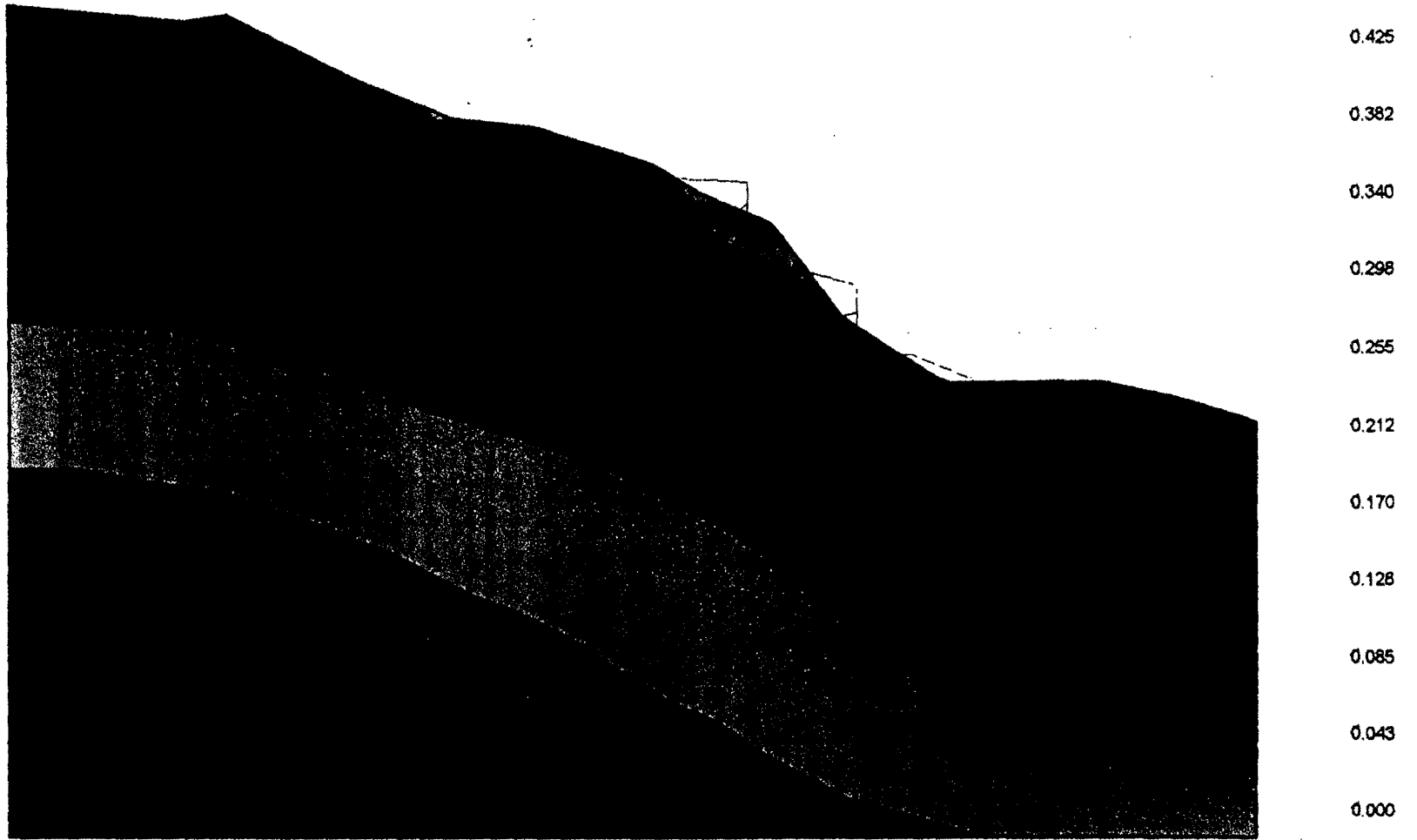


Fig. 6.18: Relative shear stress ratio contours after phase 1

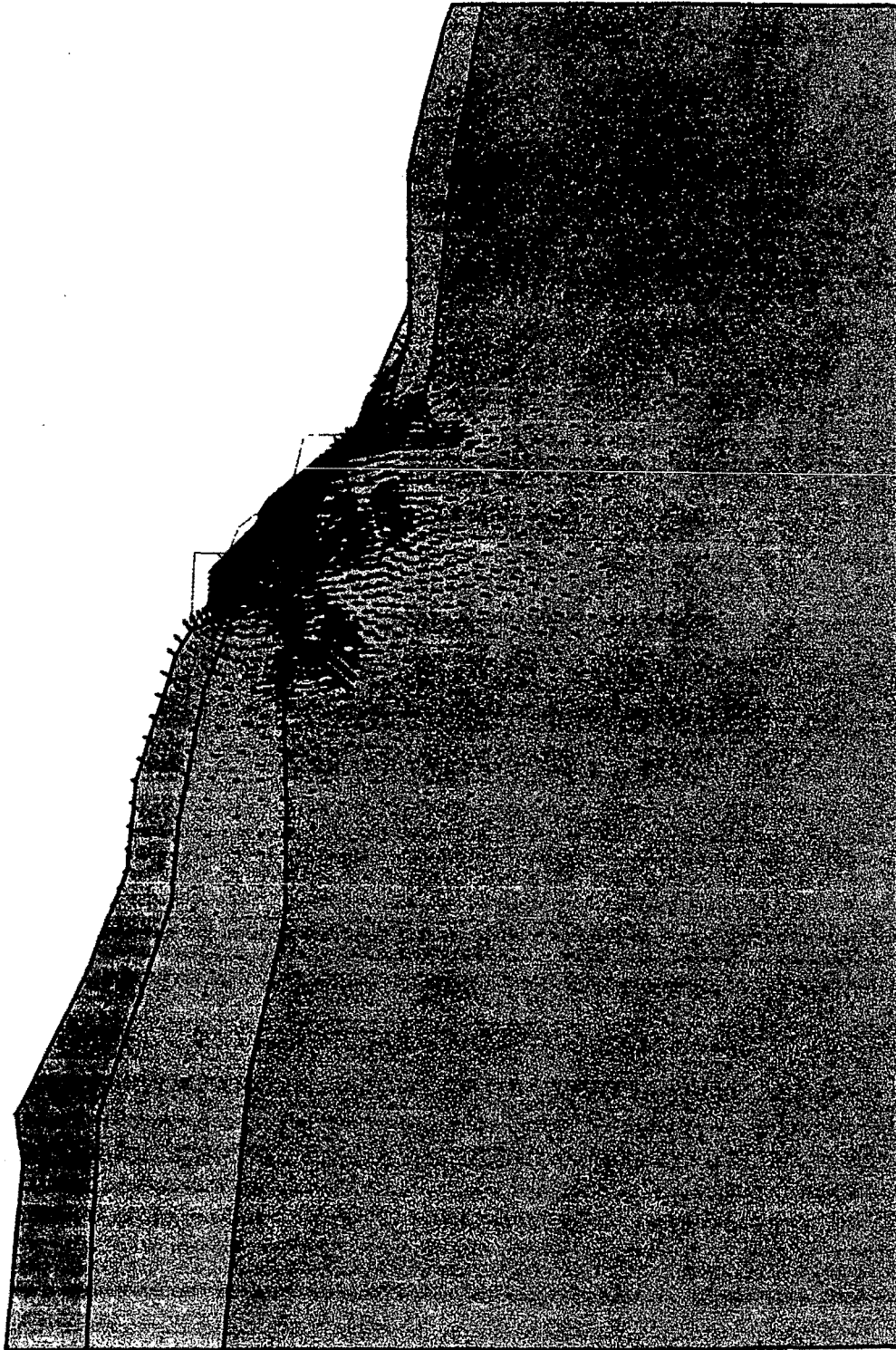


Fig. 6.19: Soil displacement vectors due to phase 2

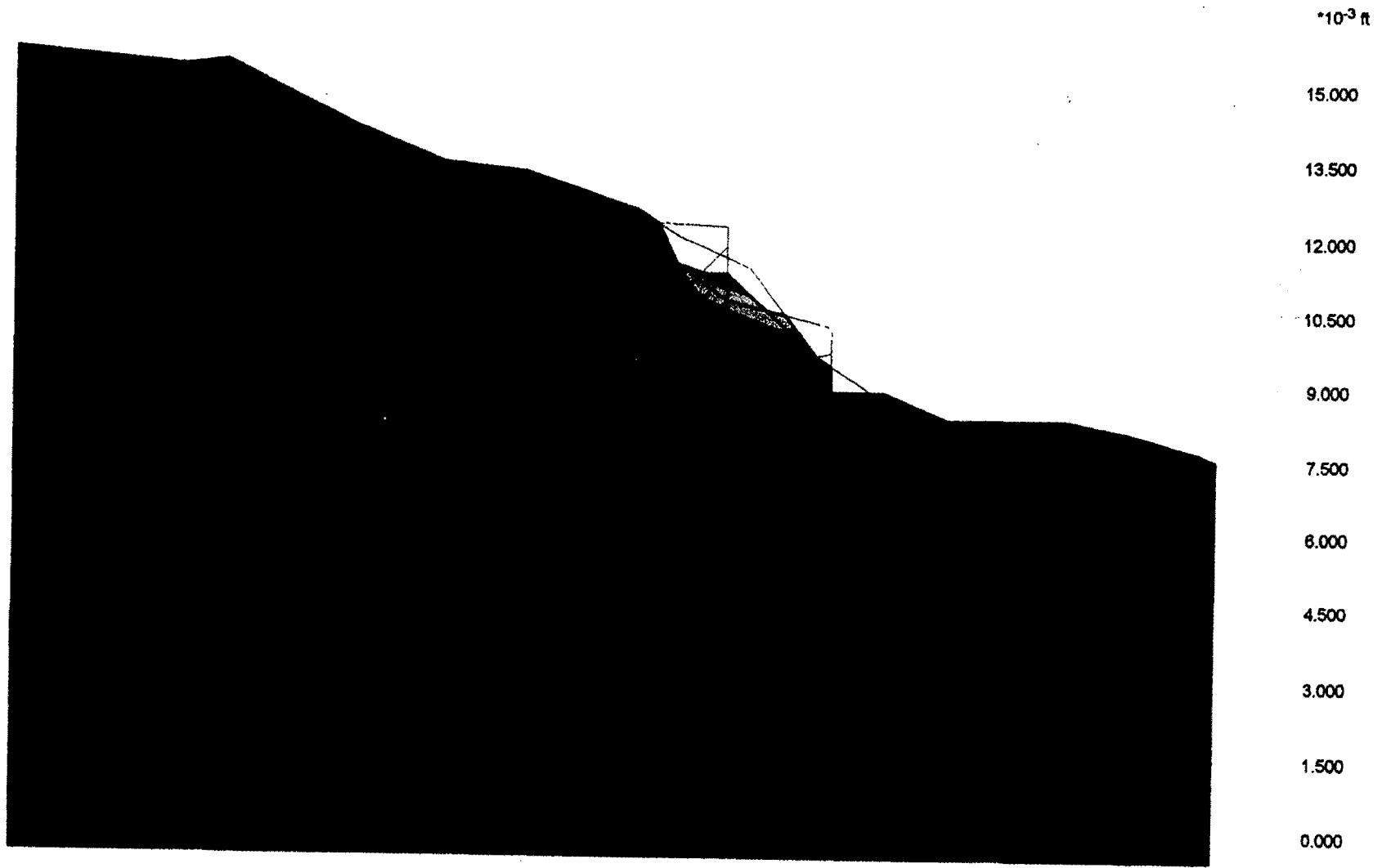


Fig. 6.20: Soil displacement contours due to phase 2

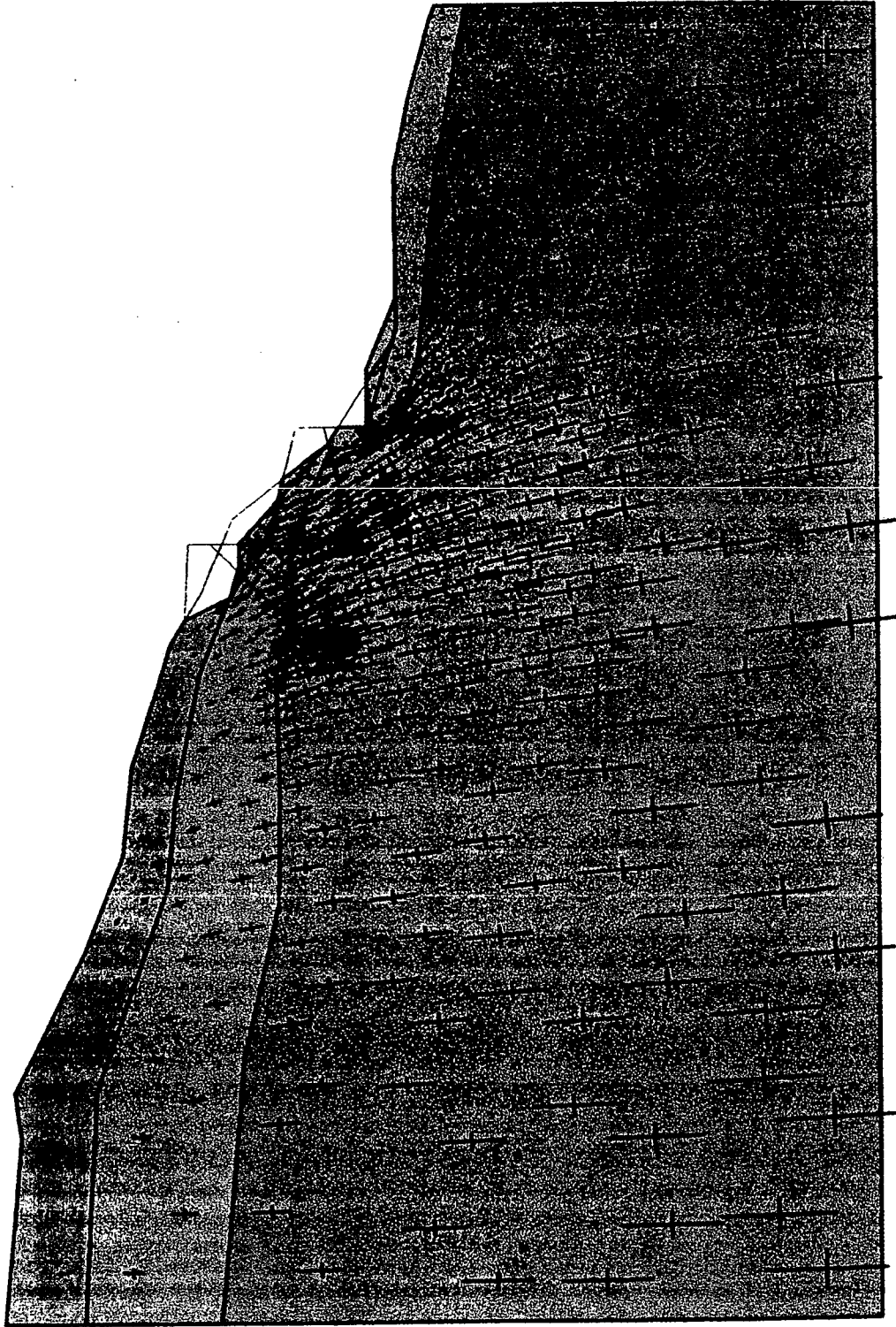


Fig. 6.21: Principal stress direction and magnitude after phase 2

VI-35

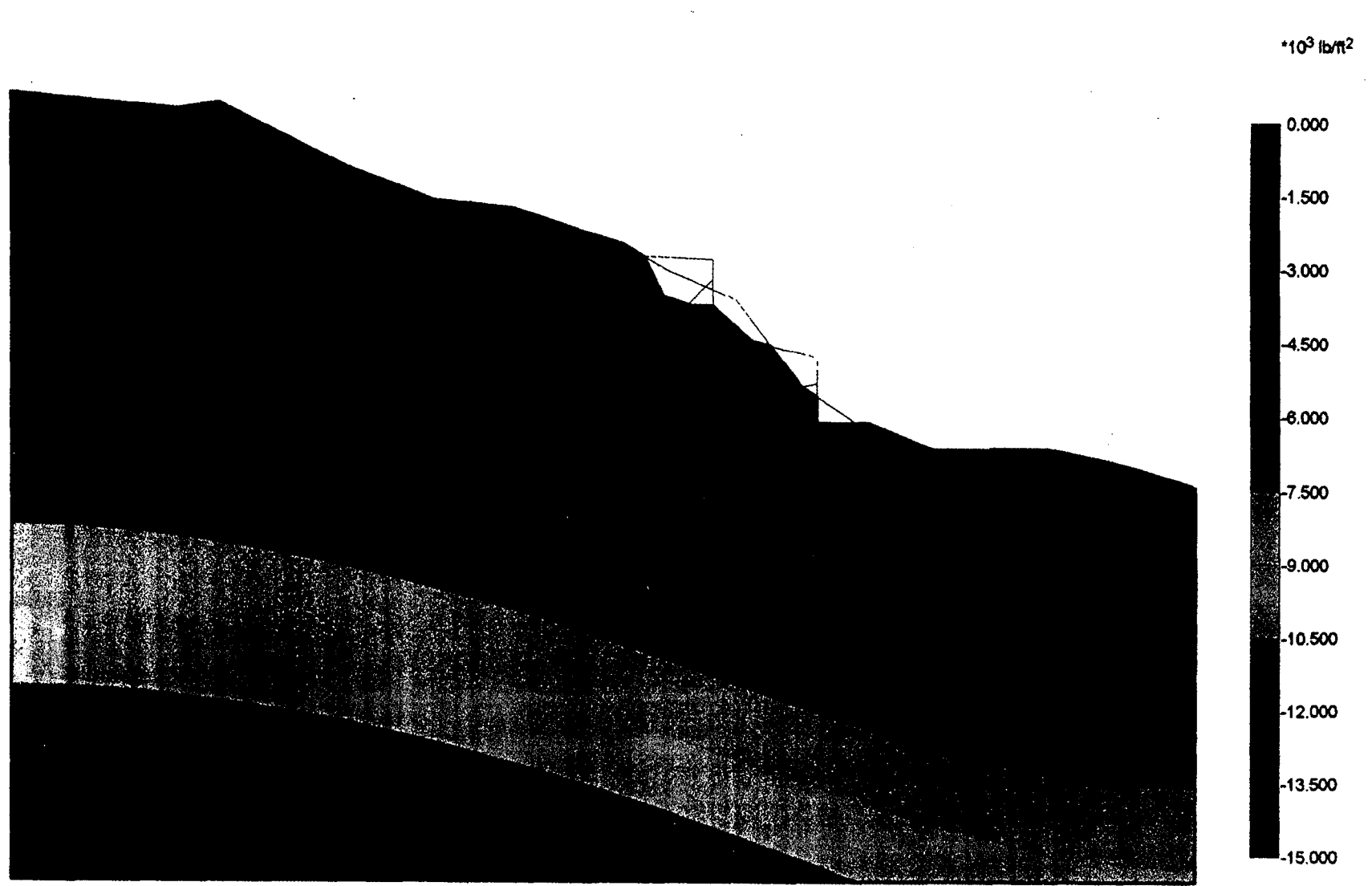


Fig. 6.22: Mean effective stress contours after phase 2

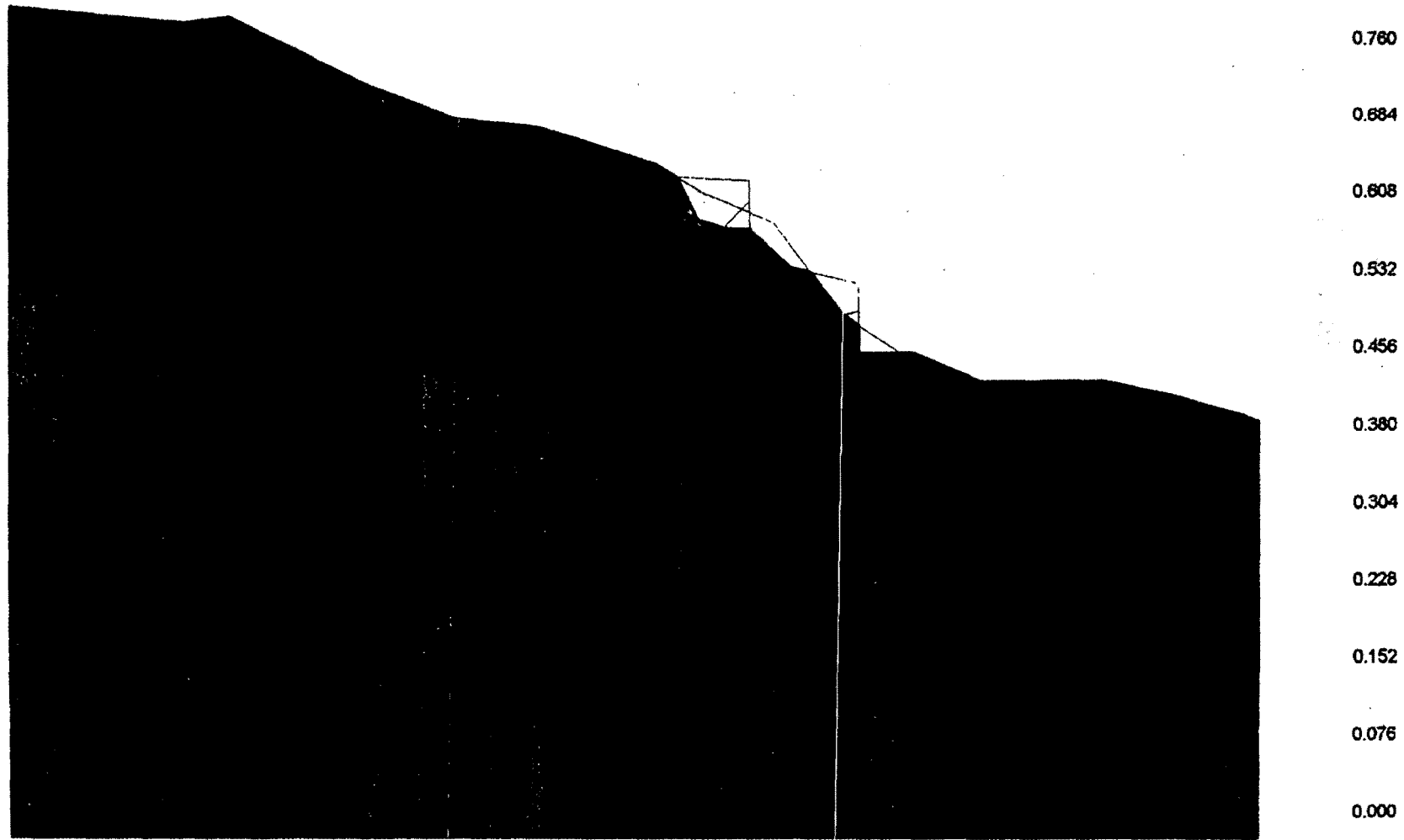


Fig. 6.23: Relative shear stress ratio contours after phase 2

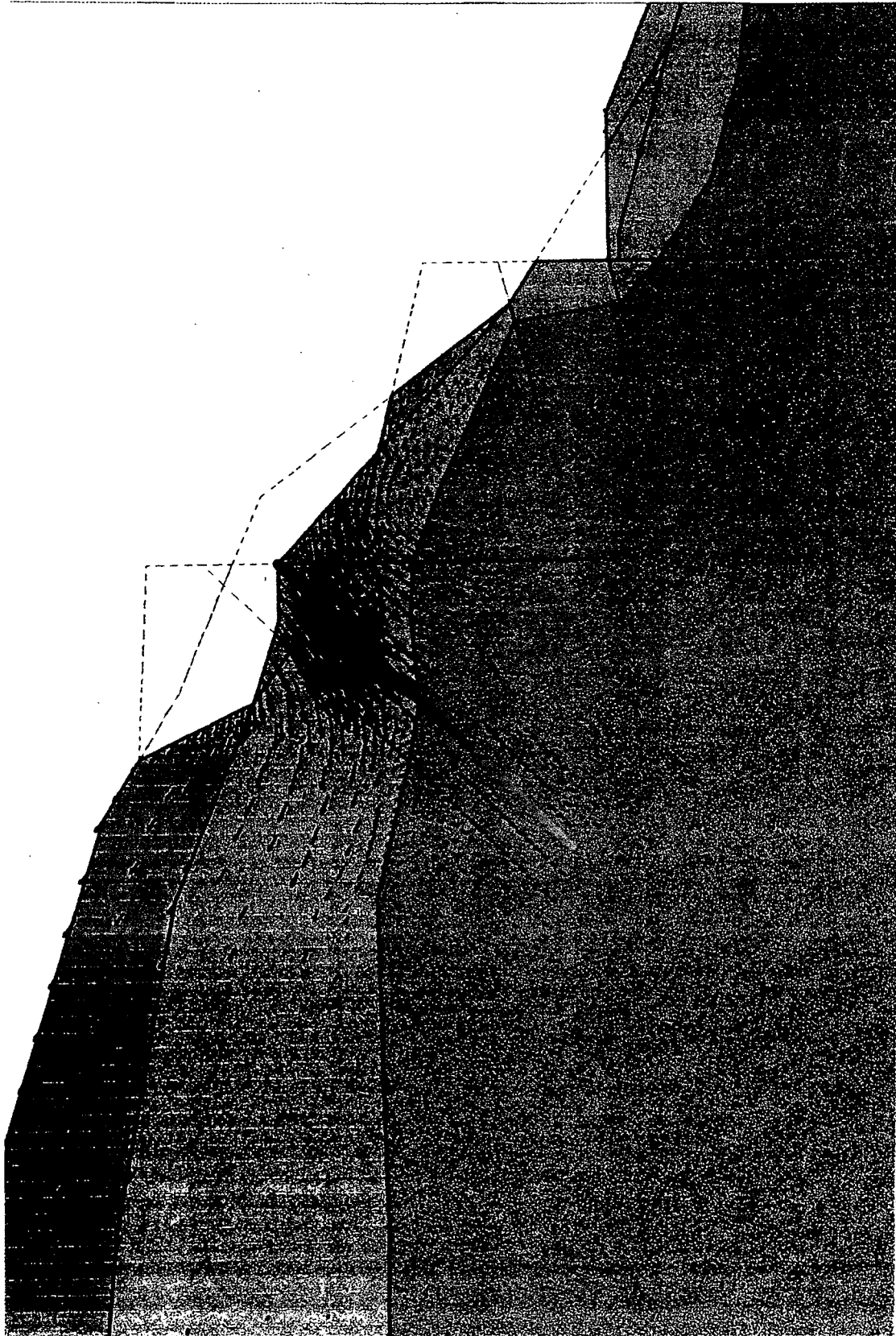


Fig. 6.24: Soil displacement vectors due to phase 3

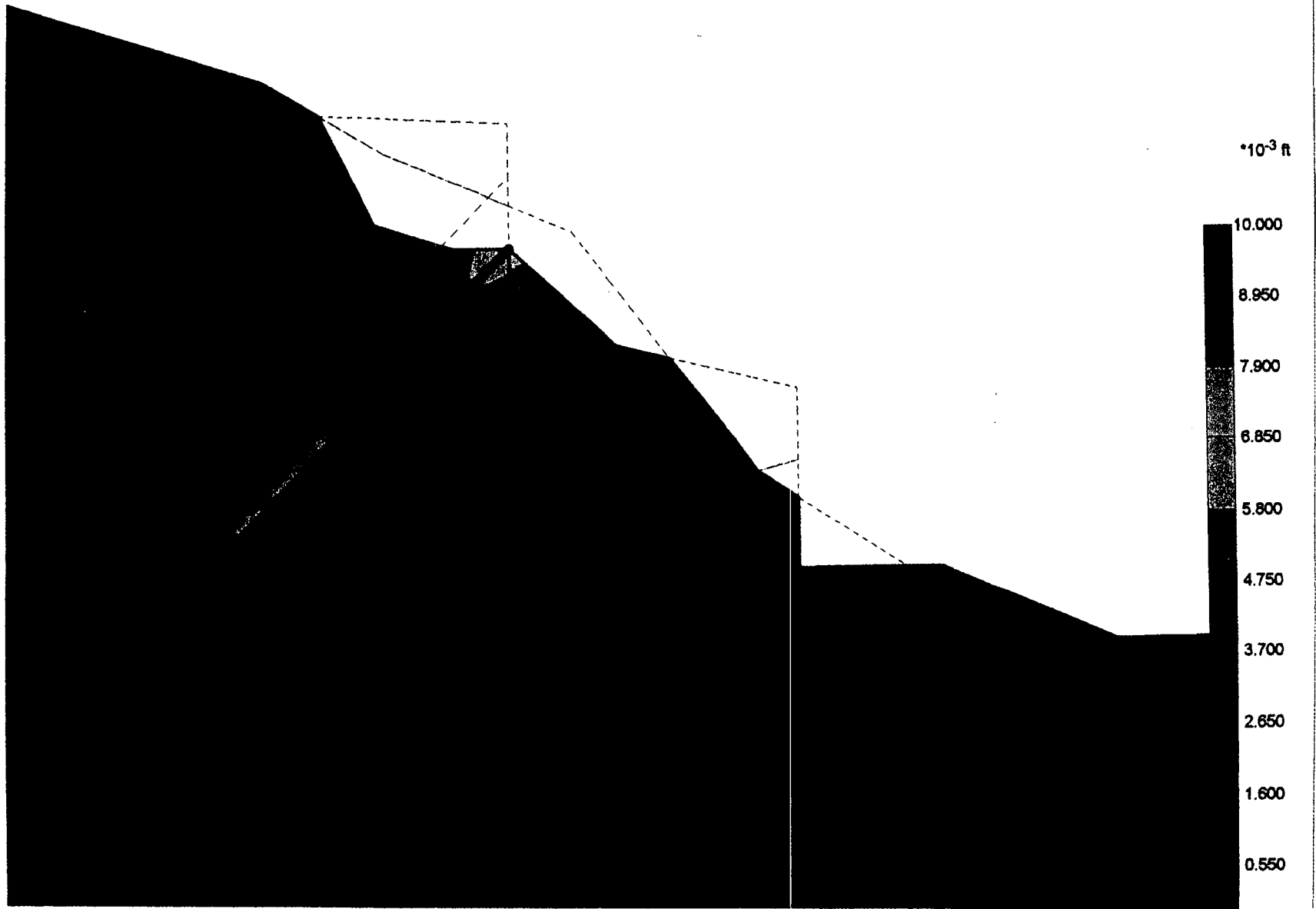


Fig. 6.25: Soil displacement contours due to phase 3

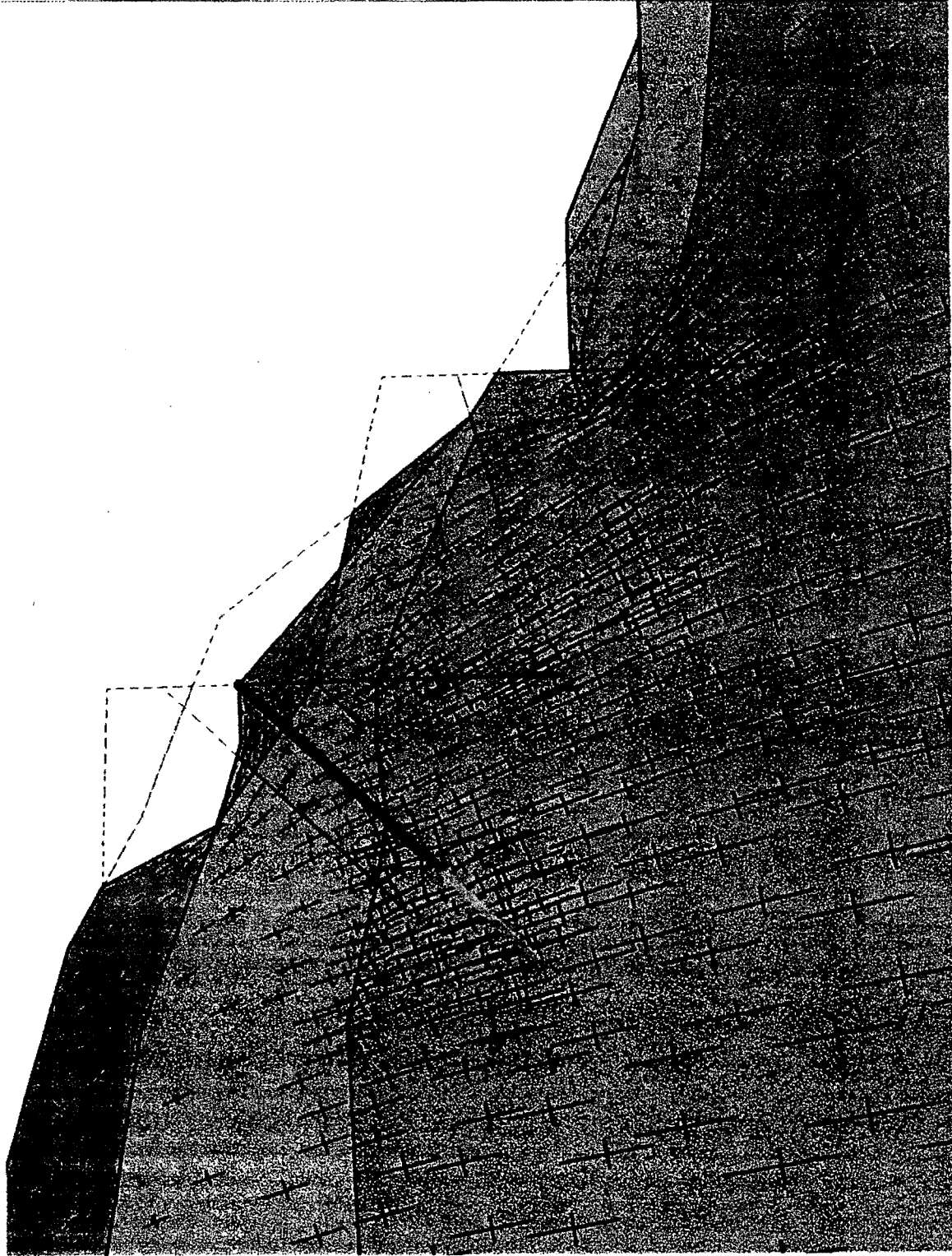


Fig. 6.26: Principal stress direction and magnitude after phase 3

VI-40

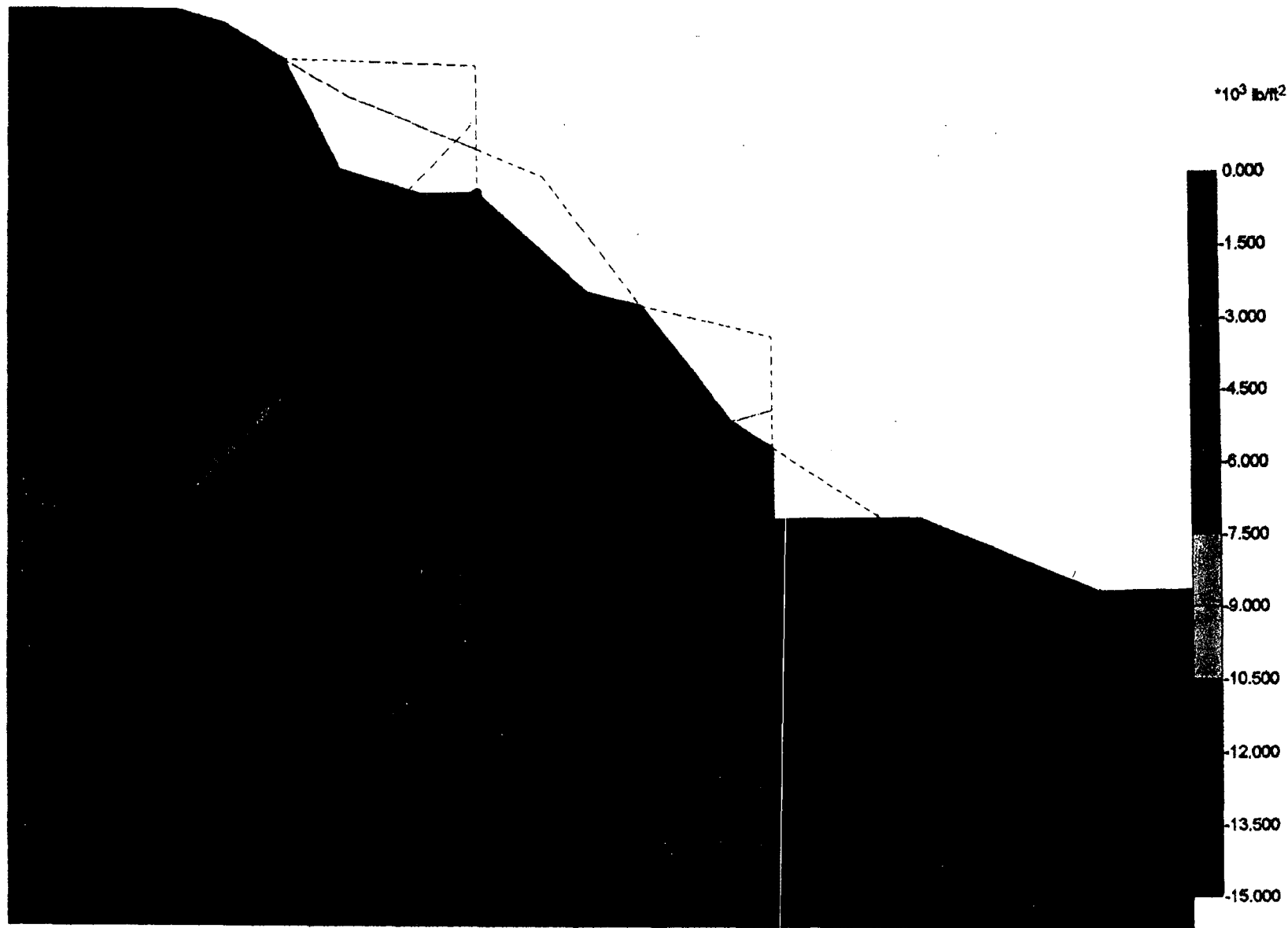


Fig. 6.27: Mean effective stress contours after phase 3

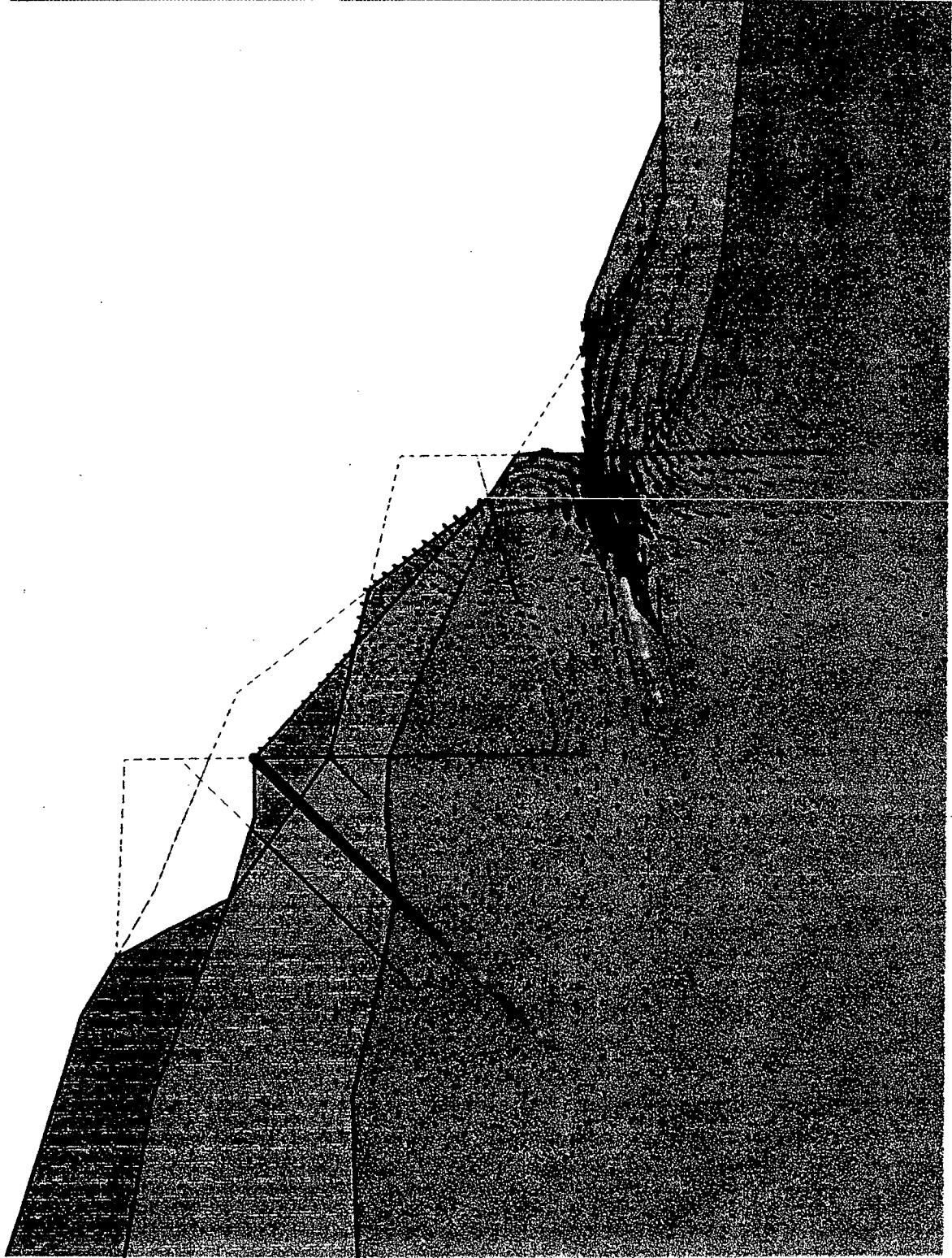


Fig. 6.29: Soil displacement vectors due to phase 4

VI-43

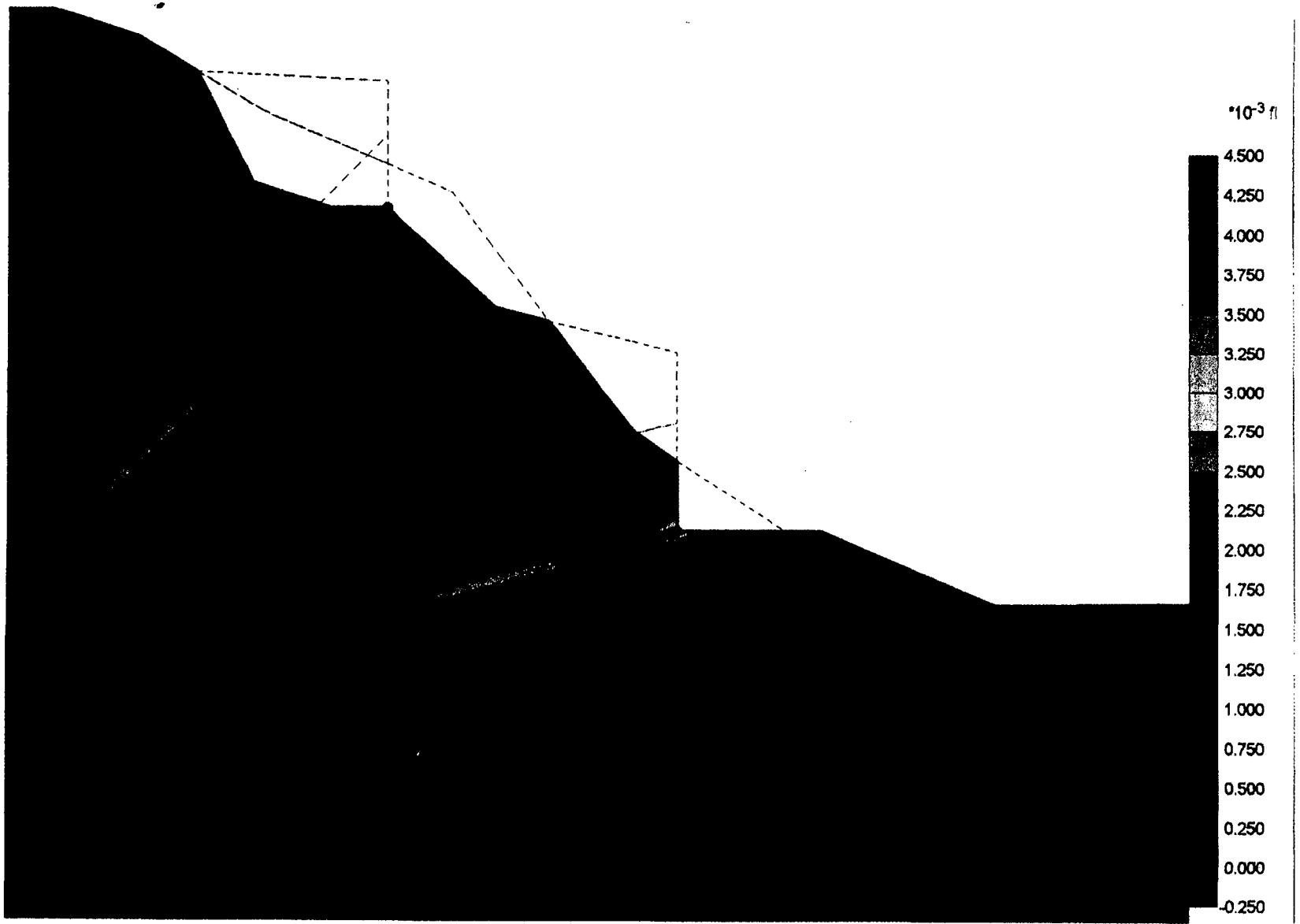


Fig. 6.30: Soil displacement contours due to phase 4

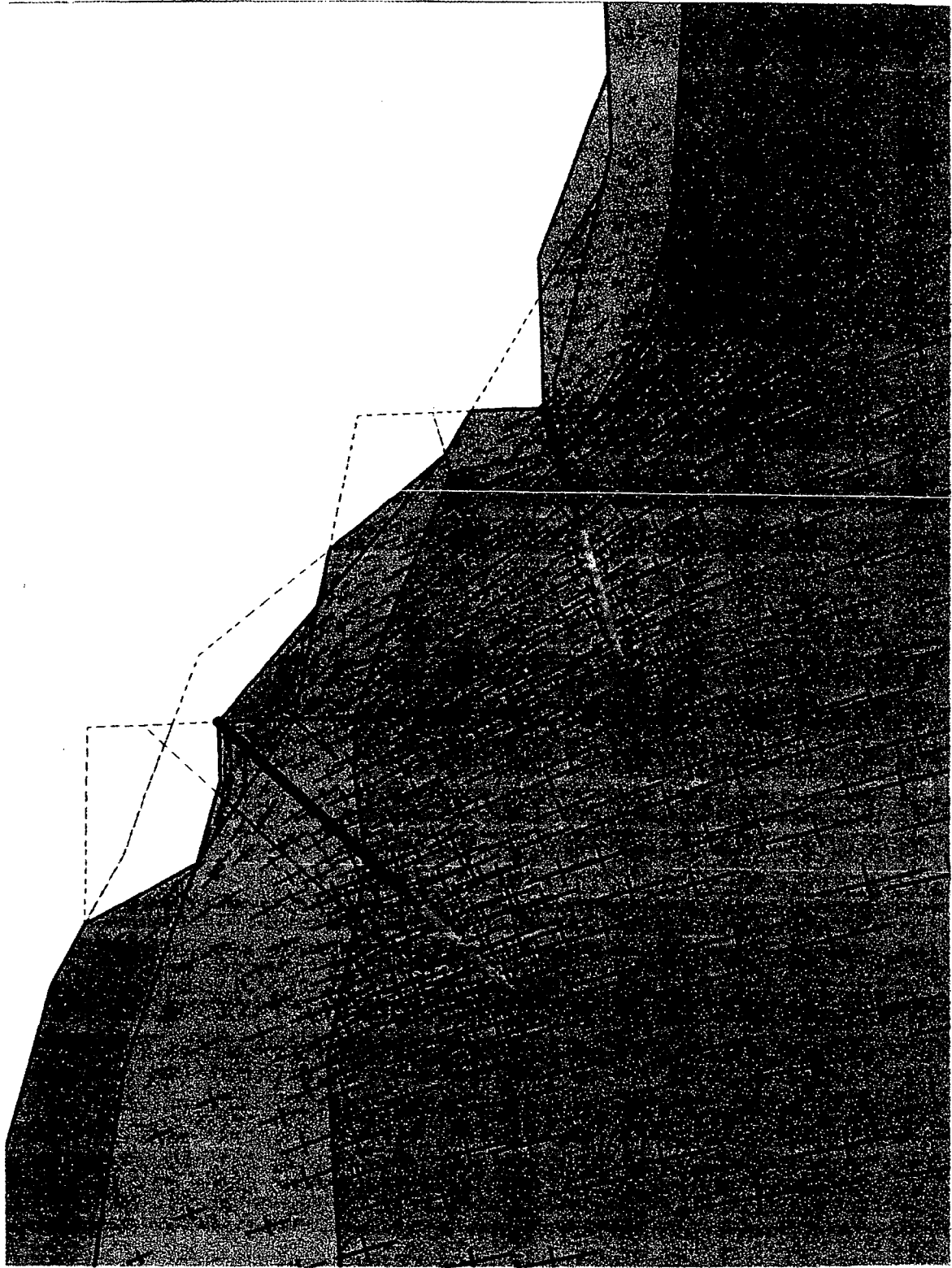


Fig 6.31: Principal stress direction and magnitude after phase 4

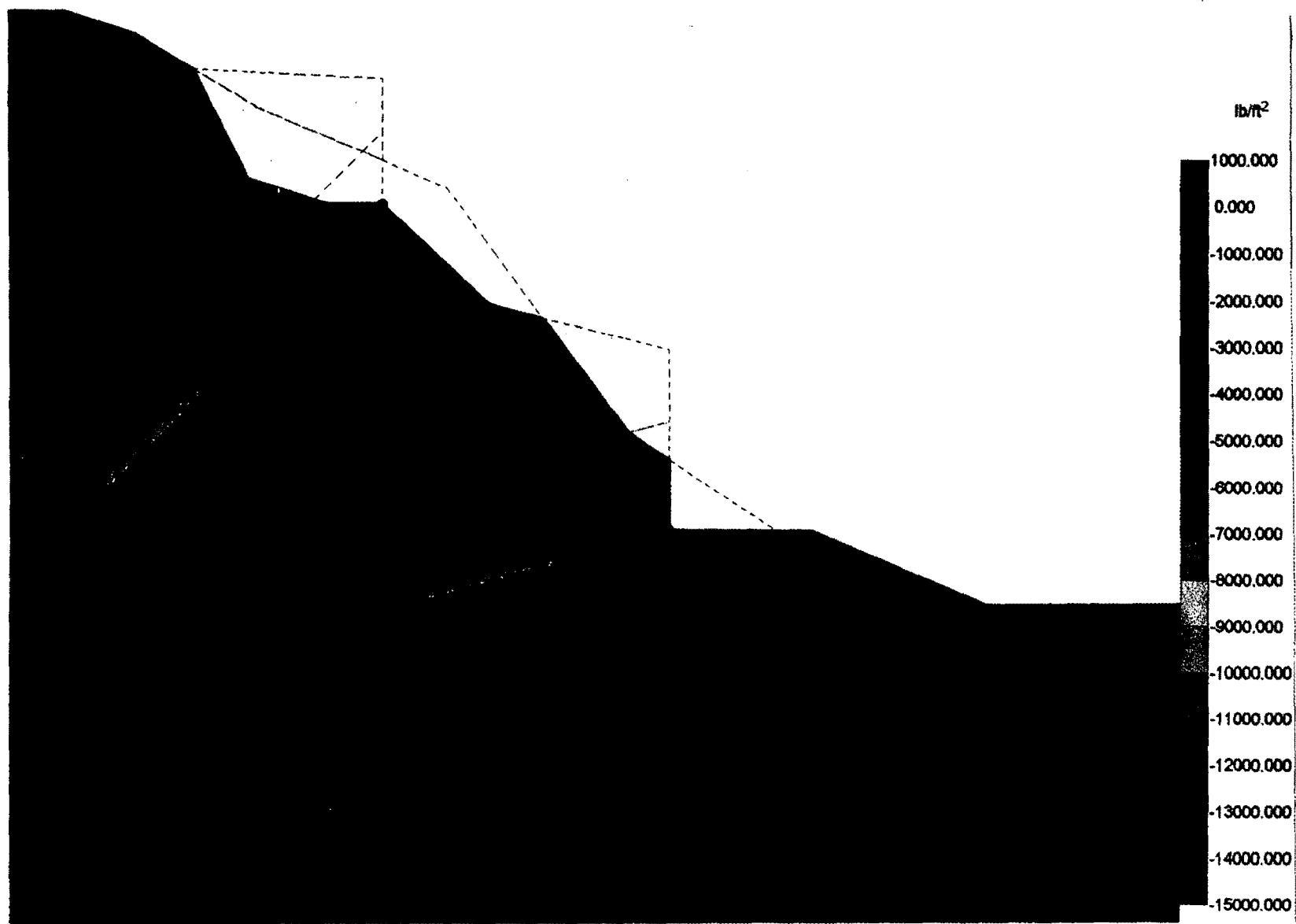


Fig. 6.32: Mean effective stress contours after phase 4

VI-46

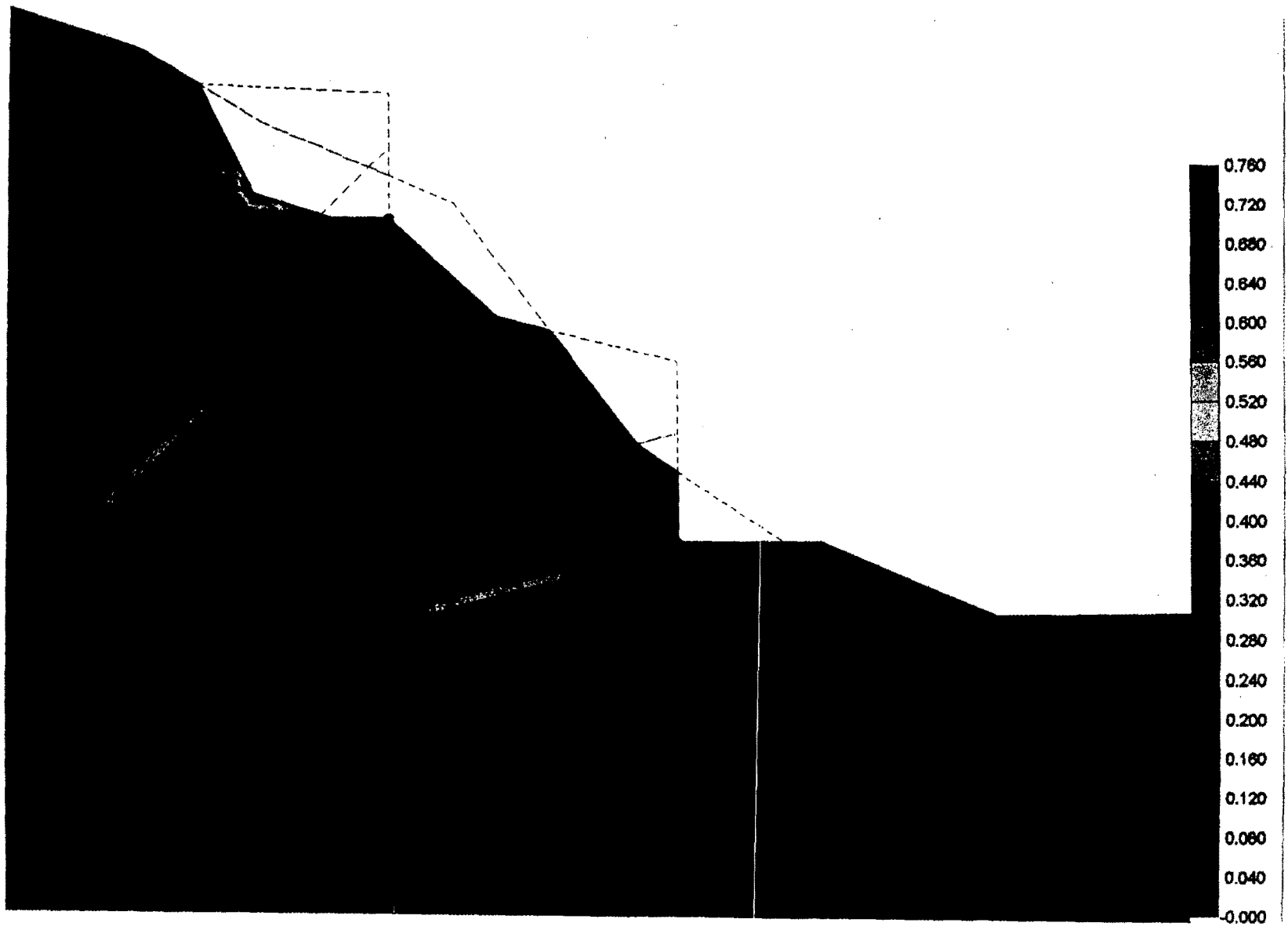


Fig. 6.33: Relative shear stress ratio contours after phase 4

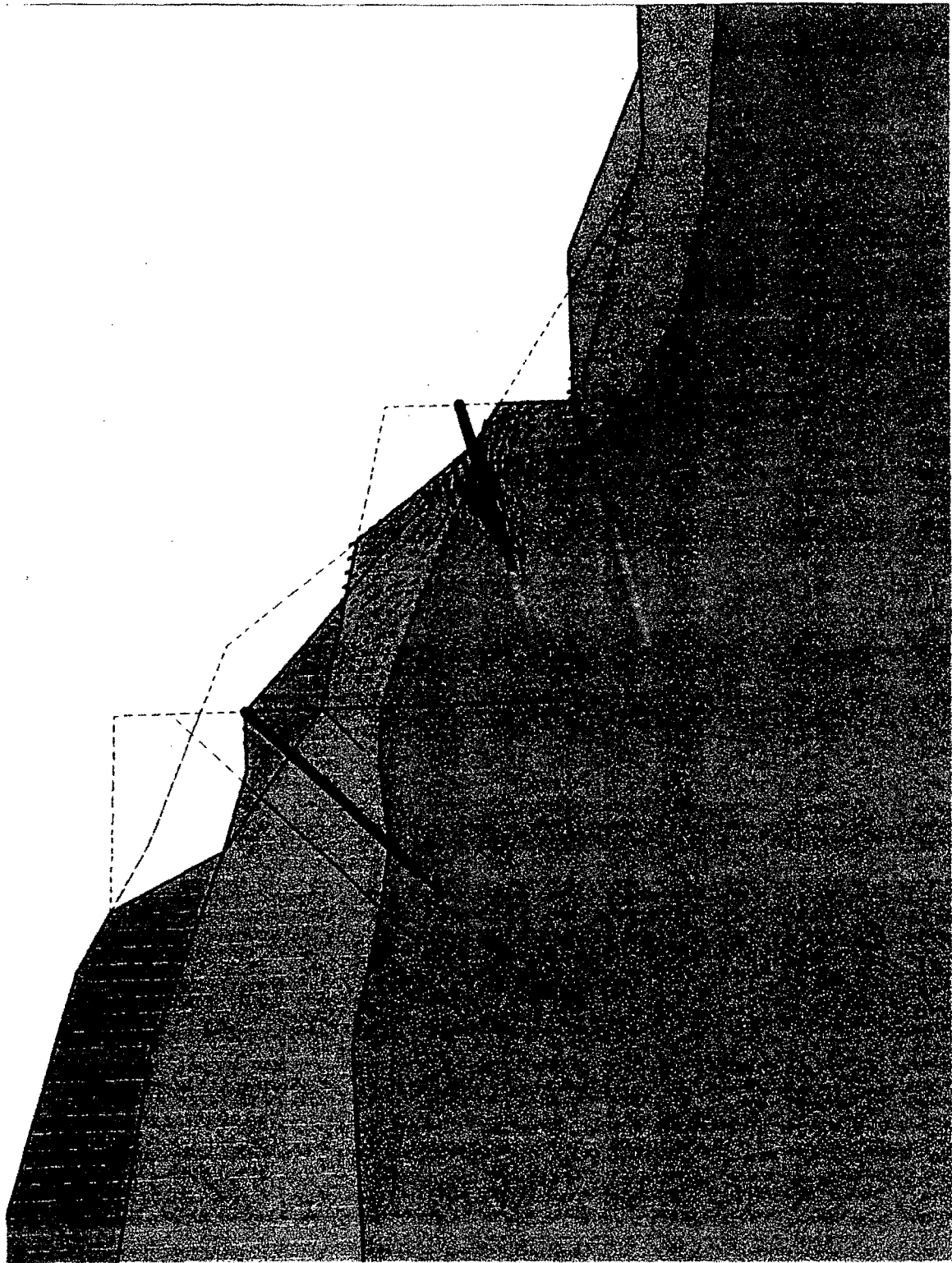


Fig. 6.34: Soil displacement vectors due to phase 5

VI-48

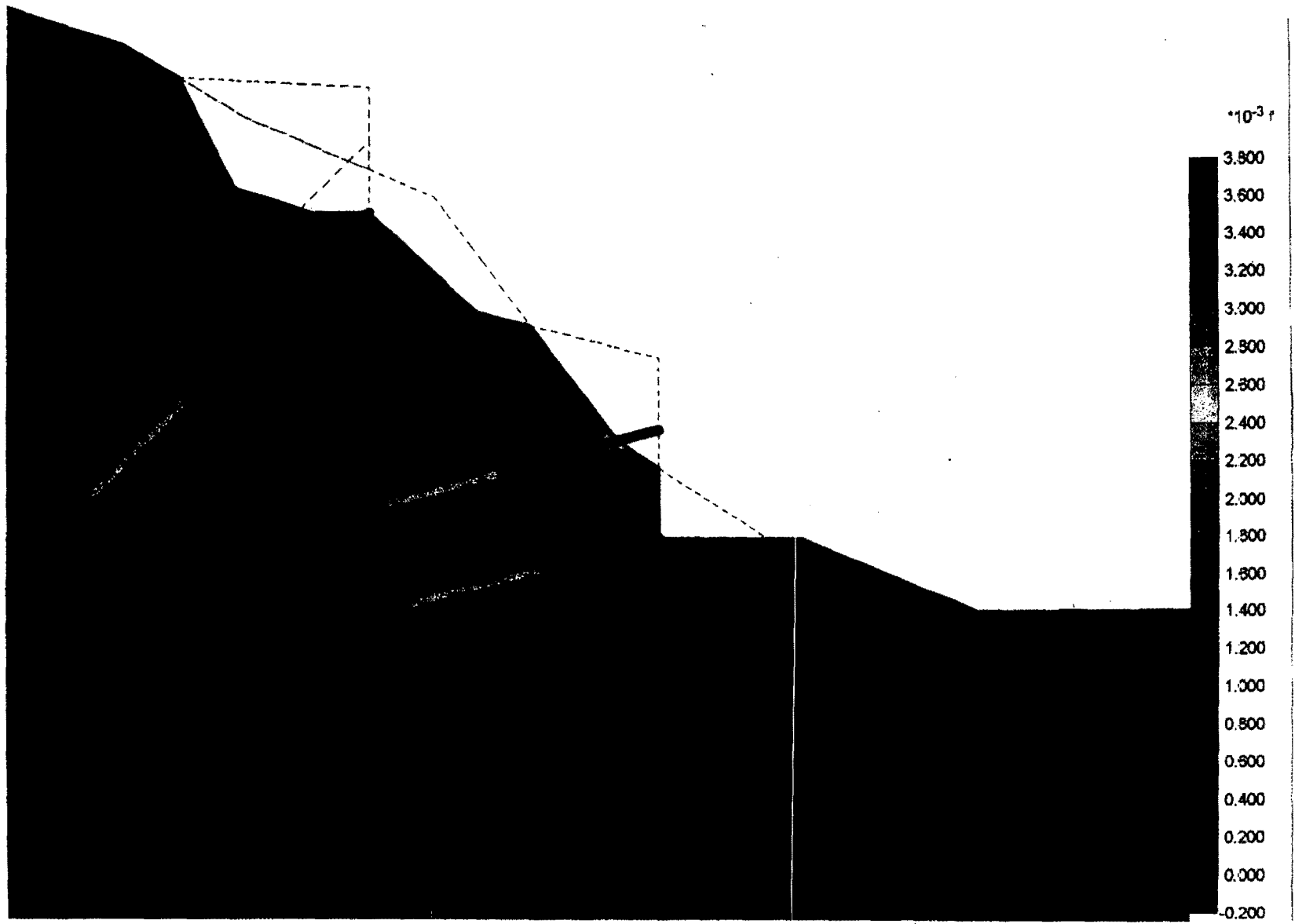


Fig. 6.35: Soil displacement contours due to phase 5

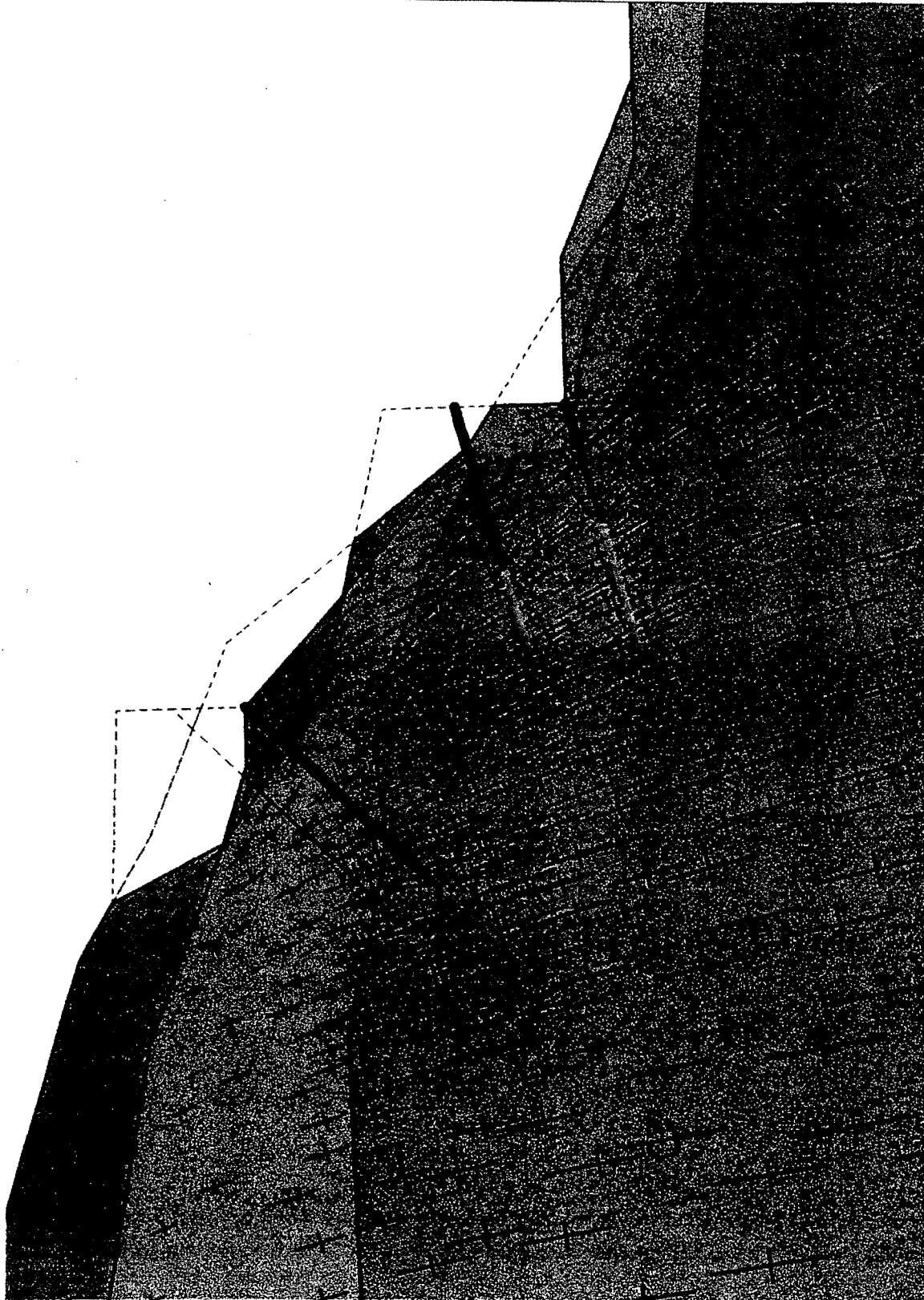


Fig. 6.36: Principal stress direction and magnitude after phase 5

VI-50

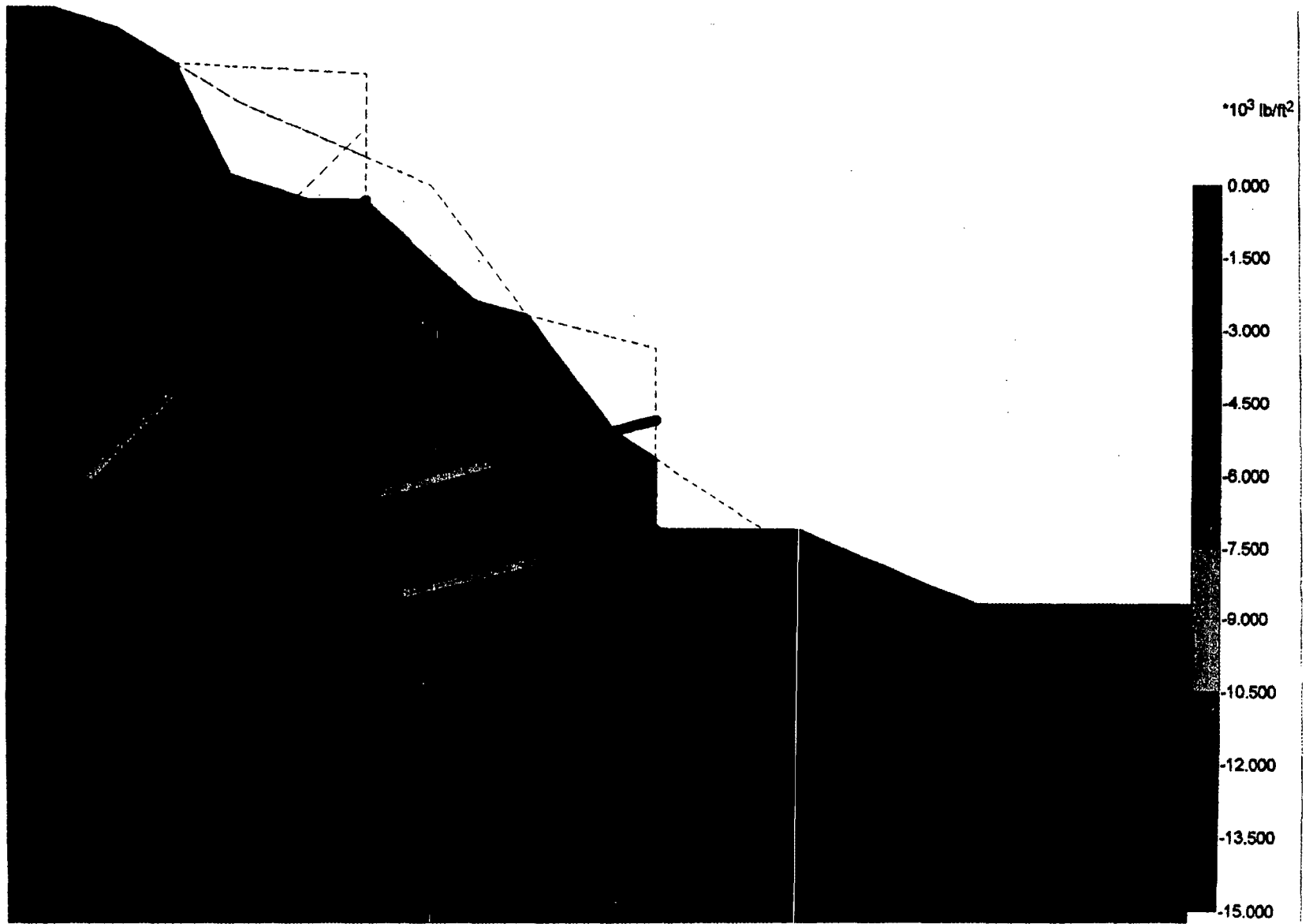


Fig. 6.37: Mean effective stress contours after phase 5

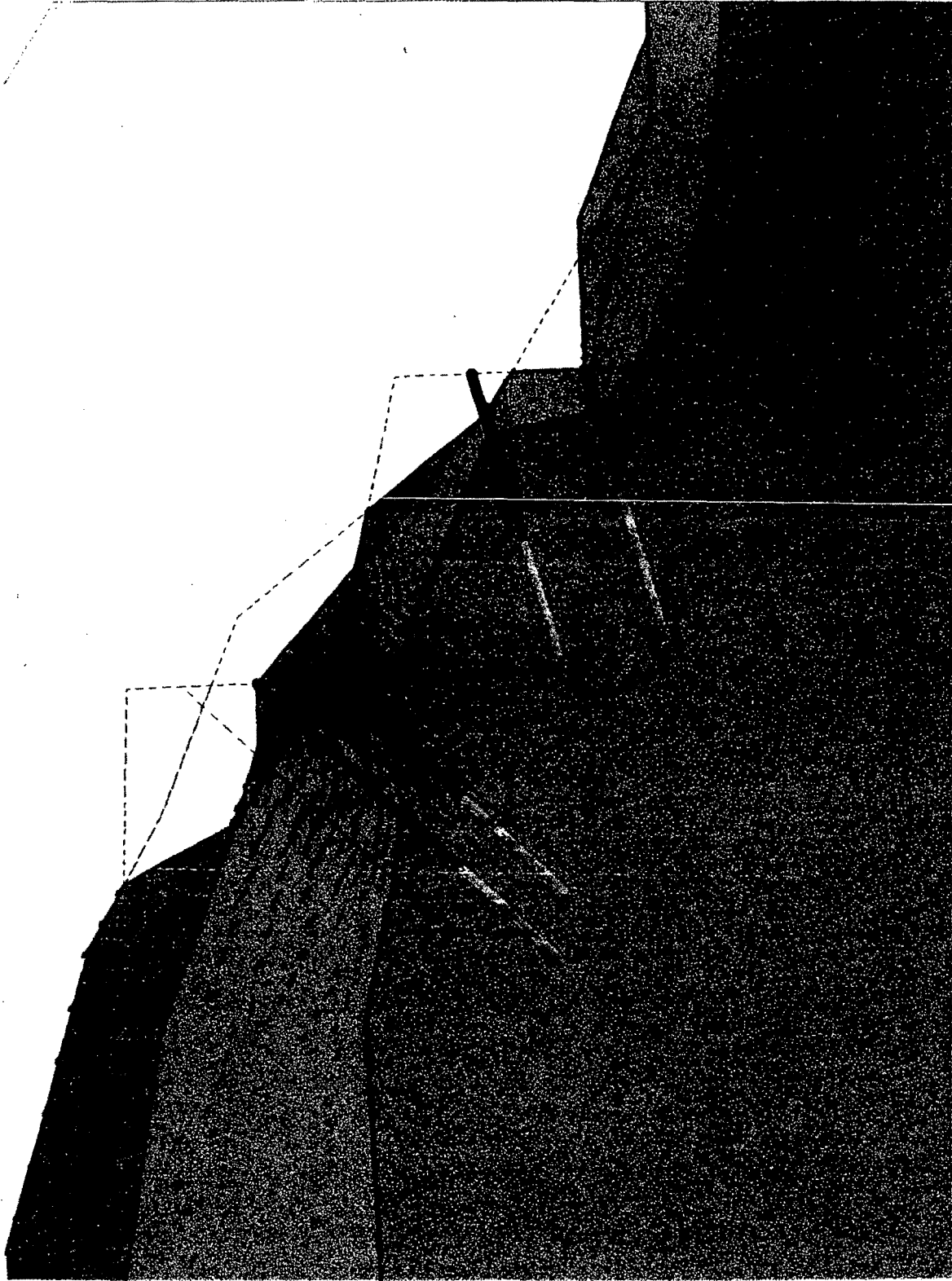


Fig. 6.39: Soil displacement vectors due to phase 6

VI-53

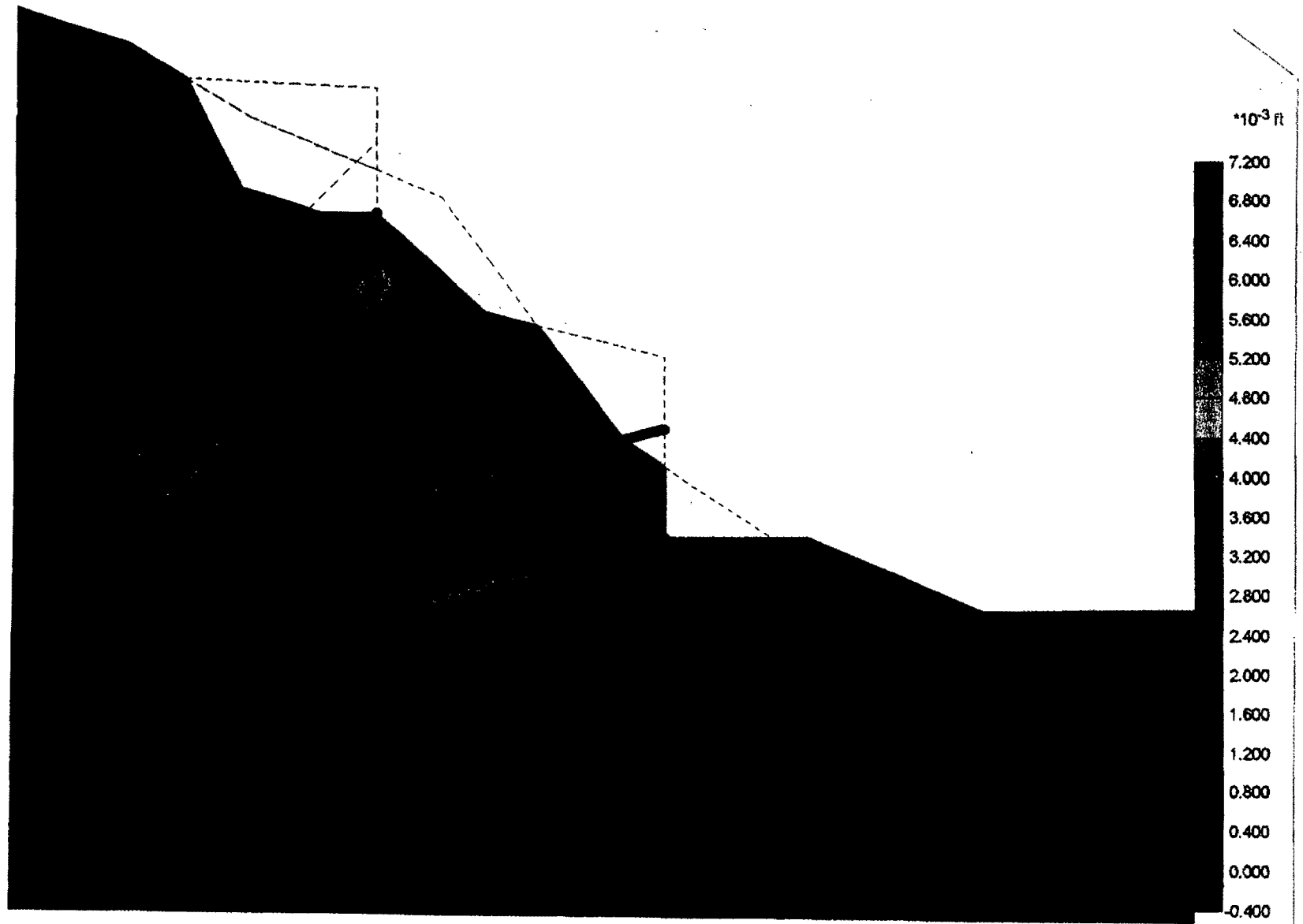


Fig. 6.40: Soil displacement contours due to phase 6

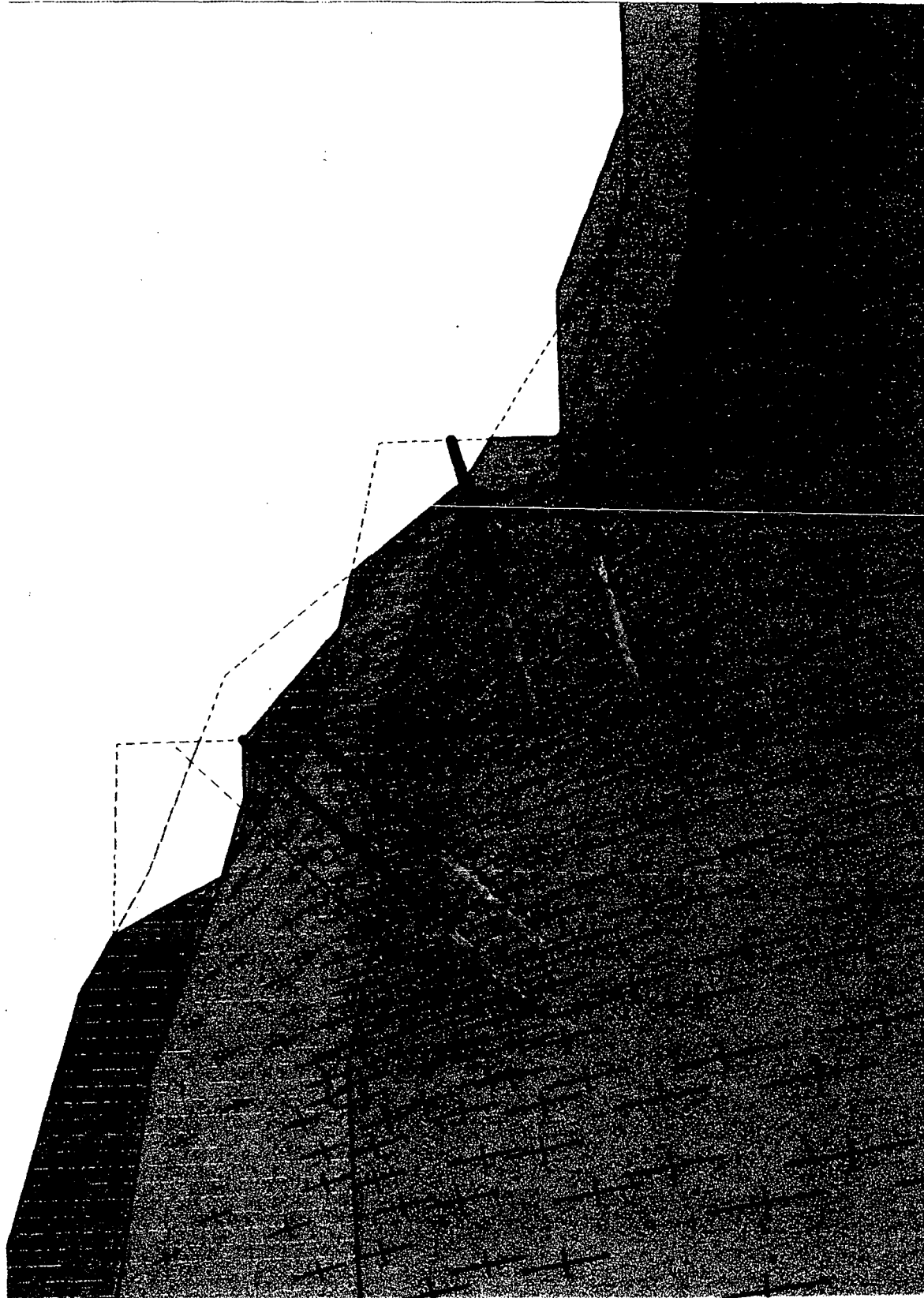


Fig. 6.41: Principal stress direction and magnitude after phase 6

VI-55

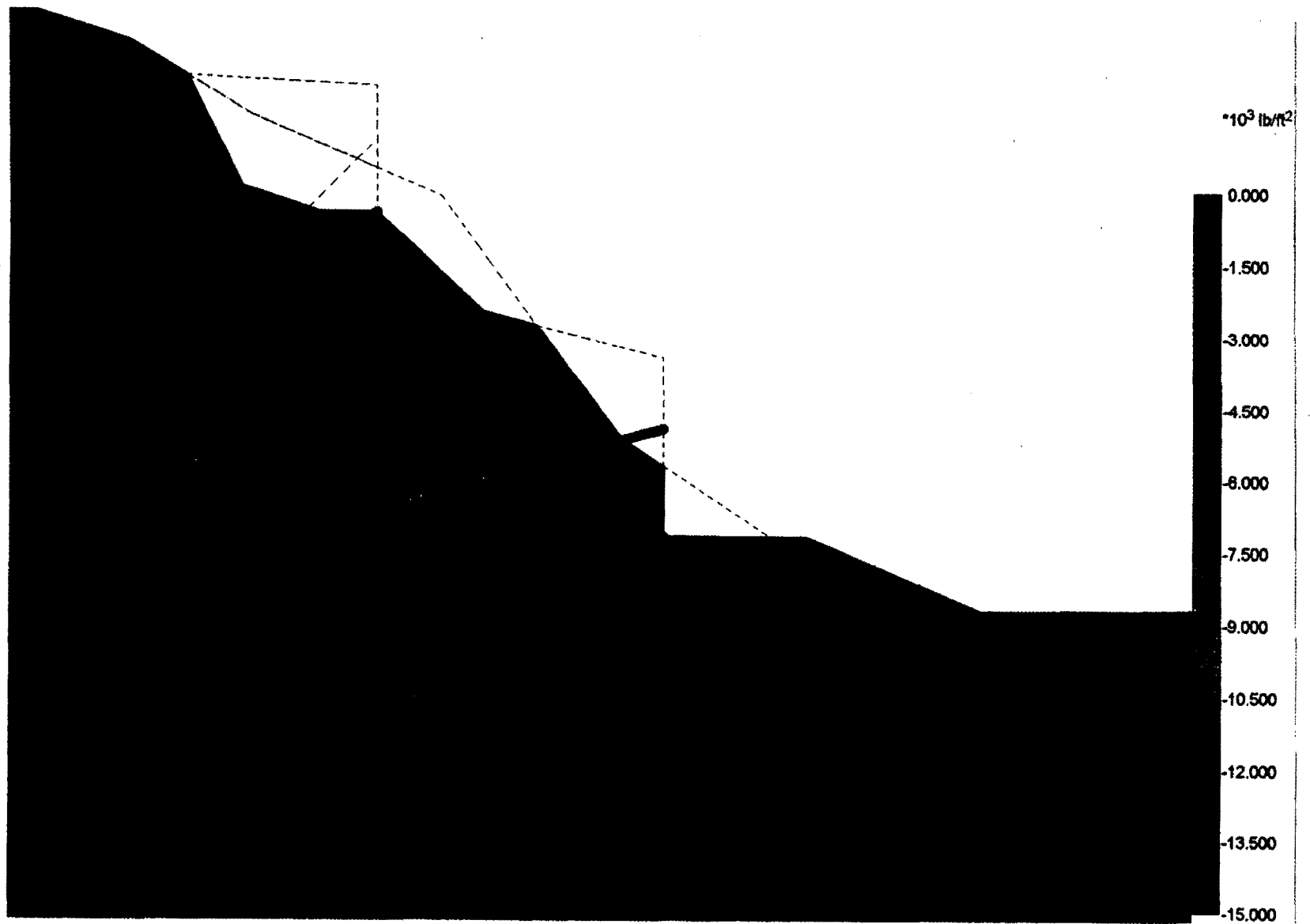


Fig. 6.42: Mean effective stress contours after phase 6

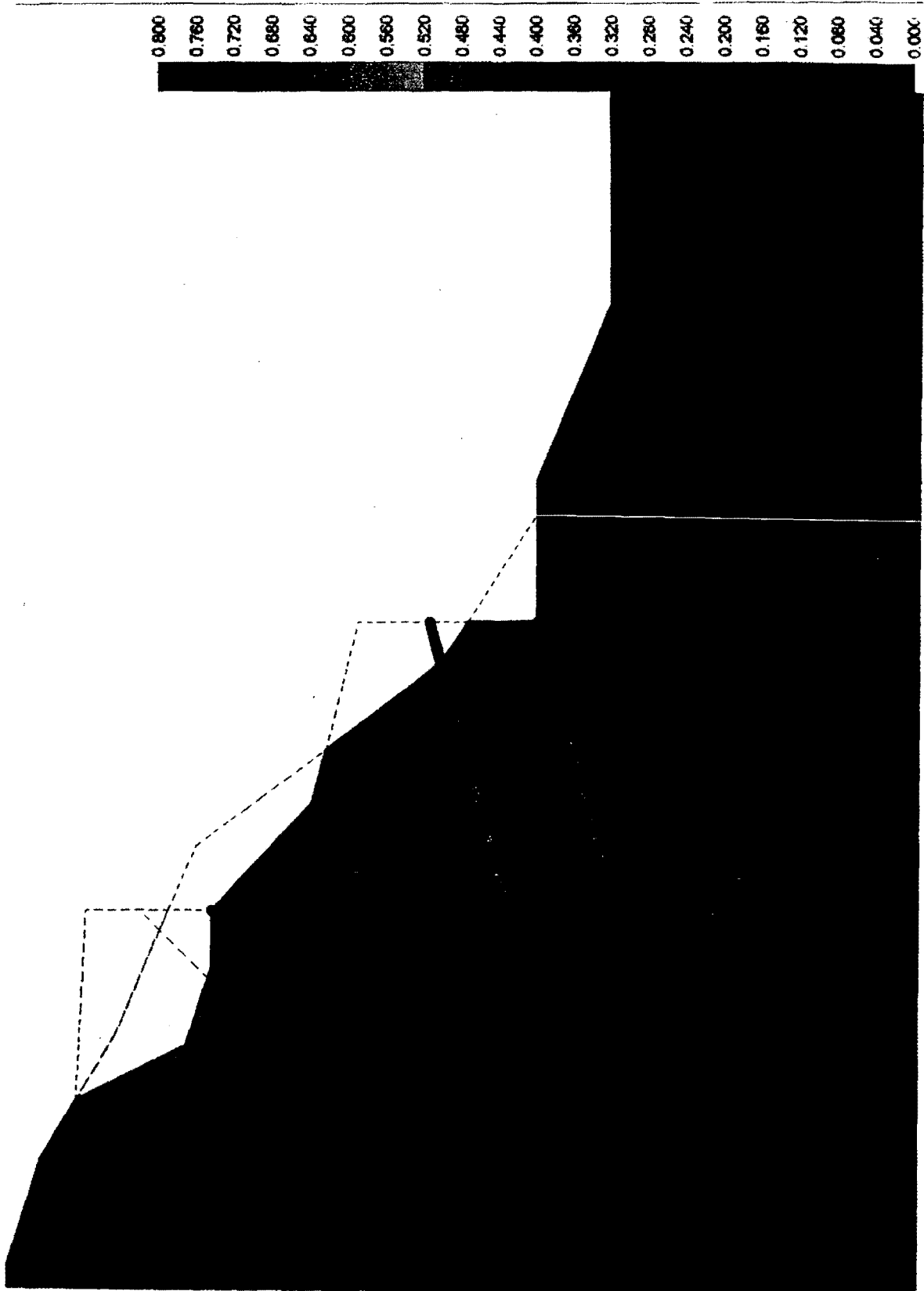


Fig. 6.43: Relative shear stress ratio contours after phase 6

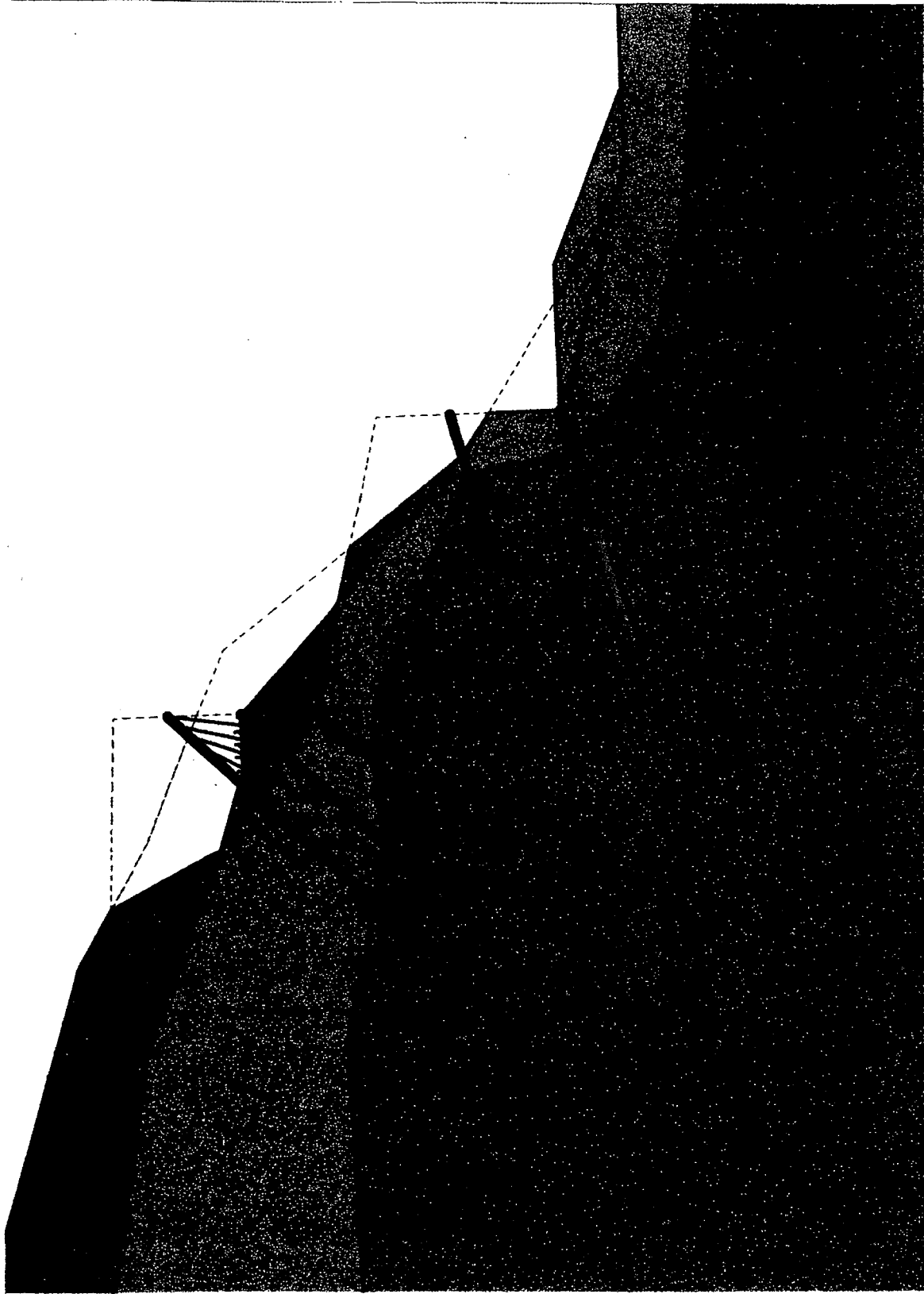


Fig. 6.44: Soil displacement vectors due to phase 7

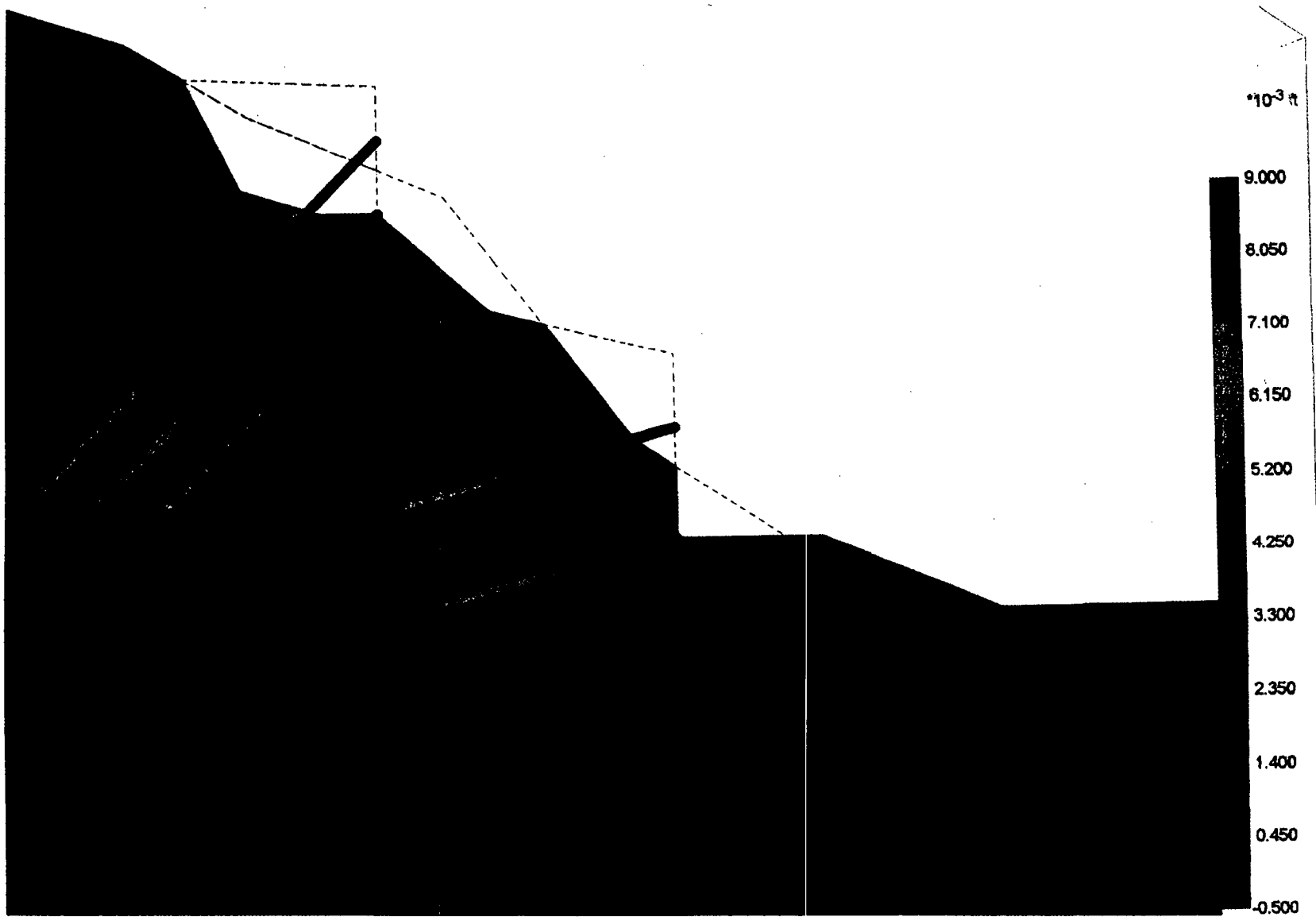


Fig. 6.45: Soil displacement contours due to phase 7

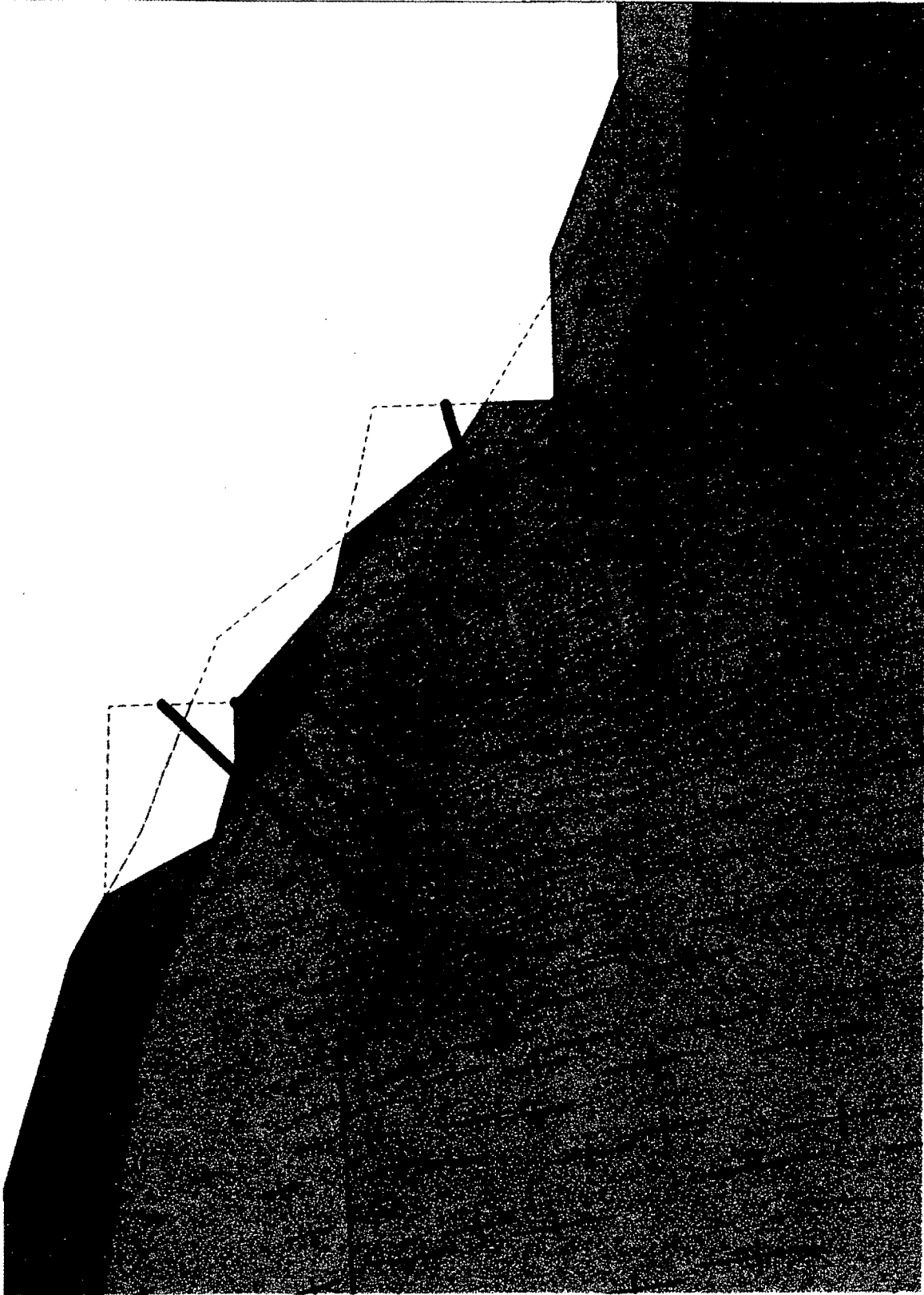


Fig. 6.46: Principal stress direction and magnitude after phase 7

09-IV

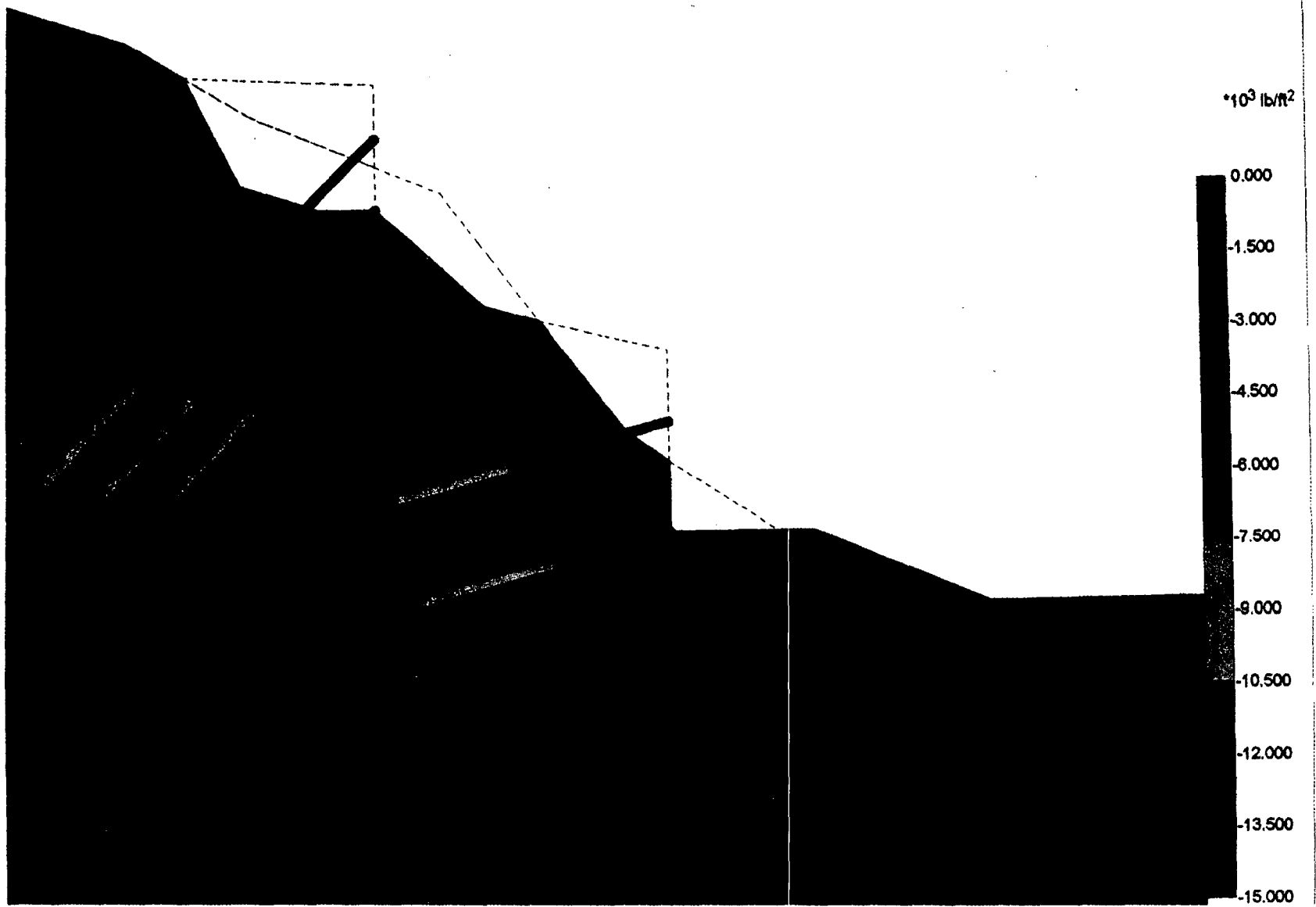


Fig. 6.47: Mean effective stress contours after phase 7

19-1A

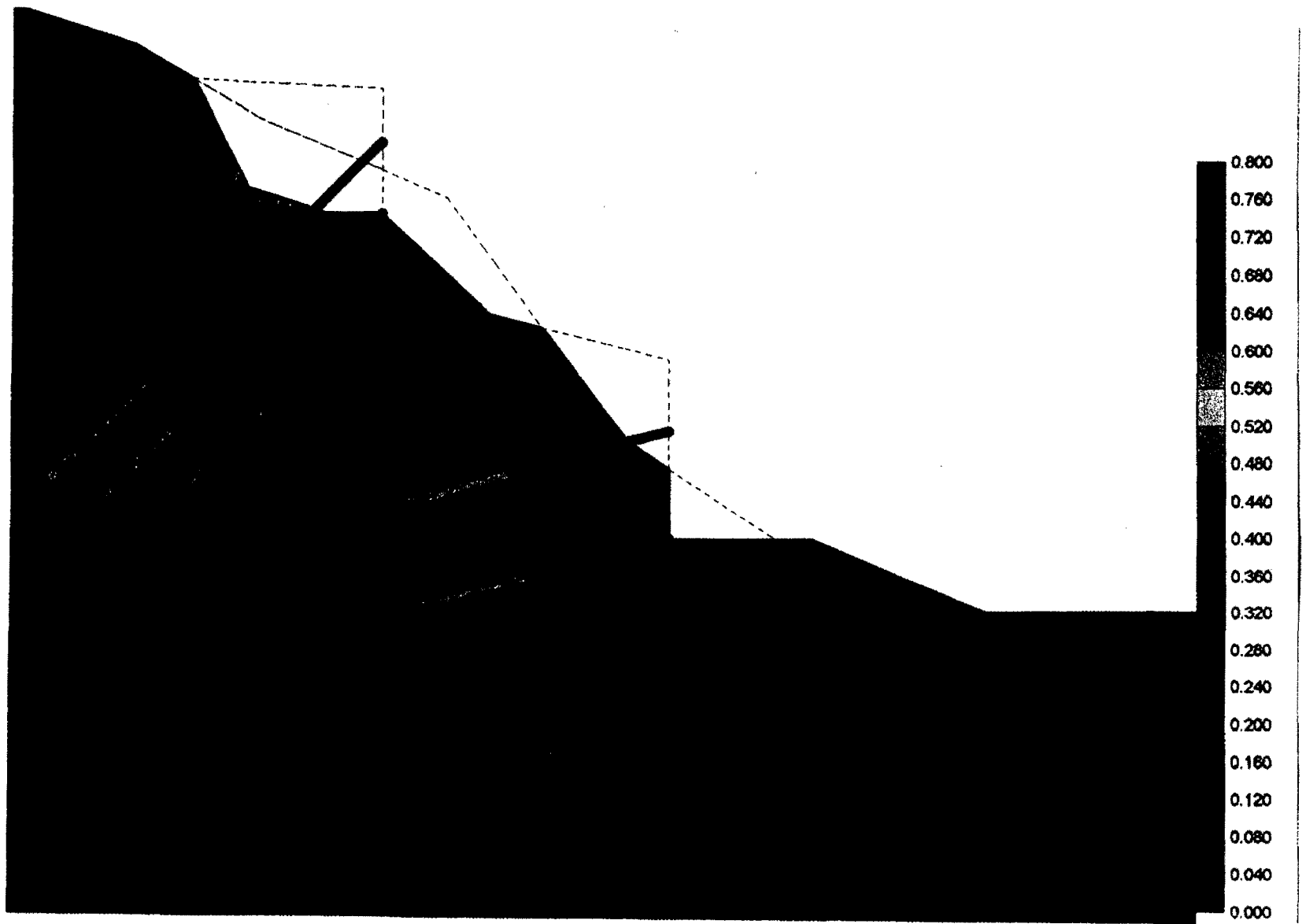


Fig. 6.48: Relative shear stress ratio contours after phase 7

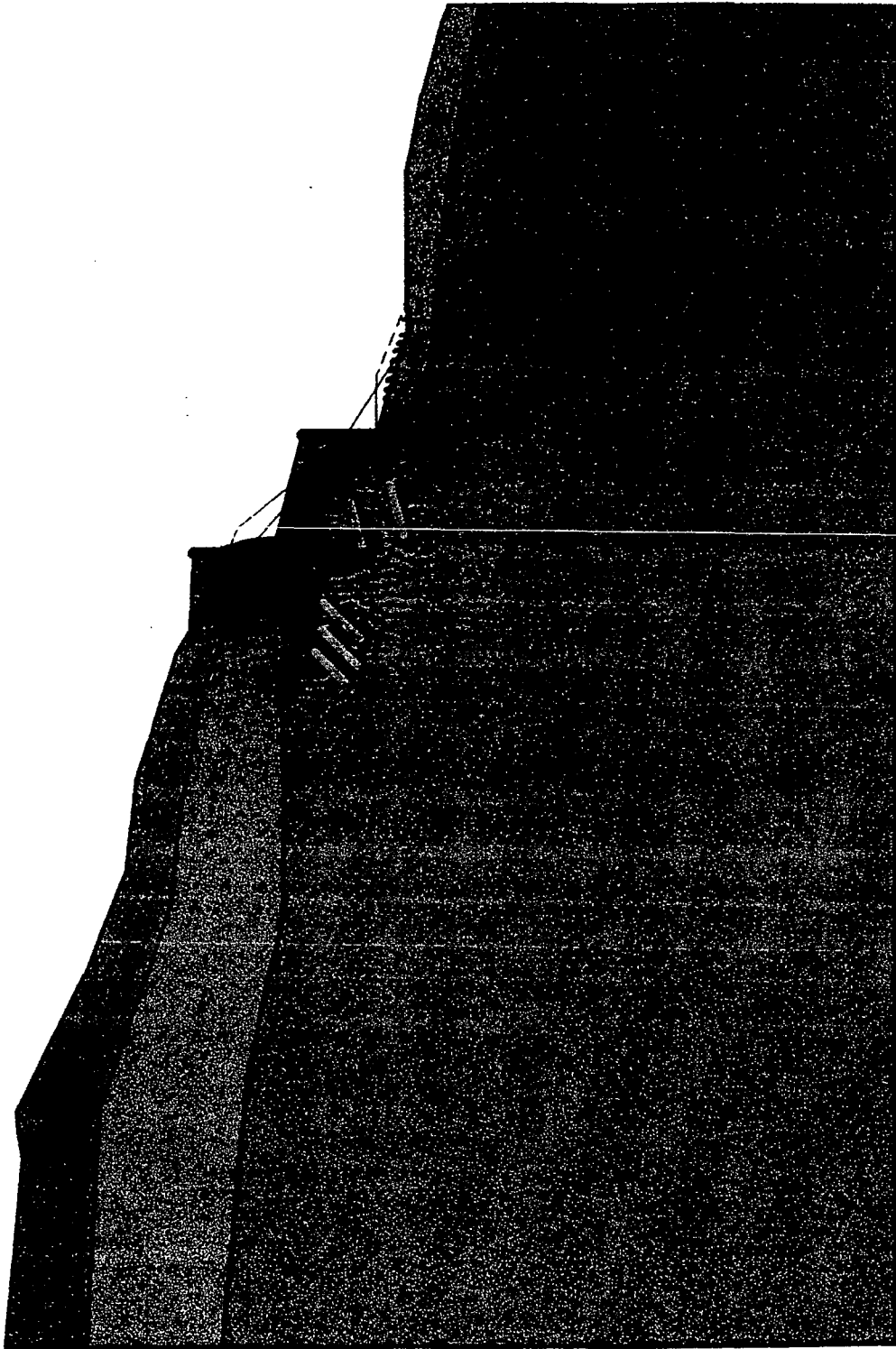


Fig. 6.49: Soil displacement vectors due to phase 9

VI-63



Fig. 6.50: Soil displacement contours due to phase 9

VI-64

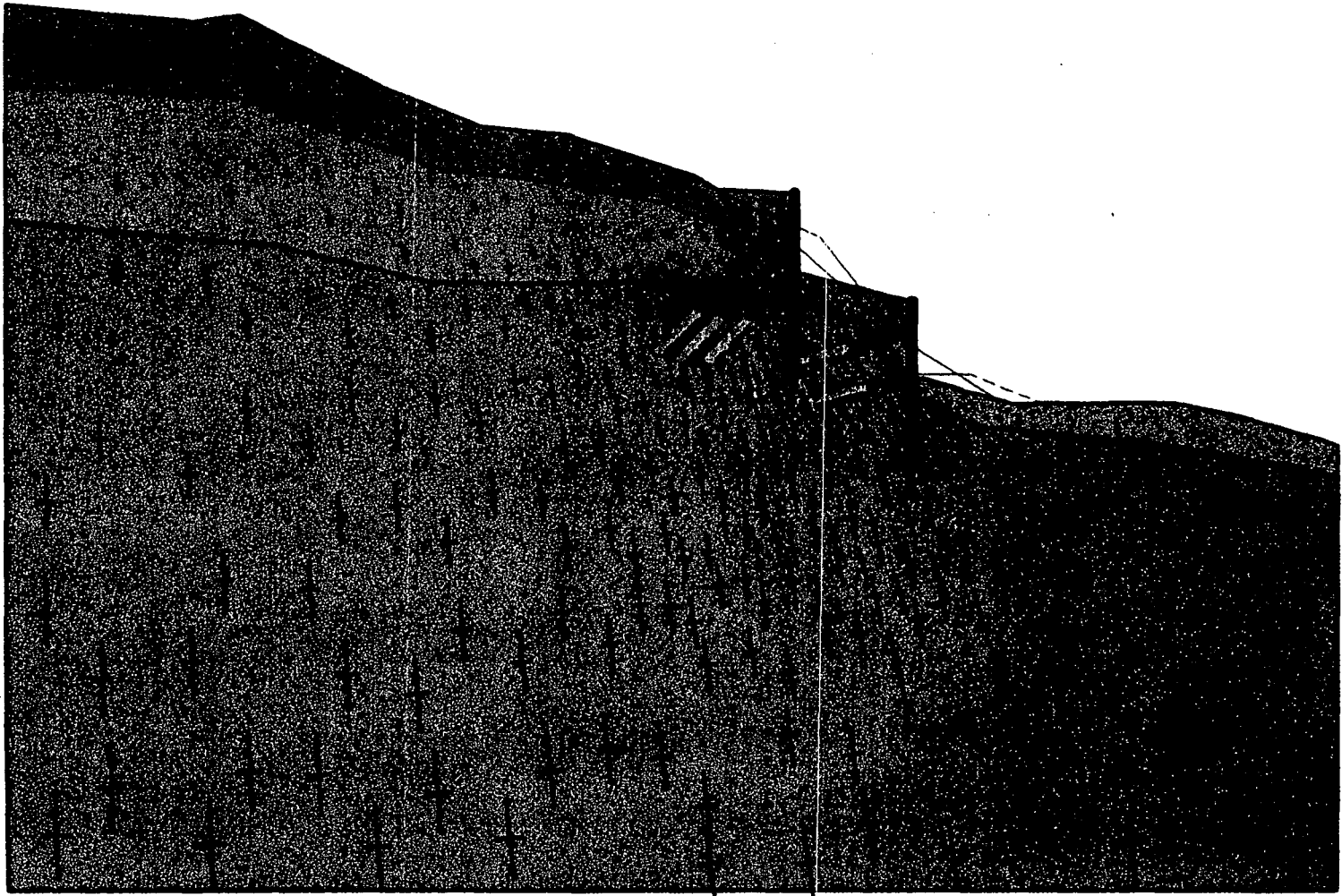


Fig. 6.51: Principal stress direction and magnitude after phase 9

VI-65

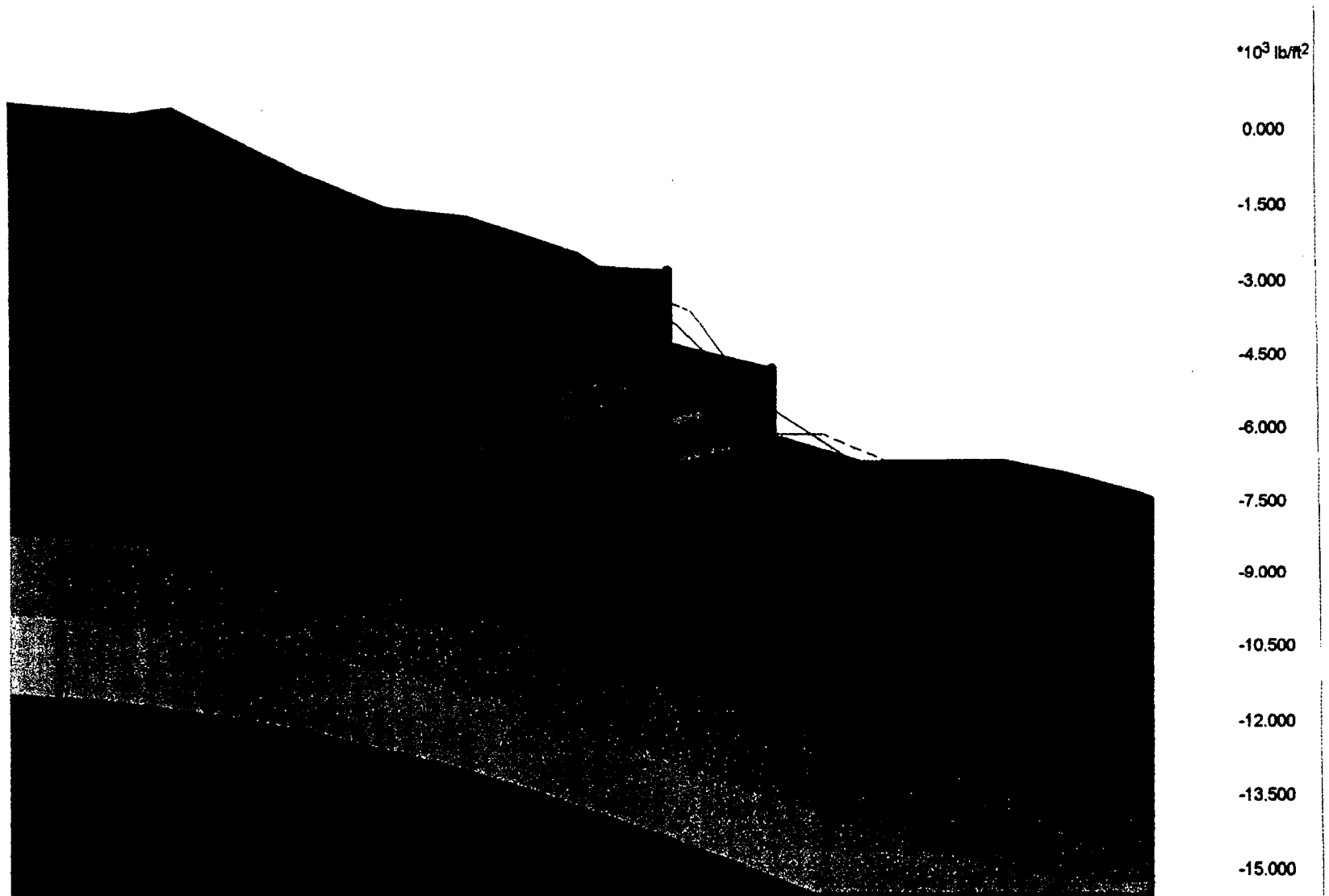


Fig. 6.52: Mean effective stress contours after phase 9

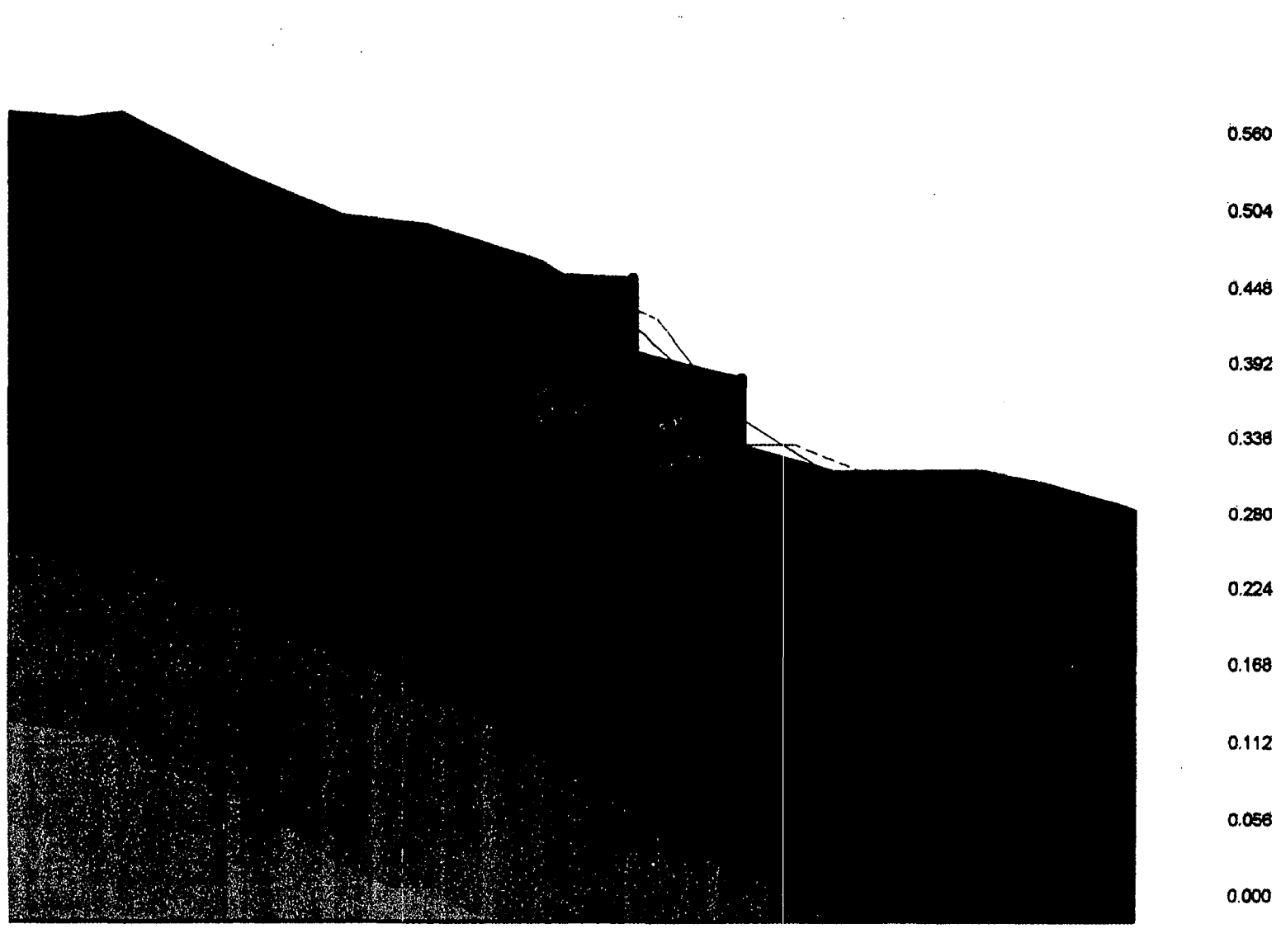


Fig. 6.53: Relative shear stress ratio contours after phase 9

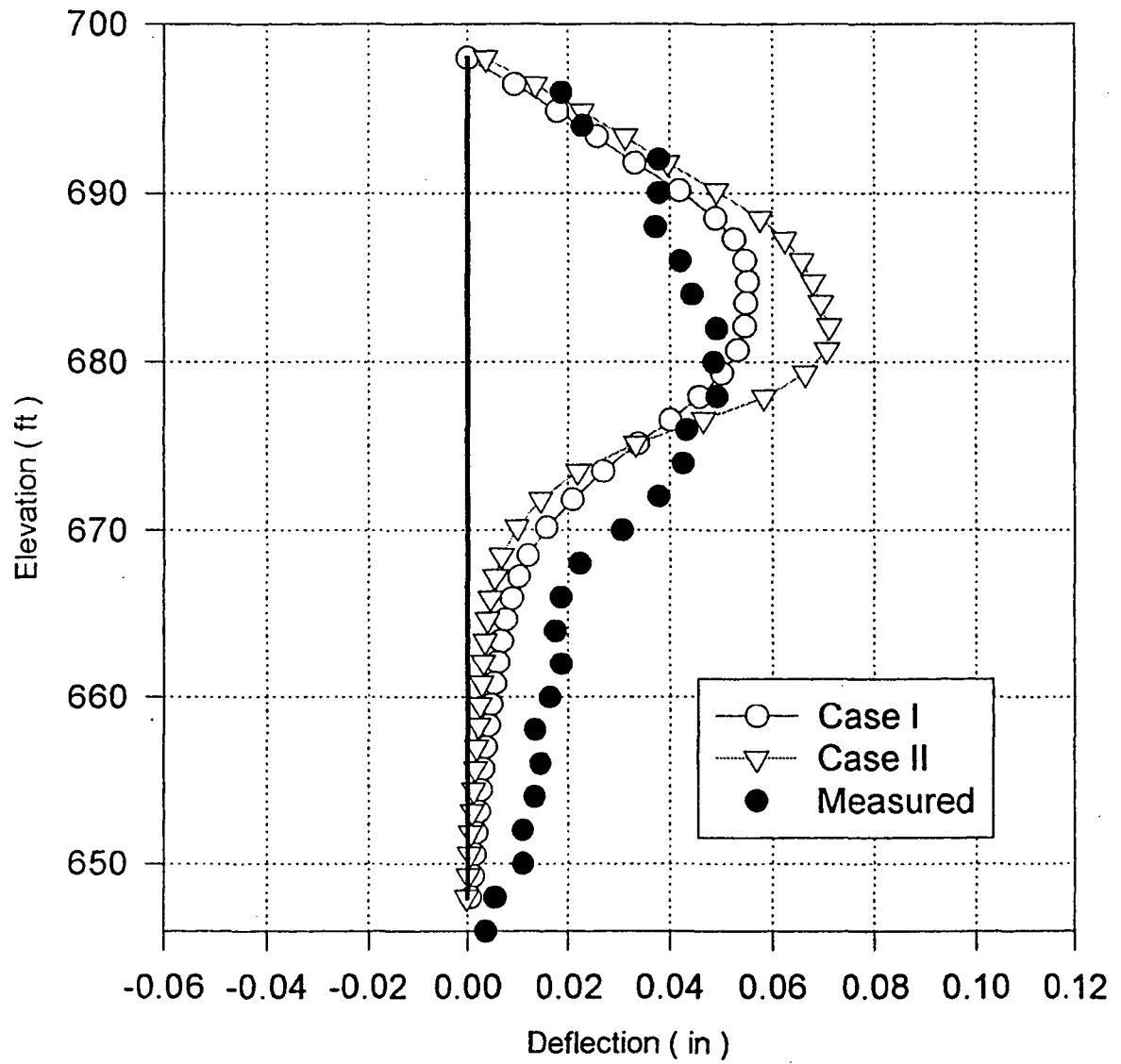
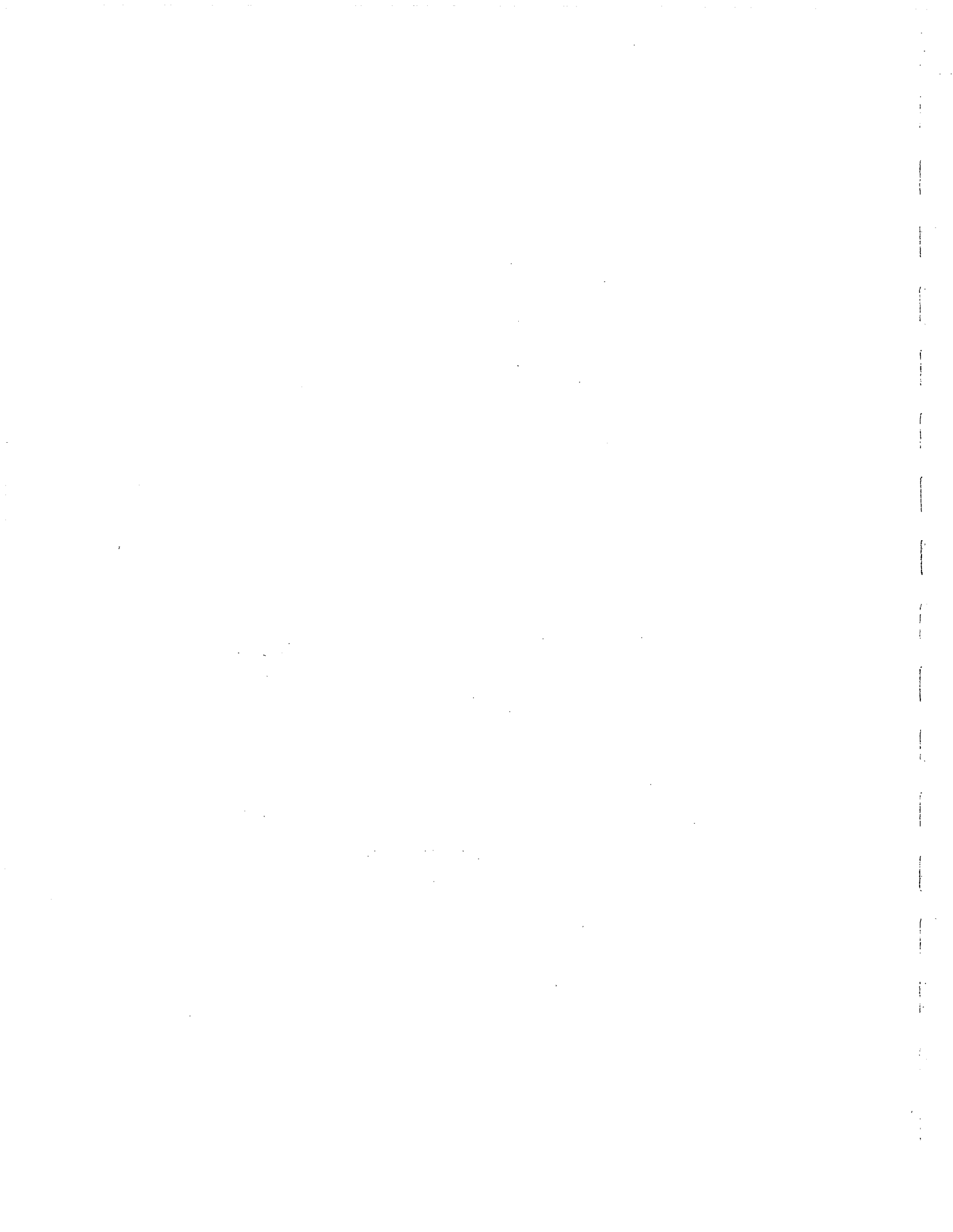


Fig. 6.54: Horizontal deflection of upper tier soldier pile



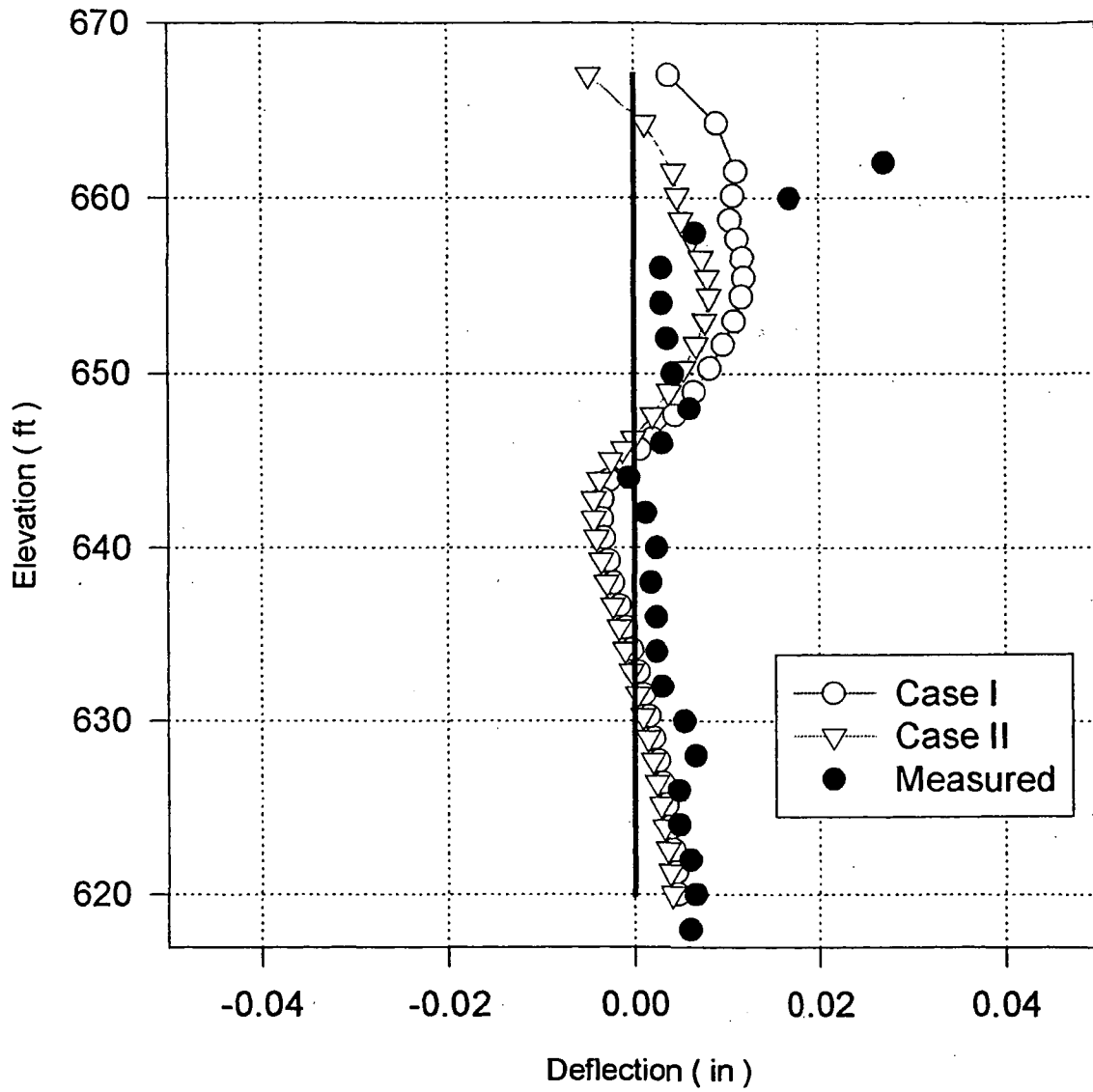


Fig. 6.55: Horizontal deflection of lower tier soldier pile

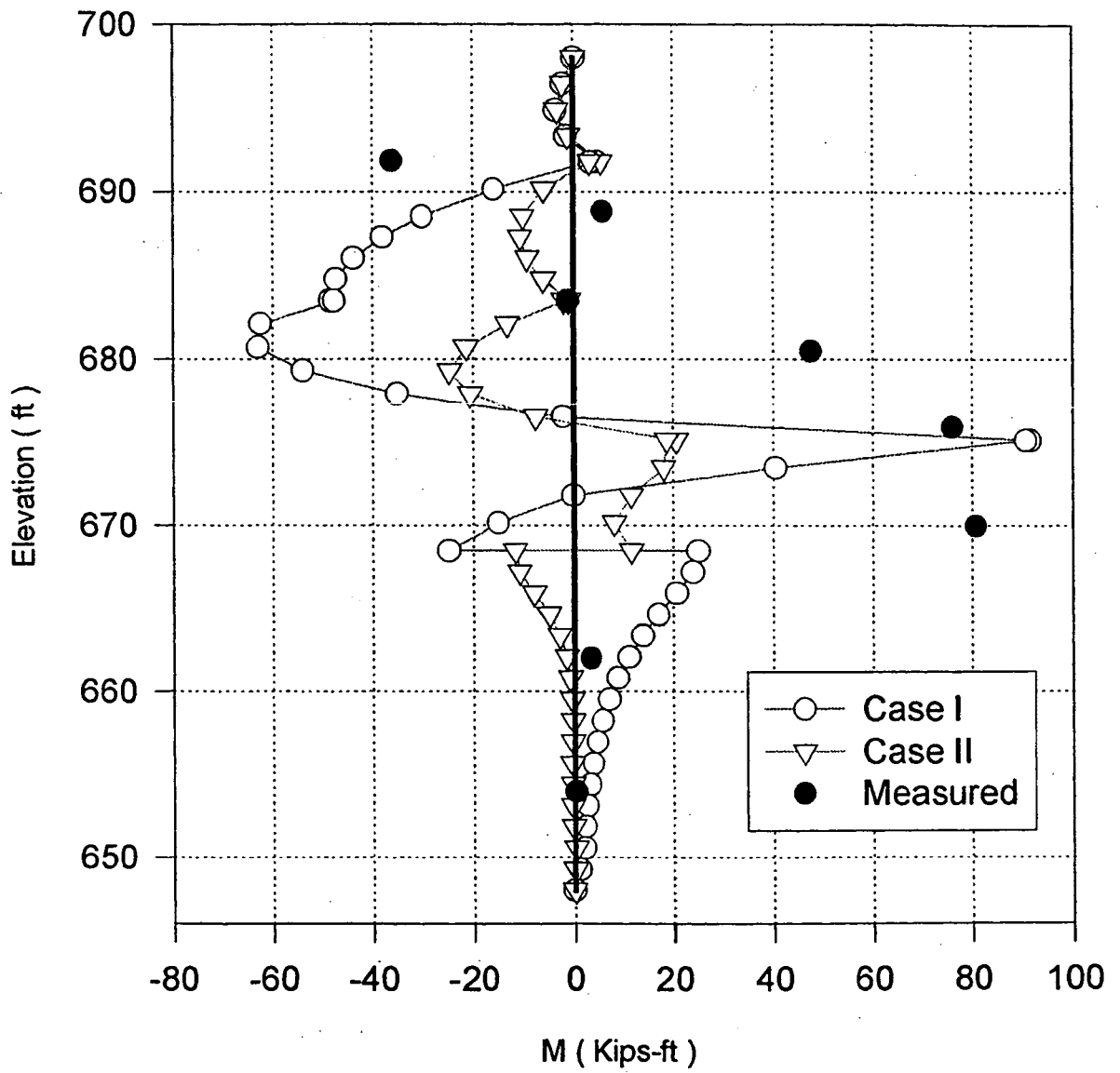


Fig. 6.56: Bending moment along pile length of upper tier pile

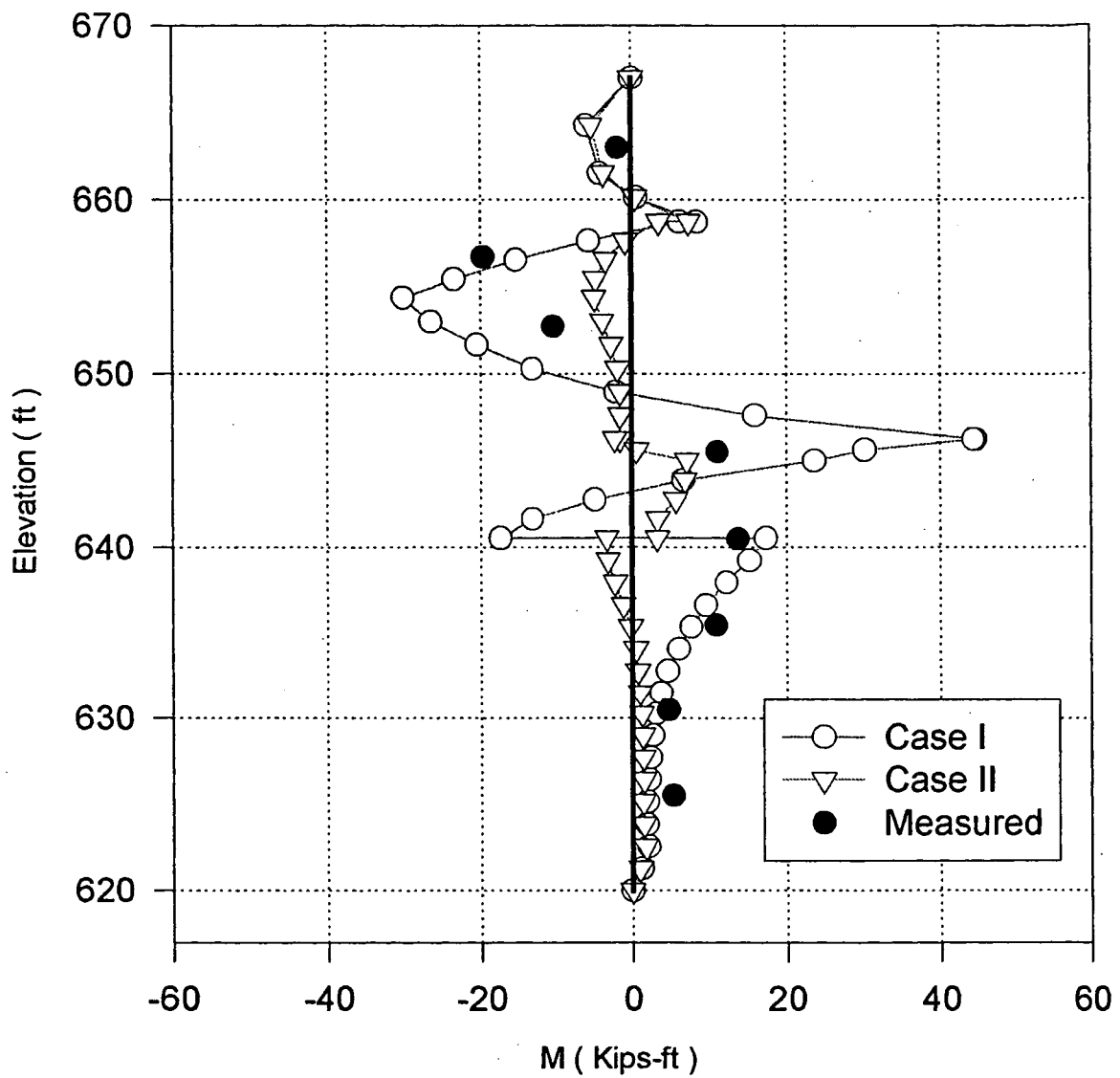


Fig. 6.57: Bending moment along pile length of lower tier pile

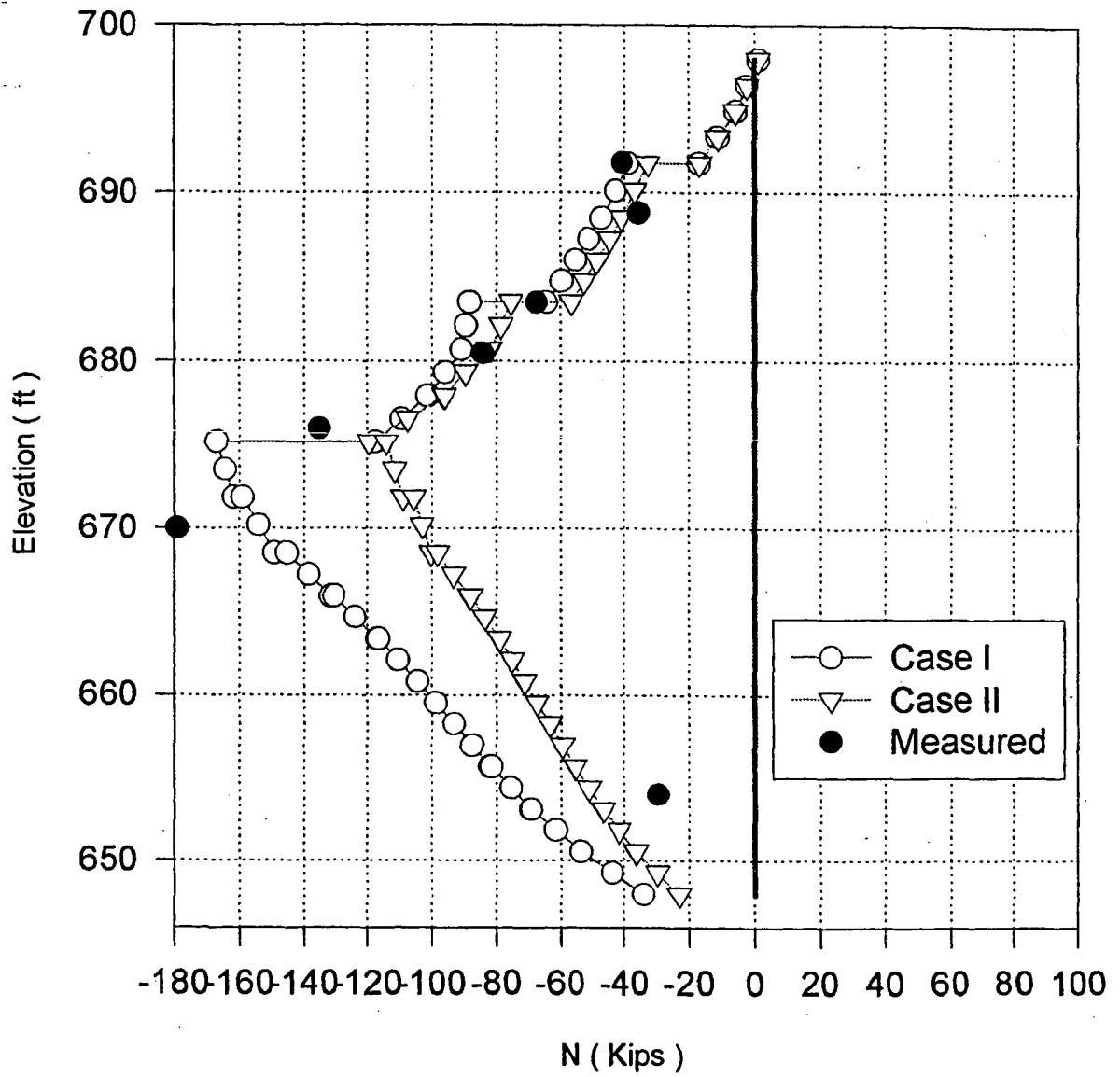


Fig. 6.58: Axial force along pile length of upper tier soldier pile

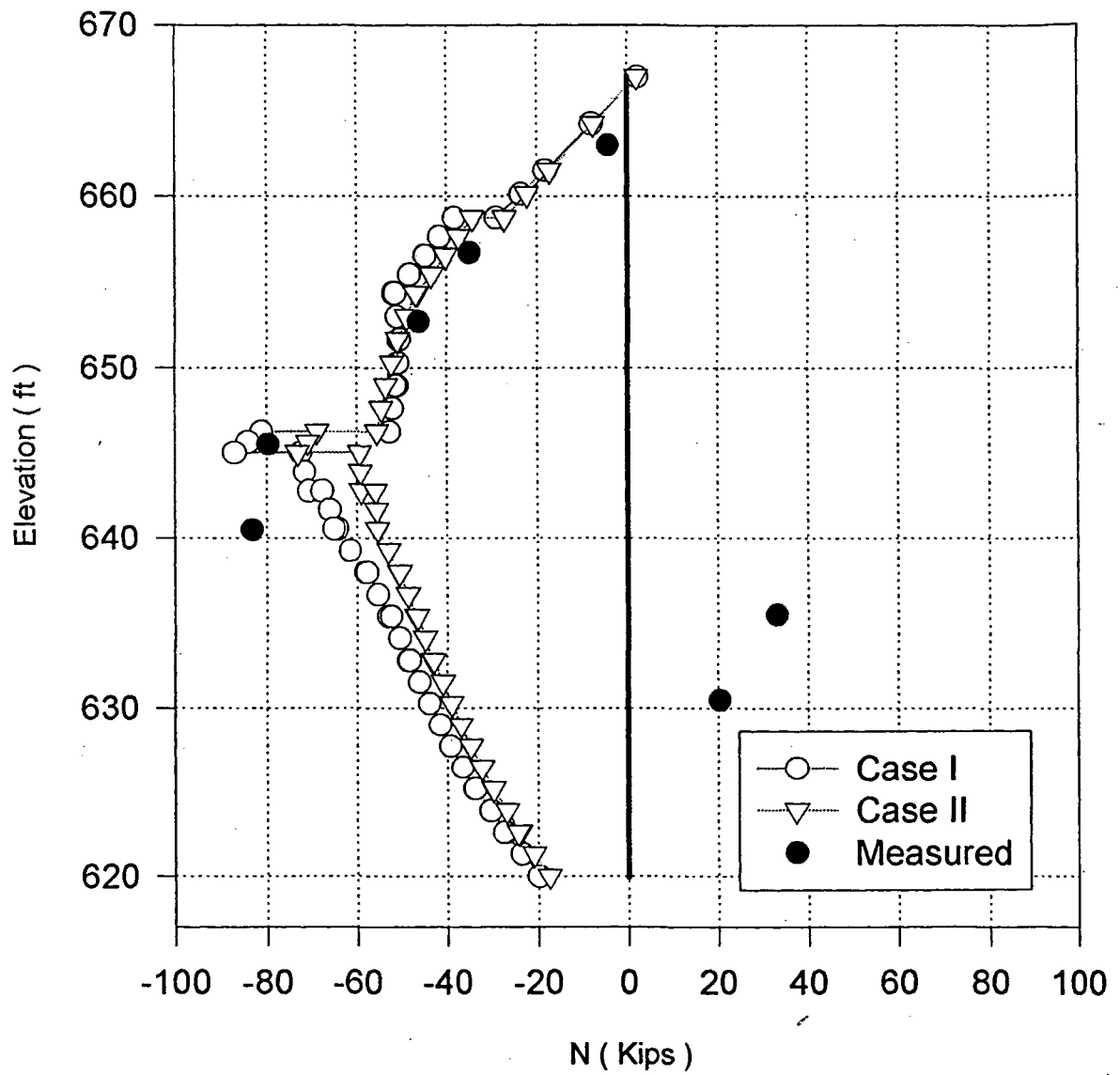


Fig. 6.59: Axial force along pile length of lower tier soldier pile

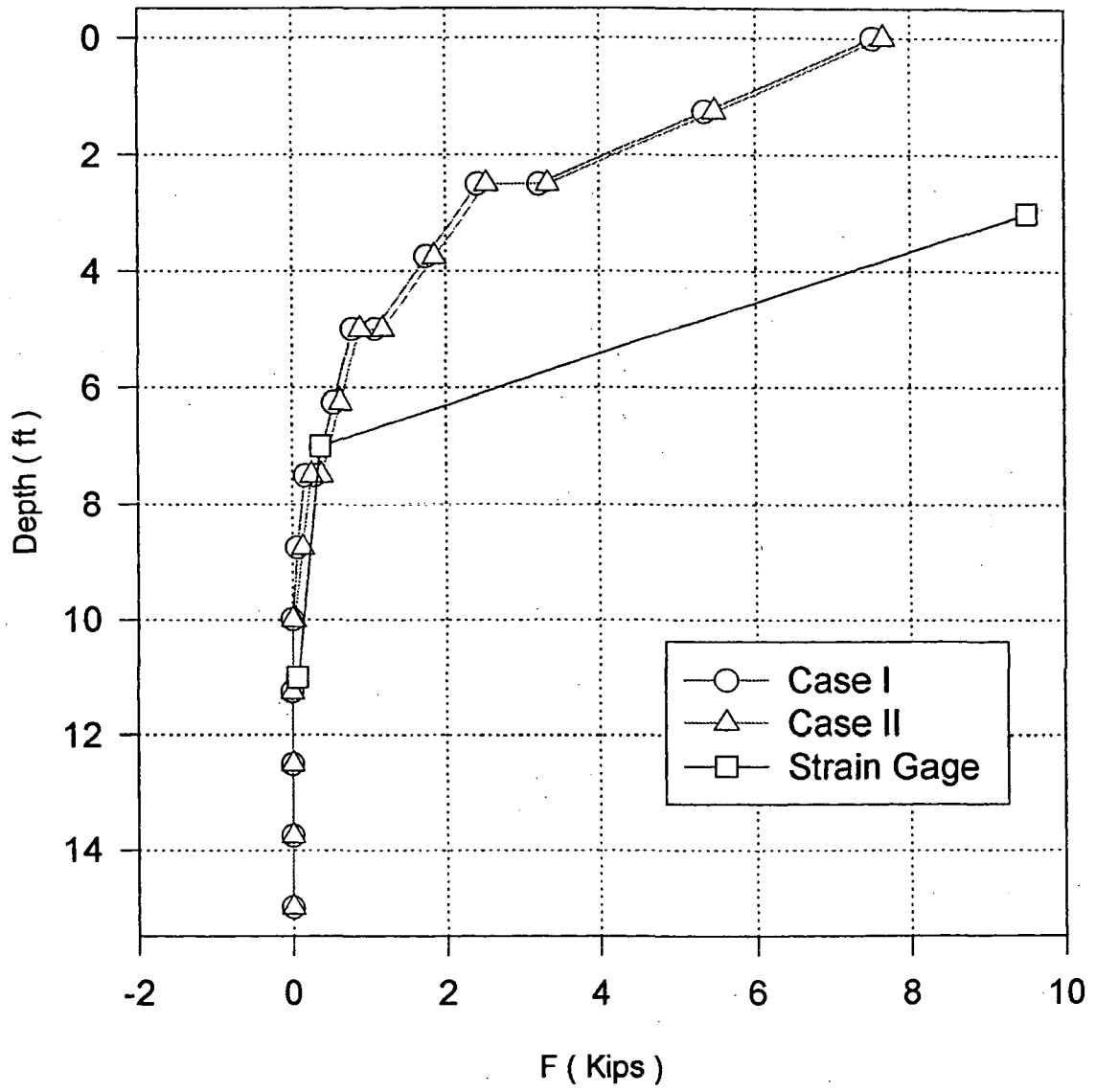


Fig. 6.60: Axial force along the bond length of ground anchor 27A

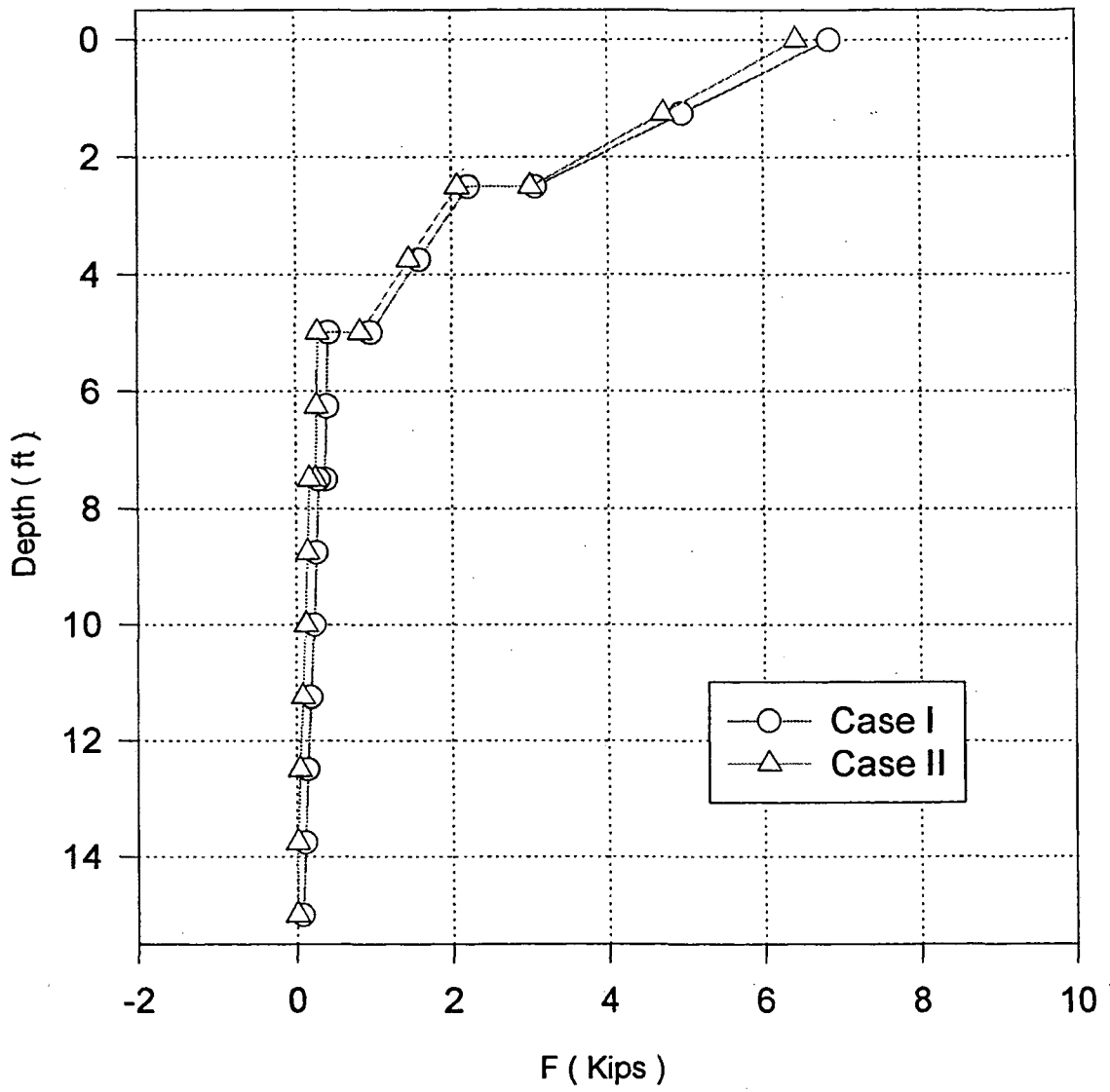


Fig. 6.61 Axial force along the bond length of ground anchor 27B

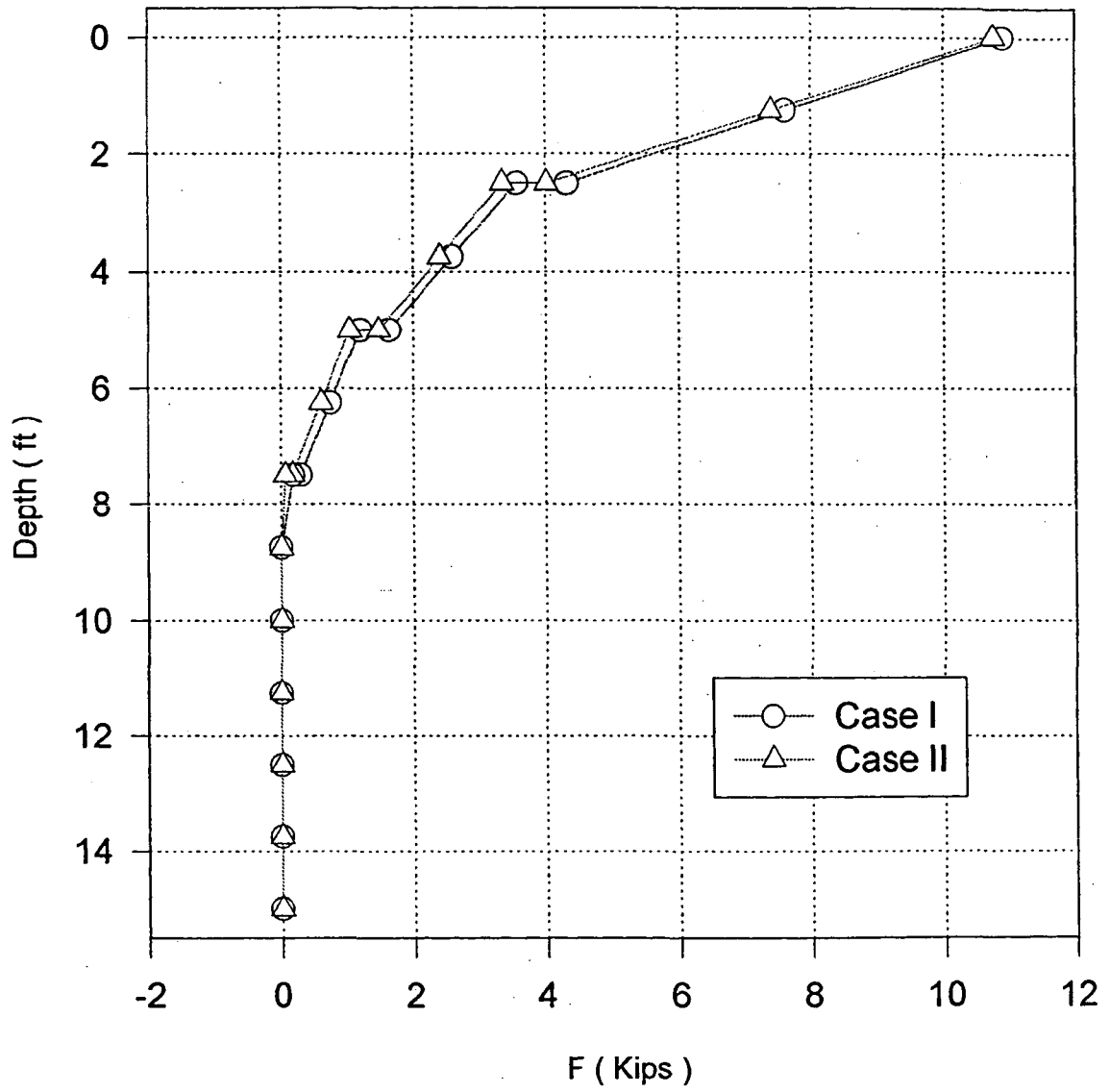


Fig. 6.62: Axial force along the bond length of ground anchor 27C

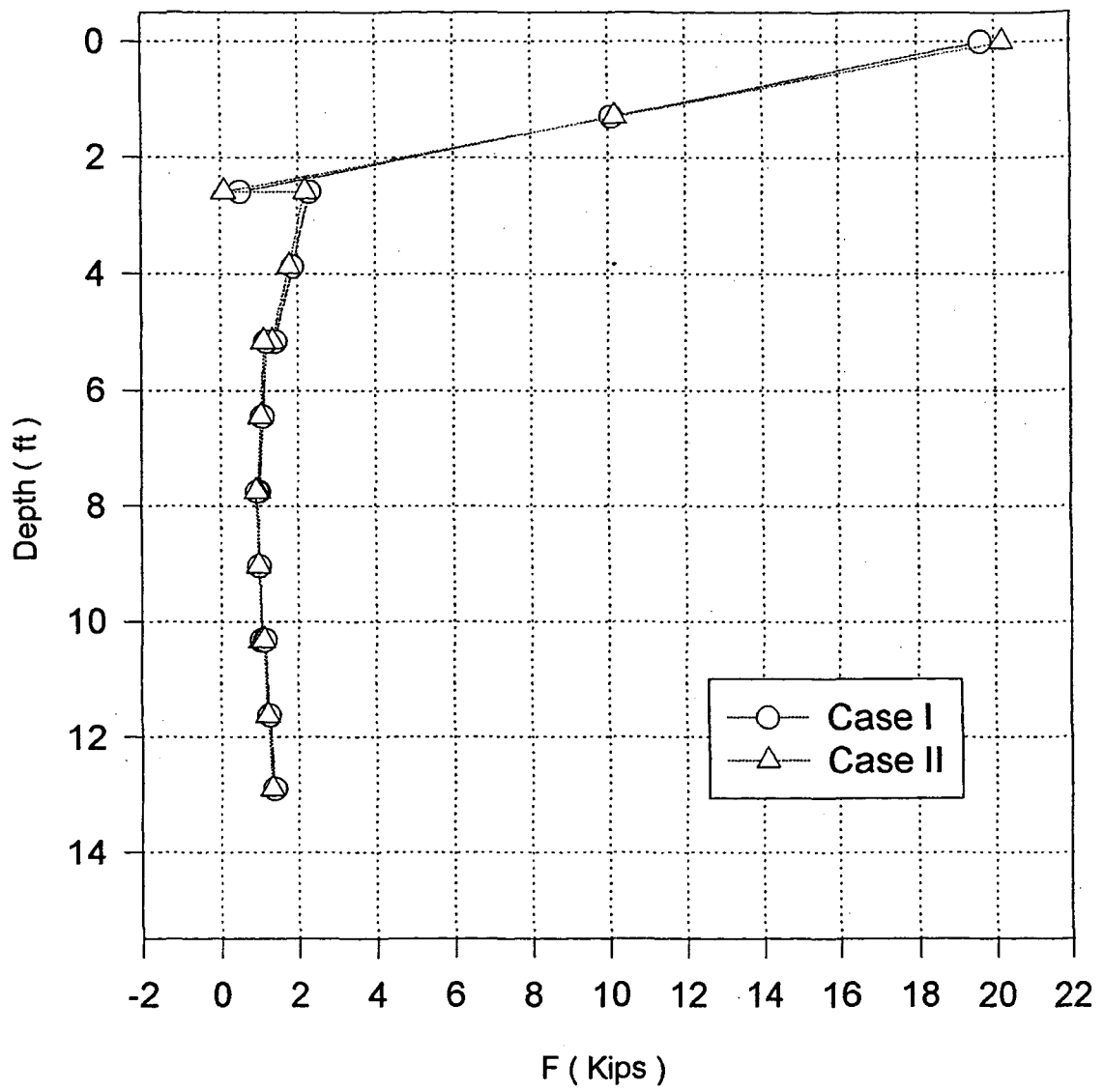


Fig. 6.63: Axial force along the bond length of ground anchor 9A

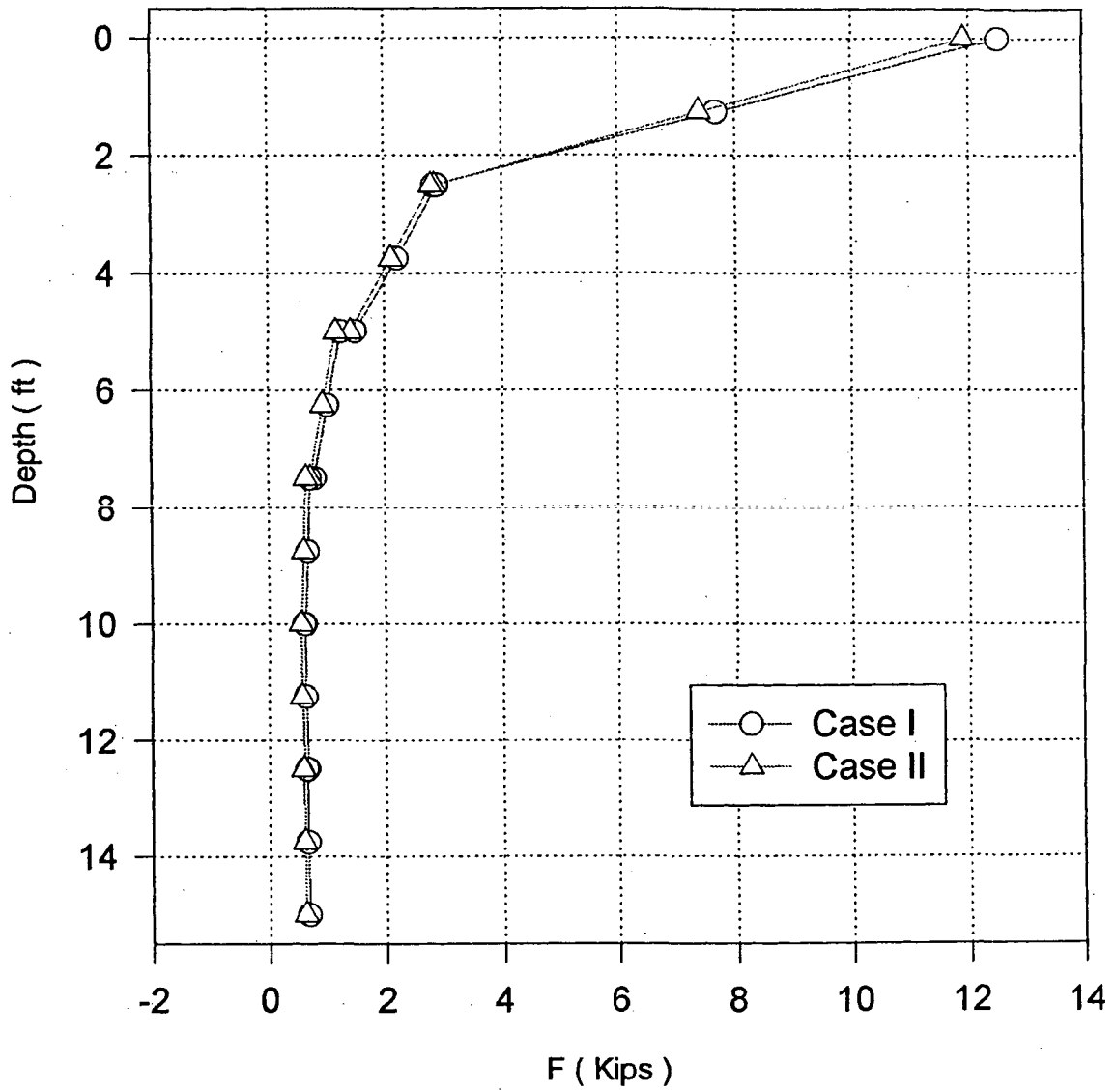


Fig. 6.64: Axial force along the bond length of ground anchor 9B

CHAPTER VII

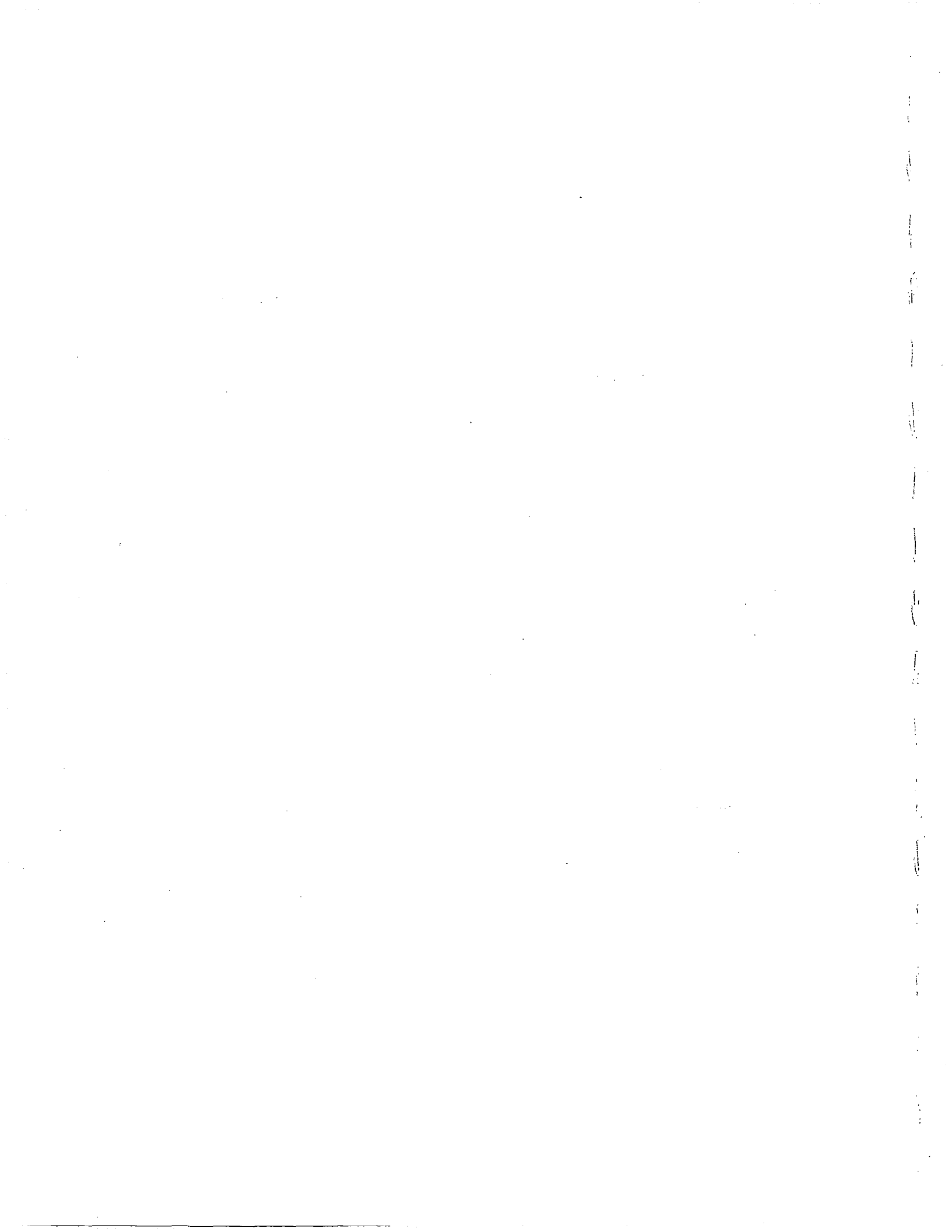
STRUCTURAL ANALYSIS OF TIEBACK WALL SYSTEM

VII.1 INTRODUCTION

Tiebacks were originally developed to anchor structures to rock foundation, and they were first introduced to engineering practice in 1933 where a permanent tie-down was installed at the Cheurfas dam, Algeria as reported by Khaova et al 1969. Later on, in the 1950's a number of tie-downs have been constructed and reported as permanent tiedowns at various dam sites, or as a part of temporary support system for some deep excavation sites (Ludwig, 1984). Later in the 1960's tieback walls began to gain more and more attraction, where research activities appeared to be more intensive and powerful than ever before. Each research group was aiming at studying either the tieback design parameters, or specific issues related to the analysis and design of tieback walls.

The increased popularity of using tiebacks in earth retaining structures and slope stabilization schemes may be attributed to:

- Availability of a variety of construction techniques for almost all types of retained materials and in various working conditions in a rather fast and economical manner that it involves less construction material, less ground losses and earth removal works, and leaving excavation grounds undisturbed.



- The capacity of a tieback is directly tested and verified on site after the completion of installation.
- The development and provision of competent corrosion seals reduced or even eliminated the risk of corrosion in steel tendons.

A tieback wall system essentially consists of three parts; namely; earth retaining unit, anchorage (provides the retaining unit by resisting forces), and free tendon (which transfer loads from either one of the two parts to the other). Earth pressures acting on the retaining unit (wall) are transferred via the unanchored tendon to the anchorage part that back transfers the loads to the earth and thus providing the resistant forces. This would necessitate that the anchors be located outside the active zone.

The global stability of a tieback requires both stability of supported mass as well as the structural stability of all working components that are functions of the geometries and stiffnesses of wall, tendon, and anchor, anchor spacing, and the anchor lock-off load.

A successful tieback design should be originally based on accurate design input (soil and structure) parameters, good understanding of ground response (stresses and strains) to excavation and construction works and sequence, the interaction between the soil and the structural elements, environmental (surface and subsurface) factors altering design options or values, as well as the satisfaction of the utmost engineering goal of construction purpose and durability.

In the subsections to come, some key issues related to tieback system will be investigated and previously related works will be reviewed and outlined.

The purpose of this chapter is manifold: (i) to present a review of available literature and previously related works, (ii) to describe a simple finite element based computational algorithm for analyzing the tieback wall response, taking into consideration of construction sequence such as excavation, installation of tiebacks, and pre-stressing of the tendon, (iii) to conduct a comparative study between field measurement and the computed results using the previous semi-empirical methods as well as the new finite element method of analysis, and (iv) to summarize the results of a series of parametric study aimed at gaining insight on the important controlling factors on the tieback wall behavior. This chapter mainly focuses on the stability issue, such as the sliding failure, the bearing capacity failure is not considered.

VII.1.1 Lateral Earth Pressure

The determination of magnitudes and distributions of stresses and accompanying strains within a soil mass either due to geostatic or imposed loads have not been universally solved. This may be attributed to many factors; such as the anisotropic, heterogeneous nature of ground material (except for water phase), shear strength variations with space, movement, and age, as well as the high porous, nonlinear compressible nature of soils.

One way to calculate the lateral (horizontal) stresses within soil mass is by expressing lateral stresses as a fraction or multiplier of the vertical or applied stress. Based on the type of the multiplier three conditions are categorized:

A) At Rest Condition, which corresponds to zero lateral strain. Thus, the vertical and horizontal stresses are actually the principal stresses (zero shear stresses on H-V planes), then

$$\sigma'_h = k_o \sigma'_v$$

k_o is derived by the theory of elasticity given that $\sigma'_1 = \sigma'_2 = \sigma'_3 = k_o \sigma'_v = k_o \sigma'_1$, and

$$\frac{\sigma_2 - \mu \sigma_1 - \mu \sigma_3}{E} = 0.0 \quad (\text{Zero Lateral Strain}), \text{ then:}$$

$$k_o = \frac{\mu}{1 - \mu} \quad (\mu \text{ is Poisson's ratio.})$$

On the other hand, the lateral earth pressure coefficient (k_o) was found to be a function of the soil's internal friction. Jaky (1948) proposed the following empirical relationship:

$$k_o = 1 - \sin \phi'$$

Wroth (1972), Myslivec (1972), and Brooker and Ireland (1965) reported that this equation could be reasonably accepted for granular soils. They further indicated that for normally consolidated (NC) clay, lateral earth pressure coefficient may be evaluated as:

$$k_o = 0.95 - \sin \phi' \quad (\phi' \text{ obtained from CD-test}).$$

Brooker and Ireland related (k_o) of NC-clay to its Plasticity Index (I_p), as follow:

$$k_o = \begin{cases} 0.4 + 0.007 I_p, & \dots \dots \dots \text{General} \\ 0.68 + 0.001 (I_p - 40), & \dots \dots \dots I_p = 40 \sim 80 \end{cases}$$

They also graphically presented (k_o) for different over-consolidation ratios, and angles of internal friction, and proposed the following relation:

$$k_{oOC} = k_{oNC} (OCR)^N \quad N = 0.5$$

Other works, however, suggested the power N to be in the range of (0.4 to 0.5).

Soil movement will alter the induced lateral stresses due to the change in stress path, as well as the shear strength. When soil is laterally loosened (moves towards free excavation or wall), the lateral (horizontal) stresses are reduced. The deviatoric (shear stress) would increase until failure point, which defines an active case of loading (Lateral extension; equivalent to axial compression). On the other hand, when the soil is acted upon by an increasing lateral stress, then the case would define a passive case of loading (Lateral compression; equivalent to Axial extension). Since the vertical stress is assumed to be constant throughout the process, the coefficient of lateral earth pressure will decrease in the former case, and increase in the later. C. A. Coulomb in 1776 presented the Coulomb's Earth Pressure Theory, where he derived equations capable of evaluating both active and passive earth pressures and earth pressures coefficients. The derivation was based on the assumptions that the soil is isotropic and homogeneous, rupture surface is plane surface, uniform distribution of friction forces along the failure plain, rigid failure wedge, and two-dimensional problem. Later, Rankine (1857) modified on Coulomb's method by introducing two simplifying assumptions, that he considered the soil to be in a state of plastic equilibrium and neglected wall-soil friction. Bell (1915) introduced the role of cohesion intercept on active/passive stresses. However, the passive stresses obtained by either Coulomb or Rankine tend to overestimate. Accordingly, Caquot and Kerisel (1948) derived earth pressure equations using the theory of Plasticity and based on non-plane failure surfaces. Later on, Janbu (1957), and Shield and Tolunay (1973) independently proposed another approach similar to the slice method, while Sokolovski (1960) introduced a finite element solution employing highly sophisticated mathematical methods.

The derivation of the existing lateral earth pressure coefficients' relations involves a lot of assumptions, thus increasing the uncertainties in all available predictive methods and relations. More importantly, it is usually difficult to decide on whether to use the at-rest, active, passive, or somewhere in between lateral earth pressure coefficient, because the lateral earth pressure coefficient is altered with soil displacement. There are many methods available in the literature in this regard (Bowles, 1988).

The distribution of earth pressure on retaining walls depends on the type of wall, since different walls require different excavation/construction techniques. For the case of tieback walls the pressures are, to some extent, different from other retaining walls due to the stage excavation/construction processes, as well as possible delays (lag times) between excavation, installation, and even between different installation stages. Bowles (1988) showed the dependence of the earth pressures imposed on a braced cofferdam (which is to some extent similar to that of the tieback walls), as shown in Figure 7.1.

There have been discussions about the suitability of the Rankine's earth pressure (triangular) envelope in the analysis and design of tiebacks or braced excavation. Schnabel (1982) reported the failure of many braced walls designed based on the Rankine's earth pressure distribution. The most frequently adopted soil pressure diagrams in the design and analyses of retaining walls are:

1. Rankine's Active Earth Pressure Diagram (Rankine, 1857):

Rankine proposed a triangular earth pressure envelope, with zero depth interception, and sloping by the active unit weight ($k_a \gamma$). But this pressure distribution was earlier discussed and not recommended in the case of anchored or braced walls.

2. Terzaghi and Peck Earth Pressure Diagram (Terzaghi and Peck, 1967):

In 1948, Terzaghi and Peck proposed two trapezoidal stress distributions for both clays and sands. Later on, in 1967, they proposed a rectangular diagram for the case of sand, and a trapezoidal one for that of clay (Figure 7.2a). The pressures were back calculated from the loads measured at the struts of the braced walls. These pressure diagrams are widely used in the analysis and design of tieback walls, though they were later noticed to be greater than the actual earth pressure.

3. Tschebotarioff's Earth Pressure Diagram (Tschebotarioff, 1973):

Tschebotarioff recommended the use of the triangular and trapezoidal earth pressure diagrams (shown in Figure 7.2b) for clays and sands, respectively.

4. Peck's Earth Pressure Diagram (Peck, 1969):

Peck proposed new pressure diagrams for sands and clays. He indirectly incorporated the effects of overconsolidation of clays by the ratio of the soil column weight to its cohesion (Figure 7.2c).

5. The US-Navy Earth Pressure Diagram (NAVFAC, 1982):

The diagrams developed by the US Navy are the same in shape as that of Terzaghi and Peck's, yet with different maximum pressure values for both sands and clays.

6. Schnabel Earth Pressure Diagram (Schnabel, 1982):

Schnabel uses a unique earth pressure diagram for all types of earth material (in the case of tieback and braced walls) that is very similar in shape to the diagram proposed by Terzaghi and Peck in 1948. His diagram assigns the maximum developed earth pressure a value depending only upon the height of excavation, which is $(25H \text{ psf})$.

7. Cheney Earth Pressure Diagram (Cheney, 1988):

Cheney (1988) incorporated the stage construction effect on the evolution of the earth pressures developed on tieback and braced walls by describing four basic pressure diagrams depending on wall deformation as shown in Figure 7.3.

Feng (1997) reported that Schnabel's diagram was noticed to be the least conservative and the closest diagram to the actual measured pressures in many cases. Schnabel (1982) reported that the preloading of tiebacks and sloping the wall make the stresses acting on the wall less than those documented in the literature, even the one he developed. He further indicated that those stresses in excess are considered as an additional safety allowance added to the overall safety factor. Moreover, for grounds having relatively higher at rest lateral pressure, the active case of loading will be reached at smaller movements in the range of (0.001 to 0.0025) times the excavated depth. Altering the wall stiffness, anchor alignment and capacity will further reduce the lateral movement- whenever suspected to be excessive.

7.1.2 Available Methods on the Analysis and Design of Tieback Wall

There are three major approaches that are frequently employed in the analysis and design of tieback walls, which are:

A. Beam-Column Method:

Although Winkler (1867), and Hetenyi (1946) put down the basic principle of this method, it was Matlock (Matlock et al, 1981) who made it practically accepted after he developed a computer program utilizing the beam column method, and Haliburton (1968) who first employed this technique in the problem of elastic retaining walls. This method is based on tieback wall deflections in the analysis procedure, and the

derived governing differential equation is solved via the Finite Difference technique. This method of analysis is quite powerful in analyzing flexible walls subjected to vertical and lateral stresses, but it becomes very restricted when it comes to predicting the behavior of the soil mass.

B. The Pressure Diagram Approach:

Using this approach, only the moment diagram and the embedment depth are obtained. Whereas, the deflection calculations can not be done, due to the simplifying assumptions encountered in each of those methods, and the fact that they all disregard the vertical anchor load component making the deflection calculations very unrealistic. The methods usually assume an empirical earth pressure diagram (at rest, or active- depending on the method), and then analyzed and solved for the bending moment and embedment depth. Of those methods are the Tributary method (Terzaghi and peck, 1967), Hinge method (Lambe and Wolfskill, 1970), Canadian Foundation Engineering Manual method (Canadian Geotechnical Society, 1985), and Cheney's method (Cheney, 1988).

B.1 Tributary Method:

In the Tributary method developed by Terzaghi and Peck (1967), the selected earth pressure diagram is divided as shown in Figure 7.4, anchor forces are calculated by applying the equilibrium conditions to each segment, separately, and then the force and bending moments diagrams are constructed. As for the wall embedment depth, it is back calculated as the equivalent soil column that will produce the same resistance (R) at the wall end that was calculated earlier via equilibrium equations.

B.2. The Hinge Method:

In the Hinge method developed by Lambe and Wolfskill (1970) and as shown in Figure 7.5, a hinge is assumed to exist at the point of application of each anchor as well as at the excavation level, unknown anchor forces are then calculated by applying the force and moment equilibrium equations to each of the segments separately, and moment diagram is constructed. The wall embedment is again assumed to be that soil column corresponding to the calculated resistance at the wall lower end.

B.3 Canadian Foundation Engineering Manual Method:

The Canadian Foundation Engineering Manual method (1985) utilizes the Rankine's pressure distributions at both sides of the tieback wall, and assumes that maximum anchor load develops just before stressing the intermediate- lower, anchor. At the first stage, the force exerted by the upper most anchor, and the passive force are assumed to be the only forces acting on the tieback wall system. For this system of forces, the anchor and passive forces are calculated simply by applying the force and moment equilibrium about the point (O) which is assumed to be a zero moment point. This procedure is repeated for other lower anchors with the assumption that the force calculated for the previous anchor(s) doesn't change throughout the calculations. The entire process is shown in Figure 7.6.

C. Finite Element Method (FEM):

The finite element approach has not been commonly used in this regard due to its complexity. It was also commonly recognized that the analysis of tieback walls

could be achieved with much less complexity and at almost the same level of predictability using other methods. Tsui (1974), and Clough (1984) employed the Finite Element technique in the analysis of tieback walls attempting to evaluate the axial loads and bending moments developed in the wall, the wall deflections, and the anchor load distribution.

In the sections to come, a simple yet powerful finite element analysis method will be introduced taking into consideration as many parameters as foreseen to be necessary.

VII.2 NUMERICAL COMPUTATIONAL ALGORITHMS

In the present formulation, the soil-pile interaction is treated as a beam-on-elastic foundation problem, with the soil reaction represented by the discrete springs. The excavation is simulated by releasing the participation of the springs connected to the beams, creating an imbalanced system. An iteration process is then evoked to seek a new balanced state, from which the anchor force, the deflection, the bending moment of the pile, and the earth pressure are calculated.

The interaction between the tieback and the pile is represented by a spring with a non-linear elastic perfectly plastic load-displacement behavior. While the anchor force can be generally decomposed into vertical and horizontal components, only the horizontal force component is considered in the present formulation.

To illustrate the analysis algorithm, a typical tieback cross-section is shown in Figure 7.7. The pile is divided into segments of the beam elements connected by the nodal points. In

addition, the soil reaction pressure is lumped into the nodal forces, calculated from the soil spring response. Thus, for a typical beam element, one can identify four internal force components: F_1 and F_2 as moment, and $(F_1 + F_2)/H$ and $-(F_1 + F_2)/H$ as shear force, as shown in Figure 7.8. The corresponding nodal forces at each node would consist of the internal shear forces and internal moments from the adjacent beam element, along with the spring reaction force due to the connected springs representing either the soil reaction force or the tieback force, or both.

Based on the elementary structure mechanism, one can establish the following relationship:

$$X = (ASA^T)^{-1} P \quad (7.1)$$

Where

X = node displacements

P = node forces

A = matrix relating external force and internal force

S = matrix relating internal force and internal displacement

The global matrix (ASA) can be derived easily from the element (ASA) by the superposition method. Thus, by given external node force, the node displacements can be obtained.

Details of the derivation of this equation and matrix A and S can be found in textbooks, such as Bowles (1988). A numerical procedure developed herein to simulate the construction sequence is described as follows.

Before the excavation, the soil mass is assumed to be subjected to initial at rest stress condition. The installation of the pile does not alter the state of stress in the soil. The first stage excavation is regarded as a release of the initial stress at the excavation side, i.e., a release of the soil springs connected to the pile above the excavation depth. The initial nodal forces is obtained by the distribution of the initial stress across the contributory area of the pile element.

For the subsequent installation of the anchors and excavations, the procedure of calculation can be summarized by the following expressions:

Stage 1:

$$[X_1]^0 = [K_1]^{-1} [P_0]^0 \quad (7.2a)$$

$$[P_1]^0 = [K_1]_{sub} [X_1]^0 \quad (7.2b)$$

$$[P_1] = [P_1]^0 + [P_0]^0 \quad (7.2c)$$

Stage 2:

$$[X_2]^0 = [K_2]^{-1} [P_1]^0 \quad (7.3a)$$

$$[P_2]^0 = [K_2]_{sub} [X_2]^0 \quad (7.3b)$$

$$[P_2] = [P_2]^0 + [P_1]^0 \quad (7.3c)$$

Stage i:

$$[X_i]^0 = [K_i]^{-1} [P_{i-1}]^0 \quad (7.4a)$$

$$[P_i]^0 = [K_i]_{sub} [X_i]^0 \quad (7.4b)$$

$$[P_i] = [P_i]^0 + [P_{i-1}]^0 \quad (7.4c)$$

where

$[X_i]^0$ = an increase of the deflection due to step i construction

$[K_i]$ = global matrix for step i construction.

$[K_i]_{sub}$ = subset of the global matrix

$[P_i]^0$ = an increase of the soil reaction force on the pile due to step i construction.

$[P_i]$ = the updated soil reaction force, which is used as an initial stress for the next construction step.

Note that the subscript is used to denote the construction stage, where stage 0 refers to the initial stress state. The superscript (⁰) is used to indicate an increment of nodal displacement and nodal force for any step i.

For each step, a checking is performed on the soil reaction force and the anchor force to see if they are outside the specified limits. If this occurs, then the corresponding springs will be disconnected from the pile, and the computation will be repeated until a convergence criterion is satisfied.

VII.2.1 Soil Reaction Model

The reaction of the soil to the pile deflection is represented by the linear elastic-perfectly plastic model as shown in Figure 7.9. The modulus of subgrade reaction K_s defines the slope, and the value of active and the passive earth pressure; P_a and P_p , marks the onset of perfect plasticity. The determination of the representation value of the modulus of the subgrade reaction has been problematic, even through a number of researchers have studied the issue (e. g. Terzaghi, et al, 1955; Bowles 1988; Briaud, 1992). Bowles (1988) suggested that the general form of the modulus of subgrade reaction could be expressed as:

$$K = A_s + B_s Z^n \quad (7.5)$$

Where:

A_s , B_s and n are constants

Z = depth of interest

However, the pressuremeter test results reported by Briaud (1992) do not support this observation. In the present formulation, the consideration of soil reaction is summarized as follows:

- (i) Each soil layer has its unique value of the subgrade modulus, which is related to the strength parameter of the soil and the depth.
- (ii) The modulus of subgrade reaction of the first soil layer increases linearly from the ground surface to the bottom of the first layer. The modulus is zero at ground surface.
- (iii) For the subsequent soil layers, a linear distribution of the modulus with depth is adopted.
- (iv) No ground water table is considered. Ground water is considered to exert insignificant effect on the value of the subgrade modulus.

A typical distribution of the modulus of the subgrade reaction with depth is shown in Figure 7.9 (b).

VII.2.2 Representation of Tiebacks

The tiebacks are represented by the spring connected to the pile. The spring is defined by the load-displacement curve obtained from the anchor pull-out test. Since the anchors in the tieback wall subjected to the preload (prestressing) and working load typically is in the

elastic range, consequently, the nonlinear elastic model as depicted in Figure 7.10 is sufficient. A piecewise linear model is actually used in the model to represent the truly nonlinear behavior.

VII.2.3 Case Study

The measurement of an instrumented full-scale tieback wall constructed at the Texas A & M University Riverside campus was used in the present comparison study. Detailed information about the field measurements, tieback wall construction, and soil condition at the site can be found in Chung (1991). The tieback wall is a soldier-beam and wood-lagging wall with pressure-injected tiebacks. It contains a one-row anchored section and a two-row anchored section. Furthermore, each section of the wall is divided into a driven soldier beams subsection and a drilled soldier beams subsection.

The test wall is 30-ft (9.1 m) high, which consists of 25-ft (7.6 m) of excavation height and 5 ft (1.5 m) of embedment depth below the excavated level. The spacing between the soldier pile is 8-ft center to center, while the horizontal spacing between the tiebacks is 8 ft and 16 ft respectively for one-row and two row anchored walls. Figs.7.11(a) and (b) show the typical cross-sections of the one-row and two-row anchored wall, respectively.

Extensive soil boring, in-situ and laboratory testing were carried out at the site. In general, the soil at the location of the wall has been classified as a medium dense clayey sand or silty sand from 0 to 10 ft, a medium dense clean poorly graded sand from 10 ft to 25 ft and a medium dense clayey sand from 25 ft to 40 ft. The water table exists at 24.5 ft to 25 ft below the natural ground level.

elastic range, consequently, the nonlinear elastic model as depicted in Figure 7.10 is sufficient. A piecewise linear model is actually used to represent the truly nonlinear behavior.

VII.2.3 Case Study

The measurement of an instrumented full-scale tieback wall constructed at the Texas A & M University Riverside campus was used in the present comparison study. Detailed information about the field measurements, tieback wall construction, and soil condition at the site can be found in Chung (1991). The tieback wall is a soldier-beam and wood-lagging wall with pressure-injected tiebacks. It contains a one-row anchored section and a two-row anchored section. Furthermore, each section of the wall is divided into a driven soldier beams subsection and a drilled soldier beams subsection.

The test wall is 30-ft (9.1 m) high, which consists of 25-ft (7.6 m) of excavation height and 5 ft (1.5 m) of embedment depth below the excavated level. The spacing between the soldier pile is 8-ft center to center, while the horizontal spacing between the tiebacks is 8 ft and 16 ft respectively for one-row and two row anchored walls. Figs.7.11(a) and (b) show the typical cross-sections of the one-row and two-row anchored wall, respectively.

Extensive soil boring, in-situ and laboratory testing were carried out at the site. In general, the soil at the location of the wall has been classified as a medium dense clayey sand or silty sand from 0 to 10 ft, a medium dense clean poorly graded sand from 10 ft to 25 ft and a medium dense clayey sand from 25 ft to 40 ft. The water table exists at 24.5 ft to 25 ft below the natural ground level.

A variety of instrumentation devices were used in the tieback wall, including strain gages, embedment strain gages, load cells, and inclinometers. The measured behavior was presented in terms of bending moment, axial force, and horizontal deflection versus depth for the three construction stages and five construction stages, corresponding to one-row and two-row wall construction, respectively.

For the purpose of the comparison between the measured behavior and the calculated results, certain assumptions and simplifications are made. They include the selection of the load-displacement curve shown in Figure 7.12 for the tieback (anchor) behavior, and the soil strength parameters: $C = 0.0$, $\phi = 32^\circ$.

The calculated pile deflection for the one-row tieback wall (Beam 15 in Chung's thesis) corresponding to three construction stages are compared with the measured in Figures 7.13(a), (b), and (c). The calculated bending moments are compared to the measured in Figure 7.14 for stage 3 (the final stage).

From Figure 7.13(c), it can be seen that the prediction results are far less than the measurements. This discrepancy is mainly due to the contribution of the system rigid movement, among other factors. In this case, if the rigid movement of the pile is evaluated as the measurement between the original pile axis and the dotted line shown in the Figure 7.13(c), it can be observed that the calculated results, the structural deflection, are very close to the measured results.

For the two-row tieback wall (Beam 7 or 8) corresponding to the five different construction stages, the calculated moment at the end of stage 5 is compared with the measured in Figure 7.15.

VII.2.4 Parametric Study

A typical tieback wall design is used in the parametric study using the developed computer program. The basic configuration of the tieback wall design is as follows: Soldier pile length = 45 ft, excavation depth = 30 ft. Two rows of tiebacks are included: one at 10 ft and the other one at 20 ft below the ground surface. The backfill soil parameters are: $C = 200$ psf, $\phi = 20^\circ$. The load-displacement curve of the tieback is shown in Figure 7.16. The prestress applied to each tieback is 3 kips. In the subsequent parametric study, several factors are investigated: (i) effect of prestress level, (ii) effect of anchor locations, (iii) effect of pile stiffness, and (iv) effect of backfill soil properties.

I. Effect of Anchor Prestressing

To see the effects of the prestress level applied to the anchor, a one row anchored wall system is analyzed. The prestress used ranges from 4 kips to 16 kips, representing 20% to 80% of the anchor pull-out capacity. The calculated results are plotted in Figure 7.17 (a), (b), and (c) for the pile deflection, the moment, and the soil reaction force, respectively. For comparison, the result for excavation to 10 ft without the anchor is also shown. As expected, the larger the prestressing, the smaller the pile deflection. However, it is expected that once the prestress level is large enough, an inward deflection of the wall will result in passive earth pressure. Obviously, this is not a desirable situation. From Figure 7.17(b), it can be seen that with an increase in the anchor prestress, the soil reaction force increases, especially at the anchor location. The distribution of the earth reaction force distribution is highly dependent

upon the level of anchor prestress. For a lower level anchor prestress, the triangle distribution is more appropriate; however, the trapezoidal shape becomes more appropriate with an increase in the prestress. From the pile moment distribution shown in Figure 7.17(c), it can be seen that the maximum moment increases with an increase of the anchor prestress. Thus, the practice of using higher prestress to control the pile deflection requires that larger pile section be used. The effect of anchor prestress can be further seen from Figure 7.18, in which an increase of anchor force due to subsequent excavation to 25 ft depth is plotted against the initial prestress. It is apparent that the larger the anchor prestress, the smaller the additional increase of anchor force due to excavation. It implies that the anchor with large prestress allows for smaller deflection at the anchor location, thus reducing significantly the potential pile deflection.

II. Effect of Anchor Location

To investigate the effect of anchor location, the depth of the first row anchor is changed from 2 ft to 10 ft, keeping others same as before. The deflection of the pile at the final excavation stage corresponding to different anchor location is shown in Figure 7.19(a). It can be seen that by shifting upward the location of the anchors, the pile deflection has been decreased. In particular, inward pile movement may result when the anchor location is close to the ground surface. The location of the second row of the anchor does not seem to have significant influence on the pile deflection pattern. It implies that the first row anchor controls the deflection of the system. The moment distribution for different anchor locations is shown in Figure 7.19(b). It can be seen that the shifting of the anchor location upward results in the shifting of the location of max. moment downward. Another way of examining the anchor

location effect is to look at the anchor force due to different anchor location as shown in Figure 7.19(c). It indicates that when the anchor is located further away from the pile top, there is more anchor force developed in the first row anchor. The variation of the developed anchor force in the second row anchor, however, is not significantly affected by the anchor locations.

III. Effect of Pile Stiffness

The effect of the pile stiffness was studied by varying the soldier pile section as follows: HP10 x 42, HP14 x 73 and HP14 x 117. The calculated results are shown in Figure 7.20(a), (b) and (c) for the pile deflection, the moment, and the soil reaction force, respectively. Although there is an order of magnitude difference in the pile's moment of inertia, the deflections calculated for the three pile sizes are relatively close to each other (refer to Figure 7.20(a)). The moment variation due to pile stiffness difference is larger than the deflection, as shown in Figure 7.20(b). From this figure, it can be found that rigid piles experience more rotation at the pile bottom than flexible piles, suggesting that the requirement for the embedment for an ideal fixed end condition is associated with the pile rigidity. The soil reaction force, shown in Figure 7.20(c), does not show any variation. It seems that the trapezoidal shape of earth force distribution is more appropriate.

IV. Effect of Soil Properties

The variation of the soil properties mainly affects the values of the soil spring model and the initial earth pressure. For sandy soil, the friction angle is varied from 10° to 30° and the

calculated pile deflection, moment, and earth reaction force, are shown in Figures 7.21(a), (b) and(c), respectively. As expected, the sand with small friction angle leads to higher pile deflection, higher moment, and higher soil reaction force calculated at the anchor locations. Similar calculation results for the cohesive clay soils with the cohesion varied from 200 to 1000 psf are shown in Figures 7.22(a), (b) and (c) for pile deflection, moment, and soil reaction force, respectively.

VII.3 ANALYTICAL STUDY OF SUMMIT 82, SOLDIER PILES

Soldier piles 30 and 31, were analyzed using different pressure diagram based methods. The "Tributary " and the "Hinge" methods were used to calculate the moments at different depths along the soldier pile, consistently with the locations of strain gages.

Figure 7.23 shows the moments obtained from these two methods using both rectangular soil distribution (Terzaghi and Peck, 1967), and the trapezoidal (Peck, 1967) for soldier pile no. 31. Based on this Figure it is clearly shown that non of these two methods could estimate the moments at different strain gage points although they gave almost the general shape (except for the tributary method using rectangular pressure envelope). This can be attributed to the fact that most of the previous methods were originally developed for the analysis of the braced excavation walls.

In the braced excavations, the ways the structural constitutive elements interact with each other and with the retained material are different from these in the case of the tieback walls. Accordingly, the moments obtained from the strain gages readings were used to back-calculate the soil pressure and other likely stresses imposed on the retaining wall.

The strain gage reading based analysis aims at evaluating the equivalent approximate soil pressure acting on the wall as well as the moments resulting from the anchor soil interaction and the prestress. So, in addition to the rectangular unknown soil pressure distribution acting on the pile, an unknown moment is placed at the point of contact between the soldier pile and the anchor. The initial anchor prestressing force and the moments calculated from the strain gages are introduced to the analysis so that the rectangular lateral earth pressure envelope and the mobilized moments are determined. Using the initial anchor prestress in such analysis enables us to correlate- whatever possible, with the initial soil conditions (γ_o , ϕ_o) making the results obtained from such analysis even more useful.

For the purpose of the research in hand, only beams number 30 and 31 will be analyzed. Soldier pile no. 31 is first analyzed to obtain the moments and the rectangular pressure intensity. These parameters are then used to calculate the moments imposed on beam no. 31 and then introduced to soldier pile no.30. Figure 7.24 shows the moments deduced from the strain gages of beam no. 31 in comparison to the measured. The first gage point on beam no. 30 was excluded from this analysis due to deviation noticed in this point. This decision can be further judged upon by the goodness of fit of the calculated moments in soldier pile no. 30. The calculated moments are plotted against the measured moments in Figure 7.25.

The calculated moments using this approach show a relatively good predictability compared to the available soil pressure diagram based methods for soldier pile no. 31 shown in Figure 7.26.

The deduced system of forces acting on the soldier pile can be therefore represented by a rectangular soil lateral force intensity of (2.21 kip/ft), and (31.86, 111.47, and 127.36 kip.ft) at the upper, middle, and lower anchor-pile point, respectively. These moments are most likely related to the anchor angle, overburden, anchor length and diameter, and the prestress. Yet, the scarcity of experimental data makes further analysis hard to achieve.

One important point is that the equivalent uniform earth pressure will be expressed in terms of the initial density and angle of friction, not the mobilized.

VII.4 SUMMARY AND CONCLUSIONS

In this chapter, different aspects of the structural analysis of tieback retaining wall for support of the deep excavation is studied. By incorporating the nonlinear anchor behavior, the analysis is developed with ability to simulate the effects of the construction stage and the anchor prestressing. The calculated results of a previously reported case study are compared with the field measurements, which showed very good agreement. Extensive parametric studies for each of the factors involved in the tieback wall system were also performed, including anchor prestressing, anchor location, pile stiffness, and soil properties. The moments measured on the soldier piles were used to back-calculate the equivalent uniform (rectangular) earth pressure diagram as well as the moment suspected at the anchor-pile point.

Based on observations from a series of parametric studies, literature review, and the analysis conducted in this chapter, the following conclusions can be made.

- (i) The deflections of tieback walls primarily occur at the early construction stage, and are controlled by the prestressing of the first row anchor. Shifting the location of

the first row anchor to near the top of the pile is an efficient way to control the total pile deflection. However, when the first row anchors are placed to the location too close to the ground surface, their capacity may be reduced due to a lack of confining stress.

- (ii) The distribution of the earth reaction force can be represented by a rectangular uniform pressure with a reasonable accuracy, although the actual soil pressure essentially be a trapezoidal.
- (iii) For the purpose of analysis of the tieback walls, the moment induced at the anchor-wall point must be considered since it considerably affects the stress distribution along the soldier pile.
- (iv) The moments developed at each anchor point can be a function of the overburden pressure, the magnitude of prestress, as well as anchor angle, length, and diameter.
- (v) The location of the maximum moment developed in the pile is usually at the anchor location or close to the bottom of excavation, depending on the anchor location, and the anchor prestress.
- (vi) Further study for the developed moments, their magnitude, and parameters encountered therein is recommended. This will enable the designer to better estimate the stresses imposed on the tieback walls and the design input parameters.
- (vii) The overlapping effect of the anchor influence zones may also be important. The vertical and horizontal anchor spacing will play a significant role in the mobilized system properties.

(viii) The prestress level at the anchor exerts more effect at the local level, namely near the anchor location. The development of the anchor working force is mainly affected by the immediate construction stage. The subsequent construction has little influence on the variation of the anchor force.

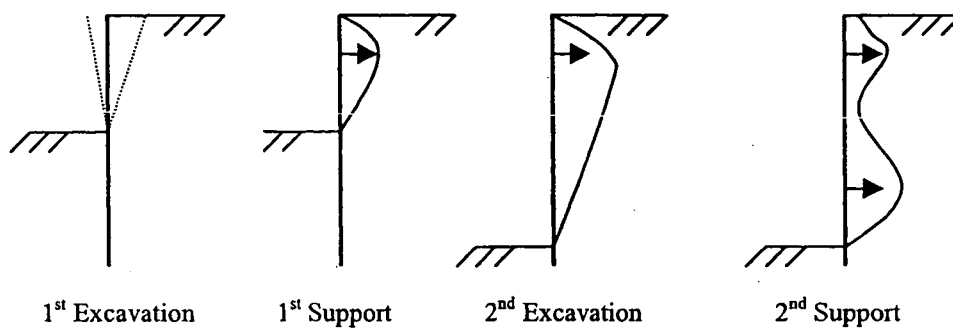


Figure 7.1 Stage Development of Earth Pressure Due to Stage Construction.

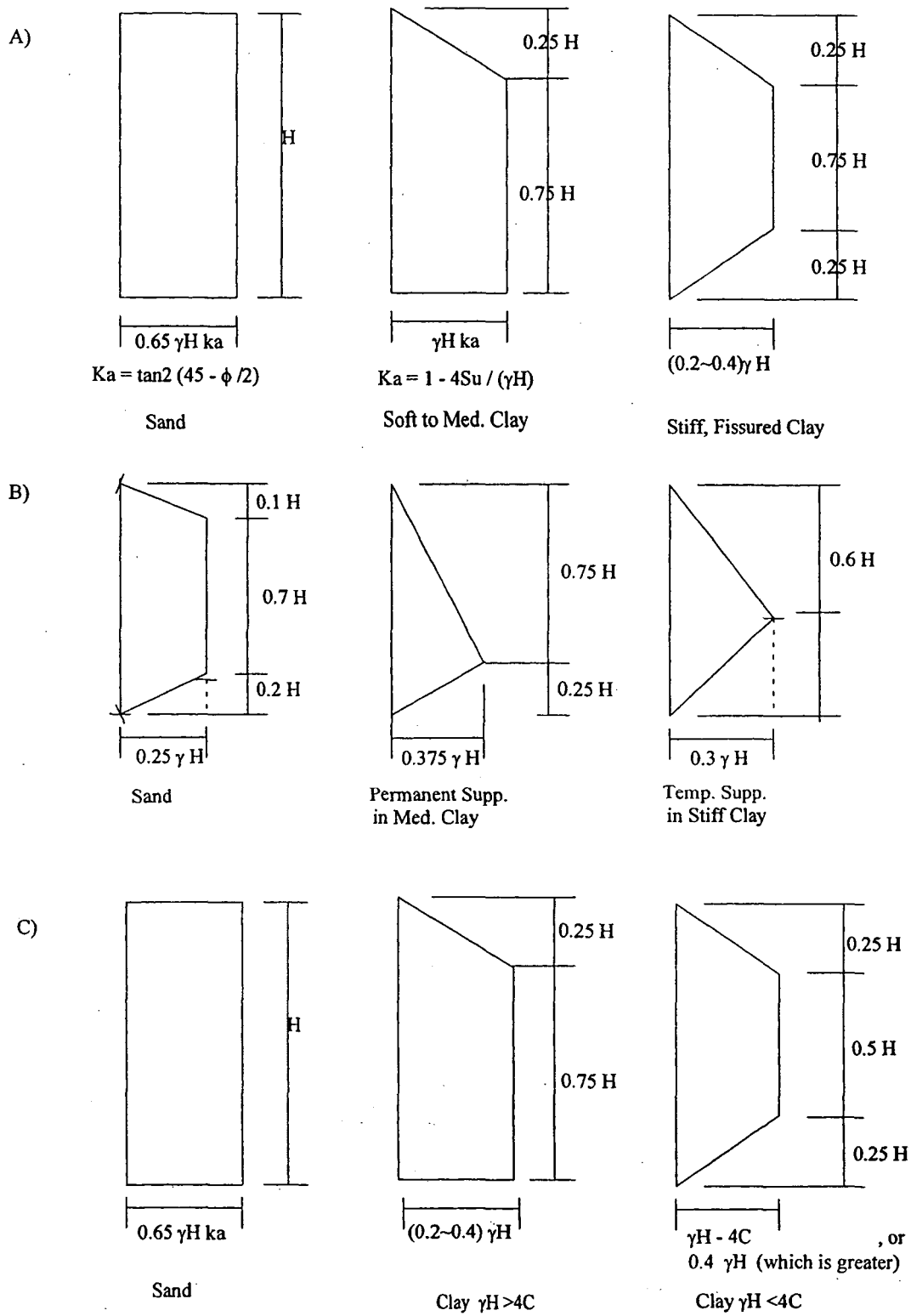
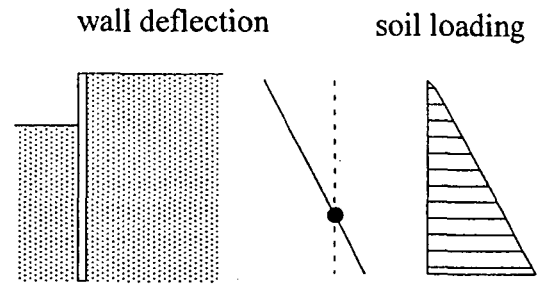
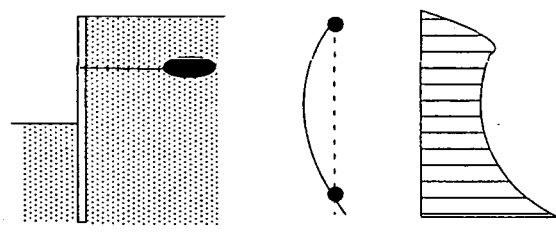


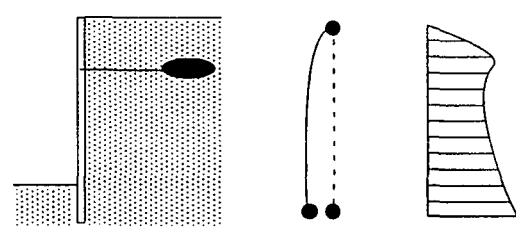
Figure 7.2 Earth Pressure Diagrams. A) Terzaghi and Peck, 1967, B) Tschebotarioff, 1973, and C) Peck, 1969.



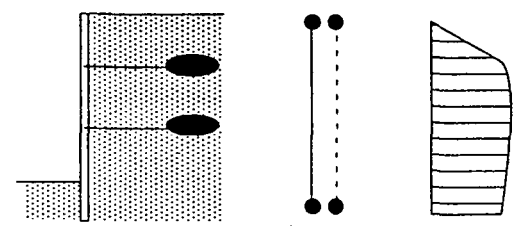
a) wall embedded in soil and not anchored (cantilever condition)



b) wall anchored at ground surfacer and embeded in soil (fixed earth support)

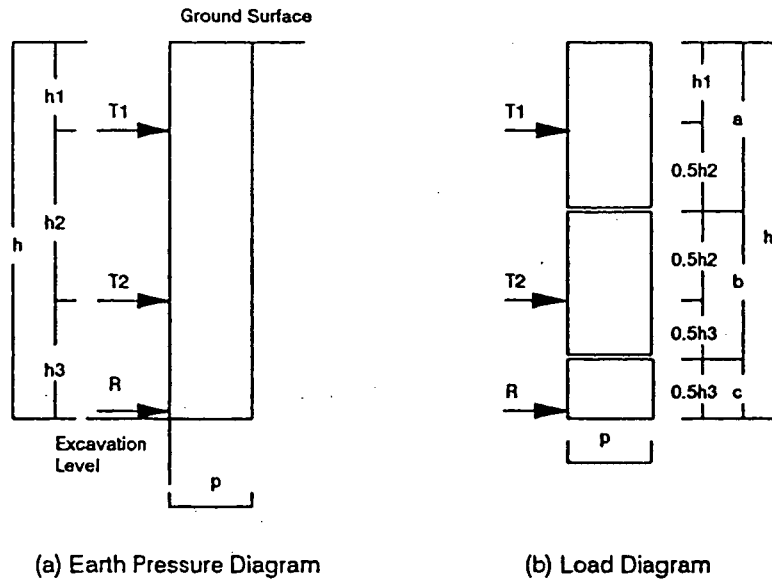


c) excvation deepened with wall anchored at ground surface



d) multiply-suported wall

Figure 7.3 Evolution of Earth Pressure (Cheney, 1982).



(a) Earth Pressure Diagram

(b) Load Diagram

The Terzaghi and Peck earth pressure diagram is used.
Anchor locations are predetermined.

p = The Terzaghi and Peck Earth Pressure (Known)
 $T1$ and $T2$ = Anchor Forces (Unknown)
 R = Soil Resistance (Unknown)
 $h = h1 + h2 + h3$ = Excavation Height (Known)

Load diagram is divided into 3 sections.

$$a = h1 + \frac{h1^2}{2}$$

$$b = \frac{h1^2}{2} + \frac{h2^2}{2}$$

$$c = \frac{h2^2}{2} + \frac{h3^2}{2}$$

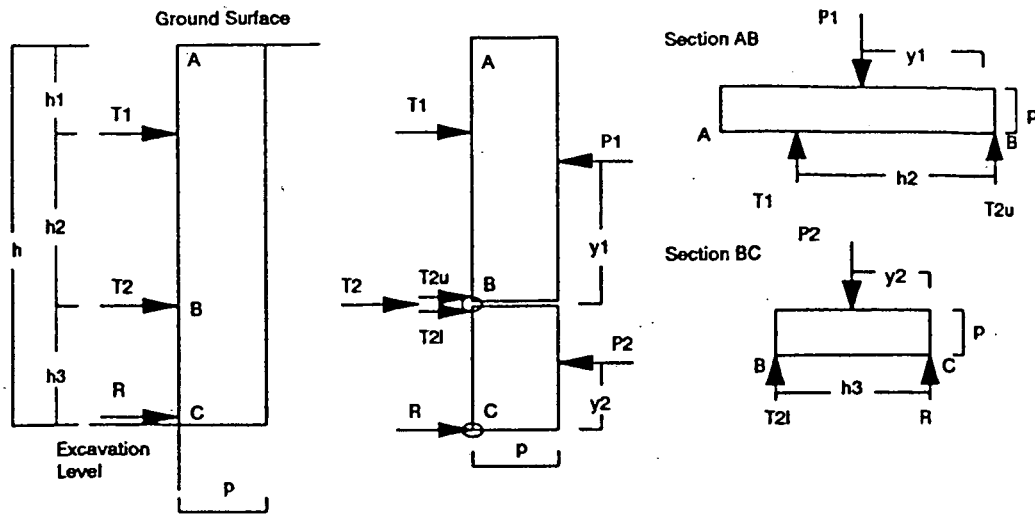
The anchor loads are given by:

$$T1 = p \times a$$

$$T2 = p \times b$$

$$R = p \times c$$

Figure 7.4 Analysis of Tieback Walls by the Tributary Method Developed by Terzaghi and Peck, 1967.



(a) Earth Pressure Diagram

(b) Load Diagram

The Terzaghi and Peck earth pressure diagram is used.

Anchor locations are predetermined.

Hinges are assumed to exist at point B and point C.

p = The Terzaghi and Peck Earth Pressure (Known)

T_1 and T_2 = Anchor Forces (Unknown) R = Soil Resistance (Unknown)

$h = h_1 + h_2 + h_3$ = Excavation Height (Known)

(1) For section AB

$$P_1 = p \times (h_1 + h_2)$$

$$\sum M_{about B} = 0, \quad \text{then} \quad T_1 = (P_1 \times y_1) / h_2$$

$$\sum F_A = 0, \quad \text{then} \quad T_{2u} = P_1 - T_1$$

(2) For section BC

$$P_2 = p \times h_3$$

$$\sum M_{about C} = 0, \quad \text{then} \quad T_{2l} = (P_2 \times y_2) / h_3$$

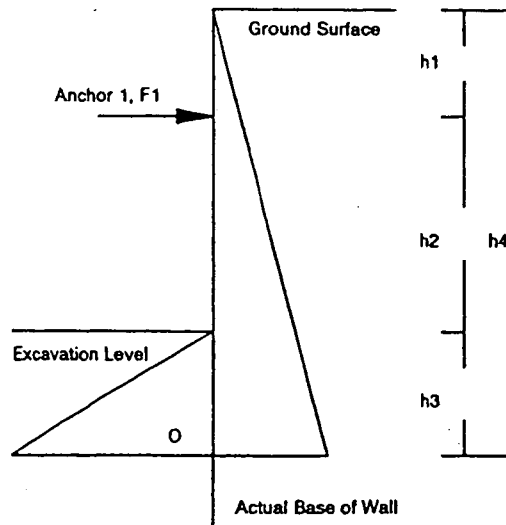
$$\sum F_A = 0, \quad \text{then} \quad R = P_2 - T_{2l}$$

(3) Anchor Loads

$$T_1 = (P_1 \times y_1) / h_2$$

$$T_2 = T_{2u} + T_{2l}$$

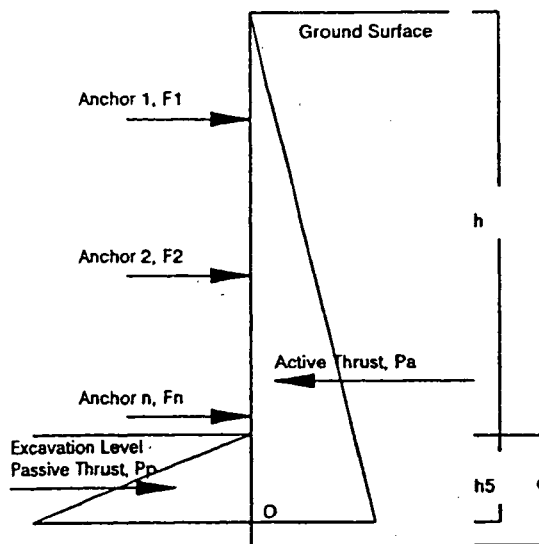
Figure 7.5 Analysis of Tieback Walls by the Hinge Method Developed by Lambe, 1970.



$h_1 + h_2 =$ Excavation depth for the next anchor (predetermined)
 $h_3 =$ Embedded depth at which the safety factor against rotation about O is 1 (unknown)
 $F_1 =$ Anchor load on Anchor 1 (unknown)

F_1 and h_3 can be calculated from
 1) Horizontal Equilibrium
 2) F.S. = 1 against rotation about the point O

(a) Analysis for First Anchor



$h =$ Final Excavation Depth
 $h_5 =$ Embedded Depth (unknown) at which the safety factor against rotation about O is 1

For $F_1 - F_n$, Use the Previously Calculated Values
 For $F_1 - F_{n-1}$, Use the Previously Calculated Values
 $F_n =$ Anchor Load on Anchor n (unknown)

h_5 and F_n are calculated from
 1. Horizontal Equilibrium
 2. F.S. = 1 against Rotation about O

Final Embedment Depth $d = 1.3 h_5$

(b) Analysis for Intermediate Anchors

Figure 7.6 Canadian Foundation Engineering manual (Equilibrium Consideration) Method- Canadian Foundation Engineering Manual, 1985.

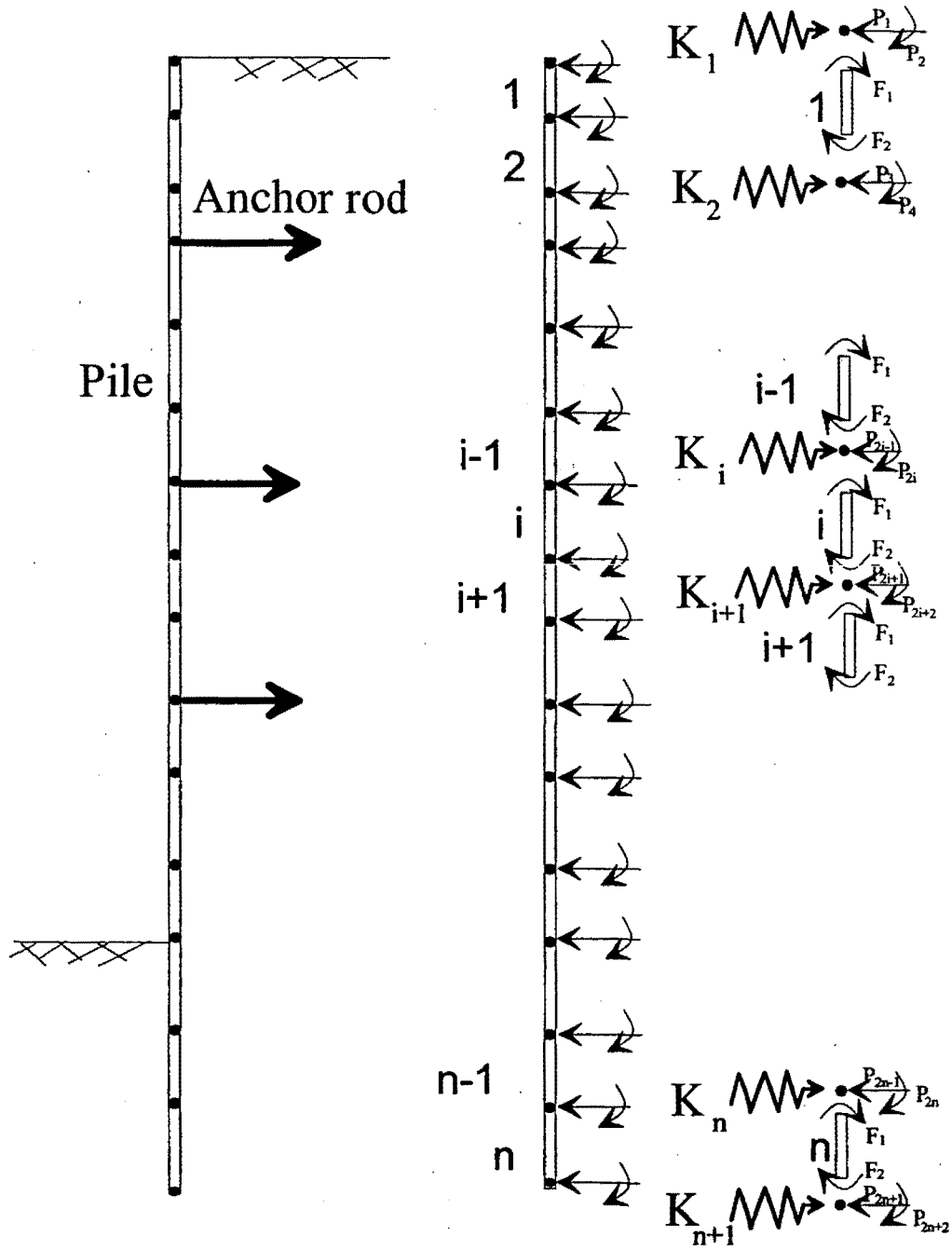


Figure 7.7 Schematic of a tieback wall elements and nodes

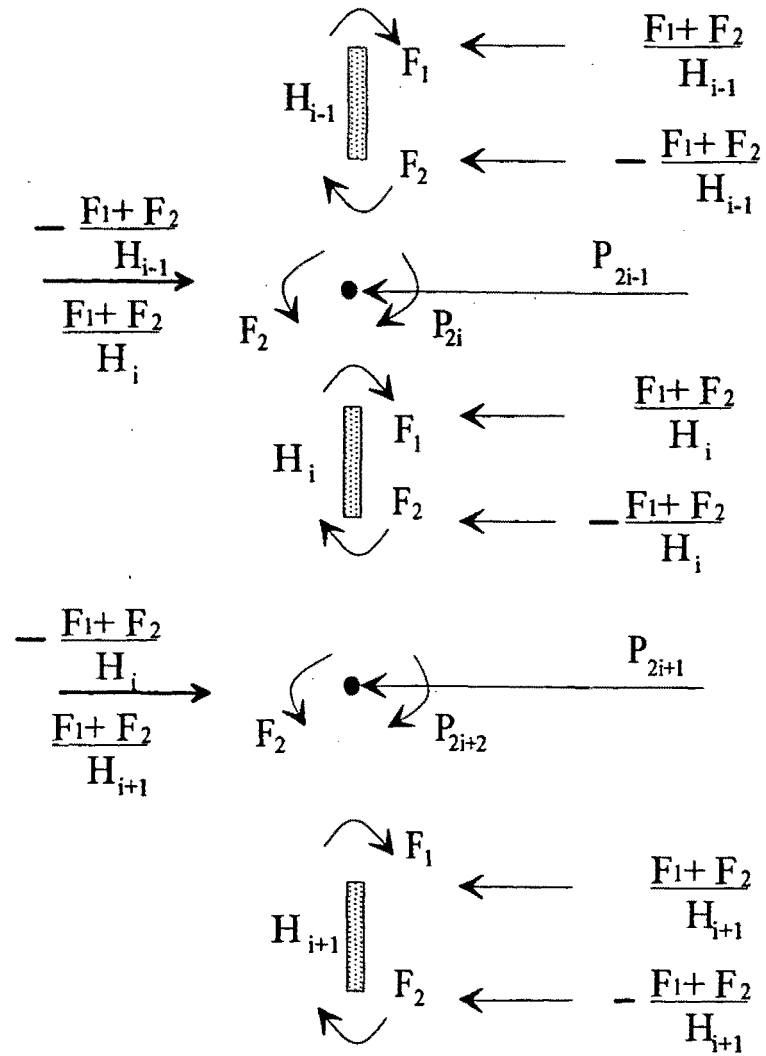


Figure 7.8 Element forces and node forces

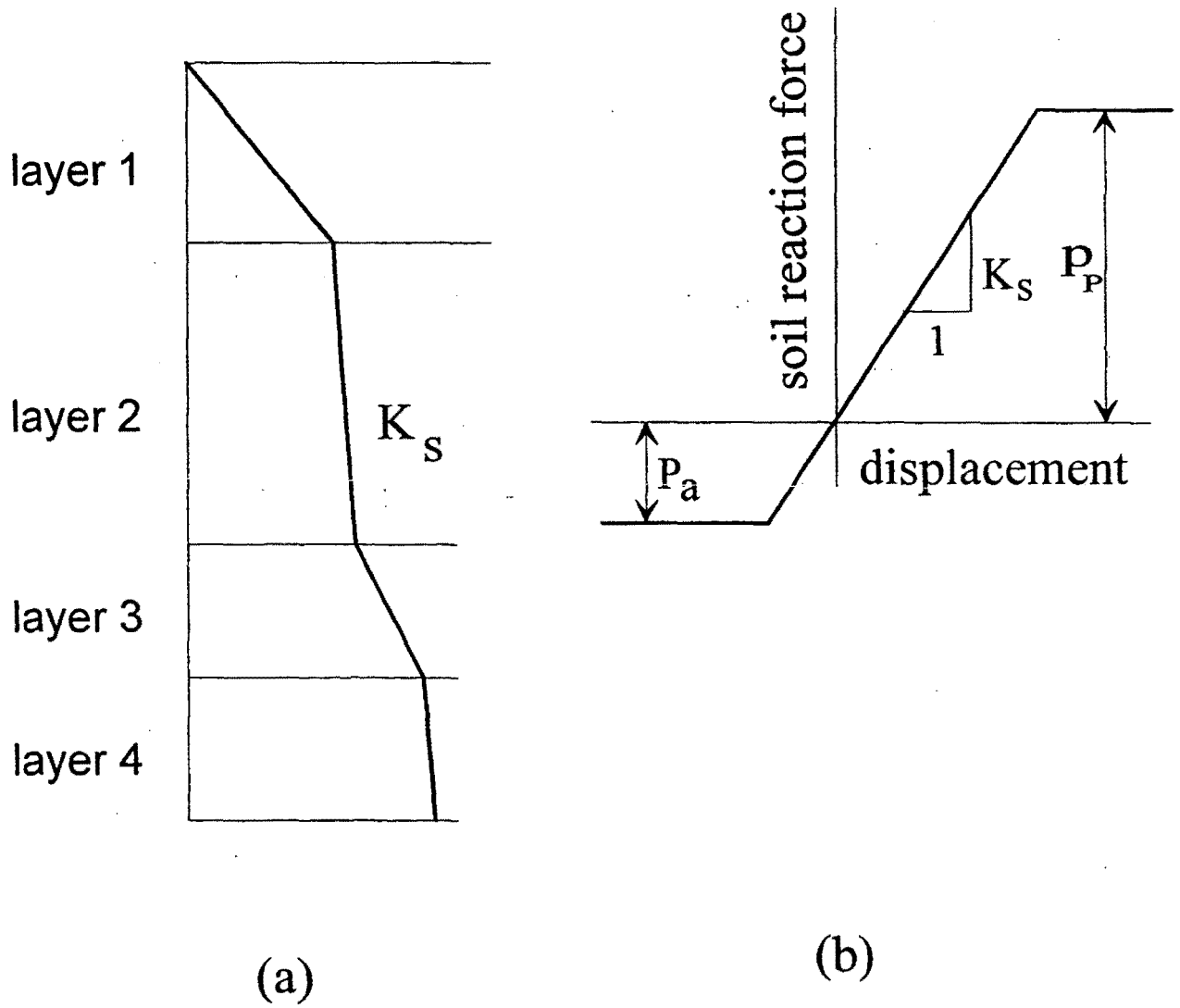


Figure 7.9 Schematic of soil subgrade modulus and soil spring model.

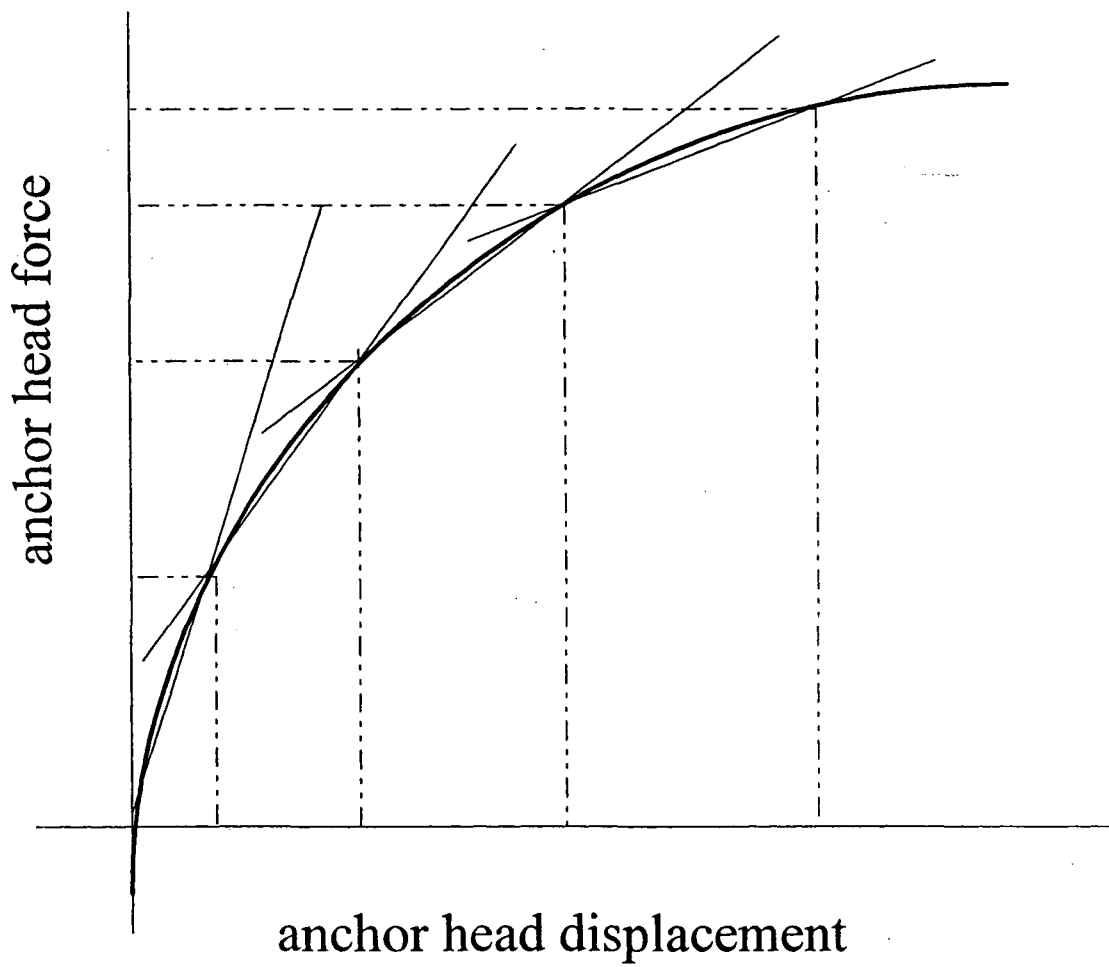


Figure 7.10 Anchor force vs. displacement representation.

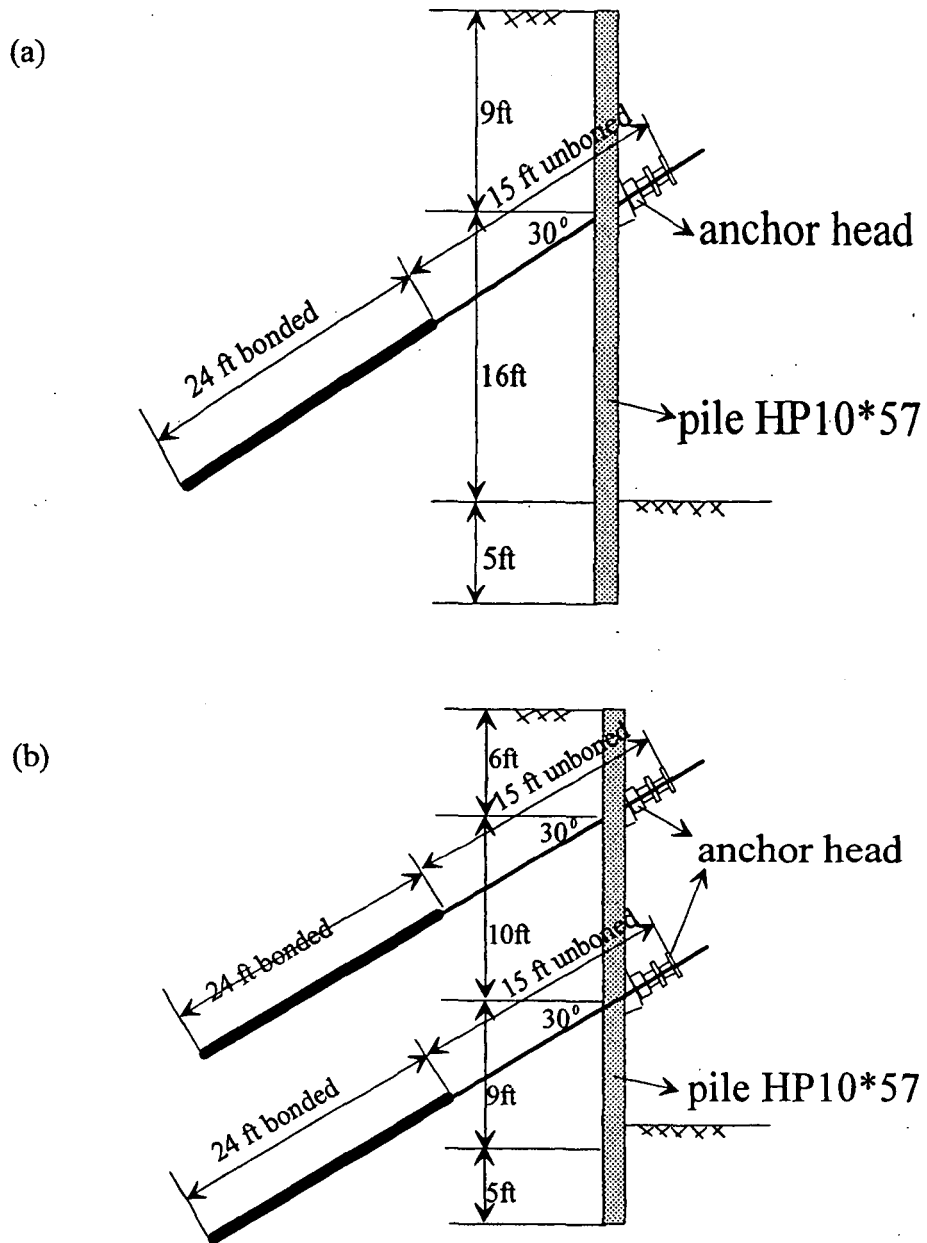


Figure 7.11 Typical cross section of the tieback wall. (Chung, M. 1991).

(a) Cross section of one row tieback wall.

(b) Cross section of two row tieback wall

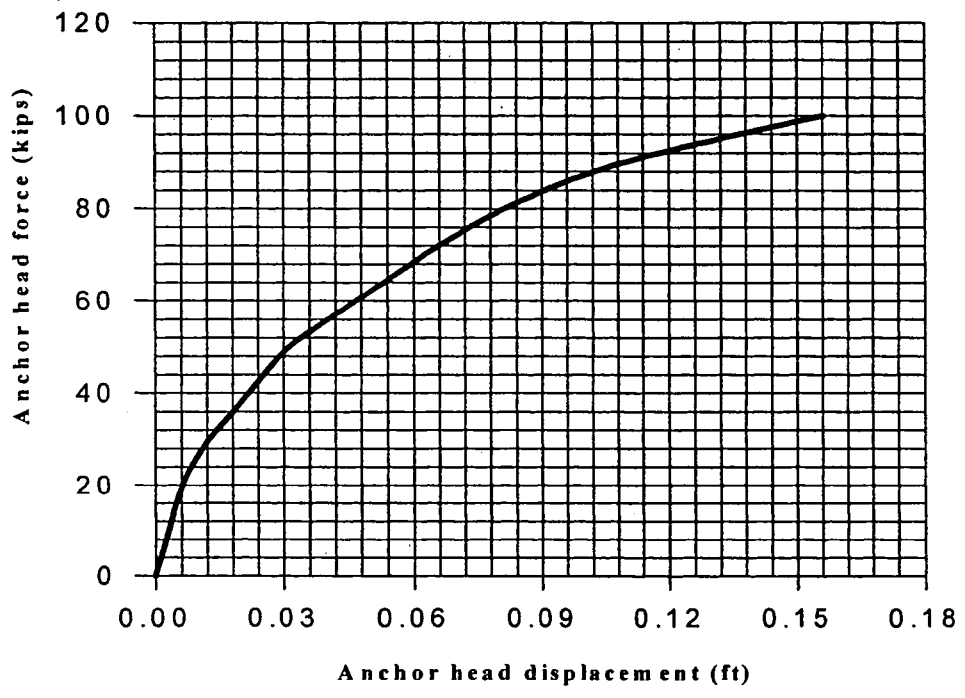


Figure 7.12 The relationship between anchor head load and displacement applied for the case history.

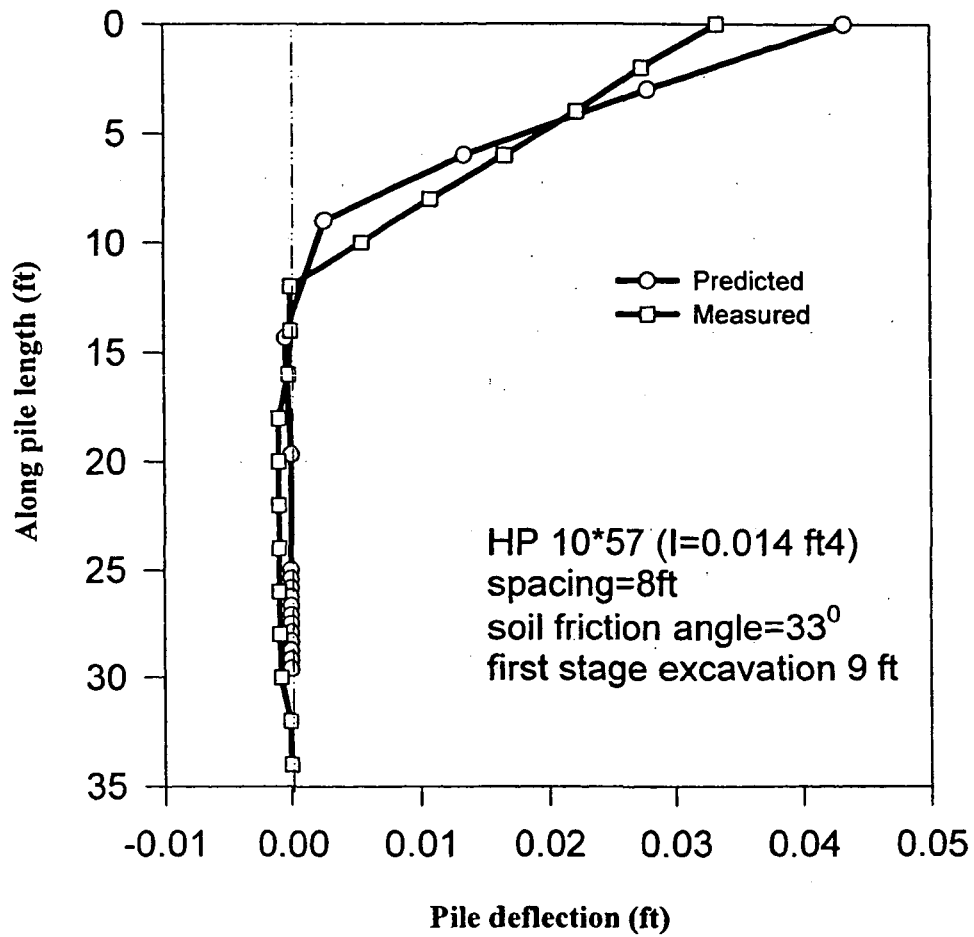


Figure 7.13 (a) Comparisons between the predicted and the measured pile deflection at stage 1, for one row tieback wall.

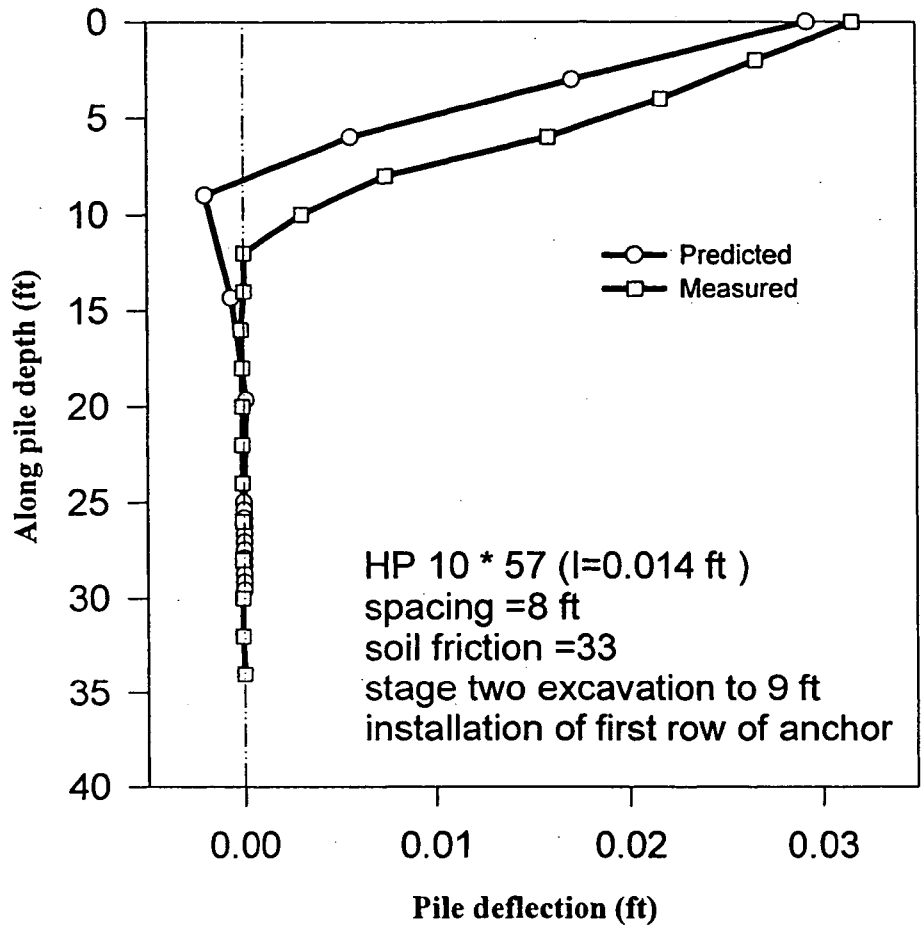


Figure 7.13 (b) Comparisons between the predicted and the measured pile deflection at stage 2, for one row tieback wall.

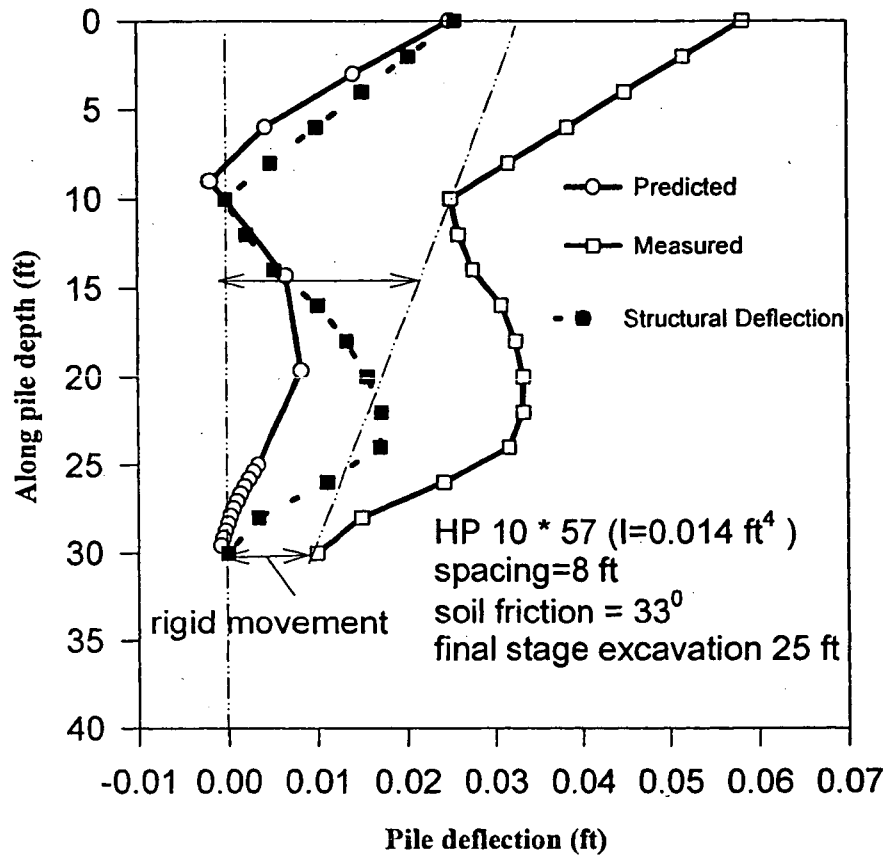


Figure 7.13 (c) Comparisons between the predicted and the measured pile deflection at stage 2, for one row tieback wall.

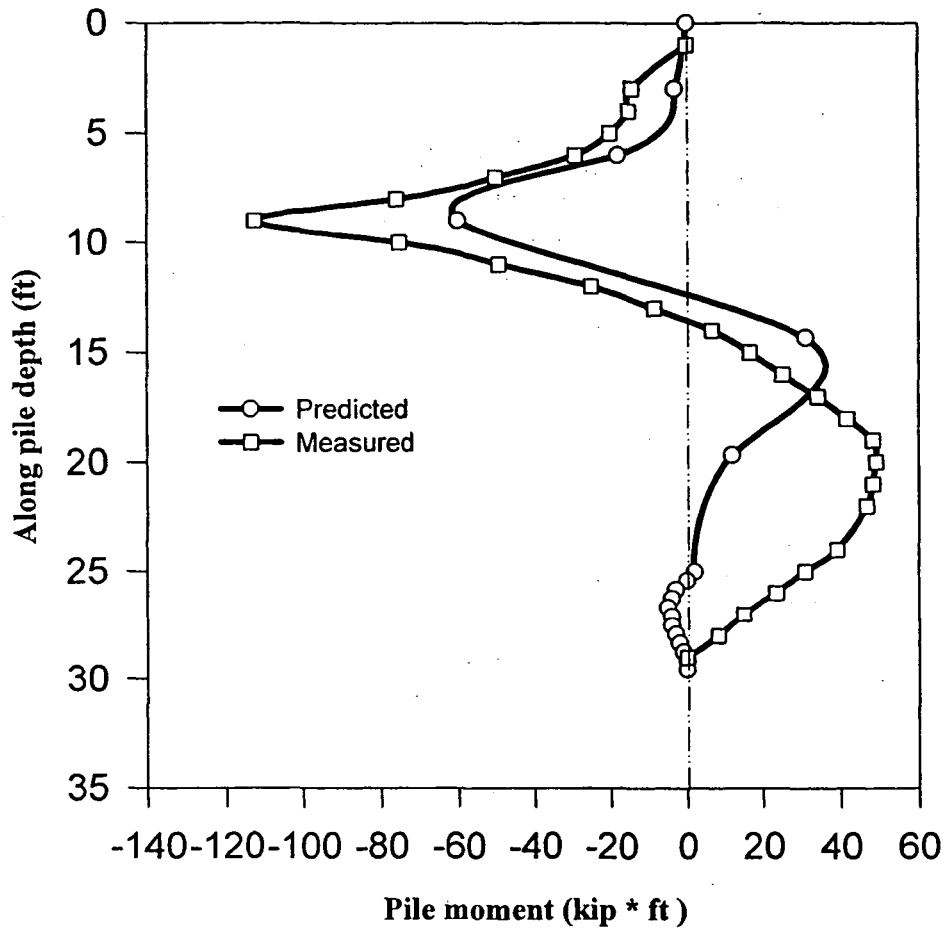


Figure 7.14 Comparison of the pile moments for one row tieback wall at stage 3.

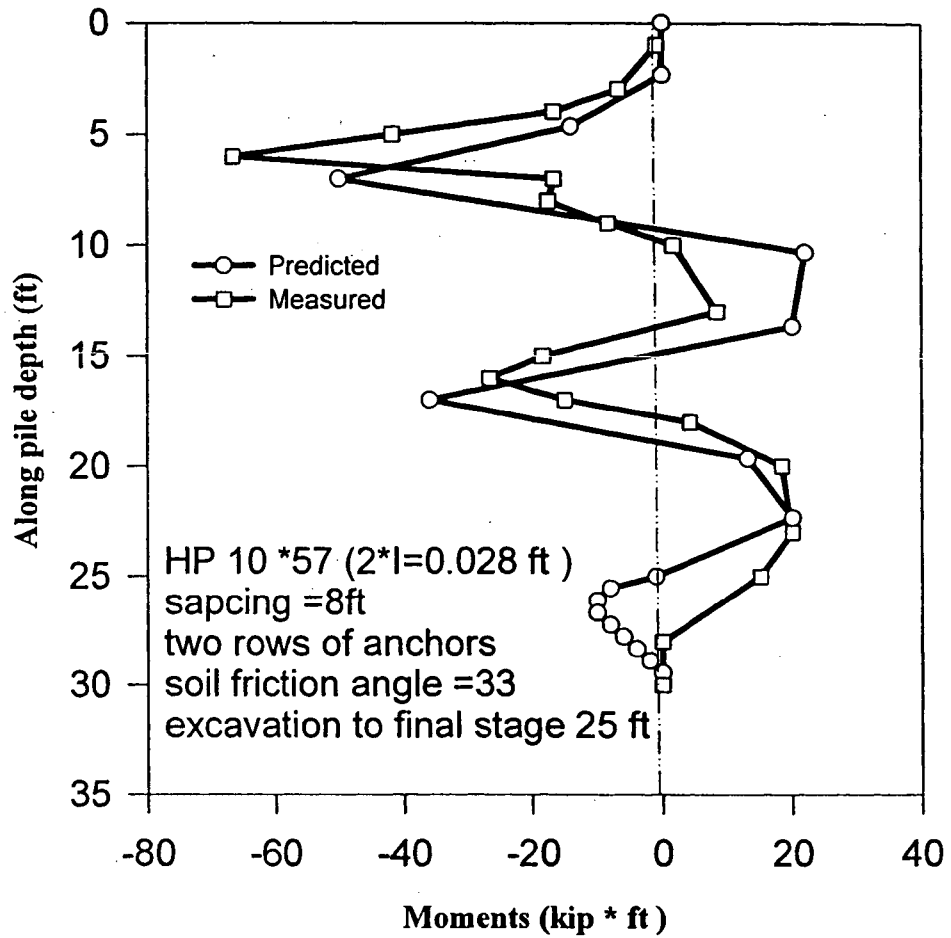


Figure 7.15 Comparison between the calculated and the measured pile moments at stage 5 for two row tieback wall.

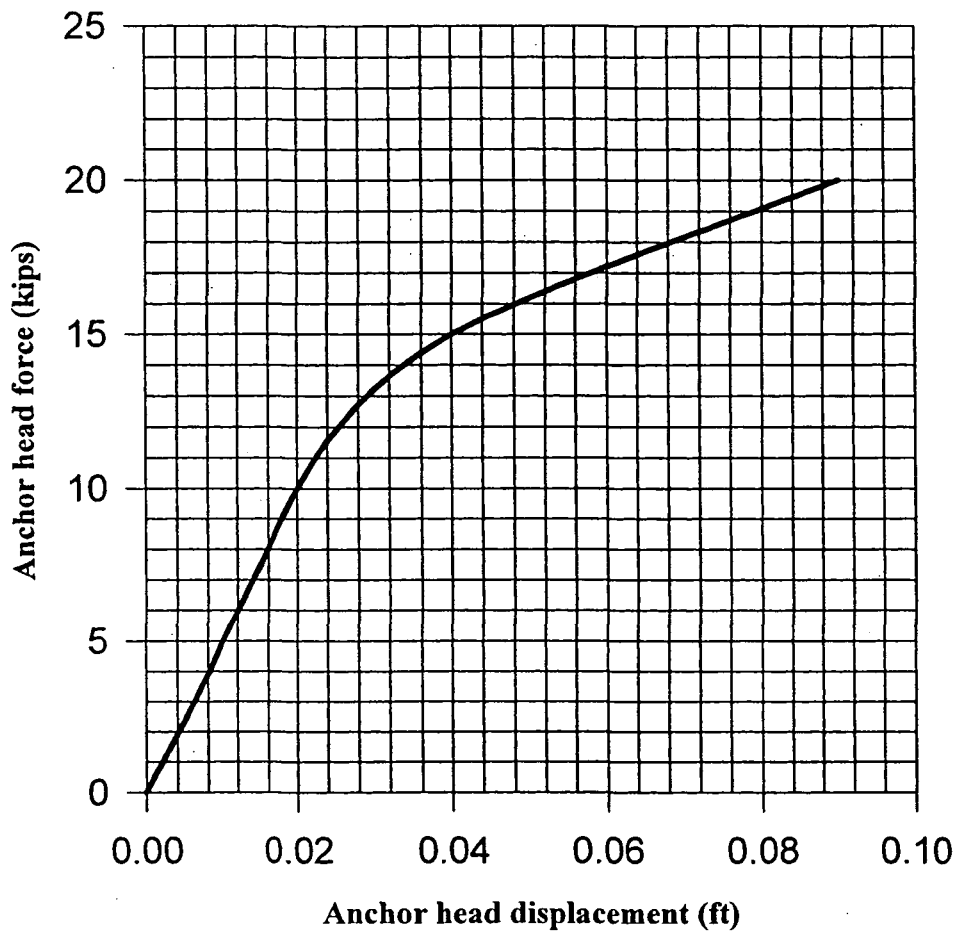


Figure 7.16 Relationship between anchor head load and displacement applied for parametric study

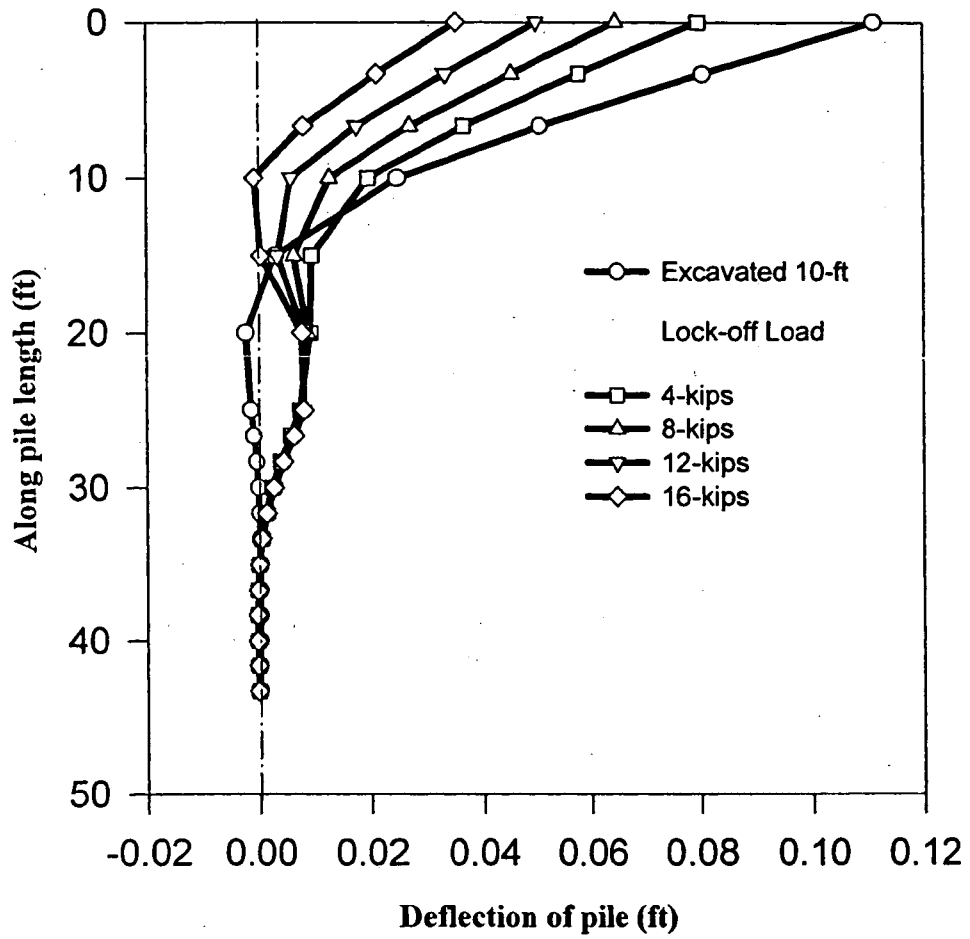


Figure 7.17 (a) Effect of lock-off loads on the structural deflections of the pile.

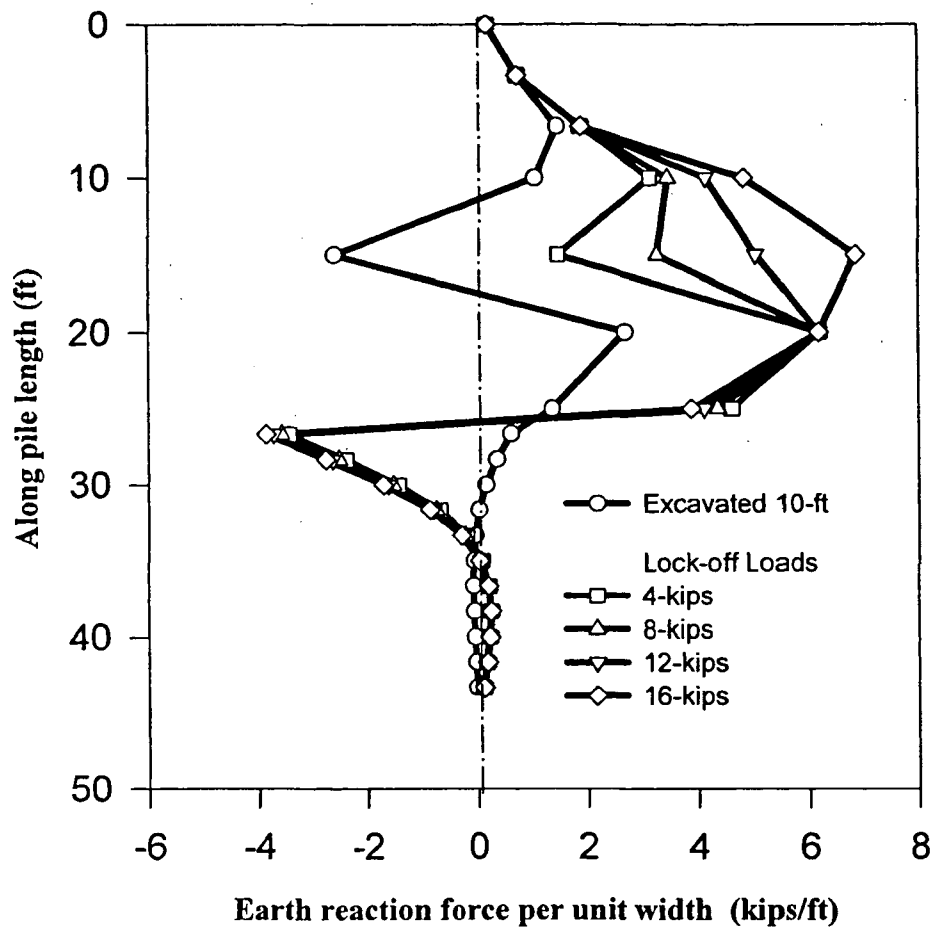


Figure 7.17 (b) Effect of lock-off loads on the soil reaction Forces.

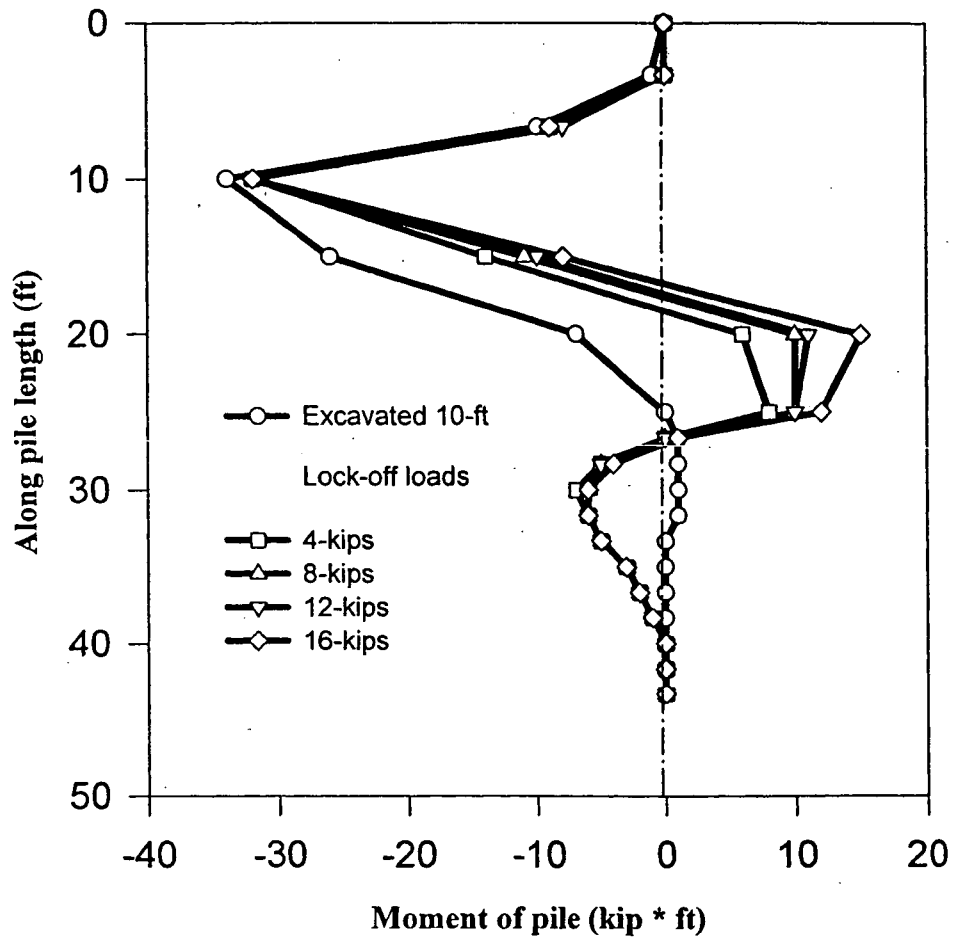


Figure 7.17 (c) Effect of lock-off loads on pile moments.

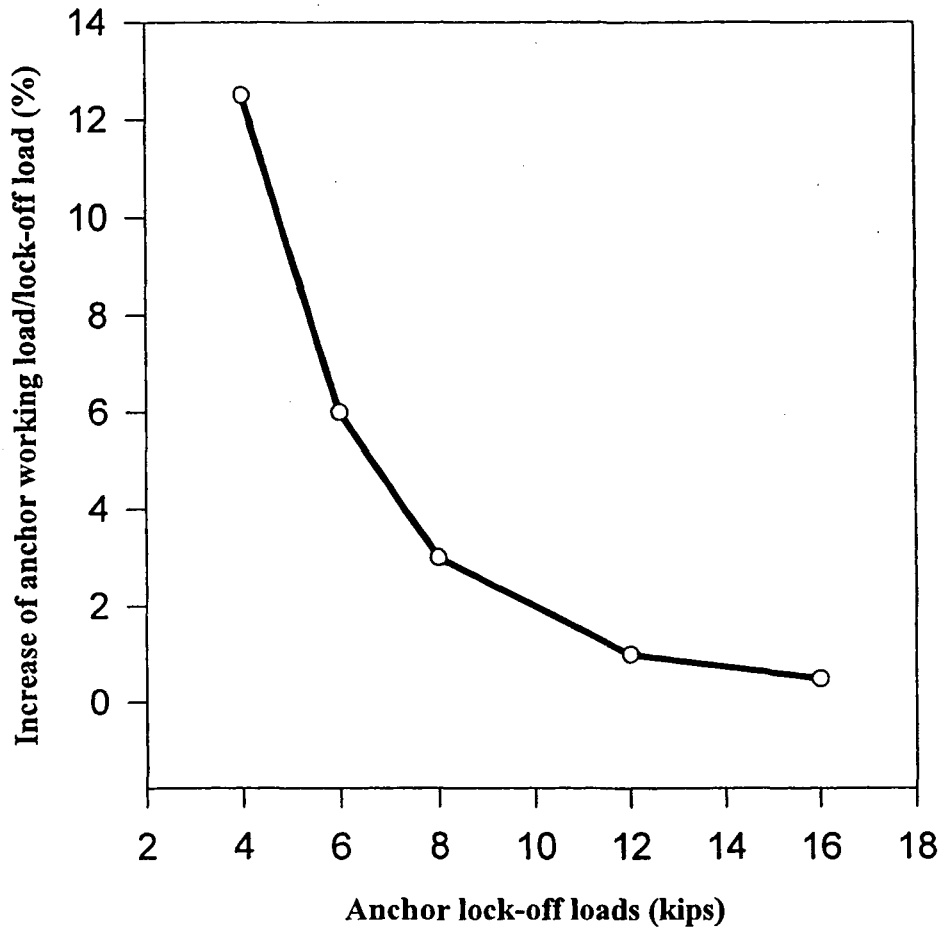


Figure 7.18 Relationship between anchor working load and anchor lock-off load.

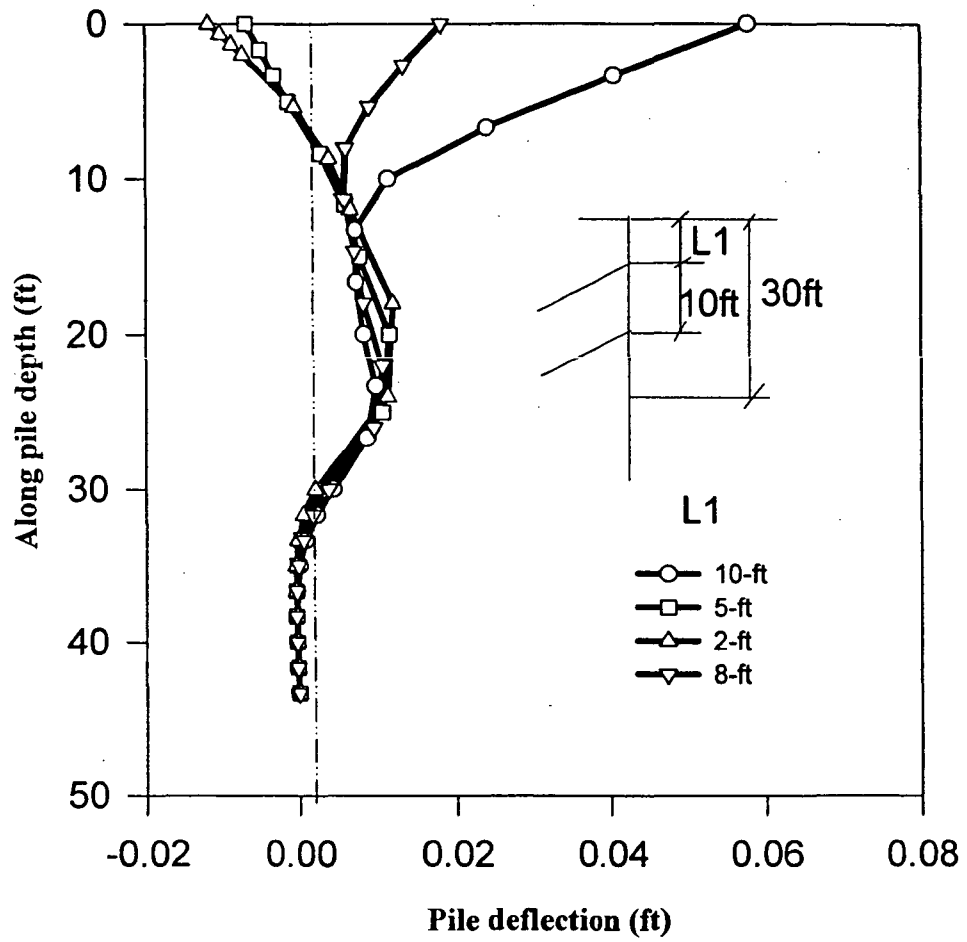


Figure 7.19 (a) Effect of anchor locations on the structural deflections of the pile.

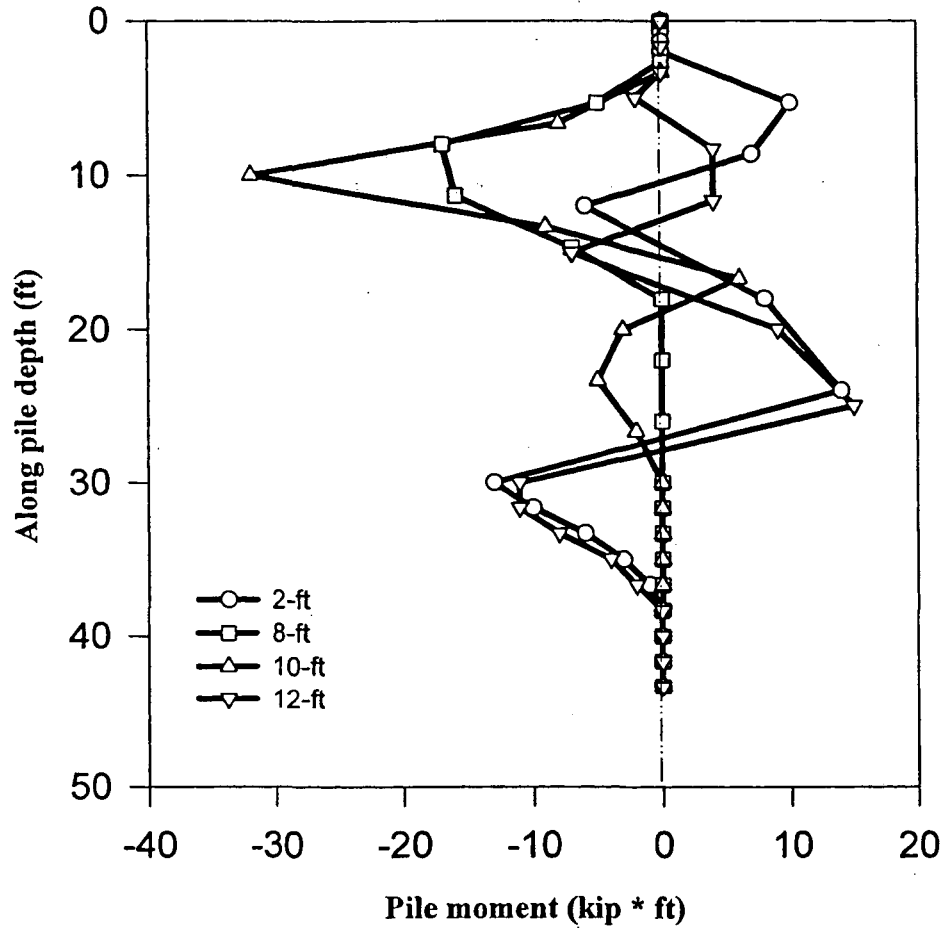


Fig.7.19 (b) Effect of anchor locations on Pile moments.

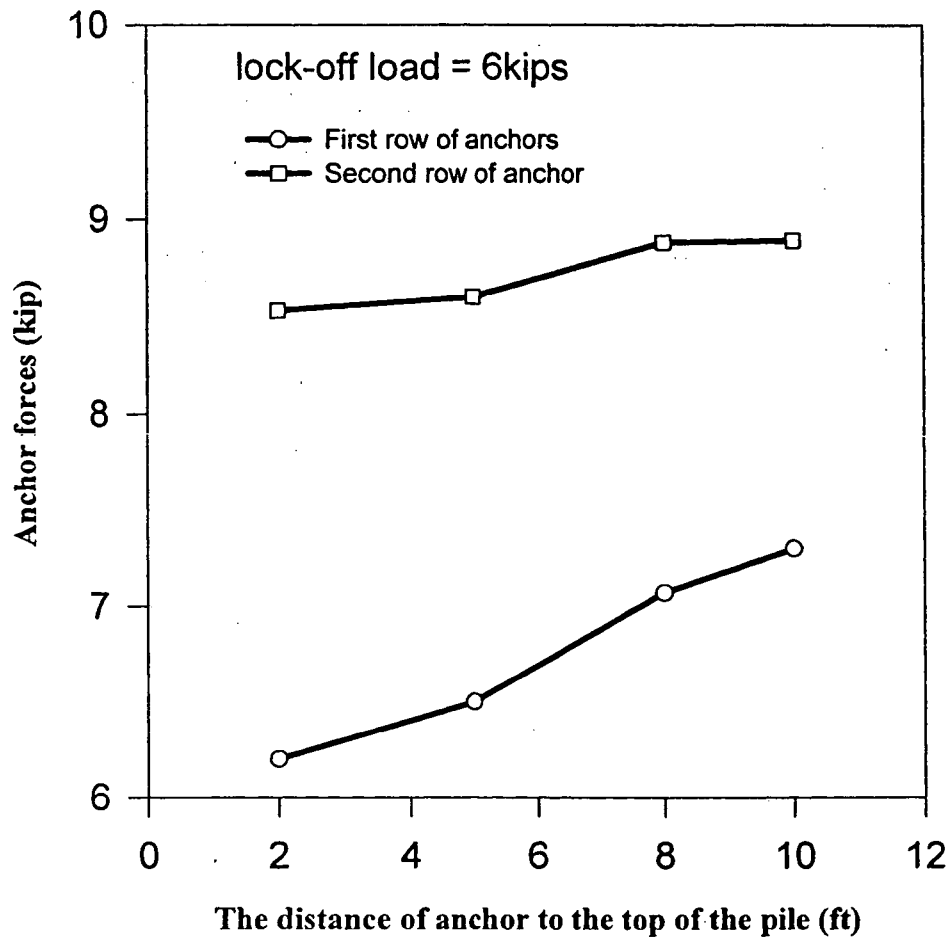


Figure 7.19 (c) Effect of anchor locations on anchor working loads.

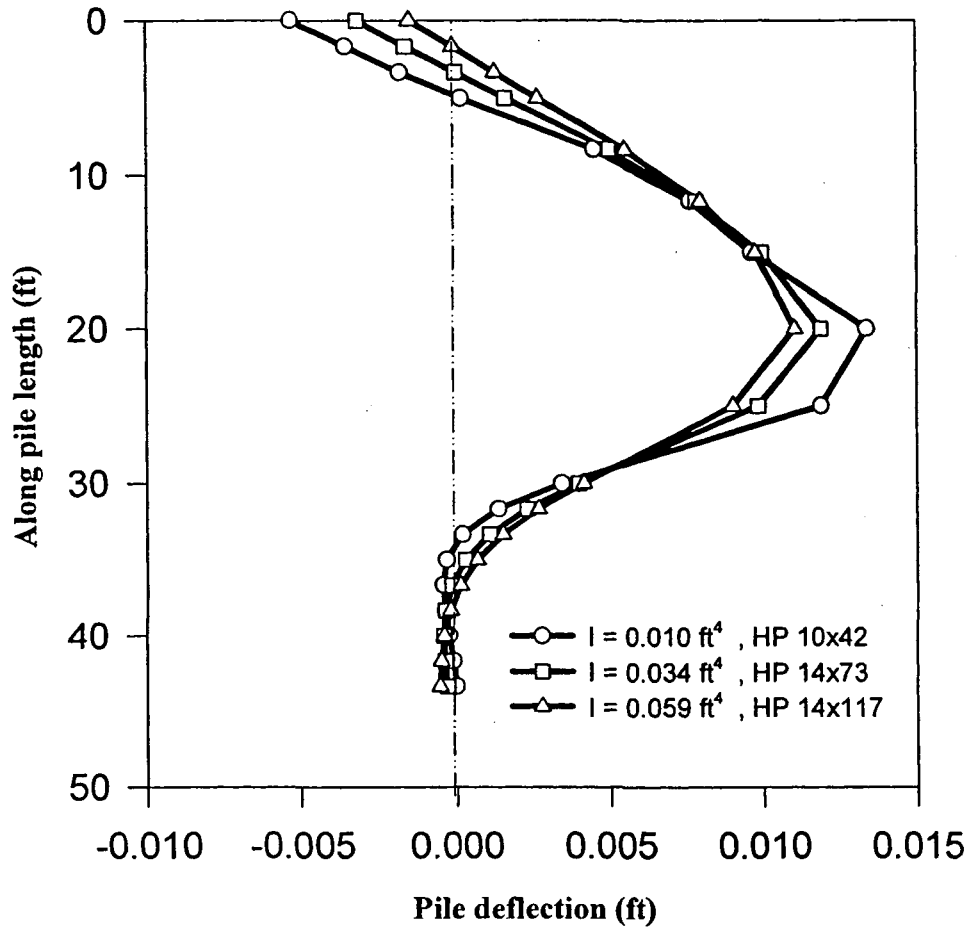


Figure 7.20 (a) Effect of pile stiffness on the structural deflections of the pile.

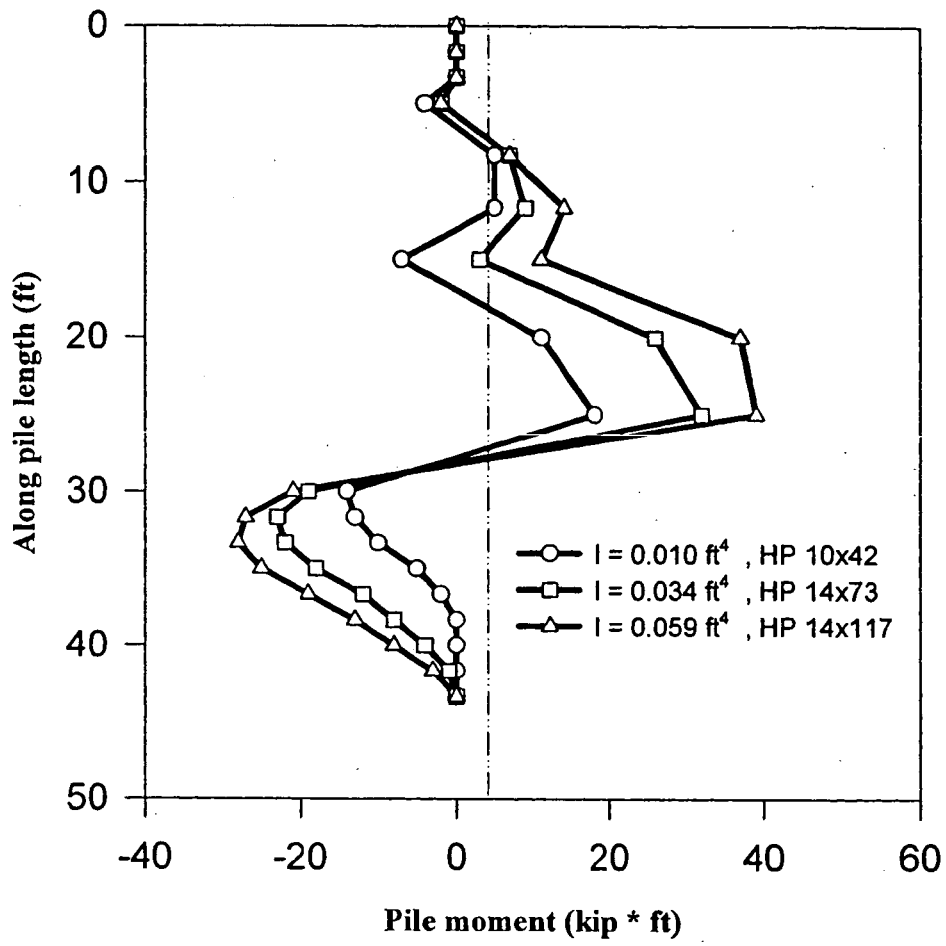


Figure 7.20 (b) Effect of pile stiffness on pile moments.

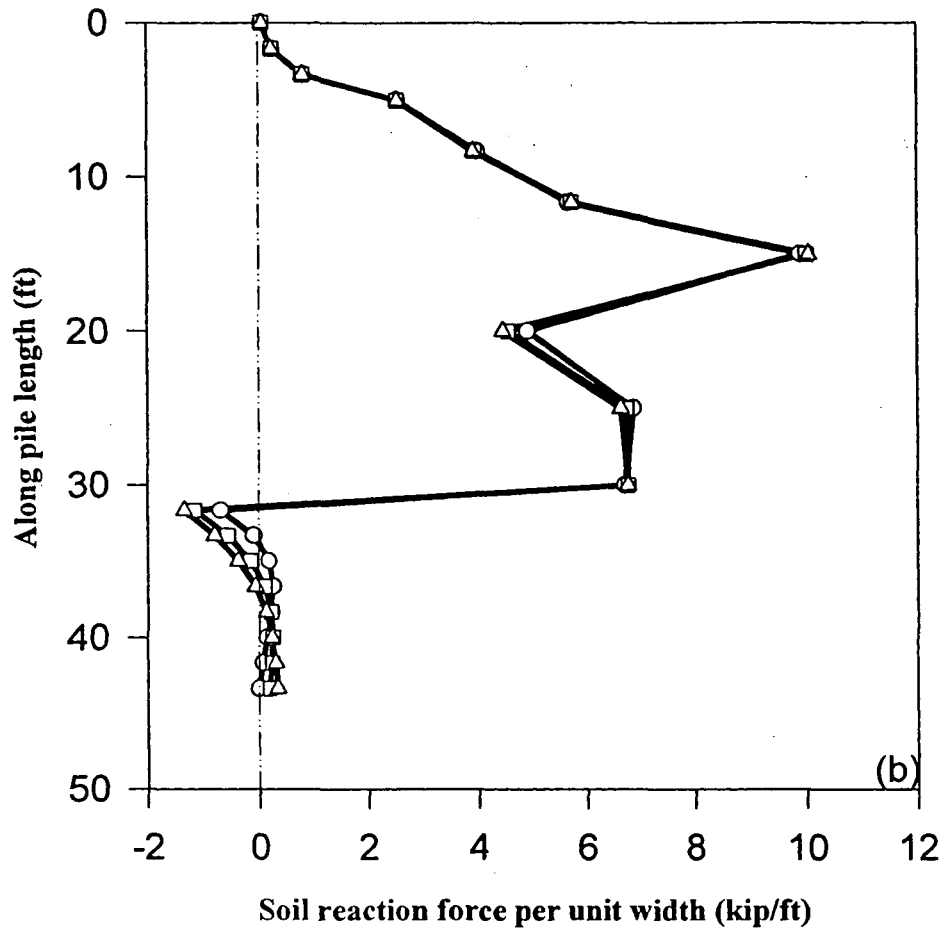


Figure 7.20 Effect of pile stiffness
 (c) Soil reaction forces under different pile stiffness

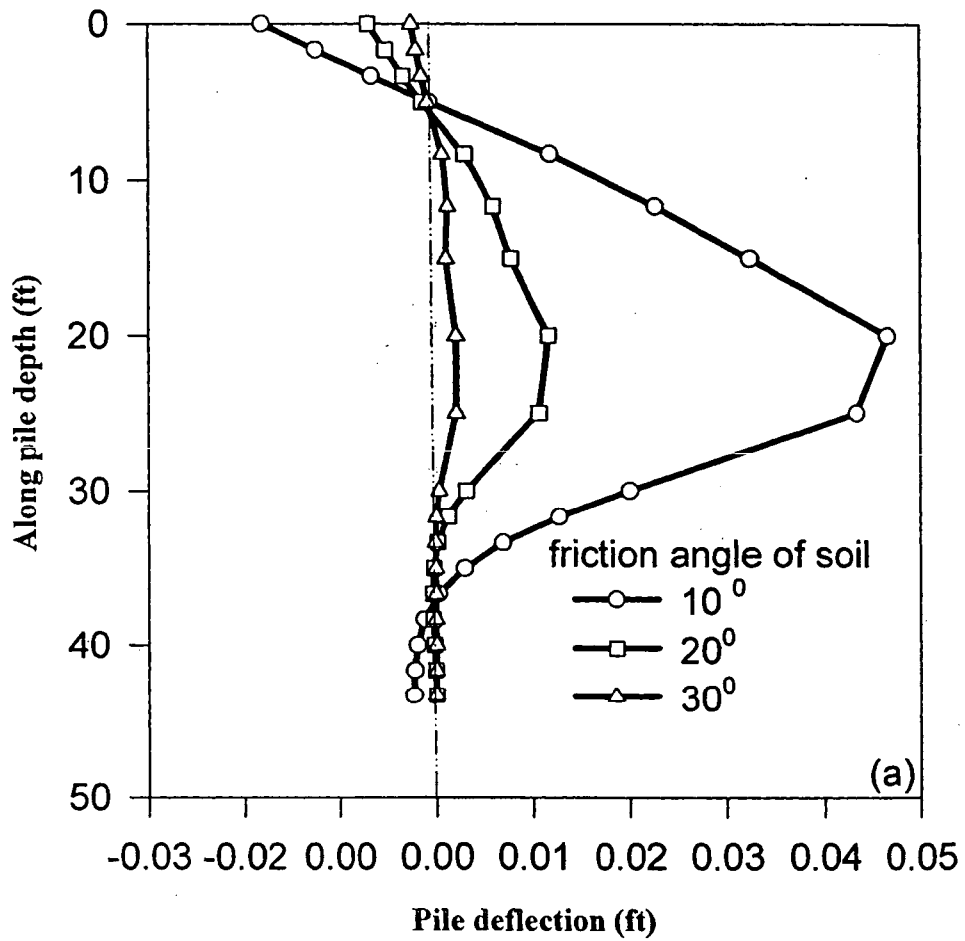


Figure 7.21 Effect of internal friction angle (C=0)
 (a) Structural deflections of the pile under different internal friction angle

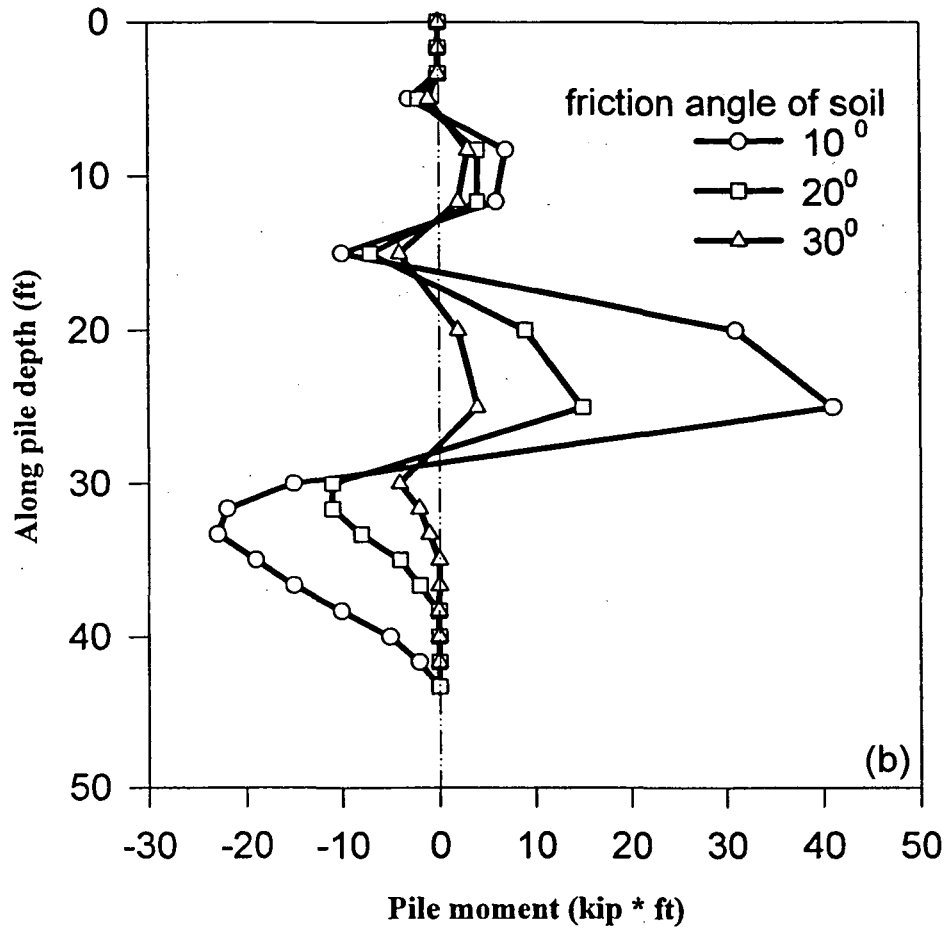


Figure 7.21 Effect of internal friction angle (C=0)
 (b) Pile moments under different internal friction angle

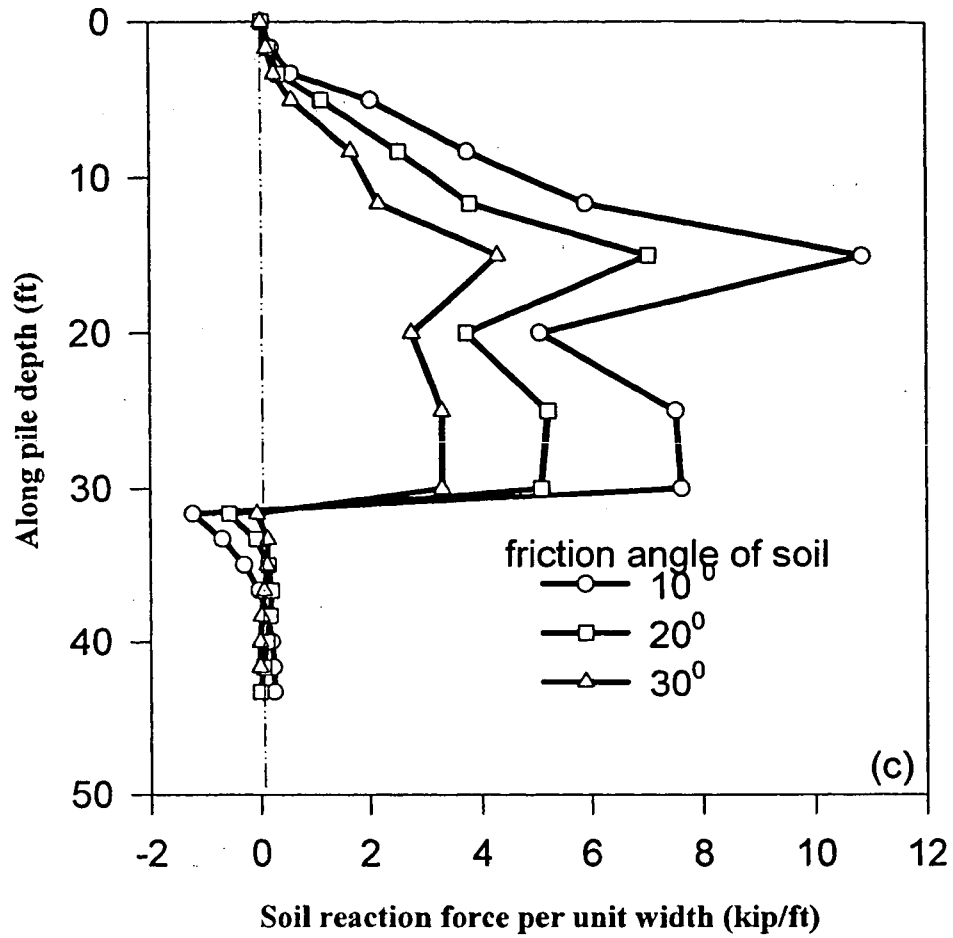


Figure 7.21 Effect of internal friction angle ($C=0$)
(c) Soil reaction forces under different internal friction angle

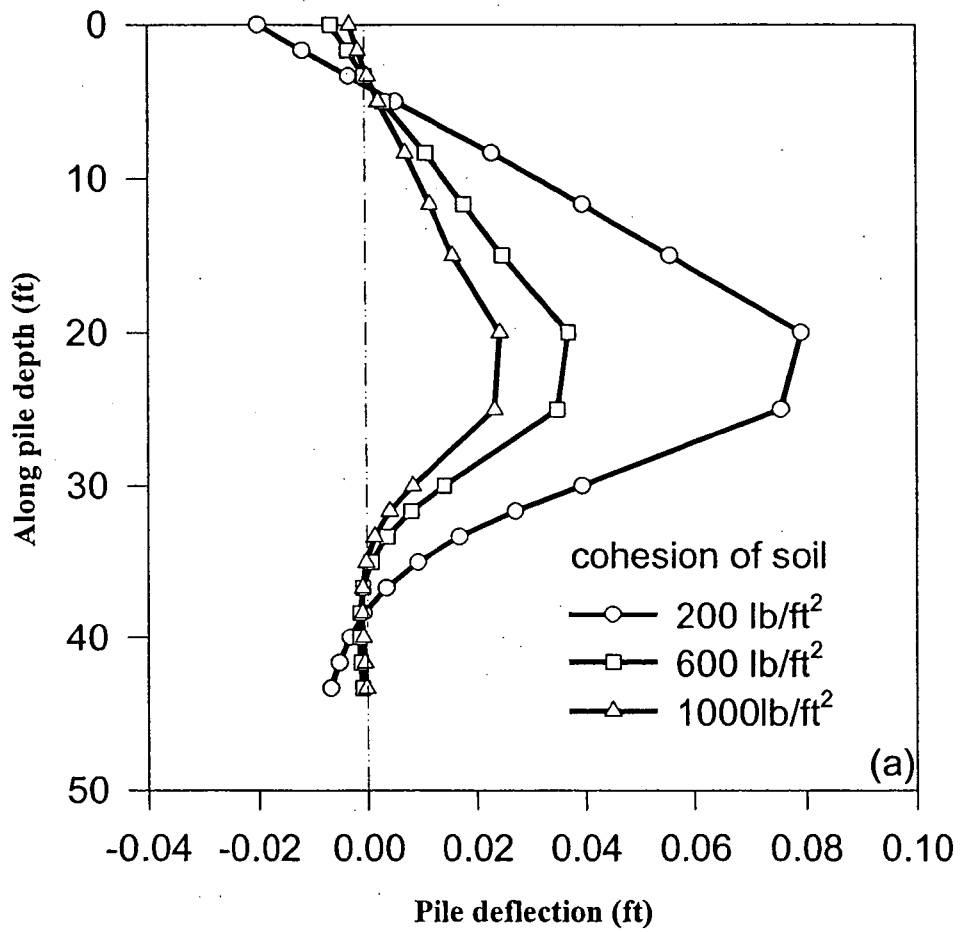


Figure 7.22 (a) Effect of cohesion ($j=0$) on structural deflections of the pile.

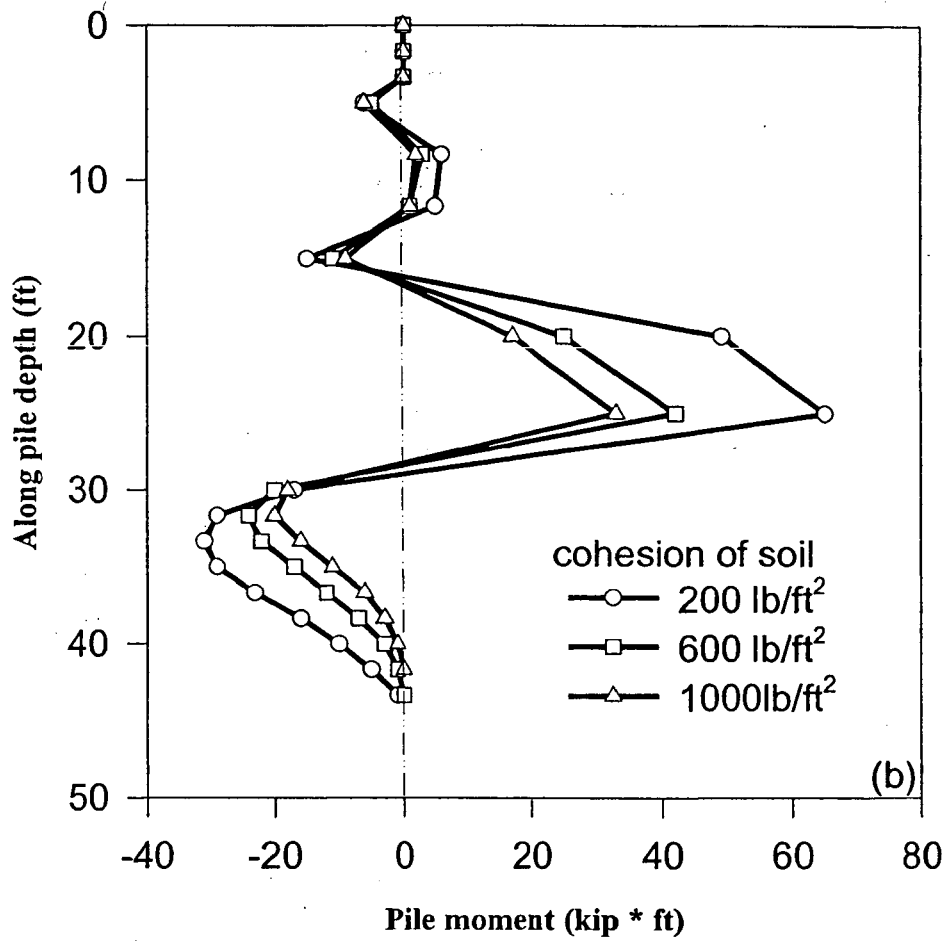


Figure 7.22 (b) Effect of cohesion ($j=0$) on pile moments.

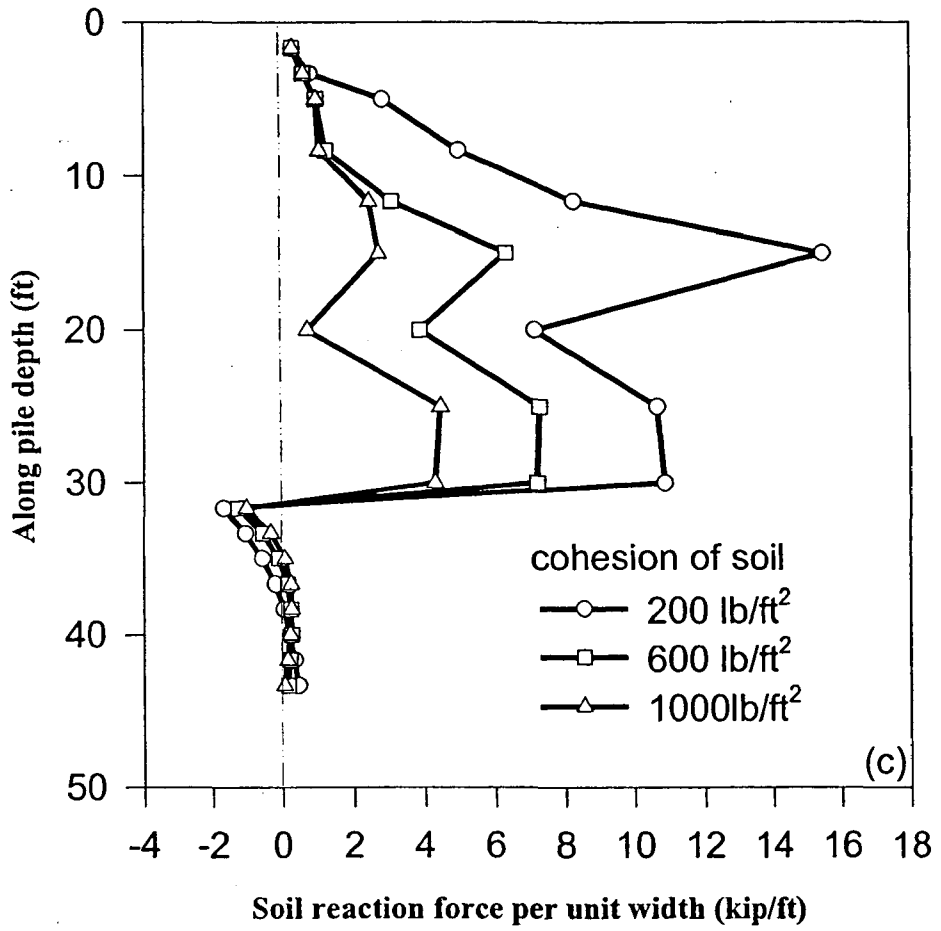


Figure 7.22 (c) Effect of cohesion ($j=0$) on soil reaction forces.

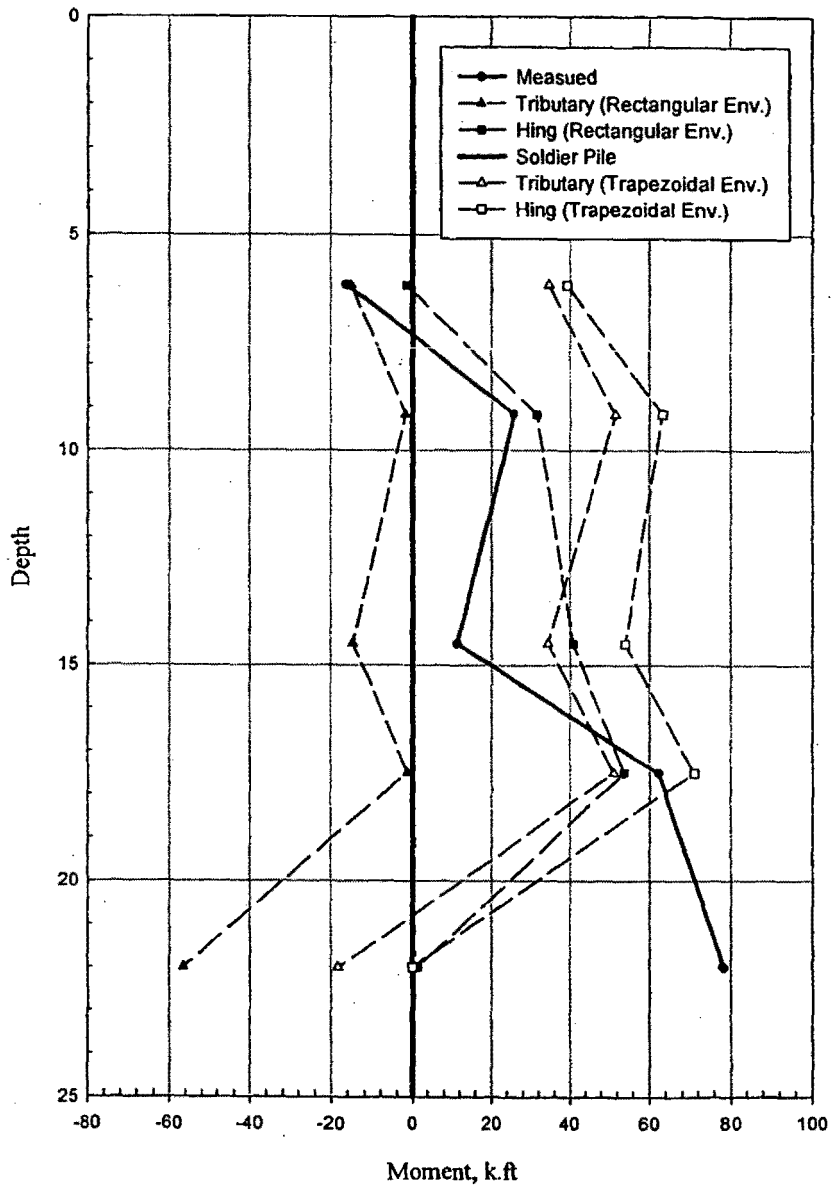


Figure 7.23 Measured moments on soldier pile no. 30 versus the moments calculated by different methods.

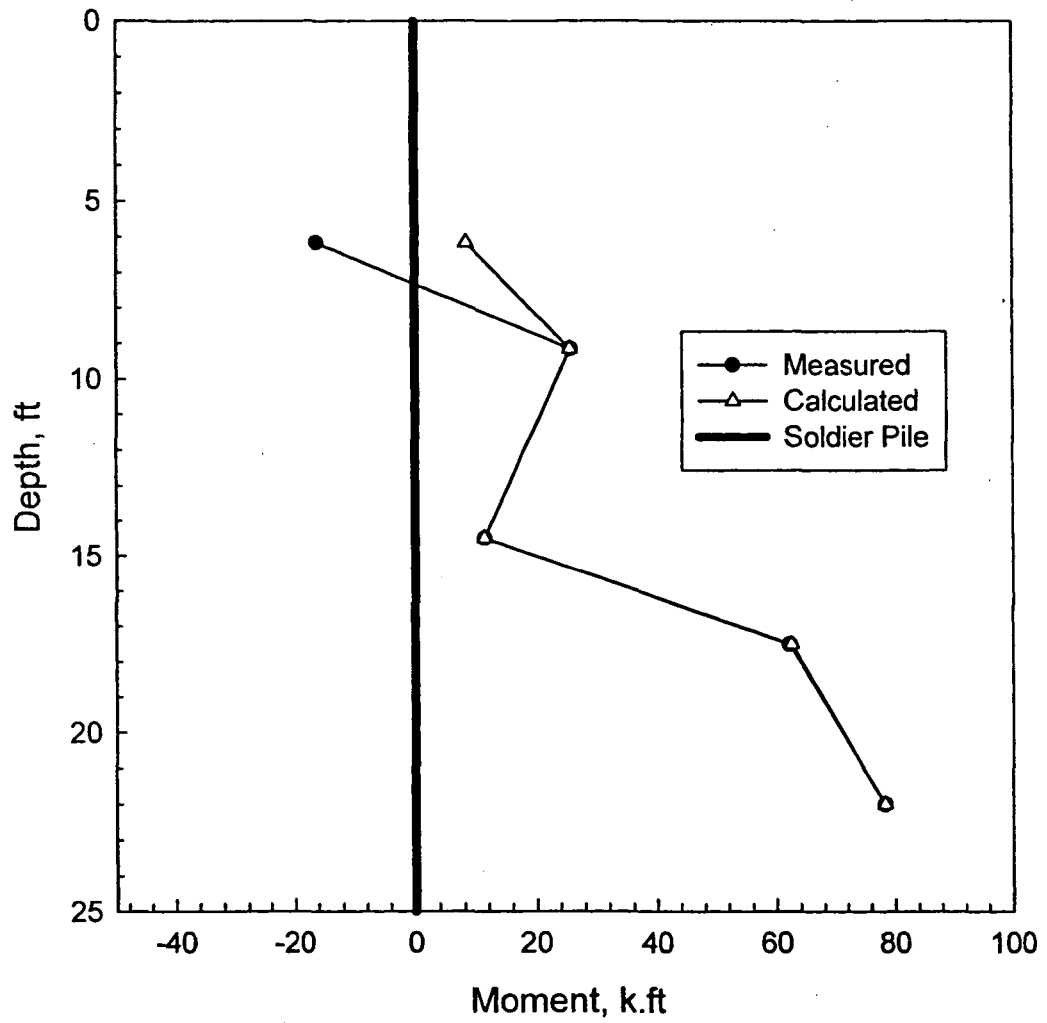


Figure 7.24 Measured moments on soldier pile no. 30 versus the moments calculated based on the derived parameters from soldier pile no. 30.

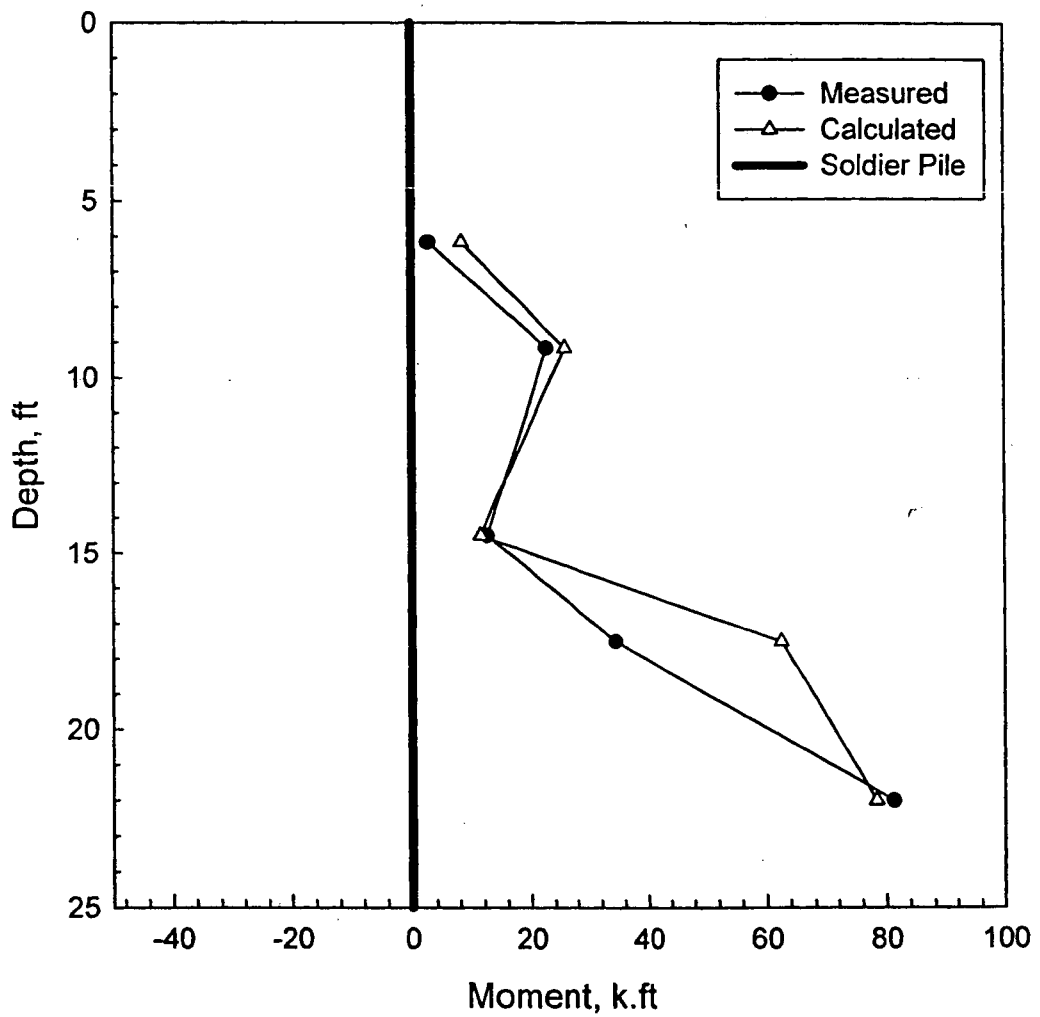


Figure 7.24 Measured moments on soldier pile no. 31 versus the moments calculated based on the derived parameters from soldier pile no. 30.

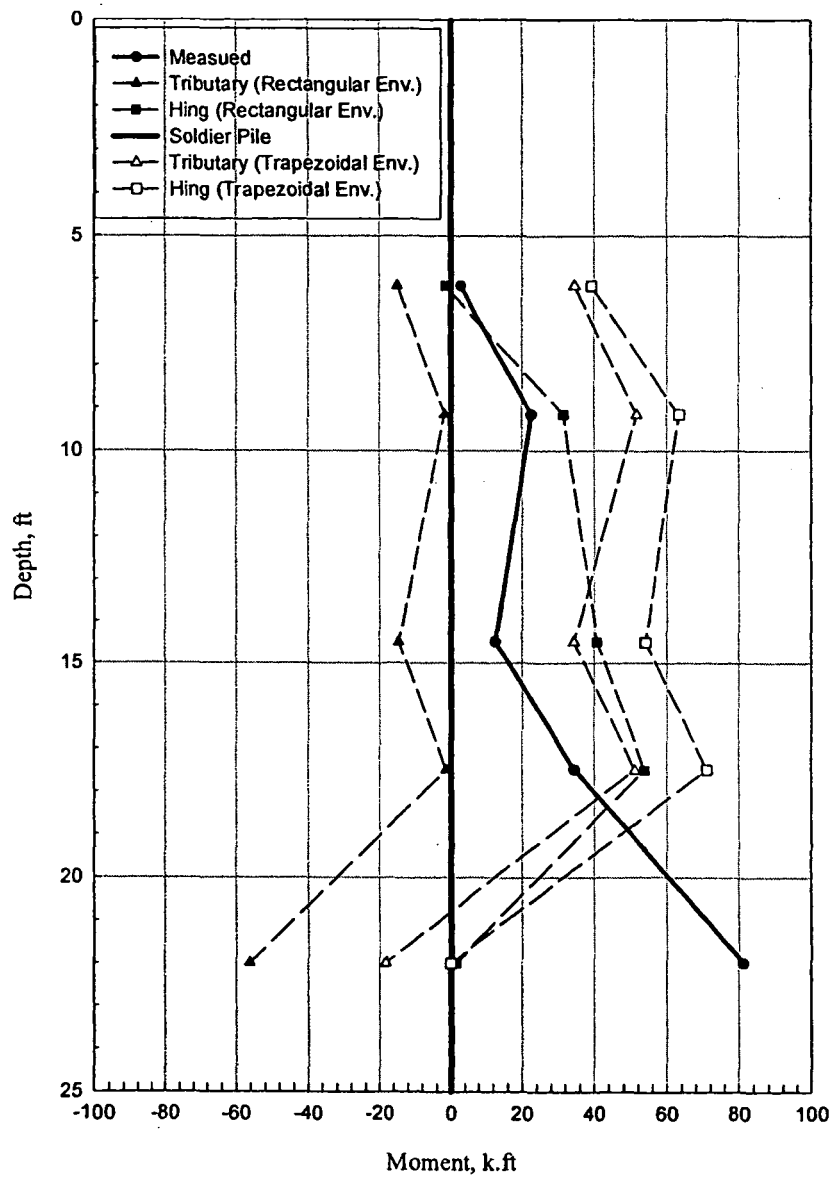


Figure 7.26 Measured moments on soldier pile no. 31 versus the moments calculated by different methods.

CHAPTER VIII

SUMMARY AND CONCLUSIONS

VIII.1 SUMMARY OF TASKS ACCOMPLISHED

During the course of this research, the following tasks have been successfully accomplished.

- a. As part of the planning process, the instrumentation plan of various types of sensors has been developed and incorporated in the final design plan.
- b. All instrumentation sensors have been individually calibrated and checked prior to deployment in the field.
- c. All sensors have been successfully installed as planned during wall construction and according to the design plans. The locations of these sensors have been clearly identified and summarized in Chapter III. The four soldier piles have been instrumented with strain gages and inclinometers. Three inclinometers were installed in the slope behind the wall, and a vibrating wire piezometer was installed at the depth of 40 ft below the ground surface to monitor the pore pressure response at the site. Each of the four soldier piles was instrumented with 16 strain gages at eight locations. Rock anchors installed in the piles #11 and #30 were each instrumented with three strain gages along the anchor length, and a load cell at the anchor head. To date, all installed strain gages have been functioning well, providing meaningful data for further analysis and interpretation.

- d. Real time monitoring of all sensors has been continuing since the sensors have been installed at the site.
- e. Two failure tests on two non-production rock anchors were performed prior to the construction of the production anchors. The failure test anchors were fully instrumented with strain gages in the bond zone as well as the load cell and the dial gage at the anchor head. The anchor pullout test results were used to confirm the adequacy of the production anchor bond length.
- f. In connection with the anchor pullout tests, a new soil-anchor interface model was introduced. The newly developed anchor-soil interface model took into account the effects of dilatancy, confining pressure, the influence zone, and the relative rigidity between the anchor and the soil. Both forward and back calculation schemes were formulated so that the soil-anchor interface model parameters can be determined by the back calculation technique via a matching process between the measured and computed anchor head load-displacement curve. Once the interface model parameters have been determined, the model can be used to predict the anchor performance in the forward calculation for different anchor bond length and size. The model has been applied to the two failure tests conducted in this research project on the lower and upper tier walls, as well as to other pull out test results available in the literature. The application documented in the report has validated the usefulness of the interface model in anchor design.
- g. The techniques for analysis of the tieback wall structures have been reviewed in this report. The various earth pressure envelopes, together with the accompanied structural analysis techniques, have been examined by comparing the calculated and the

measured bending moments in the soldier piles. In addition, a back calculated earth pressure diagram was derived from the measured strain reading in this project. In general, the proposed earth pressure diagram seemed to give better predictions when compared with the measured moments.

- h. As part of the study, a Finite Element Method (FEM) program, PLAXIS, was employed to perform a numerical simulation of the construction of the tieback walls. The FEM simulation process involved the calibration of the soil properties to match the inclinometer readings in the early stage of wall construction. Once this initial calibration was done, then the soil parameters were fixed in the subsequent analysis of various construction stages involved in the wall construction. To realistically mimic the stress-path dependency of the soil response, FEM simulation was also carefully executed in similar stages. The overall quality of the numerical simulation appeared to be very good, when the computed and the measured stresses and deflections of the soldier piles were compared. The close agreements between the measured and the simulation lend strong support to the validity of the FEM analysis techniques.
- i. As part of this research, a Finite Element Method (FEM) computer program was introduced. This program is developed to help in the structural design of the tieback walls incorporating the nonlinear anchor behavior, with the ability to simulate the combined effects of construction stage and anchor prestressing. The validity of the developed FEM program was established by comparing the predictions with the field measurements of a case study of a tieback walls constructed at the Texas A & M University Riverside campus. The detailed FEM simulation study is shown to provide

a powerful and insightful picture of the behavior of the tieback walls. A more in-depth understanding of the tieback wall performance as affected by the prestress level of the anchor, the location of the anchors, the relative rigidity of the wall, and the construction sequence were carefully studied using the newly developed FEM program in a systematic parametric study. Some of the findings from this parametric study would provide useful guidelines in future tieback wall design.

VIII.2 CONCLUSIONS

Based on the experience gained from the instrumentation and monitoring program, coupled with detailed FEM simulation results, the following conclusions can be made.

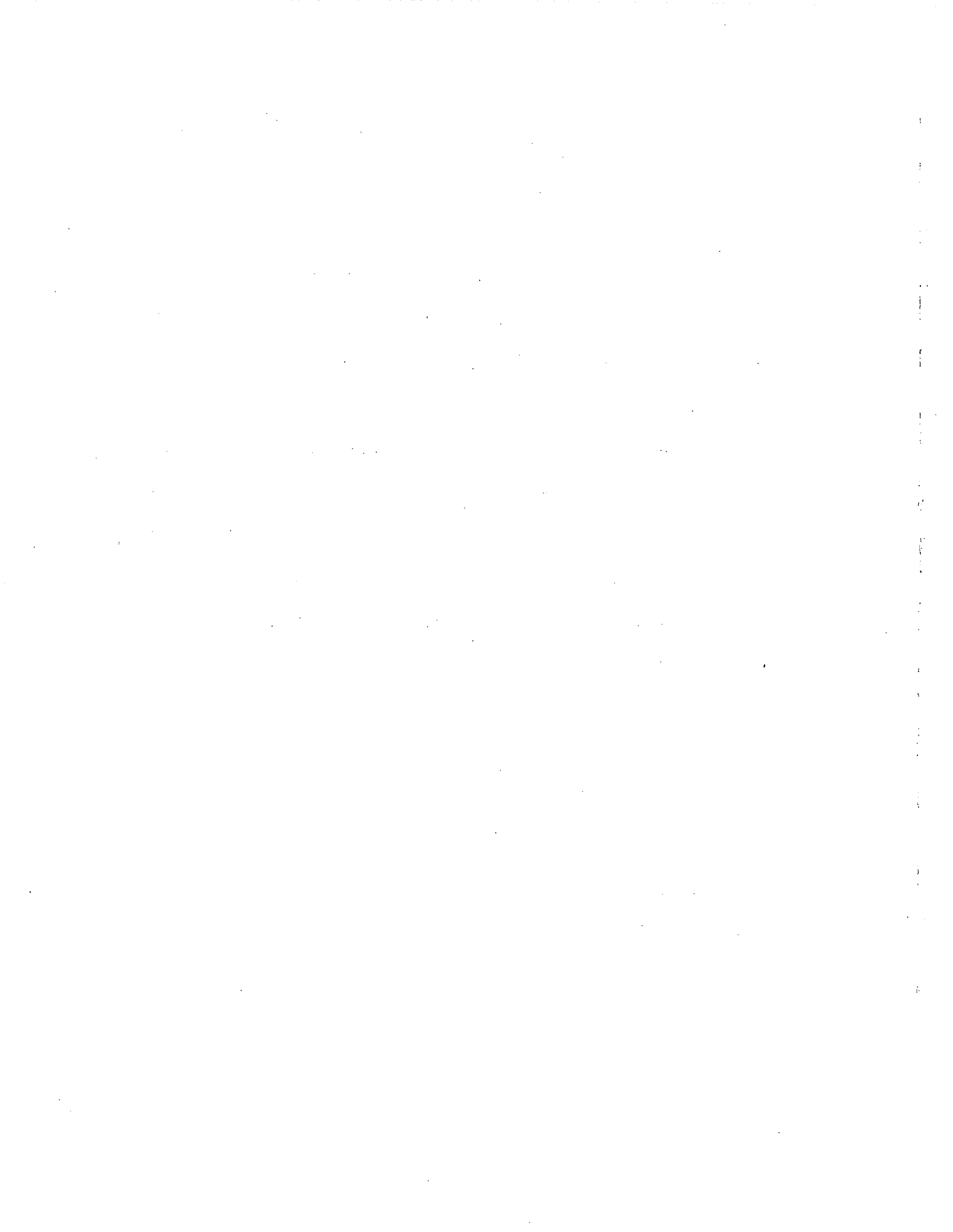
- The instrumentation of the tieback wall provided very useful data for the analysis and design of all members of the tieback walls. These data included strains, and stresses of the tieback wall, ground movement, and ground water changes.
- The performance of tieback walls is affected by anchor prestress, anchor location, layout of anchors (spacing), the relative rigidity of the wall, and the construction sequence.
- The mobilized interface shear strength is dependent upon the soil dilatancy angle and the size of influence zone. In general, an increase of either one of them would lead to an increase of the mobilized shear strength. The dilatancy, strength, and interface modulus (k) showed less contribution after reaching the definite limiting values.

- The rigidity of the anchor-soil interface increases drastically with an increase of the dilatancy angle, but decreases with an increase of the influence zone size. However, the latter factor is negligible for the dilatancy angle from 5° to 25° .
- The distribution of the mobilized anchor force along the anchor bond length is strongly dependent upon the relative rigidity of the anchor. For the case where the relative rigidity factor is larger than 1/10, the distribution is linear.
- By using the back calculation technique, the important interface model parameters can be determined accurately, which can then be used to predict the performance of the anchors with different design lengths.
- In the analysis and study of the behavior of slopes, the main parameters, such as soil properties, anchor-soil interface properties, and element types characterizing various structure components have to be carefully calibrated in a way by matching the FEM predictions with the in situ measurements obtained from two failure tests.
- With the calibrated model available, using the FEM program, two types of construction processes were fully simulated stage by stage in order to incorporate the stress path effects
- Good agreement between the calculated predictions and the measured data has verified the validity of the results obtained from the FEM- PLAXIS analysis.
- Variation in construction sequences has great impact on the bending moment distribution, both the shape and the magnitude, in the soldier piles of the retaining wall. On the other hand, different construction sequences have little influence on the ground anchor behaviors as long as the lock-off loads remain unchanged.

- The global stability of slopes is significantly improved by the installation of tieback walls. Because, both the calculated and measured results indicate that the maximum bending moments developed in the tier walls are less the design capacity, thus the structural safety of the retaining wall components is guaranteed.
- The deflections of tieback walls primarily occur at the early construction stage, and are controlled by the prestressing of the first row of anchors. Shifting the location of the first row anchor to near the top of the pile is an efficient way to control the total pile deflection. However, when the first row anchors were placed to the location too close to the ground surface, their capacity may be reduced due to a lack of confining stress.
- For the purpose of analysis of the tieback walls, the distribution of the earth reaction force can be represented by a rectangular uniform pressure with a reasonable accuracy, although the actual soil pressure is essentially trapezoidal. The moment induced at the anchor-wall point must be considered since it considerably affects the stress distribution along the soldier pile. This moments developed at each anchor point can be a function of the overburden pressure, the magnitude of prestress, as well as anchor angle, length, and diameter.
- The location of the maximum moment developed in the pile is usually at the anchor location or close to the bottom of excavation, depending on the anchor location, and the anchor prestress.
- The prestress level at the anchor exerts more effect at the local level; namely, near the anchor location. The development of the anchor working force is mainly affected by

the immediate construction stage. The subsequent construction has little influence on the variation of the anchor force.

- Further studies may be recommended. These studies are advised to be oriented at:
 - Evaluating suitable parameters for different soil/rock materials. Based on the cases analyzed earlier in this section, it was clear that the parameters of different materials differ considerably.
 - Developing a new method and standards for the analysis and design of the tieback wall. Using the available methods that were originally developed for the traditional braced excavation apparently, do not apply to the case of tieback walls. Further study for the developing moments at the anchor-pile point, their magnitude, and parameters encountered therein are recommended.
 - Studying the overlapping effect of the anchor influence zones may also be important. The vertical and horizontal anchor spacing will play a significant role in the mobilized system properties.



CHAPTER IX

REFERENCES

1. Bell, A. L., 1915, "The Lateral Pressure and Resistance of Clay, and the Supporting power of Clay Foundations", A Century of Soil Mechanics, ICE, London, pp. 93-134.
2. Bowles, J. E., 1988, "Foundation Analysis and Design", 4th ed., McGraw-Hill Book Publishing Co., NY, NY.
3. Brooker, E. W., and Ireland, H. O., "Earth Pressure At Rest Related to Stress History", CGJ, Vol. 2, no. 1, Feb., pp. 1-15.
4. Canadian Foundation Engineering Manual method (CFEM), 1985, Canadian Geotechnical Society, BiTech Publishers, Vancouver, B.C., Canada.
5. Caquot, A., and Kerisel, J., 1948, "Tables for Calculation of Passive, Pressure, Active Pressure, and Bearing Capacity of Foundations", (Translated by M. A. Bec, London), Gauthier-Villars, Paris.
6. Cheney, R. S., 1988, "Permanent Ground Anchor", FHWA-DP-68-1R, Federal Highway Administration, Washington DC.
7. Clough, W. G., 1984, "Users Manual for SOILSTRUCT", Department of of Civil Engineering, Virginia Polytechnical Institute, Blacksburg, Va.
8. Coyle, H. M., and Sulaiman, I. H., "Skin Friction For Stell Piles in Sand", Journal of Soil Mechanics and Foundation Division, ASCE, Vol. 93, No. SM6, Nov., 1967, pp. 261-278.
9. Coyle, H. M., and Reese, L. C., "Load Transfer for Axially Loaded Piles in Clay", Journal of the Soil Mechanics and Foundation Division, ASCE, Vol. 92, No. SM2, Mar., 1966, pp.1-26.
10. Feng, Y., 1997, "Fundamental Study of Single Anchor and Anchor Reinforced System", Ph.D. Thesis, The University of Akron.

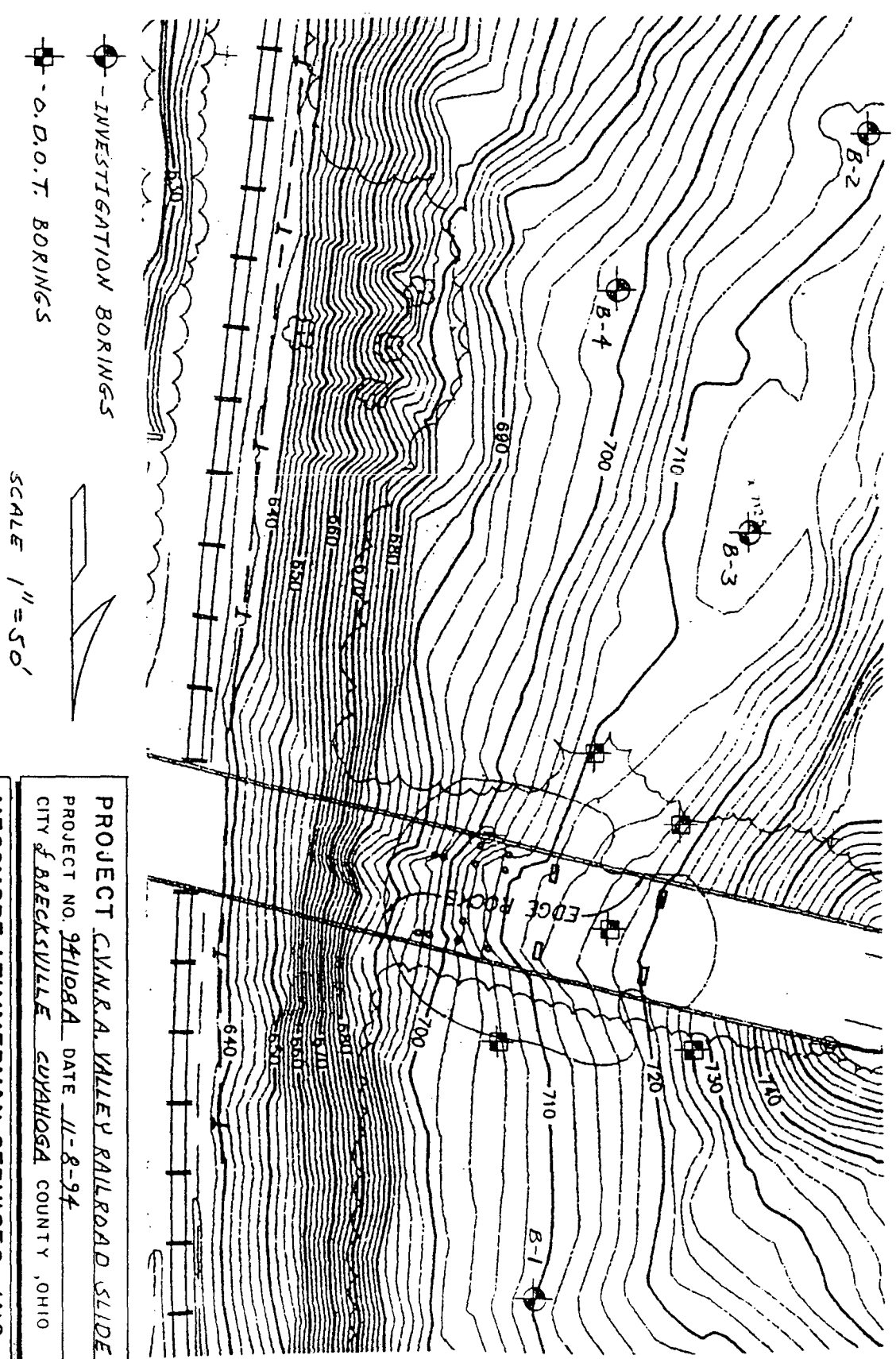
11. Haliburton, T. A., 1968, "Numerical Analysis of Flexible Retaining Structures", proc., ASCE, 94(6), 1233-1251.
12. Hetenyi, M., 1946, "Beams on Elastic Foundations", University of Michigan Press, Ann Arbor, Mich.
13. Jaky, J. (1948), "Pressure in Silos", 2nd ICSMFE, Vol. 1., pp. 103-107.
14. Janbu, N., 1957, "Earth Pressures and Bearing Capacity Calculations by Generalized Method of Slices", 4th ICSMFE, Vol. 2, pp.207-212.
15. Khaova, M., Montel, B. Civard, A., and Lauga, R., 1969, "Cheurfas Dam Anchorage: 30 Years of Controls and Recent Reinforcement", Proc. 7th ICSMFE, Mexico City, Mexico.
16. Kraft, L. M., Jr., Ray, R. P., and Kagawa, T., "Theoretical Development of t-z Curves", Journal of Geotechnical Engineering, ASCE, Vol. 107, No. GT11, 1981.
17. Lambe, T. W., and Wolfskill, A. L., 1970, "Measured Performance of Braced Excavation", J. of Soil Mechanics and Foundation Division, ASCE, 95(6), pp. 817-836.
18. Littlejohn, G. S. (1980) " Design estimation of the ultimate load-holding capacity of ground anchors", Ground engrg. (Nov.).
19. Ludwig, H., 1984, "Short Term and Long Term Behavior of Tiebacks Anchored in Clay", Ph.D. Thesis, McGill University, Montreal.
20. Matlock H., Bogard, D., and Lam, I., 1981, "BMCOL76: A Computer Program for the Analysis of Beam-Columns Under Static Uniaxial and Lateral loading", Program developed at the Univ. of Texas at Austin, under grant from Fugro, Inc., and Documented at Ertec, Inc., Long Beach, Calif.
21. Morimich Uesugh, Hideaki Kishida and Yasunori Tsubakihara, "Behavior of sand particles in sand-steel friction", Soil and Foundations, Vol. 28, No. 1, 107-118, 1988.
22. Myslivec, A., 1972, "Pressure At Rest of Cohesive Soils", Proc. 5th European Conference SMFE, Vol. 1, pp. 51-102.

23. NAVFAC DM-7.2, 1982, "foundations and Earth Structures", Department of the Navy, Naval Facilities Engineering Command, Alexandria, Va.
24. Nicholson, P. J., D. D. Uranowski, and P. T. Wycliff-Jones, 1982: "Permanent Ground Anchors, Nicholson Design Criteria", Dept. Transp. Fed. Hwy. Admin. Office of Research and Development, Washington, D.C.
25. Otta, L, Pantucek, M. and Goagnour, P. R. (1982)" Permanent ground anchors: Stump design criteria", Office of research and development, Federal highway administration, US dept. of Transportation, Washington, D. C.
26. Pfister, P., G. Evers, M. Guillaud, and R. Davidson, 1982: "Permanent Ground Anchors, Soletanche Design Criteria", Dept. Transp. Fed. Hwy. Admin. Office of Research and Development, Washington, D.C.
27. Randolph, M. F., and Wroth, C. P., "Analysis of Deformation of Vertical Loaded Piles", Journal of Geotechnical Engineering, ASCE, Vol.104, GT12, 1978.
28. Rankine, W. J. M., 1857, "On the Stability of Loose Earth", Philosophical Transactions of the Royal Society, London, Vol. 147.
29. Schnable, H. Jr., 1982, "Tiebacks In Foundation Engineering and Construction", McGraw-Hill Book Pub. Co., NY, NY.
31. Shield, D. H., and Tolunay, A. Z., 1973, "Passive Pressure Coefficients by the Method of Slices, JSMFD, ASCE, Vol. 99, SM 12, Dec., pp. 1043-1053.
32. Sokolovski, V. V., 1960, "Statics of Soil Media", Second Edition, Butterworth Scientific Publication, London.
33. Su, W and Fragaszy, R. J.(1988) "Uplift testing of Model anchors" Journal of geotechnical engineering, ASCE, vol. 114, No. 9
34. Terzaghi, K., and Peck, R. B., 1948, "Soil Mechanics in Engineering Practice", John Wiley & Sons, Inc. New York.
35. Terzaghi, K., and Peck, R. B., 1967, "Soil Mechanics in Engineering Practice", 2nd Edition, John Wiley & Sons, Inc. New York.

36. Tschebotarioff, G. P., 1973, "Foundations, Retaining and Earth Structures", 2nd ed., McGraw-Hill Book Pub. Co., NY, NY.
37. Vijivergiya, V. N., "Load-Movement Characteristics of Piles" 4th Symposium of Waterway, Port, Coastal and Ocean Division, ASCE, Vol. 2, 1977, pp. 269-284.
38. Vitton, S. J. (1991). " Local transfer mechanisms in anchored geosynthetic system." Ph. D. thesis, University of Michigan, Ann Arbor, Mich.
39. Winkler, E., 1867, "Die Lehre von Elastizitat und Festigkeit"; H. Dominicus, Prague, Czechoslovakia.
40. Wroth, C. P., 1972, "General Theories of of Earth Pressures and Deformations", 5th European Conference on SMFE, Madrid, Vol. 2, pp. 33-52.
41. Xanthakos, P. P. (1991)"Ground anchors and anchored structure", A wiley-interscience publication, John Wiley and sons Inc.
42. Yoshimi, Y., and T. Kishida, "A ring Torsion Apparatus for Evaluating Friction Between Soil and Metal Surfaces", Gotechnical Testing Journal, pp145-152, 1982.

APPENDIX A
TEST BORING LOGS

LOCATION PLAN



PROJECT C.V.M.R.A. VALLEY RAILROAD SLIDE
PROJECT NO. 94108A DATE 11-8-94
CITY of BRECKSVILLE CUYAHOGA COUNTY, OHIO
MESSMORE / TIMMERMAN SERVICES, INC.
265 E. MARKET STREET, AKRON, OHIO 44308


ABBREVIATIONS AND SYMBOLS USED ON TEST BORING LOGS

Sampling Method Abbreviations

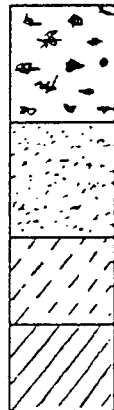
- SS: Split spoon sampler, 2" O.D. by 1-3/8" I.D. (ASTM D-1586)*
 ST: Shelby tube sampler, 3" O.D. by 2-7/8" I.D. (ASTM D-1587)
 ST2: Shelby tube sampler, 2" O.D. by 1-7/8" I.D. (ASTM D-1587)
 NX: Rock core, 2-1/8" diameter (ASTM D-2113)

* ASTM D-1586, the Standard Penetration Test, utilizes a 140 lb. hammer dropped 30" to drive the split spoon sampler.

Miscellaneous Abbreviations

- : Groundwater level at completion of boring
 Rec: Recovered length of sample
 Wn: Natural moisture content, ratio of the weight of water to the weight of solids in the sample (ASTM D-2216)
 ATV: All-terrain vehicle
 RQD: Rock Quality Designation, sum of core pieces 4" in length or greater, divided by the recovered core length

Soil Particle Sizes and Graphic Symbols

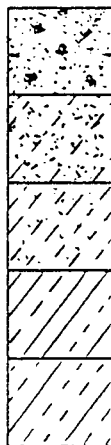


Gravel: Coarse = 3/4" to 3"
 Fine = 4.76 mm to 3/4"

Sand: Coarse = 2.0 to 4.76mm
 Medium = 0.42 to 2.00mm
 Fine = 0.074 to 0.42mm

Silt: 0.005 to 0.074mm

Clay: Finer than 0.005mm



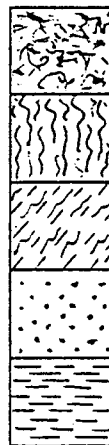
Sand and Gravel

Silty Sand

Sandy Silt

Silty Clay

Clayey Silt



Miscellaneous Fill

Peat and Organics

Organic Silt

Sandstone

Shale

Messmore/Timmerman Services, Inc.

MESSMORE/TIMMERMAN SERVICES, INC.

265 EAST MARKET STREET
AKRON, OHIO 44308

BORING NUMBER: B-1
Page 1 of 2
DATE STARTED: 9-30-94
DATE COMPLETED: 9-30-94

TEST BORING LOG

PROJECT: CVNRA Task Order #83 PROJECT NUMBER: 941108A
LOCATION: SR82 Bridge, Brecksville, Ohio DRILLER: N. Teter
BORING METHOD: 3 1/4" I.D. Hollow Stem Auger DRILL USED: D-50, ATV
SAMPLER USED: 2.0" O.D. Split Spoon WEATHER: Sunny, 55° F.
REMARKS: GROUND ELEVATION: 710±
WATER ENCOUNTER DEPTH: 44.0' WATER DEPTH ON COMPLETION: None HOLE DEPTH: 43.0'

DEPTH	SAMPLE		BLOWS/6"	REC	LOG	DESCRIPTION OF MATERIALS & REMARKS
	NO	DEPTH TYPE				
0---						6" Topsoil.
--	1.0					
--	1	SS	3-5-4	16"		Damp, stiff, brown, silty CLAY (Wn=24.5%).
--	2.5					3.0'
--	2	SS	3-2-4	17"		Damp, loose, brown SILT, some fine sand
5---	5.0					(Wn=22.2%).
--						7.5'
--	3	SS	5-5-8	17"		Damp, stiff, gray, clayey SILT
10---	10.0					(LL=30.6%, PL=19.2%, Wn=22.1%).
--						
--	4	SS	3-4-5	18"		Damp, stiff, gray, clayey SILT (Wn=21.7%).
15---	15.0					
--						
--	5	SS	3-6-7	18"		Damp, stiff, gray, silty CLAY
20---	20.0					(LL=31.9%, PL=22.0%, Wn=23.6%).
--						
--	6	SS	4-6-7	18"		Moist, stiff, gray, silty CLAY (Wn=19.8%).
25---	25.0					
--						
--	7	SS	4-5-8	18"		Moist, stiff, gray, silty CLAY
30---	30.0					(LL=28.0%, PL=18.8%, Wn=24.6%).
--						
--	8	SS	4-6-9	18"		Moist, stiff, gray, silty CLAY (Wn=16.3%).
35---	35.0					
--						
--	9	SS	12-14-22	17"		38.0' Damp, dense, gray, severely weathered SHALE
40---	40.0					(Wn=10.8%).

MESSMORE/TIMMERMAN SERVICES, INC.

265 EAST MARKET STREET
AKRON, OHIO 44308

BORING NUMBER: B-1
Page 2 of 2

PROJECT: CVNRA Task Order #83

PROJECT NUMBER: 941108A

DEPTH	SAMPLE		BLOWS/6"	REC.	LOG	DESCRIPTION OF MATERIALS & REMARKS
	NO	DEPTH TYPE				
40---						
--						
--						
--						
--	10	43.5	SS	34-50/1"	7"	Dry, compact, gray, weathered SHALE; 1" wet seam present.
45---		45.0				
--						
--						
--	11	48.5	SS	50/3.5"	2"	Dry, compact, gray, weathered SHALE.
50---		50.0				
--						
--						
55---						
--						
--						
60---						
--						
--						
65---						
--						
--						
70---						Boring terminated at 48.8 feet.
--						
--						
75---						
--						
--						
80---						
--						
--						
85---						
--						

MESSMORE/TIMMERMAN SERVICES, INC.

265 EAST MARKET STREET
AKRON, OHIO 44308

BORING NUMBER: B-2
Page 1 of 2
DATE STARTED: 9-30-94
DATE COMPLETED: 10-1-94

TEST BORING LOG

PROJECT: CVNRA Task Order #83
LOCATION: SR82 Bridge, Brecksville, Ohio
BORING METHOD: 3 1/4" I.D. Hollow Stem Auger
SAMPLER USED: 2.0" O.D. Split Spoon
REMARKS:

PROJECT NUMBER: 941108A
DRILLER: N. Teter
DRILL USED: D-50, ATV
WEATHER: Sunny, 65° F.
GROUND ELEVATION: 709±

WATER ENCOUNTER DEPTH: 13.0' WATER DEPTH ON COMPLETION: 11.5' HOLE DEPTH: 13.5'

DEPTH	SAMPLE		BLOWS/6"	REC	LOG	DESCRIPTION OF MATERIALS & REMARKS
	NO	DEPTH TYPE				
0---						
---	1.0					
---	1	2.5 SS	4-7-11	16"		Damp, very stiff, brown, clayey SILT, trace of gravel (Wn=18.2%).
---	2	3.5 SS	5-7-9	18"		Damp, very stiff, brown, clayey SILT, trace of gravel (Wn=18.3%).
5---	5.0					
---						7.0'
---	3	8.5 SS	4-4-5	17"		Moist, loose, brown, fine SAND & SILT (Wn=19.9%).
10---	10.0					

---	4	13.5 SS	3-4-5	16"		Saturated, loose, brown, fine SAND & SILT (Wn=21.4%).
15---	15.0					

---	5	18.5 SS	7-7-8	16"		Moist, medium dense, gray SILT, minor clay & fine sand (LL=30.6%, PL=20.2%, Wn=26.8%).
20---	20.0					
---						22.5'
---	6	23.5 SS	5-5-8	18"		Damp, stiff, gray, silty CLAY (Wn=29.6%).
25---	25.0					

---	7	28.5 SS	5-5-6	17"		Damp, stiff, gray, silty CLAY (LL=36.6%, PL=21.9%, Wn=23.6%).
30---	30.0					

---	8	33.5 SS	5-6-9	17"		Damp, stiff, gray, clayey SILT (Wn=27.9%).
35---	35.0					

---	9	38.5 SS	5-8-11	16"		Damp, very stiff, gray, clayey SILT (Wn=33.2%).
40---	40.0					

MESSMORE/TIMMERMAN SERVICES, INC.

265 EAST MARKET STREET
AKRON, OHIO 44308

BORING NUMBER: B-2
Page 2 of 2

PROJECT: CVNRA Task Order #83				PROJECT NUMBER: 941108A		
DEPTH	SAMPLE		BLOWS/6"	REC	LOG	DESCRIPTION OF MATERIALS & REMARKS
	NO	DEPTH TYPE				
40---						
43.5	10	SS	5-11-14	16"		Damp, very stiff, gray, clayey SILT (LL=28.0%, PL=20.7%, Wn=24.4%).
45---						
48.5	11	SS	6-11-12	17"		Damp, very stiff, gray, clayey SILT (Wn=17.9%).
50---						
53.5	12	SS	8-10-17	18"		Damp, very stiff, gray, clayey SILT (Wn=22.3%).
55---						
58.5	13	SS	11-24-40	15"		Damp, hard, gray, clayey SILT; slight shaley structure (Wn=12.3%).
60---						
63.5	14	SS	15-24-40	17"		Damp, hard, gray, clayey SILT; slight shaley structure (Wn=15.1%).
65---						
68.5	15	SS	13-36-	18"		Damp, hard, gray, clayey SILT; slight shaley structure (Wn=20.8%).
70---			60/6"			
75---						<p><u>41 Hr. Water Level Reading</u> Water Depth: 9.8' Hole Depth: 10.0'</p>
80---						Boring terminated at 70.0 feet.
85---						

MESSMORE/TIMMERMAN SERVICES, INC.

265 EAST MARKET STREET
AKRON, OHIO 44308

BORING NUMBER: B-3
Page 1 of 2
DATE STARTED: 10-3-94
DATE COMPLETED: 10-3-94

TEST BORING LOG




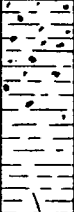
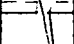
PROJECT: CVNRA Task Order #83 PROJECT NUMBER: 941108A
LOCATION: SR82 Bridge, Brecksville, Ohio DRILLER: N. Teter
BORING METHOD: 3 1/4" I.D. Hollow Stem Auger DRILL USED: D-50, ATV
SAMPLER USED: 2.0" O.D. Split Spoon WEATHER: Sunny, 50° F.
REMARKS: GROUND ELEVATION: 713±
WATER ENCOUNTER DEPTH: 11.0' WATER DEPTH ON COMPLETION: 50.0' HOLE DEPTH: 63.5'

DEPTH	SAMPLE		BLOWS/6"	REC	LOG	DESCRIPTION OF MATERIALS & REMARKS
	NO	DEPTH TYPE				
0						
1	1.0					
	2.5	SS	6-8-8	15"		Moist, medium dense, brown, fine to medium SAND, some silt (Wn=10.6%).
	3.5					
2	5.0	SS	3-5-9	17"		Moist, medium dense, brown SILT & fine SAND (Wn=18.1%).
5						
	8.5					7.5'
	10.0	SS	6-7-9	10"		Damp, medium dense, gray SILT, some fine sand (Wn=18.1%). Wet seam present from 11.0' to 12.5'.
10						
	13.5					
	15.0	SS	5-8-9	11"		Damp, medium dense, gray SILT, minor clay & fine sand (Wn=15.1%).
15						
	18.5					
	20.0	SS	7-8-10	15"		Damp, medium dense, gray SILT, minor clay & fine sand (LL=24.8%, PL=19.7%, Wn=13.6%).
20						
	23.5					
	25.0	SS	8-9-10	12"		Damp, medium dense, gray SILT, trace of fine sand (Wn=20.6%).
25						
	28.5					28.0'
	30.0	SS	3-5-6	16"		Damp, stiff, gray, clayey SILT (LL=34.6%, PL=21.1%, Wn=20.3%).
30						
	33.5					
	35.0	SS	4-6-7	18"		Damp, stiff, gray, clayey SILT (Wn=26.5%).
35						
	38.5					
	40.0	SS	4-5-7	17"		Damp, stiff, gray, clayey SILT (Wn=23.3%).
40						

MESSMORE/TIMMERMAN SERVICES, INC.

265 EAST MARKET STREET
AKRON, OHIO 44308

BORING NUMBER: B-3
Page 2 of 2

PROJECT: CVNRA Task Order #83				PROJECT NUMBER: 941108A		
DEPTH	SAMPLE		BLOWS/6"	REC	LOG	DESCRIPTION OF MATERIALS & REMARKS
	NO	DEPTH TYPE				
40---						
45---	10	43.5 SS	6-9-12	18"		Damp, very stiff, gray, silty CLAY, trace of gravel (Wn=16.7%).
50---	11	48.5 SS	5-7-10	17"		Damp, very stiff, gray, clayey SILT (Wn=21.7%).
55---	12	53.5 SS	4-5-7	17"		Damp, gray, clayey SILT. 54.0'
60---	13	58.5 SS	35-50/6	10"		Saturated, stiff, gray, silty CLAY (LL=29.2%, PL=19.0%, Wn=29.2%). 58.0'
65---	14	63.5 SS	19-34-45	13"		Dry, compact, gray, severely weathered SHALE & SILTSTONE (Wn=8.2%).
70---						<u>18 Hr Water Level Reading</u> Water Depth: 4.5' Hole Depth: 5.0'
75---						
80---						Boring terminated at 65.0 feet.
85---						

MESSMORE/TIMMERMAN SERVICES, INC.

265 EAST MARKET STREET
AKRON, OHIO 44308

BORING NUMBER: B-4
Page 1 of 1
DATE STARTED: 10-4-94
DATE COMPLETED: 10-4-94

TEST BORING LOG

PROJECT: CVNRA Task Order #83 PROJECT NUMBER: 941108A
LOCATION: SR82 Bridge, Brecksville, Ohio DRILLER: N. Teter
BORING METHOD: 3 1/4" I.D. Hollow Stem Auger DRILL USED: D-50, ATV
SAMPLER USED: 2.0" O.D. Split Spoon WEATHER: Sunny, 45° F.
REMARKS: GROUND ELEVATION: 699±
WATER ENCOUNTER DEPTH: None WATER DEPTH ON COMPLETION: None HOLE DEPTH: 26.5'

DEPTH	SAMPLE		BLOWS/6"	REC	LOG	DESCRIPTION OF MATERIALS & REMARKS
	NO	DEPTH TYPE				
0---						2" Topsoil.
--	1.0					Damp, stiff, brown, clayey SILT, trace of fine sand & gravel (Wn=18.4%).
--	1	SS	5-6-9	15"		2.5'
--	2.5					
--	2	SS	2-3-3	18"		Damp, loose, brown, fine SAND & SILT (Wn=18.8%)
5---	3.5					5.0'
--	5.0					
--	8.5					
--	3	SS	2-2-4	14"		Damp, medium stiff, gray, silty CLAY (LL=46.2%, PL=26.2%, Wn=32.9%).
10---	10.0					
--	13.5					
--	4	ST		23"		Damp, medium stiff, gray, silty CLAY (LL=44.8%, PL=25.6%, Wn=30.5%; q _u =1,460 psf).
15---	15.5					
--	18.5					
--	5	SS	4-6-9	17"		Damp, stiff, gray, clayey SILT (Wn=25.9%).
20---	20.0					
--	23.5					
--	6	SS	5-7-9	17"		Moist, stiff, gray, silty CLAY (Wn=25.2%).
25---	25.0					
--	28.5					
--	7	ST		14"		Damp, very stiff, gray, silty CLAY (Wn=21.0%; q _u =5,030 psf).
30---	30.5					
--						
35---						Boring terminated at 30.5 feet.
--						
40---						